Bull. Min. Res. Exp. (2018) 157: 1-21

Bulletin of the Mineral Research and Exploration

http://bulletin.mta.gov.tr

Geochemical and petrologic evolution of Otlakbaşı basaltic volcanism to the east of Lake Van

Vural OYAN[a*]

[a]*Yüzüncü Yıl University, Faculty of Engineering, Department of Mining Engineering, 65080, Van. orcid.org/0000-0002-1566-9749*

Research Article

Keywords:
Eastern Anatolia, Otlakbaşı volcanism, crustal contamination, partial melting, spinel peridotite.

ABSTRACT

Collision-related Otlakbaşı volcanism to the east of Lake Van occurred by eruptions from extensional fissures. In this study, new Ar-Ar age data and major, trace and rare earth elements characteristics of the Otlakbaşı basaltic volcanism are investigated. The Ar-Ar age data indicate that this basaltic volcanism erupted in Early Pliocene time in contrast to its previously known as Quaternary age. The volcanic products are basaltic composition and close to alkaline-subalkaline division line. Results of fractional crystallization accompanied by assimilation (AFC) modelling imply that fractional crystallisation can be negligible compared to crustal contamination in the evolution processes of the magma chamber and ratio of the crustal contamination to the fractional crystallisation (r values) varies from 0.1 to 0.35. Enrichment of large ion lithophile elements (LILE) and light rare earth elements (LREE) relative to high strength field elements (HFSE) and behaviour of mobile elements (Ba and Th) reveal that the mantle source region of the Otlakbaşı basaltic volcanism might have been enriched by melts that were derived from subducted sediments. Depletion in Rb and K elements of the fractionated-corrected samples indicate that amphibole and/or phlogopite could be presence in the mantle source. Results of partial melting model studies show that this basaltic volcanism can be predominantly produced by the melting of the spinel peridotite source. Metasomatized spinel bearing lithospheric mantle may be responsible for the eruption of the Otlakbaşı basaltic volcanism.

Received Date: 07.12.2017
Accepted Date: 04.02.2018

1. Introduction

Turkey is located within geodynamic belts coeval with collision, post collision and arc in the collision zone between the Gondwana and Eurasian plates. As a result, it appears to be a natural laboratory in terms of geological variety. The East Anatolian Collision Zone (EACZ) is a high plateau formed by north-south compression linked to continental collision in the stage from the Miocene on, following subduction of the Tethys ocean between the Arabian and Eurasian plates (Şengör and Kidd, 1979). As a result of this collision east-west oriented folds, reverse faults, and the strike-slip North Anatolian and East Anatolian fault systems (Figure 1a) developed in the region (Yılmaz et al., 1987). The EACZ is characterised by volcanic activity ranging from the Miocene to historical periods (Keskin et al., 2013; Oyan et al., 2016, 2017). This volcanic activity began in the south of the EACZ before 15 My (Lebedev et al., 2010). Recent studies indicate the last oceanic lithosphere in the East Anatolian region was completely subducted before 20 My (Okay et al., 2010). Additionally, Karaoğlan et al. (2016) emphasised that the collision between the Taurides and Anatolian plates occurred in the Oligocene. The tectonic regime in East Anatolia was characterised by compression-contraction until the end of the Late Miocene and Early Pliocene, then transformed to a compressional-extension in the Early-Late Pliocene (Koçyiğit et al., 2001). Many researchers have proposed different geodynamic models for the East Anatolian region and different sources for volcanism extending over large areas of the region (İnnocenti et al., 1982; Pearce et al., 1990; Keskin et al., 1998; Yılmaz et al., 1998; Keskin, 2003; Şengör et al., 2008; Allen and Armstrong, 2008; Schildgen

* *Corresponding author: Vural OYAN, vuraloyan@yyu.edu.tr*
http://dx.doi.org/10.19111/bulletinofmre.427782

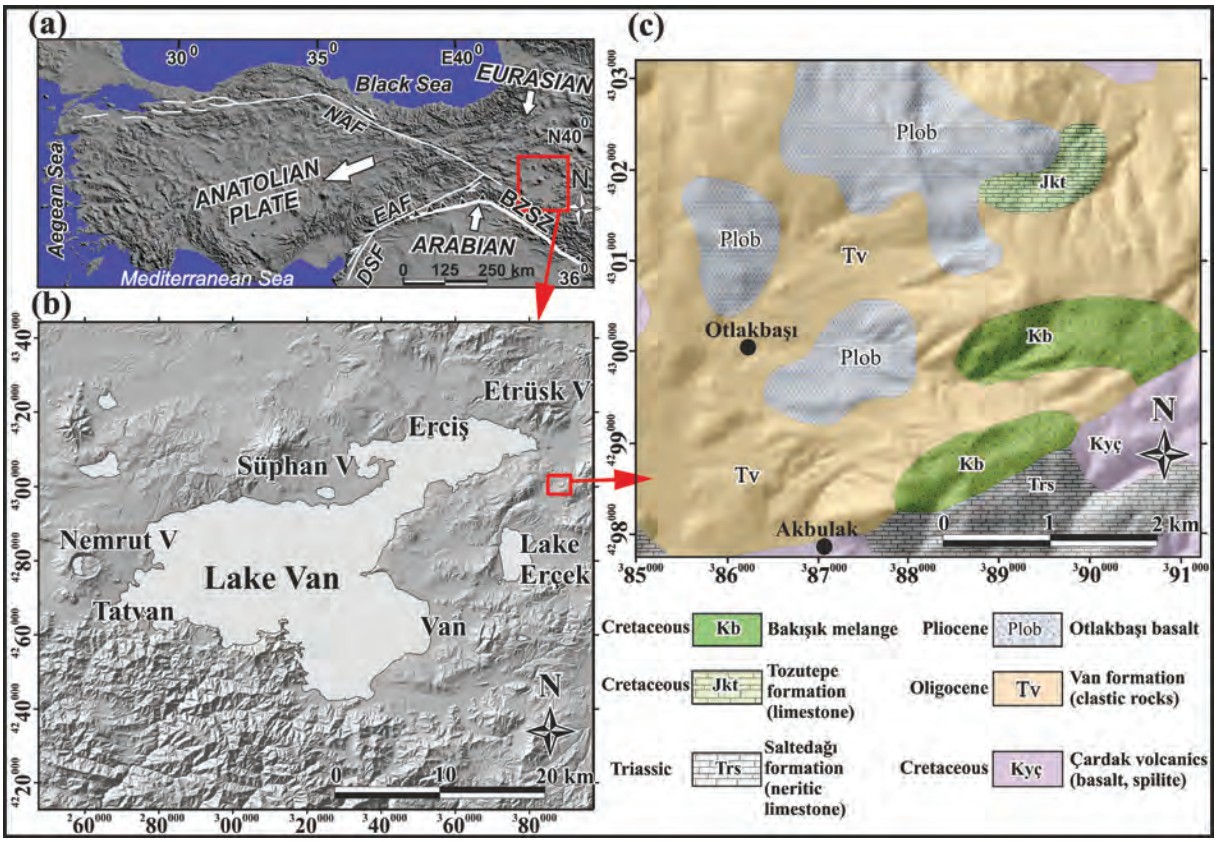

Figure 1- Location and geology maps for Otlakbaşı volcanism, a) Main neotectonic lineations in Turkey, b) Large volcanic centres in Lake Van basin and the study area (marked in red), c) Geology map of the study area (MTA, 2008, adapted from the geological report for 1/100000 scale K-51 sheet).

et al., 2014). The most important models proposed for the geodynamic evolution of the region are (1) lithospheric delamination (Pearce et al., 1990; Keskin et al., 1998); (2) oceanic crust becoming vertical and slab break-off (Keskin, 2003; Şengör et al., 2008) and (3) oceanic slab rupture (Allen and Armstrong, 2008; Schildgen et al., 2014). Studies in recent years have revealed that the volcanic activity observed in large areas on a regional scale may have formed by mixing of melts derived from lithospheric and asthenospheric mantle with different degrees of melting (Özdemir and Güleç, 2014; Oyan et al., 2016). The volcanic activity in the region reached a peak in the Pliocene, and continued with reducing volumes until the Quaternary (Oyan et al., 2016). This magmatic activity observed in the interval from the Pliocene to the Pleistocene formed volcanic centres like Nemrut, Süphan, Ağrı, Tendürek and Etrüsk (Figure 1b) and large regional-scale plateaus or basaltic lava flows locally along extensional fractures.

The Otlakbaşı lava located east of Lake Van (Figure 1) formed as lava erupting from extensional fractures. The Otlakbaşı lava cuts Cretaceous-aged limestone and Oligocene-aged clastic rocks and covers both these units and the Cretaceous ophiolite units observed over large areas in the region and Triassic-aged limestones.

In this study the aims were *(1)* to present new geochronologic, geochemical and petrologic data belonging to the Otlakbaşı volcanism east of Lake Van, *(2)* to discuss data obtained from petrologic modelling studies with magma chamber evolution processes, the nature of the mantle source area and melt processes and *(3)* to assess findings associated with regional geodynamic processes.

2. Regional Geology

The basement of the Anatolian-Iranian platform within the EACZ comprises microterranes amalgamated from the Late Cretaceous-Early Tertiary (Şengör, 1979). These microterranes are separated by ophiolitic complexes and adhesion complexes. There are 5 different tectonic blocks defined in East

Anatolia. There are *(1)* Rhodope-Pontide unit to the northeast of the region (Topuz et al., 2004); *(2)* the northwest Iran section (Karapetian et al., 2001); *(3)* the East Anatolian Accretionary Complex located between the Aras River and Bitlis-Pötürge massif (EAAC) (Şengör et al., 2008); *(4)* the Bitlis-Pötürge massif located along the Tauride belt (Şengör et al., 2008); and *(5)* the Arabian continent or autochthonous units ahead of it (Şengör et al., 2008; Keskin, 2007).

Following block uplift within the EACZ volcanism began before 15 My (Lebedev et al., 2010) with lava flows and pyroclastic products outcropping widely in the region. This volcanic activity produced three different types of eruption dynamics (effusive, extrusive, explosive). These volcanic units covered the tectonic blocks within the EACZ masking them, with volcanic products covering nearly 2/3 of the region and locally reaching 1 km thickness (Keskin, 2007).

Geophysical studies to reveal the crustal structure and geodynamic processes in the EACZ indicate the area between the Aras River and the Bitlis-Pötürge Massif has no lithospheric mantle and the East Anatolian Accretionary Complex (EAAC; Şengör et al., 2008) sits direction on asthenospheric mantle (Al-Lazki et al., 2003; Sandvol et al., 2003). As a result of geodynamic evolution, the crustal thickness is 38 km in the south section of the East Anatolian region, while it reaches 50 km in the northern section (Zor et al., 2003). In light of this data, Keskin (2003) stated the Neotethyan oceanic lithosphere ruptured while sinking into the asthenosphere and that volcanism with character varying from calc-alkali to alkali in the region may have developed due to this mechanism.

Recently some geophysical studies have indicated there may be 25-30 km of lithospheric mantle below the East Anatolia region and that the lithosphere may reach 70-75 km thickness (Angus et al., 2006; Özacar et al., 2008).

The EACZ transitioned to a compressional-extensional tectonic regime in the Early-Late Pliocene (Koçyiğit et al., 2001) and it is known that some zones of the crust displayed clear compression-thickening while other zones display extension-thinning characteristics as a result of delamination of the region below the lithospheric mantle (Göğüş and Pysklywec, 2008). Regionally, the Early Pliocene volcanism is known to have formed due to partial delamination of the lithospheric mantle (Pearce et al., 1990). Studies in recent years have revealed that volcanism began before 15 My (Lebedev et al., 2010; Oyan, 2011); additionally, a peak was reached nearly 5 My ago in terms of volume of erupted material and at this point basaltic lava forming widespread plateaus erupted in the region (Oyan, 2011). Within the scope of this study, the petrologic evolution, geochemistry and Ar-Ar age dates are presented for the rocks of the Otlakbaşı volcanism, a product of Pliocene basaltic volcanism, for the first time.

3. Analytic Techniques

Rock samples taken during field studies were prepared for petrographic, geochemical and Ar-Ar geochronologic dating analyses. Samples were first cut using a Struers brand diamond cutting disk. Cut rock samples had 30-micron thickness thin sections made for mineralogic petrographic analyses and were investigated under a polarising microscope. For geochemical analyses, samples first had the outer sections cleaned of dust, soil, moss and secondary formations. Later, a jaw crusher was used to break samples and they were powdered with the aid of an agate mortar and prepared for analysis.

Geochemical main oxides, trace elements and rare earth element analyses were performed in Acme Analytic Laboratories (Acme Labs) in Canada. Main element analyses were measured using an inductively-coupled plasma emission spectrometer (ICP-OES) with the lithium metaborate/tetraborate fusion technique. The detection limits for main elements varied from 0.001 to 0.04%. Loss on ignition (LOI) was determined with the firing method for sample separation and later obtained by measuring weight loss. For trace and rare earth element (REE) analyses, 0.2 g samples were mixed with $LiBO_2/Li_2B_4O_7$ in graphite crucibles. The prepared crucibles were fired in an oven. Later, melted samples were dissolved in 5% HNO_3 and trace element and rare earth element analyses were completed with an inductively-coupled plasma mass spectrometer (ICP-MS). For reliability of data obtained from main, trace and rare earth element analyses, standards for the analysis laboratory (reference material SO-18) were analysed at the same time as the samples. For standard SO-18, trace and rare earth elements, deviation of 5% or better was obtained. The main oxide, trace element and rare earth element results for rock samples from the Otlakbaşı volcanics and laboratory standards are given in table 1.

Table 1- Main oxides, trace elements and rare earth element analysis results for Otlakbaşı basaltic rocks.

Sample No	2015-5	2015-11	2015-12	2015-13	2015-14	2015-16	2015-19	2015-23	2015-25
Rock Type	*Basalt*	*Basalt*	*Basalt*	*Basalt*	*Basalt*	*Basalt*	*Basalt*	*Basalt*	*Basalt*
Coordinates (UTM)	***N:***4331972 ***E:***364899	***N:***4331972 ***E:***364899	***N:***4331972 ***E:***364899	***N:***4331972 ***E:***364899	***N:***4331972 ***E:***364899	***N:***4331972 ***E:***364899	***N:***4331972 ***E:***364899	***N:***4331972 ***E:***364899	***N:***4331972 ***E:***364899
SiO_2 ***%***	47.63	48.35	48.24	48.28	48.23	47.70	48.43	49.02	49.04
TiO_2	1.28	1.35	1.33	1.32	1.36	1.32	1.28	1.26	1.27
Al_2O_3	17.02	16.95	17.16	17.05	16.92	16.97	16.99	17.14	17.03
$Fe_2O_3^{TOT}$	9.47	9.62	9.64	9.52	9.74	9.42	9.13	9.17	9.19
MnO	0.16	0.16	0.15	0.15	0.16	0.16	0.15	0.16	0.15
MgO	8.77	8.26	8.39	8.34	8.35	7.59	7.55	7.13	7.76
CaO	10.85	10.35	10.38	10.59	10.25	11.08	11.13	11.27	10.89
Na_2O	3.10	3.14	3.16	3.11	3.20	3.13	3.17	3.04	3.22
K_2O	0.59	0.53	0.61	0.60	0.51	0.61	0.80	0.83	0.86
P_2O_5	0.21	0.22	0.24	0.22	0.21	0.23	0.25	0.25	0.26
LOI	0.6	0.7	0.4	0.5	0.8	1.5	0.8	0.4	0.0
Total	99.71	99.73	99.72	99.72	99.73	99.74	99.73	99.71	99.71
Mg#	0.732	0.717	0.721	0.722	0.717	0.704	0.712	0.699	0.718
V ***(ppm)***	189	193	196	186	187	193	196	205	199
Co	40.7	42.2	40.5	39.3	39.2	38.1	32.5	36.4	35.7
Ni	94.5	93.3	94.7	93.8	92.0	75.2	51.9	58.2	58.8
Sr	404.6	346.2	389.1	374.8	347.3	361.7	442.9	493.3	488.0
Rb	12.1	7.7	11.5	11.8	8.1	11.3	16.1	15.5	18.7
Ba	214	261	223	297	165	223	242	353	279
Th	2.0	1.8	2.1	2.1	1.7	2.0	2.6	3.1	3.3
Ta	0.4	0.3	0.4	0.4	0.3	0.3	0.3	0.4	0.5
Nb	5.6	5.1	6.1	6.9	4.7	5.5	6.5	7.2	7.4
Zr	126.6	129.6	118.9	119.8	128.2	114.7	123.3	131.9	131.8
Y	23.8	25.3	23.5	24.4	22.7	22.7	22.2	24.9	24.7
Hf	3.3	3.1	2.7	2.9	3.2	2.7	2.8	3.0	3.5
U	0.4	0.4	0.5	0.6	0.4	0.4	0.5	0.6	0.6
Pb	2.2	2.2	1.2	1.7	0.7	0.8	2.6	3.1	2.6
La	15.0	11.8	13.8	14.6	11.4	13.4	18.8	20.6	21.2
Ce	31.6	24.4	28.6	31.2	24.0	27.6	37.8	42.0	43.0
Pr	4.15	3.61	3.70	3.98	3.42	3.76	4.82	5.44	5.51
Nd	17.3	15.3	16.1	16.6	14.7	15.5	21.0	22.3	23.2
Sm	3.85	3.90	3.69	3.94	3.86	3.70	4.51	4.88	4.93
Eu	1.33	1.30	1.26	1.35	1.27	1.24	1.45	1.59	1.60
Gd	4.53	4.47	4.42	4.56	4.22	4.13	4.62	5.09	5.05
Tb	0.73	0.75	0.70	0.75	0.73	0.68	0.71	0.77	0.82
Dy	4.45	4.42	4.60	4.25	4.49	4.21	4.19	4.38	4.64
Ho	0.93	0.96	0.96	0.87	0.98	0.92	0.87	0.94	0.99
Er	2.74	2.70	2.65	2.93	2.68	2.46	2.56	2.66	2.68
Tm	0.40	0.39	0.37	0.41	0.38	0.37	0.37	0.41	0.43
Yb	2.36	2.54	2.66	2.62	2.58	2.25	2.54	2.70	2.55
Lu	0.38	0.39	0.41	0.41	0.40	0.38	0.37	0.42	0.42
CIPW									
Quartz	0	0	0	0	0	0	0	0	0
Orthoclase	3.54	3.185	3.652	3.599	3.067	3.694	4.81	4.97	5.13
Albite	24.624	27.035	27.103	26.705	27.551	26.086	26.063	26.07	27.126
Anorthite	31.27	31.123	31.258	31.244	30.829	31.206	30.286	31.09	29.755
Nepheline	1.095	0	0	0	0	0.573	0.669	0	0.203
Diopside	17.58	15.711	15.463	16.469	15.598	18.878	19.38	19.158	18.429
Hiperstene	0	3.745	1.367	1.522	2.651	0	0	2.345	0
Olivine	14.36	11.388	13.332	12.767	12.432	11.842	11.193	8.812	11.719
Magnetite	4.568	4.684	4.7	4.63	4.748	4.603	4.536	4.542	4.594
Ilmenite	2.469	2.61	2.56	2.545	2.628	2.57	2.473	2.425	2.435

Table 1- continued.

Sample No	**2015-27**	**2015-29**	**2015-30**	**2015-32**	**2015-33**	**2015-34**	SO-18	SO-18	SO-18
Rock Type	Basalt	Basalt	Basalt	Basalt	Basalt	Basalt	Standard	Standard	Standard
Coordinates (UTM)	**N:**4331972 **E:**364899	**N:**4331972 **E:**364899	**N:**4331972 **E:**364899	**N:**4331972 **E:**364899	**N:**4331972 **E:**364899	**N:**4331972 **E:**364899	Analysed	Analysed	Expected values
SiO_2 **%**	48.49	48.84	48.17	47.98	48.84	48.44	58.1	58.08	58.09
TiO_2	1.27	1.28	1.33	1.29	1.29	1.31	0.69	0.69	0.69
Al_2O_3	16.90	17.03	17.05	17.01	17.04	17.04	14.13	14.13	14.13
$Fe_2O_3^{TOT}$	8.99	9.17	9.65	9.43	9.49	9.56	7.61	7.61	7.6
MnO	0.15	0.15	0.15	0.15	0.15	0.15	0.39	0.39	0.39
MgO	7.29	7.46	8.26	8.53	8.50	8.04	3.33	3.33	3.33
CaO	11.45	11.18	10.34	10.31	10.32	10.28	6.36	6.37	6.37
Na_2O	3.11	3.05	3.27	3.25	3.19	3.28	3.68	3.68	3.69
K_2O	0.85	0.84	0.57	0.55	0.63	0.54	2.15	2.15	2.16
P_2O_5	0.27	0.26	0.22	0.20	0.22	0.21	0.82	0.83	0.83
LOI	0.9	0.4	0.7	1.0	0.0	0.8	1.9	1.9	1.9
Total	99.70	99.72	99.72	99.71	99.72	99.71	99.72	99.72	99.72
Mg#	0.708	0.708	0.718	0.728	0.727	0.714			
V **(ppm)**	200	199	189	177	189	183	198	198	199
Co	33.8	36.2	43.6	42.4	40.3	42.3	26.2	26.1	26.2
Ni	56.2	49.2	99.1	99.1	73.1	104.1	40	46	44
Sr	481.3	492.9	362.4	354.2	378.5	375.2	399.1	400.1	403
Rb	16.5	16.7	9.8	10.5	12.7	10.0	28	28	28.2
Ba	317	334	193	338	208	372	496	497	498
Th	3.3	3.2	2.2	1.6	2.2	1.9	9.7	9.8	9.7
Ta	0.4	0.5	0.5	0.4	0.4	0.3	7.2	7.2	7.1
Nb	7.4	8.0	5.7	4.6	6.2	5.2	21.2	20.8	21
Zr	130.3	134.6	125.8	126.3	116.8	132.1	281.5	279.9	280.8
Y	24.6	24.1	25.3	22.8	24.4	25.0	31.5	31.3	31.3
Hf	3.3	3.1	2.8	3.1	2.9	3.2	9.6	9.7	9.4
U	0.6	0.9	0.4	0.5	0.4	0.4	16	16.1	16.1
Pb	3.3	2.5	0.5	1.7	2.0	1.9			
La	20.6	20.6	14.4	12.5	14.7	12.1	11.9	11.8	12
Ce	41.2	41.6	28.5	25.6	29.6	25.8	26.5	26.9	27
Pr	5.42	5.58	3.88	3.54	4.01	3.61	3.4	3.39	3.39
Nd	22.3	21.7	16.6	15.5	17.4	15.8	13.9	13.8	13.8
Sm	4.83	5.06	3.89	3.66	4.33	3.75	2.86	2.81	2.89
Eu	1.45	1.59	1.43	1.24	1.27	1.34	0.87	0.86	0.86
Gd	5.18	5.07	4.61	4.50	4.46	4.39	2.85	2.85	2.83
Tb	0.81	0.82	0.77	0.75	0.72	0.72	0.5	0.5	0.5
Dy	4.62	4.89	4.66	4.52	4.44	4.43	2.9	2.86	2.92
Ho	0.93	0.98	0.93	0.97	0.95	0.90	0.61	0.6	0.6
Er	2.66	2.81	2.73	2.74	2.71	2.72	1.79	1.77	1.79
Tm	0.42	0.41	0.42	0.40	0.40	0.41	0.28	0.28	0.28
Yb	2.55	2.76	2.63	2.48	2.74	2.60	1.74	1.75	1.76
Lu	0.39	0.41	0.39	0.37	0.40	0.38	0.27	0.26	0.26
CIPW									
Quartz	0	0	0	0	0	0			
Orthoclase	5.118	5.029	3.422	3.315	3.758	3.25			
Albite	25.518	26.164	28.127	27.689	27.255	28.262			
Anorthite	30.191	30.71	30.663	30.794	30.611	30.724			
Nepheline	0.698	0	0	0.191	0	0			
Diopside	20.691	19.024	16.002	15.991	15.674	15.834			
Hiperstene	0	1.241	0.093	0	2.816	2.15			
Olivine	10.218	10.218	13.868	14.43	12.24	12.043			
Magnetite	4.471	4.538	4.735	4.619	4.657	4.707			
Ilmenite	2.458	2.465	2.568	2.498	2.473	2.534			

Ar-Ar dating analyses were performed in the isotope and geochronology laboratories of Nevada University (Las Vegas, United States of America). Samples for analysis were wrapped in Al foil and stacked in 6 mm internal diameter sealed fused silica tubes. Individual packets with mean 3 mm thickness were inserted with neutron flux monitors (FC-2, Fish Canyon tuff sanidine) at 5-10 mm intervals. The FC-2 sanidine standards heated together with CaF_2 and K-glass pieces were placed on a Cu sample tray in a high vacuum line and melted with a 20 W CO_2 laser. During the laser fusion, samples were imaged with a video camera system. Samples were analysed with the step-by-step heating method in a dual vacuum resistant oven similar to the design of Staudacher et al. (1978).

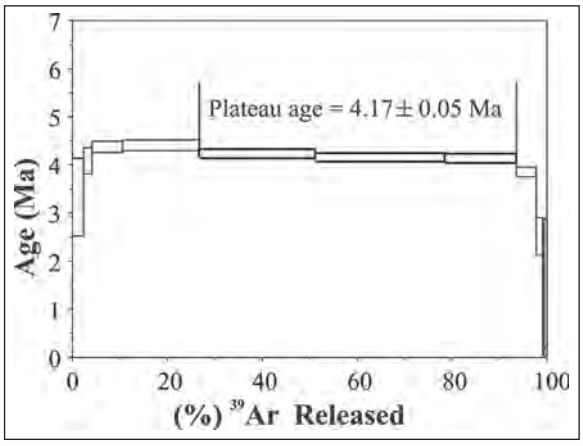

Figure 2- Ar-Ar plateau age for Otlakbaşı volcanic rocks. Best plateau formed between steps 4 and 7. Between these steps the ^{39}Ar amount released was 67%.

4. Results

4.1. Geology and Geochronology of the Area

Otlakbaşı lava comprises a basaltic-composition lava series erupted from different extensional fractures east of Lake Van. With outcrops in different locations, the Otlakbaşı lava covers a 4 km area at most and cuts clastic rocks called the Van formation (Acarlar et al., 1991) (Figure 1c). These clastic rocks comprise Oligocene-Miocene-aged sandstone, claystone and siltstone successions (Acarlar et al., 1991). The Otlakbaşı basaltic lava cuts Cretaceous-aged neritic limestones in the north of the study area (Figure 1c). This unit, called the Topuztepe formation, is formed of grey, white and dark grey colour limestone, dolomitic limestone and recrystallised limestone lithologies (Acarlar et al., 1991).

Within the study area, the Otlakbaşı lava flows unconformably overlie older ophiolitic melange units. Ophiolitic rock units are serpentinite, dunite and spilites. Covering all these lithologies, the Otlakbaşı volcanics cover a total area of nearly 15 km^2 (Figure 1c). Within rocks with black and grey colour, the largest observable feldspar and olivine microphenocrystals are nearly 0.5 cm in size.

A sample chosen to best represent the Otlakbaşı lava flow (Sample no: 2015-33) was sent for Ar-Ar dating analysis. The Ar-Ar geochronologic dating analysis of rock mass is in accordance with Ca/K. The analysed sample had total gas age of 4.14±0.004 My. Between steps 5-7, a plateau age of 4.17±0.05 My was defined (released 39Ar amount 67%) (Figure 2). Though an isochron age could not be determined for this sample, there were no alteration effects observed due to high radiogenic yield. The 4.17±0.05 My Ar-Ar age for Otlakbaşı lava indicates they erupted in the Early Pliocene (Zanclean), contrary to the known age of Quaternary. The age data belonging to the steps are given in table 2.

4.2. Mineralogy-Petrography

Rocks forming the Otlakbaşı volcanics are formed of plagioclase, olivine, pyroxene and opaque minerals (Figure 3). While olivines are observed as microphenocrystals and are iddingsitised, plagioclase phenocrystals have rod-like form, with polysynthetic twins observed. Some plagioclase microphenocrystals with cell-like structure developed were determined to have been eroded by magma along the edges. Colourless pyroxene crystals with microlith sizes, have lilac colour tones in some forms close to the titanaugite composition. Gas cavities observed in rocks are filled with secondary calcite and zeolite crystals. The groundmass of the Otlakbaşı rocks comprises microliths and volcanic glass. Generally, they display interstitial and flow textural characteristics. Glomeroporphyric texture characteristics formed by clusters of plagioclase, olivine and pyroxene minerals or plagioclase crystals were identified in the rocks (Figure 3).

4.3. Whole-rock Geochemistry

The freshest samples collected during fieldwork in locations where the Otlakbaşı volcanics outcrop were sent to ACME analytic laboratories in Canada for main oxide, trace element and rare earth element (REE) analyses. The results of analyses using ICP-AES and

Table 2- Apparent age data for steps in the Ar-Ar geochronologic dating analyses. T - temperature, My – million years, SE – standard error margin.

Step	T (^{0}C)	t (min.)	^{36}Ar	^{37}Ar	^{38}Ar	^{39}Ar	^{40}Ar	%^{40}Ar*	% ^{39}Ar	^{40}Ar*/^{39}Ar	Age (My)	1s.e.
1	560	12	0.791	0.305	0.281	7.503	228.015	3.6	2.3	1.075392	3.33	0.40
2	620	12	0.074	0.221	0.094	5.691	26.270	41.1	1.8	1.318518	4.08	0.14
3	680	12	0.071	0.647	0.281	20.928	47.161	75.0	6.5	1.411981	4.37	0.06
4	740	12	0.071	1.242	0.685	51.701	90.239	89.7	16.1	1.422654	4.40	0.06
5	800	12	0.082	1.598	1.049	78.776	127.168	90.2	24.5	1.366703	4.23	0.05
6	870	12	0.092	1.615	1.196	87.834	140.192	88.9	27.3	1.342125	4.16	0.04
7	960	12	0.092	1.005	0.695	48.507	89.309	81.7	15.1	1.335334	4.13	0.05
8	1050	12	0.109	0.928	0.292	13.554	46.317	47.1	4.2	1.243824	3.85	0.05
9	1140	12	0.136	0.627	0.136	4.298	41.850	12.7	1.3	0.811043	2.51	0.20
10	1230	12	0.171	0.263	0.068	1.190	48.898	1.4	0.4	0.417326	1.29	0.63
11	1400	12	0.487	0.463	0.147	1.850	137.305	0.8	0.6	0.497728	1.54	0.67
										Total gas age	4.14	0.04
										Plateau age	4.17	0.05

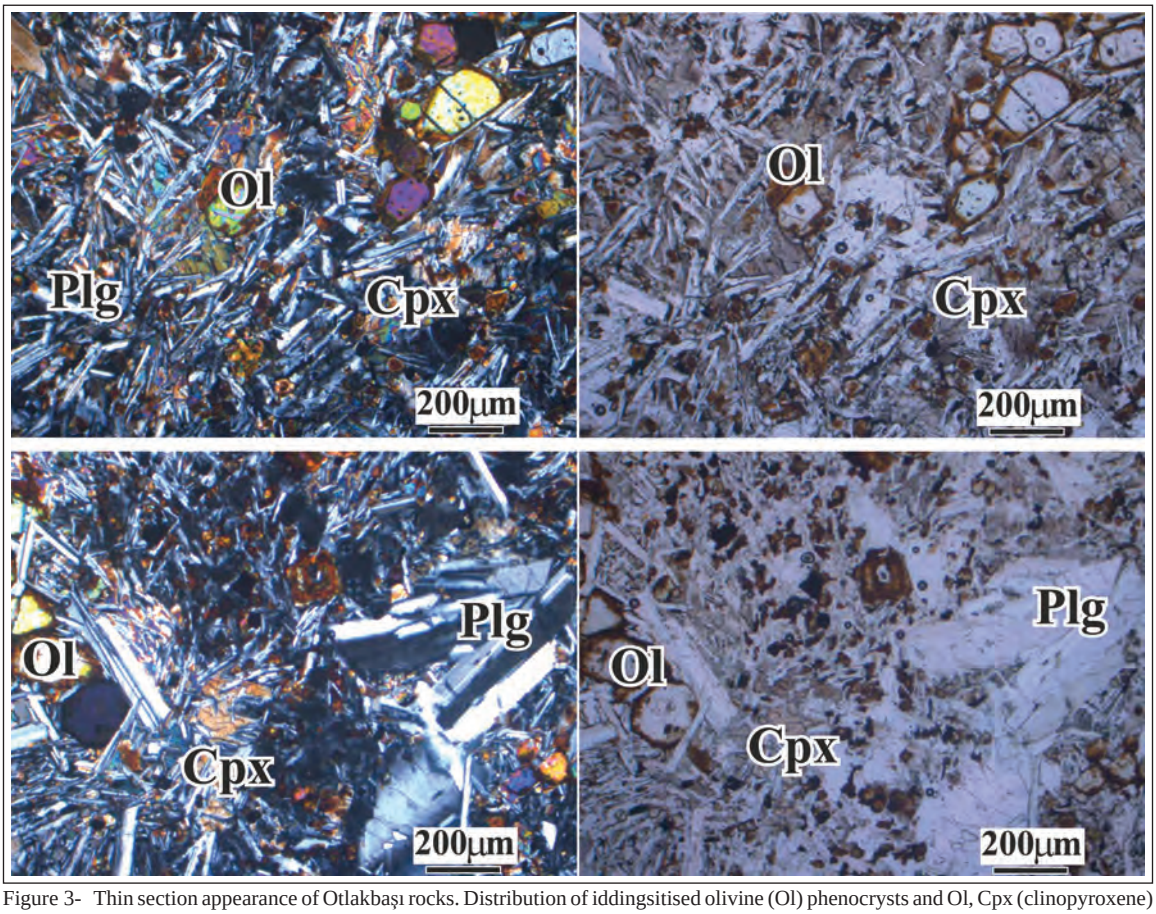

Figure 3- Thin section appearance of Otlakbaşı rocks. Distribution of iddingsitised olivine (Ol) phenocrysts and Ol, Cpx (clinopyroxene) and Plg (plagioclase) crystals in interstitial matrix

ICP-MS methods found low element mobility in rocks, with LOI (loss on ignition) values varying between 0 and 1, indicating that these rocks were fresh and not affected by alteration. Geochemical classification of these rocks was completed using values calculated for main oxide values on dry basis (distributing the water loss on ignition in proportion to the major element values). The lava erupted in the Otlakbaşı area fell in the basalt area on the total alkali (Na_2O+K_2O) – silica (TAS diagram; LeBas et al., 1986) classification diagram (Figure 4a).

With the aim of determining the character of the magma forming the rocks in the study area, the alkali-subalkali differentiation line of Irvine and Baragar (1971) was drawn on the TAS diagram and basalts fell close to the alkali-subalkali differentiation line and were located in the subalkali area. On the SiO_2 – K_2O diagram of Peccerillo and Taylor (1976), the rocks were located in the medium K series area (Figure 4b).

While the SiO_2 content of the Otlakbaşı basaltic samples varied in a narrow interval from 47.63-49.04%, the MgO contents varied from 7.13 to 8.77% with Mg# values varying from 0.699 to 0.732. As the SiO_2 content of the Otlakbaşı basaltic rocks varies in a narrow interval, they do not provide very clear information on the Harker variation diagrams. As a result, to produce more productive data for basaltic rocks on the Harker diagram the solidification index MgO values were used. The MgO binary Harker variation diagrams for some chosen main oxides are given in figure 5a and b. Though there are no very clear trends observed on MgO against main oxide variation diagram, there is a negative trend between MgO and SiO_2 and a positive trend with Fe_2O_3.

The MgO binary Harker variation diagrams for some trace elements from the basaltic samples are given in figure 5 c-f. Together with the fall in MgO in basaltic rocks, the Ni and Co elements have a negative trend, Sr and Y elements display close to horizontal or slightly positive trends. The traces of other trace elements and main oxide elements against MgO on Harker variation diagrams have irregular distribution or display completely horizontal trends.

The location of Otlakbaşı basaltic rock samples on primitive mantle (PM)-normalised multi-element diagrams is given in figure 6a. On these diagrams, all samples appear to be severely depleted in high field strength elements (HFSE), compared to large ion lithophile elements (LILE) and light rare earth elements (LREE). Samples presenting typical trends for active continental margin volcanism display enrichment in Pb and Sr compared to neighbouring elements. Medium and heavy rare earth elements in the primitive mantle-normalised rock samples are parallel to the PM line. The same samples on Sun and McDonough's (1989) chrondrite-normalised rare earth element (REE) spider diagrams (Figure 6b) display enrichment in all samples for LREE elements compared to medium rare earth elements (MREE) and heavy rare earth elements (HREE). The MREE and HREE plot parallel or close to parallel with primitive mantle values.

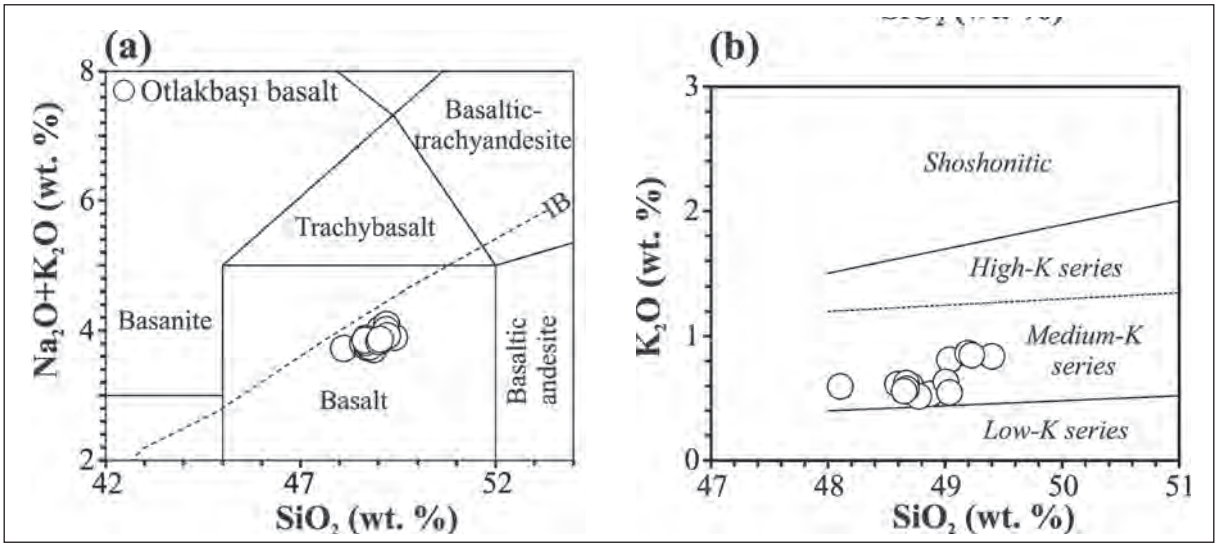

Figure 4- For Otlakbaşı volcanic rocks a) total alkali-silica (TAS: LeBas et al., 1986) classification diagram, b) SiO_2 (%)-K_2O (%) variation diagram (Peccerillo and Taylor, 1976).

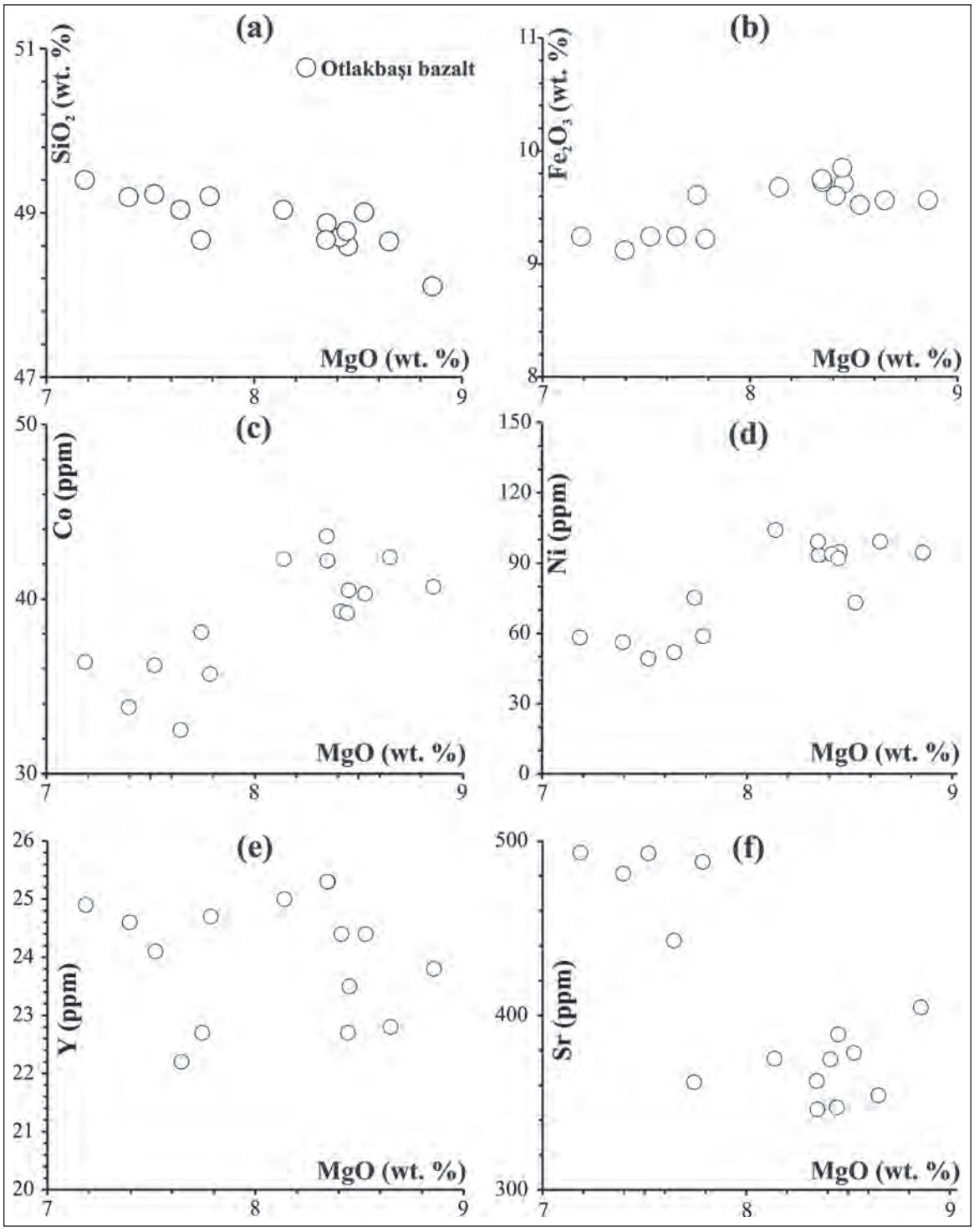

Figure 5- Selected main oxide and trace elements against MgO for Otlakbaşı basaltic rocks on Harker binary variation diagrams.

5. Discussion

5.1. Fractional Crystallisation

As the MgO and SiO_2 values for Otlakbaşı basaltic lava vary within a very narrow range on Harker variation diagrams against MgO values (Figure 5), the trends indicating fractional crystallisation could not be clearly observed. Only Fe_2O_3, Co and Ni had slightly positive trends against MgO, which indicates that the evolution of these rocks may have been partly affected by fractional crystallisation processes of

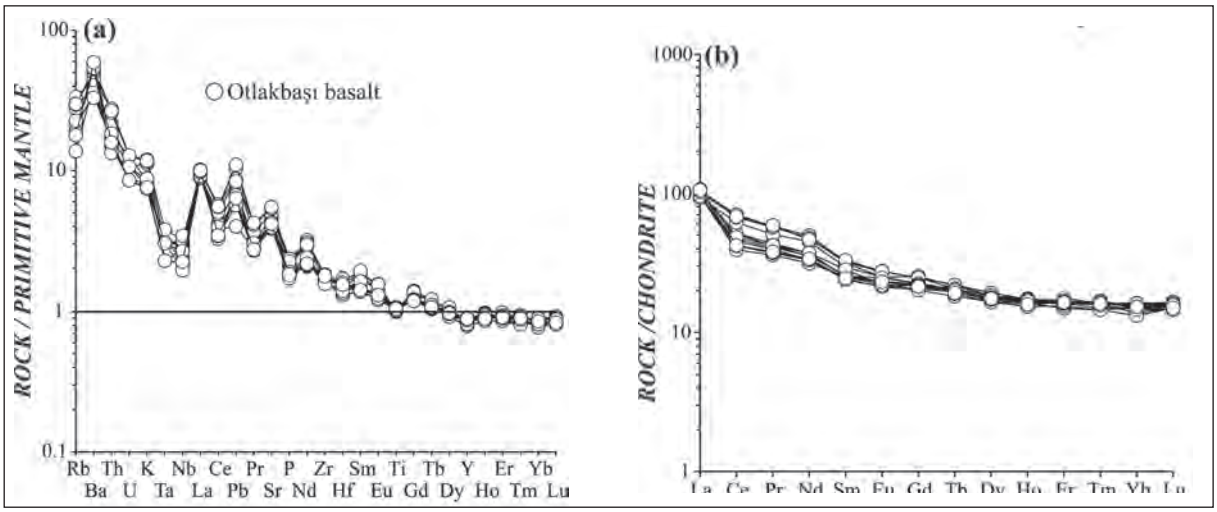

Figure 6- For Otlakbaşı basaltic lava a) multi element spider diagrams normalised to primitive mantle (PM), b) rare earth element (REE) spider diagrams normalised to chrondrite. Normalised values taken from Sun and McDonough (1989) for both diagrams.

ferromagnesian minerals like olivine and pyroxene. Together with the fall in MgO values, the slight increasing trend in SiO_2 indicates that fractional crystallisation may have affected the evolution of the rocks, though only slightly.

The positive trend of Y and Sr with MgO shows that amphibole and plagioclase were not affected by fractional crystallisation processes. To test whether fractional crystallisation was an effective evolutionary process for Otlakbaşı basaltic volcanism, Th-Co and Rb-Y binary variation diagrams were produced using the Rayleigh fractionation equation (Figure 7). On these diagrams, the fractional crystallisation trends for magmas with different mineralogic composition were drawn. On the Th against Co diagram for Otlakbaşı

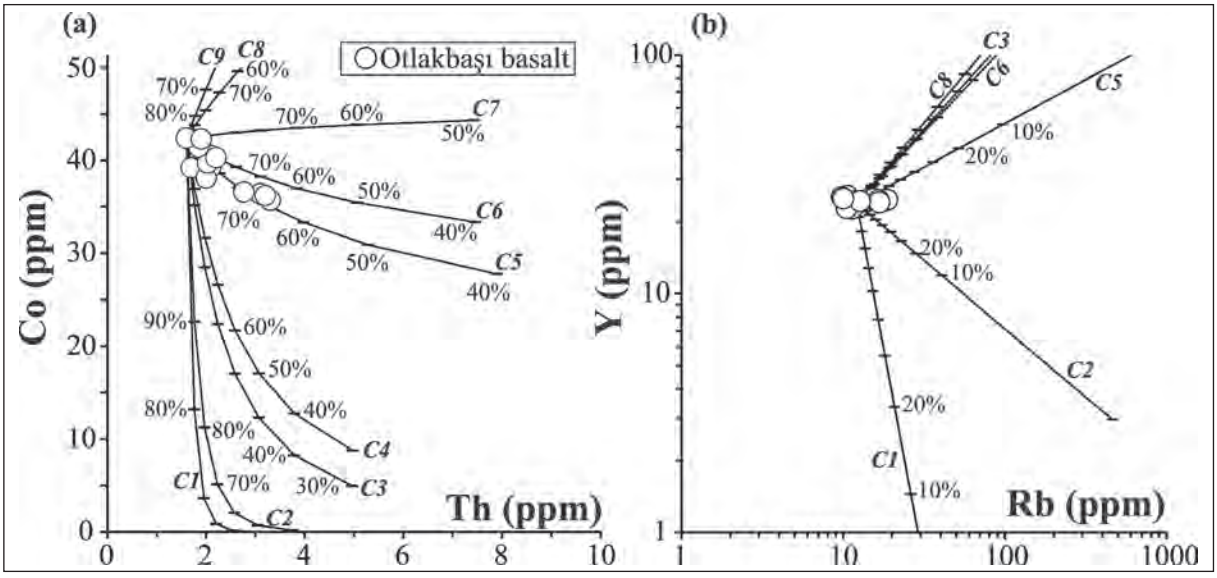

Figure 7- Co-Th normal – normal and Rb-Y log – log variation diagrams. Each curve modelled on the diagrams was calculated characterised by crystallisation of mineral assemblages given below according to Rayleigh crystallisation and traced on the diagram. % values given on the curves indicate post-crystallisation with remaining melt % indicated. ***C1***-$Amp_{0.2}$+$Plg_{0.5}$+$Cpx_{0.1}$+$Bio_{0.1}$+$Sn_{0.1}$, ***C2***-$Amp_{0.1}$+$Plg_{0.7}$+$Cpx_{0.1}$+$Bio_{0.05}$+$Sn_{0.05}$, ***C3***-$Plg_{0.5}$+$Cpx_{0.5}$, ***C4***-$Ol_{0.1}$+$Amp_{0.15}$+$Plg_{0.5}$+$Opx_{0.15}$+$Cpx_{0.1}$, ***C5***-$Ol_{0.2}$+$Plg_{0.6}$+$Cpx_{0.2}$, ***C6***-$Plg_{0.7}$+$Opx_{0.1}$+$Cpx_{0.2}$, ***C7***-$Amp_{0.1}$+$Plg_{0.65}$+$Bio_{0.05}$+$Sn_{0.1}$+$Cpx_{0.1}$, ***C8***- $Amp_{0.1}$+$Plg_{0.6}$+$Opx_{0.2}$+$Cpx_{0.1}$, ***C9***- $Plg_{0.5}$+$Opx_{0.5}$ (Amp; amphibole, Plg; plagioclase, Ol; olivine, Opx; orthopyroxene, Cpx; clinopyroxene, Bio; biotite, Sn; Sanidine). Discriminant coefficient values (Kd) used to obtain the curves taken from Geochemical Earth Reference website (http://www.earthref.org).

basaltic lava, the line falls on curves C5 and C6. This diagram shows that for magmatic systems comprising mineral assemblages of olivine (20%), plagioclase (60%) and clinopyroxene (20%), nearly 20% fractional crystallisation may create the Otlakbaşı lava. Additionally, for the fractional crystallisation model using Rb-Y elements, samples fall close to the C5 curve with 80% F value. This modelling clearly indicates that olivine and pyroxene minerals were affected by fractionation of the magma system, while crystallisation of other minerals was unimportant for Otlakbaşı basaltic volcanism.

5.2. Continental Contamination

Continental contamination processes occur as hot magma melts colder continental crust material and absorbs the material as it moves through the continental crust or while in a magma chamber and this event is reflected in the melt geochemistry (DePaolo, 1981). On multielement spider diagrams for Otlakbaşı basaltic lava (Figure 6a), there is clear enrichment of LILE and LREE compared to HFSE elements which may reflect the effects of continental contamination or continental contamination combined with fractional crystallisation (assimilation fractional crystallisation-AFC). Additionally, the Ta/Zr and Rb/Th element ratios are clearly enriched in continental crust compared to the mantle and are high in some Otlakbaşı basaltic lava samples. This data indicates that continental contamination may have been an effective process in the evolution of the Otlakbaşı volcanism. With the aim of revealing whether AFC effects were an important evolutionary process for Otlakbaşı basaltic lava, modelling studies were completed using DePaolo's (1981) AFC equations.

DePaolo's (1981) AFC modelling reveals the ratio of crustal contamination (M_a) to the ratio of fractional crystallisation (M_c) and this is shown as the assimilation fractional crystallisation ratio **"***r* (M_a/M_c)". Another parameter used in these equations is the ratio of remaining magma mass after fractional crystallisation (M_m) to original magma (M_m^0) and is shown by "*F* (M_m / M_m^0)". With DePaolo's (1981) equations, curves may be modelled for different ***r*** values for trace element and isotope ratios and interpretations may be made about the true r value of rock samples. Rb, Th, Ta and Zr elements were used in the AFC modelling systematic derived for the Otlakbaşı basaltic lavas and different *r* values were produced with Rb-Rb/Th and Ta-Ta/Zr AFC modelling curves (Figure 8). With the crystallisation of the trace elements given above as some accessory minerals in acidic-character magmas, the Zr, Th and mica minerals, apart from Rb, are incompatible with minerals in most of the magma

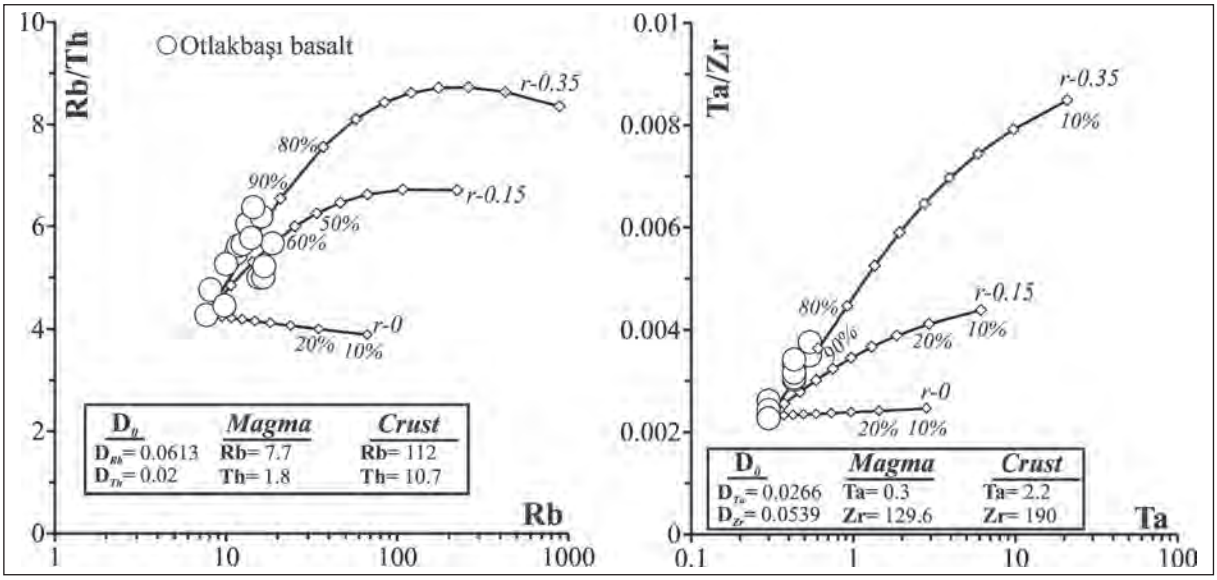

Figure 8- AFC modelling curves using DePaolo's (1981) equations. Values on the curves for r show the ratio of crustal contamination to fractional crystallisation. Percentage values on the model curves represent the F value of the original magma ratio in the residual magma mass after fractional crystallisation. The parameters used for formulation of modelling are given in the figure. Discriminant coefficient values taken from McKenzie and O'Nions (1991) and Adam and Green (2006). Total discriminant coefficients (D_0) for elements calculated on the basis of less evolved lava with olivine$_{(0.2)}$ +plagioclase$_{(0.6)}$ +clinopyroxene$_{(0.2)}$ mineralogic composition.

(D<<1). As a result, these trace elements are not affected by fractional crystallisation processes in most magma systems. Data presented in the mineralogy-petrography section and on figure 3 reveals the minerals mentioned above did not fractionate during the evolution of Otlakbaşı volcanism and that no differentiation process developed for these minerals. For these reasons, the variation in these elements and element ratios will be controlled by continental contamination. During Rb and Ta element modelling, fractionation indices, Ta/Zr and Rb/Th element ratios are selected as the continental contamination index and the samples were traced on binary variation diagrams for different r values (Figure 8).

As can be seen on figure 8, some of the basaltic rock samples fall along the curve with r values varying from 0-0.35. These samples, especially, are basaltic rocks with low MgO values reflecting the trace of continental contamination. Another noteworthy data point on the modelling curves is that fractional crystallisation varied from 0 to 10% for samples with low MgO values. This data indicates that for the Otlakbaşı basaltic lava, samples with low MgO values may have undergone an evolutionary process with significant continental contamination, but fractional crystallisation remained at negligible levels compared to continental contamination. Trends obtained from Harker variation diagrams that do not indicate fractional crystallisation are consistent with the data obtained from these modelling studies.

5.3. Mantle Source Area and Enrichment

On multielement spider diagrams normalised to primitive mantle, Otlakbaşı basaltic lava (Figure 6) is clearly depleted in Nb and Ta elements compared to neighbouring LILE and LREE, with clear enrichment in Pb, typically indicating the presence of subduction components in the mantle source area. Additionally, this effect may be reflected in the traces of continental contamination and fractional crystallisation in the magma chamber. In the magma chamber evolution processes of the Otlakbaşı basaltic volcanism, AFC processes play an effective role in samples with low MgO values with this effect not observed in samples with high MgO values. Due to these reasons, on multielement spider diagrams normalised to primitive mantle, the trends mentioned above reflect clear traces of subduction components for primitive lava with high MgO values in the Otlakbaşı volcanism. Ta/Yb – Th/Yb binary variation diagrams were produced with the aim of revealing the mantle source area of rock samples (Figure 9). Ta/Yb and Th/Yb ratios have nearly fixed values in asthenospheric mantle and small-volume melts derived from the asthenosphere and in enriched lithospheric mantle (Pearce et al., 1990). At the same time, Th and Ta elements with similar incompatibility have nearly the same differentiation coefficients in mantle melt and fractional crystallisation processes. High values for both Ta/Yb and Th/Yb elements indicates high degrees of mantle melting, with lavas with these values falling in the mantle area (or mantle metasomatisation) on source diagrams. However, sources containing subduction components or sources enriched in these components are enriched in Th and Ba elements, with increasing Th/Yb or Ba/Yb ratios deviating linked to the mantle area.

When figure 9 is examined, basaltic samples from the study area have increasing Th/Yb and nearly stable Ta/Yb values, with increasing Th/Yb ratios indicating they deviate from the mantle area. This data indicates

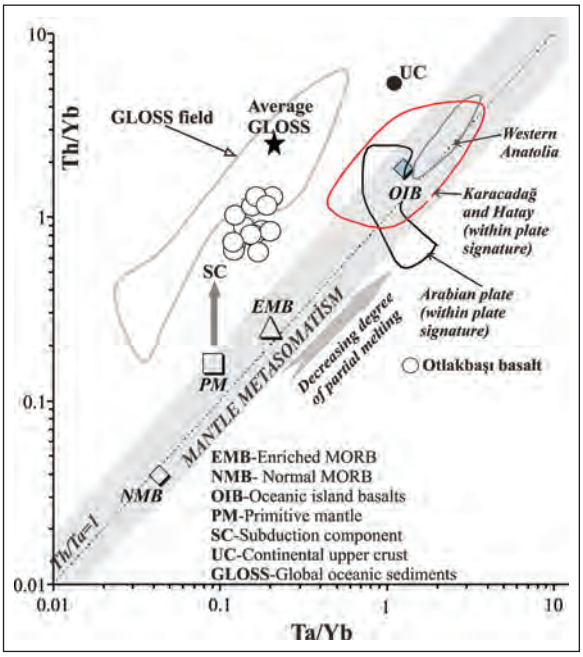

Figure 9- Location of Otlakbaşı basaltic lava on Ta/Yb-Th/Yb binary variation diagrams. PM, EMB, NMB and OIB values taken from Sun and McDonough (1989). UC and GLOSS (subducting oceanic sediment) values taken from Taylor and McLennan (1985) and Plank and Langmuir (1998), respectively. Values for the Arabian plate taken from Lustrino and Wilson (2007), Shaw et al. (2003) and Krienitz et al. (2006). Data for Karacadağ and Hatay taken from Keskin et al. (2012), Parlak et al. (2000) and Bağcı et al. (2011). Western Anatolia area taken from Aldanmaz et al. (2007). Mantle area shown on figures drawn according to values obtained from Pearce et al. (2005) and Sun and McDonough (1989).

the presence of subduction components in the mantle source area for the least evolved rock samples from Otlakbaşı basaltic volcanism. The process of adding subduction components into the mantle source area is described in two ways. These are (1) via the effects of fluids derived from altered oceanic crust (Tatsumi et al., 1986; Hawkesworth et al., 1997; Turner. 2002) or subducted sediments (Class et al., 2000; Elburg et al., 2002) or (2) via partial melting of altered oceanic crust or subducted sediments (Elliott et al., 1997; Hawkesworth et al., 1997). With these mechanisms, volcanic rocks erupting from magmas derived from enriched mantle have significant differences in their geochemical traces (Hawkesworth et al., 1997; Class et al., 2000; Foley et al., 2002; Kessel et al., 2005). Some LILE elements (Ba, Sr, Rb, U) are mobile in fluids, while HFSE and rare earth elements and Th are immobile in fluids but act in more mobile fashion in sediment or altered oceanic crust melts (Turner, 2002; Elburg et al., 2002; Foley et al., 2002; Kessel et al., 2005). As a result, ratios of elements enriched in fluid phase or sediment (or altered oceanic crust) melts may be used to determine enrichment processes in the source area. With this aim, Ba/Yb and Th/Yb binary variation diagrams recommended by Oyan et al. (2017) were produced (Figure 10). While Th is mobile in sediment or altered oceanic crust melts, Ba is mobile and enriched in the fluids released from these. Yb acts immobile in both cases, so slightly increasing Ba/Yb ratios compared to Th/Yb ratios indicate enrichment with fluids or metasomatisation processes, while Th/Yb ratios slightly increased compared to Ba/Yb ratios indicates enrichment processes with sediment melts. Situations when both values are low reflect melting or altered oceanic crust or metasomatisation processes with fluids released from this (Oyan et al., 2017). As seen in figure 10, the Otlakbaşı basaltic lava samples trend towards increasing Th/Yb ratios and reflect enrichment with dominantly sediment melts and metasomatisation processes. However, it should be noted that some samples fall between the curves for fluid from sediment (SF) and sediment melts (SM) and this indicates that metasomatisation processes with low rates (compared to sediment melts) of enrichment from fluids derived from sediments may have been effective. Another noteworthy trend is that some samples fall between primitive mantle and upper crust composition. As discussed in the continental contamination section, this complies with the continental contamination effects during the evolution of Otlakbaşı basaltic volcanism.

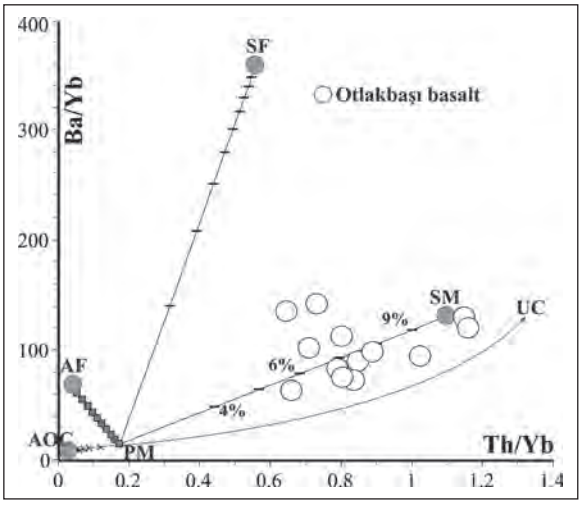

Figure 10- Th/Yb-Ba/Yb (Oyan et al., 2017) diagram for Otlakbaşı basaltic rocks. Three members used on the diagram taken from Oyan et al. (2017). SM – subducting sediment melts, SF – sediment derived fluids, AF – altered oceanic crust derived fluids, AOC – altered oceanic crust, PM – primitive mantle and UC – continental upper crust.

All this data indicates the presence of subduction components in less evolved samples from Otlakbaşı basaltic volcanism, and that these subduction components formed due to the effect of sediment melts dominantly with lower rates of fluids derived from sediments.

5.4. Partial Melting Process

To research and determine the partial melting processes for Otlakbaşı basaltic volcanism, partial melting models using rare earth elements (REE) were produced. During partial melting processes, REEs in source areas with spinel peridotite and/or garnet peridotite mineralogy have different solid-mineral/melt coefficients and thus behave differently and are very useful in conceptualising partial melt modelling. Melting processes in mantle source areas with garnet or spinel peridotite mineralogy initially enrich in light rare earth elements (LREE) and partial melting in the garnet peridotite facies produces slightly higher LREE/HREE ratios compared to melting in the spinel peridotite facies (Shaw et al., 2003). Additionally, MREE/HREE ratios only occur in the residual phase if there is garnet present ($^{Garnet\text{-}melt}D_{Yb} \sim 4$; $^{Garnet\text{-}melt}D_{MREE} \sim 0.21\text{-}1$; McKenzie and O'Nions, 1991). This situation produces high MREE/HREE ratios in melts from mantle with garnet peridotite mineralogy, while contrarily partial melts from mantle source areas with spinel peridotite mineralogy have lower rates of MREE/HREE in melt fractionation and source and

melt ratios are similar ($^{Spinel-melt}D_{Yb}$ ~ 0.01; $^{Spinel-melt}D_{MREE}$ ~ 0.01; $^{Clinopyroxene-melt}D_{Yb}$ ~ 0.28; $^{Clinopyroxene-melt}D_{MREE}$ ~ 0.30; McKenzie and O'Nions, 1991). In light of this information, as the effects of partial melting of mantle with different source mineralogy varies in terms of REEs, they ensure clear observation of partial melting area and melting degree.

With the aim of determining partial melting processes of the Otlakbaşı basaltic rocks, partial melting was modelled using La/Yb against Tb/Yb element ratios. As shown in figure 11, the La/Yb – Th/Yb diagram illustrates 7 source areas with different mineralogies. Among these models are the phlogopite-rich garnet and spinel peridotite reflecting metasomatism effects, with amphibole-rich garnet and spinel peridotite curves. Partial melt modelling was created using nonmodal melting equations proposed by Shaw (1970). The parameters used in modelling are given in table 3. As seen on the diagram, only spinel and/or garnet-rich sources could not have formed the Otlakbaşı basaltic volcanism. Samples fall between the mixing curves obtained for different rates and degrees of melts from source areas with phlogopite- and/or amphibole-rich garnet peridotite and spinel peridotite mineralogy, with the condition that the spinel contribution is dominant. This modelling reveals that the Early Pliocene Otlakbaşı basaltic volcanism was produced from low partial melting degrees from residual mineral phase amphibole- and/or phlogopite-rich spinel peridotite mantle source area.

While fluids or sediment/AOC melts formed by subduction component effects enrich mantle source areas, residual phase minerals like amphibole and/or phlogopite are included in the mantle source area due to metasomatism processes. Considering the Otlakbaşı basaltic volcanism mantle source area was metasomatised by dominantly sediment melts with lesser rates of fluids, the question occurs of whether

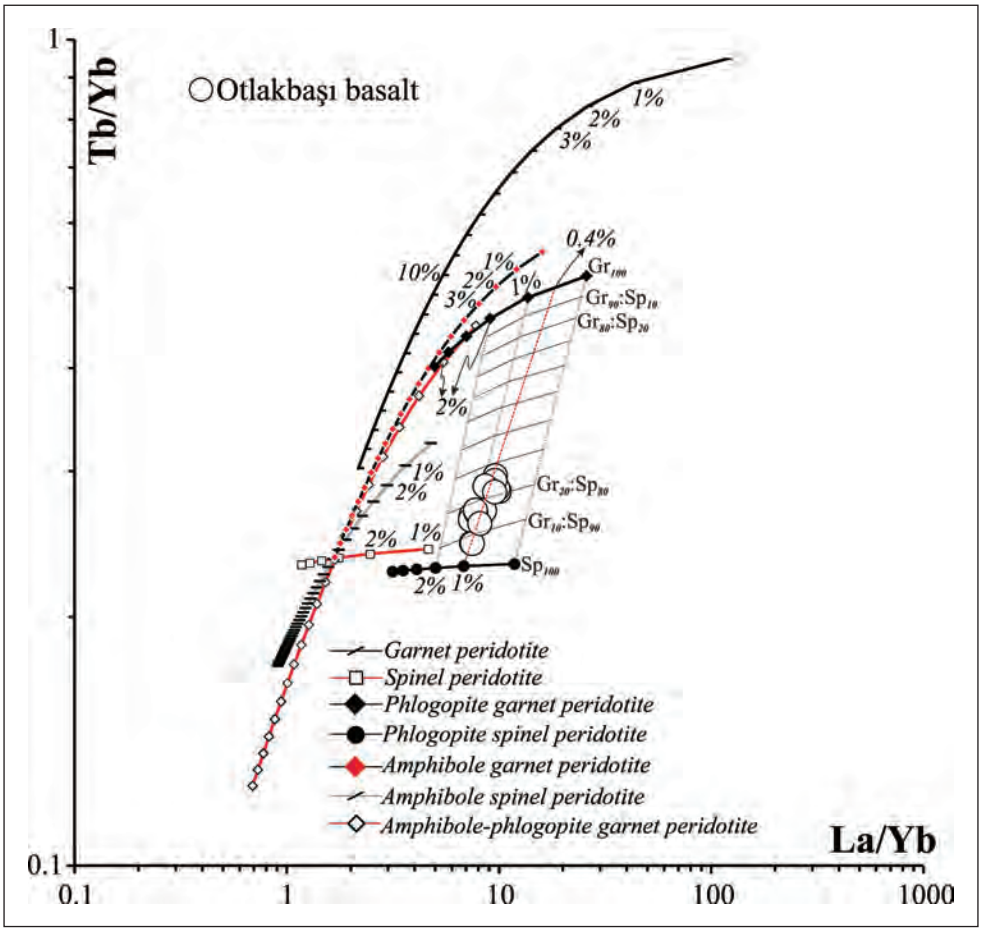

Figure 11- Partial melting model curves using La/Yb-Tb/Yb element ratios. The mineralogy and parameters used in modelling are given in table 2. To reduce AFC process effects to a minimum, samples were drawn after confirming 8% MgO value fractionation.

Table 3- Parameters used in non-modal mass balance melting given in figure 11. Discriminant coefficients taken from McKenzie and O'Nions (1992), Ionov et al. (2002) and Adam and Green (2006). Source mode and melt mode mineralogic compositions taken from Oyan et al. (2017).

	Olivine	*Orthopyroxene*	*Clinopyroxene*	*Spinel*	*Garnet*	*Amphibole*	*Phlogopite*	*Total*
	Garnet peridotite (PM source)[1]							
Source mode	0.598	0.211	0.076		0.115			1
Melt mode	0.05	0.2	0.3		0.45			1
	Amphibole garnet peridotite (PM source)[5]							
Source mode	0.794	0.123	0.03		0.011	0.042		1
Melt mode	0.15	0.15	0.22		0.15	0.33		1
	Phlogopite garnet peridotite (PM source)[5]							
Source mode	0.55	0.22	0.15		0.03		0.05	1
Melt mode	0.05	0.05	0.65		0.05		0.20	1
	Amphibole phlogopite garnet peridotite (PM source)[4]							
Source mode	0.55	0.20	0.15		0.05	0.04	0.01	1
Melt mode	0.05	0.05	0.20		0.20	0.40	0.10	1
	Spinel peridotite (PM source)[1]							
Source mode	0.578	0.27	0.119	0.033				1
Melt mode	0.10	0.27	0.5	0.13				1
	Phlogopite spinel peridotite (PM source)[5]							
Source mode	0.48	0.30	0.18	0.02			0.02	1
Melt mode	0.10	0.35	0.47	0.02			0.06	1
	Amphibole spinel peridotite (PM source)[3]							
Source mode	0.794	0.123	0.03	0.011		0.042		1
Melt mode	0.15	0.15	0.22	0.06		0.42		1

amphibole and/or phlogopite were present in the mantle source area. The answer to this question may be identified from the variation in trace element chemistry of the rocks. As K element is highly compatible with phlogopite and amphibole, if these minerals are present in the mantle wedge as residual phase in partial melting processes, then at low partial melting degrees K element is held by these minerals and does not enrich in the melt. With the increase in the degree of partial melt, the melt begins to enrich in K in direct correlation with the consumption of residual mineral phases in the source area. If these minerals are not present in the mantle wedge, dry melt conditions are present and K acts highly incompatibly and remains fixed with the variation in melting degree. In light of this information, to test whether residual mineral phase melting occurred in the mantle source area of the Otlakbaşı basaltic lava, K/K* (K anomaly) – La/Yb binary variation diagrams were produced (Figure 12). On this diagram, there is a negative trend with the increasing partial melt degrees for Otlakbaşı basaltic lava. This negative trend shows there may have been

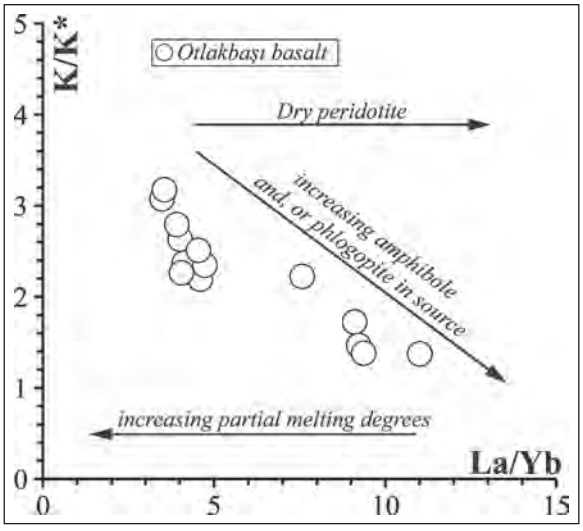

Figure 12- La/Yb against K/K* variation diagram for Otlakbaşı basaltic lava [$K/K^*=K_{PM}$ / $(Nb_{PM}*Th_{PM})^{½}$; PM values normalised to primitive mantle]. Falling partial melting degrees in basaltic lava towards positive K/K* values. This data is associated with the presence of phlogopite or amphibole in the mantle source area. To reduce AFC process effects to a minimum, samples were drawn after confirming 8% MgO value fractionation.

aqueous minerals like phlogopite and/or amphibole in the source area as residual mineral phase.

For samples from the Otlakbaşı basaltic volcanism considered less evolved and not affected by AFC processes, primitive mantle normalised multielement spider diagrams show depletion of Ba compared to Rb indicating phlogopite was more dominant in the source area compared to amphibole. The most important reason for this is that phlogopite has higher discriminant coefficient for Ba compared to Rb compared to amphibole (Green and Ringwood, 1967). With the aim of determining the presence of phlogopite or amphibole in the mantle source area, primitive mantle normalised Ba/Rb – Rb/Sr binary variation diagrams were created. Ba, Rb and Sr have different discriminant coefficients for amphibole and phlogopite, so elevated Ba/Rb and low Rb/Sr element ratios reflect the traces of amphibole while high Rb/Sr and low Ba/Rb ratios reflect phlogopite. Additionally, Sr has higher discriminant coefficient values for amphibole compared to phlogopite. As seen on figure 13, falling Ba/Rb and increasing Rb/Sr values for lava from Otlakbaşı basaltic volcanism indicates the possible presence of typical phlogopite in the mantle source area.

Alternatively, the variation in the ratios of incompatible elements of Ba and Rb in Otlakbaşı basaltic rock samples may be caused by exposure to fractional crystallisation of phlogopite in the magma chamber. With the aim of revealing these effects, the solidification index of MgO values against primitive mantle normalised Ba/Rb ratio diagrams were produced. As seen in figure 13b, there was no good correlation observed between MgO values and Ba/Rb_{PM} values and this situation reveals that phlogopite did not crystallise during magma chamber evolution processes. As a result, the presence of phlogopite appears not to be related to the magma chamber but may be related to metasomatisation processes in the mantle source area.

Experimental melt results for phlogopite-rich peridotite (spinel or garnet) source have revealed a phase with phlogopite, forsterite, hypersthene, diopside, spinel and steam (phlogopite spinel lherzolite) forming at nearly 15 kbar pressure and nearly 1000 ºC and equilibrium fluid contains 0.5 to 1% K_2O content (thus low alkali and low potassic). But at 30 kbar pressure and nearly 1100-1200 ºC, the fluid in equilibrium with phlogopite, forsterite, hypersthene, diopside, garnet

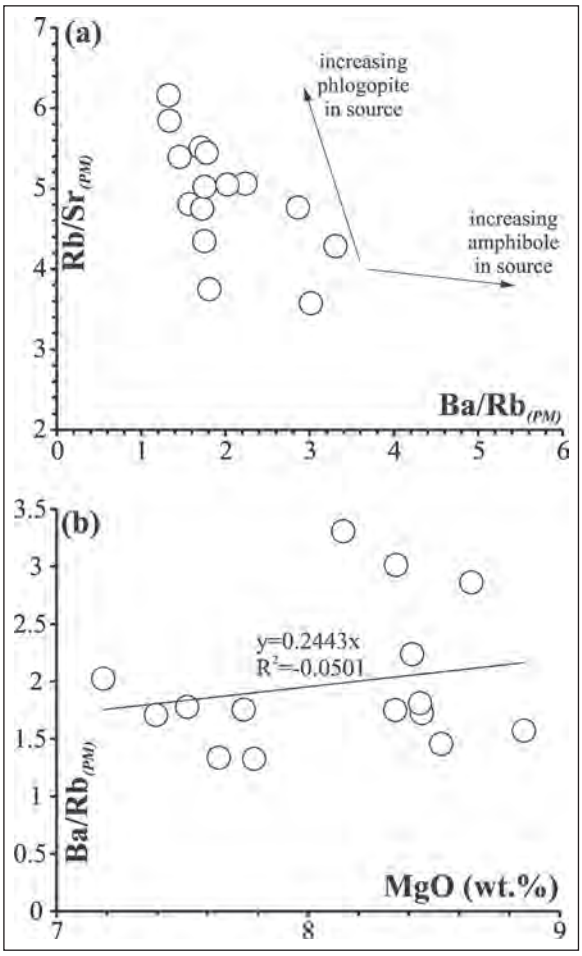

Figure 13- a) Variation of Rb/Sr trace element ratios normalised to primitive mantle (Furham and Graham, 1999), b) Ba/Rb trace element ratios normalised to primitive mantle against MgO.

and steam (phlogopite garnet lherzolite) phase had nearly 2.5% K_2O content (thus alkali, possibly high, and high potassic) (Bravo and O'Hara, 1975). When it is considered that Otlakbaşı lava derived from a spinel peridotite dominant mineralogy with melting in shallow conditions (nearly 50-60 km, 15-20 kbar), it supports the view that alkali rates in the experimental data may not be very high. An experimental study by Condamine et al. (2016) stated that phlogopite-rich silica-saturated lavas may produce high K lava and the melt formed in this situation will have silica amounts from 52-63%. However, this study also showed that in experimental conditions melting of a phlogopite-rich spinel peridotite source may not contain phlogopite in the melt phase but may contain olivine and pyroxene with spinel. In this situation, as phlogopite does not enter the melt, the K amounts may remain low. If there is phlogopite in the residual mineral phase

during production of tholeiitic melts, phlogopite will have a tendency to buffer the K concentration in the melt and then K and Rb elements may display compatible behaviour in the magmatic system rather than incompatible behaviour (Hofmann and Hart, 1978). Additionally, if the amount of phlogopite in the source is greater than the amount in melt, then low partial melting degrees will leave phlogopite as residual phase in the source; thus, the K content of the melt may be low. All this data supports the view that phlogopite and/or amphibole existed as residual mineral phase in the mantle source area for Otlakbaşı basaltic volcanism and that phlogopite may have been more dominant compared to amphibole.

5.5. Geodynamics

Nearly 2/3 of the EACZ is covered with young volcanic rocks (from Miocene to historical periods) and is mean ~2 km above sea level (Şengör et al., 2008). With compression-contraction tectonic regime dominant until the Late Miocene-Early Pliocene, the EACZ entered a compression-extensional tectonic regime in the Early-Late Pliocene (Koçyiğit et al., 2001). Though different geodynamic models have been proposed for the EACZ by many researchers (Innocenti et al., 1982; Pearce et al., 1990; Yılmaz et al., 1998; Keskin 2003 and 2007; Şengör et al., 2008), the most important of these models may be summarised as partial delamination of lithospheric mantle (Pearce et al., 1990; Oyan et al., 2016, 2017), steepening and breaking of subducting oceanic lithosphere (Keskin, 2003; Şengör et al., 2008) or regional-scale broad volcanism as a result of elevation of enriched asthenospheric mantle.

Latest studies about the source area and root of intense volcanic activity in the region have focused on mixture of different melt degrees and different proportions of asthenospheric and lithospheric mantle to form the volcanism (Özdemir and Güleç, 2014; Oyan et al., 2016). Quaternary volcanism north of Lake Van was determined to have formed from amphibole-rich garnet peridotite melt and delamination of the lithospheric mantle may have been responsible for this (Pearce et al., 1990; Oyan et al., 2016). Studies of volcanism in the region indicate a mantle source area with EM2 type enrichment of isotopic and trace element concentrations in most primitive lava and the presence of significant amounts of subduction components (Pearce et al., 1990; Yılmaz et al., 1998; Keskin et al., 1998; Keskin, 2003; Özdemir et al., 2006; Özdemir and Güleç, 2014; Oyan et al., 2016, 2017). The majority of these studies mention the presence of subduction components, while Oyan et al. (2016, 2017) revealed that subduction components derived from sediment melts and metasomatisation processes were dominant in nearly 2 to 10% of sediment melts, based on petrologic modelling. This data may explain the regional-scale volcanism processes as a mixture of lithospheric and asthenospheric mantle via lithospheric delamination and clear metasomatisation of sediment melts in lithospheric mantle.

Geophysical studies with the aim of determining the crustal structure of the EACZ have reported that there is no or very thin lithospheric mantle below the region; as a result, the EAAC sits directly on asthenospheric mantle (Al-Lazki et al., 2003; Gök et al., 2003; Sandvol et al., 2003). Additionally, Angus et al. (2006) and Özacar et al. (2008) indicated there may be 70-80 km thickness of lithosphere below the region. When it is considered the crust below the EACZ has mean 45 km thickness (Zor et al., 2003), it may be that there is 30-35 km thin lithospheric mantle below the region. Partial melting models of Otlakbaşı basaltic volcanism indicate the presence of spinel-rich mantle in the source area of these lavas. Considering the spinel and garnet transition zone is nearly 80 km depth (Takahashi and Kushiro, 1983), it is understood the spinel-rich mantle source for the EACZ derived from lithospheric mantle. Oyan et al. (2016) studied the Pliocene basaltic rocks in the region and found lavas forming broad plateaus erupted in a narrow time interval of 4.9 to 4.5 My, with character transitioning from alkali to subalkali and an increase in spinel peridotite melts over time. This data is compatible with melt results for the Pliocene-aged Otlakbaşı basaltic lava. Data support the opinion that the source area forming the volcanism formed from partial melting of spinel-rich lithospheric mantle and metasomatised zones containing dominantly phlogopite over amphibole.

6. Conclusion

The Otlakbaşı volcanism located east of Lake Van has different output centres and basaltic composition. Ar-Ar dating results indicate this volcanism erupted in the Early Pliocene-Zanclean (4.14 My), contrary to the known age of Quaternary. Petrologic modelling completed with the aim of determining magma chamber evolution reveal that continental contamination was effective in the magma chamber

of this volcanism, though fractional crystallisation effects were slightly less than crustal contamination.

The primitive mantle-normalised trace element characteristics of the least evolved rock samples from the Otlakbaşı basaltic volcanism were determined to be clearly depleted in HFSE elements compared to LILE and LREE elements and enriched in Pb compared to neighbouring elements. This finding shows enrichment of the mantle source area in terms of subduction components. Subduction components came from dominantly sediment melts and fluids from sediments to a lesser extent.

Melt modelling to determine the nature of the mantle source area indicate the source forming this basaltic volcanism may have formed from dominantly metasomatised 1% spinel peridotite facies melts. Delamination of lithospheric mantle within the EACZ with metasomatised spinel-rich melts in shallow zones in the lithospheric mantle may be responsible for the Otlakbaşı basaltic volcanism in the Pliocene period.

Acknowledgements

This study was supported by Van Yüzüncü Yıl University SRP project number 2012- HIZ-MİM001 and TÜBİTAK project number 113Y406. The author wishes to thank Dr. İrfan Temizel, Dr. Fatih Karaoğlan, Dr. Kurtuluş Günay and anonymous reviewers for contributing their constructive criticism and opinions of the manuscript.

References

Acarlar, M., Erkal, T., Güner, E., Şen, A., Umut, M., Elibjol, E., Gedik, İ., Hakyemez, Y., Uğuz, F. 1991. Van Gölü Doğu ve Kuzeyinin Jeolojisi, Maden Tetkik ve Arama Genel Müdürlüğü, Rapor No: 9469, 94 s. Ankara (unpublished).

Adam, J., Green, T. 2006. Trace element partitioning between mica- and amphibole-bearing garnet lherzolite and hydrous basanitic melt: 1. Experimental results and the investigation of controls on partitioning behavior. Contributions to Mineralogy and Petrology 152, 1-17.

Aldanmaz, E., Yalınız, M.K., Güçtekin, A., Göncüoğlu, M.C. 2007. Geochemical characteristics of mafic lavas from the Neotethyan ophiolites in western Turkey: implications for heterogeneous source contribution during variable stages of ocean crust generation. Geological Magazine 145, 37-54.

Al-Lazki, A., Seber, D., Sandvol, E., Türkelli, N., Mohamad, R., Barazangi, M. 2003. Tomographic Pn velocity and anisotropy structure beneath the Anatolian plateau (eastern Turkey) and the surrounding regions, Geophysical Research Letter 30, 8043.

Allen, M., Armstrong, H. A. 2008. Arabia-Eurasia collision and the forcing of mid-Cenozoic global cooling. Palaeogeography, Palaeoclimatology, Palaeoecology 265, 52-58.

Angus, D.A., Wilson, D.C., Sandvol, E., Ni, J.F. 2006. Lithospheric structure of the Arabian and Eurasian collision zone in Eastern Turkey from S-wave receiver functions. Geophysical Journal of International 166, 1335-1346.

Bağcı, U., Alpaslan, M., Frei, R., Kurt, M.A., Temel, A. 2011. Different Degrees of Partial Melting of the Enriched Mantle Source for Plio-Quaternary Basic Volcanism, Toprakkale (Osmaniye) region, Southern Turkey. Turkish Journal of Earth Science 20, 115-135.

Bravo, M.S., O'Hara, M.J. 1975. Partial melting of phlogopite–bearing synthetic spinel– and garnet–lherzolites. Physics and Chemistry of the Earth 54, 845-854.

Class, C., Miller, D. M., Goldstein, S. L., Langmuir, C. H. 2000. Distinguishing melt and fluid subduction components in Umnak volcanics: Aleutian arc. Geochemistry, Geophysics, Geosystems (3G) 1, 1-34.

Condamine, P., Medard, E., Devidal, J.L. 2016. Experimental melting of phlogopite-peridotite in the garnet stability field. Contribution to mineralogy and petrology 95, 1-26.

DePaolo, D. J. 1981. Trace element and isotopic effects of combined wall-rock assimilation and fractional crystallization. Earth and Planetary Science Letters 53, 189–202.

Elburg, M. A., Bergen, M. V., Hoogewerff, J., Foden, J., Vroon, P., Zulkarnain, I., Nasution, A. 2002. Geochemical trends across an arc–continent collision zone: magma sources and slab–wedge transfer processes below the Pantar Strait volcanoes, Indonesia. Geochimica et Cosmochimica Acta 66, 2771–2789.

Elliott, T., Planck, T., Zindler, A., White, W., Bourdon, B. 1997. Element transport from slab to volcanic front at the Mariana arc. Journal of Geophysical Research 102, 14991–15019.

Foley, S. F., Tiepolo, M., Vannucci, R. 2002. Growth of early continental crust controlled by melting of amphibolite in subduction zones. Nature 417, 837– 840.

Furham, T., Graham, D. 1999. Erosion of lithospheric mantle beneath the East African Rift system: geochemical evidence from the Kivu volcanic province. Lithos, 48, 237-262.

Green, D. H., Ringwood, A. E. 1967. The stability fields of aluminous pyroxene peridotite and garnet peridotite. Earth and Planetary Science Letters 3, 151-160.

Göğüş, O. H., Pysklywec, R. N. 2008. Mantle lithosphere delamination driving plateau uplift and synconvergent extension in eastern Anatolia. Geology 36, 723-726.

Gök, R., Sandvol, E., Türkelli, N., Seber, D., Barazangi, M. 2003. Sn attenuation in the Anatolian and Iranian plateau and surrounding regions, Geophysical Research Letter 30, 8038 -8042.

Hawkesworth, C. J., Turner, S. P., McDermott, F., Peate, D. W., Van Calsteren, P. 1997. U–Th isotopes in arc magmas: implications for element transfer from the subducted crust. Science 276, 551–555.

Hofmann, A.W., Hart, S. 1978. An assessment of local and regional ısotopic equilibrıum in the mantle. Earth and Planetary Science Letters 38, 44-62.

Innocenti, F., Mazzuoli, R., Pasquaré, G., Radicati di Brozolo, F., Villari, L. 1982. Tertiary and Quaternary volcanism of the Erzurum-Kars area (Eastern Turkey): Geochronological data and geodynamic evolution. Journal of Volcanology and Geothermal Research 13, 223-240.

Irvine, T. N., Baragar, W. R. A. 1971. A guide to the chemical classification of the common volcanic rocks. Canadian Journal of.Earth Sciences 8, 523-548.

Ionov, D.A., Bodinier, J.-L.,Mukasa, S.B. Zanetti, A. 2002. Mechanisms and sources of mantle metasomatism: major and trace element compositions of peridotite xenoliths from Spitsbergen in the context of numerical modelling. Journal of Petrology 43, 2219–2259.

Karaoğlan, F., Parlak, O., Thöni, M., Klötzli, U., Koller, F. 2016. The temporal evolution of the active margin along the Southeast Anatolian Orogenic Belt (SE Turkey): Evidence from U–Pb, Ar–Ar and fission track chronology. Gondwana Research 33, 190-208.

Karapetian, S.G., Jrbashian, R.T., Mnatsakanian, A.K. 2001. Late collision rhyolitic volcanism in the north-eastern part of the Armenian Highland, Journal of Volcanology and Geothermal Research 112, 189-220.

Keskin, M. 2003. Magma generation by slab steepening and breakoff beneath a subduction-accretion complex: An alternative model for collision-related volcanism in Eastern Anatolia, Turkey. Geophysical Research Letters 30, 8046-8050.

Keskin, M., 2007. Eastern Anatolia: a hot spot in a collision zone without a mantle pluma. In:Foulger, G.R., and Jurdy, D., (eds) Plates, Plumes and Planetary Processes. Geological Society of America, Special papers 430, 693-722.

Keskin, M., Pearce, J. A., Mitchell, J. G. 1998. Volcano-stratigraphy and geochemistry of collision-related volcanism on the Erzurum-Kars Plateau, North Eastern Turkey. Journal of Volcanology and Geothermal Research 85, 355-404.

Keskin, M., Genç, Ş. C., Aysal, N., Özeren, M. S., Sharkov, E. V., Lebedev, V. A., Chugaev, A. V., Oyan, V., Özdemir, Y., Ünal, E., Karaoğlu, Ö., Duru, O., 2013. Tectono-magmatic processes across the Arabian-Eurasian collision zone and their geodynamic significance: an integrated geological, petrological, geochemical and geochronological study of the post-collisional Cenozoic volcanic units displaying a transition from orogenic to anorogenic nature across a geotraverse from Caucasus to Arabian foreland, Unpublished report of TÜBİTAK-RFBR project #108Y222.

Kessel, R., Schmidt, M., Ulmer, P., Pettke, T. 2005. Trace element signature of subduction-zone fluids, melts and supercritical liquids at 120-180 km depth. Nature 437, 724-727.

Koçyiğit, A., Yılmaz, A., Adamia, S., Kuloshvili, S. 2001. Neotectonics of East Anatolian plateau (Turkey) and lesser caucasus: Implication for transition from thrusting to strike-slip faulting. Geodinamica Acta 14, 177-195.

Krienitz, M. S., Haase, K.M., Mezger, K., Eckardt, V., Shaikh-Mashail, M. A. 2006. Magma genesis and crustal contamination of continental intraplate lavas in northwestern Syria. Contribution of Mineralogy and Petrology 151, 698–716.

Le Bas, M.J., Le Maitre, R.W., Streckeisen, A., Zanettin, B. 1986. A chemical classification of volcanic rocks based on the total alkali-silica diagram. Journal of Petrology 27, 745–750.

Lebedev, V.A., Sharkov, E.V., Keskin, M., Oyan, V. 2010. Geochronology of the Late Cenozoic volcanism in the area of Van Lake (Turkey): an example of the developmental dynamics for magmatic processes. Doklady Earth Sciences 433, 1031–1037.

Lustrino, M., Wilson, M. 2007. The circum-Mediterranean anorogenic Cenozoic igneous province. Earth Science Reviews 81, 1-65.

Mc Kenzie, D. P., O'Nions, R. K. 1991. Partial melt distributions from inversion of rare earth element concentrations. Journal of Petrology 32, 1021-1091.

MTA. 2008. 1/100000 ölçekli Başkale K-51 paftası. Maden Tetkik ve Arama Genel Müdürlüğü, Ankara.

Okay, A. I., Zattin, M., Cavazza, W. 2010. Apatite fission-track data for the Miocene Arabian-Eurasia collision. Geology 38, 35-38.

Oyan, V. 2011. Vocanostratigraphy, Petrology and Magmatic Evolution of the Etrusk Volcano and Surrounding Areas (North of Lake Van, Turkey). PhD thesis, Yüzüncü Yıl Universtiy, 362 s.Van, Turkey.

Oyan, V., Keskin, M., Lebedev, V.A., Chugaev, A.V., Sharkov, E.V. 2016. Magmatic evolution of the Early Pliocene Etrüsk stratovolcano, Eastern Anatolia collision zone, Turkey. Lithos 256-257, 88-108.

Oyan, V., Keskin, M., Lebedev, V.A., Chugaev, A.V., Sharkov, E.V., Ünal, E. 2017. Petrology and Geochemistry of the Quaternary Mafic Volcanism in the northeast of Lake Van, Eastern Anatolian Collision Zone, Turkey. Journal of Petrology DOI: https://doi.org/10.1093/petrology/egx070.

Özacar, A.A., Gilbert, H., Zandt, G. 2008. Upper mantle discontinuity structure beneath East Anatolian Plateau (Turkey) from receiver functions. Earth and Planetary Science Letters 269, 426-434.

Özdemir, Y., Karaoğlu, Ö., Tolluoğlu, A.Ü., Güleç, N. 2006. Volcanostratigraphy and petrogenesis of the Nemrut stratovolcano (East Anatolia High Plateau): The most recent post-collisional volcanism in Turkey. Chemical Geology 226, 189-211.

Özdemir, Y., Güleç, N. 2014. Geological and Geochemical evoluation of Suphan Stratovolcano Eastern Anatolia, Turkey: Evidence for the lithosphere-asthenosphere interaction on post collisional volcanism. Journal of Petrology 55, 37-62.

Parlak, O., Delaloye, M., Kozlu, H., Fontıgnie, D. 2000. Trace element and Sr-Nd isotope geochemistry of the alkali basalts observed along the Yumurtalık Fault (Adana) in southern Turkey. Yerbilimleri 22, 137-148.

Pearce, J.A., Bender, J.F., De Long, S.E., Kidd, W.S.F., Low, P.J., Güner, Y., Şaroğlu, F., Yılmaz, Y., Moorbath, S., Mitchell, J.G. 1990. Genesis of collision volcanism in Eastern Anatolia, Turkey. Journal of Volcanol and Geothermal Research 44, 189-229.

Pearce, J.A., Stern.R.J., Bloomer, H.S., Fryer, P. 2005. Geochemical mapping of the Mariana arc-basin system: Implications for the nature and distribution of subduction components. Geochemistry, Geophysics, Geosystem (3G) 6, 1-27.

Plank, T., Langmuir, C. H. 1998. The chemical composition of subducting sediment and its consequences for the crust and mantle. Chemical Geology 145, 325–394.

Peccerillo, A., Taylor, S.R., 1976. Geochemistry of Eocene calc-alkaline volcanic rocks from the Kastamonu area. Northern Turkey. Contributions to Mineralogy and Petrology 58 63–81.

Sandvol, E., Türkelli, N., Barazangi, M. 2003. The Eastern Turkey Seismic Experiment: The study of a young continent-continent collision. Geophysical Research Letter 24, 8038-8041.

Shaw, J.E., Baker, J.A., Menzies, M.A., Thirlwall, M.F., İbrahim, K.M. 2003. Petrogenesis of the largest intraplate volcanic field on the Arabian Plate (Jordan): a mixed lithosphere–asthenosphere source activated by lithospheric extension. Journal of Petrology 44, 1657– 1679.

Staudacher,Th., Jessberger, E. K., Dorflinger, D., Kiko, J. 1978. A refined ultra-high vacuum furnace for rare gas analysis. Journal of Physics E: Scientific Instruments 11,781-784.

Şengör, A.M.C., Kidd, W.S.F. 1979. Post – collisional tectonics of the Turkısh – Iranian plateau and a comparison with tibet. Tectonophysisics 55, 361-376.

Şengör, A.M.C., Özeren, M.S., Keskin, M., Sakınç, M., Özbakır, A.D., Kayan, I. 2008. Eastern Turkish high plateau as a small Turkic-type orogen: implications for post-collisional crust-forming processes in Turkic-type orogens. Earth Science Reviews 90, 1-48.

Schildgen, T.F., Yildirim, C., Cosentino, D., Strecker, M.R. 2014. Linking slab break-off, Hellenic trench retreat, and uplift of the central and Eastern Anatolian plateaus. Earth Science Reviews 128, 147–168.

Shaw, D.M. 1970. Trace element fractionation during anatexis. Geochimica et Cosmochimica Acta 34, 237-243.

Sun, S.S., McDonough, W.F. 1989. Chemical and isotopic systematics of oceanic basalts: implications for mantle composition and processes. In: Saunders, A.D. & Norry, M.J. (ed.) In Magmatism in Ocean Basins, Geological Society of London Special Publication 42, 313-345.

Takahashi, E., Kushiro, I. 1983. Melting of a dry peridotite at high pressures and basalt magma genesis. American Mineralogist 68, 859-879.

Tatsumi, Y., Hamilton, D.J., Nesbitt, R. W. 1986. Chemical characterization of fluid phase released from a subducted lithosphere and origin of arc magmas: Evidence from high-pressure experiments and natural rocks. Journal of Volcanology and Geothermal Research 29, 293–309.

Taylor, S.R., McLennan, S.M. 1985. The continental crust: its composition and evolution, Geoscience Texts. Blackwell Scientific Publications, London.

Topuz, G., Altherr, R., Kalt, A., Satır, M., Werner, O., Schwarz, W.H. 2004. Aluminous granulites from the Pulur complex, NE Turkey: a case of partial melting, efficient melt extraction and crystallization, Lithos 72, 183-207.

Turner, S. P. 2002. On the time-scales of magmatism at island-arc volcanoes. Philosophical Transactions of the Royal Society of London, Mathematical, Physical and Engineering Sciences 360, 2853–2871.

Yılmaz, Y., Şaroğlu, F., Güner, Y. 1987. Initation of the neomagmatism in East Anatolia. Tectonophysics 137, 177-199.

Yılmaz, Y., Güner, Y., Şaroğlu, F. 1998. Geology of the Quaternary volcanic centres of the East Anatolia. Journal of Volcanology and Geothermal Research 85,173-210.

Zor, E., Gürbüz, C., Türkelli, N., Sandvol, E., Seber, D., Barazangi, M. 2003. The crustal structure of the East Anatolian Plateau from receiver functions. Geophysical Research Letters 30, 8044-8047.

Bulletin of the Mineral Research and Exploration

http://bulletin.mta.gov.tr

The Relationship of Landslides with lithological units and fault lines occurring on the East Anatolian Fault Zone, between Palu (Elazığ) and Bingöl, Turkey

Vedat AVCI[a*] and Murat SUNKAR[b]

[a]*Bingöl University, Faculty of Science and Literature, Dept. of Geography, Bingöl, Turkey. orcid.org/0000-0003-1439-3098*

[b]*Fırat University, Faculty of Humanity and Social Sciences, Dept. of Geography, Elazığ, Turkey. orcid.org/0000-0002-4479-5023*

Research Article

Keywords:
East Anatolian Fault Zone, Palu, Bingöl, landslide, Gökdere uplift.

ABSTRACT

In this study, the relationship of landslides with lithological units and fault lines on the East Anatolian Fault Zone (EAFZ) between Palu (Elazığ) and Bingöl, was evaluated. In the study area, which is located within the EAFZ, Göynük to the northeast, Palu Segment to the southwest, Genç Segment to the south of Bingöl plain and Gökdere Uplift in the intersection area form the main tectonic structures. In addition, the Karakoçan Fault Zone (KFZ) cutting the EAFZ in NW-SE direction between Palu and Bingöl corresponds to another important structure (system). The area, which is located in a region where a number of faults intersect, is tectonically very active. This situation has affected the morphology and caused the formation of many landslides along fault lines. In order to determine the relationship between the landslides observed in this area and lithological and tectonic structures, landslide magnitude and distribution analyses were performed by means of Geographical Information Systems. For this purpose, the landslide inventory map and the database were reproduced controlling the satellite images in field studies. Similarly; geological and tectonic maps were prepared considering previous studies. Landslides created in vector format were converted into raster format and overlain with lithological and tectonic maps, and then the relationship between landslides and lithology-fault lines were determined. According to these results, 59% of landslides occur in Upper Miocene-Pliocene agglomerate and tuff units and 10% of them in Eocene carbonate units. According to these data, almost 70% of the landslides in the study area occurred in two units. Considering the relationship between landslides and fault lines 64% of the landslides are observed at 0-1000 m distances to the fault lines. As a result, there is an important relationship between lithological features and fault lines. The fact that landslides have occurred along the fault lines in the north of Murat Valley shows that the landslides are triggered more by earthquakes when compared with those triggered by the hydro meteorological events.

Received Date: 22.09.2017
Accepted Date: 24.05.2018

1. Introduction

In this study, the relationship between the landslides on the EAFZ and the lithology and fault lines in the Palu western and Bingöl western regions were investigated. The study area corresponding to Palu-Bingöl has an important and very complex position in terms of tectonics. The eastern, western and the southern parts part of this area in the EAFZ consist of structures named as; Göynük, Palu and Genç Segment, respectively. The area between Göynük and Palu segments in the east of Bingöl Plain is the Gökdere uplift and the area to the north is the Karakoçan Fault Zone (KFZ) (Figure 1).

The East Anatolian Fault System (EAFS) is located between the Karlıova County in the north and Karataş (Adana) and Samandağ (Antakya) in the southwest. This system is approximately 30 km wide and 700 km long, large shear zone with a left lateral strike slip in the NE direction between Anatolian in NW and the Arabian-African plates in SE (Arpat and Şaroğlu, 1972; Koçyiğit et al., 2003; Aksoy et al., 2007). Though EAFS have not been investigated as well as

* *Corresponding author: Vedat AVCI, vavci@bingol.edu.tr*
http://dx.doi.org/10.19111/bulletinofmre.428277

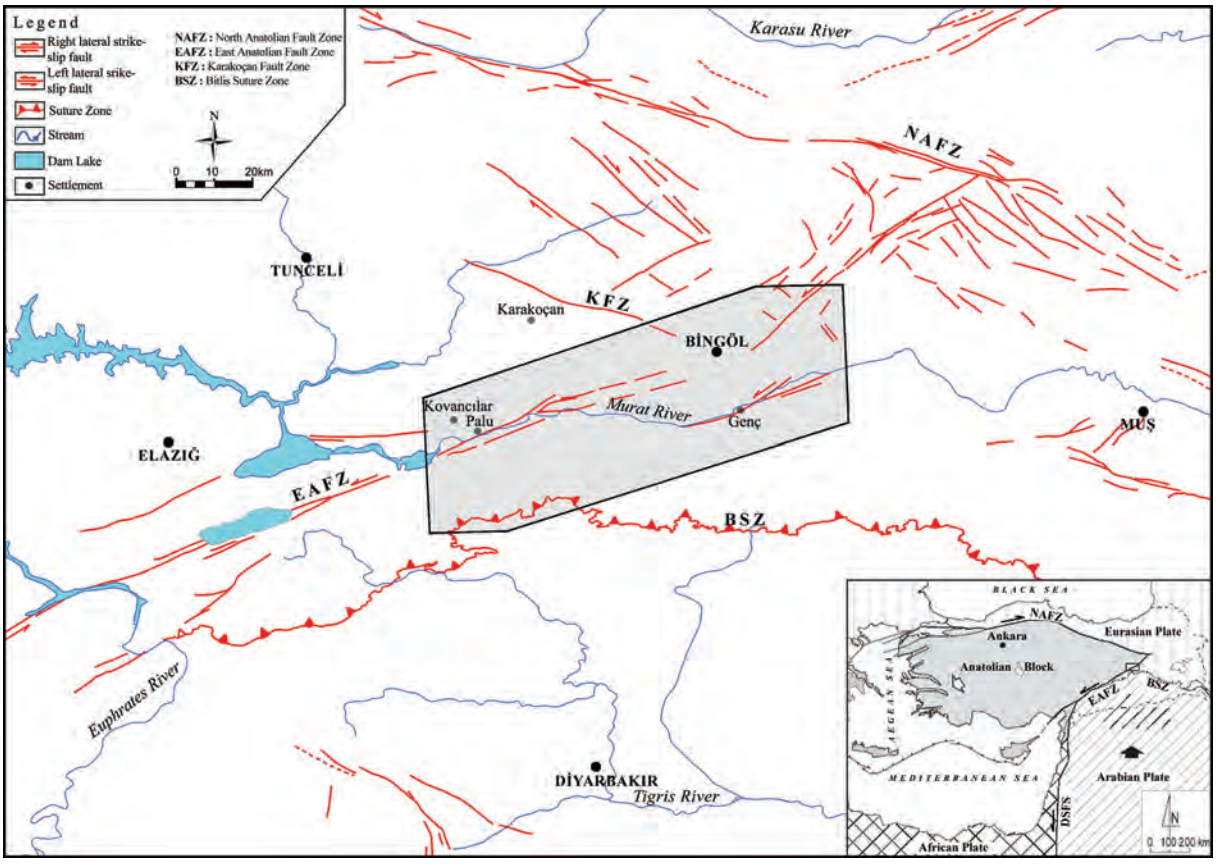

Figure 1- The location map of Palu-Bingöl interval (Faults were taken from Emre et al., 2012; Duman et al., 2012).

the North Anatolian Fault System (NAFS), numerous geological and seismological studies have been carried out on EAFS (Arpat and Şaroğlu, 1972; Gülen et al., 1987; Şaroğlu et al., 1987; Tatar, 1987; Herece and Akay, 1992; Reilinger et al, 1997; Ambraseys and Jakson, 1998; Koçyiğit et al., 2003).

The area between Palu and Bingöl corresponds to the intersection area of the EAF (Eastern Anatolian Fault) and the Karakoçan Fault (KF). Due to this intersection and compression effect, the area has been fragmented and uplifted to form the Karaömer Mountain (2460 m). In the south of this mountain the Murat River has been settled into EAFZ. The Murat River merges with the Göynük stream near the Genç District and then enters a 40-45 km long cut valley to Palu. The strait is considered to be epigenetic in this area as it is mainly buried in young volcanic units overlying metamorphics in the basement and ophiolites in the west (Atalay, 1974-1977; Tonbul, 1990; Tonbul and Özdemir, 1994; Özdemir and İnceöz, 2003; Avcı and Sunkar, 2016). Although the Murat River in east of the Eski Palu was emplaced into an epigenetic strait (Genc-Palu Strait), it flows along a valley with wide bottom varying between 750-1000 m in the Eski Palu vicinity and in the far west where sharp meanders are drawn (Tonbul and Özdemir, 1994).

There is an average elevation difference of 1500 m between Palu and Bingöl, and 1600-1700 m between Palu and the mountainous areas in the south. The fact that the area has been cut by numerous faults and the Murat River has been cut by deep and steep valleys has made the slope value high in the slopes. In the mountainous areas between Palu and Bingöl the slope reaches 45^{o} and above. In some canyon shaped valleys this value even reaches 90^{o}. This elevation difference at short distances, high slope, young cover units, faulty structures and the rainfall have caused the occurrence of landslides in this area.

Özdemir and Tonbul (1990) indicated that the EAF to form a weak zone near Palu in the Murat River Valley, unstable rocks such as the claystone and marl to crop out on valley slopes and the Murat River to erode convex slopes of the Murat River and the strong slope angle have caused landslides. Atalay (1974-1977) stated that active mass movements along the Murat valley between Muş-Palu had caused the

Elazığ-Mus railway to deteriorate and train accidents to occur. Due to the dams built between Palu and Genç in the Murat Valley, the railway line that remained in this area has been changed. Despite this change made in recent years, the railway transportation is affected by the recurrent mass movements (Figure 2).

Palu-Bingöl is one of the areas where landslides are most intensely seen; it is due to the fact that in this region, all conditions for landslide formation are available. Because of this feature of the field, such a study was carried out with the thought that each of the parameters affecting the landslide is very well analyzed. For this purpose, the distribution of landslides according to geomorphologic units has been investigated previously (Avcı and Sunkar, 2016). In this study, the relationships between landslides and lithological units besides the distance to the fault lines were analyzed. The fact that the landslides observed in this study are arranged along the fault lines indicate that there is a close relationship between the fault lines and the distribution of landslides. These seismically active faults are followed by large-scale landslides. Again, the accumulation of landslides on certain lithologies shows that lithology along with the fault is also important.

Active and passive landslides, which were examined according to the landslide inventory map prepared by the MTA, cover a wide area (Duman et al., 2009). In geomorphological studies carried out in the region other than the inventory map, a large number of landslides have been mapped around Palu-Bingöl and their properties have been explained (Atalay, 1974-1977; Tonbul, 1990; Tonbul and Özdemir, 1994; Özdemir and İnceöz, 2003). Active and passive groupings of landslides in the field were made according to current literature and field observations. The landslides are regarded as active when the carvings at the toe causes the mass movement, however the landslides in which the movement is not visible are accepted as passive. Furthermore, it was observed that cracks and swelling structures were visible in active landslide areas in geomorphologic observations carried out as well as in passive landslides, the vegetation covered the surface and there were no cracks'.

2. General Geological and Geomorphological Features of the Area Between Palu and Bingöl

The study area corresponds to the Murat valley located in between Palu and Bingöl, which has an important place in EAFS. Palu western and Bingöl east were included in the study area and it was aimed to reveal the relation between lithological units and fault lines in the distribution of landslides. The survey area covers an area of 3280 km^2 within the specified boundaries and landslide susceptibility analyzes were performed in some small basins located within these boundaries (Avcı, 2016).

According to data of Bingöl meteorological station located at 1177 m elevation, the mean temperature

Figure 2- The landslide that occurred on 19 March 2017 at the exit of the tunnel on the new railway between Genç Beyhan and Süveran Locality, which had been built after Beyhan Dam, caused the locomotive to come out of the way (http://www.hurriyet.com.tr/heyelan-nedeniyle -yuk-treni-raydan-çikti-40400338 19 Mart 2017).

has been 12.1°C for long years (1961-2016) and for the same period the average amount of rainfall has been 943.6 mm. Monthly average maximum rainfall in January and the minimum values in August were measured as; 138.5 mm and 3.2 mm, respectively. (Table 1, MGM, 2017).

The lithological units within the study area have been studied in detail in different studies (Sirel et al., 1975; Naz, 1979; Sungurlu et al., 1985; Herece and Akay, 1992; Yüksel, 2006). Precambrian gneisses and schists, which outcrop in large areas to the east of Akdağ and south of Murat River, are the oldest units. The Upper Paleozoic marbles, which are exposed in Bingöl northeast and Akdağ, are the second oldest units. The ophiolites formed by gabbros and diabases cut by EAF and Murat Valley are Mesozoic aged rocks. Apart from these units, the units consisting of volcanic and sedimentary rocks (Lower-Middle Eocene), clastic rocks and carbonates (Middle-Upper Eocene and Upper Miocene), clastic and carbonates (Oligocene, Lower Miocene) crop out. The Upper Miocene-Pliocene units composed of agglomerate, tuffs and basalts in the vicinity of Bingöl to the east of Karaömer Mountain are the lithologies having the largest area. Quaternary alluvials observed at the bottom of the Murat River valley and in the Kovancılar and Bingol plains correspond to the youngest units (MTA, 2002, Figure 3).

Table 1- Bingöl Central Meteorology Station long period (1961-2016) monthly temperature and precipitation averages (MGM, 2017).

BİNGÖL	January	February	March	April	May	June	July	August	September	October	November	December	Annual
Temperature **(°C)**	-2.4	-1.3	4.0	10.8	16.3	22.1	26.8	26.4	21.1	14.0	6.6	0.5	12.1
Rainfall Amount (mm)	138.5	134.6	128.7	116.8	74.5	21.3	5.6	3.2	11.7	66.2	107.9	134.6	943.6

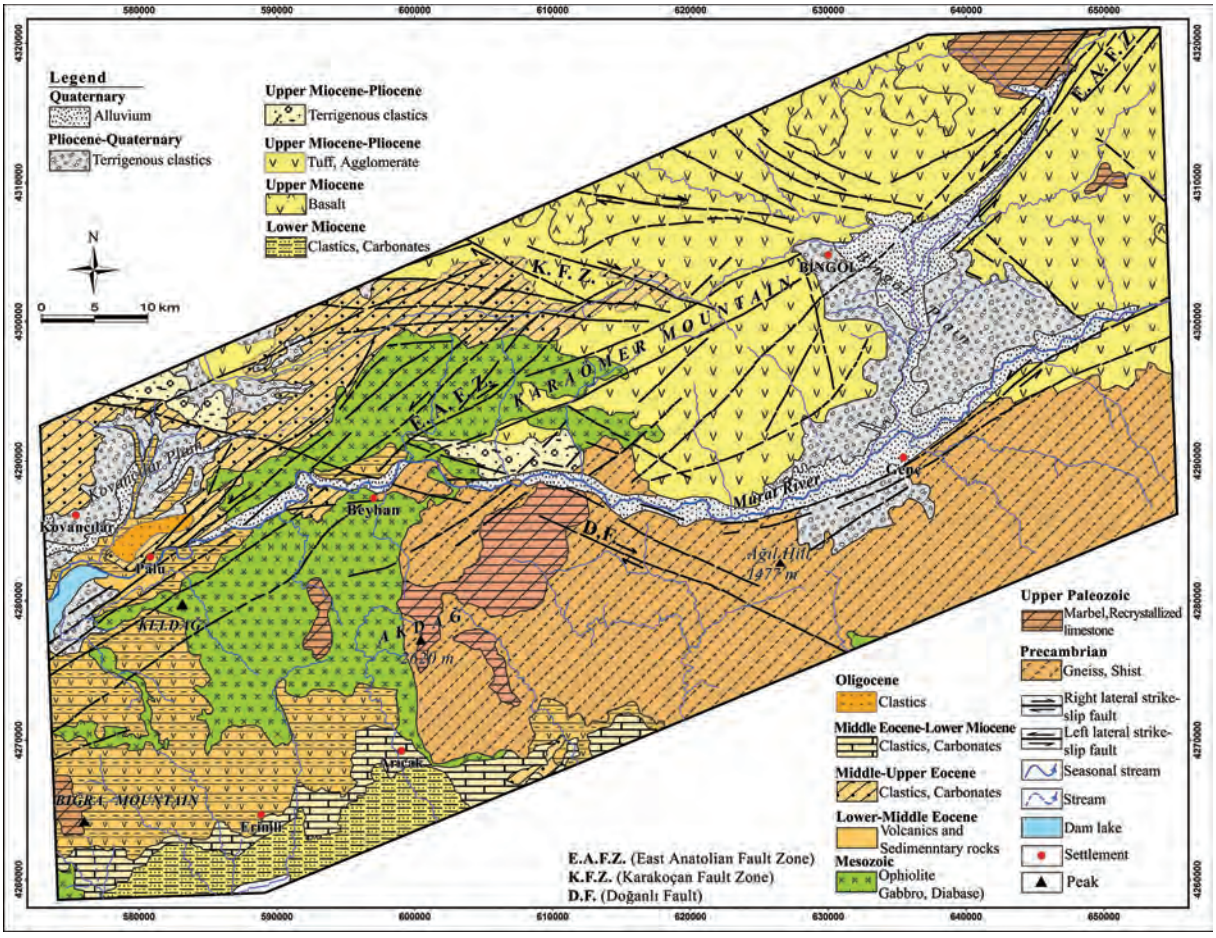

Figure 3- Geological map of the area remaining in the EAFZ between Bingol and Palu (from MTA 1/500000 scale Geological Map of Turkey, Erzurum sheet).

The area between Palu and Bingöl exhibits tectonically very complex structure and constitutes the biggest compressional stepover in EAFZ (Arpat and Şaroğlu, 1972). The Karaömer Mountain, which corresponds to the compression and stepover area between Göynük and Palu segment, is named as the Gökdere Uplift. The Gökdere Uplift was cut by KFZ at the same time (Figures 1 and 3).

EAFZ is divided into different segments according to its geometrical characteristics and slip of faults (Arpat and Şaroğlu; 1972, 1975). Hempton et al. (1981) classified EAFZ into 5 segments according to its fault behavior and slip; however, Barka and Kadinsky-Cade (1988) divided this zone into 14 segments according to fault geometry, earthquake activity and surface fractures. Şaroğlu et al. (1992) investigated the EAFZ in 6 structural segments ranging from 45-145 km in length. The Gökdere uplift between Karlıova-Bingöl and Palu-Hazar Lake sections and the Sincik uplift between the Hazar Lake-Sincik and Çelikhan-Erkenek sections correspond to morphotectonic structures which developed from compressional stepovers between the main sections of the fault (Şaroğlu et al., 1987, 1992; Herece, 2008).

The Karakoçan Fault Zone, which limits the Gökdere Uplift in the east is a new active 6-10 km wide, 50 km long, right lateral strike slip intra-plate structure in NW direction. This zone consists of a large number of closely spaced (100 m), parallel to sub parallel structural fault segments with lengths ranging from 0,5-17 km. The most important structure developed within the Karakoçan Fault Zone is the Karakoçan pull-apart basin where the Karakoçan county and numerous towns are located. The oldest basin fill that continues its development under the control of the Karakoçan Fault is the Late Pliocene Kızılca travertine. Therefore, the age of the fault is Plio-Quaternary (Koçyiğit, 2003).

The area between Palu and Bingöl geomorphologically corresponds to mountainous areas. Bingöl and Palu surrounds on the other hand form tectonic basins that form between these areas. The highest peak in the investigated area is Akdağ (2620 m) and the lowest area is the Murat valley near Palu (845 m). The average slope value in the area is 16,70° and the slope of the fault planes and steep valleys reach 70-90°. Mountainous areas, which formed by folding, have then faulted and uplifted under compressional regime. The mountainous areas to the east of Bingöl were formed by volcanic activity and later cut by EAF. The fact that the site was cut by EAFS and KFZ caused the formation of numerous landslides. New landslides are formed with earthquakes occurring in the region and old landslides become active and affect settlement and access roads.

3. Material and Method

In the preparation of the landslide inventory map used in this study, the landslide inventory map of 1/500.000 scale Erzurum Sheet prepared by the General Directorate of Mineral Research and Exploration (MTA) was used (Duman et al., 2009). However, not all landslides are shown in this inventory map because of the wide area, scale difference of the inventory map, and ignorance of some landslides. Considering this situation, a landslide inventory map showing the landslides in the study area was prepared based on satellite images (Landsat Image 8, dated 4 June 2013), 1/25.000 scale digital topography maps and field observations.

Landslide areas were identified by defining morphological features of the land from satellite images and topography maps. The boundaries of the landslides, and their activity were assessed during field studies. In addition, the ground truth of the existing landslide inventory map was carried out. Inventory maps are the simplest mapping method in direct mapping methods and are important in pointing out the locations of known landslides (Hansen, 1984).

Previously digitized landslide inventory map was corrected by Digital Elevation Model (DEM) and isohypse curves obtained from the topography. The landslides in the inventory map were grouped as active and passive, then converted from raster to vector format. Lithological information was taken from Altınlı (1963) and the geological map was updated by using 1/500.000 scale Geological Map of Turkey, Erzurum Sheet. Some of the information regarding faults was taken from investigations carried out by MTA (Emre et al., 2012; Duman et al., 2012) and of some from geological studies carried out in the region (Çetin et al., 2003; Aksoy et al., 2007; Sarp, 2014). Especially the faults between Palu and Bingöl were determined based on satellite images, DEM data and geomorphological observations.

By using geological maps, the lithology map was prepared and lithological units and landslides were correlated based on this map. Apart from lithology,

the spatial relation of active faults and landslides was investigated by buffer analysis. After preparing the numerical data of the field, the distance map to the fault lines from the tectonic map was produced. The lithology and the distance maps of fault lines of the landslides were aligned with the landslide inventory map in the same cell size (10x10 m), and the pixel numbers with/without landslides of layer subgroups were detected. By using these data, the distribution of landslides based on the lithological units and the distance to fault lines was determined and their distributions according to slope and elevation were statistically analyzed.

4. Findings and Discussion

4.1. Distribution of Landslides between Palu and Bingöl

Knowledge of the factors that control the spatial distribution, characterization and formation of existing and potential mass movements is necessary to take preventive measures and reduce harm (Cihangir and Görüm, 2016). When losses caused by mass movements are taken into consideration the necessity of such a study is better justified.

Simplification was made in mapping very small scale landslides and landslides that had been intertwined during the digitization process. Small scale landslides were combined with the nearest landslide, and intertwined landslides were shown as single landslide. For example, there are tens of landslides in the large active and passive landslide areas seen in the northeast of Bingöl. As the landslides in such areas are interconnected and have similar characteristics, they were shown as one landslide. By making such a digitization approximately 30% of landslides were simplified. In this way, within the boundaries of the study area, a total of 718 landslides, 164 passive and 554 active, were mapped. Active landslides cover a total of 144.07 km^2, whereas passive landslides cover a total area of 70.25 km^2. The total area of the landslides is 214.32 km^2, corresponding to a total of 6.5% of the study area. The sizes of the landslides range from 0.01 km^2 to 13.95 km^2 with an average area of 0.29 km^2. When the classification made by Cihangir and Görüm (2016) for the Kelkit downstream is taken into consideration, 3 of the landslides in the study area are very large (13.95-5.1 km^2), 19 are large (5.1-1.0 km^2), 475 are medium 1.0-0.1 km^2), 221 are smaller (0.1-0.001 km^2) (Figure 4a). Considering the slope aspect, 632 (93%) of the landslides are observed on the northern slopes and 86 (7%) of the landslides are observed on the southern slopes (Figure 4b).

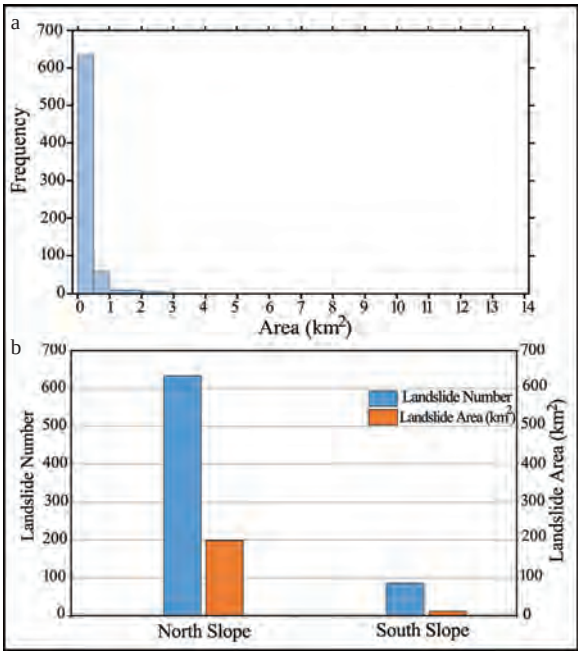

Figure 4- (a) The areal frequency of landslides observed between Palu-Bingöl, (b) number and areal distribution according to northern and southern slopes.

The landslides in the area show formation characteristics in the form of flow, fall and slide. Apart from landslides, which are mostly in slide type, the landslides that occur along formation boundaries and fault lines are in fall type, and the landslides on steep slopes where debris accumulates are in flow type. Atalay (1974-1977) emphasized that there were a continuous debris flow and transportations in areas where agglomerate, sandy and pebbly slope deposits in the Murat Valley were present. In order to determine the range of impact of landslides between Palu and Bingöl long and short axis ratios of them were calculated. According to these calculations, the long-short axis ratios of the landslides between Palu and Bingöl range between 1.0 and 3.6. Furthermore, according to the analysis results, it was concluded that circular failures were more abundant (Figure 5).

Geomorphological factors such as slope, aspect, and failure grade in the region are predominant for the mass movements in the region. More than 50% of the landslides in the study area are observed in slopes with a slope of 15-45° (Avcı and Sunkar, 2016). When the

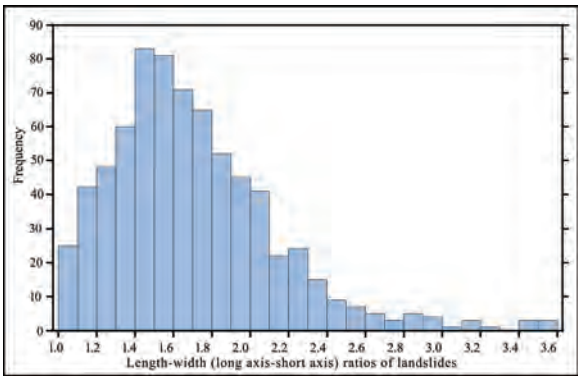

Figure 5- Length-width (long axis-short axis) ratios of landslides observed between Palu-Bingöl.

relationship between landslide and geomorphologic factors is evaluated, the average slope in the studied area is 16.69°, while the average slope of landslide areas is 18.29°. The fact that the slope is nearly 1.5° higher in the landslide areas is due to the slope of landslides. When this situation is ignored, the mean slopes of the landslide fields and the average slope values of the study area are in compatible. The median value of the slope in landslide areas is 17.2°, the landslides decrease after this value (Figure 6a).

The average elevation between Palu and Bingöl is 1401 m and the approximate height of the landslide fields (1520 m) is very close to this value. According to the results of the analysis, the median value of elevation in landslide areas is 1488 m. It is seen that landslides become dense in 1200-1400 m and 1700-1800 m contours. There is a close relationship between the aspect, slope and elevation features located in geomorphological parameters summarized above and the distribution of landslides (Figure 6b). As the relationship between geomorphological factors and landslides between Palu and Bingöl was evaluated in detail by Avcı and Sunkar (2016), only the density analyses of slope and elevation factors were analyzed in this study.

Except for this general situation, the mass movements and landslides become dense along the steep valley slopes of Murat River and fault lines. To the west of Palu Castle, Gökyamaç corresponds to a landslide area, and mud flows, failures and slip types indicate that the landslide is active (Tonbul and Özdemir, 1994, Figure 7a).

In areas where landslides occur in the form of slide that develop towards the end of spring, large cracks might form in the upper parts. Cracks in 1 m width

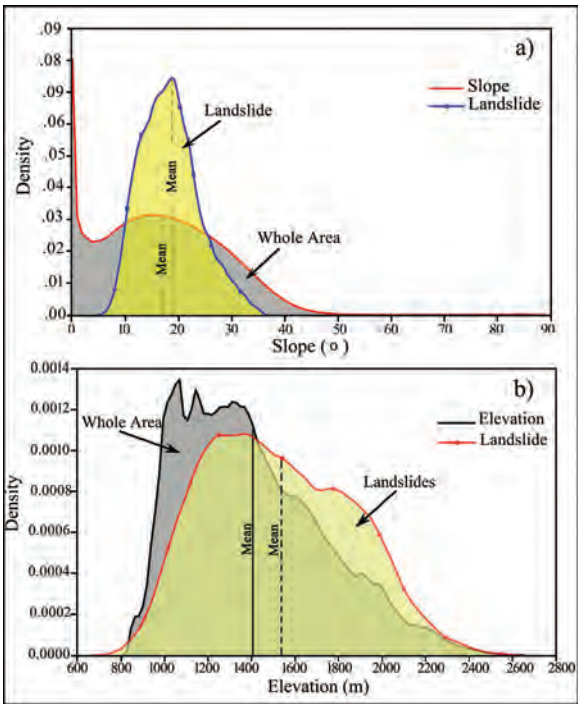

Figure 6- Probability estimates of landslides observed between Palu-Bingöl according to slope (a) and elevation (b) based on the kernel density analysis.

and 2-3 m depth were formed at the end of 2017 spring in the east of Genç, due to the slide seen at Çaytepe Duşmalan Locality (Figure 8).

4.2. Relationship between Lithological Units and Landslides

Lithology is one of the most important parameters affecting the slopes and their stabilities because the shear strength and permeabilities of different lithological units are different from each other. Therefore, the sensitivity of these units to sliding is also different (Dağ, 2007). Different degree of disintegration on the same lithological unit produce different sensitivity. For this reason, the degree of disintegration should be considered as another property that affects the slide. In the study carried out in Rize Fındıklı, an area of approximately 25 km^2, 85% of the observed landslides have been found to be formed on completely disintegrated rocks. The increase in clay content in these disintegrated rocks in these areas also led to an increase in the number of landslides (Bulut et al., 1995). In another study carried out in Rize, Çayeli, 87% of the landslides were formed within the disintegrated rocks (Dağ et al., 2006). The depth of the disintegrated material is also effective in the formation of landslides (Ercanoğlu and Gökçeoğlu, 2002).

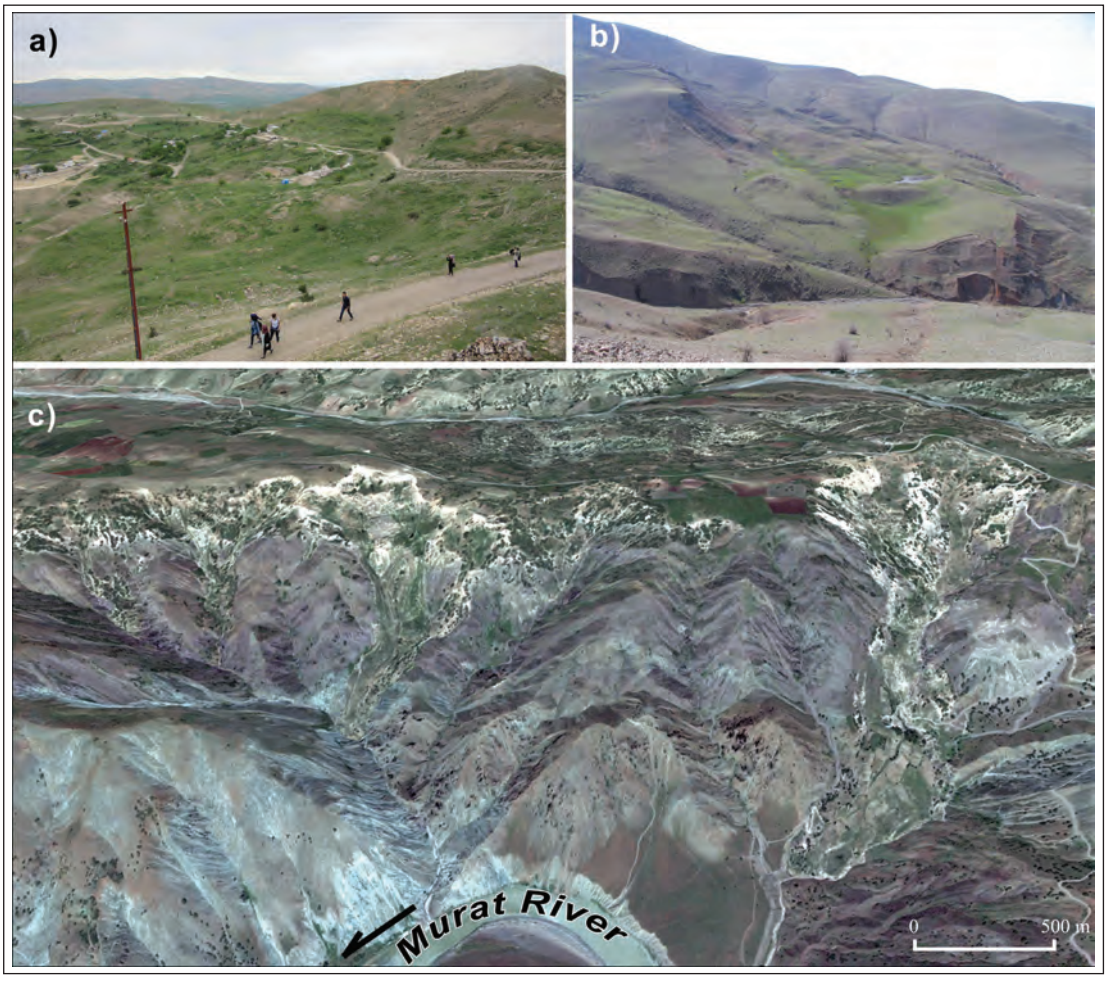

Figure 7- Landslides observed on EAFZ between Palu-Bingöl; a) Slide type landslide affecting Eski Palu to the east of Palu, b) Bahçecik Landslide developed in detachment type on the south of Karakoçan and c) flow type landslides observed in Google Earth image on the southern slope of the Murat Valley, south of Palu).

Figure 8- Large cracks were formed at Çaytepe Duşmalan Locality, the east of Genç, due to the slide that occurred in early summer of 2017.

Tuffy, clayey and marly structures in our country are the lithologies where landslides are seen the most. However, landslides are less commonly observed in lithologies such as limestone and basalt (Erinç, 2012). The distribution of landslides between Palu and Bingöl in lithological units is particularly compatible with this.

When the distribution of the landslides to lithological units in the study area is examined, most of the landslides are found on the Upper Miocene-Pliocene volcanics. This is followed by the unit consisting of Middle-Upper Eocene clastic and carbonates (Figure 9). When lithological units are examined, Upper Miocene Pliocene volcanics occur in 24% of the study area, Middle-Upper Eocene clastic and carbonates in 7% of the study area. Gneiss and schists of the Pre-Cambrian period, which are exposed to the south of Murat Valley, are not very important

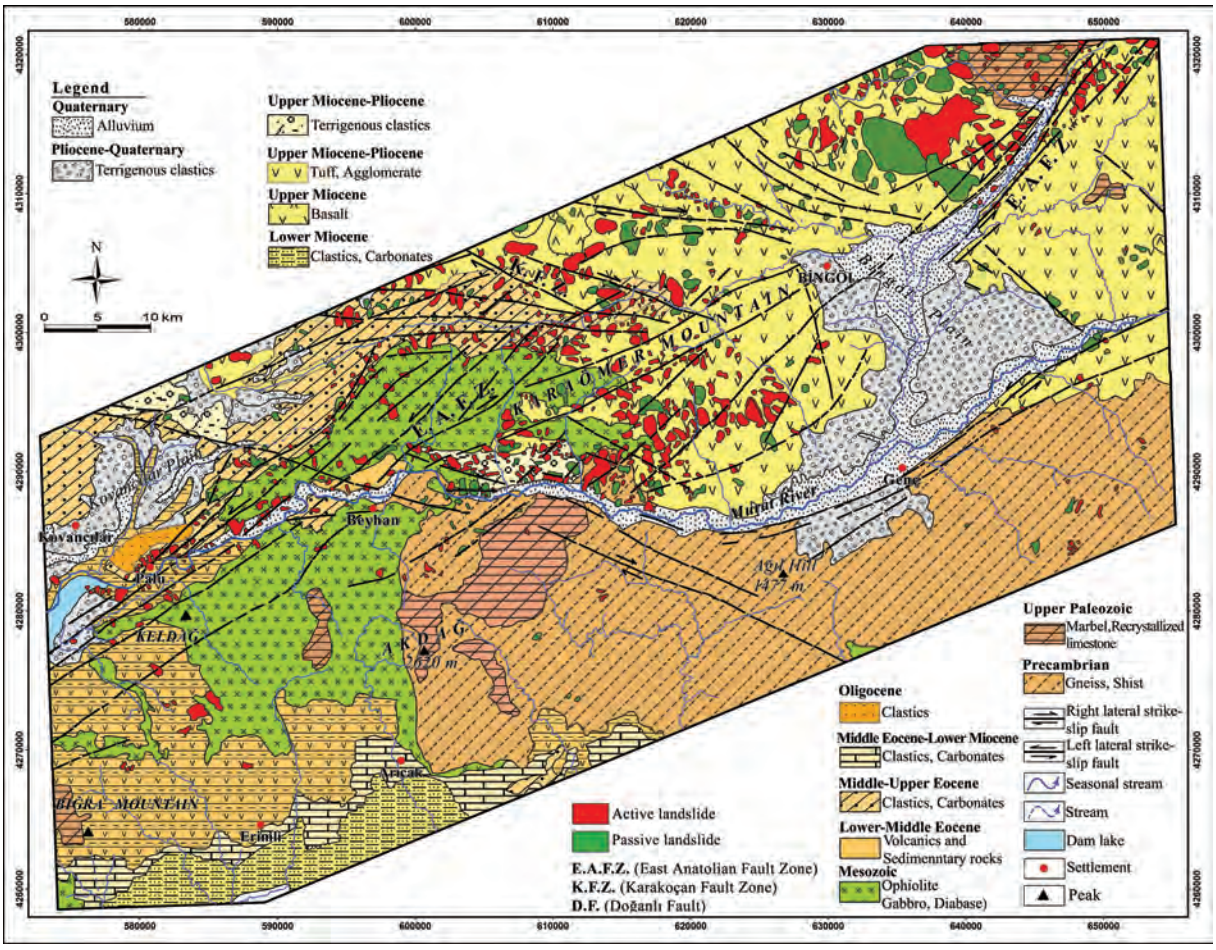

Figure 9- Distribution map of the landslides in the EAFZ between Palu and Bingöl with respect to lithological units.

in the distribution of landslides though they cover an area of 24% (Figures 9 and 10).

All other lithological units except the two lithologies in the southwest of the study area were cut and deformed by active faults. It is thought that lithology is important as well as being affected by these deformations in the formation of landslides. Because although the unit, which is formed by gneiss and schist in the south of Murat Valley, is cut by faults, the landslide density is very low. 66% of the landslides in the study area are observed in areas where the Upper Miocene-Pliocene agglomerates, tuffs and basalts are exposed. Apart from this unit, 10% of the landslides occurred on Middle-Upper Eocene and 8% of them occurred on Mesozoic (ophiolites) units. According to this distribution, more than 80% of the landslides were gathered over 4 lithologies and show the effect of lithology on landslide formation (Table 2, Figure 11).

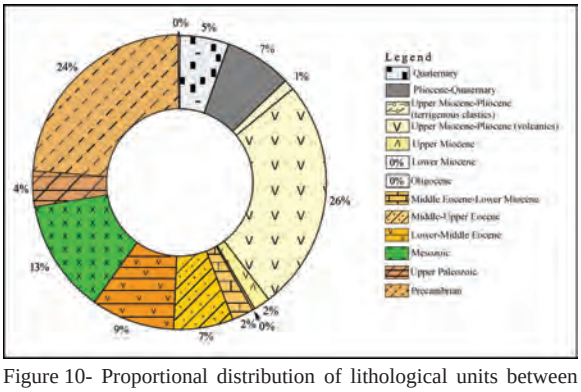

Figure 10- Proportional distribution of lithological units between Palu and Bingöl.

As stated by Atalay (1974-1977), the equilibrium angle was spoiled in areas where the volcanic tuff, sand and agglomerates were failed in the Murat Valley and on branches of its side steep slopes. The fact that these units together with river valleys were cut by faults and the presence of clayey structures have made reach the liquid limit quickly and accelerates the formation of landslide.

Table 2- Densities of lithological units and landslides with respect to lithological units.

Lithological Units	Study Area			All landslides in the study area		
	km²	%	Density in the study area	km²	%	Density in the study area
Quaternary	177,83	5,41	0,054	4,15	1,92	0,001
Pliocene-Quaternary	238,71	7,19	0,070	0,96	0,44	0,000
Upper Miocene-Pliocene (terrigenous clastics)	39,054	1,16	0,011	6,34	2,95	0,001
Upper Miocene-Pliocene (Tuff, Agglomerate)	838,15	25,54	0,255	126,45	58,93	0,036
Upper Miocene	59,83	1,77	0,017	16,00	7,45	0,004
Lower Miocene	90,12	2,67	0,026	0	0	0
Middle-Upper Eocene	215,04	6,39	0,062	20,90	9,74	0,006
Lower-Middle Eocene	301,49	8,96	0,087	6,49	3,02	0,001
Middle Eocene-Lower Miocene	77,93	2,31	0,022	0	0	0
Oligocene	8,38	0,24	0,002	0	0	0
Mesozoic	410,45	12,20	0,119	16,32	7,60	0,004
Upper Paleozoic	40,205	1,22	0,012	6,305	2,93	5,168
Precambrian	775,35	23,68	0,236	10,511	4,89	0,003
Dam Lake	7,9850	0,23	0,002	0,11	0,052	3,306
Total	3280,52	100	1	214,32	100	0,062

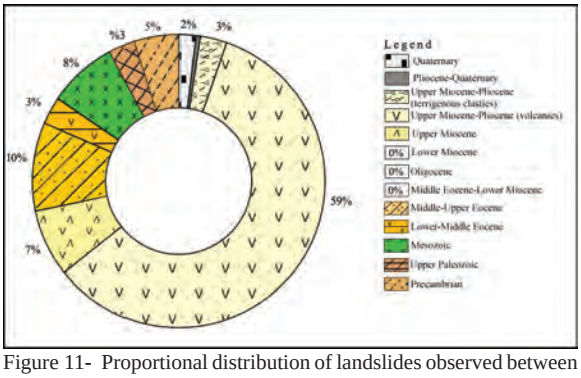

Figure 11- Proportional distribution of landslides observed between Palu and Bingöl with respect to lithological units.

Frequency ratio method was used to statistically explain the relationship between landslides and lithology. This method reveals the relationship between the position of existing landslides and the factors affecting the landslide. The frequency ratio method has a probability model and can be defined as the ratio of the likelihood of occurrence of an event to the probability of unlikelihood (Erener and Lacasse 2007; Yilmaz, 2009; Akıncı et al., 2010). Frequency values higher than one (1) indicate meaningful relation with landslide. It is observed that the frequency in the investigated area is high in areas where the Upper Miocene-Pliocene terrigenous clastics and volcanic rocks are exposed. In addition, the landslide frequency values are high in areas where the Eocene and Mesozoic units with clayey structures are exposed (Table 3).

The landslides in the study area appear to be concentrated on the EAFZ and in certain areas. These areas are the Palu surround from the southwest to the northeast, the Karaömer Mountain and the Göynük stream valley in northeast of the Bingöl Plain. The landslide density at the formation boundaries of clayey lithologies around Palu is high. In particular, landslides occur in areas where clayey structures on ophiolites are cut. The Karaömer Mountain, which corresponds to Gökdere uplift, corresponds to the junction of EAF and KF. Due to this tectonic structure, high angled steep slopes were formed. Also the lithology to be in agglomerated, tuff and clayey structures caused the formation of landslides on almost all slopes cut by faults. Because of fault, slope and lithology, the landslides in this area are both wide based and active. The landslides, which develop generally in the form of slides, move slowly and they are in the form of intertwined because of this formation.

The widespread occurrence of landslides around Palu in the Murat River Valley is due to the high angle values and the widespread presence of clayey ophiolitic rocks and Eocene clay and marls. In addition, the presence of many spring waters on slopes facilitates this formation (Özdemir and Tonbul, 1990).

Table 3- Relation of landslides between Palu and Bingöl with lithology based on frequency ratio.

Lithology	Sub Grup Area (m^2)	Total Area (m^2)	Total Area Percentage (a)	Landslide Area (m^2)	Total Landslide Area (m^2)	Landslide area Percentage (b)	Frequency ratio (b/a)
Quaternary	177712200	3280521800	5.4171931	4157300	214325800	1.940616	0.3582327
Pliocene-Quaternary	238732100	3280521800	7.27726	891200	214325800	0.41601	0.0571657
Upper Miocene-Pliocene (terrigenous clastics)	39054900	3280521800	1.1905088	6328700	214325800	2.954219	2.4814763
Upper Miocene-Pliocene (Tuff, Agglomerate)	838151000	3280521800	25.54932	126496600	214325800	59.04826	2.3111479
Upper Miocene	59834900	3280521800	1.8239446	15995600	214325800	7.466701	4.0937104
Lower Miocene	90121200	3280521800	2.7471605	0	214325800	0	0
Middle-Upper Eocene	215047500	3280521800	6.5552834	20903300	214325800	9.757602	1.4885095
Lower-Middle Eocene	301228200	3280521800	9.1823258	6498700	21432580	3.033575	0.3303711
Middle Eocene-Lower Miocene	77942100	3280521800	2.3759056	0	214325800	0	0
Oligocene	8385200	3280521800	0.2556057	0	214325800	0	0
Mesozoic	410439800	3280521800	12.511418	16313300	214325800	7.615002	0.6086442
Upper Paleozoic	40205900	3280521800	1.2255947	6030700	214325800	2.815114	2.296937
Precambrian	775353800	3280521800	23.63508	10515500	214325800	4.908606	0.207683
Dam Lake	7985200	328052180	0.2434125	11450	21432580	0.053448	0.219579

4.3. Relationship between The Distance to Fault Lines and Lanslides

When we look at the distribution of the landslides between Palu and Bingöl, it seems that it is directly parallel to the extension of EAFZ. Starting from Palu west, almost all active landslides were arrayed along a line until the Göynük Valley in the east of Bingöl (Figure 12). This general distribution is directly related to active faults and earthquakes experienced. With snow and rainfall seepages into blocks, which cut and uplifted, facilitated the slip of masses on clayey layers. This formation is also affected by the degradation of the slope balance due to the abrasion of the rivers located in fault lines.

The most important structural elements in the study area are EAFZ and KFZ. Apart from these faults, the Doğanlı Fault (DF) and Genç Fault (GF) constitute other structural elements and are not as effective as EAF and KF. The cut of the EAF by the KF between Palu and Bingöl caused this area to uplift and deform.

The Gökdere uplift passes through the south of the study area. The right slip of the Palu segment with respect to the Göynük segment causes the region between these two segments to rise. The area, which is called as the Gökdere uplift, covers 15 km wide, 30 km long area starting from north of Beyhanlı village in the west to the Ormanardı village in the east. The uplift of the Gökdere compressional zone, deep excavations in the valley basins and alluvial fans and the heights of the Early Pleistocene deposits today show that the area between Palu and Bingöl uplifted in the Quaternary (Herece, 2008). In this area, which corresponds to the Gökdere Uplift, a significant expansion has occurred in EAFZ. The EAFZ forms a 15 km wide zone in the east of Palu, which corresponds to the area where the uplift occurred, and a 5 km wide zone in east of Bingöl. There is also observed an increase in the number of landslides parallel to this expansion. On the other hand, as moving further away from fault zones, the number of landslides decreases and gains a density value close to zero to the south of the Murat Valley. Gupta and Joshi (1990) have also stated that the density of landslides increased as approaching the fault and decreased as moving away from the fault. Moreover, it has been stated that if you are close to fault zones, then it will cause the break up in the rocks, which will negatively affect the slope balance.

The intersection area and close vicinity of the EAF and KF correspond to a risky and mobile area in terms of both the seismicity and mass movements (Avcı and Sunkar, 2016). In this area, the offset of the Murat River Valley to the south is seen as the reflection of the two fault to the morphology. Again, the high asymmetry between the northern and southern sides of the Murat Valley in the distribution of landslides is due to faults.

In order to determine the distribution of landslides with respect to fault lines in the study area, 7 classes

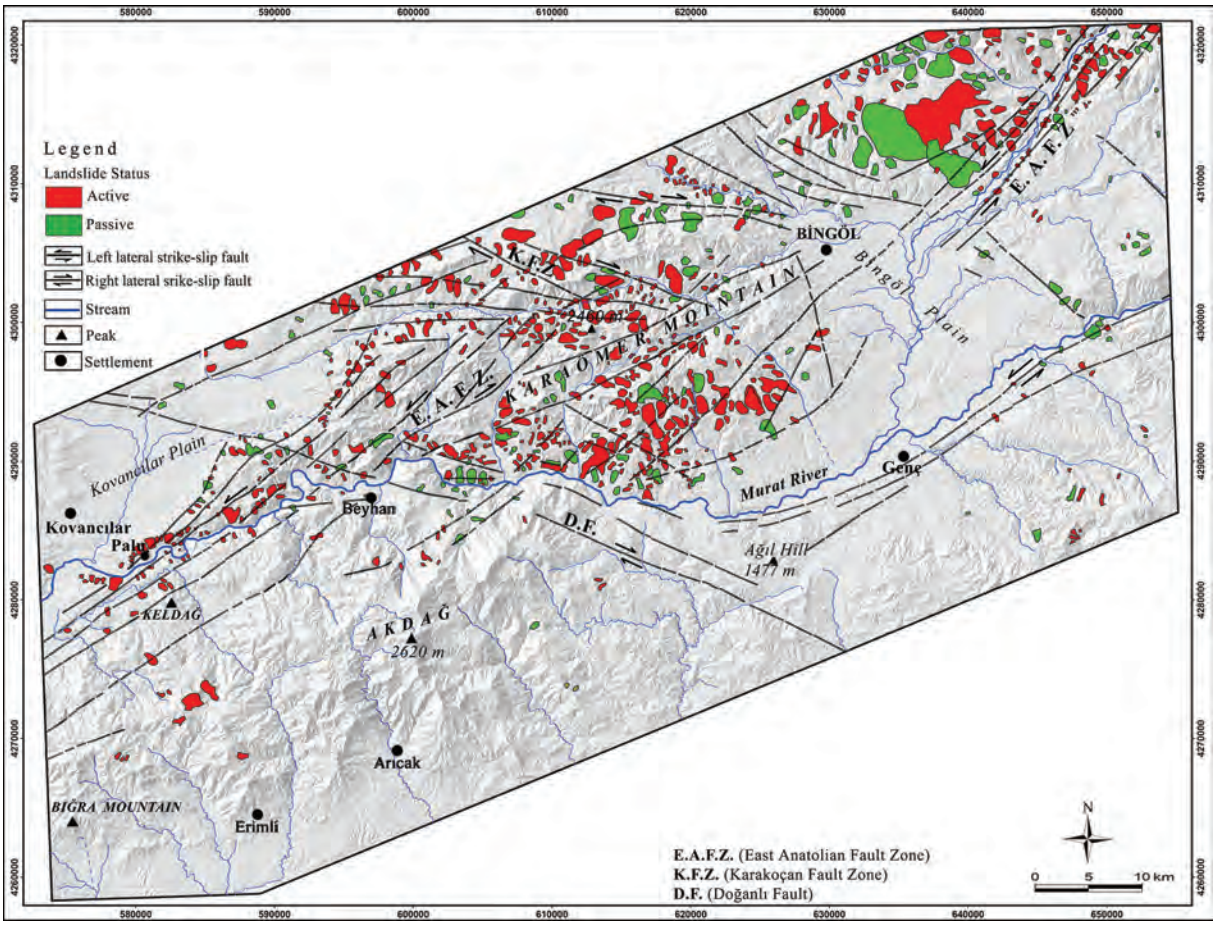

Figure 12- Distribution map of the landslides in the EAFZ between Palu and Bingöl with respect to active fault lines.

were created as; 0-50, 50-100, 100-150, 150-200, 200-250, 250-1000 and 1000 m away. According to the buffer analysis performed, the ratios of the landslide areas with related distances to fault lines are given as follows; 0-50 m 3%, 50-100 m 2%, 100-150 m 3%, 200-250 m 3%. According to this, the ratio of the landslide areas 0-250 m away from the fault lines of the Murat valley is 14%. The areas 250-1000 m away from the fault lines are 29%, and the ratio of areas at 1000 m and more distant from the fault lines is 57% (Figures 13 and 14).

When the width of the fault zones in the region is considered, it is seen that the distribution of distances to the fault lines of the overall study area is not significant, because the width of the fault zones varies from 5 to 15 km. However, in order to determine the spatial relation between active faults and landslides, it is important to carry out the buffering analysis of these classes to reveal the fault lines and the distribution of landslides. According to the results of this analysis, 24% of the landslides are observed at distances of 0-250 m, 40% at 250-500 m and 36% at distances more than 1000 m to the fault lines (Figure 15). According to the results of analyzes, it was determined that the frequency of the landslides was high in areas close to fault lines and low as they moved away from the fault lines. According to these results, there is observed a significant relationship between the fault lines and distribution of landslides (Table 4).

A major part of the active landslides between Palu and Bingöl is closely related with frequently occurring earthquakes in the region. The earthquakes occurring in this area trigger landslides and negatively affect the settlement and access roads. Numerous landslides have occurred in the area investigated in the Kovancılar-Okçular (Elazığ) earthquake that occurred in March 8, 2010. It was observed that new landslides with 15 km in width had occurred in an area, which is about 45 km away from the earthquake epicenter and the existing landslides had been triggered and reactivated

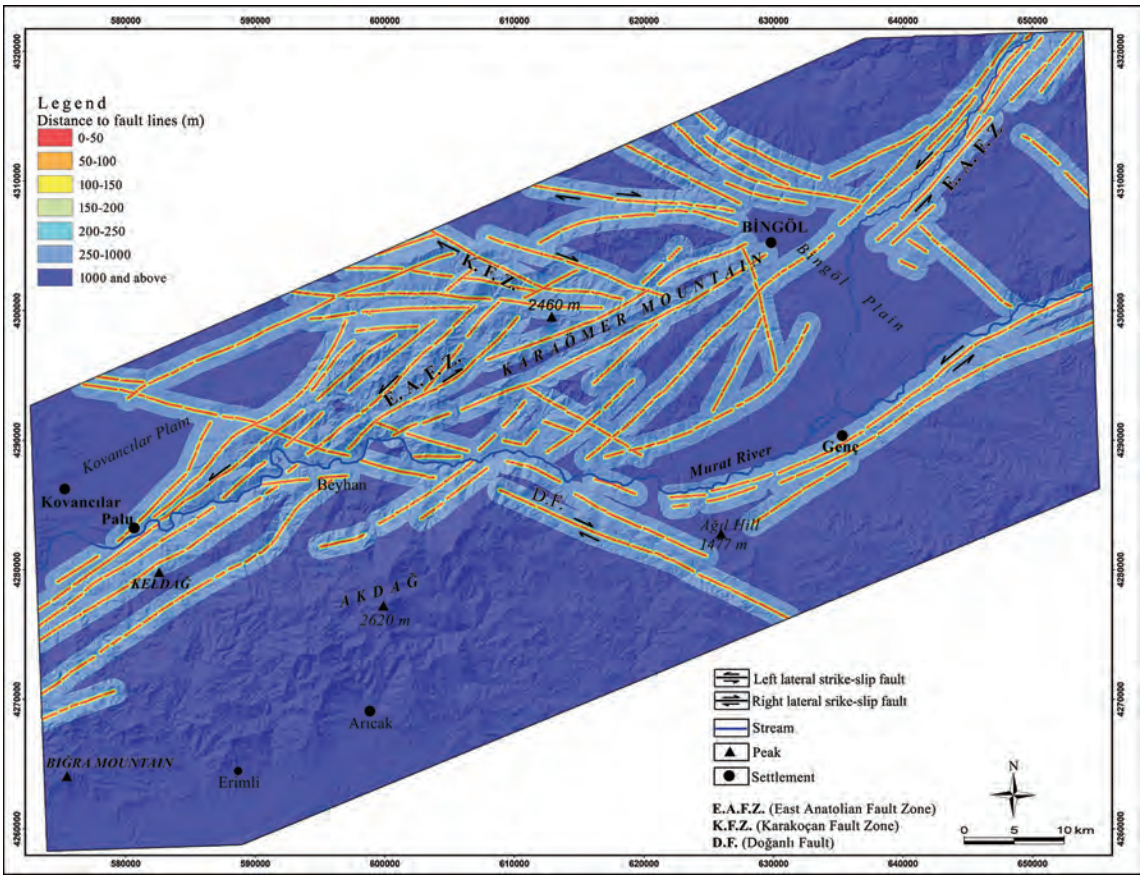

Figure 13- Distance map of the area within the EAFZ between Palu and Bingöl with respect to fault lines.

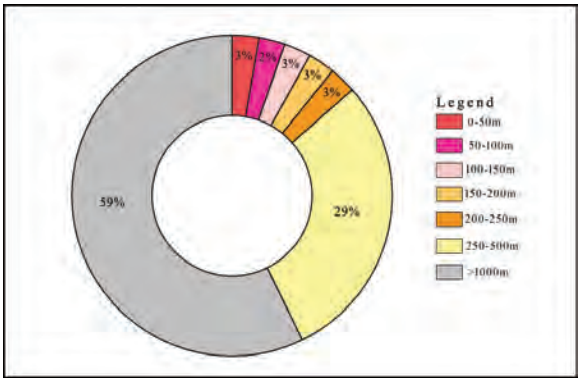

Figure 14- The proportional distribution of the area between Palu and Bingöl with respect to the fault line distance groups.

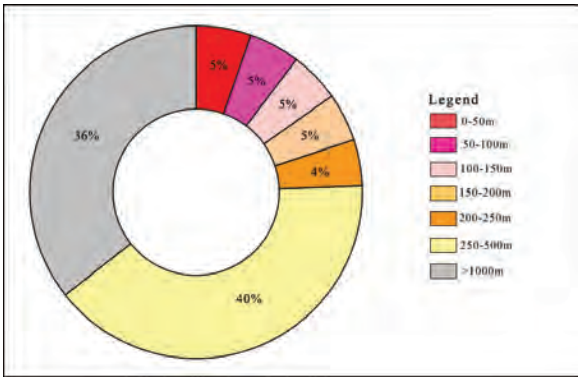

Figure 15- The proportional distribution of the landslides between Palu-Bingöl with respect to fault lines.

Table 4- Frequency Relation with respect to the Distance to the Fault Lines of the Landslides Between Palu and Bingöl.

Distance to Fault Lines (m)	Sub Grup Area (m^2)	Total Area (m^2)	Total Area Percentage (a)	Landslide Area (m^2)	Total Landslide Area (m^2)	Landslide area Percentage (b)	Frequency ratio (b/a)
0-50	89611600	3280521800	2.731626	11484700	214325800	5.361026	1.962577
50-100	87045600	3280521800	2.653407	10610400	214325800	4.952905	1.866621
100-150	90127500	3280521800	2.747353	10470300	214325800	4.887507	1.778988
150-200	90366400	3280521800	2.754635	10066000	214325800	4.69878	1.705772
200-250	89892900	3280521800	2.740201	9669900	214325800	4.513882	1.647281
250-1000	958688800	3280521800	29.22367	85657400	214325800	39.98463	1.368228
1000>	1874789000	3280521800	57.14911	76267200	214325800	35.60131	0.622955

by the earthquake. The newly developed or existing landslides have been responsible in the damage distribution in Okçular and Yukarı Kanatlı villages and İsa Ağa Area, where there had been much casualty and damage in the earthquake. It was also seen that the landslides, which occurred or reactivated during the earthquake had not only been responsible for damage of buildings but also deteriorated structures like road and bridge (Emre et al., 2010; Sunkar, 2011).

5. Results

The area between Palu and Bingöl at the intersection of EAF and KF is tectonically very active and complicated. The EAFZ is observed in a 5-15 km wide zone in the East of Palu and intersects with KFZ in the area where the Karaömer Mountain is located. The Karaömer Mountain was sliced and uplifted by this cut. Due to the fact that the area has been cut by numerous faults and the development of landslides along the fault lines has deformed fault planes. This area, which corresponds to Gökdere uplift is located at the intersection of two fault zones and corresponds to a tectonically very active area.

Considering the factors that control the formation of landslides between Palu and Bingöl, the characteristics such as; lithology, active faults, slope and climate come out. Due to these features, numerous landslides formations in the form of landslide, fall, and flow were observed. The distribution of landslides creates a great asymmetry on northern and southern slopes. It was determined that 93% of the existing landslides occurred in the north and 7% in the southern slopes.

Looking at the landslides occurring between Palu-Bingöl, 59% of them were formed on the Upper Miocene-Pliocene volcanics, 10% in the Middle-Upper Eocene clastic and carbonates, 8% in the ophiolites and 7% in the Upper Miocene basalts. Despite having 15 lithological units in the mapped area, 84% of the landslides were collected on 4 units. These ratios and the frequency analysis results are consistent with each other. It is observed that the elevation and slope factor are effective in the formation of landslides developing in flow and fall types and the effect of these two factors is not apparent in the formation of slide landslides. In addition, the effect of relief is also evident in slide and fall type landslides.

The uplift of the tectonically active field and the downward cutting of the bed of the Murat River caused the formation of different reliefs on the field. The deeper erosion of the rivers have rejuvenated landslides on slopes of Murat and Göynük valleys. The formation of numerous, wide based intertwined landslides were observed with this effect of the rivers and earthquakes. It was observed that the current landslides had been activated by earthquakes, especially at the end of winter and the beginning of spring. In Kovancılar-Okçular Earthquake in March 8, 2010, the damage and loss of lives were higher in settlements built on landslides.

As a result, a close relationship has been observed between the distribution of landslides between Palu and Bingöl and faults. Even all the landslides seen in the south of the Kovancılar Plain remain on the fault line in this area. Very large landslides have developed in the shear zone of the faults, in the Karaömer Mountain and the north of the Bingöl Plain located in the intersection areas of EAF and KF. In this development the intersection of the faults and with this intersection the uplift and lithological features have become effective.

References

Akıncı, H., Doğan, S., Kılıçoğlu, C., Keçeci, S. B. 2010. Samsun İl Merkezinin Heyelan Duyarlılık Haritasının Üretilmesi. Harita Teknolojileri Elektronik Dergisi, 2 (3), 13-27.

Aksoy, E., İnceöz, M., Koçyiğit, A. 2007. Lake Hazar Basin: A Negative Flower Structure on the East Anatolian Fault System (EAFS), SE Turkey, Turkish Journal of Earth Sciences, 16, 319-338.

Altınlı, E. 1963. 1/500.000 Ölçekli Türkiye Jeoloji Haritası Erzurum Paftası İzahnamesi, Maden Tetkik ve Arama Enstitüsü Yayınları, No: 131, Ankara.

Ambraseys, N. N., Jackson, J. A. 1998. Faulting associated with historical and recent earthquakes in the Eastern Mediterranean region. Geophysical Journal International, 133, 390-406.

Arpat, E., Şaroğlu, F. 1972. Doğu Anadolu Fayı ile İlgili Gözlemler ve Düşünceler. Maden Tetkik ve Arama Enstitüsü Dergisi, 78, 44-50.

Arpat, E., Şaroğlu, F. 1975. Türkiye'deki Bazı Önemli Genç Tektonik Olaylar. Türkiye Jeoloji Kurumu Bülteni, 18, 29–41.

Atalay, İ. 1974-1977. Muş-Palu Arasındaki Murat Vadisi Boyunca Oluşan Kütle Hareketleri. İstanbul Üniversitesi Coğrafya Enstitüsü Dergisi, 20-21, 263-279.

Avcı, V. 2016. Gökdere Havzası ve Çevresinin (Bingöl Güneybatısı) Frekans Oranı Metoduna Göre Heyelan Duyarlılık Analizi. Marmara Coğrafya Dergisi, 34, 160-177.

Avcı, V., Sunkar, M. 2016. The Distribution of Landslides Observed in Murat River Valley Between Bingöl and Palu (Elazığ) by Geomorphological Factors, (Ed. Recep EFE, İsa CÜREBAL, Gülnara NYUSSUPOVA, Emin ATASOY) Recent Research in Interdisciplinary Sciences (Chapter 31), Sofia University, St Klement Ohridsky-Publishing House, ISBN 978-954-07-4141-3.

Barka, A. A., Kadinsky-Cade, K. 1988. Strike-slip fault geometry in Turkey and its influence on earthquake activity. Tectonics, 7(3), 663–684.

Bulut, F., Boynukalın, S., Tarhan, F., Ataoğlu, E. 1995. Fındıklı ilçesi (Rize) Doğu Yöresindeki Heyelanların Nedenleri. II. Ulusal Heyelan Sempozyumu Bildiriler Kitabı, Adapazarı, 143-152.

Cihangir, M. E., Görüm, T. 2016. Kelkit Vadisi'nin Aşağı Çığırında Gelişmiş Heyelanların Dağılım Deseni ve Oluşumlarını Kontrol Eden Faktörler, Türk Coğrafya Dergisi, 66, 19-28.

Çetin, H., Güneyli, H., Mayer, L. 2003. Palaeoseismology of the Palu-Lake Hazar segment of the East Anatolian Fault Zone, Turkey. Tectonophysics, 374, 163-197.

Dağ, S. 2007. Çayeli (Rize) ve Çevresinin İstatistiksel Yöntemlerle Heyelan Duyarlılık Analizi. Karadeniz Teknik Üniversitesi Fen Bilimleri Enstitüsü, Trabzon, Doktora Tezi, 241 s (Unpublished).

Dağ, S., Bulut, F., Akgün, A. 2006. İki Değişkenli İstatistiksel Analiz Yöntemi ile Çayeli (Rize) ve Çevresindeki Heyelanların Değerlendirilmesi, 1. Heyelan Sempozyumu, Trabzon, Bildiriler Kitabı, 84.

Duman, T. Y., Olgun, Ş., Çan T., Nefeslioğlu, H. A., Hamzaçebi, S., Elmacı, H., Durmaz, S., Çörekçioğlu, Ş. 2009. Türkiye Heyelan Envanteri Haritası 1/500.000 Ölçekli Erzurum Paftası. Maden Tetkik ve Arama Genel Müdürlüğü Özel Yayın Serisi-16, 26 s. Ankara.

Duman, T. Y., Emre, Ö., Özalp, S., Elmacı, H., Olgun, Ş. 2012. 1/250.000 Ölçekli Türkiye Diri Fay Haritası Serisi, Elazığ (NJ 37-7) Paftası Seri No: 45, Maden Tetkik ve Arama Genel Müdürlüğü, Ankara.

Emre, Ö., Duman, T., Özalp, S., Elmacı, H. 2010. 8 Mart 2010 Başyurt-Karakoçan (Elazığ) Depremi Değerlendirme Raporu. Maden Tetkik Arama Enstitüsü Jeoloji Etütleri Dairesi, Ankara.

Emre, Ö., Duman, T. Y., Olgun, Ş., Özalp, S., Elmacı, H. 2012, 1/250.000 Ölçekli Türkiye Diri Fay Haritası Serisi Muş (NJ 37-8) Paftası. Seri No: 49, Maden Tetkik ve Arama Genel Müdürlüğü, Ankara.

Ercanoğlu, M., Gökçeoğlu, C. 2002. Assessment of Landslide Susceptibility for a Landslide-Prone Area (North of Yenice, NW Turkey) by Fuzzy Approach. Environmental Geology, 41, 720-730.

Erener A., Lacasse S. 2007. Heyelan Duyarlılık Haritalamasında Cbs Kullanımı. Ulusal Coğrafi Bilgi Sistemleri Kongresi Bildiriler Kitabı içinde. Trabzon: Türk Mühendis ve Mimar Odaları Birliği Harita ve Kadastro Mühendisleri Odası

Erinç, S. 2012. Jeomorfoloji I (6. Baskı). (Güncelleştirenler: A. Ertek ve C. Güneysu) Der Yayınları.

Gupta, R. P., Joshi, B. C. 1990. Landslide Hazard Zoning Using the GIS Approach- A Case Study From the Ramganga Catchment, Himalayas. Engineering Geology, 28, 119-131.

Gülen, L., Barka, A., Toksöz, M. N. 1987. Continental collision and related complex deformation; Maraş triple junction and surrounding structures in SE Turkey. Hacettepe University Earth Sciences 14, 319-336.

Hansen, A. 1984. Landslide Hazard Analysis, In. D. Brunsden and D.B. Prior (Ed.), Slope Instability, John Wiley and Sons, New York, p. 523-602.

Hempton, M. R., Dewey, J. F., Şaroğlu, F. 1981. The East Anatolian transform fault: along strike variations in geometry and behavior. Trans Am Geophys Union EOS 62:393.

Herece, E., Akay, E. 1992. Karlıova-Çelikhan arasında Doğu Anadolu fayı (East Anatolian Fault between Karlıova and Çelikhan). Abstracts, 9th Petroleum Congress of Turkey, 361-372.

Herece, E. 2008. Doğu Anadolu Fayı (DAF) Atlası, Maden Tetkik ve Arama Genel Müdürlüğü, Özel Yayın Serisi, No: 13.

Koçyiğit, A. 2003. Karakoçan Fay Zonu: Atımı, Yaşı, Etkin Stres Sistemi ve Depremselliği, ATAG-7 Aktif Tektonik Araştırma Grubu 7. Toplantısı, Sayfa: 9-10 Yüzüncüyıl Üniversitesi Jeoloji Mühendisliği Bölümü, 01-03 Ekim 2003.

Koçyiğit, A., Aksoy, E., İnceöz, M. 2003. Basic Neotectonic Characteristics of the Sivrice Fault Zone in the Sivrice-Palu area, East Anatolian Fault System (EAFS), Turkey. Excursion Guide Book, International Workshop on the North Anatolian, East Anatolian and Dead Sea Fault Systems: Recent Progress in Tectonics and Palaeoseismology, 31 August to 12 September 2003, METU (Ankara, Turkey).

MGM, 2017, Meteoroloji Genel Müdürlüğü, Bingöl Meteoroloji İstasyonu Meteorolojik Verileri.

MTA, 2002. 1/500.000 Ölçekli Türkiye Jeoloji Haritası, Erzurum Paftası.

Naz, H. 1979. Elazığ-Palu Dolayının Jeolojisi. Türkiye Petrolleri Anonim Ortaklığı Rapor No: 1360, (unpublished).

Özdemir, M. A., Tonbul S., 1990. Kovancılar Ovası ve Palu Çevresinin (Elazığ Doğusu) Uygulamalı Jeomorfoloji Bakımından İncelenmesi. Fırat Üniversitesi Sosyal Bilimler Enstitüsü Dergisi, 4(2).

Özdemir, M. A., İnceöz, M. 2003. Doğu Anadolu Fay Zonu'nda (Karlıova-Türkoğlu Arasında) Akarsu Ötelenmelerinin Tektonik Verilerle Karşılaştırılması. Afyon Kocatepe Üniversitesi, Sosyal Bilimler Enstitüsü Dergisi, 5(1), 89-114.

Reilinger, R. E., Mcclusky, S. C., Oral, M. B., King, R.W., Toks, Z, M. N. 1997. Global Positioning System measurements of present-day crustal movements in the Arabia-Africa-Eurasian plate collision zone. Journal of Geophysical Research 102, 9983-9999.

Sarp, G. 2014. Evolution of neotectonic activity of East Anatolian Fault System (EAFS) in Bingöl pull-apart basin, based on fractal dimension and morphometric indices. Journal of Asian Earth Sciences, 88, 168–177.

Sirel, E., Metin, S., Sözeri, B. 1975. Palu (KD Elazığ) Denizel Oligosen'in Stratigrafisi ve Mikro Palaeontolojisi. Türkiye Jeoloji Kurumu Bülteni, 18 (2), 175-180.

Sungurlu, O., Perinçek, D., Kurt, G., Tuna, E., Dülger, S., Çelikdemir, E., Naz, H. 1985. Elazığ-Hazar-Palu alanının jeolojisi (Geology of Elazığ-Hazar-Palu area). Petrol İşleri Genel Müdürlüğü Dergisi 29, 83-191.

Sunkar, M. 2011. 8 Mart 2010 Kovancılar-Okçular (Elazığ) Depremi; Yapı Malzemesi ve Yapı Tarzının Can ve Mal Kayıpları Üzerindeki Etkisi, Türk Coğrafya Dergisi, 56, 23-37.

Şaroğlu, F., Emre, Ö., Boray, A. 1987. Türkiye'nin Diri Fayları ve Depremsellikleri. Maden Tetkik Arama Enstitüsü Genel Müdürlüğü, Rapor No: 8174.

Şaroğlu, F., Emre, Ö., Kuşçu, Ü. 1992. The East Anatolian Fault Zone of Turkey. Annales Tectonicae 6, 99-125.

Tatar, Y. 1987. Elazığ Bölgesinin genel tektonik yapıları ve Landsat fotoğrafları üzerine yapılan bazı gözlemler. Hacettepe Üniversitesi Yerbilimleri, Dergisi, 14, 295-308.

Tonbul, S. 1990. Bingöl Ovası ve Çevresinin Jeomorfolojisi ve Gelişimi. Atatürk Dil ve Tarih Yüksek Kurulu Coğrafya Araştırmaları Dergisi 1(2), 229–359.

Tonbul, S., Özdemir, M. A. 1994. Doğu Anadolu Fayı'nın Palu Civarında (Elazığ Doğusu) Jeomorfolojik Birimlere Yansıması Üzerine Gözlemler. Ankara Üniversitesi Türkiye Coğrafyası Araştırma ve Uygulama Merkezi Dergisi, 3, 275-290.

Yılmaz, I. 2009. Landslide susceptibility mapping using frequency ratio, logistic regression, artificial neural networks and their comparison: A case study from Kat landslides (Tokat-Turkey). Computers and Geosciences, 35, 1125-1138.

Yüksel, S. 2006. Okçular (Kovancılar/Elazığ) Alanının Stratigrafisi. Adana: Çukurova Üniversitesi Fen Bilimleri Enstitüsü Jeoloji Mühendisli Anabilim Dalı, Yüksek Lisans Tezi (Unpublished).

http://www.hurriyet.com.tr/heyelan-nedeniyle-yuk-treni-raydan-cikti-40400338 19 Mart 2017).

Bull. Min. Res. Exp. (2018) 157: 39-57

Bulletin of the Mineral Research and Exploration

http://bulletin.mta.gov.tr

Post-Glacial Terraces of The Marmara Sea and Water Exchange Periods

Vedat EDİGER[a*], Emin DEMİRBAĞ[b], Semih ERGİNTAV[c], Sedat İNAN[d] and Ruhi SAATÇILAR[e]

[a]*The Scientific and Technological Research Council of Turkey, Marmara Research Center, Earth and Marine Sciences Institute, Gebze-Kocaeli, Turkey. orcid.org/0000-0003-4388-7951*

[b]*Istanbul Technical University, Department of Geophysics, Maslak-Istanbul, Turkey. orcid.org/0000-0001-8448-8741*

[c]*Boğazici University Kandilli Observatory Earthquake Research Institute Department of Geodesy Çengelköy-Istanbul/Turkey. orcid.org/0000-0001-5094-6599*

[d]*Saudi Aramco, EXPEC Advanced Research Center, Dhahran 31311, Saudi Arabia. orcid.org/0000-0001-5639-6831*

[e]*Department of Geophysical Engineering, Faculty of Engineering, Sakarya University, Sakarya 54187, Turkey. orcid.org/0000-0001-6739-1702*

Research Article

Keywords:
Marmara Sea, morphology, marine terraces, sea-level changes, paleo-lagoon.

ABSTRACT

Semi enclosed Marmara Sea is a passage between the Aegean Sea (Northeastern Mediterranean Sea) and the Black Sea. The Marmara Sea is connected to the Black Sea and Aegean Sea through the İstanbul Strait (Bosphorus) and Çanakkale Strait (Dardanelles), respectively. Despite the fact that the late Pleistocene-Holocene connections between the seas have been explored by many scientists, there are still uncertainties about the nature and timing of the connections. Within the scope of this study, a new approach has been displayed for post-glacial connections between the Black Sea, Marmara Sea and Aegean Sea. This study is based on 80 shallow seismic reflection lines, multibeam bathymetric data and 15 short gravity cores collected from the northeastern shelf of the Marmara Sea (between Silivri and Golden Horn). The sea bottom and sub-bottom morphology have a highly chaotic structure at the exit of the Büyükçekmece/Küçükçekmece lagoons and further east near the Marmara- İstanbul Strait junction. This chaotic bottom and sub-bottom surface morphologies are mainly controlled by the structure of the basin, current regime of the shelf, coastal drainage systems and by the sea/lake water level changes controlled by climate and the sill depths of the two straits, which in turn determined the water exchange between the seas. The sedimentological interpretation of the seismic reflection profiles and core sediments have allowed us to distinguish five stratigraphic units (S1-S5) and four sedimentary layers (A-D) over the acoustic basement. The lower stratigraphic unit and sedimentary layer are separated from the overlying acoustic basement by a chaotic to parallel and by a high amplitude seismic reflector. Seaward dipping units of the acoustic basement are inferred to be the seaward continuation of the Oligocene–Upper Miocene units widely exposed on land. The presence of three different marine terraces distinguished (T1-T3) along the northeastern shelf of the Marmara Sea have been associated with the six different curves of the post-glacial sea-level changes. From statistical point of view, the most significant terraces occur from -78 m to -80 m (T1), -58 m to -62 m (T2) and -28 m to -32 m at (T3). Considering the global sea level curves, these terraces can be dated 9.25, 12.25 and 13.75 Cal kyr BP, respectively.

Received Date: 09.10.2017
Accepted Date: 27.02.2018

1. Introduction

The Marmara Sea is an inland sea with a surface area of approximately 11,350 km^2 which is connected to the Black Sea and the Mediterranean Sea through the İstanbul Strait and Çanakkale Strait respectively (Figure 1). The Istanbul Strait is about 30 km long and its width varies between 0.7 and 3.7 km with water depth varies from 36 to 124 m. Çanakkale Strait is about 61 km long and 1-6 km wide with mean water depth of 55 m (Beşiktepe et al., 1994; Polat and Tuğrul, 1996).

* *Corresponding author: Vedat EDİGER, vedat.ediger@tubitak.gov.tr*
http://dx.doi.org/ 10.19111/bulletinofmre.401208

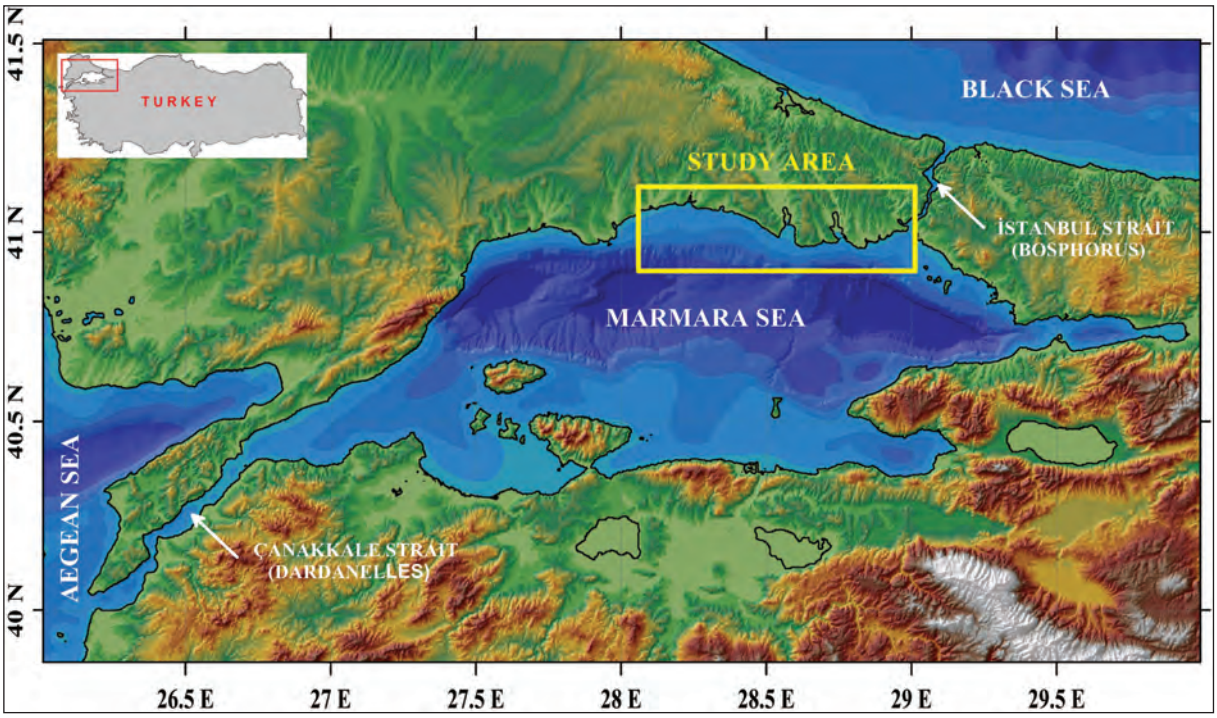

Figure 1- Sea bottom morphology (General Bathymetric Chart of the Oceans; GEBCO), topography of landmass (Shuttle Radar Topography Mission; SRTM) and location of the study area. Coastline data are taken from the Istanbul Metropolitan Municipality.

The Marmara Sea and the strait system regulate the oceanographic conditions and sea-level differences between the Black Sea and the Mediterranean Sea. At present, the Black Sea level is high (~30 cm above the Marmara Sea) due to high discharge of major European and Asian rivers, resulting in outflow through the Istanbul Strait (net outflow is ~300 km^3/yr) (Ünlüata et al., 1990; Oğuz et al., 1990; Beşiktepe et al., 1994). The present water exchange across the Çanakkale and İstanbul Straits occurs as a two-layer flow. A cooler and lower salinity (‰ 17-20) Black Sea water exits southward at the surface while warmer and higher salinity (‰ 38-39) Mediterranean Sea water flows northward at depth through the straits (Polat and Tuğrul, 1996; Özsoy et al., 2001). The water column of the Marmara Sea is characterized by two distinct layers with different temperature and salinity levels: the upper layer (salinity <25psu) and the deeper layer (salinity=38.7psu), separated by a steep halocline located between 20 – 25 m (Beşiktepe et al., 1994). Major rivers flow into the Marmara Sea only from the south and discharge ~$2.2x10^6$ tons/yr of suspended sediment (EIE, 1993). The Marmara Sea has strong surface and relatively strong bottom currents (Beşiktepe et al., 1994) and a small tidal range (8-10 cm, DAMOC, 1971; Alpar and Yüce, 1998).

The reconnections among the Black, Marmara and Mediterranean Seas after the Last Glaciation have been discussed in recent literature. Various scenarios have been proposed for the modes and periods of the connections e.g., Ryan et al. (1997); Gökaşan et al. (1997); Görür et al. (2001); Aksu et al. (2002*a*, *b* and *c*); Kaminski et al. (2002); Myers et al. (2003); Polonia et al. (2004); Major et al. (2006); Hiscott et al. (2002, 2007 and 2008); Meriç and Algan (2007); Eriş et al. (2007 and 2008); Martin et al. (2007); McHugh et al. (2007); Çağatay et al. (2000, 2003,2009, 2015). Myers et al. (2003) examined the catastrophic flood hypothesis through the İstanbul Strait proposed by Ryan et al. (2003) by means of a series of simple hydraulic calculations to investigate some of the questions associated with the Holocene reconnection of the Black Sea with the Mediterranean Sea through the Turkish Straits System. The same hydraulic model was also used to elucidate the more traditional connection hypothesis of continuous freshwater outflow from the Black Sea, and slowly increasing saline water inflow from the Mediterranean Sea beginning around 8-9 Cal kyr BP (Myers et al., 2003). According to an alternative outflow hypothesis, the Black Sea level was at -40 m (i.e., the bedrock sill depth in the Istanbul Strait), Black Sea waters were cascading down slope into the rising Marmara Sea from 10 to 9 Cal kyr BP and finally constructing the

outflow delta at the southern exit of the strait (Hiscott et al., 2002; Aksu et al., 2002*b*). However, the same delta was claimed to have been formed by sediments transported by the Kurbağalıdere River during the middle Holocene (Eriş et al., 2007).

The main objective of this study is to investigate the Late Quaternary sub-marine terraces on the northern shelf of the Marmara Sea between Silivri and Golden Horn and its implications for sea-level change (Figure 1). We also would like to identify the effects of the sea-level rise on the sediment supply and paleo-oceanographic conditions of the region using sedimentological, geochemical, seismic reflection and bathymetric data.

Four different chronostratigraphic sedimentary layers and five different seismic units have been distinguished over the acoustic basement in the Northern Shelf of the Marmara Sea. Three distinct terraces are clearly identified in the interpreted seismic reflection profiles. The latest connection between the Mediterranean and Marmara Seas was established as the sea-level reached the sill depth of the Çanakkale Strait. At the end of this wet period, Mediterranean saline water invaded the Marmara Sea bottom and gradually established anoxic conditions (Çağatay et al., 1999 and 2000). Further rise of the sea-level during the next warm period reached the depth of the Istanbul Strait and the latest connection between the Marmara, Black and Aegean Seas was established.

2. Materials and Methods

In this study, geophysical (shallow seismic and bathymetric) and sedimentological (gravity cores) data collected from the northeastern shelf of the Marmara Sea were used. Total of 94 seismic reflection profiles with 1100 km length were acquired during the cruise of the R/V Koca Piri Reis in October 2007 and fifteen gravity cores were collected during the cruise of the R/V Arar in March 2008 (Figure 2).

Continuous seismic reflection surveying was carried out by using a standard side mounted (SeaBed 3010 Mp; frequency: 3-7 kHz) and a deep-towed chirp (GeoChirp II Sub-bottom Profiler; frequency: 1 kHz-12 kHz) sub-bottom profilers. The seismic reflection data along 80 lines (Figure 2) are used to map the sub-bottom features such as total sediment thickness and paleo-topography of the acoustic basement. In interpretation of the reflection patterns in the seismic reflection data, methods defined by Mitchum et al. (1977); Vail et al. (1977); Brown and Fisher (1980); Sangree and Widmier (1977); Badley (1985) and Boggs (1987) were followed. Depth conversions were made using a sound velocity of 1500 m/s for the sea water depth and 1600 m/s for the Late Quaternary sediment thickness (Ediger et al., 1993; Okyar et al., 1994). A Differential Global Positioning System (DGPS) was used for navigation during the cruises.

Total of 12.579 surface depth values (in meter) of the acoustic basement with 5 m interval from a total of

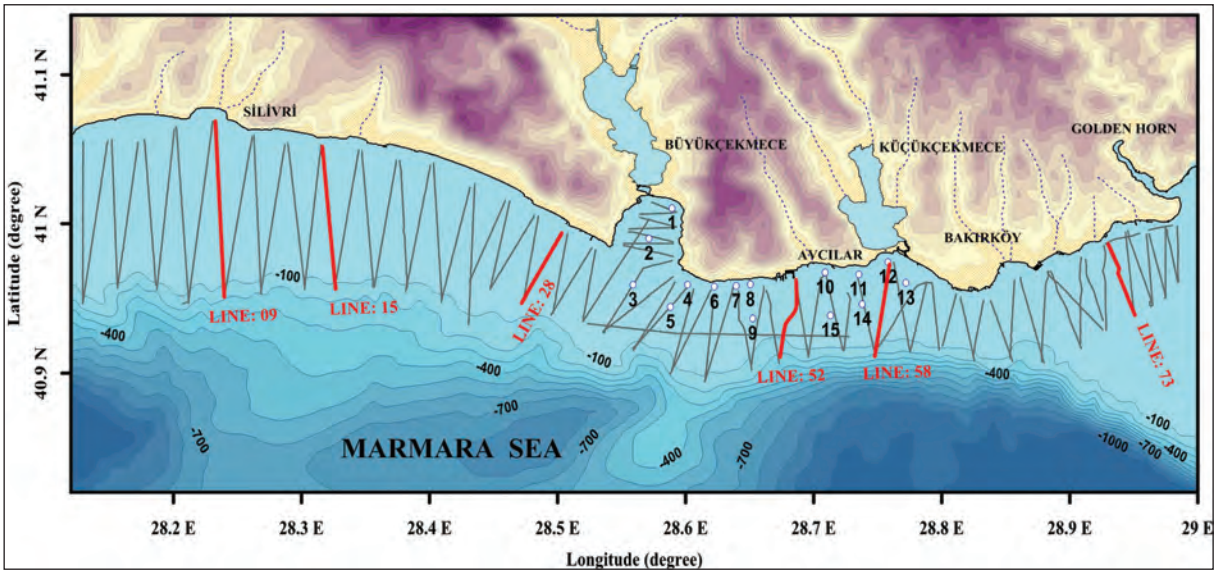

Figure 2- General bathymetry (100 m intervals) (General Bathymetric Chart of the Oceans; GEBCO), coastal topography (20 m intervals) (Shuttle Radar Topography Mission; SRTM), coastal drainage system, shallow seismic lines and sediment core locations are shown along the northeastern Marmara shelf. Bold red lines indicate seismic sections and bold white dots indicates sediment core locations.

40 interpreted shallow seismic reflection profiles are sampled to find the prominent topographic features and determine the most significant terraces in the northeastern shelf of the Marmara Sea. The clarity and the coverage area (depth intervals) of the terraces along the seismic reflection profiles have been considered in determining the number of depth measurements on each of the terraces.

A total of 15 sediment cores were obtained using a standard gravity corer along the inner Marmara shelf area between the Büyükçekmece and Küçükçekmece bays where the maximum water depth is 76 m (Figure 2). The cores were opened in the laboratory for visual observation of lithology and sedimentary structure. For this study, 12 sub-samples were selected based on colour, grain size, shell contents and layers (A1, A2 and A3) within the top layers of the cores (Figure 3). Each sample was dried and powdered for geochemical analysis. Approximately 80 mg of the samples were weighed for TOC analysis using a Rock-Eval 6 Pyrolysis device at the TÜBİTAK Marmara Research Center, Environmental and Petroleum Geochemistry Lab (Figure 3).

A chronology was established based on ^{14}C analysis from five molluscs and one *Lithothamnium* samples (Figure 3; Unit B). Radiocarbon analysis was carried

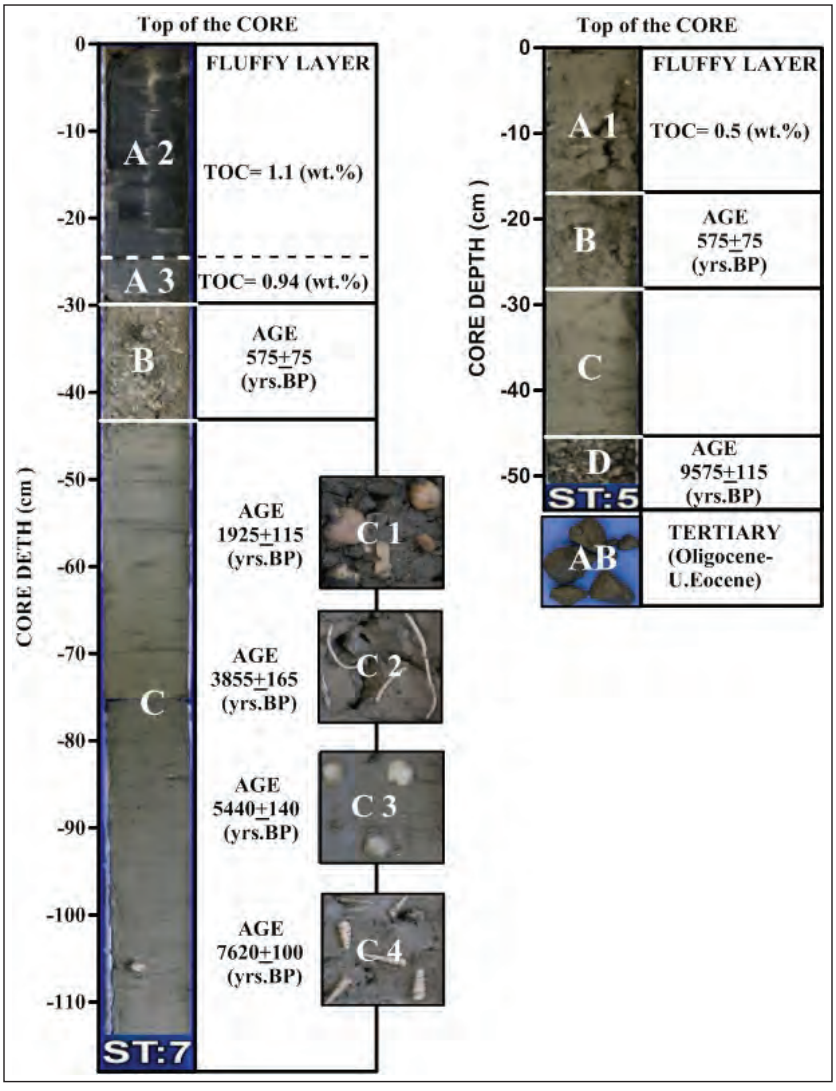

Figure 3- The generalized columnar section showing the units and subunits distinguished by the examination of 15 gravity cores (St. 1-15). A (subunits: A1-A3), B, C (subunits: C1-C4) and D are the main Late Quaternary sediment units and AB is the rocky acoustic basement. TOC values of the A1-A3 and age of the B, C (subunits: C1-C4) and D units are given at figure.

out at the NOSAMS Facility at Woods Hole, MA. The age variability of the sediments is reported as both calibrated (Keven, 2002) years BP and radiocarbon years BP (Figure 3). Finally, the ages were converted to calendar years. CALIB makes the conversion from radiocarbon age to calibrated calendar years by calculating the probability distribution of the sample's true age. (Stuiver and Reimer, 1993).

Four (bivalve, gastropod and *Lithothamnium*) samples were cleaned powdered and analysed for oxygen isotope values ($\delta^{18}O$). Oxygen isotope analysis was conducted using EA-GC/IRMS (Micromass UK) at the TÜBİTAK Marmara Research Center, Environmental and Petroleum Geochemistry Lab. IAEA standards were used to calibrate the instrument. Pore waters were extracted from the same depths as the samples (bivalve, gastropod and *Lithothamnium*) collected for the radiocarbon dating analyses. Pore-water salinity measured by salinometer (WTW, ph/ Cond 340i).

3. Results and Interpretations

3.1. Sea Bottom Topography and Depth Analysis

The studied shelf area becomes narrower and deeper from west to east direction (Figure 4). Most significant four depth intervals of the sea bottom topography (between -10m and -12m, -24 m and -26m, -54 and -58m and -76 and -80 m) along the shelf were distinguished as a result of data interpretation by using the depth distribution bar-graphs shown in figure (4). It can be clearly seen that the most predominant depth range along the shelf is between -54m and -58m. Morphological characteristics varies considerably from west to east, which are likely to be due to the structural characteristics, distance to the NAF, coastal morphology, bottom current system and coastal sedimentary processes.

3.2. Seismic Stratigraphy and Sediment Thickness

According to the basic seismic stratigraphic principles, three distinct main boundary reflector surfaces (R1-R3) and two unconformity surfaces (U1

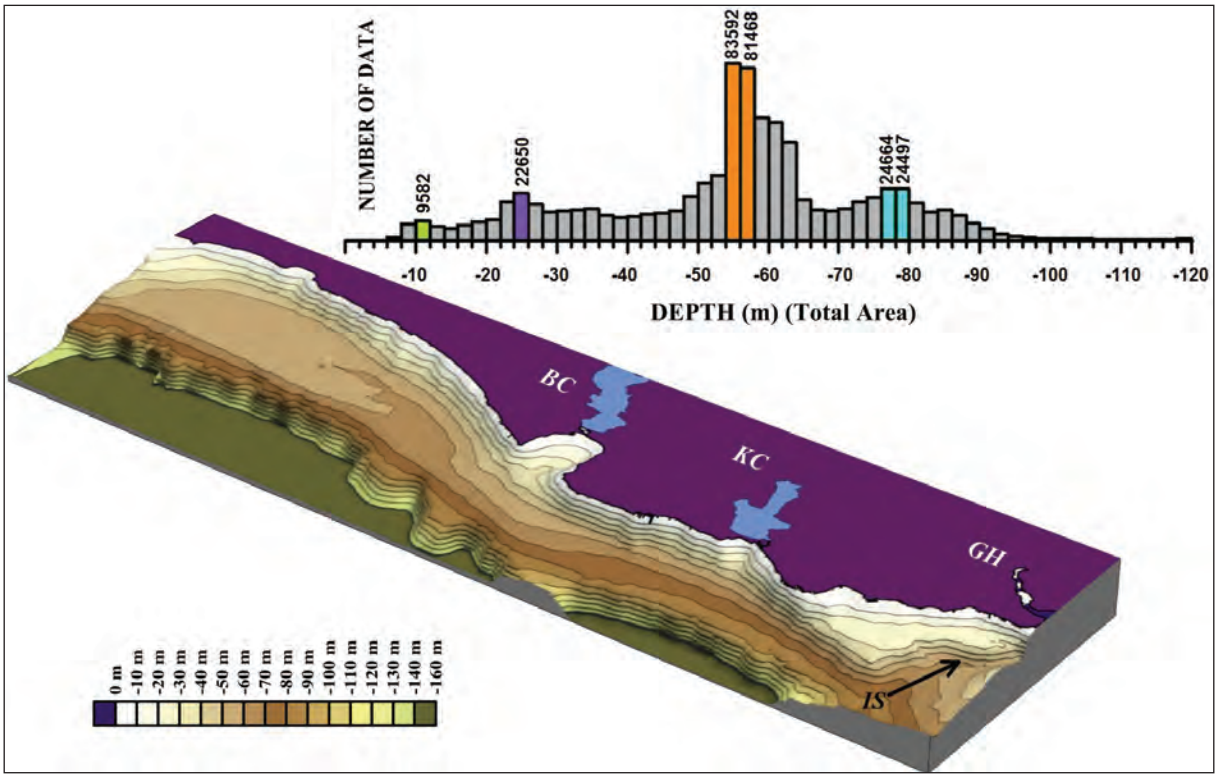

Figure 4- Total depth prevalence analyses with bar graph of the water depth Frequency distribution based on approximately 178,000 depth measurements. The horizontal axis is the measured depths from the echosounder; the vertical axis is the number of depth measurement for a given bin (bin size is 2 m.). From statistical point of view, the most significant depth intervals occur between -10 m and -12 m, -24 m and -26 m, -54 and -58 m and -76 and -80 m. BC: Büyükçekmece, KC: Küçükçekmece, GH: Golden Horn and IS: İstanbul Strait (Bosphorus).

and U2) were identified within the five sedimentary seismic units (S1-S5) overlying the acoustic basement (AB) (Figures 2 and 5).

The beds of the acoustic basement underlying the sedimentary units (S1-S5) dip towards southeast and have strong and irregular surfaces reflection configuration (Figure 5). The top of the sedimentary acoustic basement (Figures 5 and 6) is an erosional unconformity (U1) formed during the Last Glacial Maximum (LGM) period. The oldest seismic unit (S5; Layer-D) fills the paleo-depression and channel over the unconformity surface U1 (Figures 3, 5 and 6). Unit S5 is generally represented by a strong chaotic reflection, having internal reflection characteristics indicative of relatively coarse-grained sediments over the top of the AB in depression. Gravelly and well-rounded sediments (Unit-S5) might have been concentrated under the winnowing and washing processes of the high energy (regressive) conditions during the Last Glacial regressive period. Another prominent unconformity surface U2 occurs at the top of the Unit S5. This unconformity is partially erosional and was formed during the post-glacial wet period. It is overlain by the onlapping transgressive unit S4 and S3 with the well-developed bioherms at the bottom of Unit S4 and top of Unit S5 (Hiscott et al., 2007, Çağatay et al., 2009 and Eriş et al., 2011) (Figure 6).

Mud dominated and weakly stratified S4, S3, S2, and S1 units above the unconformity surfaces (U1 and U2) consist of weak-reflection and acoustically transparent internal structure. Moreover, these units are separated by conformable R3, R2 and R1 reflectors from each other, respectively (Figure 5). Units S3, S2 and S1 are significantly thicker at the eastern depression of the shelf and on the margins. These units thin considerably as close to the shore and on the south side of the shelf.

Sedimentary deposits overlying the regional unconformity surface (U1) are identified as Holocene sediment having calibrated ages younger than 9575 ± 115 Cal yr BP for which the total thickness along the shallow seismic reflection lines was calculated and

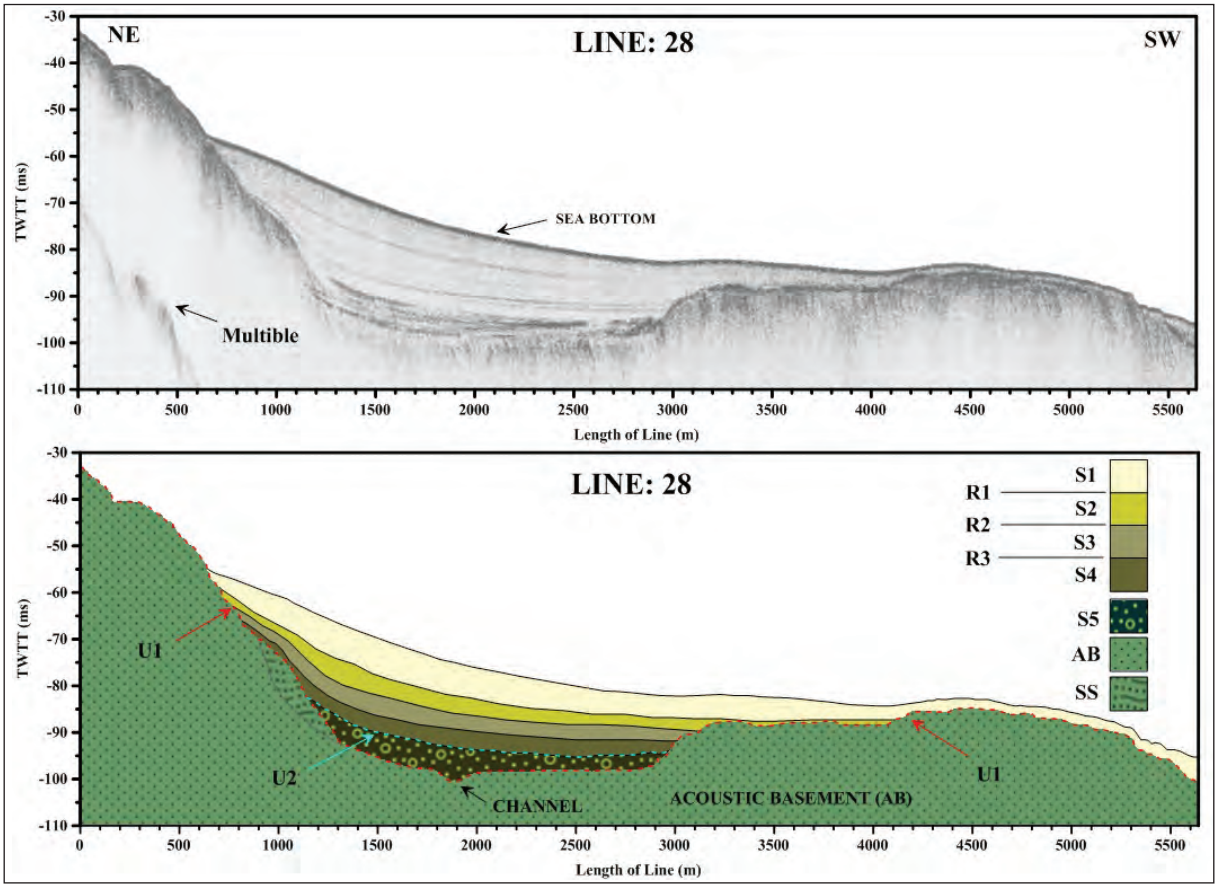

Figure 5- High resolution seismic section from Line-28 (top). Seismic stratigraphy and interpretation of the Line-28 (bottom). Location of the line is given in Fig. 2. S1, S2, S3, S4 and S5 are the main sedimentary units; SS is a kind of slumping/sliding deposit; AB is Acoustic Basement; R1, R2 and R3 are the main transgressive and U1 and U2 are erosional surfaces.

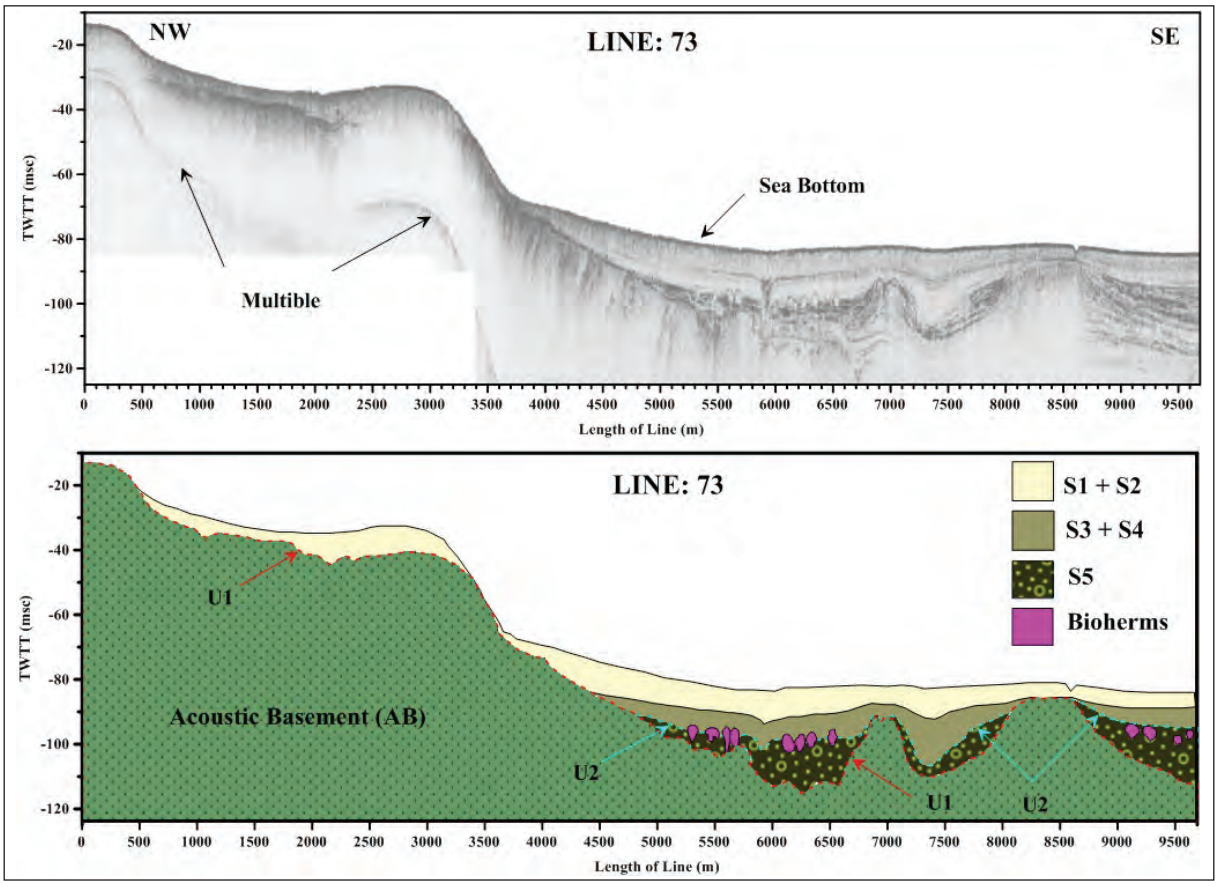

Figure 6- High resolution seismic section from Line-73 (top) and the interpreted section (bottom). Location of the line is given in figure 2. S1, S2, S3, S4 and S5 are the main sedimentary units.

mapped (Figures 3 and 5). Figure 7 shows the thickness map of Holocene sediments over the acoustic basement. Thickness variations in sediment cover are strongly controlled by the sediment sources, sedimentary processes and topography of the underlying erosional surface. Areas of thick sediment deposition generally occur over localized bedrock troughs, near the coastal zone, at the edge of the shelf and at the Istanbul Strait-Marmara Sea junction (Figure 7). Notable examples of 10 to 15 m thick sedimentary deposition occur filling depressions in the eastern and central part of the area. The thickest deposits (15-30 m) are located at the inner part of the Büyükçekmece Bay and western depressed mid-shelf area (Figure 7). Sediment cover is thin in most of the central part where this part is not completely devoid of sediment (Figure 7). High resolution seismic reflection profiles indicate that the Holocene sediments with less than 5 m thickness are common throughout the study area. There are some localities where the sediment cover drops down to less than 2 m thick due to probable sediment removal by bottom currents (Figure 7).

3.3. Acoustic Basement Topography and Terraces

From the shallow seismic reflection lines (80 lines) collected from the study area, only those standing perpendicular to the shore and those parallel to one another (40) lines) were selected for the morphological analysis of the acoustic basement. The sub-bottom morphology of the shelf, most probably controlled by the North Anatolian Fault (NAF) and its side and secondary effects in the south of the study area, is narrowing and deepening from west to east direction (Figure 8).

The frequency distribution of the measured depths was plotted by using 2 m wide depth bins (Figure 8). The depth frequency histogram optimally separates five modes indicating presence of 3 distinct terraces along the shelf. From figure (8), it is clear that the most significant depths occur between “-78 and -80 m” (-79 ± 1 m; blue area), “-58 and -62 m” (-60 ± 2 m; red area) and “-28 and -32 m” (-30 ± 2 m; green area) intervals of the acoustic basement. The T2 terrace

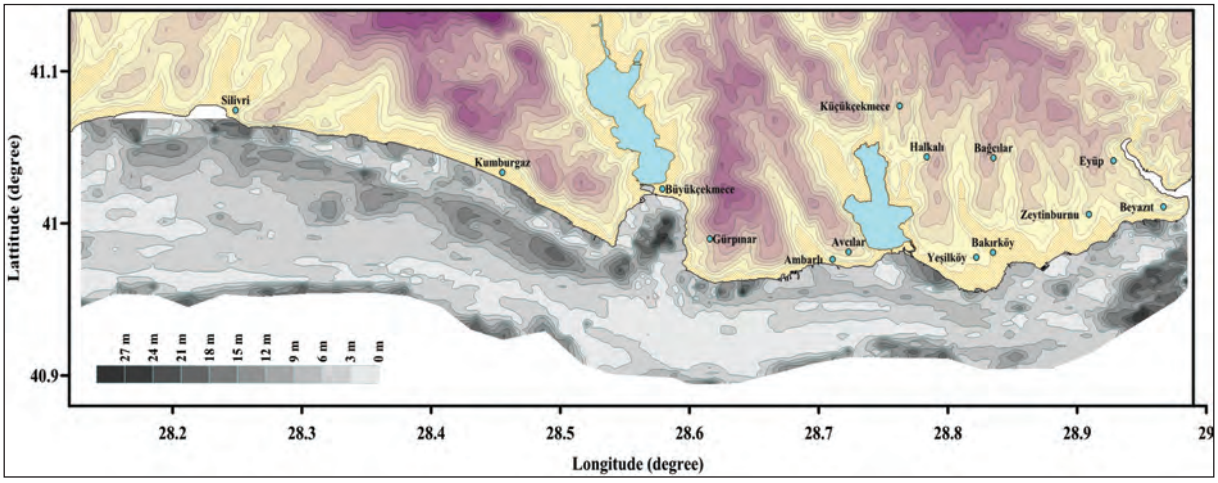

Figure 7- Coastal topography and total Late Quaternary sediment thickness of the northeastern Marmara shelf.

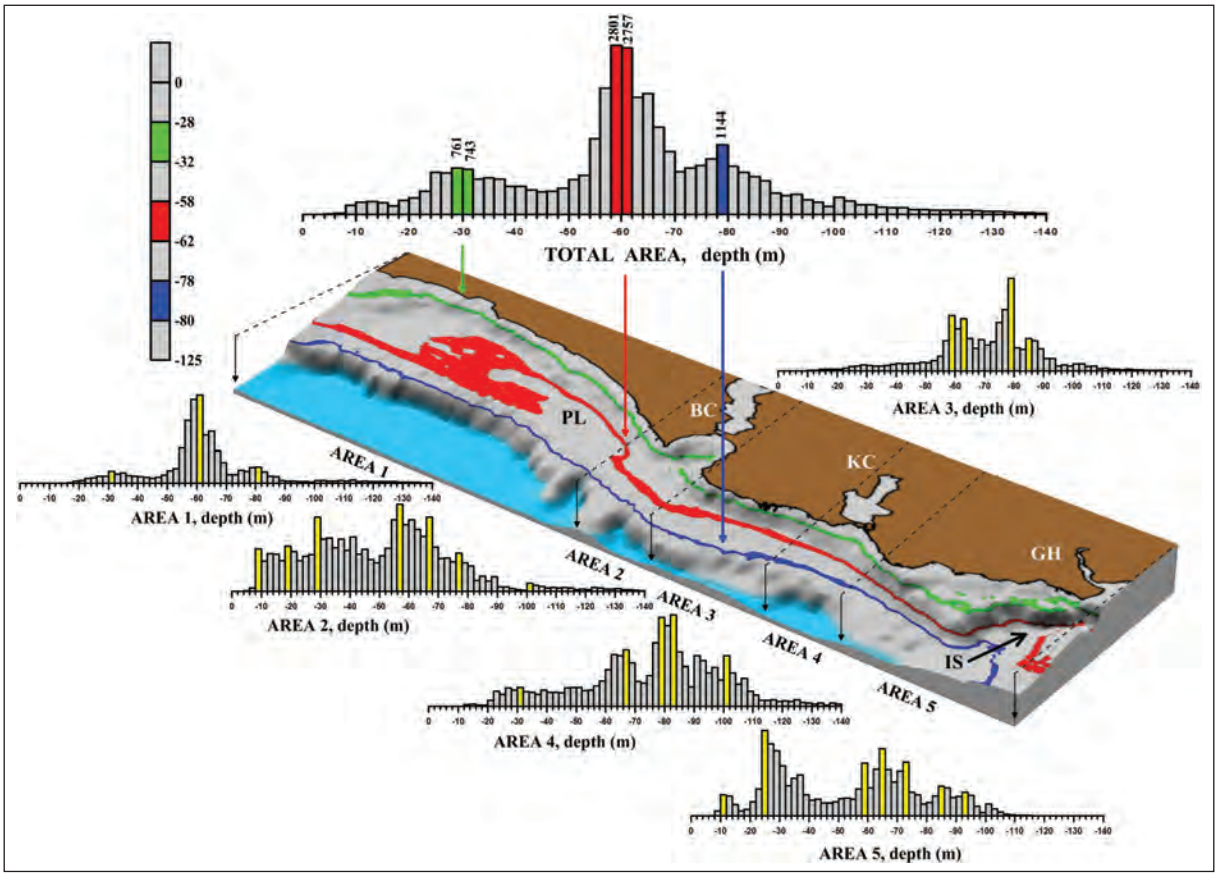

Figure 8- Total depth prevalence analyses with bar graph of the acoustic basement Frequency distribution of the terrace depths based on approximately 12579 samples. The horizontal axis is the measured depths from the reconstructed seismic sections; the vertical axis is the number of depth measurement for a given bin (bin size is 2 m.). From statistical point of view, the most significant terraces occur at T1 (-78 m to -80 m), T2 (-58 m to -62 m) and T3 (-28 m to -32 m). Depth prevalence analyses of the five different parts of the acoustic basement (Areas 1-5) with bar graphs are also given in this figure. BC: Büyükçekmece, KC: Küçükçekmece, GH: Golden Horn, IS: İstanbul Strait (Bosphorus) and PL: Paleo-Lagoon.

located between -58 and -62 m water depths covers the widest and most significant area along the eastern and central mid-shelf (Figure 8). These terraces are also clearly identified on the seismic reflection profiles (and histogram) and labelled T1 (blue), T2 (red) and T3 (green) respectively (Figures 8 and 9).

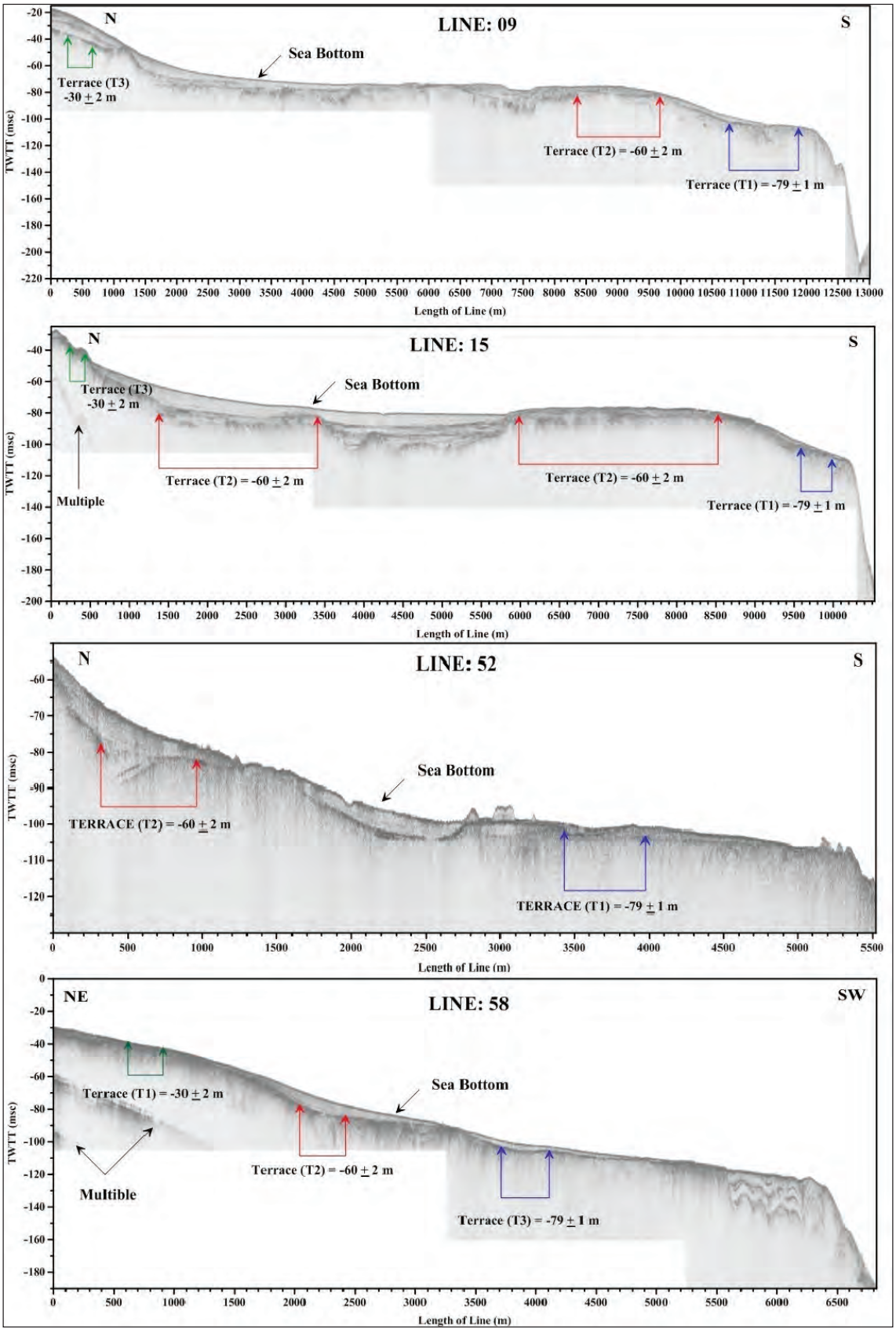

Figure 9- High resolution seismic sections (Lines 15, 52 and 58) and terraces locations. Location of the lines are given in figure 2.

In order to investigate the morphological properties of the sub-bottom in detail, the study area is divided into five different sectors (A1-A5) and bar-graphs of depth values corresponding to these sectors are prepared and separately processed (Figure 8). Morphological characteristics of each shelf sector are considerably different from each other, considering their structural characteristics, distance to NAF, coastal morphology, current system and features of coastal sedimentary processes. The presence of terraces and their depths were identified at -85 m (Çağatay et al 2009, 2003; Polonia et al., 2004; Eriş et al., 2007, 2008; McHugh et al., 2008), -80 m (Kuprin et al., 1974; Shimkus et al., 1980; Dimitrov, 1982; Ballard et al., 2000) and-65 m (Çağatay et al., 2009, 2003; Newman, 2003; Polonia et al., 2004; Eriş et al., 2007, 2008; McHugh et al., 2008) in previous studies. The main reason for these differences may be due to that fact that the seismic reflection data analysed belong to different areas of the Sea of Marmara which could have been affected by different uplift-subsidence rates.

3.4. Lithostratigraphy, Chronostratigraphy and Geochemistry

Four different chronostratigraphic sedimentary layers (A, B, C and D) are distinguished over the acoustic basement (AB) in the cores (Figure 3). Layer-A represents the youngest top sedimentary layer (younger than 575 ± 75 Cal yr BP) and has characteristics of marine deposits (Figure 3). This layer consists of three different sub-layers (A1, A2, and A3) based on the color variations and TOC contents (Figure 3). Dark olive green and brownish homogeneous mud layers (A1) have a maximum of 12 cm thickness at the top of the cores (St-5, St-9, St-11, St-13, St-14 and St-15; Figure 2) and has the lowest TOC content (0.5 wt %; Figure 3). These sediments could be provided by slide and slump of coastal cliffs which are observed along the coastal areas of the studied shelf (Ergintav et al., 2011). In some places, at the bottom of this sub-layer, dark gray to black colored sediments (A2) are present as seen in cores St-1, St-2, St-7, St-8, St-10 and St-12 (Figure 2). These sediments have homogeneous to finely-laminated internal structure (maximum 15 cm thick) and higher TOC contents (1.1 wt %; Figure 3). Sub-layer A3 consists of gray, finely laminated muddy sediments (A3) which are sampled from cores St-7, St-8, St-10 and St-12 and has relatively lower TOC value (0.94 wt %; Figure3) than that of the upper sub-layer (A2).

Layer-B has irregular top and bottom boundaries. It is observed in the cores St-6, St-7 and St-8. Layer B has a high amount of partially eroded *Lithothamnium* grains, carbonate coated terrigenic and biogenic grains and carbonate nodules in dark green muddy matrix. Layer B is dated as 575 ± 75 Cal yr BP (Figure 3). These kinds of sediment mixtures are approximately 22 cm thick in the cores. *Lithothamnium* is reported to dwell in shallow-water areas with sandy and rocky bottoms (Milliman et al., 1972; Campbell, 1982; Alavi et al., 1989). Although both warm and cold marine conditions may provide appropriate environmental conditions for growth of coralline algae, Ergin et al. (1991) noted that most of these organisms live in warm and saline waters in tropical and sub-tropical zones.

Layer-C is made up of as much as 130 cm thick silt dominated and well stratified olive gray sediments which have some micro-sized silt lenses with mica flakes. Layer C is separated into four different sub-layers. Sub-layers C1 through C4 are dated as 1925 ± 115, 3855 ± 165, 5440 ± 140 and 7620 ± 100 Cal yr BP, respectively (Figure 3). Pelecypods (C1 and C3), gastropods (C4) and worm tubes (C2) are observed in the silty muddy matrix at different locations of these sub-layers (Figure 3).

The location of core St-5 on seismic reflection Line-44 is shown in figure 2. This core location is selected for sampling the oldest Holocene sediments (Layer-D) which are deposited over the acoustic basement (AB; Oligocene-U. Eocene) of the northern Marmara shelf. Layer-D, which is dated as 9575 ± 115 Cal yr BP, is deposited over the erosional surface (U1) of the acoustic basement (AB) and composed of washed rounded gravel-sized terrigenic and biogenic grains without matrix in cores St-3 and St-5 (Figures 2 and 3). The presence of the same kinds of sediments and interpretation of their depositional patterns in İzmit Bay (eastern Marmara Sea) were previously discussed by Polonia et al. (2004).

During the deposition of the sediments along the northeastern shelf of the Marmara Sea, sedimentation rates ranged from 0.02 m/kyr to 0.34 m/kyr. The high sedimentation rates are representative of the areas where the water from the coastal rivers (with highly suspended sediments during the flood time) enter into the Marmara Sea and the suspended sediments are rapidly flocculated and then deposited on sea floor during the Holocene.

Bivalve, gastropod and *Lithothamnium* oxygen isotope and pore water salinity values are plotted on the oxygen isotope ratio-salinity diagram of Rank et

al. (1999) in figure 10. Pore water data plot close to the oxygen isotope-salinity line, with two samples each located in the Marmara Sea and the Black Sea sectors. However, a gradual increase of salinity with time are not completely conformable with bivalve, gastropod and *Lithothamnium* ages. This discrepancy may be due to the "vital" effects on the oxygen isotope composition of bivalve, gastropod and *Lithothamnium* caused by growth rate, size and age (Wefer and Berger, 1981). Despite this discrepancy, the bivalve, gastropod and *Lithothamnium* data suggest that the transition from brackish water conditions to the present day marine conditions in the Marmara Sea took place sometime between 5400 and 3800 Cal yr BP.

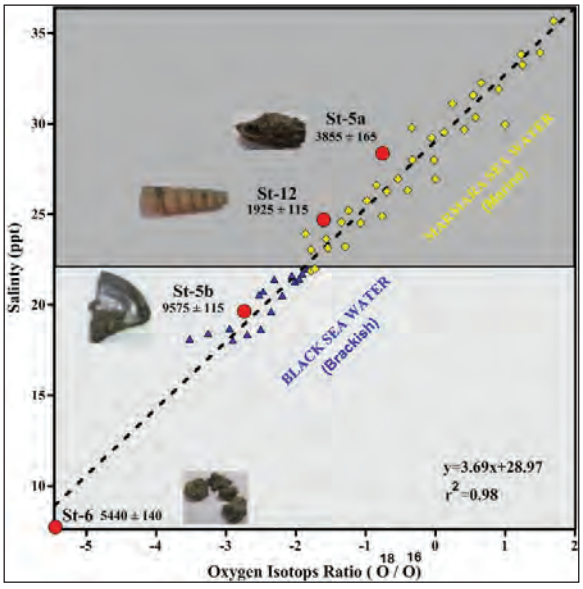

Figure 10- Relationship between salinity (‰) and the Oxygen Isotops Ratio ($^{18}O/^{16}O$) in the Marmara Sea, Black Sea (adapted from Rank et al., 1999) and along the cores.

4. Discussion

In this section, we discuss the ages of the terraces (T1, T2, T3) and the water exchanges between the Mediterranean, the Marmara Sea and the Black Sea, based on the high-resolution shallow seismic reflection profiles, sediment cores and post-glacial sea-level curves (Figures 3, 8 and 11).

It is generally accepted that the minimum sill depths of the bedrocks in the Çanakkale and İstanbul Straits have controlled the connections between the Aegean Sea, Marmara Sea and Black Sea (e.g., Eriş et al., 2008, Çağatay et al., 2009, Gökaşan et al., 2010). Previous studies suggest that the Çanakkale (Yaltırak et al., 2002) and İstanbul Straits and shelf of the Marmara Sea were exposed during the LGM, with fluvial erosion lowering the depths of the straits (Eriş et al., 2007, 2008; McHugh et al., 2007; Çağatay et al., 2009; Gökaşan et al., 2010) and shelf areas. Sea-level fluctuations in the Aegean Sea, Marmara Sea and Black Sea were associated with the global climate and sea level change, size of the drainage basins and depth of the straits. Sea-level started to rise, during the post-glacial warm and wet periods (WWP) after the last glacial maximum (LGM), which took place after 22 Cal kyr BP (Gornitz, 2009) (Figure 11). Before the beginning of the late glacial period, Aegean Sea level stood at -120 m, Marmara Sea level around -105 m and the Black Sea level between -60 m and -90m (Eriş et al., 2011).

In today's climatic and oceanographic conditions of the Aegean, Marmara and Black Seas, the only relatively semi-enclosed Black Sea has positive freshwater balance because of the high ratio of drainage to surface area (D/S) of the Black Sea (4 times greater than Marmara Sea and 2 times greater than the Mediterranean Sea). This provides the Marmara Sea and Aegean Sea with a Black Sea outflow through the İstanbul and Çanakkale straits. A one-way outflow from the Black Sea most likely operated during the late glacial due to the glacier melt waters. Such a continuous Black Sea outflow hypothesis during the late glacial and early Holocene is supported by our study as well as by some previous studies (Degens and Ross 1974; Lane-Serff et al. 1997; Aksu et al., 2002c; Hiscott et al., 2002). However, some other researchers have argued an evaporative drawdown of the Black Sea level during the late-glacial period (Ryan et al., 1997; Ballard et al., 2000).

As a result, there is no consensus among the scientists about the timing of the water connections between the Aegean Sea and Black Sea during the post glacial period. The water-level would have changed at different rates in different basins, depending on the climate, latitude of the basin, the values of D/S ratio and the connection with the local basins. The first sea-level rise period started after the LGM (22 Cal kyr BP) during the late glacial (Figures 11 and 12 A). The level of the Black Sea reached the minimum depth of İstanbul Strait (around -30m; Major et al., 2006) between the 13.7-22 Cal kyr BP (Figures 11 and 12 B), which could have then started a one-way flow

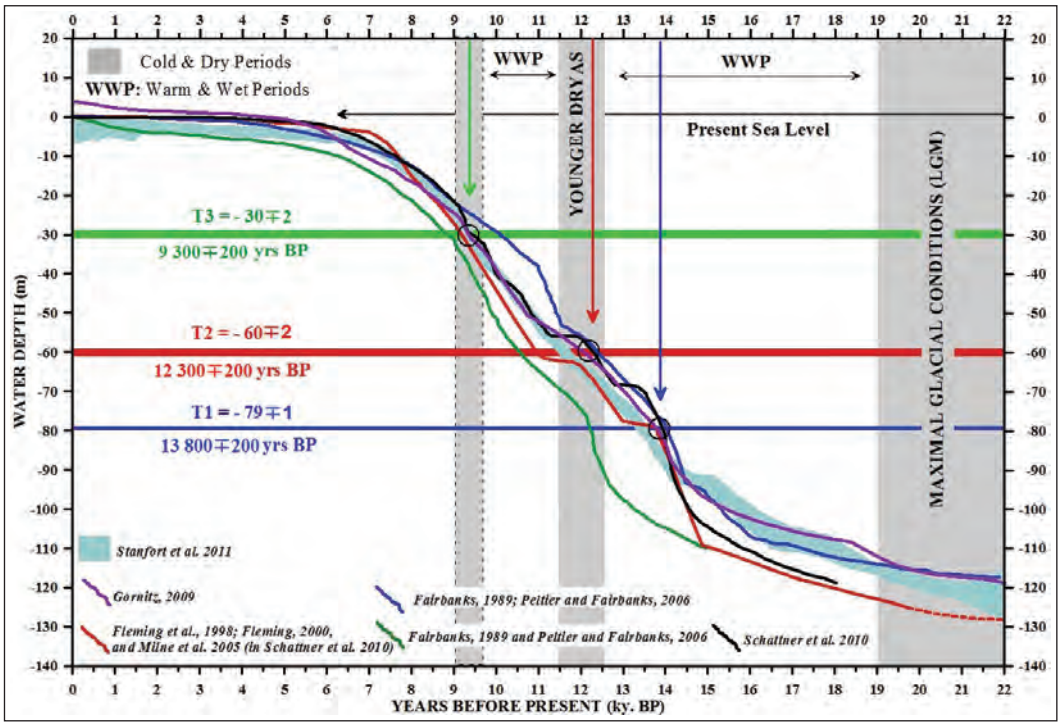

Figure 11- Sea-level rise (depth-time) since the end of the last glacial maximum (Fairbanks, 1989, Fleming et al., 1998, Fleming, 2000, Gornitz, 2009, Milne et al., 2005, Peltier and Fairbanks, 2006, Schattner et al., 2010, Stanford et al., 2011 and http://www.globalwarmingart.com) and terrace depths, LGM: Last Glacial Maximum. Colored arrows and black circles indicate times and depths of the three different terraces.

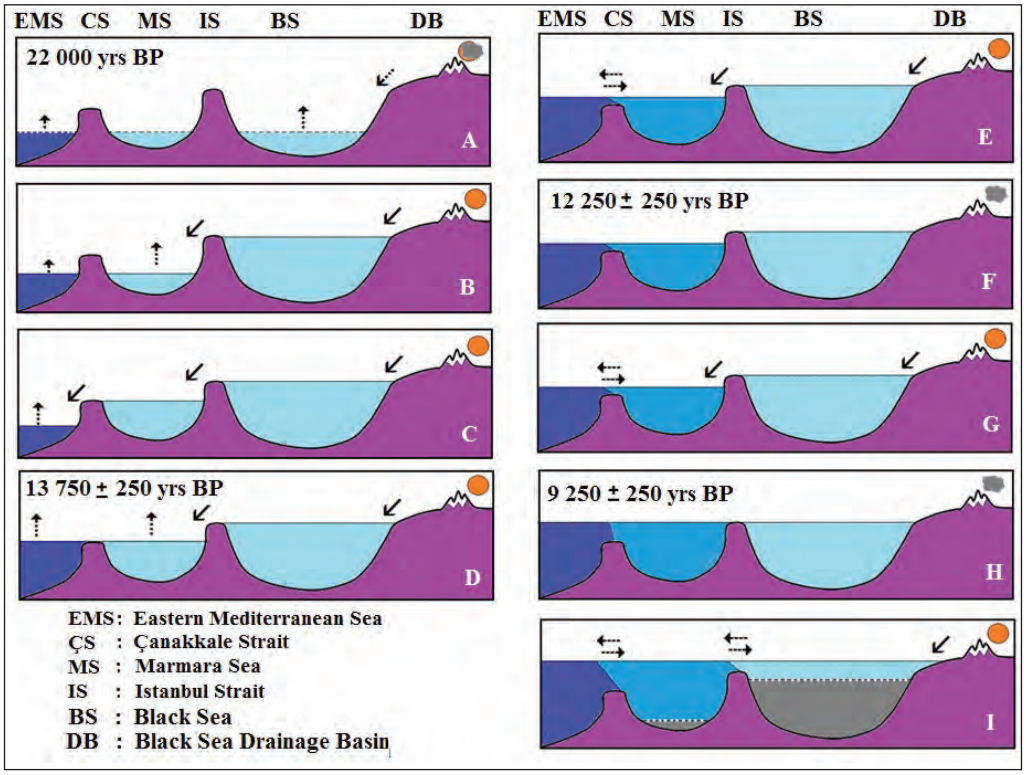

Figure 12- Sketch of Late Quaternary sea-level changes and water exchange among the Marmara, Mediterranean and Black Seas, based on interpretations of seismic reflection profiles, subbottom topography and previous sea-level change curves (phases A to I).

into the Marmara Sea along the İstanbul Strait (Figure 12 B). At the end of this one-way flow regime from Black Sea to Marmara Sea, Marmara Sea should have filled with fresh Black Sea water to the sill depth of the Çanakkale Strait during the first WWP (Figure 12 B). This one way flow regime should have continued until the global sea level in the Aegean Sea reached to the sill depth of Çanakkale Strait (Figure 12 C and D). Afterwards, the Marmara Sea level would rise in tandem with global sea level (Figure 12 D).

First terrace of the Marmara Sea (T1) was formed by truncation of the Marmara Sea shelf by the wave and current action at the sill depth of Çanakkale Strait (i.e., at -79 ± 1 m) around 13.7 Cal kyr BP when the Marmara Sea was fresh-brackish water lake during the time interval for establishing the first two way connection between Aegean Sea and Marmara Sea (Figures 8, 11 and 12 E). It was the result that the depth of the T1 terrace was controlled by the depth of the Çanakkale Strait. However, when the previous studies were examined, it was observed that the depth of the Çanakkale Strait varied between -65 m and -85 m (Smith et al., 1995; Ryan et al., 1997; Hiscott et al., 2002, 2008; Yaltırak et al., 2002; Aksu et al., 2002*c*; Polonia et al., 2004; Major et al., 2006; Gökaşan et al., 2008; Eriş et al., 2007, 2008; McHugh et al., 2008; Çağatay et al., 2000, 2003, 2009). It has been reported by Çağatay et al. (2000) that the Marmara basin was last inundated by Aegean waters around 12 Cal kyr BP. Areal distribution of the T1 along the slope of the region are given in figure (13 A). Despite the suggestion of Ryan et al. (2003) and Ryan (2007) that the amount of evaporation in the Black Sea kept the water level below the sill of İstanbul Strait during that time, we advocate that the waters produced by glaciers melting during the warm period kept the Black Sea level around the sill depth of İstanbul Strait during the late glacial period.

Truncation of the terrace T1 was completed along the northern Marmara shelf and the two-way flow regime established between the Aegean Sea and the Marmara Sea after 13.7 Cal kyr BP (Figures 12 E). Subsequently, the density stratification and suboxic to anoxic bottom conditions gradually established in the Marmara Sea after the Aegean Sea (Mediterranean Sea) connection. These conditions led deposition the sapropel and sapropelic layers dated as ~12-7 and 5-3 Cal kyr BP in the Marmara Sea cores (Çağatay et al., 1999; 2000, 2009, 2015; Tolun et al., 2002; Aksu et al., 2002*c* and 2008). The cold and dry period of Younger Dryas (YD) was period of sea level still stand (Fairbanks, 1989), that resulted in slow down of the unidirectional flow from Black Sea to Marmara Sea and the bidirectional flow from Aegean Sea to Marmara Sea (Figure 11; 12F) (Lane-Serff et al., 1997). The Marmara Sea level during the YD, in tandem with global sea level, was around -60 m according to the global sea level curves. This was the period when the second terrace (T2) was truncated at around -60 ± 2 m by strong current and wave action (Figures 11, 12 F). Throughout this period, the Black Sea water must have been fresh and that of the Marmara Sea partially brackish. This second terrace at -60 ± 2 m water depth is statistically the most significant and morphologically the most common of all the terraces along the northern Marmara shelf (Figures 8, 11). The depth of the Marmara Sea terrace (T2) was claimed to be around -65 m in previous studies (in Newman, 2003; Polonia et al., 2004; Eriş et al., 2007, 2008; McHugh et al., 2008; Çağatay et al., 2003, 2009). The areal distribution of terrace T2 and the presence of a paleo-lagoon along the northern shelf is shown in figure (13 B). Paleo-lagoon and some coastal lakes probably had been filled with the melt fresh waters at the end of this period. Also, bioherms probably developed over the unconformity surfaces (U1) around the western side of the Marmara Sea-İstanbul Strait junction (Figure 6). The YD age of terrace T2 is supported by radiocarbon dating of a broad wave-cut terrace in the Princes' Islands shelf (Eriş et al., 2010).

Some researchers have proposed a gradual connection between the Marmara Sea and Black Sea (e.g., Aksu et al., 2002*a*, *b*; Hiscott et al., 2002, 2007), whereas others have suggested an abrupt connection (Ryan et al., 1997, 2003; Major et al., 2002, 2006; Myers et al., 2003; Siddall et al., 2003). During the early Holocene warm and wet period (~11.7-9.3 Cal kyr BP) after the Younger Dryas, the sea-level gradually rose to the level of the İstanbul Strait's sill and the first Mediterranean transgression of the Black Sea took place at around 9.3 Cal kyr BP (Major et al., 2002; Ryan, 2007). A two-way flow connection was established between the Aegean Sea and Marmara Sea via the Çanakkale Strait during this WWP (Figures 12 G and H). Terrace T3 corresponds to the İstanbul Strait's sill depth and was most likely controlled by a short sea level still stand around 9.3 Cal kyr BP (Figures 12 H, 13). However, when the previous studies were examined, it was observed that the depth of the İstanbul Strait varied between -35 m and -45 m (Fairbanks, 1989; Görür et al., 2001; Hiscott et al.,

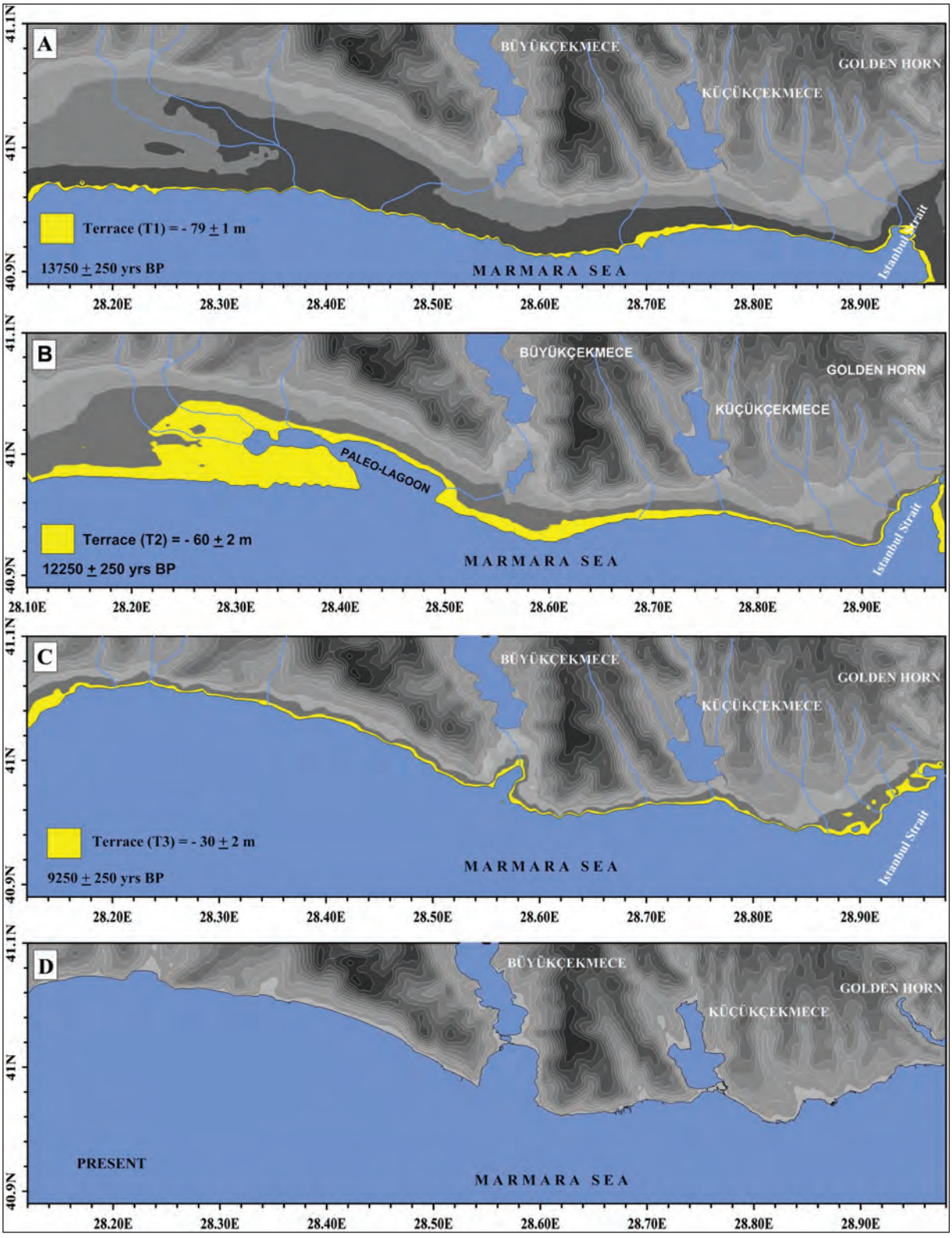

Figure 13- Paleo shorelines along the northeastern Marmara shelf during the low-stand periods of the sea at -78 m to -80 m, -58 m to -62 m, -28 m to -32 m and present condition. Black solid lines represent shore-lines. Coastal drainage networks (blue lines) are given in these figures.

2002; Yaltırak et al., 2002; Aksu et al., 2002*a*; Major et al., 2006; McHugh et al., 2008; Eriş et al., 2007, 2008; Çağatay et al., 2000, 2003, 2009). Areal distribution of the T3 along the shelf of the region are given in figure (13 C).This still stand may have been due to hydraulic conditions between the initially opposing flows of Mediterranean and Black Sea waters and/or climatic causes.

The present day two-way flow system along the straits and anoxic Black Sea bottom conditions were established after 9.3 Cal kyr BP (Figure 12I). Present day geometry of the coastal zone has been shaped after about 6 Cal kyr BP when the sea-level stabilized near the present sea level (Figures 11 and 13 D).

5. Conclusions

By using high resolution shallow seismic reflection data and applying basic seismic stratigraphic techniques, three distinct main boundary reflector surfaces (R1, R2 and R3) and two unconformity surfaces (U1 and U2) were identified among the five sedimentary seismic units (S1-S5) over the acoustic basement (AB).

Four different chronostratigraphic sedimentary layers (A, B, C and D; younger than 9575 ± 115 Cal yr BP) have been distinguished over the acoustic basement (AB) in the Northern Shelf of the Marmara Sea. Total thickness of the Late Quaternary deposits reaches up to 30 m in the eastern depression of the shelf and Büyükçekmece Bay. The central part of the shelf is not completely devoid of sediment, but most of the deposits are less than 2 m thick. Sedimentation rates on the northeastern shelf of the Marmara Sea range from 0.05 m/kyr to 0.34 m/kyr. The distribution of acoustic basement depth values on the density bar-graph shows the presence of three basic terraces (T1, T2 and T3) at depths of -79 ± 1, -60 ± 2 and -30 ± 2 respectively.

The Black Sea level should have gradually increased since the last glacial maximum and one-way flow regime from Black Sea to Marmara Sea should have been established after filling of Black Sea basin due to higher water inputs during the late glacial melt water events. With the Black Sea outflow, the Marmara Sea water level reached the depth of the Çanakkale Strait and established a one-way outflow from Marmara Sea to Aegean Sea (13.7 Cal kyr BP). The one-way flow from Marmara Sea to Aegean Sea continued until the global sea level reached the depth of Çanakkale Strait around 13.7 Cal kyr BP. The depth of the Marmara Sea level stabilized at the sill depth of Çanakkale Strait that controlled the formation of the T1 terrace (at -79 ± 1 m) by wave and current truncation under lacustrine conditions of the Marmara Sea. Subsequent to the marine connection at 13.7 Cal kyr BP, water stratification and anoxic sea bottom conditions were established during this transgressive period.

The overflow from the Black Sea to Marmara Sea was probably gradually stopped and two way flow regime degenerated between the Aegean Sea and Marmara Sea around the 12.3 Cal kyr BP during the Younger Dryas (Fairbanks, 1989) at the end of the first warm and wet period. During the Younger Dryas, the second terrace (T2) might have been truncated around -60 ± 2m depth intervals by strong coastal erosion and sediment reworking processes by the currents and waves during the cold and dry period (Younger Dryas). Throughout this period, the Black Sea water must have been fresh and that of the Marmara Sea partially brackish. Paleo-lagoon and some coastal lakes were developed and filled with the fresh melt waters at the end of this period. Also, bioherms developed over the unconformity surfaces (U1) around the western side of the Marmara Sea-İstanbul Strait junction.

At the end of the Younger Dryas, the sea-level started to rise gradually in the Aegean Sea and Marmara Sea and the two-way flow regime between Aegean Sea and Marmara Sea and one-way flow regime from Black Sea to Marmara Sea were established. Overflow probably gradually stopped from the Black Sea to Marmara Sea and the two-way flow regime re-established between the Aegean Sea and Marmara Sea after the 9.3 Cal kyr BP as a result of the beginning of the second cold and dry period. The sea-level reached -30±2 m (sill depth of the İstanbul Strait) around 9.3 Cal kyr BP when the T3 terrace of the Marmara Sea was formed by wave and current truncation.

The present day two-way flow system along the straits and anoxic Black Sea bottom conditions were established after 9.3 Cal kyr BP. Present day geometry of the coastal zone has been shaped after about 6 Cal kyr BP when the sea-level stabilized near the present sea level.

Acknowledgements

This research was supported by the "Scientific and technical cooperation protocol within the scope of investigating probable faults in land areas of İstanbul and developing landslide detection and monitoring methods through multidisciplinary research of priority landslide areas; 509770" project, funded by Istanbul Metropolitan Municipality (İBB) and the Scientific and Technological Research Council of Turkey (TÜBİTAK) Marmara Research Center (MRC). The authors also express their sincere thanks to the project teams of the İBB-Earthquake and Ground Research Directorate and TÜBİTAK MRC-Earth and Marine Sciences Institute for their kind effort in providing the data during surveys. The authors thank the officers, crew and scientific staff on the R/V Koca Piri Reis (Dokuz Eylül University) and R/V Arar (İstanbul University) for invaluable assistance during a succession of successful cruises. We thank Prof. Dr. Namık Çağatay, Dr. Christopher Sorlien and an anonymous reviewer for valuable suggestions and contributions that improved our paper.

References

Aksu, A.E., Hiscott, R.N., Yaşar, D., Işler, F.I., Marsh, S. 2002*a*. Seismic stratigraphy of Late Quaternary deposits from the southwestern Black Sea shelf: evidence for non-catastrophic variations in sea-level during the last 10,000 years. Mar. Geol. 190, 61–94.

Aksu, A.E., Hiscott, R.N., Mudie, P.J., Rochon, A., Kaminski, M.A., Abrajano, T., Yaşar, D. 2002*b*. Persistent Holocene outflow from the Black Sea to the Eastern Mediterranean contradicts Noah's Flood hypothesis. GSA Today 12 (5), 4–10.

Aksu, A.E., Hiscott, R.N., Kaminski, M.A., Mudie, P.J., Gillespie, H., Abrojano, T., Yaşar, D. 2002*c*. Last glacial–Holocene paleoceanography of the Black Sea and Marmara Sea: stable isotopic, foraminiferal and coccolith evidence. Mar. Geol. 190, 119–149.

Aksu, A.E., Jenner, G., Hiscott, R.N., İşler, E.B. 2008. Occurrence, stratigraphy and geochemistry of Late Quaternary tephra layers in the Aegean Sea and the Marmara Sea Mar. Geol. 252, 174–192.

Alavi, S.N., Ediger, V., Ergin, M. 1989. Recent sedimentation on the shelf and upper slope in the Bay of Anamur, southern coast of Turkey, Mar. Geol.i 89: 29-56. Fli.igel, E. 1978. Mikrofazielle Untersuchungsmethoden yon Kalken. Springer, Berlin, 454 p.

Alpar, B., Yüce, H. 1998. Sea-level variations and their interactions between the Black Sea and the Aegean Sea. Estuar Coast Shelf Sciences, 46, 609-619.

Badley, M.E. 1985. Practical Seismic Interpretation. Prentice-Hall, Englewood Cliffs, N J, 266 p.

Ballard, R.D., Coleman, D.F., Rosenburg, G. 2000. Further evidence of abrupt Holocene drowning of the Black Sea shelf: Marine Geology 170, 253–261.

Beşiktepe, Ş., Sur, H.I., Özsoy, E., Latif, M.A., Oğuz, T., Ünlüata, Ü. 1994. The circulation and hydrography of the Marmara Sea. Prog. Oceanogr. 34, 285-334.

Boggs, S. Jr. 1987. Principles of Sedimentology and Stratigraphy. Macmillan, New York, 784 p.

Brown, Jr., L.F., Fisher, W.L. 1980. Seismic Stratigraphic Interpretation and Petroleum Exploration. AAPG Continuing Education Course Note Series 16, Tulsa, Oklahoma, 125 p.

Campbell, A.C. 1982. The Hamlyn Guide to the Flora and Fauna of the Mediterranean Sea. Hamlyn, London, p. 320.

Çağatay, M.N., Algan, O., Sakınç, M., Eastoe, C.J., Egesel, L., Balkis, N., Ongan, D., Caner., H. 1999. A mid-late Holocene sapropelic sediment unit from the southern Marmara sea shelf and its palaeoceanographic significance, Quaternary Science Reviews 18 (1999) 531-540.

Çağatay, M.N., Görür, N., Algan, O., Eastoe, C., Tchalaliga, A., Ongan, D., Kuhşl, T., Kuşçu, İ. 2000. Late Glacial-Holocene paleoceanography of the Sea of Marmara: timing of connections with the Mediterranean and the Black Sea. Mar. Geol. 167, 191–206.

Çağatay, M.N., Görür, N., Polonia, A., Demirbağ, E., Sakınç, M., Cormier, M.-H., Capotondi, L., McHugh, C.M.G., Emre, Ö., Eriş, K. 2003. Sea-level changes and depositional environments in the İzmit Gulf, eastern Marmara Sea, during the late glacial–Holocene period. Mar. Geol. 202, 159–173.

Çağatay, M.N., Eriş, K., Ryan, W.B.F., Sancar, Ü., Polonia, A., Akçer, S., Biltekin, D., Gasperini L, Görür, N., Lericolaris, G., Bard, E. 2009. Late pleistocene-holocene evolution of the northern shelf of the Sea of Marmara, Mar. Geol. 265, 87-100.

Çağatay, M.N., Wulf, S., Guichard, F., Özmaral, A., Henry, P., Gasperini, L. 2015. Tephra record from the Sea of Marmara for the last 71 ka and its paleoceanographic implications. Marine Geology, 361: 96-110.

DAMOC, 1971. Master plan and feasibility report for water supply and sewerage for Istanbul region. Prepared by the DAMOC Consortium for WHO, Los Angeles, CA, vol. III, part II and III.

Degens, E.T., Ross, A. 1974. The Black Sea-Geology, chemistry, and biology. American Association of Petroleum Geologists, Tulsa, Oklahoma, 633 p.

Dimitrov, P. 1982. Radiocarbon datings of bottom sediments from the Bulgarian Black Sea shelf. Bulg. Acad. Sci. Oceanol. 9, 45-53.

Ediger, V., Okyar, M, Ergin, M. 1993. Seismic stratigraphy of the fault-controlled submarine canyon/valley system on the shelf and upper slope of Anamur Bay, Northeastern Mediterranean Sea. Mar. Geol. 15, 129-142.

EIE, 1993. Sediment data and sediment transport amount for surface water in Turkey. Türkiye Elektirik İşleri Etüd Dairesi Genel Müdürlüğü, Ankara, EIE Publ., No.68. 56 p.

Ergin, M., Bodur, M.N., Ediger, V. 1991. Distribution of surficial shelf sediments in the northeastern and southwestern parts of the Sea of Marmara: Strait and canyon regimes of the Dardanelles and Bosphorus. Mar. Geol. 96, 313-340.

Ergintav, S., Demirbağ, E., Ediger, V., Saatçılar, R., Inan, S., Cankurtaranlar, A., Dikbaş, A., Baş, M. 2011. Structural framework of onshore and offshore Avcılar, ˙Istanbul under the influence of the North Anatolian fault. Geophys. J. Int. 185, 93–105.

Eriş, K.K., Ryan, W.B.F., Çağatay, M.N., Sancar, U., Lericolais, G., Ménot, G., Bard, E. 2007. The timing and evolution of the post-glacial transgression across the Sea of Marmara shelf south of İstanbul. Mar. Geol. 243 (1-4), 57-76.

Eriş, K.K., Ryan, W.B.F., Çağatay, M.N., Lericolais, G., Sancar, Ü., Menot, G, Bard, E. 2008. Reply to Comment on "The timing and evolution of the post-glacial transgression across the Sea of Marmara shelf south of İstanbul" by Hiscott et al., Mar. Geol. 248 228-236.

Eriş, K.K., Çağatay, M.N., Akçer, K., Luca, G., Yosi., M. 2010. Late glacial to Holocene sea-level changes in the Sea of Marmara: new evidence from high-resolution seismics and core studies. Geo-Mar Lett 31:1–18.

Eriş, K.K., Çağatay, M., Sena, A., Gasperini, L., Mart, Y. 2011. Late glacial to Holocene sea-level changes in the Sea of Marmara: new evidence from high-resolution seismics and core studies, Geo-Marine Letters, V:31, N:1, 1-18.

Fairbanks, R.G. 1989. A 17,000 year glacio-eustatic sea-level record: Influence of glacial melting rates on the Younger Dryas event and deep-ocean circulation: Nature, v. 342, p. 637-642.

Fleming, K. M. 2000. Glacial Rebound and Sea-level Change Constraints on the Greenland Ice Sheet. Australian National University. PhD Thesis.

Fleming, K., Johnston, P., Zwartz, D., Yokoyama, Y., Lambert, K., Chappell, J. 1998. Refining the eustatic sea-level survey since the Last Glacial Maximum using far- and intermediate-field sites. Earth Planet. Sci. Lett. 163, 327–342.

Gökaşan, E., Demirbağ, E., Oktay, F.Y., Ecevitoğlu, B., Şimşek, M., Yüce, H. 1997. On the origin of the Bosphorus. Mar. Geol. 140, 183–199.

Gökaşan, E., Ergin, M., Özyalva Ç. M., İbrahim Sur, H., Tur, H., Görum, T., Ustaömer, T., Gül Batuk, F., Alp, H., Birkan, H., Türker, A., Gezgin, E., Özturan, M.., 2008. Factors controlling the morphological evolution of the Canakkale Strait (Dardanelles, Turkey). Geo-Mar Letters 28, 107–129.

Gökaşan E., Tur, H., Ergin, M., Görüm, T., Batuk F.G., Sağcı, N., Ustaömer, T., Emem, O., Alp, H. 2010. Late Quaternary evolution of the Çanakkale Strait region (Dardanelles, NW Turkey): implications of a major erosional event for the postglacial Mediterranean-Marmara Sea connection. Geo-Mar Lett (2010) 30:113-131.

Gornitz, V. 2009. Sea level change, post-glacial. In Encyclopedia of Paleoclimatology and Ancient Environments. V. Gornitz, Ed., Encyclopedia of Earth Sciences Series. Springer, 887-893.

Görür, N., Çağatay, M.N., Emre, Ö., Alpar, B., Sakınç, M., Islamoğlu, Y., Algan, O., Erkal, T., Keçer, M., Akkök R., Karlık, G. 2001. Is the abrupt drowning of the Black Sea shelf at 7150 yr BP a myth? Mar. Geol. 176, 65-73.

Hiscott, A.E., Aksu, R.N, Mudie, P.J, Kaminski, M.A., Abrajano, T., Yaşar, D., Rochon, A. 2007. The Marmara Sea gateway since 16 ky BP: non-catastrophic causes of paleoceanographic events in the Black Sea at 8.4 and 7.15 ky BP. In: Yanko-Hombach, V., Gilbert, A.S., Dolukhanov, P.M. (Eds.), The Black Sea Flood Question. Springer, The Netherlands, 89–117.

Hiscott, R.N., Aksu, A.E, Yaşar, D., Kaminski, M.A., Mudie, P.J., Kostylev, V.E., MacDonald, J.C., İşler, F.I., Lord, A.R. 2002. Deltas south of the Bosphorus Strait record persistent Black Sea outflow to the Marmara Sea since ~10 ka. Mar. Geol. 190:95-118.

Hiscott, R.N., Aksu, A.E., Mudie, P.J. 2008. Comment on "The timing and evolution of the post-glacial transgression across the Sea of Marmara shelf south of Istanbul" by Eriş et al., Mar. Geol. 243, 57–76 Mar. Geol., Volume 248, Issues 3-4, 25 February 2008, Pages 228-236.

http://www.globalwarmingart.com

Kaminski, M.A., Aksu, A.E., Box, M., Hiscott, R.N., Filipescu, S., Al-Salameen, M. 2002. Late glacial to Holocene benthic foraminifera in the Marmara Sea: implications for Black Sea-Mediterranean Sea connections following the last deglaciation. Mar. Geol. 190: 165–202.

Keven, G. 2002. Archaeology: An Introduction. Philadelphia: University of Pennsylvania Press. Pages. 165–167.

Kuprin, P.N., Scherbakov, F.A., Morgunov, I.I. 1974. Correlation, age and distribution of the postglacial continental terrace sediments of the Black Sea. Baltica 5, 241-249.

Lane-Serff, G.F., Rohling, E.J., Bryden, H.L., Charnock, H. 1977. Postglacial connection of the Black Sea to the Mediterranean and its relation to the timing of sapropel formation. Paleoceanography Volume 12, Issue 2. Pages 169–174.

Major, C., Ryan, W., Lericolais, G., Hajdas, I. 2002. Constraints on Black Sea outflow to the Sea of Marmara during the last glacial–interglacial transition. Mar. Geol. 190, 19–34.

Major, C.O., Goldstein S.L., Ryan, W.B.F., Lericolais, G., Piotrowski, A.M., Hajdas, I. 2006. The co-evolution of Black Sealevel and composition through the last deglaciation and its paleoclimatic significance. Quat. Sci. Rev. 25, 2031–2047.

Martin, R. E., Leorri, E., McLaughlin, P.P. 2007. Holocene sea level climate change in the Black Sea: Multiple marine incursions related to freshwater discharge events. 2007 Quaternary International 167-168, 61-72.

Meriç, E., Algan, O. 2007. Paleoenvironments of the Marmara Sea (Turkey) Coasts from paleontological and sedimentological data. Quaternary International 167-168, 128-148.

McHugh, W.D., Hansell, D.A., Morgana, J. A. 2007. Reprint of Dissolved organic carbon and nitrogen in the Western Black Sea. Marine Chemistry 105 (1-2), 140-150.

McHugh, C.M.G., Gurung, D., Giosan, L., Ryan, W.B.F., Mart, Y., Sancar, U., Burckle, L., Çağatay, M.N. 2008. The last reconnection of the Marmara Sea (Turkey) to the World Ocean: a paleoceanographic and paleoclimatic perspective. Mar. Geol 255 (1-2), 64-82.

Milliman, J.D., Weiler Y., Stanley D.J. 1972. Morphology and carbonate sedimentation on shallow banks in the Alborian Sea. In: D.J. Stanley (Editor), The Mediterranean Sea A Natural Sedimentation Laboratory. Dowden, Hutchinson and Ross, Stroudsburg, Pa., 241, 259 p.

Mitchum, R.M., Vail, P.R., Sangree, J.B. 1977. Seismic stratigraphy and global changes of sea level, part 6: Stratigraphic interpretation of seismic reflection patterns in depositional sequences. In: C.E. Payton (Editor), Seismic Stratigraphy--Applications to Hydrocarbon Exploration. AAPG Mem., 26: 117-133.

Myers, P.G., Wielki, C., Goldstein, S.B, Rohling, E.J. 2003. Hydraulic calculations of postglacial connections between the Mediterranean and the Black Sea. Mar. Geol. 201, 253-267.

Newman, K.R. 2003. Using Submerged Shorelines to Constrain Recent Tectonics in the Marmara Sea, Northwestern Turkey. Department of Geology, Senior Thesis, Smith College. 49 pp.

Oğuz T., Özsoy E., Latif M., Sur H.I., Ünlüata Ü. 1990. Modeling of hydraulically controlled exchange flow in the Bosphorus Strait. J. Phys. Oceanogr., 20: 945-965

Okyar, M., Ediger, V., Ergin, M. 1994. Seismic stratigraphy of the southeastern Black Sea shelf from high-resolution seismic records. Mar. Geol., Volume 121, Issues 3-4, November 1994, Pages 213-230.

Özsoy, E., Di Iorio, D., Gregg, M., Backhaus, J.O. 2001. Mixing in the Bosphorus Strait and the Black Sea continental shelf: observations and a model of the dense water outflow J. Mar. Syst., 31 (2001), pp. 99-135

Peltier, W.R., Fairbanks, R.G. 2006. Global glacial ice volume and Last Glacial Maximum duration from an extended Barbados sea level record. Quaternary Science Reviews 25 (23-24), 3322-3337.

Polat, Ç., Tuğrul, S. 1996. Chemical exchange between the Mediterranean and Black Sea via the Turkish Straits. In: Briand, F. (Ed.), Dynamics of Mediterranean Straits and Channels. Bulletin de l'Institut Oce.anographique, Monaco, Special No. 17, CIESME Science Series 2, 167-186.

Polonia, A., Gasperini, L., Amorosi, A., Bonatti E., Bortoluzzi, G., Çağatay, N., Capotondi, L., Cormier, M.H., Görür, N., McHugh, C., Seeber, L. 2004. Holocene slip rate of the North Anatolian Fault beneath the Sea of Marmara. Earth Planet. Sci. Lett. 227, 411–426.

Rank, D., Özsoy, E., Salihoğlu I. 1999. Oxygen -18, deuterium and tritium in the Black Sea and the

Sea of Marmara. J. Environ. Radioact. 43, 231-245.

Ryan, W.B.F. 2007. Status of the Black Sea Flood hypothesis. Yanko-Hombach, V., Gilbert, A.S., Panin, N., Dolukhanov, P. (Edit.), The Black Sea Flood Question-Changes in Coastline, Climate and Human Settlement, Springer, Dordrecht, 63-88.

Ryan, W.B.F., Pitman III, W.C., Major, C.O., Shimkus, K., Moskalenko, V., Jones, J.A., Dimitrov, P., Görür, N., Sakınç, M., Yüce, H. 1997. An abrupt drowning of Black Sea shelf. Mar. Geol. 138, 119–126.

Ryan, W.B.F., Major, C.O., Lericolais, G., Goldstein, S.L. 2003. Catastrophic flooding of the Black Sea. Annual Review of Earth and Planetary Sciences 31: 525-554.

Sangree, J.B., Widmier. J.M. 1977. Seismic stratigraphy and global changes of sea level, part 9: Seismic interpretation of clastic depositional facies. In: C.E. Payton (Editor), Seismic Stratigraphy--Applications to Hydrocarbon Exploration. AAPG Mem., 26: 165-184.

Schattner U., Lazar M., Tibor G. 2010. Filling up the shelf – A sedimentary response to the last post-glacial sea rise. Marine Geology 278: 165–176.

Shimkus, K.M., Evsyukov, Y.D., Solovjeva, R.N. 1980. Submarine terraces of the lower shelf zone and their nature. In: Malovitsky, Y.P., Shimkus, K.M. (Eds.), Geological and Geophysical Studies of the Pre-Oceanic zone. P.P. Shirshov Inst. Of Oceanology Acad Sci USSR, Moscow, pp 81-92.

Siddall, M., Rohling, E.J., Almogi-Labin, A., Hemleben, Ch., Meischner, D., Schmelzer. I. Smeed. D.A. 2003. Sea-level fluctuations during the last glacial cycle. Nature 423, 853-858.

Smith, A. D., Taymaz, T., Oktay, F., Yüce, H., Alpar, B., Başaran, H., Jackson, J. A., Kara,S., Şimşek, M. 1995. High-resolution seismic profiling in the Sea of Marmara (northwest Turkey): Late Quaternary sedimentation and sea-level changes. Geological Society of America Bulletin, August 1995 923-936

Stanford, J. D., Hemingway, R., Rohling, E. J., Challenor, P. G., Medina-Elizade, M., Lester, A. J. 2011. Sea-level probability for the last deglaciation: A statistical analysis of far-field records, Global Planet. Change, 79, 193–203.

Stuiver, M., Reimer, P.J. 1993: Extended 14C data base and revised CALIB 3.0 14C age calibration program . Radiocarbon 35, 215-230

Tolun, L., Çağatay, M. N., Carrigan, W. J. 2002. Organic geochemistry and origin of late Glacial-Holocene sapropelic layers and associated sediments in Marmara Sea, Mar. Geol., 190, 47 – 60

Ünlüata Ü., Oğuz T., Latif M., Özsoy E. 1990. On the physical oceanography of the Turkish Straits. *In*: Pratt L.J. (ed.). The physical oceanography of sea straits, Kluwer Academic Publishers, Boston, pp 25-60.

Vail, P.R., Mitchum, Jr.R.M., Thompson, S.III. 1977. Seismic stratigraphy and global changes of sea level, part 3: Relative changes of sea level from coastal onlap. In: C.E. Payton (Editor), Seismic Stratigraphy--Applications to Hydrocarbon Exploration. AAPG Mem., 26: 63-81.

Wefer, G., Berger, W.H., 1981. Stable isotopes composition of benthic calcareous algae from Bermuda: Journal of Sedimentary Petrology, v. 51. 0459-0465 p.

Yaltırak, C., Sakınç, M., Aksu, A.E., Hiscott, R.N., Galleb, B., Ülgen, U.B. 2002. Late Pleistocene uplift history along the southwestern Marmara Sea determined from raised coastal deposits and global sea-level variations. Mar. Geol. 190:283-305.

Bull. Min. Res. Exp. (2018) 157: 59-74

Bulletin of the Mineral Research and Exploration

http://bulletin.mta.gov.tr

Geology and critical review of the Upper Cretaceous Zagros chalky limestone (Kometan Formation) from Sulaimani Governorate, Northeastern Iraq

Kamal Haji KARIM[a*], Sherzad Tofeeq AL-BARZINJY[b] and Polla Azad KHANAQA[c]

[a]*Department Geology, College of Science, University of Sulaimani, New camp, Siulaimani city, Iraq. orcid.org/0000-0003-0685-3103*
[b]*Department Geology, College of Science, University of Sulaimani, New camp, Siulaimani city, Iraq. orcid.org/0000-0002-8010-1551*
[c]*Institution for Strategic Studies and Scientific Research, Qrga, Sulaimani city, Iraq. orcid.org/0000-0003-1045-8720*

Research Article

Keywords:
Chalky limestone, Late Cretaceous, Zagros geology, pseudo-bedding, depositional bedding, Kometan Formation, Thalassinoides.

ABSTRACT

The chalky limestone (Kometan Formation) is aged Late Turonian–Middle Campanian and cropping out in the High, Imbricate and Thrust Zones of northeastern Iraq, Sulaimani area. It laterally changes to Bekhme and Mushurah formations toward northwest and west Iraq respectively and its reefal equivalents occurs too in subsurface of Central Iraq in the oil fields. Stratigraphically, it is located between Shiranish Formation (Middle-Late Campanian), at the top, and Gulneri Formation (Late Cenomanian-Early Turonian) at its base. It has the thickness of about 40-120 meter and deposited in pelagic realm. All previous studies have defined it as well bedded and fine grain limestone of deep marine facies with concentration of chert nodules and stylolites on or near bedding surfaces. The only recorded fossils are nannofossils, planktonic forms and rare benthonic forams. On the contrary, a most recent study has declined all the above features and changed lithology to massive, homogenous limestone with abundant *Thalassinoides* trace fossils. It additionally concluded that the bedding surfaces are not true bedding (pseudo-bedding) and formed by stylolization not by deposition. The present study is focusing on update the geology of the Cretaceous chalky limestone and critical review in addition to comparison of all the above ideas and introducing new ones. The features of the *Thalassinoides*, massiveness and pseudo-bedding of previous authors discussed and their absence confirmed and justified by field and laboratory works. Moreover, the massiveness is refused and well bedding (relatively has thin beds) is proved as an intrinsic characteristic of the formation in all section. The study also shows absence of relation of the chert nodules and chert bedding with traces fossils due to absence of bioturbation, detrital clasts, bioclasts, sorting, lamination and color change. Moreover, the idea of deposition of Kometan Formation in Zagros Foreland basin refused and assumed as deposition of continental margin of Neo-Tethys Sea (or ocean) before ophiolitic obduction and foreland generation.

Received Date: 02.10.2017
Accepted Date: 16.03.2018

1. Introduction and Geological Setting

Chalky limestone Kometan (Ilam in Iran) Formation (Late Turonian–Middle Campanian) exposed mainly along the limbs of the anticlines in the High, Imbricate and Thrust Zones of northern Iraq (Figure 1). In Central Iraq, its neritic equivalents (Khasib and Tanuma formations) occur as oil reservoir in the East Baghdad fields (Al-Ameri, 2011). In northern Iraq, it changes laterally to Mushurah Formation toward northwest (Buday, 1980; Jassim and Goff, 2006).Stratigraphically, it is located between Shiranish Formation (Late Campanian) and Gulneri Formation (Late Cenomanian-Early Turonian) at its top and base respectively. According to Dunnington, (1953 in Bellen et al., 1959), the formation consists of thin-bedded globigerinal-oligosteginal limestones and they added that HV Dunnington first defined the formation in 1953. The type locality located in the Naudasht valley 18 km to the north of Ranyia town near Kometan village within Imbricated Zone.

* *Corresponding author: Kamal Haji KARIM, kamal.karim@univsul.edu.iq*
http://dx.doi.org/10.19111/bulletinofmre.428342

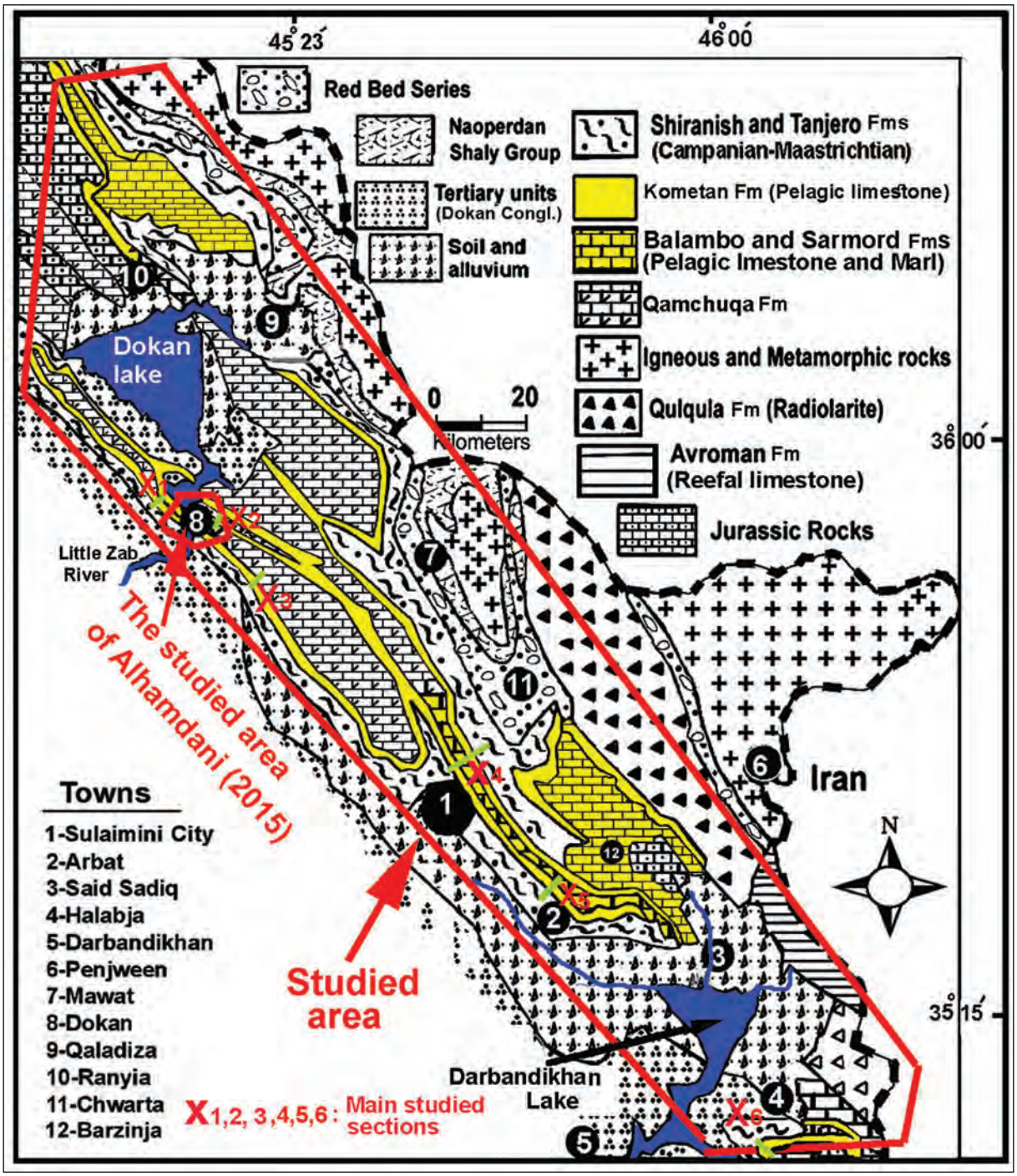

Figure 1- Geological map of the studied area (modified from Sissakian, 2000 and Karim et al., 2011).

Lithologically, it consists of 40-120 m of fine-grained (pelagic) chalky limestone and shows a crowd of planktonic forams, mainly including Globotruncana and oligostegina species. In many place it contains association of nodules and bands of the chert in addition to high amplitude stylolites. The cherts nodules shapes include branched, non-branched, cylindrical or irregular and randomly arranged with 1-7 and 5-25 cm in thickness and length respectively. The area of its exposure is mainly restricted to Sulaimani Governorate (Sulaimanyiah on the map). While toward Arbil and Dohuk governorates, it laterally changes to dolomite and dolomitic limestone of reefal Bekhme Formation (Karim et al., 2012 and Karim, 2013).

In the past, a Portland cement company quarried (used) the formation for cement raw materials near Sulaimani city. This using is due to its minerological constituents, which consist of about 84%, and 7% of microcrystalline calcite and silica respectively, with about 9% clay minerals. In Turkey, the deposition of Turonian- Campanian was continuous too and named Bey Dağları formation which consisted of neritic and hemipelagic carbonates (Sari and Özer, 2001; Sarı et al., 2004). Lithologically, the formation is more similar to Bekhme Formation than Kometan in the latter country.

In southern Anatolia, the equivalents of Kometan Formation are Derdere and Karababa formations (Late Cenomanian-Early Turonian). The former formation consists of dolomites at the base, dolomitic limestone in the middle, and bioclastic at the top. The latter one composed of about 100 m of dark brown, gray and very fine-grained limestone and bioclastic limestone (Mülayim et al., 2015). In Eastern Iran (on the Kopet-Dogh range) the Upper Cretaceous chalky limestone is Abderaz Formation (Hadavi and Moghaddam, 2011) while in Zagros belt it called Ilam Formation which include both deep and shallow facies (Adabi and Mehmandosti, 2008).

In the earlier studies such as Bellen et al. (1959) and Buday (1980) assigned the boundaries of the formation as unconformable. The same idea is discussed by Lawa et al. (2013) and Lawa and Gharib (2010) which mentioned that Gulneri and Dokan formations are absent between Kometan and Qamchuqa Formations and the unconformity lasted 4.7 million years. Conversely, some recent studies such as Karim et al. (2008), Taha and Karim, (2009), Al-Badrani, et al. (2012) and Karim et al. (2012) conclude gradational boundaries in their studied areas.

Bromley and Ekdale (1984) and Mortimorene et al. (2001) summarize the characteristics of Upper Cretaceous chalks of Europe and when the geology of these chalks compared with Zagros Chalky limestone, they are nearly similar in many aspects. The similarities include age (Cenomanian-Maastrichtian), color, bedding pattern, chert nodule content, presence of beds of glauconite, association of both with marl beds and hardground. However, the differences are softer and cocoliths content of the European chalk instead of planktonic foraminiferas (Figure 2). Another difference is deposition of Europe chalk in shallower and more circulated water.

The present study is aiming to update the geology and objectively review the Zagros chalky limestone (Kometan Formation) and introduce many new ideas about the formation. The given ideas are depending on field, thin section and boundary condition studies of the formation including both lateral and vertical facies (lithological) changes. Additionally, the present study discussed the tectonic setting in detail.

1.1. Location and Geomorphology

The studied area is located between the northern latitudes of 35° 09′ 20″ and 36° 31′ 40″ and eastern longitudes of 46° 56′ 45″ and 44° 15′ 43″ in Sulaimani Governorate, northeastern Iraq (Figure 1). The area includes High, Imbricate and part of Thrust Zone of

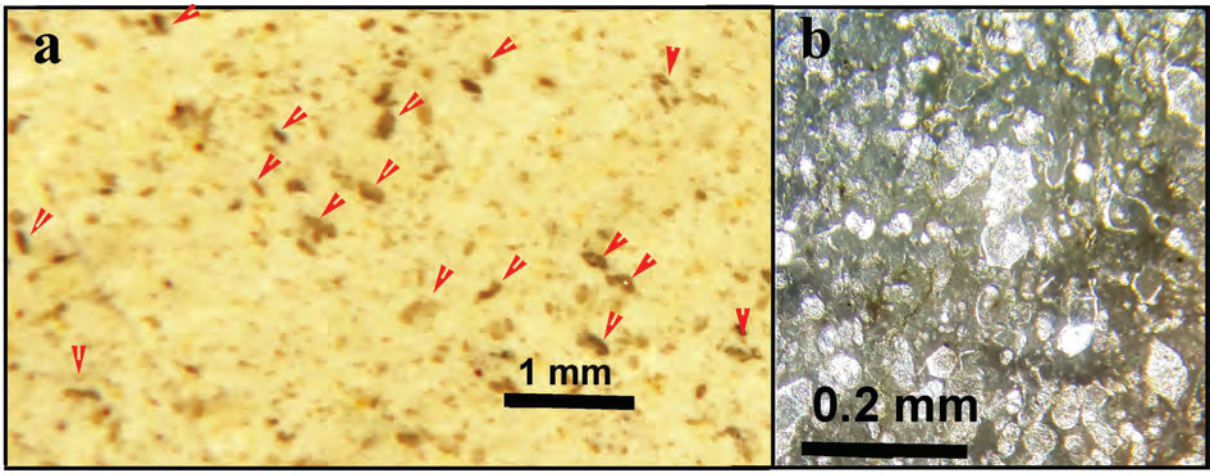

Figure 2- (a) fracture (breakage) surface of the Kometan Formation shows the planktonic foraminiferas (most of them indicated by red arrows) under stereoscope microscope (b) thin section of the formation shows planktonic foraminiferas under polarizing microscope.

Buday (1980); Jassim and Goff (2006). It includes towns such as Ranyia, Dokan, Chwarta, Barzinja, Said Sadiq and Halabja towns from northwest to southwest respectively (Figure 1). The main mountains of the area are Karokh, Makok, Kewa Rash, Asos, Kosrat, Azmir, Goizha, Askawta Rash, Kato, Kachali, Pantaw, Greza Bamo and Shinarwe. The highest mountains are Piramagrun and Kura Kazhaw that are about 2300 m high above the sea level. The Kometan Formation mostly cropped out along the sides of these mountains and there are deep and narrow subsequent or consequent valleys between the mountains, which have dendritic drainage pattern. The annual rainfall is more than 650 mm and drained mostly by emepheral streams to the Darbandikhan and Dokan lakes (reservoirs) (Figure 1).

1.2. Materials and Methodology

The study of the chalky limestone depends on the fieldwork and microscopic studies. The Kometan Formation is surveyed and inspected lithologically and stratigraphically in the complete studied area by the eyes and hand lens. In the area, six sections are selected and sampled for further laboratory studies (Figure 1). From the sampled specimens, 20 petrographic thin sections prepared for inspection under polarizer and stereoscopic microscopes by which the lithology and its constituents are indicated and photographed. During the fieldwork, the authors studied the boundary condition (all lateral and vertical changes) of the formation in addition to its beds, chert nodules and trace fossils contents. The locations of the sections are plotted on the geological map (Figure 1) and stratigraphic columns of three sections are drawn. The field and thin section photos are compared with the previous studies to establish objective argument about origin and mutual relations between features such as chalky limestone, chert nodules, *Thalassinoides* and stylolites. The previous conclusions (in previous studies) about the materials of the current study are checked and critically analyzed in the field and laboratory.

2. Results

This chapter is concerned with new description and analysis of outcomes in the field and laboratory and compares them with previous studies and then the data critically analyzed with documentation of the newest published ideas about Kometan Formation.

2.1. Well Bedded Versus Massiveness of The Chalky Limestone (Kometan Formation)

In the literature, all previous studies have indicated that the Kometan Formation is well-bedded succession of pelagic limestone. The most important studies are Bellen et al. (1959), Buday (1980), Jassim and Goff (2006), Karim et al. (2008), Taha (2008), Taha and Karim, (2009) Al-Badrani et al. (2012), Karim et al. (2012), Ghafor et al. (2012), and Karim et al. (2013).

Conversely, Alhamdani (2015) concluded massiveness and homogeneity of the formation in Dokan (Dukan) Area (area around Dokan Town, see Figure 1).This article added that bedding planes of the Kometan Formation are pseudo-bedding and formed by pressure solution stylolites in a massive `homogeneous pelagic limestones. This latter study further added that the beds visibility, on weathered outcrops, is deceptive and due to removal of friable clayey stylolite seams by erosion.

The results of the fieldwork in the present study in the entire northeastern Iraq revealed that Kometan Formation is actually well bedded (not massive) and the origin of the layers are sedimentary not diagenesis. The thickness of the sedimentary bedding ranges from 7-25 cm (Figure 3). This true bedding is very clear in all part of studied area which is more than 50 times large (in surface area) than Dokan area where Alhamdani (2015) recorded massiveness and pseudo-bedding properties. In the same area, Al-Barzinjy (2008) showed well-developed and high amplitude stylolites, which are mainly distributed along or around the bedding planes and commonly associated with chert nodules. The latter study mentioned the presence of widespread chert nodules and stylolites in Dokan area and absence in other areas.

2.2. True and Pseudo-Bedding

The non-sedimentary (pseudo) beds and laminations, in Kometan Formation, are mentioned near Said Sadiq town (at 43km to the east of Sulaimani city) by Ghafor et al (2012) (Figure 4). They showed that the laminations have secondary origins which is developed by pressure and flexure slip during folding. The present study confirms the above statement of Ghafor et al. (2012) about presence of the secondary lamination in the Kometan Formation. In Said Sadiq area, the secondary (pseudo) bedding can be distinguished easily from true (depositional) ones which are about 5 times thicker than the secondary lamination (or bedding) (Figure 5a).

Figure 3- Sedimentation (true) bedding of Kometan Formation in Sirwan valley along upstream of Diala River. These beds are not associated with stylolite and chert nodules.

Figure 4- Vertical sections on the Ashbolagh hill near Said Sadiq town, a) shows crenulation and secondary lamination of Kometan Formation, which are modulating (superimposed on) true bedding. (b) Close up view shows crenulation of non-depositional lamination with depositional beds of limestone and cherts (Ghafor et al., 2012).

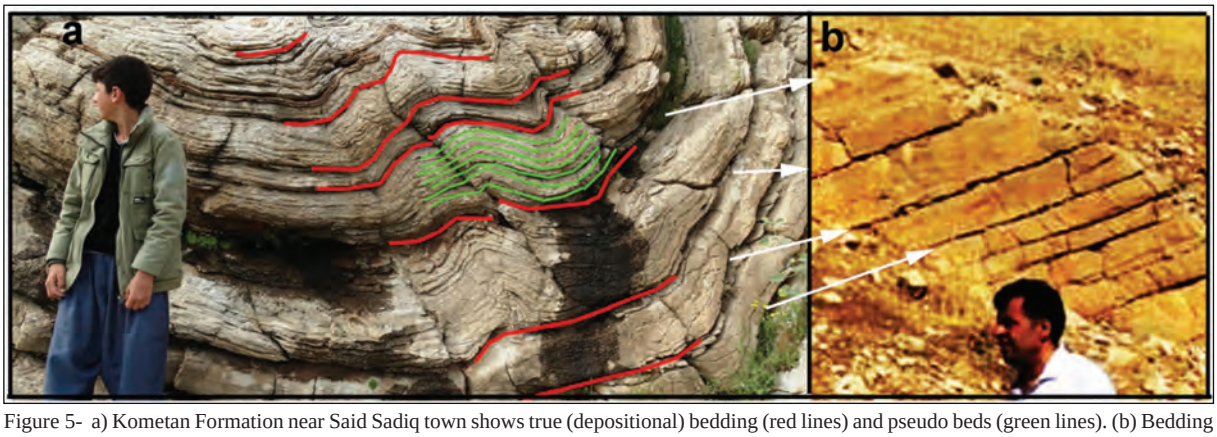

Figure 5- a) Kometan Formation near Said Sadiq town shows true (depositional) bedding (red lines) and pseudo beds (green lines). (b) Bedding of Kometan Formation in Dokan area that envisaged being pseudo-bedding by Alhamdani (2015). Comparison with photo (a) indicates that they are true ones which shown by white arrow.

The true beds have clear, thick and eroded bedding interface while the secondary ones have faint and thin surfaces (Figure 5a). The true beds, in the figure (5), are observable in bold lines and have nearly same thickness of the beds indicated by Alhamadani (2015) as pseudo-bedding (Figure 5b). The comparison of photo (5a) with photo (5b) shows that they are true ones, while the latter study which assumed them as pseudo-bedding. Unfortunately, the latter study not compared or differentiated between the claimed pseudo- and true-bedding in Dokan area. The true beds must be more clearly expressed than those formed by stylolization.

2.3. Relation of Chert Nodules with *Thalassinoides* Burrows

In Kometan Formation, Al-Barzinjy (2008) and Taha (2008) discussed in detail the origins of stylolites, bedding and chert nodules in the Dokan area. However, Alhamdani (2015) neither discussed nor mentioned these later two works and concluded that chert nodules are controllable chiefly by pre-existing *Thalassinoides* burrow. This later study further added that the association of silicified burrows (chert nodules) with stylolite veins refers to regressive discontinuity surfaces.

The present study inspected all the outcrops of the Kometan Formation and showed that *Thalassinoides* burrow and signs of the relation with chert nodules are not observable in all outcrops. Although the Kometan Formation is rich with planktonic foraminifera and nannofossils but any other fossil shells or their pellets that are responsible for claimed *Thalassiniodes* of Alhamdani (2015) are not observable. Another observation, under hand lens and microscope, is absence of colors or lithologic changes, dolomitization, or sorting of the sediment, around the claimed *Thalassinoides* or chert nodules. Giannetti, et al. (2007) mentioned that the organisms that dwell in *Thalassinoides* traces are belonging to crustaceans, fish and worms genera. If these traces are true in the formation, they must associated with, at least, more than one of these structures which are mentioned by many authors such as (Kennedy, 1967, Figure 6) McCal (1982), Pak and Pemberton (2003) and Myrow (1995).

In the studied area and in the upper part of Kometan Formation (directly below Shiranish Formation) there are *Thalassinoides* and planolite traces, which are associated with the lithologic and color changes (Figure 7) and pelecypod shells. In the figure (7a), the traces have cross cutting relation and they have not silicified to chert nodules and not similar in shape and size to chert nodule in the formation. With the traces, there are chert nodules too but they have not relation with the traces (Figure 7b). Karim et al. (2001)

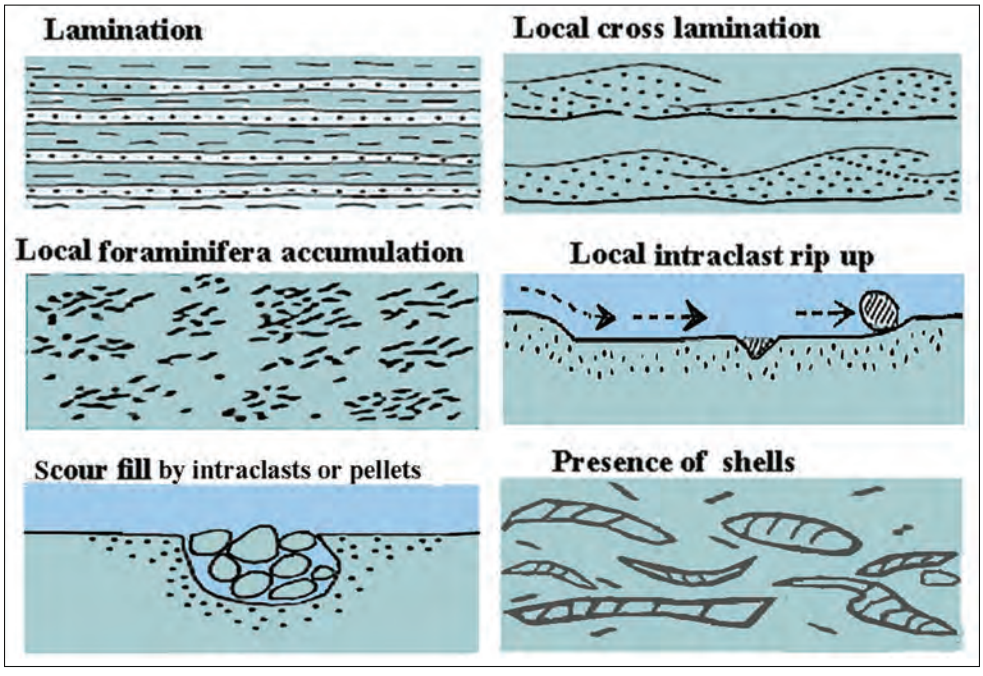

Figure 6- At least one of these structures must be associated with chert nodule (supposed to be *Thalassinoides*) but non of them are recorded in the present study (drawn from description of Kennedy, 1967)

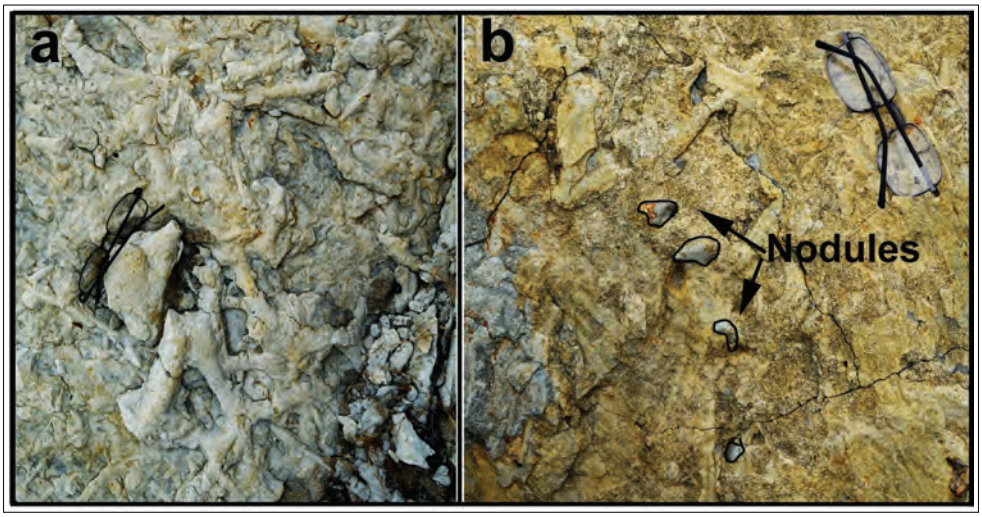

Figure 7- Trace fossils (possibly planolite or *Thalassinoides*) in the contact between Kometan and Shiranish Formation in Dokan area. It is clear that neither they silicified nor related to chert nodules. Scale: the glass is 12cm long.

studied these traces and they found hard ground and *Glossifungite* ichnofacies at the contact between the latter two formations.

3. Discussion

3.1. Problem of the Association of The Pseudo-Bedding, *Thalassinoides* and Chert Nodules

The massiveness and homogeneity of Kometan Formation as stated by Alhamdani (2015) are problematic when one reviews literature of the formation. This is due to nine facts, the first is according to Walness (1979) high amplitude stylolites (such as those of Kometan Formation) not formed in homogenous (clean) limestone but non-seam solution occurs. Arthur et al. (1986) described North American and European Upper Cretaceous pelagic carbonate sequences as rhythmic bedding. They added that such bedding rhythms could result from climatic cycles that are linked to variations in the Earth's orbital characteristics (Milankovich cycles). Therefore, the Kometan formation is not homogenous and contains interbed materials, which act as discontinuities for solution circulation that are necessary for chert nodule nucleation and stylolites generation.

The second is establishment of a relation of Thalassinoides with canyon margin in Dokan area by Alhamdani (2015). The critique on this point is neither present study nor Alhamdani (2015) or any other studies proved occurrence of canyon margins in Dokan area. In the formation, the present authors did not find evidences of the canyon, these evidences are such as calci-and siliciclastic turbidites, extensive bioturbation by macrobenthos, mega breccia and coarse detrital limestone. Instead, the Formation contains only planktonic foraminifera and nannofossils while it barren of signs of current actives. Moreover, in the formation, no one has recorded color change, clastic sediments, fecal pellet and shell accumulation, effect of current (lamination, cross bedding or sign of reworking such as intraclast and bioclasts sediments). Stevens et al. (2014) referred to these characteristics of sediments in canyon margin setting and in Upper Cretaceous chalks of England by Kennedy (1967). In the current study, the thin section and hand lens inspections revealed very poorness in benthonic foraminifera and above structures are not observable. Therefore, the mentioned canyon margin by Alhamdani (2015) is not supportable by the present study.

The third fact is the problem of the presence of more than 40 horizons rich in chert nodules in a succession of massive limestone about 100 meters thick (as seen from part of the section in the Figure 8A of Alhamadani, 2015). If these horizons are *Thalassinoides*, they are actually evidence of true beds which separated by thin marl interbed. The most remarkable result of Alhamdani (2015) is record of the repeated *Thalassinoides* horizons and omission surfaces in Dokan area, if these repetitions are true, they indicate true bedding because repetitions of traces horizons and occurrence of omission surfaces are good indications of true bedding which are burrowed during changes of rate of sedimentation and sea level.

It is possible that the marl has compacted and dewatered during early diagenesis and supplied $CaCO_3$ ions for early cementation and lithification of a part of limestone layers that are directly adjacent to the bedding surfaces. Due to this process, the high amplitude stylolization and chert nodules have developed mostly along and near to the interbed horizon in the limestone beds due to their early cementation. Field study shows that the source of silica is closely related to the development of the stylolites since, in many cases, the chert nodules are trailing the line of stylolite not bedding surface (bedding plane) (Figure 9). In the same cases, it appears that nodules have mostly the oval shape and resemble river gravel and granules not *Thalassinoides*. In Kometan Formation, the marl interbed increase in thickness toward its boundary with Shiranish Formation and in the contact, the thickness of the marl and limestone become nearly equal (Figure 8).

This lithological change and equality of thickness between the two formations is clear evidence for true bedding of Kometan Formation which is shown in several localities by Karim et al. (2008) (Figure 8). If the layers, in Shiranish Formation, are depositional (true) bedding, then those of the Kometan must be the same also. The same thing is true for Gulneri Formation, which is underlying Kometan Formation. The same type of bedding of Kometan Formation continuously passes down and upward to Gulneri and Shiranish Formations respectively.

The fourth critique is that Alhamdani (2015) not used thin section to prove if the growth of the chert nodules is displacive or replacive and only assumed, without evidence, that they are replacing *Thalassinoides* traces. Conversely, thin section study by Al-Barzinjy (2008) showed clearly that the nodules developed by both replacement and displacement during deep burial. The displacement occurred by force of crystallization of silica and the sources of silica are well documented by the later author.

The fifth criticism against the massiveness of Kometan Formation is presence of bedding plane even in massive limestone succession. However, and unfortunately, Alhamdani (2015) has not differentiated between the true and false beds in the Dokan area. In the latter area, all bedding surfaces (or interbeds) are similar in term of thickness and type of expression. The similarity is evidence for depositional origin of the beds because their interbed are thicker and better expressed in outcrop, which is observable near Said Sad town (Figure 5a and b). The sixth point is that in most areas of the northern Iraq the Kometan bedding pattern is similar and not associated with high amplitude stylolite or chert nodules, only in Dokan area associated with the stylolite. Therefore, the well bedding (relatively thin bedding) of the Kometan Formation is not requiring presence of stylolite and occur in all areas of northeastern Iraq (Figure 3 and 9).

The seventh point is closeness of all traces to each other on bedding surfaces (or in interbeds) and their shape and size are very different. If the traces belong to crustaceans as cited by the latter study, they must have nearly same shape (oval, elongate, or irregular) and size (the size of granule or cobble) (Figure 8, 9 and 10). The comparison of these figures with (7) shows the actual *Thalassinoides* traces have nearly similar

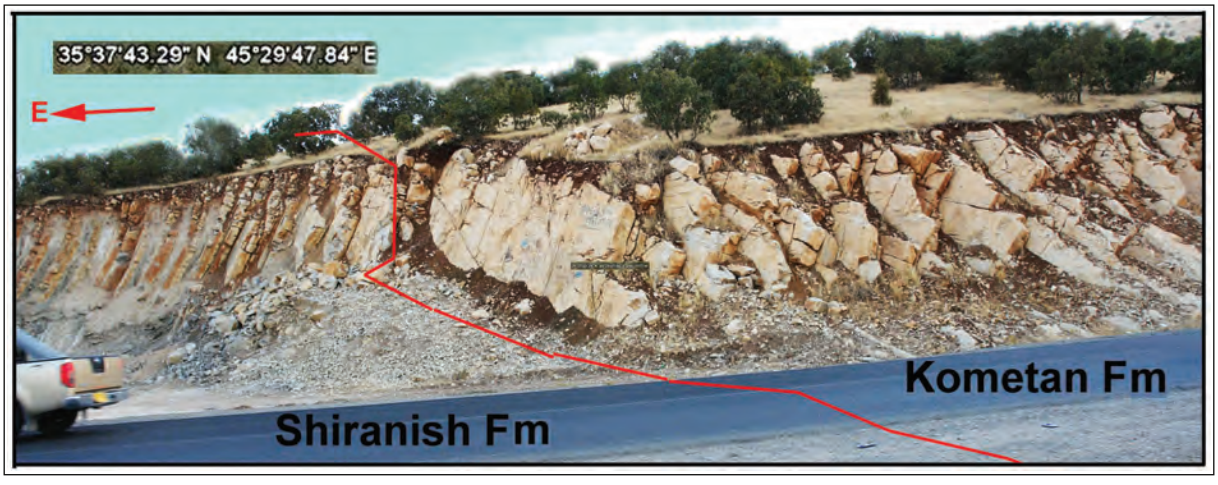

Figure 8- Gradational boundary between Kometan and Shiranish Formation on northeastern limb of Azmir anticline, northeast of Sulaimani city shows alternation of well-bedded limestone and marl of the two formations.

Figure 9- spherical nodules are trailing the stylolite line along a vertical of a bed of Kometan Formation at 2 km southwest of Dokan town.

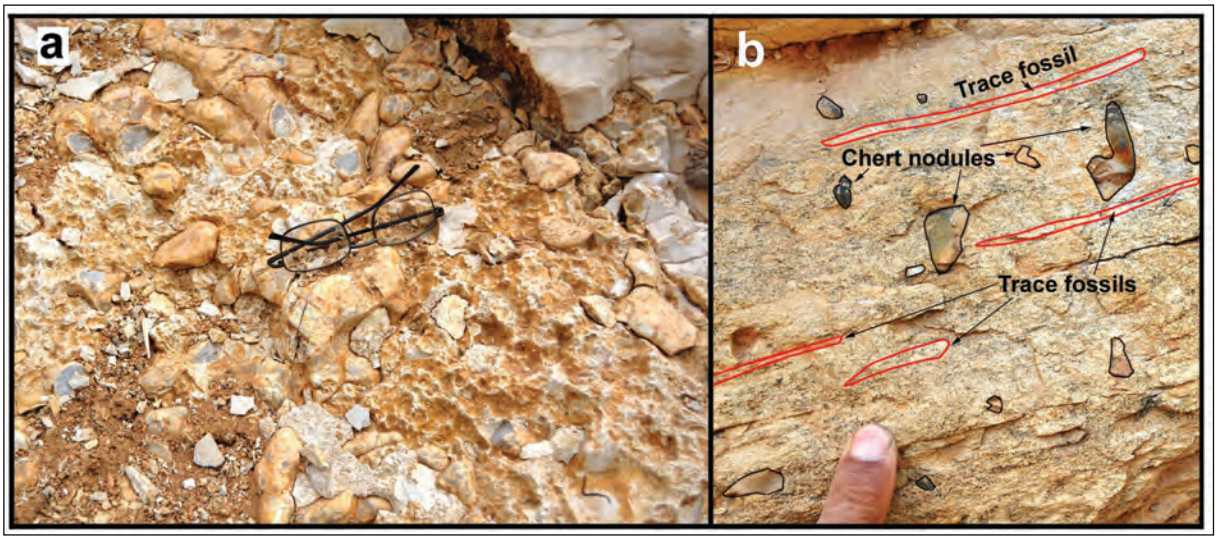

Figure 10- (a) Bedding surface shows stylolite peaks and pebble-sized chert nodules which are neither in shape nor in size related to *Thalassinoides* (b) A vertical section of a bed of glauconitic limestone at the top of Kometan Formation shows chert nodules lined vertical to the trace fossils (red lines).

sizes and shape of those located at the top of Kometan Formation. The shapes and size of chert nodules are highly variable in the formation, which are thinning or thickening suddenly and they coexist together (Figure 10 and 11). Thin section study in the present study and other studies of the present authors and others have not recorded fecal pellets and bioclasts. Why do all observed traces, (chert nodules) are not associated with fecal pellets? The answer to this question is that the nodules are not relatable to *Thalassinoides* in Kometan Formation.

In Europe Sieveking and Hart (2011) has collected many research articles in a book in which the relations between of chert nodules and *Thalassinoides* are documented. Some of these articles mentioned that the chert nodules are replacement of latter traces. The authors such asBromely (1967); Bromley and Ekdale (1984) found many evidence of relation between the latter nodules and traces. The evidences are such as nodule digitation, gradation from pure to partially silicified traces and lamellae of spreites in addition to spires around nodules and *Thalassinoides* activities boxworks.

In chalky limestone of Zagros (Kometan Formation), the authors have not found above features since the shapes and external sculpture of the European chert are different from ones of the present study. Moreover than that the present ones are associated

Figure 11- Various shape and sizes of chert nodules in Kometan Formation in Dokan area, (a) top view on the bedding plane, and (b) cross section view.

with stylolites and in literature Wangen (2010, p.369) discussed the silica concentration (development of chert nodules) by stylolization due to increase of local silica concentration.

The eighth criticism is presence of chert beds and lamination inside the Kometan Formation in many places (Figure 12). These sedimentary structures are visible clearly around Sharazoor plain where Al-Khafaf, (2014) has well studied the formation. These beds have thickness of 3-7 cm and continuous for ten of meters. The color of bedded chert is back or dark brown and not showing signs of nodules content (Figure 12). Therefore, the attributions of the chert nodules to replacement of *Thalassinoides* are disagreeing with bedded chert and indicate that chert, as nodules or beds, are a property of Kometan Formation and has not related to the *Thalassinoides*.

The ninth issue is widely using of Kometan Formation for building stone inside Sulaimani city. The quarries were usable for more than 50 years (called Sherkozh quarries) and located directly to the northwest of city in the Chachaq valley. In the city and the quarries, vast fractured and exposed surfaces are available for accurate study. The critique is on these surfaces, neither trace fossils nor high amplitude stylolites are observable and instead, randomly distributed pyrite nodules are common but they are unrelated to bedding planes or *Thalassionides* (Figure 13). The inter-beds clayey or marly materials are full of small pyrite crystals.

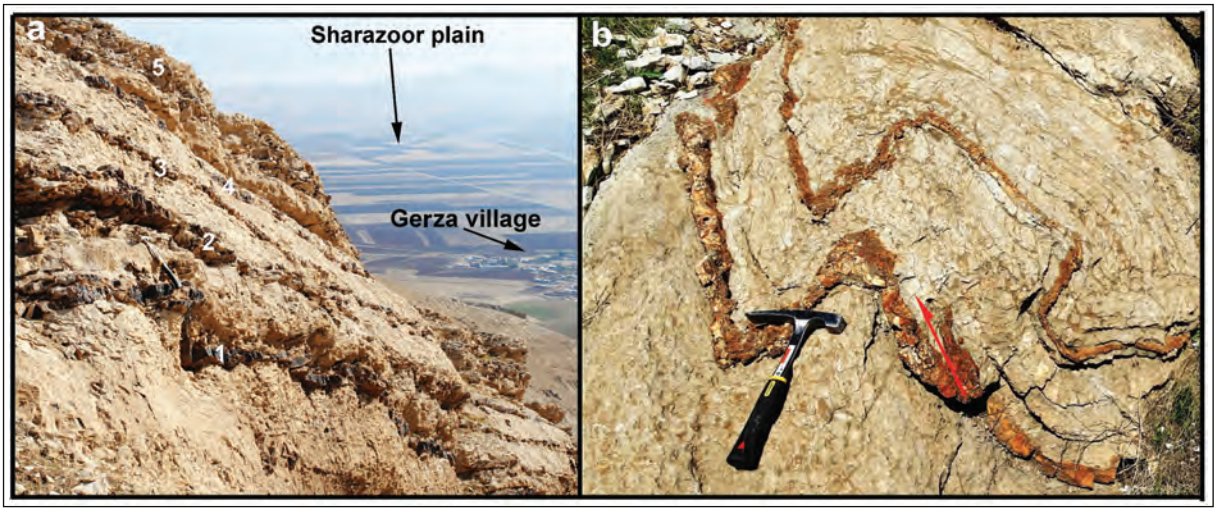

Figure 12- (a) Occurrence of five chert beds in an interval of 3m thick inside Kometan Formation on Greza Mountain. (b) Two folded chert beds in the latter formation near Said Sadiq town

Figure 13- (a) Weathered and (b) fresh nodules of pyrite inside Kometan Formation directly at the west of Sulaimani city (Sherkozh Quarries).

3.2. Tectonic Setting of Zagros Chalky Limestone (Kometan Formation)

There are agreement among researchers that the New Tethys sea (or ocean) is tectonically divided to oceanic and foreland basin episodes (Alavi 2004, Karim, 2004; Karim, and Surdashy, 2005; Jassim and Goff, 2006). The tectonic position of Kometan Formation within two episodes is controversial since some authors put the formation in the foreland basin while others placed it on continental margin of oceanic episode. Taha and Karim (2009), Karim (2013) and Karim et al. (2016) have put Kometan Formation on continental margin of New Tethys Ocean in a pre-obduction (collision) phase. On the other hand, Al-Qayim, et al. (2012) and Lawa et al. (2011 in Al-Hakari, 2011) have cited that the foreland had developed before Turonian, which means that Kometan Formation deposited in the foreland episode.

Based on absence of fossils, Omer et al. (2015) indicated an unconformity that represented by disappearance of Dokan (late Cenomanian) and Gulneri Formations (Early Turonian). This research further added that during this unconformity ophiolite had obducted on Arabian passive margin. During the early Turonian, Lawa et al. (2011 in Al-Hakari, 2011) have mentioned that the Qulqula Radiolarian and main igneous complexes were uplifted and acted as Hinterland for Kuudistan Foreland basin. Under the title of "Turonian (base-AP9) Unconformity" Lawa et al. (2013, p81) documented an unconformity formed as a result of uplift associated with the emplacement of allochthonous thrust sheets (Mawat ophiolites, Qulqula Group and Avroman Limestone) over the Arabian passive margin. They further added that thrust loading resulted in the formation of the North foreland basin in which Kometan Formation has deposited (see p92 of latter article). However, Lawa (2018, p13) opposed his earlier ideas and mentioned that the obduction occurred during Middle Campanian which previously conformed by Taha and Karim (2009, Figure 15a).

The present study does not agree with above timing of the Foreland basin since it had developed after

Figure 14- Gulneri Formation along road cut on Salta Re hill at 3 km north of Sulaimani City, it consists of grey marly limestone and laminated red marl

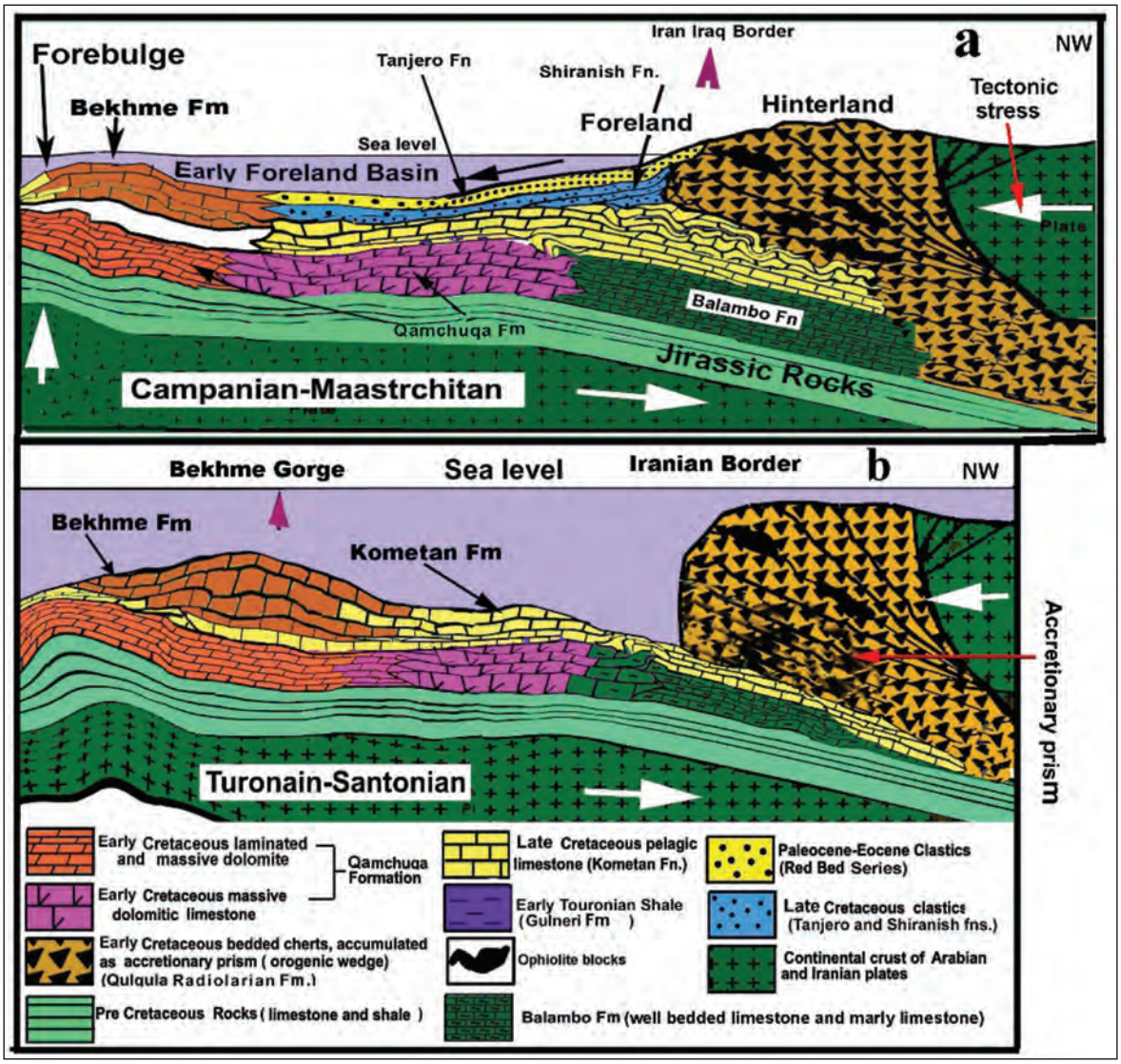

Figure 15- Tectonic mode shows deposition of Kometan Formation on continental margin of Neo-Tethys Ocean (a) before generation of Foreland basin (b), modified from Taha and Karim (2009) and Karim (2013).

deposition of Kometan Formation (during Campanian-Maastrichtian) (Figure 15). This timing aided by many paleontological and sedimentological evidences such 500 m boulder and gravel conglomerate with red clastics that deposited during Maastrichtian and studied by Karim (2004), Karim, and Surdashy (2005) and Karim et al. (2013).

Paleontologically, Khafaf, (2014), Karim et al. (2013) and Karim et al. (2016) concluded that both Dokan and Gulneri Formation are occurring in all area of northeastern Iraq and there is no unconformity in the sequence of Upper Cretaceous (Figure 14, 15 and 16). Baziany (2014) found the radiolarian of Cenomanian inside Qulqula Radiolarian Formation at Chwarta area, which mentioned continuous deposition of radiolarites (very deep facies) up to middle Cenomanian. In this connection, Ali et al. (2016) have aged crystallization ofKata Rash volcanic rocks, in Penjween area, to be Albian in Supra Subduction Zone setting. They added that it crystalized in the Neotethys Ocean rather than at a continental margin. Thus the Ophiolite obduction during Cenomanian, in northern Iraq, does not agree with result of Ali et al (op cit).

There are three other facts that do not aid deposition of the Kometan Formation during foreland episode. The first one is deposition of similar facies (Chalk Group) in Europe during Cenomanian (Mortimore, 2001) and more before development of Foreland basin in Europe. In Iran, Razin et al. (2010) did not record unconformity during study of the sequence stratigraphy of the Cenomanian and Turonian. The study added that the thickness of the Late Cenomanian-Early Turonian rocks ranges 15-35 m and consist of bioclastic facies of platform margin and intra-shelf basinal facies. In Syria Ghanem and Kuss (2013) record the biozones of the boundary of the latter two ages. The second fact is that no one has shown photo or direct evidence to indicate unconformity below Kometan Formation. The third fact is that in the field the present authors - distinguished easily the presence of Gulneri and Dokan Formations (Figure 14).

4. Conclusions

1- The previous studies attributed presences of extensive chert nodules to replacement of *Thalassinoides*, however, the present study does not aid this replacement.

2- The previous massiveness of the Turonian-Middle Campanian chalky limestone is refused and changed to the well bedding.

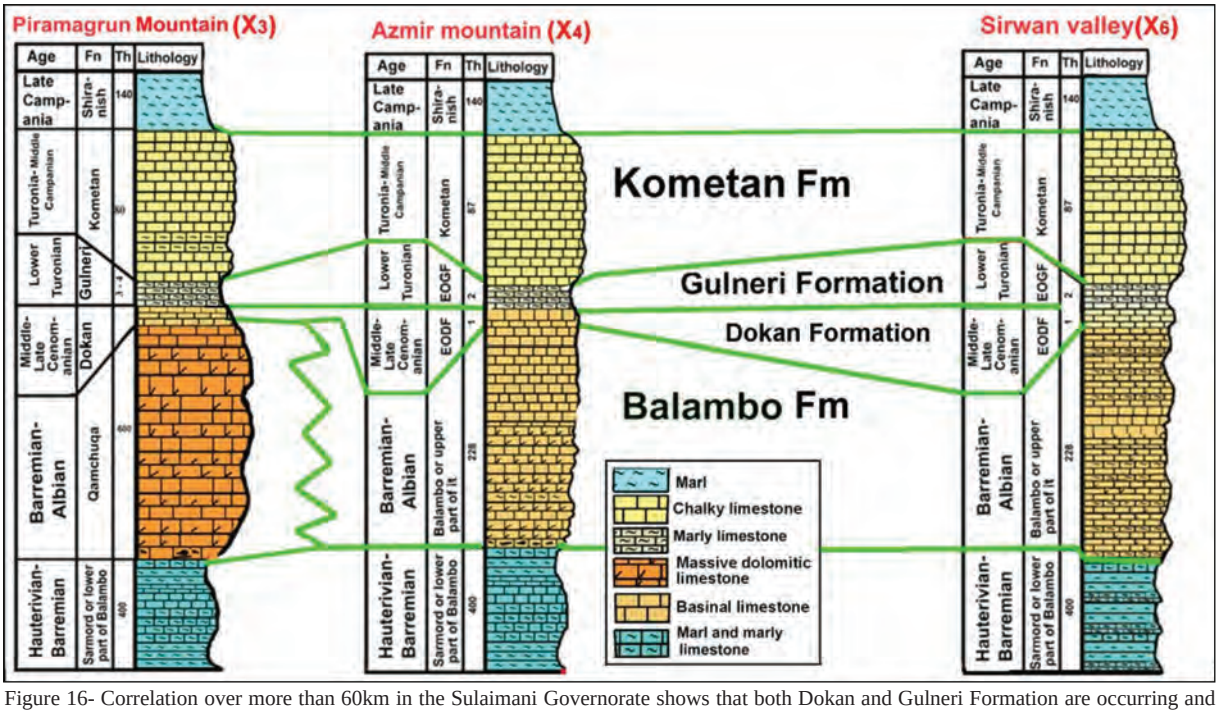

Figure 16- Correlation over more than 60km in the Sulaimani Governorate shows that both Dokan and Gulneri Formation are occurring and absence of unconformity. On the figure 1, the sections are indicated by X_3, X_4 and X_6 for Piramagrun, Azmir and Sirwan valley sections respectively.

3- The chert nodules and stylolites are formed during burial of the rocks and not related to *Thalassinoide burrow* .

4- The depositional well bedding property of Kometan Formation is intrinsic characteristic of the formation in its entire outcrops without exception and differentiable from pseudo-bedding.

5- In addition of nodules, Kometan Formation contains beds and laminae of chert.

6- Kometan Formation has deposited on continental margin of Neo-Tethys Ocean (sea) not in Zagros Foreland Basin as cited by many previous researchers.

References

Alavi, M. 2004. Regional Stratigraphy of the Zagros Fold-Thrust Belt of Iran and Its Proforeland Evolution, American Journal of Science, 304: 1-20.

Al-Ameri, T.K. 2011. Khasib and Tannuma oil sources, East Baghdad oil field, Iraq, Marine and Petroleum Geology, 28(4): 880-894.

Al-Badrani, O.A., Karim, K.H., Ismail, K.M. 2012. Nannofossils biozones of contact between Kometan and Shiranish Formations, Chaqchaq Valley, Sulaimanyia, NE- Iraq. Iraqi Bulletin of Geology and Mining, 8(1): 19-29.

Al-Barzinjy, S.T. 2008. Origin of chert nodules in Kometan Formation from Dokan area, Northeast Iraq. Iraqi Bulletin of Geology and Mining, 4(1): 95-104.

Al-Hakari, S.H.S. 2011. Geometric Analysis and Structural Evolution of NW Sulaimani Area, North Region, Iraq. Unpublished PhD Thesis, University of Sulaimani, 309p.

Alhamdani, A.M. 2015. Pseudo-bedding and burrow silicification in the Kometan Formation of the Dokan area, Northeastern Iraq. Arab J Geosci, 8:325–333.

Ali, S. A., İsmail, S.A., Nutman, A. P., Bennett, V. C., Jones, B. G., Buckman, S. 2016. The intra-oceanic Cretaceous (~108 Ma) Rata–Rash arc fragment in the North segment of Iraqi Zagros suture zone: Implications for Neo-Tethys evolution and closure, Lithos 260: 154–163.

Al-Khafaf, A. O. 2014. Biostratigraphic contribution to the differentiation of the Lower-Middle Cretaceous units in the Imbricated Zone of Sulaimani Governorate, North Region, NE Iraq, PhD thesis, University of Sulaimani, 230p.

Al-Qayim, B. 2012. Foreland Basin System of the Northeastern Arabian Margin, North Region, Iraq ; Impact on Oil Accumulations, EAGE Workshop on Iraq, Hydrocarbon Exploration & Field Development, IR03,Istanbul,Turkey, (earthdoc.eage.org/publication/-download/?publication=58878).

Al-Qayim, B., Ömer, A., Koyi, H. 2012. Tectonostratigraphic overview of the Zagros Suture Zone, North Region, Northeast Iraq, GeoArabia, 17(4):109-156.

Arthur, M.A., Bottjer, D.J., Dean, W.E., Hattin, D.E., Kauffman, E.G., Pratt, L.M., Scholle, P.A. 1986. Rhythmic bedding in Upper Cretaceous pelagic carbonate sequences: Varying sedimentary response to climatic forcing. Geology, 14 (2): 153-156

Baziany, M.M. 2014. Depositional Systems and Sedimentary Basin Analysis of the Qulqula Radiolarian Formation of the Zagros Suture Zone, Sulaimani Area, Iraqi North Region. PhD Thesis, College of Science, University of Sulaimani, 200p.

Bellen, R.C.V., Dunnington, H.V., Wetzel, R., Morton, D. 1959. Lexique Stratigraphique, Interntional. Asie, Iraq, Vol. 3c. 10a, 333p.

Bromley, R. G. 1967. Some observations on burrows of Thalassinidean Crustacea in chalk hardgrounds. Geological Society of London Quarterly Journal, 123:157-182.

Bromley, R.G., Ekdale, A. A. 1984. Trace fossil preservation in flint in the European chalk, Journal of Paleontology, 58(2): 298-311.

Buday, T. 1980. the Regional Geology of Iraq, Volume 1: Stratigraphy and Paleogeography, Kassab II.M and Jassim SZ. (Eds.), GEOSURV, Baghdad, Iraq, 445p.

Ghafor, I.M., Karim, K.H., Baziany, M.M. 2012. Age determination and origin of crenulated limestone in the eastern part of Sulaimaiyah Governorate, North Region, NE-Iraq. Iraqi Bulletin of geology and Mining, 8 (2):21-30.

Ghanem, H., Kuss, J. 2013. Stratigraphic control of the Aptian–Early Turonian sequences of the Levant Platform, Coastal Range, northwest Syria, GeoArabia, Gulf PetroLink, Bahrain, 18(4): 85-132.

Giannetti, A., Monaco, P., Caracuel, J.E., Soria, J.M., Yébenes, A. 2007. Functional morphology and ethology of decapod crustaceans gathered by Thalassinoides branched burrows in Mesozoic shallow water environments.3rd Symposium on Mesozoic and Cenozoic Decapod Crustaceans -

Museo di Storia Naturale di Milano, Volume 35, Fascicolo 2.

Hadavi, F., Moghaddam, M. N. 2011. Calcareous nannofossils from chalky limestone of upper Abderaz Formation and lower part of Abtalkh Formation in the Kopet-Dogh range NE Iran, Arabian Journal of Geosciences 4(7): 1041–1049.

Jassim, S.Z., Goff, J.C. 2006. Geology of Iraq. Dolin, Prague and Moravian Museum, Berno. 341pp.

Karim, K.H. 2004. Basin analysis of Tanjero Formation in Sulaimaniya area, NE-Iraq, PhD thesis, University of Sulaimani, 135p.

Karim, K.H. 2013. New geologic setting of the Bekhme Formation. Journal of Zankoy Sulamani (JZS), 15 (3): 23-38.

Karim, K.H., Surdashy, A.M. 2005. Tectonic and depositional history of Upper Cretaceous Tanjero Formation in Sulaiumanyia area, NE-Iraq. Journal of Zankoy Sulaimani, 8(1):1-20.

Karim, K.H, Lawa FA., Ameen, BM. 2001. Upper Cretaceous Glauconite filled boring from Dokan area. North Region (NE-Iraq), North Acadimician Journal (KAJ) 1 (1): 1-10.

Karim, K.H., İsmail, K. M., Ameen, B.M. 2008. Lithostratigraphic study of the Contact between Kometan and Shiranish Formations (Upper Cretaceous) from Sulaimani Governorate, North Region, NE-Iraq. Iraqi Bulletin of Geology and Mining 4 (2): 16 -27.

Karim, K.H., Koyi, H., Baziany, M.M., Hessami, K. 2011. Significance of angular unconformities between Cretaceous and Tertiary strata i n t he northwestern segment of the Zagros fold–thrust belt, North Region, NE- Iraq. Geological Magazine, Cambridge University Press, 148 (5-6):925-939.

Karim, K.H., Al-Hamadani, R.K., Ahmad, S.H. 2012. Relations between deep and shallow stratigraphic units of the Northern Iraq during Cretaceous. Iranian Journal of Earth Sciences, Islamic Azad University, Mashhad Branch, 4(2): 93-103.

Karim, K.H., Salih, A.O., Ahmad, S.H. 2013. Stratigraphic Analysis of Azmir-Goizha anticline by Nannofossils. Journal of Zankoy Sulamani (JZS), 15 (2):103-124.

Karim, K.H., Al-Khafaf, A.O., Sharbazheri, K.I. 2016. Critical analysis of the type section of the Balambo Formation (Valanganian-Turonian), Sirwan valley, North Region, NE-Iraq, Journal of Zankoy Sulaimani – Part A, special issue.

Kennedy, W. J. 1967. Burrows and surface traces from the Lower Chalk of Southern England. Bulletin of the British Museum (Natural History) Geology, London. 15 (3):127-166.

Lawa, F. A. 2008. Late Campanian–Maastrichtian sequence stratigraphy from Northforeland basin, NE/Iraq, Journal of Petroleum Exploration and Production Technology, https://doi.org/10.1007/s13202-017-0424-1.

Lawa, F.A., Gharib, H. 2010. Cretaceous Sequence Stratigraphy of Western Zagros Outcrops from North Region, N. Iraq. AAPG GEO 2010 Middle East Geosciences Conference & Exhibition March 7-10, 2010–Manama, Bahrain (only abstract available).

Lawa, F.A., Koyi, H., Ibrahim, A. 2013. Tectono-stratigraphic evolution of the NW segment of the Zagros fold-thrust Belt, North, NE Iraq. Journal of Petroleum Geology 36 (1): 75–96.

Mangen, W. 2010. Physical principles of Sedimentary basins analysis, Cambrigde University Press, p.379.

McCall,1982. Animal-Sediment Relations: The Biogenic Alteration of Sediments. Springer Science & Business Media, Nov 11 - Science - 336 p.

Mehmandosti, E. A., Adabi, M. H., 2008. Microfacies and geochemistry of the Ilam Formation in the Tang-E Rashid area, Izeh, S.W. Iran. Journal of Asian Earth Sciences, 33: 267–277.

Mortimore, R.N., Wood, C.J., Gallois, R.W. 2001. British Upper Cretaceous Stratigraphy, Geological Conservation Review Series, No. 23, Joint Nature Conservation Committee, Peterborough, 558 pages, see: http://www.jncc.gov.uk/page-2969.

Mülayim, O., Mancini, E., Çemen, İ., Yılmaz, İ. Ö. 2015. Upper Cenomanian-Lower Campanian Derdere and Karababa formations in the Çemberlitaş oil field, southeastern Turkey: their microfacies analyses, depositional environments, and sequence stratigraphy, Turkish Journal of Earth Sciences, 24: 1-17.

Myrow, P.M. 1995. Thalassinoides and the Enigma of Early Paleozoic Open-Framework Burrow Systems. PALAIOS, 10: 58-74.

Omar, A.A., Lawa, F.A., Sulaiman, S.H. 2015. Tectonostratigraphic and structural imprints from balanced sections across north-western Zagros fold-thrust belt, North Region, NE Iraq. Arab J Geosci. 8 (10):8107-8129

Pak, R., Pemberton, S.G. 2003. Ichnology of the Yeoman Formation; in Summary of Investigations, Volume 1, Saskatchewan Geological Survey.

Razin, P. Taati, F., van Buchem, F.S.P. 2010. An outcrop reference model for the Arabian Plate platform margins (Sarvak Formation) in the High Zagros, SW Iran: Sequence stratigraphy of Cenomanian-Turonian carbonate. Geological Society, London, Special Publications, 329: 187-218

Sarı, B., Özer, S. 2002. Upper Cretaceous stratigraphy of the Beydagları carbonate platform, Korkuteli area (Western Taurides, Turkey). Turkish Journal of Earth Sciences 11: 39-59.

Sarı, B., Steuber, T., Özer, S. 2004. First record of Upper Turonian rudists (Mollusca, Hippuritoidea) in the Bey Dağları carbonate platform, Western Taurides (Turkey): taxonomy and strontium isotope stratigraphy of Vaccinites praegiganteus (Toucas, 1904). Cretaceous Research, 25: 235-248.

Sieveking, G. de G., Hart, M. B. 2011.The Scientific Study of Flint and Chert: Proceedings of the Fourth International Flint Symposium, Cambridge University Press, 306pp.

Sissakian, V.K. 2000. Geological map of Iraq. Sheets No.1, scale 1:1 000 000, 3rd edit., GEOSURV, Baghdad, Iraq.

Stevens, T., Paull, C.K., Ussler W.I.I., McGannn, M., Buylaert. J.P., Lundsten, E. 2014. The timing of sediment transport down Monterey Submarine Canyon, offshore California. Geological Society of America. Bulletin, 126(1-2): 103-121.

Taha, Z. 2008. Sedimentology of Late Cretaceous Formation from North Region, NE−Iraq, Unpublished, M.Sc thesis, University of Suilaimani.150 pp.

Taha, Z.A., Karim, K.H. 2009. Tectonical history of Arabian platform during Late Cretaceous An example from North region, NE Iraq. Iranian Journal of Earth Sciences, 1(1): 1-14.

Walness, H.R. 1979. Limestone response to stress: Pressure solution and dolomitization. Journal of Sedimentary Petrology, 49(2): 436 – 462.

Wangen, M. 2010. Physical principles of sedimentary basin analysis, Cambridge University Press.

Bulletin of the Mineral Research and Exploration

http://bulletin.mta.gov.tr

Petrography, mineral chemistry and crystallizatıon conditions of cenozoic plutonic rocks located to the north of Bayburt (Eastern Pontides, Turkey)

Abdullah KAYGUSUZ[a*], Cem YÜCEL[b], Mehmet ARSLAN[c], Ferkan SİPAHİ[d], İrfan TEMİZEL[e], Gökhan ÇAKMAK[f] and Z. Samet GÜLOĞLU[g]

[a]*Gümüşhane University, Department of Geological Engineering, Gümüşhane. orcid.org/0000-0002-6277-6969*
[b]*Gümüşhane University, Department of Mining Engineering, Gümüşhane. orcid.org/0000-0001-7220-9397*
[c]*Karadeniz Technical University, Department of Geological Engineering, Trabzon. orcid.org/0000-0003-0816-4168*
[d]*Gümüşhane University, Department of Geological Engineering, Gümüşhane. orcid.org/0000-0002-4072-4834*
[e]*Karadeniz Technical University, Department of Geological Engineering, Trabzon. orcid.org/0000-0002-6293-8649*
[f]*Bayburt Provincial Special Administration, Directorate of Water and Channelisation Services, Bayburt. orcid.org/0000-0001-6991-0545*
[g]*Gümüşhane University, Department of Geological Engineering, Gümüşhane. orcid.org/0000-0002-7171-6810*

Research Article

Keywords:
Mineral chemistry, geothermobarometer, Cenozoic plutonic rocks, eastern Pontides, Bayburt, Turkey.

ABSTRACT

The Eastern Pontides comprise many intrusive bodies varying in composition, size and age from Palaeozoic to Cenozoic. Especially Cenozoic aged bodies are commonly observed in the southern part, while they are rarely exposed in the northern part of the Eastern Pontides. In this study, the petrography and mineral chemistry of the Cenozoic aged Çiçekli, Somarova, Sorkunlu, Şaşurluk, Aydıntepe, Kemerlikdağı and Pelitli plutons located to the north of Bayburt are determined, and the crystallisation conditions of the studied bodies were estimated by means of thermobarometer calculations. The studied plutons extend mostly in NE-SW directions and are approximately ellipsoid in shape. The contacts between the plutons and surrounding rocks are sharp, and plutons commonly contain mafic microgranular enclaves (MMEs) of different sizes. Petrographic and mineral chemistry studies reveal some disequilibrium textures reflecting the magma mixing process. Based on modal mineralogy, the plutonic rocks are gabbroic diorite, diorite, tonalite, granodiorite and monzogranite in composition. The rocks have fine to medium granular, porphyric, monzonitic, poikilitic, occasionally myrmekitic and micrographic textures. The main minerals are labradorite and albite (An_{68-02}), magnesiohornblende and actinolite (Mg# = 0.6-0.9), diopside and augite (Wo_{44-46}), clinoenstatite (En_{53-57}) and Fe-Ti oxide minerals. Crystallization temperatures calculated from amphibole, biotite, clinopyroxene, magnetite and ilmenite minerals are 405°C to 1161°C, pressure values are 0.1 to 2.7 kbar, and oxygen fugacity (log10 fO_2) is -20 to -12. Estimation of water content calculated by using amphiboles is between 2.9 and 6.8%. Based on obtained data, it is suggested that the studied plutons were emplaced at shallow depths (~ 1-8 km).

Received Date: 18.06.2017
Accepted Date: 09.04.2018

1. Introduction

The Eastern Pontides (NE Turkey), located within the Alpine-Himalayan orogenic belt, are a significant area where volcanic and plutonic rocks are commonly observed (Arslan et al., 2000, 2013; Kaygusuz et al., 2006; Kaygusuz, 2009; Saydam Eker et al., 2012; Aslan et al., 2014; Sipahi et al., 2014; Aydınçakır, 2014; Alemdağ, 2015; Temizel et al., 2012, 2016; Kaygusuz and Şahin, 2016; Özdamar, 2016; Yücel et al., 2014, 2017). There are numerous various sized plutons in the region with a broad age range varying from Permo-Carboniferous to Eocene in the region and types varying from mainly gabbro to granite (Figure 1). These plutons intruded mainly at three different time period including Paleozoic, Cretaceous and Eocene. Of these Palaeozoic-aged plutons intruded

* *Corresponding author: Abdullah KAYGUSUZ, abdullah.kaygusuz@gmail.com*
http://dx.doi.org/10.19111/bulletinofmre.427829

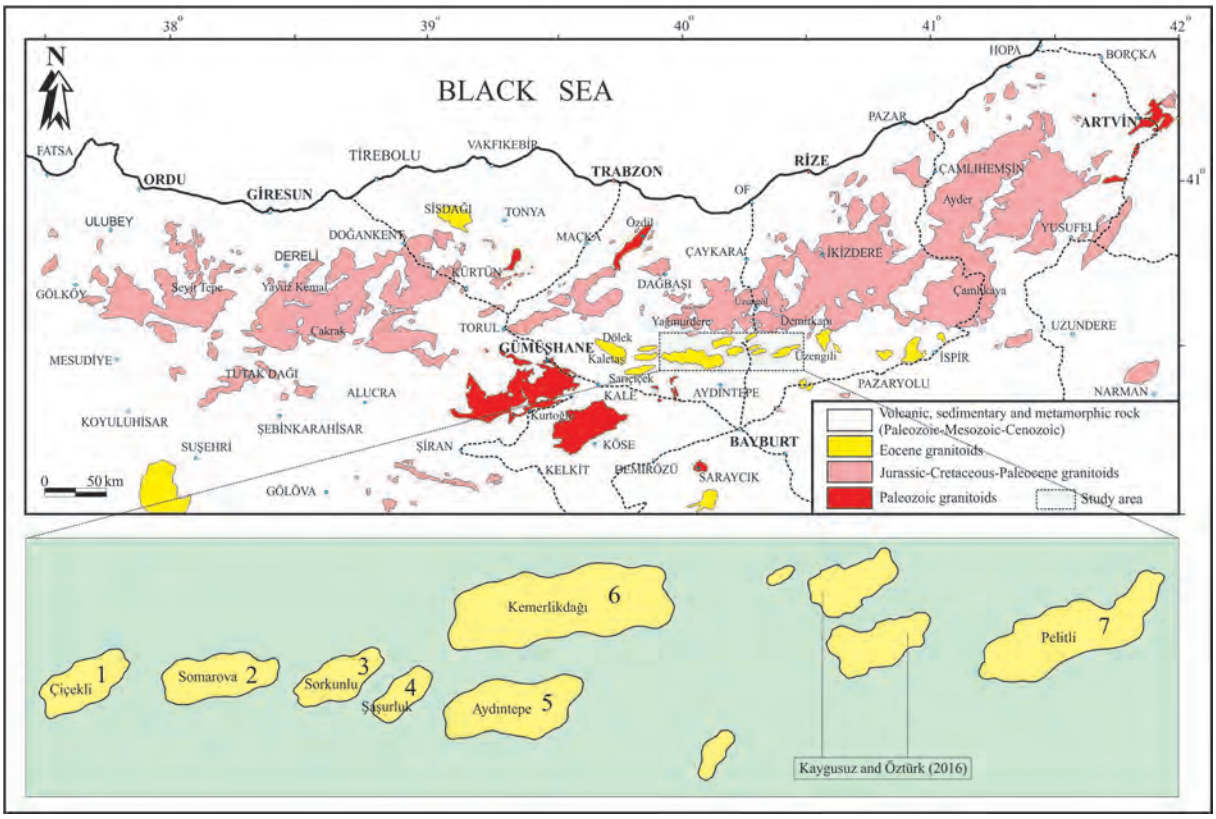

Figure 1- Geologic map showing distribution of Cenozoic-aged plutons in the Eastern Pontides and investigated plutons (1: Çiçekli, 2: Somarova, 3: Sorkunlu, 4: Şaşurluk, 5: Aydıntepe, 6: Kemerlikdağı, 7: Pelitli) (based on 1/500,000 scale MTA map).

into the metamorphic rocks (Yılmaz, 1972; Çoğulu, 1975; Topuz et al., 2010; Dokuz, 2011; Kaygusuz et al., 2016; Karslı et al., 2017), Cretaceous plutons intruded into the subduction-related volcanic and/or volcanoclastic rocks (Köprübaşı et al., 2000; Şahin et al., 2004; Boztuğ et al., 2006; İlbeyli, 2008; Kaygusuz et al., 2010, 2013; Karslı et al., 2010; Kaygusuz and Aydınçakır, 2011; Kaygusuz and Şen, 2011; Sipahi et al., 2017), and Eocene and later plutons are intruded in a narrow area cutting all former series (Yılmaz and Boztuğ, 1996; Aslan et al., 1999; Topuz et al., 2005; Arslan and Aslan, 2006; Karslı et al., 2007; Kaygusuz and Öztürk, 2015; Eyüboğlu et al., 2013, 2017; Özdamar et al., 2017).

There are limited studies about Eocene-aged plutons in the Eastern Pontides (Figure 1), where the age of many plutons relatively identified according to contact relations and stratigraphic relationships. The age of the Saraycık Pluton situated south of the study area was determined as 66 Ma (Rb-Sr, Aslan, 1998) and 52 Ma (Ar-Ar, Topuz et al., 2005); in the west of the study area, the age of the Kaletaş Pluton is 44 Ma (U-Pb, Arslan and Aslan, 2006), the age of the Dölek Pluton is 44 Ma (U-Pb, Arslan and Aslan, 2006), with ages of the Dölek and Sarıçiçek plutons 42-43 Ma (K-Ar, Karslı et al., 2007) and the age of the Sarıçiçek Pluton is 44 Ma (U-Pb, Eyuboğlu et al., 2017).

The Eocene-aged intrusive rocks located within the area of the studied plutons were named the Rize Pluton by Keskin et al. (1989) and Önenç et al. (2005). Çakmak and Kaygusuz (2014), reported the age of the Pelitli Pluton as 46 Ma (U-Pb). Kaygusuz and Öztürk (2015) reported the age of the Kılıçkaya and Kozluk Plutons located in the study area as 46 Ma (U-Pb). Eyuboğlu et al. (2017) reported the age of the Sorkunlu Pluton as 44 Ma (U-Pb), the age of the Üzengili Pluton as 45 Ma (U-Pb) and the age of the Kozluk Pluton as 44 Ma (U-Pb).

The aim of this study is to determine the petrographic and mineral chemistry features of the Cenozoic-aged plutonic rocks outcropped north of Bayburt, and to determine thermobarometer conditions (pressure (P) – temperature (T)) during the crystallisation of the pluton with mineral chemistry data and to contribute to the literature about emplacement conditions.

2. Geological Setting and Field Characteristics of Plutons

The basement of the study area, located south of the Eastern Pontides and dominated by generally sedimentary, volcanic and plutonic rocks, is formed by conglomerates, marl, shale, sandstone, siltstone, tuff, tuffite, and red-coloured fossiliferous limestones along with acidic-basic lava, dykes and sills of the Liassic-aged Hamurkesen formation (Ağar, 1977). The Hozbirikyayla formation, comprising Dogger-Malm-Lower Cretaceous-aged oolitic limestone, dolomitic limestones, sandy limestone, limestone with sandstone-siltstone interlayers, carbonates with chert bands and nodules, conformably overlies this formation (Ağar, 1977). The Upper Cretaceous-aged Çatıksu formation, comprising sandstone, pelagic limestone, mudstone and claystone alternations overlies the Hozbirikyayla formation with an angular unconformity (Keskin et al., 1989). The Arduç Volcanic rocks comprising Upper Cretaceous andesite and basalt lavas, andesitic-basaltic agglomerates, tuff and tuffite (Keskin et al., 1989) lies above the Çatıksu formation. The Eocene-aged Sırataşlar formation comprising nummulitic limestone, sandstone, occasional marl and sandy limestone, unconformably overlies the Arduç Volcanic rocks (Ağar, 1977). The Ypresian-Lutetian-aged andesite-basalt lavas, andesitic-basaltic agglomerates and tuff alternations of the Yazyurdu formation (Keskin et al., 1989) unconformably overlie the Sırataşlar formation. The Cenozoic-aged plutonic rocks cut the Yazyurdu formation (Figure 3) and the youngest unit in the study area is Quaternary-aged alluvium (Figure 2).

The long axes of the studied plutons extend in the northeast-southwest direction and are generally ellipse in shapes (Figure 2). Çiçekli and Somarova plutons contain small sized (0.5-2 cm) and minor amount of mafic microgranular enclaves; whereas Sorkunlu, Şaşurluk, Aydıntepe, Kemerlikdağı and Pelitli plutons contain large amounts of angular, partially rounded mafic magmatic enclaves ranging in size from 1 to 10 cm. The enclaves are finer grained and darker than the host rock.

The Çiçekli Pluton outcrops over an area of about 6 km^2, with 3-4 km length and 1-2 km width. The pluton intruded into the Eocene-aged Yazyurdu formation at northern boundary, while intruded into the Upper Cretaceous-aged Arduç Volcanic rocks at the east-west and southern boundaries (Figure 2 and 3a). At contacts with the wall rocks, volcanic rocks have been transformed to metavolcanics, while at contacts with sedimentary rocks, limestone has been transformed into crystallised limestone and occasionally marble. The Somarova Pluton, which extends an area of about 8 km^2 (4-5 km in length, 2-3 km in width), cuts the Eocene-aged Yazyurdu formation at north- northwest boundary, and cuts the Upper Cretaceous-aged Arduç Volcanic rocks at the south-southeast boundary (Figure 2 and 3b). The Sorkunlu Pluton is of the same size as the Çiçekli Pluton, with length of 3-4 km and width of 1-2 km (about 6 km^2). The pluton cuts the Eocene-aged Yazyurdu formation at the northern boundary, cuts the Upper Cretaceous-aged Arduç Volcanic rocks at the east-west boundary, and cuts the Liassic-aged Hamurkesen formation at the southern boundary (Figure 2 and 3c).

The Şaşurluk Pluton has the smallest size of these intrusive rocks, and outcrops about 3 km^2 area (2-3 km long, 1-2 km wide). The pluton cuts Eocene-aged Yazyurdu formation at its northern boundary, cuts

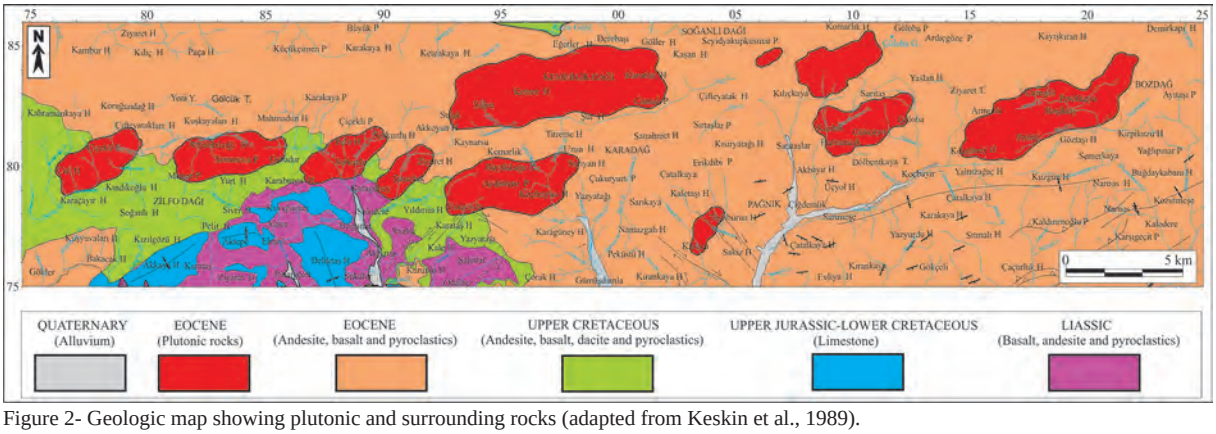

Figure 2- Geologic map showing plutonic and surrounding rocks (adapted from Keskin et al., 1989).

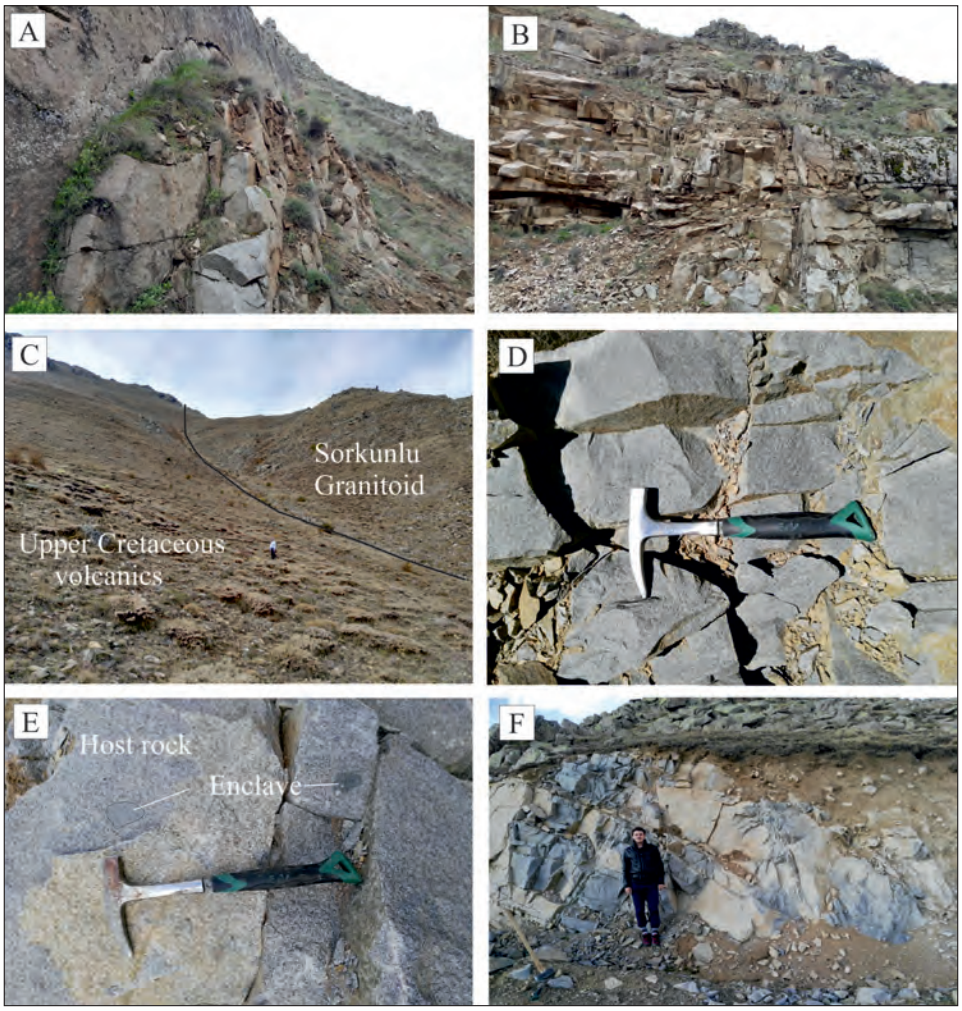

Figure 3- Field photograps of the studied plutonic rocks (a) Çiçekli, (b) Somarova, (c) Sorkunlu, (d) Aydıntepe, (e) Kemerlikdağı, (f) Pelitli.

Upper Cretaceous Arduç Volcanics at its east-west boundaries and cuts the Liassic-aged Hamurkesen formation at its southern boundary. The Aydıntepe Pluton outcrops over an area of about 12 km^2 with 5-6 km length and 2-3 km width. The pluton cuts the Eocene-aged Yazyurdu formation at the north-east and west edges, while cuts the Upper Cretaceous-aged Arduç Volcanic rocks at the south edge (Figure 2 and 3d). The Kemerlikdağı Pluton has the largest outcrop in the study area (nearly 22 km^2) with 7-8 km length and 2-3 km width. The pluton cuts the Eocene-aged Yazyurdu formation where the metavolcanics developed along contacts with volcanic wall rocks. The Pelitli Pluton outcropping over nearly 16 km^2 area, the length is 5-6 km with width of 3-4 km. The pluton cuts the the Eocene aged Yazyurdu formation with metavolcanics developed along the contacts (Figure 2 and 3f).

3. Analytical Methods

Under the scope of this study, thin sections were prepared from 450 rock samples obtained in the field and detailed petrographic characteristics were determined with a polarising microscope and modal analyses of 162 samples were performed. For modal analyses, in samples with grain size 0.5-0.8 mm 1000-1300 points were counted, and for samples with grain size 1.0-1.5 mm, 1300-1700 points were counted. Counted samples had counts calculated with the count error formulae and 8 samples had counts repeated.

Microprobe analyses performed on twenty samples from the studied intrusives at the Geology and Mineral Research Laboratory of the New Mexico Institute of Mining and Technology (USA). Microprobe analyses were performed on plagioclase, K-feldspar, biotite,

amphibole, pyroxene and Fe-Ti oxide minerals using a CAMECA-SX 100 brand microprobe-3 wavelength dispersive (WD) spectrometry device. The working conditions of the device were 15 kV voltage and 20 nA. Analyses were completed with a 10 µm laser diameter and the count time was fixed at 10 s for Si, Al, Ti, Fe, Mn, Mg, Ca, Na and K elements. Point laser of 1 µm was chosen for amphibole and pyroxene analyses. Considering sodium evaporation in feldspar and plagioclase analyses, very slightly defocused light (10 µm) was used to prevent or reduce losses to a minimum. During measurements, caersuitite (UCB), diopside (UCB), orthoclase (UCB), albite (UCB), anorthite (UCB), biotite and magnetite (UCB) standards were used.

4. Results

4.1. Petrography of Plutons

The general petrographic characteristics of the studied plutonic rocks are given in table 1, QAP diagrams based on modal analysis shown in figure 4. The zoning map prepared based on modal composition of rocks forming the plutons is shown in figure 5.

The modal analysis results of the samples from the Çiçekli Pluton show monzogranite, granodiorite and tonalite composition in the QAP diagram (Streickeisen, 1976) (Figure 4). Monzogranites are located in zones close to the centre of the pluton, while tonalite and granodiorite are located in the margin zones. Monzogranites cut granodiorite and tonalites, with less distribution (Figure 5a). The rocks of the Somarova Pluton are granodiorite, tonalite and diorite in composition (Figure 4). The granodiorites are mainly in the central zone, with diorites located around the edges. The granodiorites

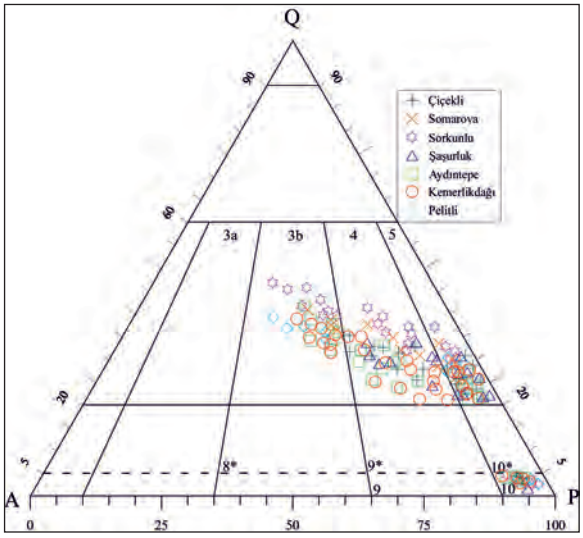

Figure 4- Location of rock samples from the plutons on QAP diagram (Streckeisen, 1976).

Table 1- General petrographic characteristics of studied plutonic rocks.

Pluton	Çiçekli (n=15)	Somarova (n=22)	Sorkunlu (n=19)	Şaşurluk (n=16)	Aydıntepe (n=34)	Kemerlikdağı (n=29)	Pelitli (n=27)
Rock unit	mg, gd, to	gd, to, di	gd, to, di, gbrdi	mg, to, di	mg, gd, to, di, gbrdi	mg, gd, to, di, gbrdi	mg, gd, to, di
Texture	granular, porphyric, monzonitic, poikilitic, myrmekitic	granular, porphyric, poikilitic, myrmekitic	granular, porphyric, poikilitic, myrmekitic, micrographic	granular, porphyric, monzonitic, poikilitic, myrmekitic, micrographic	granular, porphyric, monzonitic, poikilitic, myrmekitic, micrographic, graphic	granular, porphyric,, monzonitic, poikilitic, myrmekitic, micrographic, graphic	granular, porphyric, monzonitic, poikilitic, myrmekitic, micrographic
Grain size	fine-moderate, occasionally porphyric	fine-moderate, occasionally porphyric	fine-moderate, occasionally porphyric	fine-moderate, occasionally porphyric	fine-moderate, occasionally porphyric	fine-moderate, occasionally porphyric	fine-moderate, occasionally porphyric
Modal min (%)	min-max (mean)	min-max (mean)	min-max (mean)	min-max (mean)	min-max (mean)	min-max (mean)	min-max (mean)
Plagioclase	29-59 (46)	38-81 (57)	41-79 (55)	25-81 (53)	30-79 (53)	29-80 (52)	23-80 (51)
Quartz	21-37 (28)	3-31 (22)	1-29 (19)	2-37 (20)	2-37 (22)	3-38 (21)	2-46 (29)
Ortoclase	4-24 (11)	1-22 (9)	1-18 (7)	2-32 (11)	1-28 (13)	2-26 (12)	2-30 (12)
Amphibole	1-8 (3)	2-14 (7)	3-17 (9)	1-14 (7)	2-16 (7)	1-14 (8)	0-9 (4)
Biotite	4-10 (7)	1-5 (3)	1-10 (5)	1-9 (5)	1-10 (4)	1-10 (4)	0-5 (2)
Pyroxene	3-5 (4)	4 (4)	2-10 (5)	1-4 (3)	1-5 (3)	2-3 (3)	2-4 (3)
Opaque minerals	1-5 (2)	1-4 (2)	1-4 (2)	2-6 (3)	1-4 (2)	1-4 (3)	0-4 (2)
Accessory Minerals	apatite, zircon	apatite, zircon, sphene	apatite, zircon, sphene	apatite, zircon, sphene	apatite, zircon, sphene, allanite	apatite, zircon, sphene, allanite	apatite, zircon, sphene
Secondary Minerals	Sericite, chlorite, epidote, calcite, clay minerals	Sericite, chlorite calcite, clay minerals	Sericite, chlorite clay minerals	Sericite, chlorite clay minerals	Sericite, chlorite calcite, clay minerals	Sericite, chlorite calcite, clay minerals	Sericite, chlorite calcite, clay minerals
mg: monzogranite, gd: granodiorite, to: tonalite, di: diorite, gbrdi: gabbrodiorite, n: number of samples							

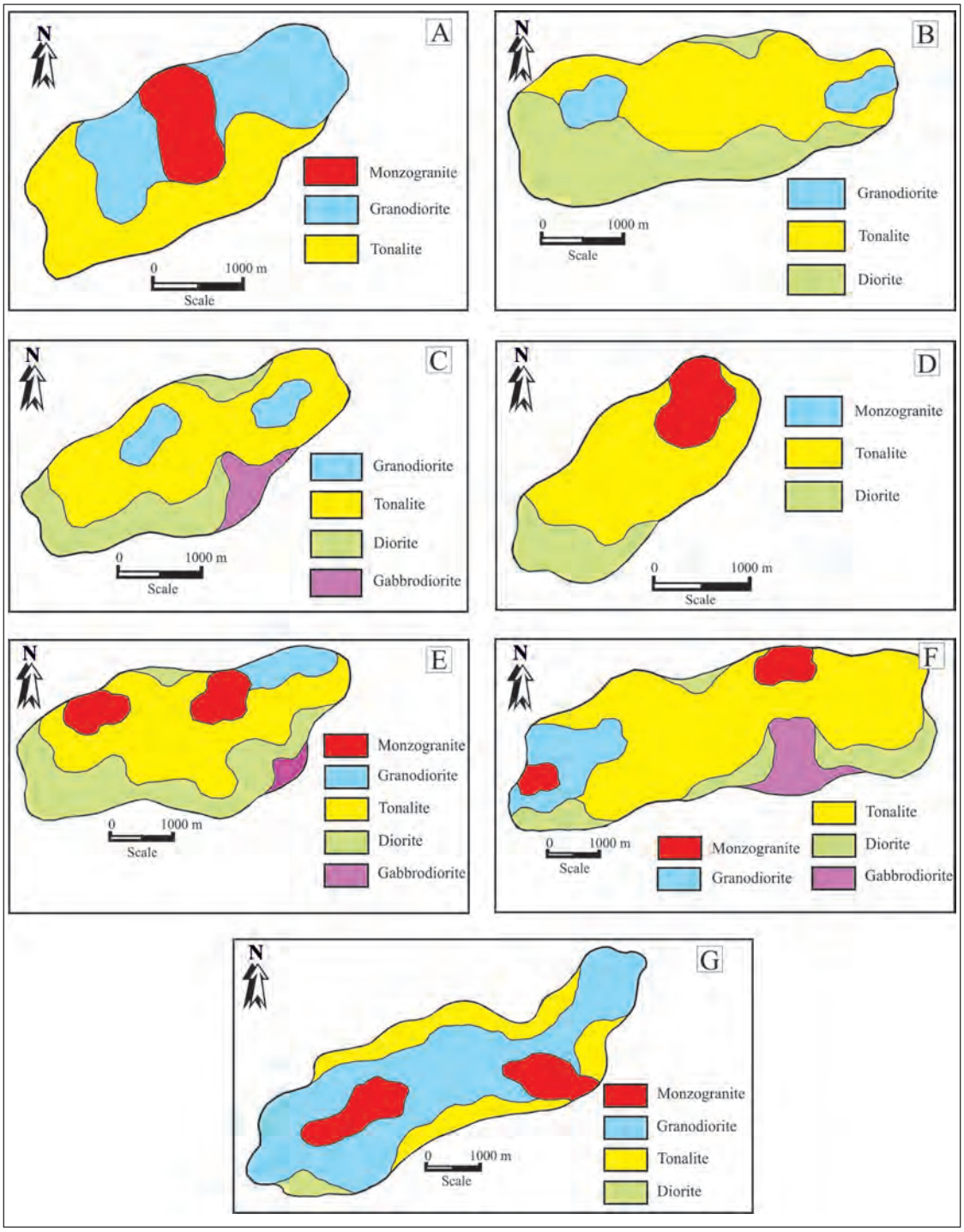

Figure 5- Maps showing locations of rocks forming the plutons a) Çiçekli, b) Somarova, c) Sorkunlu, d) Şaşurluk, e) Aydıntepe, f) Kemerlikdağı, g) Pelitli.

have less distribution (Figure 5b). The rocks of the Sorkunlu Pluton are modally granodiorite, tonalite, diorite and gabbrodiorite in composition (Figure 4). The granodiorites are generally in central sections, while gabbro diorite and diorites are located in the edge sections. The distribution of gabbro diorite and granodiorites are less (Figure 5c). The Şaşurluk Pluton is modally composed of monzogranite, tonalite and diorite (Figure 4). The monzogranites are generally in central sections with diorites around the

edges. Tonalites have highest distribution of all rocks within the pluton (Figure 5d). The Aydıntepe Pluton comprises monzogranite, granodiorite, tonalite, diorite and gabbro diorite composition rocks (Figure 4). Monzogranites concentrate close to the centre of the pluton with diorite and gabbro diorites around the edges and in a surrounding zone (Figure 5e). Tonalites are the most common rock in the pluton. Samples from the Kemerlikdağı Pluton modally comprise monzogranite, granodiorite, tonalite, diorite and gabbro diorite composition rocks (Figure 4). The monzogranites are located in areas close to the centre of the pluton with diorite and gabbro diorites located near the edges (Figure 5f). Tonalites have highest distribution in the pluton. The Pelitli Pluton comprises monzogranite, granodiorite, tonalite and diorite (Figure 4). Monzogranites are located close to the centre of the pluton while diorites and tonalites are located near the edges (Figure 5g). Diorites have the lowest distribution with tonalites having the highest distribution.

Microscopic studies of plutons show fine-medium granular, porphyric, monzonitic, poikilitic, occasionally myrmekitic, micrographic and graphic textures (Figure 6a-f). In samples with monzonitic textures, euhedral and subhedral large and small plagioclase crystals were found surrounded by anhedral orthoclase crystals. Granular, monzonitic and poikilitic textures were commonly observed. Porphyric texture was rarely observed.

The main minerals comprise plagioclase, quartz, K-feldspar, biotite, amphibole, pyroxene and opaque minerals. Apatite, zircon and sphene comprise accessory minerals. Secondary mineral phases include sericite, calcite, chlorite, epidote and clay minerals.

Plagioclases form euhedral and subhedral laminated prismatic crystals and are seen in all samples. Sizes are from 0.2 to 2.5 mm. Large plagioclase crystals contain small amphibole and opaque mineral inclusions. In terms of importance, they show albite and albite-carlsbad twins. Zoned crystals generally have oscillatory zoning, with occasional sieve texture (Figure 6a). In some of the large crystals, the margins have been lost and replaced by other plagioclase crystals with different appearance, twinning and zoning. In some samples there are myrmekites similar to small bullets with potassium feldspar around the margins. Some plagioclases are less fractured and partially sericitised. The overall ratio within the studied intrusives is 23-81% with the highest proportion in the Somarova Pluton (mean 57%) and the lowest in the Çiçekli Pluton (mean 46%) (Table 1).

K-feldispar is generally anhedral with sizes both large (2.5-3 mm) and small crystals (Figure 6b). Generally fibrous perthitic texture is observed and, in some sections, carlsbad twins were clear. In those with poikilitic texture, small plagioclase, biotite and opaque mineral inclusions are present (Figure 6c-d). In some sections, myrmekites are observed at boundaries with plagioclase. Some are fractured and partly argillised. The ratio of the feldspar within the studied intrusive rocks is 1-32%, with the highest rates in the Aydıntepe Pluton (mean 13%) and the lowest rates in the Sorkunlu Pluton (mean 7%) (Table 1).

Quartz comprises large and small anhedral crystals, filling in the gaps between other minerals. On some sections wavy extinction is observed. Generally, they have fractured and broken structures. They comprise 1-46% of the studied intrusive rocks, with the highest rates in Pelitili Pluton (mean 29%) and the lowest rates in the Sorkunlu Pluton (mean 19%) (Table 1). Amphiboles are euhedral and subhedral large laminated and small crystals. They comprise 0-17% of the studied intrusive rocks, with highest rates in the Sorkunlu Pluton (mean 9%) and lowest rates in the Çiçekli Pluton (mean 3%) (Table 1).

Biotite appears as euhedral and subhedral rod-like prismatic crystals. Poikilitic texture minerals contain smaller plagioclase and opaque minerals (Figure 6e). In some sections, they observed to be partially altered and transformed to chlorite. The iron, released due to alteration, forms opaque oxide clusters along cleavages. In the studied granitoid rocks, they comprise 0-10%, with highest rates in the Çiçekli Pluton (mean 7%) and lowest rates in the Pelitli Pluton (mean 2%) (Table 1).

Pyroxenes are subhedral and anhedral laminated crystals. They are found in some sections and occasionally. In some sections they have been altered to chlorite and calcite. They comprise 1-10% of the granitoid rocks, with highest rates in the Sorkunlu Pluton (mean 5%) (Table 1).

Apatites are generally needle-like and found as inclusions in quartz and feldspar (Figure 6g). Zircon is observed in nearly all rocks as small euhedral prismatic crystals (Figure 6g). Opaque minerals are found as euhedral and subhedral both large and small

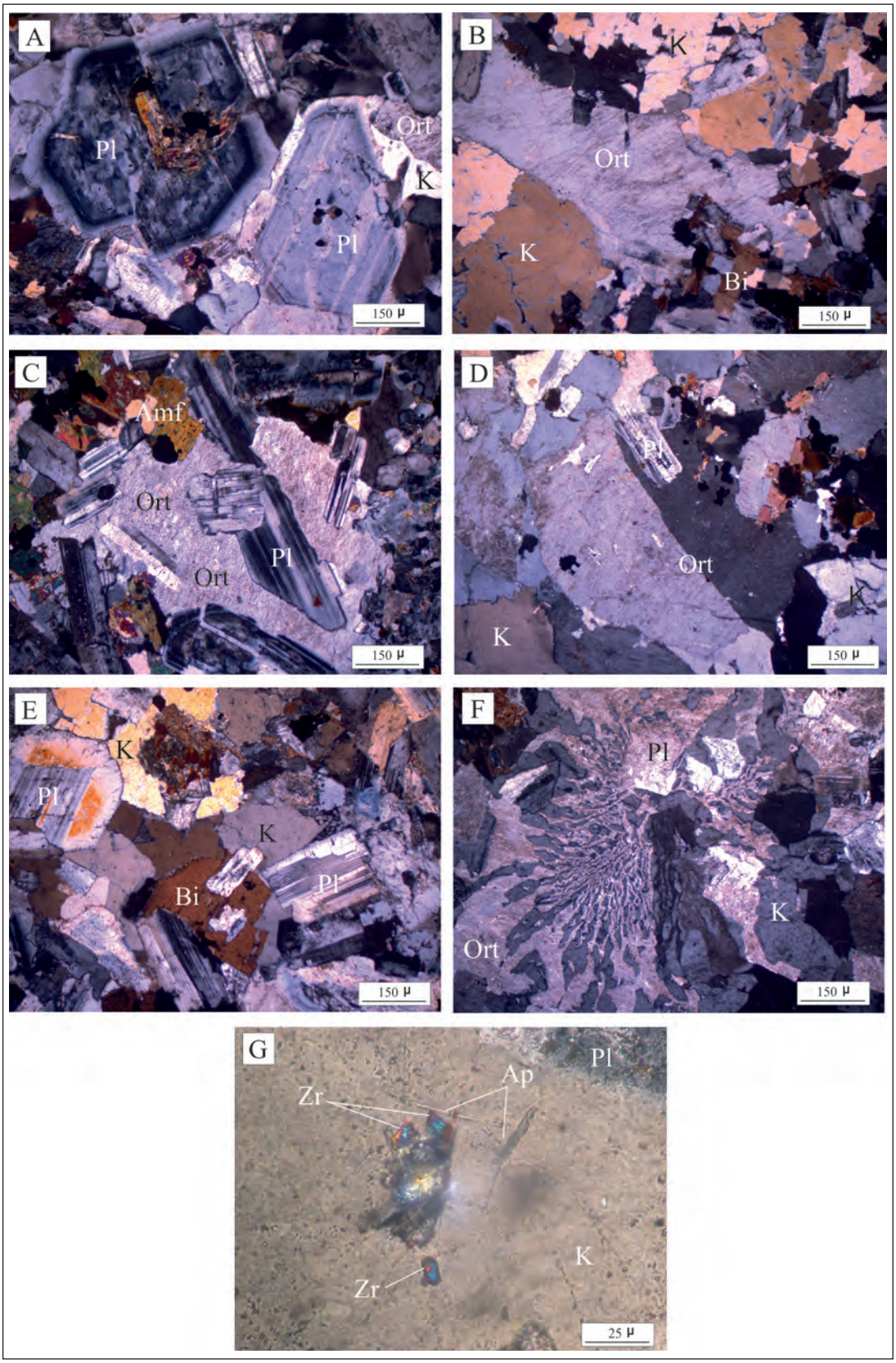

Figure 6- Microscopic characteristics of rocks from the plutons (a) zoned plagioclase minerals, (b) granular texture and large orthoclase minerals, (c-d) poikilitic orthoclase, (e) poikilitic biotite (f) micrographic texture (crossed polars, Pl: plagioclase, K: quartz, Ort: orthoclase, Bi: biotite, Amf: amphibole, Zr: zircon, Ap: apatite).

crystals. Generally, they are observed more densely in sections containing biotite and amphibole crystals. They are found at rates of 0-6% of the granitoid rocks studied (Table 1).

4.2. Mineral Chemistry of Plutons

4.2.1. Plagioclase

The minimum, maximum and mean values for plagioclase minerals found in the plutons according to microprobe analysis are given in table 2.

The An content of plagioclase in the pluton is varying from 68 to 02 (Table 2) with these values varying from An_{68-19} in the Çiçekli Pluton; An_{57-13} in the Somarova Pluton; An_{66-13} in the Sorkunlu Pluton: An_{63-03} in the Şaşurluk Pluton; An_{59-13} in the Aydıntepe Pluton; An_{64-04} in the Kemerlikdağı Pluton and An_{60-02} in the Pelitli Pluton (Table 2; Figure 7). The plagioclase of the Kemerlikdağı Pluton has the lowest An content (mean 32), while the Çiçekli Pluton has the highest An content (mean 44) (Table 2; Figure 7).

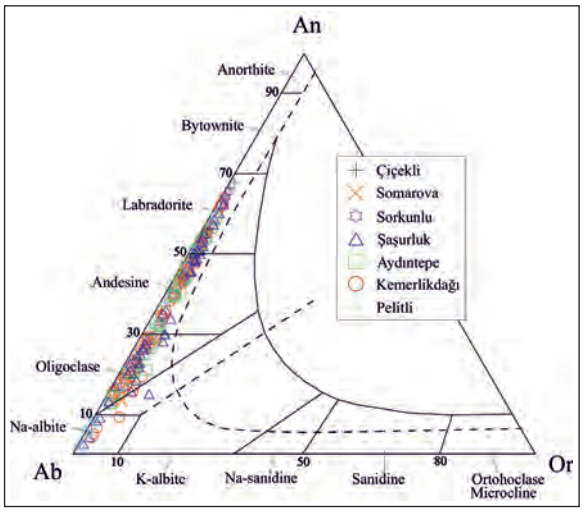

Figure 7- An-Ab-Or ternary diagram (Smith and Brown, 1988) showing plagioclase composition of studied plutons (Symbols as in figure 4).

Occasional oscillatory zoning is observed in plagioclase, with the An content of zoned crystals observed to be variable (Figure 8).

Table 2- Minimum, maximum and mean values for microprobe analyses of plagioclase.

Pluton	SiO_2	Al_2O_3	FeO	CaO	Na_2O	K_2O	BaO	SrO	Total	Si	Al	$Fe^{(ii)}$	Ca	Na	K	Ba	Sr	An	Ab	Or
Kemerlikdağı (n=57)																				
min	51.22	20.14	0.03	0.92	4.10	0.13	0.00	0.01	98.98	2.34	1.03	0.00	0.04	0.36	0.01	0.00	0.00	4.05	35.37	0.74
max	67.63	30.40	0.80	13.40	11.79	0.98	0.15	0.23	101.83	2.95	1.63	0.03	0.65	1.00	0.06	0.00	0.01	63.89	94.01	5.42
mean	59.91	25.03	0.36	6.77	7.76	0.37	0.05	0.09	100.34	2.67	1.32	0.01	0.33	0.67	0.02	0.00	0.00	32.14	65.80	2.06
Aydıntepe (n=54)																				
min	52.57	18.12	0.09	2.62	4.40	0.14	0.00	0.00	98.39	2.41	0.92	0.00	0.12	0.39	0.01	0.00	0.00	12.48	39.78	0.77
max	71.42	29.14	0.61	11.73	10.74	1.00	0.09	0.19	101.95	3.07	1.58	0.02	0.58	0.91	0.06	0.00	0.00	58.61	85.69	5.47
mean	58.70	25.81	0.31	7.60	7.18	0.38	0.03	0.09	100.10	2.63	1.36	0.01	0.37	0.62	0.02	0.00	0.00	36.36	61.49	2.15
Sorkunlu (n=34)																				
min	50.96	20.57	0.08	2.61	3.76	0.14	0.00	0.01	98.82	2.34	1.07	0.00	0.12	0.34	0.01	0.00	0.00	12.51	33.44	0.81
max	66.44	30.67	0.62	13.33	9.92	0.55	0.08	0.17	100.53	2.92	1.65	0.02	0.66	0.85	0.03	0.00	0.00	65.51	86.06	3.04
mean	56.54	26.80	0.36	8.97	6.37	0.32	0.04	0.10	99.50	2.56	1.43	0.01	0.44	0.56	0.02	0.00	0.00	43.16	55.04	1.80
Çiçekli (n=18)																				
min	50.23	22.56	0.22	4.06	3.46	0.13	0.00	0.02	99.07	2.31	1.17	0.01	0.19	0.31	0.01	0.00	0.00	19.06	31.26	0.76
max	63.69	30.96	0.63	13.59	9.10	0.65	0.09	0.17	100.39	2.81	1.68	0.02	0.67	0.78	0.04	0.00	0.00	67.85	77.31	3.63
mean	56.55	26.89	0.42	9.09	6.21	0.33	0.03	0.09	99.61	2.55	1.43	0.02	0.44	0.54	0.02	0.00	0.00	44.15	53.97	1.88
Somarova (n=29)																				
min	52.97	21.63	0.09	2.91	4.92	0.15	0.00	0.00	98.75	2.41	1.13	0.00	0.14	0.43	0.01	0.00	0.00	13.20	42.43	0.85
max	64.94	29.42	0.54	11.90	10.28	0.78	0.08	0.15	101.39	2.86	1.57	0.02	0.58	0.88	0.04	0.00	0.00	56.72	84.41	4.31
mean	58.24	25.88	0.33	7.82	7.25	0.39	0.04	0.09	100.04	2.61	1.37	0.01	0.38	0.63	0.02	0.00	0.00	36.78	61.05	2.17
Şaşurluk (n=53)																				
min	51.71	19.37	0.00	0.51	3.93	0.12	0.00	0.00	97.62	2.39	1.00	0.00	0.02	0.35	0.01	0.00	0.00	2.49	36.08	0.78
max	68.68	29.42	0.56	12.34	10.94	1.45	0.08	0.16	101.05	3.01	1.60	0.02	0.61	0.92	0.08	0.00	0.00	62.60	96.47	8.98
mean	59.02	25.31	0.26	7.24	6.84	0.40	0.03	0.08	99.18	2.65	1.35	0.01	0.35	0.59	0.02	0.00	0.00	36.04	61.56	2.40
Pelitli (n=21)																				
min	50.16	18.58	0.04	0.38	4.46	0.02	0.00	0.01	98.73	2.32	0.99	0.00	0.02	0.40	0.00	0.00	0.00	1.77	38.90	0.11
max	69.25	29.98	0.71	12.75	11.52	0.64	0.13	0.16	101.00	3.00	1.61	0.03	0.63	0.98	0.04	0.00	0.00	60.06	97.81	3.32
mean	61.60	23.58	0.32	5.28	8.77	0.22	0.04	0.07	99.90	2.74	1.24	0.01	0.26	0.76	0.01	0.00	0.00	24.57	74.20	1.23

min: minimum values, max: maximum values, mean: average values

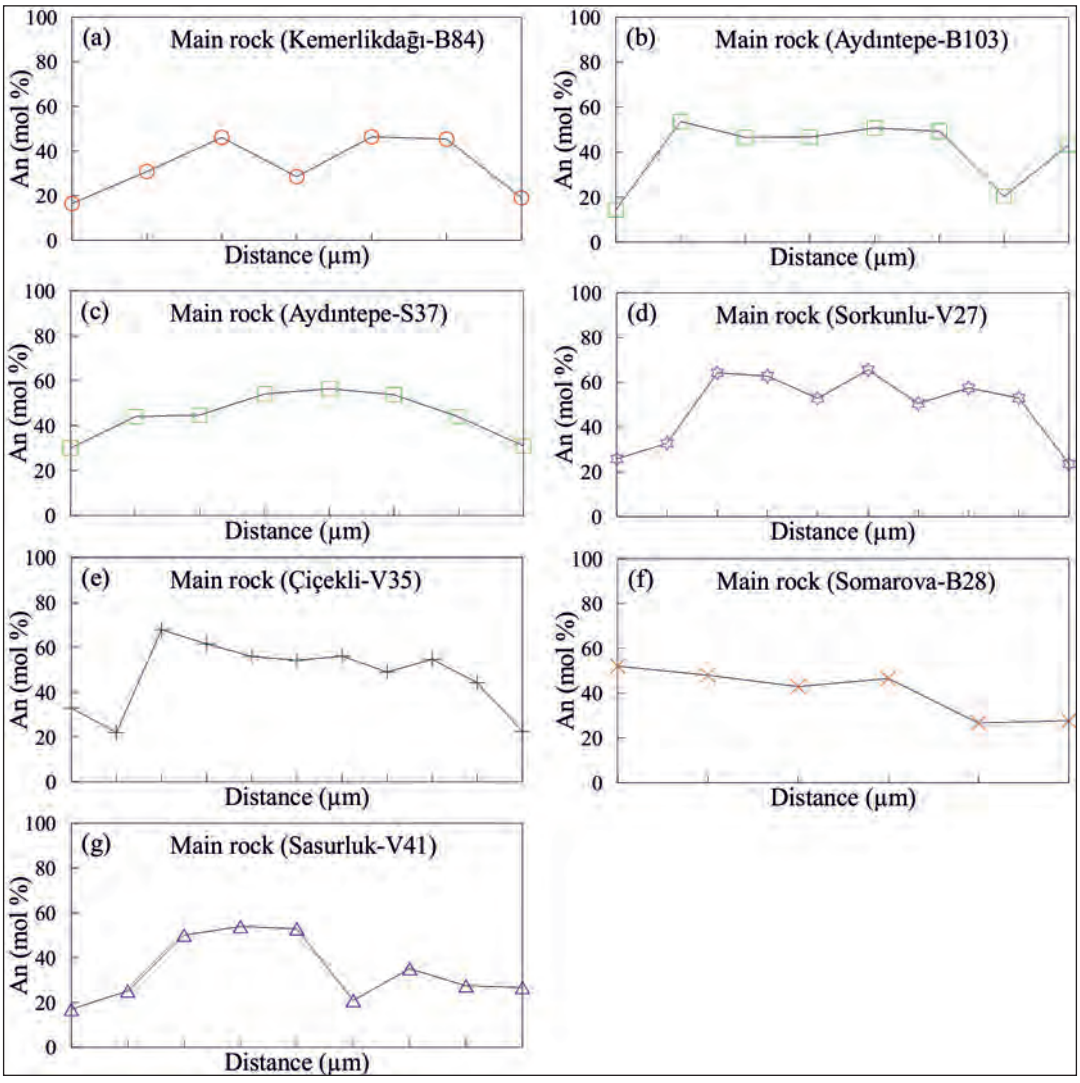

Figure 8- An (%) variations in the zoned plagioclase from the studied plutons (Symbols as in figure 4).

4.2.2. K-Feldspar

The minimum, maximum and mean values for the microprobe analyses of K-feldspar in the studied plutons are given in table 3. The Or content of K-feldspar is between 1 and 96, without any chemical zoning in the crystals. The Çiçekli Pluton has Or_{87-58}, Somarova Pluton has $Or_{93-02;}$ Sorkunlu Pluton has Or_{94-01}; Şaşurluk Pluton has Or_{96-01}; Aydıntepe Pluton has Or_{93-70}; Kemerlikdağı Pluton has Or_{96-01} and the Pelitli Pluton has Or_{96-79} (Figure 9). When the Or content of the K-feldspar is examined, the Somarova Pluton has lowest content (mean 76), while the Pelitli Pluton has highest Or content (mean 90) (Table 3; Figure 9).

Table 3- Minimum, maximum and mean values of microprobe analyses of K-feldspar

	SiO_2	Al_2O_3	FeO	CaO	Na_2O	K_2O	BaO	SrO	Total	Si	Al	$Fe^{(ii)}$	Ca	Na	K	Ba	Sr	An	Ab	Or
Kemerlikdağı (n=22)																				
min	63.64	18.81	0.01	0.01	0.49	0.21	0.00	0.01	100.10	2.92	0.99	0.00	0.00	0.04	0.01	0.00	0.00	0.05	4.40	1.24
max	70.04	20.69	0.24	0.96	11.30	16.18	1.60	0.10	101.97	3.01	1.08	0.01	0.04	0.94	0.95	0.03	0.00	4.77	95.75	95.55
mean 65.21		19.25	0.12	0.15	2.02	13.92	0.21	0.04	100.92	2.97	1.03	0.00	0.01	0.17	0.81	0.00	0.00	0.73	17.85	81.42
Aydıntepe (n=25)																				
min	64.06	18.86	0.02	0.00	0.74	12.06	0.02	0.01	99.93	2.95	1.02	0.00	0.00	0.07	0.70	0.00	0.00	0.00	6.60	69.71
max	65.71	19.56	0.38	0.25	3.36	15.98	1.06	0.10	101.60	2.98	1.06	0.01	0.01	0.30	0.94	0.02	0.00	1.26	29.52	93.18
mean	64.89	19.19	0.12	0.09	1.80	14.26	0.26	0.04	100.64	2.97	1.03	0.00	0.00	0.16	0.83	0.00	0.00	0.44	15.99	83.58
Sorkunlu (n=17)																				
min	63.23	8.15	0.03	0.02	0.64	0.17	0.00	0.01	98.93	2.88	0.40	0.00	0.00	0.06	0.01	0.00	0.00	0.10	5.69	1.03
max	85.91	21.74	0.30	1.75	10.48	16.12	1.36	0.09	101.20	3.59	1.12	0.01	0.08	0.89	0.95	0.02	0.00	8.02	93.00	94.22
mean	65.70	18.53	0.11	0.24	2.17	13.08	0.29	0.05	100.17	3.00	1.00	0.00	0.01	0.19	0.77	0.01	0.00	1.24	20.27	78.48
Çiçekli (n=11)																				
min	63.04	18.72	0.10	0.03	1.28	9.70	0.01	0.01	99.94	2.92	1.02	0.00	0.00	0.12	0.57	0.00	0.00	0.15	11.59	58.17
max	65.33	19.70	0.20	0.29	4.43	14.66	2.82	0.10	100.72	2.98	1.08	0.01	0.01	0.39	0.87	0.05	0.00	1.46	40.37	87.31
mean	64.61	19.11	0.14	0.16	2.38	13.25	0.68	0.06	100.37	2.96	1.03	0.01	0.01	0.21	0.78	0.01	0.00	0.77	21.27	77.96
Somarova (n=17)																				
min	64.21	18.98	0.03	0.03	0.79	0.32	0.00	0.00	99.92	2.90	1.03	0.00	0.00	0.07	0.02	0.00	0.00	0.15	7.03	1.77
max	68.11	21.46	0.41	1.35	11.25	15.85	0.40	0.12	101.71	2.98	1.11	0.02	0.06	0.94	0.92	0.01	0.00	6.38	94.34	92.82
mean	65.04	19.42	0.12	0.19	2.67	12.98	0.22	0.05	100.69	2.96	1.04	0.00	0.01	0.23	0.76	0.00	0.00	0.91	23.20	75.88
Şaşurluk (n=24)																				
min	63.09	18.16	0.00	0.00	0.35	0.18	0.00	0.01	99.19	2.93	1.00	0.00	0.00	0.03	0.01	0.00	0.00	0.00	3.15	1.04
max	68.57	20.50	0.32	0.51	10.94	16.28	1.92	0.12	100.92	3.00	1.08	0.01	0.02	0.92	0.97	0.03	0.00	2.49	96.47	96.26
mean	64.47	19.09	0.10	0.12	1.55	14.40	0.37	0.06	100.16	2.97	1.04	0.00	0.01	0.14	0.85	0.01	0.00	0.58	13.94	85.48
Pelitli (n=17)																				
min	61.98	17.89	0.01	0.02	0.47	13.54	0.01	0.01	97.00	2.96	1.00	0.00	0.00	0.04	0.81	0.00	0.00	0.09	4.21	78.92
max	64.14	18.50	0.36	0.13	2.35	16.11	1.17	0.11	99.36	2.99	1.03	0.01	0.01	0.21	0.98	0.02	0.00	0.65	20.84	95.59
mean	62.98	18.22	0.11	0.05	1.07	15.31	0.37	0.05	98.16	2.98	1.01	0.00	0.00	0.10	0.92	0.01	0.00	0.26	9.59	90.14

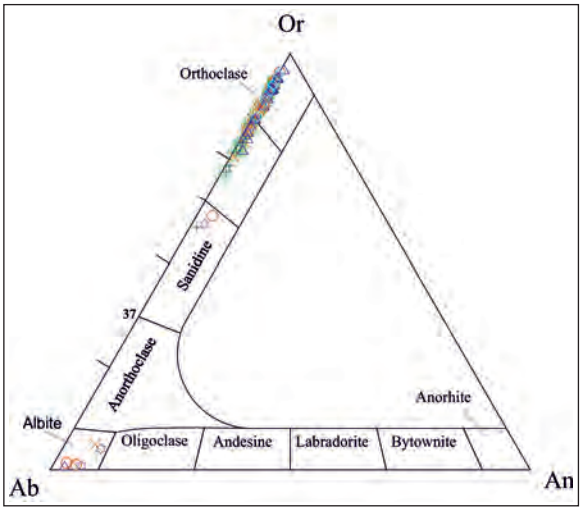

Figure 9- An-Ab-Or ternary diagram (Smith and Brown, 1988) for K-feldspars of the studied plutons (Symbols as in figure 4)

4.2.3. Biotite

The minimum, maximum and mean values of the microprobe analyses of biotite observed in plutonic rocks is given in table 4.

Biotites are solid melt products between the end members of phlogopite and annite and are close to the magnesium-rich phlogopite end (Figure 10).

Table 4- Minimum, maximum and mean values of microprobe analyses of biotite.

	SiO_2	TiO_2	Al_2O_3	FeO	MnO	MgO	CaO	Na_2O	K_2O	Cl	F	Total	Si	Ti	Al	$Fe^{(ii)}$	Mn	Mg	Ca	Na	K	Cl	F
Kemerlikdağı (n=15)																							
min	36.51	4.18	12.12	16.19	0.18	11.46	0.04	0.08	8.87	0.22	0.31	93.83	5.59	0.47	2.13	2.03	0.02	2.56	0.01	0.02	1.72	0.06	0.15
max	38.81	5.26	12.82	20.30	0.30	14.31	0.52	0.18	9.64	0.56	0.60	97.59	5.69	0.59	2.27	2.54	0.04	3.15	0.09	0.05	1.84	0.14	0.28
mean	37.55	4.58	12.50	18.26	0.23	12.83	0.14	0.12	9.23	0.39	0.42	96.24	5.63	0.52	2.21	2.29	0.03	2.87	0.02	0.03	1.76	0.10	0.20
Aydıntepe (n=23)																							
min	36.18	3.39	12.81	16.14	0.28	12.34	0.01	0.07	8.96	0.15	0.39	94.44	5.46	0.38	2.28	1.99	0.04	2.79	0.00	0.02	1.72	0.04	0.19
max	38.02	5.05	13.57	18.44	0.46	14.66	0.20	0.21	9.67	0.33	0.78	97.20	5.61	0.57	2.39	2.29	0.06	3.23	0.03	0.06	1.83	0.08	0.37
mean	36.97	4.35	13.20	17.36	0.38	13.40	0.10	0.14	9.31	0.25	0.57	96.02	5.53	0.49	2.33	2.17	0.05	2.99	0.02	0.04	1.78	0.06	0.27
Sorkunlu (n=23)																							
min	35.67	4.06	11.78	17.57	0.17	11.12	0.03	0.11	8.67	0.19	0.14	93.26	5.49	0.47	2.14	2.17	0.02	2.55	0.00	0.03	1.69	0.05	0.07
max	37.91	5.23	13.04	20.30	0.33	13.84	2.47	0.18	9.54	0.48	0.44	97.30	5.73	0.61	2.36	2.58	0.04	3.05	0.41	0.05	1.84	0.12	0.21
mean	37.01	4.47	12.51	18.85	0.25	12.28	0.22	0.14	9.18	0.32	0.29	95.52	5.62	0.51	2.24	2.40	0.03	2.78	0.04	0.04	1.78	0.08	0.14
Çiçekli (n=9)																							
min	37.23	4.41	12.13	16.06	0.10	13.46	0.02	0.14	9.15	0.45	0.71	95.17	5.53	0.49	2.14	2.00	0.01	2.95	0.00	0.04	1.73	0.11	0.33
max	37.56	4.99	12.91	17.05	0.14	14.13	0.13	0.23	9.60	0.54	0.86	96.98	5.58	0.55	2.24	2.12	0.02	3.14	0.02	0.07	1.81	0.14	0.40
mean	37.44	4.64	12.55	16.55	0.12	13.78	0.06	0.20	9.40	0.48	0.81	96.03	5.56	0.52	2.20	2.05	0.01	3.05	0.01	0.06	1.78	0.12	0.38
Somarova (n=19)																							
min	36.44	3.41	12.01	17.42	0.20	12.10	0.03	0.11	7.24	0.23	0.39	94.12	5.55	0.39	2.11	2.17	0.03	2.74	0.00	0.03	1.41	0.06	0.19
max	38.32	4.65	13.05	19.23	0.39	14.01	0.75	0.24	9.59	0.53	0.53	97.79	5.70	0.53	2.31	2.42	0.05	3.13	0.12	0.07	1.82	0.13	0.25
mean	37.45	4.22	12.53	18.33	0.27	12.93	0.14	0.18	9.21	0.31	0.46	96.02	5.63	0.48	2.22	2.30	0.03	2.90	0.02	0.05	1.76	0.08	0.22
Şaşurluk (n=14)																							
min	36.34	3.18	11.98	17.63	0.17	10.92	0.01	0.09	7.48	0.30	0.23	94.11	5.60	0.37	2.15	2.20	0.02	2.50	0.00	0.03	1.48	0.08	0.11
max	37.87	4.53	12.94	21.65	0.30	13.64	0.24	0.20	9.63	0.73	0.40	96.60	5.67	0.52	2.33	2.81	0.04	3.04	0.04	0.06	1.85	0.19	0.19
mean	37.03	4.24	12.50	19.40	0.22	12.05	0.08	0.14	9.15	0.43	0.30	95.55	5.63	0.48	2.24	2.47	0.03	2.73	0.01	0.04	1.77	0.11	0.15
Pelitli (n=8)																							
min	37.50	4.24	12.38	16.13	0.19	13.43	0.08	0.06	8.71	0.06	0.35	97.31	5.51	0.46	2.12	1.95	0.02	2.89	0.01	0.02	1.60	0.02	0.16
max	39.35	5.36	13.92	19.46	0.27	14.96	0.29	0.27	9.37	0.40	0.81	98.92	5.68	0.59	2.37	2.38	0.03	3.26	0.04	0.08	1.75	0.10	0.38
mean	38.44	4.74	12.88	17.33	0.23	14.21	0.21	0.19	9.04	0.18	0.53	97.96	5.61	0.52	2.21	2.12	0.03	3.09	0.03	0.05	1.68	0.04	0.24

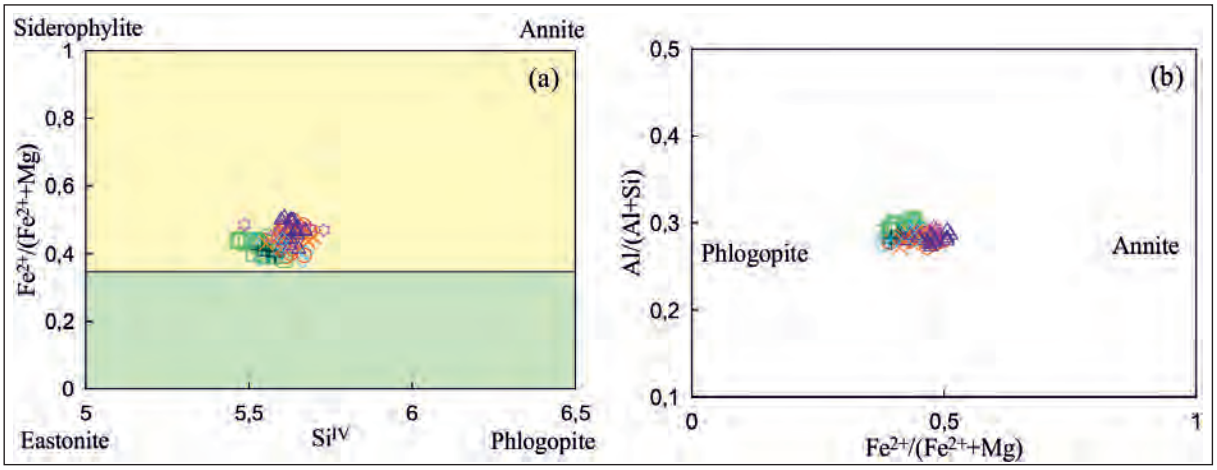

Figure 10- Biotite composition of the studied plutonic rocks on (a) Si^{IV}-(Fe^{2+}/Fe^{2+}+Mg) diagrams, (b) (Fe^{2+}/Fe^{2+}+Mg)-Al/(Al+Si) diagrams (Parsons et al., 1991) (Symbols as in figure 4).

4.2.4. Amphibole

The minimum, maximum and mean values of microprobe analyses for amphiboles in the studied plutons are given in table 5.

All of the amphiboles in the plutons are calcic amphiboles (Figure 11a) and are mainly magnesium hornblende with a small amount with actinolite composition on the Leake et al. (1997) classification diagram (Figure 11b).

Table 5- Minimum, maximum and mean values of microprobe analyses of amphiboles.

	SiO_2	TiO_2	Al_2O_3	FeO	MnO	MgO	CaO	Na_2O	K_2O	Total	Si	Ti	Al	$Fe^{(ii)}$	Mn	Mg	Ca	Na	K
Kemerlikdağı (n=32)																			
min	47.97	0.17	1.51	10.11	0.27	12.47	10.70	0.31	0.09	96.86	6.99	0.02	0.25	1.18	0.03	2.70	1.67	0.17	0.02
max	55.42	1.37	5.46	15.44	0.91	18.31	12.89	1.54	0.60	98.55	7.73	0.15	0.94	1.88	0.11	3.86	1.98	0.87	0.11
mean	50.58	0.89	4.31	13.51	0.53	15.00	11.55	1.00	0.39	97.78	7.27	0.10	0.73	1.63	0.06	3.21	1.78	0.56	0.07
Aydıntepe (n=21)																			
min	48.35	0.11	1.50	10.15	0.50	14.33	11.13	0.23	0.08	97.26	6.95	0.01	0.25	1.21	0.06	3.10	1.67	0.13	0.01
max	54.07	1.74	6.50	13.33	0.89	18.12	12.77	1.56	0.67	98.65	7.70	0.19	1.10	1.60	0.11	3.82	1.95	0.87	0.12
mean	51.37	0.65	4.43	11.77	0.64	16.19	11.84	0.87	0.34	98.09	7.29	0.07	0.74	1.40	0.08	3.42	1.80	0.48	0.06
Sorkunlu (n=21)																			
min	47.14	0.12	3.16	14.03	0.37	12.97	10.90	0.63	0.24	96.97	6.88	0.01	0.54	1.69	0.05	2.83	1.68	0.35	0.04
max	50.97	1.30	6.20	16.59	0.57	15.01	11.73	1.50	0.66	98.35	7.38	0.14	1.07	2.01	0.07	3.22	1.83	0.85	0.12
mean	49.11	0.88	4.96	15.42	0.49	13.89	11.21	1.17	0.48	97.62	7.12	0.10	0.85	1.87	0.06	3.00	1.74	0.66	0.09
Çiçekli (n=13)																			
min	47.92	0.40	2.01	10.28	0.30	13.10	10.77	0.22	0.09	96.53	7.00	0.04	0.34	1.23	0.04	2.87	1.68	0.12	0.02
max	53.81	1.13	5.64	15.82	0.88	16.89	12.30	1.47	0.63	97.44	7.64	0.12	0.98	1.94	0.11	3.61	1.90	0.83	0.12
mean	50.87	0.78	4.32	12.73	0.55	15.19	11.35	1.03	0.37	97.17	7.32	0.08	0.73	1.53	0.07	3.26	1.75	0.58	0.07
Somarova (n=16)																			
min	47.34	0.17	1.00	12.18	0.46	12.81	11.00	0.22	0.11	96.67	6.92	0.02	0.17	1.43	0.06	2.79	1.66	0.12	0.02
max	54.58	1.24	6.34	16.35	0.76	17.05	12.15	1.56	0.76	98.82	7.78	0.14	1.09	2.00	0.09	3.57	1.86	0.88	0.14
mean	50.90	0.67	4.09	14.56	0.58	14.37	11.50	0.84	0.35	97.87	7.33	0.07	0.69	1.75	0.07	3.08	1.77	0.47	0.06
Şaşurluk (n=18)																			
min	47.80	0.23	2.06	13.09	0.43	12.77	10.45	0.62	0.19	96.70	7.00	0.02	0.34	1.54	0.05	2.81	1.57	0.34	0.03
max	53.47	1.27	5.86	16.59	0.60	16.77	12.27	1.35	0.65	98.51	7.56	0.14	1.01	2.03	0.07	3.51	1.91	0.77	0.12
mean	49.41	0.90	4.84	15.25	0.53	13.83	11.28	1.08	0.48	97.59	7.17	0.10	0.83	1.85	0.07	2.99	1.75	0.61	0.09
Pelitli (n=21)																			
min	50.21	0.19	1.73	11.14	0.37	15.15	10.58	0.28	0.19	96.98	7.06	0.02	0.29	1.31	0.04	3.20	1.58	0.15	0.03
max	52.90	0.94	5.19	14.40	0.88	17.25	11.89	1.27	0.48	98.72	7.50	0.10	0.86	1.71	0.11	3.62	1.80	0.70	0.09
mean	51.41	0.71	4.16	12.71	0.56	16.03	11.28	0.73	0.30	97.88	7.28	0.08	0.69	1.50	0.07	3.38	1.71	0.40	0.05

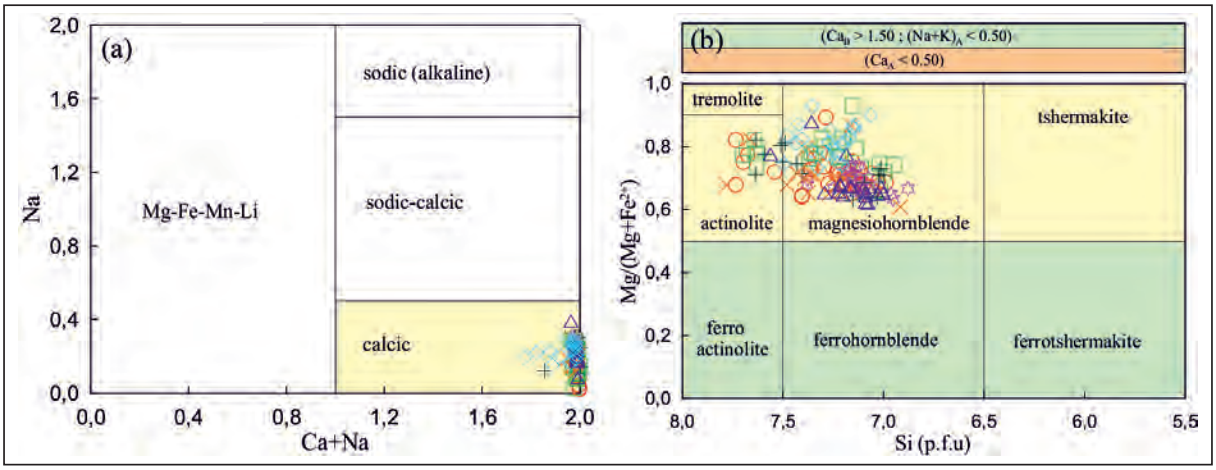

Figure 11- Composition of amphiboles (Leake et al., 1997) (Symbols as in figure 4).

4.2.5. Pyroxene

Pyroxene has been observed in some plutons and the microprobe analyses of pyroxenes are given in table 6 as minimum, maximum and mean values. All pyroxenes are calcic (Wo_{44-46}) in composition except clinoenstatite (En_{53-57}) orthorhombic pyroxenes observed in some thin-sections of Aydıntepe (Figure 12a). Calcic pyroxenes are generally augite, with lesser amounts of diopside composition (Figure 12a). Clinoenstatite and diopside composition is rare, while augite compositions are abundantly observed. On the

Table 6- Minimum, maximum and mean values of microprobe analyses of pyroxene.

	SiO_2	TiO_2	Al_2O_3	FeO	MnO	MgO	CaO	Na_2O	Total	Si	Ti	Al	$Fe^{(ii)}$	Mn	Mg	Ca	Na	Wo	En	Fs
Kemerlikdağı (n=12)																				
min	51.00	0.11	0.38	8.07	0.26	13.04	19.97	0.30	98.28	1.87	0.00	0.02	0.25	0.01	0.73	0.79	0.02	40.34	37.06	13.40
max	53.49	0.71	3.15	12.13	0.38	15.69	22.44	0.39	100.93	1.99	0.02	0.14	0.38	0.01	0.86	0.89	0.03	45.39	44.44	19.82
mean	51.85	0.51	1.96	9.14	0.33	14.91	20.92	0.35	99.97	1.92	0.01	0.09	0.28	0.01	0.82	0.83	0.03	42.68	42.31	15.01
Aydıntepe (n=19)																				
min	51.13	0.07	0.19	8.75	0.39	13.23	0.93	0.00	97.02	1.96	0.00	0.01	0.28	0.01	0.74	0.04	0.00	1.88	37.58	15.31
max	52.58	0.29	0.66	27.17	1.07	20.23	21.89	0.28	100.08	2.00	0.01	0.03	0.87	0.03	1.15	0.89	0.02	45.75	56.99	44.78
mean	51.86	0.14	0.45	16.96	0.68	15.75	12.97	0.16	98.98	1.98	0.00	0.02	0.54	0.02	0.89	0.53	0.01	26.85	45.01	28.14
Sorkunlu (n=9)																				
min	51.04	0.34	1.22	8.15	0.24	14.62	20.52	0.22	98.68	1.89	0.01	0.05	0.26	0.01	0.81	0.81	0.02	41.46	41.49	13.58
max	52.61	0.67	2.59	10.01	0.48	15.59	20.79	0.56	100.48	1.98	0.02	0.11	0.31	0.02	0.86	0.83	0.04	43.19	44.31	16.60
mean	52.04	0.51	1.76	8.84	0.38	15.08	20.63	0.36	99.60	1.94	0.01	0.08	0.28	0.01	0.84	0.82	0.03	42.29	43.01	14.69
Çiçekli (n=11)																				
min	51.27	0.10	0.42	8.42	0.38	12.77	21.01	0.21	97.55	1.97	0.00	0.02	0.27	0.01	0.73	0.85	0.02	43.27	36.80	14.57
max	52.79	0.20	0.86	11.30	0.54	13.85	22.21	0.35	99.61	2.00	0.01	0.04	0.36	0.02	0.78	0.91	0.03	45.96	40.03	18.70
mean	52.19	0.15	0.60	9.80	0.45	13.44	21.68	0.28	98.59	1.98	0.00	0.03	0.31	0.01	0.76	0.88	0.02	44.83	38.67	16.50
Şaşurluk (n=13)																				
min	51.00	0.03	0.12	7.12	0.24	12.77	0.93	0.00	97.02	1.87	0.00	0.01	0.22	0.01	0.73	0.04	0.00	1.88	36.80	11.87
max	53.06	0.19	0.88	8.92	0.56	14.86	23.88	0.45	99.38	1.99	0.01	0.04	0.28	0.02	0.83	0.96	0.03	47.88	41.93	15.35
mean	52.79	0.15	0.67	8.26	0.45	14.19	22.18	0.27	98.95	1.98	0.00	0.03	0.26	0.01	0.80	0.89	0.02	45.53	40.52	13.95
Pelitli (n=4)																				
min	51.25	0.16	0.64	8.18	0.34	13.32	19.99	0.29	97.01	1.91	0.00	0.03	0.26	0.01	0.76	0.80	0.02	41.32	39.33	13.78
max	52.87	0.62	2.51	9.02	0.42	15.32	22.32	0.37	99.22	2.00	0.02	0.11	0.29	0.01	0.85	0.90	0.03	45.98	44.07	15.65
mean	52.21	0.28	1.21	8.63	0.40	14.13	21.45	0.33	98.64	1.97	0.01	0.05	0.27	0.01	0.79	0.87	0.02	44.55	40.82	14.63

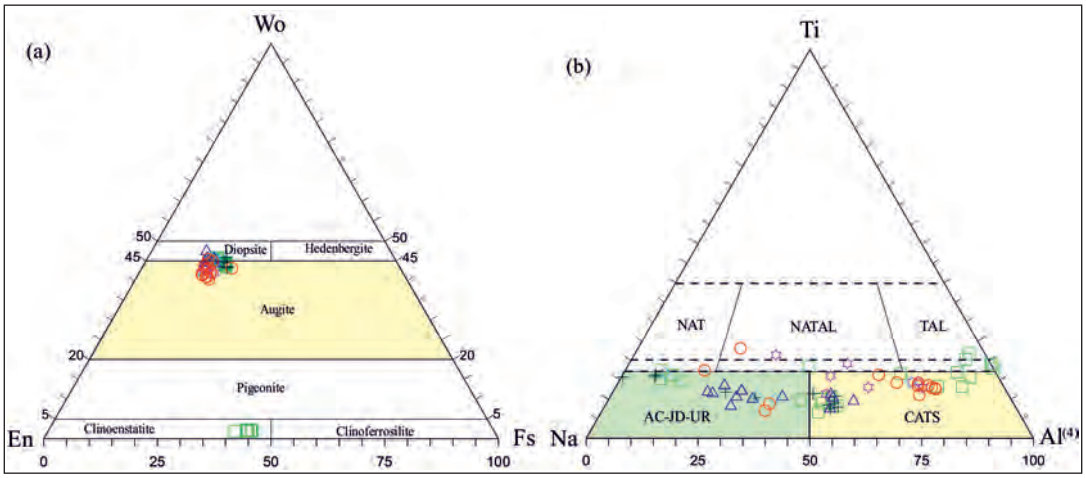

Figure 12- Pyroxenes on a) Wo-En-Fs (Morimoto, 1988), b) Ti-Na-$Al^{(4)}$ (Papike et al., 1974) diagrams (Symbols as in figure 4).

Ti-Na-Al^4 diagram for the studied rocks (Papike et al., 1974), they vary between the poor in Ti and rich in Na and $Al^{(4)}$ end members (Figure 12b).

4.2.6. Fe-Ti Oxides

The Fe-Ti oxides in the studied plutons are mainly magnetite with lower amounts of ilmenite. Microprobe analysis results for magnetite and ilmenite are given in tables 7 and 8 as minimum, maximum and mean values.

The studied magnetites are ulvospinel-magnetite solid melt products and have compositions close to the magnetite end (Figure 13a). Ilmenites are generally located at the ilmenite end of the ilmenite-hematite solid melt (Figure 13b).

Table 7- Minimum, maximum and mean values of microprobe analyses of magnetites.

	SiO_2	TiO_2	Al_2O_3	Cr_2O_3	Fe_2O_3	FeO	MnO	MgO	CaO	Total	Si	Ti	Al	Cr	$Fe^{(ii)}$	Mn	Mg	Ca
Kemerlikdağı (n=12)																		
min	0.03	0.06	0.06	0.01	60.27	30.62	0.02	0.00	0.02	96.97	0.01	0.02	0.03	0.00	28.62	0.01	0.00	0.01
max	0.71	3.39	1.23	0.12	67.92	33.07	1.14	0.10	0.15	100.37	0.29	1.00	0.57	0.04	31.76	0.38	0.06	0.06
mean	0.11	1.27	0.38	0.08	65.02	31.66	0.34	0.02	0.06	98.95	0.05	0.38	0.18	0.03	30.68	0.12	0.01	0.02
Aydıntepe (n=10)																		
min	0.01	0.05	0.06	0.05	67.52	31.05	0.05	0.00	0.02	99.68	0.00	0.02	0.03	0.02	31.37	0.02	0.00	0.01
max	0.07	0.42	0.40	0.07	69.54	31.50	0.15	0.03	0.14	101.51	0.03	0.13	0.19	0.02	31.82	0.05	0.02	0.06
mean	0.04	0.18	0.19	0.06	68.73	31.33	0.08	0.01	0.05	100.67	0.02	0.05	0.09	0.02	31.64	0.03	0.01	0.02
Sorkunlu (n=10)																		
min	0.03	0.09	0.15	0.08	48.72	29.93	0.03	0.00	0.02	95.36	0.01	0.03	0.07	0.03	26.22	0.01	0.00	0.01
max	2.34	8.51	1.28	0.15	69.01	36.31	2.38	0.42	0.47	101.13	0.93	2.50	0.60	0.05	31.68	0.78	0.25	0.20
mean	0.30	1.98	0.36	0.10	63.11	32.31	0.44	0.06	0.09	98.74	0.12	0.58	0.17	0.03	30.07	0.14	0.04	0.04
Çiçekli (n=5)																		
min	0.02	0.31	0.63	0.06	60.44	30.31	0.08	0.05	0.03	96.52	0.01	0.10	0.31	0.02	29.40	0.03	0.03	0.01
max	0.06	2.36	1.27	0.08	65.40	31.95	0.30	0.13	0.05	97.94	0.02	0.72	0.61	0.03	31.18	0.10	0.08	0.02
mean	0.04	1.17	0.93	0.07	63.49	31.06	0.18	0.09	0.04	97.07	0.02	0.36	0.45	0.02	30.40	0.06	0.06	0.02
Somarova (n=8)																		
min	0.01	0.43	0.18	0.07	37.23	30.96	0.06	0.00	0.02	96.09	0.00	0.13	0.09	0.02	22.52	0.02	0.00	0.01
max	0.14	13.58	2.24	0.10	68.43	41.08	1.67	0.11	0.12	101.42	0.06	3.69	0.95	0.03	31.44	0.51	0.06	0.05
mean	0.07	2.16	0.56	0.08	63.33	32.59	0.28	0.02	0.05	99.14	0.03	0.60	0.25	0.03	30.20	0.09	0.01	0.02
Şaşurluk (n=15)																		
min	0.04	0.25	0.08	0.05	57.86	30.81	0.04	0.00	0.01	97.28	0.02	0.08	0.04	0.02	28.04	0.01	0.01	0.00
max	0.50	4.49	2.42	0.17	67.01	34.16	0.63	0.19	0.32	99.15	0.20	1.34	1.12	0.05	31.58	0.21	0.11	0.14
mean	0.12	1.80	0.68	0.10	63.07	32.05	0.21	0.05	0.08	98.16	0.05	0.54	0.32	0.03	30.15	0.07	0.03	0.03
Pelitli (n=14)																		
min	0.08	0.19	0.08	0.04	56.31	29.92	0.04	0.01	0.01	96.00	0.03	0.06	0.04	0.01	28.18	0.01	0.01	0.00
max	0.72	4.98	0.63	0.55	66.03	34.26	0.69	0.18	1.02	100.05	0.29	1.49	0.30	0.18	31.48	0.23	0.12	0.44
mean	0.17	2.37	0.36	0.14	61.70	32.24	0.28	0.04	0.12	97.42	0.07	0.72	0.17	0.05	29.92	0.10	0.02	0.05

Table 8- Minimum, maximum and mean values of microprobe analyses of ilmenite.

	SiO_2	TiO_2	Al_2O_3	Cr_2O_3	FeO	MnO	MgO	CaO	Total	Si	Ti	Al	Cr	$Fe^{(ii)}$	Mn	Mg	Ca
Kemerlikdağı (n=8)																	
min	0.00	44.85	0.00	0.01	41.78	2.97	0.02	0.02	97.09	0.00	9.62	0.00	0.00	9.97	0.71	0.01	0.01
max	0.09	47.25	0.04	0.02	47.50	11.16	0.11	0.16	98.42	0.03	10.03	0.01	0.00	11.22	2.69	0.05	0.05
mean	0.04	46.31	0.02	0.02	45.36	5.74	0.08	0.07	97.64	0.01	9.88	0.01	0.00	10.76	1.38	0.03	0.02
Aydıntepe (n=3)																	
min	0.04	46.57	0.04	0.02	47.15	1.64	0.27	0.03	96.51	0.01	10.00	0.01	0.00	11.19	0.40	0.11	0.01
max	0.05	47.27	0.05	0.02	47.89	1.70	0.28	0.12	96.63	0.01	10.09	0.02	0.00	11.43	0.41	0.12	0.04
mean	0.05	46.92	0.05	0.02	47.52	1.67	0.28	0.08	96.57	0.01	10.05	0.02	0.00	11.31	0.40	0.12	0.02
Çiçekli (n=4)																	
min	0.01	44.38	0.03	0.02	48.09	2.18	0.39	0.02	95.52	0.00	9.70	0.01	0.00	11.69	0.54	0.17	0.01
max	0.03	44.66	0.04	0.03	48.67	2.29	0.45	0.03	95.80	0.01	9.77	0.01	0.01	11.82	0.56	0.19	0.01
mean	0.02	44.52	0.04	0.03	48.38	2.24	0.42	0.03	95.66	0.01	9.73	0.01	0.01	11.76	0.55	0.18	0.01
Somarova (n=3)																	
min	0.03	46.36	0.02	0.02	43.98	4.85	0.07	0.04	96.86	0.01	9.90	0.01	0.00	10.32	1.16	0.03	0.01
max	0.19	47.97	0.05	0.03	44.36	6.63	0.14	0.06	97.51	0.05	10.13	0.02	0.01	10.52	1.59	0.06	0.02
mean	0.09	47.26	0.04	0.03	44.15	5.54	0.10	0.05	97.27	0.03	10.05	0.01	0.01	10.44	1.33	0.04	0.01
Şaşurluk (n=4)																	
min	0.01	47.02	0.00	0.01	43.06	3.75	0.06	0.02	95.43	0.00	10.04	0.00	0.00	10.30	0.90	0.03	0.01
max	0.06	48.38	0.04	0.03	46.12	5.06	0.10	0.09	97.50	0.02	10.28	0.01	0.01	10.95	1.21	0.04	0.03
mean	0.03	47.70	0.02	0.02	44.49	4.44	0.09	0.06	96.83	0.01	10.16	0.01	0.00	10.53	1.06	0.04	0.02
Pelitli (n=3)																	
min	0.04	47.66	0.02	0.01	44.01	4.48	0.06	0.05	96.83	0.01	10.14	0.01	0.00	10.41	1.07	0.03	0.02
max	0.04	47.84	0.04	0.05	44.51	4.73	0.10	0.10	96.91	0.01	10.18	0.01	0.01	10.53	1.13	0.04	0.03
mean	0.04	47.75	0.03	0.03	44.26	4.61	0.08	0.08	96.87	0.01	10.16	0.01	0.01	10.47	1.10	0.03	0.02

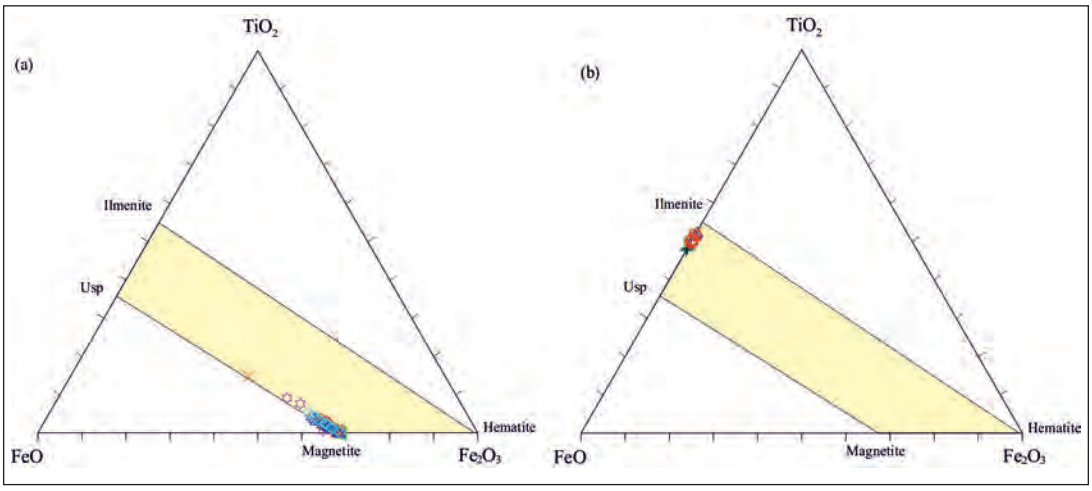

Figure 13- TiO_2-FeO-Fe_2O_3 discrimination diagrams for Fe-Ti oxides from the plutons (Bacon and Hirschmann, 1988), a) Magnetite, b) Ilmenite (Symbols as in figure 4).

4.3. Thermobarometer Calculations for the Plutons

4.3.1. Amphibole-Plagioclase thermometer

The amphibole-plagioclase thermometer recommended by Blundy and Holland (1990) was used to estimate the crystallisation temperature of the magmas. This thermometer calculates temperature with the formula T= 0.667 P - 48.98 + Y/- 0.0429 - 0.008314 LnK. The pressure (P) is calculated from amphibole minerals that developed in contact with plagioclases at equilibrium crystallisation. For X_{ab} > 0.5, Y=0. If X_{ab} < 0.5, then Y= -8.06 + 25.5(1- X_{ab})^2 is used. The K value is a special number, with (Si-4/8-Si) X_{ab} used. For the use of this thermometer, firstly amphibole–plagioclase equilibrium crystallisation should be accompanied by biotite, quartz, K-feldspar, pyroxene, Fe-Ti oxides ± sphene minerals. The thermometer reactions are chosen as edenite + 4 quartz = tremolite + albite and pargasite + 4 quartz = amphibole + albite. Plagioclase should have less calcic character than An_{92} and the cationic Si content of the amphibole developing in contact with plagioclase should be lower than 7.8. Additionally, this type of thermometer is sensitive for temperatures between 500 and 1100°C.

The temperatures calculated for the plutons were between 625 and 824°C (Table 9) and varied from 625 to 789ºC for Çiçekli Pluton, 659-768ºC for Somarova Pluton, 713-824ºC for Sorkunlu Pluton, 652-797ºC for Şaşurluk Pluton, 625-815ºC for Aydıntepe Pluton, 642-802ºC for Kemerlikdağı Pluton and 666-767ºC for Pelitli Pluton (Table 9). When mean values are examined, Sorkunlu Pluton has the highest (mean 761ºC), and the Çiçekli Pluton has the lowest values (mean 710ºC) (Table 9).

4.3.2. Amphibole Thermometer

Amphibole thermometer calculations were done by using the formula proposed by Ridolfi et al. (2010) and Ridolfi and Renzulli (2012) and the results are given in table 10. According to Ridolfi et al. (2010), the mean temperature values are; 681-802ºC for Aydıntepe Pluton, 693-788ºC for Çiçekli Pluton, 719-796ºC for Kemerlikdağı Pluton, 723-778ºC for Pelitli Pluton, 672-770ºC for Samarova Pluton, 696-767ºC for Şaşurluk Pluton and 710-797ºC for Sorkunlu Pluton (Table 10).

The amphibole temperatures calculated using the equations recommended by Ridolfi and Renzulli (2012) were between 645 and 842ºC for Aydıntepe Pluton, 627-792ºC for Çiçekli Pluton, 674-816ºC for Kemerlikdağı Pluton, 707-766ºC for Pelitli Pluton, 668-753ºC for Samarova Pluton, 727-774ºC for Şaşurluk Pluton and 724-804ºC for Sorkunlu Pluton (Table 10).

Table 9- Minimum, maximum and mean values for temperature and pressure calculated from amphiboles.

	P1 (kbar) (Hammarstrom and Zen, 1986)	P2 (kbar) (Hollister et al., 1987)	P3 (kbar) (Schmidt, 1992)	T°C Blundy and Holland (1990)
Çiçekli (n=13)				
min	0.2	0.2	0.9	625
max	1.0	0.7	1.6	789
mean	0.7	0.5	1.3	710
std (±)	0.2	0.2	0.2	51
Somarova (n=17)				
min	0.1	0.1	0.4	659
max	1.6	1.4	2.2	768
mean	0.5	0.5	1.0	722
std (±)	0.5	0.6	0.5	34
Sorkunlu (n=22)				
min	0.1	0.1	0.1	713
max	1.4	1.3	2.1	824
mean	0.5	0.5	1.1	761
std (±)	0.4	0.4	0.5	28
Şaşurluk (n=18)				
min	0.1	0.1	0.7	652
max	1.2	0.9	1.8	797
mean	0.5	0.5	1.2	759
std (±)	0.4	0.3	0.3	38
Aydıntepe (n=22)				
min	0.1	0.2	0.7	625
max	1.6	1.4	2.2	815
mean	0.5	0.6	1.1	727
std (±)	0.5	0.5	0.5	57
Kemerlikdağı (n=25)				
min	0.1	0.1	0.1	642
max	0.8	0.5	1.5	802
mean	0.3	0.3	0.9	746
std (±)	0.2	0.1	0.3	40
Pelitli (n=21)				
min	0.1	0.1	0.7	666
max	0.4	0.1	1.1	767
mean	0.2	0.1	0.9	721
std (±)	0.1	0.1	0.1	31
min: minimum, max: maksimum, mean: average, std: standard deviation				

4.3.3. Clinopyroxene Thermometer

Putirka et al. (1996, 2003) and Putirka (1999, 2005, 2008) were studied the equilibrium between clinopyroxene and the melt, in order to calculate the temperature and pressure of rock crystallisation. Putirka (2008) calculated the Fe-Mg variability constant as $K_D(Fe–Mg)^{cpyr\text{-}melt} = 0.27 \pm 0.03$ based on experimental observations to test the necessary equilibrium state between clinopyroxene and the melt. To calculate the clinopyroxene crystallisation temperature, it is necessary to know the melt

Table 10- Temperature, pressure, hydrometer and oxygen fugacity values obtained from amphiboles.

	Ridolfi et al. (2010)						Ridolfi and Renzulli (2012)			
	T°C	P (kbar)	ΔNNO	fO_2	H_2O		T°C	P (kbar)	ΔNNO	H_2O
Çiçekli (n=8)										
min	693	0.3	1.3	-14.4	3.1		627	0.4	-0.2	4.2
max	788	0.8	2.4	-12.3	5.5		792	0.9	1.7	5.6
mean	736	0.6	2.0	-13.4	4.0		719	0.6	0.9	4.7
std (±)	37	0.2	0.4	0.7	0.7		66	0.2	0.6	0.5
Somarova (n=8)										
min	672	0.3	1.5	-14.7	3.5		668	0.4	-0.3	4.5
max	770	0.7	2.7	-12.3	5.8		753	0.8	0.8	5.9
mean	723	0.5	1.9	-13.7	4.4		708	0.6	0.1	5.0
std (±)	32	0.2	0.4	0.7	0.7		33	0.1	0.4	0.5
Sorkunlu (n=10)										
min	710	0.4	1.3	-14.2	3.8		724	0.7	-0.1	4.5
max	797	0.9	2.1	-12.5	4.5		804	1.0	1.0	5.6
mean	753	0.7	1.7	-13.2	4.2		748	0.8	0.5	4.9
std (±)	23	0.1	0.3	0.5	0.2		24	0.1	0.3	0.4
Şaşurluk (n=11)										
min	696	0.3	1.2	-14.1	3.8		727	0.7	0.0	4.6
max	767	0.8	2.3	-13.3	4.5		774	0.9	0.8	5.4
mean	748	0.7	1.5	-13.6	4.2		749	0.8	0.3	4.8
std (±)	20	0.1	0.3	0.2	0.2		15	0.1	0.3	0.2
Aydıntepe (n=9)										
min	681	0.3	1.7	-14.3	3.2		645	0.3	-0.1	4.1
max	802	0.9	3.0	-12.0	5.7		842	1.3	2.4	6.6
mean	745	0.6	2.1	-13.0	4.0		762	0.8	1.5	4.6
std (±)	39	0.2	0.4	0.6	0.8		77	0.3	0.8	0.8
Kemerlikdağı (n=11)										
min	719	0.6	1.2	-14.6	3.4		674	0.5	-1.7	3.7
max	796	0.7	2.1	-12.2	6.8		816	0.9	1.2	5.4
mean	749	0.6	1.7	-13.3	4.3		747	0.7	0.5	4.6
std (±)	25	0.0	0.2	0.7	1.0		42	0.1	0.8	0.5
Pelitli (n=13)										
min	723	0.3	1.9	-13.6	2.9		707	0.6	0.4	4.6
max	778	0.6	2.7	-11.6	5.1		766	0.9	1.7	5.1
mean	749	0.6	2.3	-12.7	4.1		740	0.7	1.0	4.8
std (±)	18	0.1	0.3	0.6	0.7		21	0.1	0.6	0.2

composition in equilibrium with clinopyroxene. While electron microprobe analysis results are used for the clinopyroxene composition, the microprobe analyses of glass or data obtained from whole rock analyses may be used for the melt composition. In this study, the thermobarometer which calibrated based on clinopyroxene and melt composition and proposed by Putirka (2008) was used and the results are given in table 11.

The crystallisation temperatures calculated according to Putirka (2008) are between 1118 and 1127ºC for Aydıntepe Pluton, 1118 and 1122ºC for Çiçekli Pluton, 1104 and 1137ºC for Kemerlikdağı Pluton, 1121 and 1161ºC for Pelitli Pluton, 1129 and 1142ºC for Şaşurluk Pluton, and 1139 and 1158ºC for Sorkunlu Pluton (Table 11).

4.3.4. Biotite Thermometer

Using biotites from the studied plutonic rocks, biotite thermometer were calculated based on the formula proposed by Luhr et al. (1984) (Table 12). The crystallisation temperatures calculated according to Luhr et al. (1984) were between 726 and 793ºC for Kemerlikdağı Pluton, 709 and 795ºC for Aydıntepe

Table 11- Temperature and pressure values obtained from clinopyroxene (Putirka, 2008).

Clinopyroxene-liquid thermobarometer (Putirka, 2008)	P (32b. kbar)	T (ºC)	K_D (Ab-An)
Çiçekli (n=5)			
min	0.4	1118	0.26
max	0.9	1122	0.26
mean	0.6	1120	0.26
std (±)	0.2	2	0.00
Sorkunlu (n=5)			
min	0.8	1139	0.26
max	2.5	1158	0.27
mean	1.8	1151	0.27
std (±)	0.7	7	0.00
Şaşurluk (n=5)			
min	0.7	1129	0.26
max	1.4	1142	0.26
mean	1.0	1136	0.26
std (±)	0.3	5	0.00
Aydıntepe (n=3)			
min	0.2	1118	0.26
max	1.1	1127	0.26
mean	0.7	1123	0.26
std (±)	0.4	4	0.00
Kemerlikdağı (n=9)			
min	0.4	1104	0.25
max	2.6	1137	0.26
mean	1.6	1127	0.26
std (±)	0.7	16	0.00
Pelitli (n=4)			
min	0.6	1121	0.26
max	2.7	1161	0.27
mean	1.5	1138	0.27
std (±)	1.0	17	0.00

Table 12- Temperature, pressure and oxygen fugacity values obtained from biotite.

	P (kbar) Uchida et al. (2007)	T (°C) Luhr et al. (1984)	(fO_2) Wones (1989)
Çiçekli (n=7)			
min	0.2	780	-14.4
max	0.3	800	-13.8
mean	0.2	789	-14.2
std (±)	0.1	8	0.2
Somarova (n=17)			
min	0.1	698	-16.9
max	0.4	777	-14.5
mean	0.2	745	-15.4
std (±)	0.1	22	0.7
Sorkunlu (n=20)			
min	0.1	719	-16.2
max	0.4	783	-14.3
mean	0.2	750	-15.3
std (±)	0.1	22	0.6
Şaşurluk (n=11)			
min	0.1	708	-16.6
max	0.4	768	-14.7
mean	0.2	741	-15.5
std (±)	0.1	20	0.6
Aydıntepe (n=13)			
min	0.4	709	-16.5
max	0.7	794	-14.0
mean	0.5	758	-15.0
std (±)	0.1	27	0.8
Kemerlikdağı (n=13)			
min	0.1	726	-16.0
max	0.3	793	-14.0
mean	0.2	763	-14.9
std (±)	0.1	24	0.7
Pelitli (n=8)			
min	0.1	754	-15.1
max	0.7	801	-13.8
mean	0.3	778	-14.5
std (±)	0.2	19	0.5

Pluton, 719 and 783ºC for Sorkunlu Pluton, 780 and 800ºC for Çiçekli Pluton, 698 and 777ºC for Samarova Pluton, 708 and 768ºC for Şaşurluk Pluton and 754 and 801ºC for Pelitli Pluton (Table 12).

4.3.5. Ilmenite-Magnetite Thermometer

The ILMAT program prepared by Lepage (2003) linked to the chemical composition of magnetite and ilmenite minerals in plutonic rocks was used to calculate temperature and oxygen fugacity values for the studied plutonic rocks. When calculating the temperature values, the approaches recommended by Powell and Powell (1977), Spencer and Lindsley (1981) and Andersen and Lindsley (1985) were used.

The mean crystallisation temperatures calculated according to Powell and Powell (1977) were as follows: 406-661ºC for Kemerlikdağı Pluton, 496-582ºC for Çiçekli Pluton, 409-592ºC for Şaşurluk Pluton, 463-497ºC for Somarova Pluton and 595-628ºC for Pelitli Pluton (Table 13).

According to Spencer and Lindsley (1981), the temperatures were as follows; 550-719ºC for Kemerlikdağı Pluton, 618-668ºC for Çiçekli Pluton, 540-661ºC for Şaşurluk Pluton, 583-615ºC for Somarova Pluton and 648-668ºC for Pelitli Pluton (Table 13).

The temperatures according to Andersen and Lindsley (1985) were 556-734ºC for Kemerlikdağı

Table 13- Temperature and oxygen fugacity values obtained from magnetite and ilmenite pairs.

	Powell and Powell (1977)	Spencer and Lindsley (1981)		Andersen and Lindsley (1985)	
	T (°C)	T (ºC)	$\log_{10} fO_2$	T (ºC)	$\log_{10} fO_2$
Çiçekli (n=3)					
min	496	618	-15.6	629	-15.4
max	582	668	-15.1	684	-14.9
mean	541	645	-15.4	658	-15.1
std (±)	43	25	0.3	28	0.3
Somarova (n=4)					
min	463	583	-18.1	592	-17.7
max	497	615	-16.3	626	-15.9
mean	477	599	-17.0	609	-16.6
std (±)	18	16	1.0	17	1.0
Şaşurluk (n=6)					
min	409	540	-19.7	545	-19.3
max	592	661	-16.3	680	-15.9
mean	508	603	-18.2	616	-17.7
std (±)	83	51	1.5	57	1.5
Kemerlikdağı (n=6)					
min	406	550	-17.8	556	-17.5
max	661	719	-13.6	734	-13.5
mean	521	627	-16.0	638	-15.8
std (±)	118	79	2.0	84	1.9
Pelitli (n=3)					
min	595	648	-17.5	668	-17.1
max	628	668	-16.9	689	-16.4
mean	612	658	-17.2	679	-16.7
std (±)	24	14	0.4	15	0.4

Pluton, 629-684ºC for Çiçekli Pluton, 545-680ºC for Şaşurluk Pluton, 592-626ºC for Somarova Pluton and 668-689ºC for Pelitli Pluton (Table 13).

4.3.6. Amphibole-plagioclase Barometer

The total aluminium content of amphiboles increases linearly with increasing pressure and temperature (Hammarstrom and Zen, 1986; Hollister et al., 1987; Johnson and Rutherford, 1989; Schmidt, 1992). Especially the $Al^{(T)}$ content of amphiboles crystallising from granitoid magmas is known to be an indicator of pressure and used in pressure calculations with various calibrations. In granitoid rocks, the $Al^{(T)}$ content of amphiboles are used with the calibrations used for pressure estimation given below:

P (kbar)= 4.76 $Al^{(T)}$ - 3.01 (Schmidt, 1992); P (kbar)= 5.03 $Al^{(T)}$ - 3.92 (Hammarstrom and Zen, 1986)

P (kbar)= 5.64 $Al^{(T)}$ - 4.76 (Hollister et al., 1987); P (kbar)= 4.28 $Al^{(T)}$ - 3.54 (Johnson and Rutherford, **1**989)

Of these, the calibration of Johnson and Rutherford (1989) was produced especially for the volcanic rocks and is used for rocks formed at very high pressures. The other three calibrations may be used for granitoid rocks. However, the calibrations of Hammarstrom and Zen (1986) and Hollister et al. (1987) provide best results for granitoid rocks crystallising under high pressure conditions, while the Schmidt (1992) calibration provides better results for rocks formed at low pressures. For pressure estimations, the amphibole crystals with $Al^{(T)}$ variations used should have formed in plagioclase, amphibole, biotite, pyroxene, K-feldspar, magnetite, ilmenite ± sphene equilibrium crystallisation.

The pressures calculated based on the aluminium-hornblende barometer in amphiboles are given in Table 9. The lowest pressures were obtained with the Hammarstrom and Zen (1986) calibration, while the highest pressures were obtained with the Schmidt (1992) calibration (Table 9).

The crystallisation pressures calculated for the studied plutons have very close values to each other

(Table 9). While the crystallisation pressures for the studied plutonic rocks vary from 0.1 to 2.2 kbar, these values are as follows for the individual plutons; 0.2-1.6 kbar for Çiçekli Pluton, 0.1-2.2 kbar for Somarova Pluton, 0.1-2.1 kbar for Sorkunlu Pluton, 0.1-1.8 kbar for Şaşurluk Pluton, 0.1-2.2 kbar for Aydıntepe Pluton, 0.1-1.5 kbar for Kemerlikdağı Pluton and 0.1-1.1 kbar for Pelitli Pluton (Table 9).

4.3.7. Amphibole Barometer

Using amphiboles in the studied plutonic rocks, amphibole barometer calculations were done based on the formula proposed by Ridolfi et al. (2010) and Ridolfi and Renzulli (2012) and the values are given in table 10.

The crystallisation pressures calculated according to Ridolfi et al. (2010) are between 0.3 and 0.9 kbar for Aydıntepe Pluton, 0.3-0.8 kbar for Çiçekli Pluton, 0.6-0.7 kbar for Kemerlikdağı Pluton, 0.3-0.6 kbar for Pelitli Pluton, 0.3-0.7 kbar for Samarova Pluton, 0.3-0.8 kbar for Şaşurluk Pluton and 0.4-0.9 kbar for Sorkunlu Pluton (Table 10).

According to Ridolfi and Renzulli (2012), the calculated crystallisation pressures are as follows; 0.3-1.3 kbar for Aydıntepe Pluton, 0.4-0.9 kbar for Çiçekli Pluton, 0.5-0.9 kbar for Kemerlikdağı Pluton, 0.6-0.9 kbar for Pelitli Pluton, 0.4-0.8 kbar for Samarova Pluton, 0.7-0.9 kbar for Şaşurluk Pluton and 0.7-1 kbar for Sorkunlu Pluton (Table 10).

4.3.8. Clinopyroxene Barometer

Pyroxene barometer formula proposed by Thompson (1977) was used to determine under which pressure the magma of the plutonic rocks were uprise. (Figure 14). Thompson (1977) stated the high crystallisation pressure in magmas was linked to high Al^T content. Thus, based on the Al^T and Ti contents of clinopyroxene, the crystallisation pressure of clinopyroxene can be estimated.

The low Al^T and Ti content of clinopyroxene in the studied plutonic rocks indicates that these minerals crystallised at a lower temperature according to Thompson (1977), with the values for these plutonic rocks below 5 kbar (Figure 14).

Thermobarometer calculations proposed by Putirka (2008) for hydrous melts and calibrated based on clinopyroxene and melt composition are given in

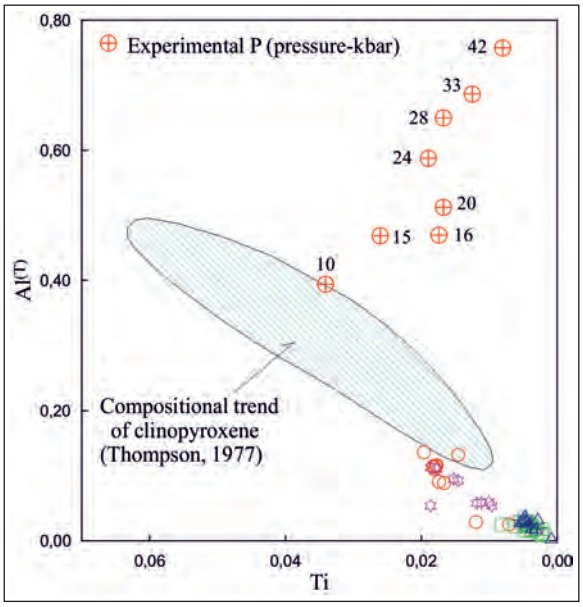

Figure 14- Correlation between Ti-Al^T related to clinopyroxenes from the plutons (For symbols see figure 4).

table 11. Accordingly, the crystallisation pressures were as follows; 0.2-1.1 kbar for Aydıntepe Pluton, 0.4-0.9 kbar for Çiçekli Pluton, 0.4-2.6 kbar for Kemerlikdağı Pluton, 0.6-2.7 kbar for Pelitli Pluton, 0.7-1.4 kbar for Şaşurluk Pluton and 0.8-2.5 kbar for Sorkunlu Pluton (Table 11).

4.3.9. Biotite Barometer

The empirical equation for determination of the crystallisation pressures for biotites proposed by Uchida et al. (2007) was calibrated according to the calculated $Al^{(T)}$ amount according to 11 oxygen using microprobe analysis results obtained from biotites.

Using this formula recommended by Uchida et al. (2007), the pressures were between 0.1 and 0.3 kbar for Kemerlikdağı Pluton, 0.4 and 0.7 kbar for Aydıntepe Pluton, 0.1 and 0.4 kbar for Sorkunlu Pluton, 0.2 and 0.3 kbar for Çiçekli Pluton, 0.1 and 0.4 kbar for Somarova Pluton, 0.1 and 0.4 kbar for Şaşurluk Pluton and 0.1and 0.7 kbar for Pelitli Pluton (Table 12).

4.3.10. Amphibole Oxygen Fugacity

Using amphiboles from the studied plutonic rocks, oxygen fugacity calculations were performed with the formulae proposed by Ridolfi et al. (2010) and Ridolfi and Renzulli (2012) and the results obtained are given in table 10.

The amphibole oxygen fugacity (ΔNNO) calculated according to Ridolfi et al. (2010) vary as follows; 1.7 to 3 for Aydıntepe Pluton, 1.3 to 2.4 for Çiçekli Pluton, 1.2 to 2.1 for Kemerlikdağı Pluton, 1.9 to 2.7 for Pelitli Pluton, 1.5 to 2.7 for Samarova Pluton, 1.2 to 2.3 for Şaşurluk Pluton and 1.3 to 2.1 for Sorkunlu Pluton (Table 10).

Using the temperature and pressure values obtained by Ridolfi et al. (2010), the oxygen fugacity (fO_2) values calculated with the approach proposed by Wones (1989) were as follows; -14.3 to -12 for Aydıntepe Pluton, -14.4 to -12.3 for Çiçekli Pluton, 14.6 to -12.2 for Kemerlikdağı Pluton, -13.6 to -11.6 for Pelitli Pluton, -14.7 to -12.3 for Samarova Pluton, -14.1 to -13.3 for Şaşurluk Pluton and -14.2 to -12.5 for Sorkunlu Pluton (Table 10).

The oxygen fugacity values (ΔNNO) calculated using the equations of Ridolfi and Renzulli (2012) were between -0.1 to 2.4 for Aydıntepe Pluton, -0.2 to 1.7 for Çiçekli Pluton, -1.7 to 1.2 for Kemerlikdağı Pluton, 0.4 to 1.7 for Pelitli Pluton, -0.3 to 0.8 for Samarova Pluton, 0 to 0.8 for Şaşurluk Pluton and -0.1 to 1 for Sorkunlu Pluton (Table 10).

4.3.11. Biotite Oxygen Fugacity

The oxygen fugacity values (fO_2) calculated by using the pressure values recommended by Wones (1989) and calculated by Luhr et al. (1984) (Table 12) and using the temperature values by Uchida (2007) (Table 12) are given in table 12 and are as follows: -16 to -14 for Kemerlikdağı Pluton, -16.5 to -14 for Aydıntepe Pluton, -16.2 to -14.3 for Sorkunlu Pluton, -14.4 to -13.8 for Çiçekli Pluton, -16.9 to -14.5 for Samarova Pluton, 16.6 to -14.7 for Şaşurluk Pluton and -15.1 to -13.8 for Pelitli Pluton.

4.3.12. Ilmenite-magnetite Oxygen Fugacity

The oxygen fugacity values were calculated using the ILMAT program prepared by Lepage (2003) linked to the chemical composition of magnetite and ilmenite minerals in studied plutonic rocks.

The oxygen fugacity values calculated according to Spencer and Lindsley (1981) and Andersen and Lindsley (1985) were as follows; -17.8 to -13.6 for Kemerlikdağı Pluton, -15.6 to -15.1 for Çiçekli Pluton, -19.7 to -16.3 for Şaşurluk Pluton, -18.1 to -16.3 for Samarova Pluton and -17.5 to -16.9 for Pelitli Pluton (Table 13).

The oxygen fugacity values calculated according to Andersen and Lindsley (1985) are given in Table 13 and were as follows; -17.5 to -13.5 for Kemerlikdağı Pluton, -15.4 to -14.9 for Çiçekli Pluton, -19.3 to -15.9 for Şaşurluk Pluton, -17.7 to -15.9 for Samarova Pluton and -17.1 to -16.4 for Pelitli Pluton (Table 13).

4.3.13. Amphibole Hydrometer

Using amphiboles in the studied plutonic rocks, hydrometer calculations were performed using formulae recommended by Ridolfi et al. (2010) and Ridolfi and Renzulli (2012) and the results are given in table 10.

The mean water content calculated according to Ridolfi et al. (2010) is 3.2-5.7% for Aydıntepe Pluton, 3.1-5.5% for Çiçekli Pluton, 3.4-6.8% for Kemerlikdağı Pluton, 2.9-5.1% for Pelitli Pluton, 3.5-5.8% for Samarova Pluton, 3.8-4.5% for Şaşurluk Pluton and 3.8-4.5% for Sorkunlu Pluton (Table 10).

According to Ridolfi and Renzulli (2012), the calculated mean water contents were as follows; 4.1-6.6% for Aydıntepe Pluton, 4.2-5.6% for Çiçekli Pluton, 3.7-5.4% for Kemerlikdağı Pluton, 4.6-5.1% for Pelitli Pluton, 4.5-5.9% for Samarova Pluton, 4.6-5.4% for Şaşurluk Pluton and 4.5-5.6% for Sorkunlu Pluton (Table 10).

5. Discussion

The Eastern Pontides, forming from the Palaeozoic to the present day, have been under a compressional regime dominated by nearly N-S orientation especially since the beginning of the Mesozoic, with NE-SW and NW-SE oriented fracture systems developed related to this regime. Generally, the long axes of plutons in the Eastern Pontides align with these main fracture orientations. The correlation of pluton emplacement with main fracture lines was first determined by Gedikoğlu (1978), with new studies in the region clarifying these correlations (Kaygusuz et al., 2008, 2012). The studied plutonic rocks are generally emplaced parallel to the NE-SW oriented fracture lines. The plutons generally have ellipsoidal shape, with sharp and unconformable contacts with wall rocks and fine-grained contact facies with these rocks. At contacts with wall rocks, porphyritic and granophyritic textures are observed and a small number of xenoliths from the wall rocks are observed. All these characteristics indicate the studied plutonic rocks were emplaced at shallow depths of the crust.

The mineral content of the studied plutonic rocks allowed the chance to use amphibole-plagioclase (Hammarstrom and Zen, 1986; Hollister et al., 1987; Johnson and Rutherford, 1989; Schmidt, 1992), amphibole (Ridolfi et al., 2010; Ridolfi and Renzulli, 2012), biotite (Uchida et al., 2007) and clinopyroxene (Putirka, 2008) geobarometers; amphibole-plagioclase (Blundy and Holland, 1990), amphibole (Ridolfi et al., 2010; Ridolfi and Renzulli, 2012), ilmenite-magnetite (Powell and Powell, 1977, Spencer and Lindsley, 1981; Andersen and Lindsley, 1985), biotite (Luhr et al., 1984) and clinopyroxene (Putirka, 2008) geothermometers; amphibole (Ridolfi et al., 2010; Ridolfi and Renzulli, 2012), biotite (Wones, 1989) and ilmenite-magnetite (Spencer and Lindsley, 1981; Andersen and Lindsley, 1985) oxygen fugacity calculations and amphibole hydrometry (Ridolfi et al., 2010; Ridolfi and Renzulli, 2012).

The amphibole-plagioclase and amphibole barometers used in this study reveals similar values (0.1-2.2 kbar), while the values obtained from the biotite barometer are lower (0.1-0.7) and the values obtained from the clinopyroxene barometer are higher (0.2-2.7). When compared with other Eocene-aged plutonic rocks in the Eastern Pontides, the pressure values for these plutonic rocks are similar to values identified for the Dölek-Sarıçiçek plutons (1-3.8 kbar, Karslı et al., 2007), whereas, they have lower values compared to the Dölek, Sarıçiçek, Sorkunlu, Üzengili and Arslandede plutons (0.3-8.2 kbar, Eyüboğlu et al., 2017). As mentioned previously, the amphiboles in the studied plutonic rocks are calcic amphiboles with $Al^{(t)}$ values lower than 2.0. According to Hammarstrom and Zen (1986), hornblendes having $Al^{(t)} \leq 2.0$ values generally indicate shallow depth intrusion. Additionally, the textural properties like graphic-growth supporting shallow intrusion of the plutons are noteworthy in the studied plutons. The solidus temperature given by thermometers like amphibole-plagioclase is generally >700°C (Anderson, 1996). If the solidus temperature obtained from amphibole--plagioclase thermometers is lower than this temperature (~700°C), subsolidus re-equilibration occurs (Moazzen and Droop, 2004).

Calculations made on minerals in the studied plutonic rocks indicate temperature values ranging between 625 and 842°C for amphibole-plagioclase, amphibole and biotite thermometers, while the values indicate that the clinopyroxene thermometer are higher (1104-1161°C) and values for the magnetite-ilmenite thermometer are lower (406-719°C). Compared with other plutonic rocks with similar age in the Eastern Pontides, the studied plutons have similar temperature values to those calculated for the Dölek-Sarıçiçek plutons (617-768°C, Karslı et al., 2007) and are lower than those of the Dölek, Sarıçiçek, Sorkunlu, Üzengili and Arslandede plutons (388-1196°C, Eyüboğlu et al., 2017).

The biotites from the studied plutons have average values of Al^4 (2.42-2.54 fbb) and partly high Mg# (0.43-0.55), posses close values to the biotites in the plutons formed by mantle-sourced magma products (Al^4 = 2.3-2.4; Mg# > 0.60) and partly different values (Figure 15). As shown in figure 15, the biotites of studied plutons remain separate from mantle-derived melt and meta-sedimentary melt mixing curve. This leads to the consideration that the source rock was not purely mantle. Additionally, the observation of textural data indicating disequilibrated crystallisation in the studied samples and the common mafic magmatic enclaves observed in most of the plutons indicates magma mixing.

As the original oxygen fugacity of granitic magmas cannot be determined due to slow cooling, only relative approaches and calculations may be made (Wones, 1989; Anderson and Smith, 1995; Kemp, 2004). In the studied samples, the oxygen fugacity values ($\log_{10} fO_2$) are between -20 and -12, similar to the values identified for the Eocene-aged Dölek-Sarıçiçek plutons (-15 to -21, Karslı et al., 2007)

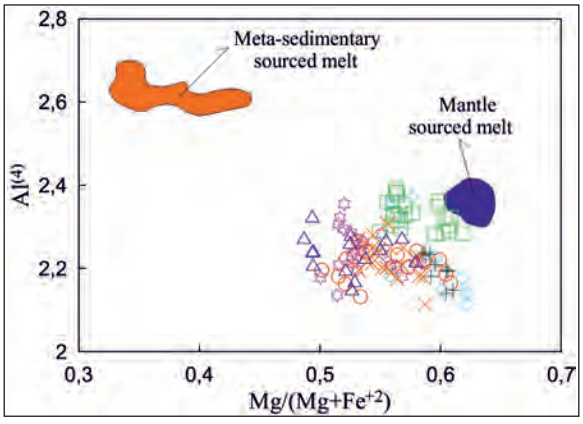

Figure 15- Correlation between Al^4-Mg/(Mg+Fe^{+2}) in biotites from the plutons and comparison with meta-sedimentary sourced melts and mantle sourced moderate-felsic melts [meta-sedimentary melt area from Kemp (2001), mantle sourced melt area taken from Kemp (2004)] (For symbols see figure 4).

The water content of magmas containing amphiboles is controversial, with variation between 2-3% according to Luhr et al. (1992), mean 5% according to Eggler (1972), Helz (1973) and Naney (1983) and mean 6% according to Merzbacher and Eggler (1984). In the studied samples, the water content calculated from the amphiboles was 2.9 to 6.8. The presence of hydrous mafic minerals (amphibole, biotite), titanite and apatite in the samples indicates high water and volatile contents in magma. The high temperature magmas in this content may rise to shallow depths in continental crust without completely crystallising (Helmy et al., 2004).

Finally, according to thermobarometric calculations based on mineral chemistry data, the studied rocks have pressure values between 0.1 and 2.7 kbar and temperature values from 406 to 1161°C. When all these characteristics are noted, it is proposed that the studied plutons were emplaced at shallow depths (1-8 km) within Eastern Pontide continental crust thickened after collision in the Cenozoic period.

6. Conclusions

The investigated Cenozoic plutons generally have NE-SW orientation and nearly ellipsoid shapes. The sizes of the plutons vary from 3 to 22 km^2 with the smallest Çiçekli Pluton (3 km^2) and the largest Kemerlikdağı pluton (22 km^2). The Çiçekli and Şaşurluk plutons are slightly more altered compared to the other plutons. The composition of the studied plutons ranges from gabbroic diorite to monzogranite. The main minerals in the rocks are plagioclase, K-feldspar, quartz, amphibole, biotite, pyroxene and Fe-Ti oxides. The rocks have fine-moderate granular, porphyric, monzonitic, poikilitic, occasionally myrmekitic, micrographic and graphic textures. Additionally, there are some special mixing textures observed indicating magma mixing. The An content of plagioclase in the studied plutonic rocks varies from 2 to 69, with the highest in the Sorkunlu Pluton and the lowest in the Şaşurluk Pluton. The Or content of K-feldspar varies from 1 to 96, with the lowest content in the Somarova Pluton and highest in the Şaşurluk Pluton. The biotite in the rocks is a solid melt product between the phlogopite-annite end members and is rich in magnesium. Amphiboles are calcic amphiboles, with magnesium-rich hornblende and actinolite in composition. Pyroxenes are calcic clinopyroxenes, apart from Aydıntepe Pluton containing clinoenstatite orthorhombic pyroxenes. Calcic pyroxenes are generally augite, with low rates of diopside in composition. Fe-Ti oxides comprise magnetite and ilmenite. According the thermobarometer calculations, the studied plutons have pressures from 0.1 to 2.7 kbar, temperature from 406 to 1161°C, oxygen fugacity values between -20 and -12 and water content of 2.9-6.8%. When field, petrographic and thermobarometric data are considered together, it may be concluded that the studied plutons were intruded at shallow depths (~1-8 km) in continental crust.

Acknowledgements

This study was supported by TÜBİTAK project number 115Y154. We thank Emre Topçu and Damla Selvi for their help during field studies. We gratefully acknowledge Pınar Şen, Fatih Karaoğlan, Şenel Özdamar and two anonymous reviewers for their contributions during the review and assessment stages of this manuscript.

References

Ağar, Ü. 1977. Demirözü (Bayburt) ve Köse (Kelkit) bölgesinin jeolojisi. Doktora Tezi, İstanbul Üniversitesi Fen Fakültesi, 59 s, İstanbul.

Alemdağ, S. 2015. Assessment of bearing capacity and permeability of foundation rocks at the Gumustas waste dam site, (NE Turkey) Using empirical and numerical analysis. Arabian Journal of Geosciences, 8, 1099-1110.

Andersen, D.J., Lindsley, D.H. 1985. New (and final) models for the Ti-magnetite/ilmenite geothermometer and oxygen barometer. Abstract AGU 1985 Spring Meeting Eos Transactions. American Geophysical Union, 66 (18), 416.

Anderson, J.L. 1996. Status of thermobarometry in granitic batholiths. Trans Royal Society Edinburgh, Earth Sciences, 87, 125-138.

Anderson, J.L., Smith, D.R. 1995. The effects of temperature and fO_2 on the Al-inhornblende barometer. American Mineralogist, 80, 549-559.

Arslan, M., Aslan, Z. 2006. Mineralogy, petrography and whole-rock geochemistry of the Cenozoic granitic intrusions in the Eastern Pontides (Turkey). Journal of Asian Earth Sciences, 27, 177-193.

Arslan, M., Şen, C., Aliyazıcıoğlu, İ., Kaygusuz, A., Aslan, Z. 2000. Trabzon ve Gümüşhane yörelerinde (KD, Türkiye) yüzeylenen Eosen (?) volkanitlerinin karşılaştırılmalı jeolojisi, mineralojisi ve Petrolojisi. Cumhuriyetin 75. Yıldönümü Yerbilimleri ve Madencilik Kongresi Bildiriler Kitabı, 39-53.

Arslan, M., Temizel, İ., Abdioğlu, E., Kolaylı, H., Yücel, C., Boztuğ, D., Şen, C. 2013. ^{40}Ar-^{39}Ar dating, whole-rock and Sr-Nd-Pb isotope geochemistry of post-collisional Eocene volcanic rocks in the southern part of the Eastern Pontides (NE Turkey): Implications for magma evolution in extension-induced origin. Contributions to Mineralogy and Petrology, 166, 113-142.

Aslan, Z. 1998. Saraycık-Sarıhan Granitoyidleri (Bayburt) ve çevre kayaçlarının petrolojisi, jeokimyası ve Sarıhan Granitoyidinin jeokronolojik incelenmesi. Doktora Tezi, KTÜ Fen Bilimleri Enstitüsü, Trabzon.

Aslan, Z., Arslan, M., Şen, C. 1999. Doğu Pontidlerin kuzey ve güney zonlarında yüzeylenen Eosen yaşlı granitik sokulumların karşılaştırılmalı jeolojik, petrografik ve jeokimyasal özellikleri. 52. Türkiye Jeoloji Kurultayı Bildiriler Kitabı, 223-230.

Aslan, Z., Arslan, M., Temizel, İ., Kaygusuz, A. 2014. K-Ar dating, whole-rock and Sr-Nd isotope geochemistry of calc-alkaline volcanic rocks around the Gümüşhane area: implications for post-collisional volcanism in the Eastern Pontides, Mineralogy and Petrology, 108, 254-267.

Aydınçakır, E. 2014. The Petrogenesis of Early-Eocene non-adakitic volcanism in NE Turkey: Constraints on geodynamic implications. Lithos, 208, 361-377.

Bacon C.R. Hirschmann, M.M. 1988. Mg/Mn partitioning as a test for equilibrium between coexisting Fe-Ti oxides. American Mineralogist, 73, 57-61.

Blundy, J.D., Holland, T.J.B. 1990. Calcic amphibole equilibria and a new amphibole-plagioclase geothermometer. Contributions to Mineralogy and Petrology, 208-224.

Boztuğ, D., Erçin, A.İ., Kuruçelik, M.K., Göç, D., Kömür, İ., İskenderoğlu, A. 2006. Geochemical characteristics of the composite Kaçkar batholith generated in a Neo-Tethyan convergence system, eastern Pontides, Turkey. Journal of Asian Earth Sciences, 27, 286-302.

Çakmak, G., Kaygusuz, A. 2014. Pelitli (Bayburt) Plütonunun petrografik ve jeokimyasal özellikleri. Gümüşhane Üniversitesi, Fen Bilimleri Enstitüsü Dergisi, 4 (1), 46-63.

Çoğulu, E. 1975. Gümüşhane ve Rize bölgelerinde petrolojik ve jeokronometrik araştırmalar. İ.T.Ü. Yayını, 1034, İstanbul, 112 s.

Dokuz, A. 2011. A slab detachment and delamination model for the generation of Carboniferous high-potassium I-type magmatism in the eastern Pontides, NE Turkey: Köse composite pluton. Gondwana Research, 19; 926-944.

Eggler, D.H. 1972. Water-saturated and undersaturated melting relations in a Paricutin andesite and an estimate of water content in the natural magma, Contributions to Mineralogy and Petrology, 34, 261-271.

Eyüboğlu, Y., Dudas, F.O., Thorkelson, D., Zhu, D.C., Liu, Z., Chatterjee, N., Yi, K., Santosh, M. 2017. Eocene granitoids of northern Turkey: Polybaric magmatism in an evolving arc-slab window system, Gondwana Research, 50, 311-345.

Eyüboğlu, Y., Dudas F.O., Santosh, M., Y.I.K., Kwon, S., Akaryalı, E. 2013. Petrogenesis and U-Pb zircon chronology of adakitic porphyries within the Kop ultramafic massif (Eastern Pontides Orogenic Belt, NE Turkey). Gondwana Research, 24, 742-766.

Gedikoğlu, A. 1978. Harşit granit karmaşığı ve çevre kayaçları. Doçentlik Tezi, KTÜ Yer Bilimleri Fakültesi, Trabzon 161 p (unpublished).

Hammarstrom, J.M., Zen, E. 1986. Aluminum in amfibole: An empirical igneous geobarometer. American Mineralogist, 71, 1297-1313.

Helmy, H.M., Ahmed, A.F., El Mahallawi, M.M., Ali, S.M. 2004. Pressure, temperature and oxygen fugacity conditions of calc-alkaline granitoids, Eastern Desert of Egypt, and tectonic implications. Journal of African Earth Sciences, 38, 255-268.

Helz, RT. 1973. Phase relations of basalts in their melting ranges at PH_2O=5 kb as a function of oxygen fugacity, Journal of Petrology, 14, 249-302.

Hollister, L.S., Grisson, G.C., Peters, E.K., Stowell, H.H., Sisson, V.B. 1987. Confirmation of the empirical calibration of aluminum in amfibole with pressure of solidification of calc-alkaline plutons. American Mineralogist, 72, 231-239.

İlbeyli, N. 2008. Geochemical characteristics of the Şebinkarahisar granitoids in the eastern Pontides, northeast Turkey: petrogenesis and tectonic implications. International Geology Review, 50, 563-582.

Johnson, M.C., Rutherford, M.J. 1989. Experimental calibration of the aluminiun-in amfibole geobarometer with application to Long Valley Caldera (California) volcanic rocks. Geology, 17,837-841.

Karslı, O., Chen, B., Aydın, F., Şen, C. 2007. Geochemical and Sr-Nd-Pb isotopic compositions of the Eocene Dölek and Sarıçiçek plutons, Eastern Turkey: Implications for magma interaction in the genesis of high-K calc-alkaline granitoids in a post-collision extensional setting. Lithos, 98, 67-96.

Karslı, O., Dokuz, A., Uysal, İ., Aydın, F., Chen, B., Kandemir, R., Wijbrans, J. 2010. Relative contributions of crust and mantle to generation of Campanian high-K calc-alkaline I-type granitoids in a subduction setting, with special reference to the Harşit Pluton (Eastern Turkey), Contributions to Mineralogy and Petrology, 160, 467-487.

Karslı, O., Dokuz, A., Kandemir, R. 2017. Subduction-related Late Carboniferous to Early Permian magmatism in the Eastern Pontides, the Camlik and Casurluk plutons: Insights from geochemistry, whole-rock Sr-Nd and in situ zircon Lu-Hf isotopes, and U-Pb geochronology. Lithos, doi: 10.1016/j.lithos.2016.10.007.

Kaygusuz, A. 2009. K/Ar ages and geochemistry of the collision related volcanic rocks in the Ilıca (Erzurum) area, eastern Turkey. Neues Jahrbuch Für Mineralogie, 186/1, 21-36.

Kaygusuz, A., Şen, C. 2011. Calc-alkaline I-type plutons in the eastern Pontides, NE Turkey: U-Pb zircon ages, geochemical and Sr-Nd isotopic evidence. Chemie der Erde Geochemistry, 71, 59-75.

Kaygusuz, A., Aydınçakır, E. 2011. Petrogenesis of a Late Cretaceous composite pluton from the Eastern Pontides: the Dağbaşı Pluton, NE Turkey. Neues Jahrbuch Für Mineralogie, 188/3, 211-233.

Kaygusuz, A., Öztürk, M. 2015. Geochronology, geochemistry, and petrogenesis of the Eocene Bayburt intrusions, Eastern Pontide, NE Turkey: implications for lithospheric mantle and lower crustal sources in the high-K calc-alkaline magmatism. Journal of Asian Earth Sciences, 108, 97-116.

Kaygusuz, A., Şahin, K. 2016. Petrographical, geochemical and petrological characteristics of Eocene volcanic rocks in the Mescitli area, Eastern Pontides (NE Turkey). Journal of Engineering Research and Applied Science, 5 (2), 473-486.

Kaygusuz, A., Şen, C., Aslan, Z. 2006. Torul (Gümüşhane) volkanitlerin petrografik ve petrolojik özellikleri (KD Türkiye); Fraksiyonel kristallenme ve magma karışımına ilişkin bulgular. Türkiye Jeoloji Bülteni, 49, 49-82.

Kaygusuz, A., Wolfgang, S., Şen, C., Satır, M. 2008. Petrochemistry and petrology of I-type granitoids in an arc setting: the composite Torul pluton, Eastern Pontides, NE Turkey. International Journal of Earth Sciences, 97, 739-764.

Kaygusuz, A., Wolfgang, S., İlbeyli, N., Arslan, M., Satır, M., Şen, C. 2010. Insight into magma genesis at convergent plate margins - a case study from the eastern Pontides (NE Turkey). Neues Jahrbuch Für Mineralogie, 187/3, 265-287.

Kaygusuz, A., Arslan, M., Wolfgang, S., Sipahi, F., İlbeyli, N. 2012. Geochronological evidence and tectonic significance of Carboniferous magmatism in the southwest Trabzon area, eastern Pontides, Turkey. International Geology Rew, 54 (15), 1776-1800.

Kaygusuz, A,. Sipahi, F,. İlbeyli, N,. Arslan, M,. Chen, B., Aydınçakır, E. 2013. Petrogenesis of the Late Cretaceous Turnagöl intrusion in the eastern Pontides: Implications for magma genesis in the arc setting. Geoscience Frontiers, 4, 423-438.

Kaygusuz, A., Arslan, M., Sipahi, F., Temizel, İ. 2016. U-Pb zircon chronology and petrogenesis of Carboniferous plutons in the northern part of the Eastern Pontides, NE Turkey: constraints for Paleozoic magmatism and geodynamic evolution. Gondwana Research, 39, 327-346.

Kemp, A.I.S. 2001. Petrogenesis of granitic rocks: A source based perspective. PhD Thesis, Autralian National University, Canberra, Australia (unpublished).

Kemp, A.I.S. 2004. Petrology of high-Mg, low-Ti igneous rocks of the Glenelg River Complex (SE Australia) and the nature of their interaction with crustal melts, Lithos, 119-156.

Keskin, İ., Korkmaz, S., Gedik, İ., Ateş, M., Gök, L., Küçümen, Ö., Erkal, T. 1989. Bayburt Dolayının Jeolojisi. Maden Tetkik ve Arama Genel Müdürlüğü rap. No: 8995,129 s, Ankara (unpublished).

Köprübaşı, N., Şen, C., Kaygusuz, A. 2000. Doğu Pontid adayayı granitoyidlerinin karşılaştırılmalı petrografik ve kimyasal özellikleri, KD Türkiye. Uygulamalı Yerbilimleri Dergisi, 1, 111-120.

Leake, E.B., Wooley, A.R., Arps, C.E.S., Birch, W.D., Gilbert, M.C., Grice, J.D., Hawthorne, F.C., Kato, A, Kisch, H.J., Krivovichev, V.G., Linthout, K., Laird, J., Mandarino, J., Maresch, W.V., Nickhel, E.H., Rock, N.M.S., Schumacher, J.C., Smith, D.C., Stephenson, N.C.N., Ungaretti, L., Whittaker, E.J.W., Youzhi, G. 1997. Nomenclature of amphiboles report of the subcommittee on amphiboles of the International Mineralogical Association Commission on New Minerals and Mineral Names. European Journal of Mineralogy, 9, 623-651.

Lepage, L.D. 2003. ILMAT: an excel worksheet for ilmenite-magnetite geothermometry and geobarometry. Computer Geosciences, 29 (5), 673-678.

Luhr, J.F., Carmichael, I.S.E., Varekamp, J.C. 1984. The 1982 eruptions of El Chicón Volcano, Chiapas, Mexico: Mineralogy and petrology of the anhydrite-

bearing pumices. Journal of Volcanology and Geothermal Research, 23, 69-108.

Merzbacher, C., Eggler, D.H. 1984. A magmatic geohygrometer: application to Mount St. Helens and other dacitic magmas, Geology, 12, 587-590.

Moazzen, M., Droop, G.T.R. 2004. Application of mineral thermometers and barometers to granitoid igneous rocks: the Etive Complex, W Scotland. Mineralogy and Petrology, 83, 27-53.

Morimoto, M. 1988. Nomenclature pyroxenes. Mineralogical Magasine, 52, 535-550.

Naney, MT. 1983. Phase equilibria of rock-forming ferromagnesian silicates in granitic systems, American Journal of Science, 283, 993-1033.

Önenç, D.İ., Altınbaş, A.F., Erkanol, D., Tulukçu, A. 2005. Bayburt taşı ve doğal taş potansiyeli. Maden Jeolojisi Raporu, Maden Tetkik ve Arama Müdürlüğü, Ankara, 155 s.

Özdamar, Ş. 2016. Geochemistry and geochronology of Late Mesozoic volcanic rocks in the northern part of the Eastern Pontide Orogenic Belt (NE Turkey): implications for the closure of the Neo-Tethys Ocean. Lithos, 248-251, 240-256.

Özdamar, Ş., Roden, M.F., Billor, M.Z. 2017. Petrology of the shoshonitic Çambaşı Pluton in NE Turkey and implications for the closure of the Neo-Tethys Ocean: insights from geochemistry, geochronology and Sr-Nd isotopes. Lithos, 284 (285), 477-492.

Papike, J.J., Cameron, K.L. Baldwın, K. 1974. Amphiboles and pyroxenes: Characterization of other than quadrilateral components and estimates of ferric iron from microprobe data. Geological Society of America, 6, 1053-1054.

Parsons, I., Mason, R.A., Becker, S.M., Finch, A.A. 1991. Biotite equilibria and fluid circulation in the Klokken Intrusion. Journal of Petrology, 32, 1299-1333.

Powell, R., Powell, M. 1977. Geothermometry and oxygen barometry using coexisting iron-titanium oxides: a reappraisal. Mineralogical Magazine, 41 (318), 257-263.

Putirka, K.D. 1999. Clinopyroxene+liquid equilibrium to 100 kbar and 2450 K. Contributions to Mineralogy and Petrology, 135, 151-163.

Putirka, K.D. 2005. Igneous thermometers and barometers based on plagioclase + liquid equilibria: Tests of some existing models and new calibrations. American Mineralogist, 90, 336-346.

Putirka, K.D. 2008. Thermometers and barometers for volcanic systems. In: Putirka K.D., Tepley, F., (eds). Reviews in Mineralogy, 69, 61-120.

Putirka, KD., Johnson, M., Kinzler, R., Walker, D. 1996. Thermobarometry of mafic igneous rocks based on clinopyroxene-liquid equilibria, 0-30 kbar. Contributions to Mineralogy and Petrology, 123, 92-108.

Putirka, K.D., Ryerson, F.J., Mikaelian, H. 2003. New igneous thermobarometers for mafic and evolved lava compositions, based on clinopyroxene + liquid equilibria. American Mineralogist, 88, 1542-1554.

Ridolfi F., Renzulli, A. 2012. Calcic amphiboles in calc-alkaline and alkaline magmas: thermobarometric and chemometric empirical equations valid up to 1,130°C and 2.2 Gpa. Contributions to Mineralogy and Petrology, 163, 877-895.

Ridolfi, F., Renzulli, A., Puerini, M. 2010. Stability and chemical equilibrium of amphibole in calc-alkaline magmas: an overview, new thermobarometric formulations and application to subduction- related volcanoes. Contributions to Mineralogy and Petrology, 160, 45-66.

Saydam Eker, Ç., Sipahi, F., Kaygusuz, A. 2012. Trace and rare earth elements as indicators of provenance and depositional environments of Lias cherts in Gumushane, NE Turkey. Chemie der Erde Geochemistry, 72, 167-177.

Schmidt, M.W. 1992. Amphibole composition in tonalite as a function of pressure: An experimental calibration of the Al-in amfibole barometer. Contributions to Mineralogy and Petrology, 110, 304-310.

Sipahi, F., Sadıklar, M.B., Şen, C. 2014. The Geochemical and Sr-Nd isotopic characteristics of Murgul (Artvin) volcanics in the Eastern Black Sea region (NE Turkey). Chemie der Erde/Geochemistry, 74, 331-342.

Sipahi, F., Kaygusuz, A., Saydam Eker, Ç., Vural, A., Akpınar, İ. 2017. Late Cretaceous arc igneous activity: The Eğrikar Monzogranite example. International Geology Review, 60 (3), 382-400.

Smith, J.V., Brown, W.L. 1988. Feldspar minerals. 2nd review and extended edition Book (ISBN 0387176926), Springer-Verlag, Berlin.

Spencer, K.J., Lindsley, D.H. 1981. A solution model for coexisting iron-titanium oxides. American Mineralogist, 66 (11-12), 1189-1201.

Streckeisen, A. 1976. To each plutonic rock its proper name. Earth Sciences Review, 12, 1-33.

Şahin, S.Y., Güngör, Y., Boztuğ, D. 2004. Comparative petrogenetic investigation of composite Kaçkar Batholith granitoids in eastern Pontide magmatic arc (Northern Turkey). Earth Planets Space, 56, 429-446.

Temizel, İ., Arslan, M., Ruffet, G., Peucat, J.J. 2012. Petrochemistry, geochronology and Sr-Nd isotopic systematics of the Tertiary collisional and post-collisional volcanic rocks from the Ulubey (Ordu) area, eastern Pontide, NE Turkey: implications for extension-related origin and mantle source characteristics. Lithos, 128, 126-147.

Temizel, İ., Arslan, M., Yücel, C., Abdioğlu, E., Ruffet, G. 2016. Geochronology and geochemistry of Eocene-aged volcanic rocks around the Bafra (Samsun, N Turkey) area: constraints for the interaction of lithospheric mantle and crustal melts. Lithos, 258-259, 92-114.

Thompson, R.N. 1977. Primary basalts and magma genesis. Contributions to Mineralogy and Petrology, 60, 91-108.

Topuz, G., Altherr, R., Schwarz, W.H., Siebel, W., Satır, M., Dokuz, A. 2005. Post-collisional plutonism with adakite-like signatures: the Eocene Saraycık Granodiorite (Eastern Pontides, Turkey). Contributions to Mineralogy and Petrology, 150, 441-455.

Topuz, G., Altherr, R., Siebel, W., Schwarz, W.H., Zack, T., Hasözbek, A., Barth, M., Satır, M., Şen, C. 2010. Carboniferous high-potassium I-type granitoid magmatism in the Eastern Pontides: the Gümüşhane Pluton (NE Turkey). Lithos, 116, 92-110.

Uchida, E., Endo, S., Makino, M. 2007. Relationship between solidification depth of granitic rocks and formation of hydrothermal ore deposits. Resource Geology, 57, 47-56.

Wones, D.R. 1989. Significance of the assemblage titanite + magnetite + quartz in granitic rocks. American Mineralogist, 74, 744-749.

Yılmaz, S., Boztuğ, D. 1996. Space and time relations of three plutonic phases in the Eastern Pontides (Turkey). International Geology Review, 38, 935-956.

Yılmaz, Y. 1972. Petrology and structure of the Gümüşhane Granite and surraunding rocks, North-Eastern Anatolia. PhD Thesis, University of London, 260 s.

Yücel, C., Arslan, M., Temizel, İ., Abdioğlu, E. 2014. Volcanic facies and mineral chemistry of Cenozoic volcanics in the northern part of the Eastern Pontides, Northeast Turkey: Implications for pre-eruptive crystallization conditions and magma chamber processes. Mineralogy and Petrology, 108, 439-467.

Yücel, C., Arslan, M., Temizel, İ., Abdioğlu Yazar, E., Ruffet, G. 2017. Evolution of K-rich magmas derived from a net veined lithospheric mantle in an ongoing extensional setting: Geochronology and geochemistry of Eocene and Miocene volcanic rocks from Eastern Pontides (Turkey). Gondwana Research, 45, 65-86.

Bull. Min. Res. Exp. (2018) 157: 103-120

Bulletin of the Mineral Research and Exploration

http://bulletin.mta.gov.tr

Petrography and petrology of The Yürekli (Balıkesir) volcanics: an example of post-collisional felsic volcanism in the Biga peninsula (NW Turkey)

Ece Simay SAATCI[a] and Zafer ASLAN[b*]

[a]*Died in a traffic accident on 08 August 2017*

[b]*Balıkesir University, Faculty of Engineering, Department of Geological Engineering, Çağış Campus, 10145 Altıeylül/Balıkesir.*
orcid.org/0000-0002-3418-4368

Research Article

Keywords:
Calc-alkaline rocks, geochemistry, fractional crystallization, tectonic setting, NW Anatolia.

ABSTRACT

In this study, it is aimed to determine to petrographical, geochemistry and sources of the Yürekli volcanics (Biga Peninsula, NW Turkey). Tertiary volcanism is widespread in Western Anatolia (NW Turkey), is an important area where tectonic and magmatic events are observed together. Yürekli volcanic rocks composed of dacitic lavas and pyroclastics. Dacitic lavas show porphyric and hyalo-porphyric texture, and consisting of plagioclase, quartz, amphibole, biotite, sanidine and Fe-Ti oxide minerals with apatite and zircon accessory minerals. Petrologically, it is high-potassic and calc-alkaline in characteristic. Yürekli volcanics show enrichment in large ion litophile elements (LILE) while depletion in high field strength elements (HFSE) on the N-MORB normalized diagram. On the chondrite-normalized rare earth element (REE) plot, light rare earth elements are enriched but heavy rare earth elements are depleted in the rocks. Besides, REE patterns are concave shaped (mean LaN/LuN=16–25), and show a slight negative Eu anomalies (0.66–0.81). Plagioclase, amphibole and biotite fractional crystallization and crustal assimilation are important in the evolution of the Yürekli volcanics. According to all data, it can be argued that the Yürekli volcanics is formed in the post-collisional setting, and their parental magmas have derived from the melts of enriched lithospheric mantle.

Received Date: 21.11.2017
Accepted Date: 26.03.2018

1. Introduction

Turkey is divided into four main tectonic zones of the Sakarya zone, Tauride-Anatolide block, Intra-Pontide suture zone and Zagros suture zone (Okay and Tüysüz, 1999). The İzmir-Ankara-Erzincan suture zone (Figure 1a) is bounded by the Sakarya zone to the north and the Tauride-Anatolide block to the south (Şengör and Yılmaz, 1981; Yılmaz, 1990; Okay and Tüysüz, 1999). NW Anatolia is an important belt within the Alpine-Himalayan orogenic belt where magmatic activity is observed together with tectonic events (Aldanmaz et al., 2000; Altunkaynak and Genç, 2008).Thus, there are many studies performed on the general geology and petrology of the NW Anatolian Region (Bingöl, 1976; Ercan, 1979; Şengör and Yılmaz, 1981; Bingöl et al., 1982; Ercan and Günay, 1984; Yılmaz, 1990; Harris et al., 1994; Okay et al., 1996; Genç, 1998; Altunkaynak and Genç, 2008; Yılmaz et al., 2001; Altunkaynak and Dilek, 2013; Erdem, 2015; Aslan et al., 2017).

After closure of the Neo-Tethys Ocean, the Sakarya and Tauride-Anatolide continents collided in the Eocene period (Şengör and Yılmaz, 1981; Okay et al., 1996; Okay and Tüysüz, 1999; Altunkaynak and Dilek, 2006; Okay 2008) and as a result widespread magmatism formed in Northwest Anatolia (Yılmaz, 1989; Güleç, 1991; Ercan et al., 1995; Seyitoğlu and Scott, 1996; Genç and Yılmaz, 1997; Altunkaynak and Dilek, 2006; Okay and Satır, 2006; Karacık et al., 2008) (Figure 1b). In this period, intrusive rocks with granitic character and volcanic rocks with andesitic, dacitic and basalt character are commonly

* *Corresponding author: Zafer ASLAN, zaslan@balikesir.edu.tr*
http://dx.doi.org/ 10.19111/bulletinofmre.428294

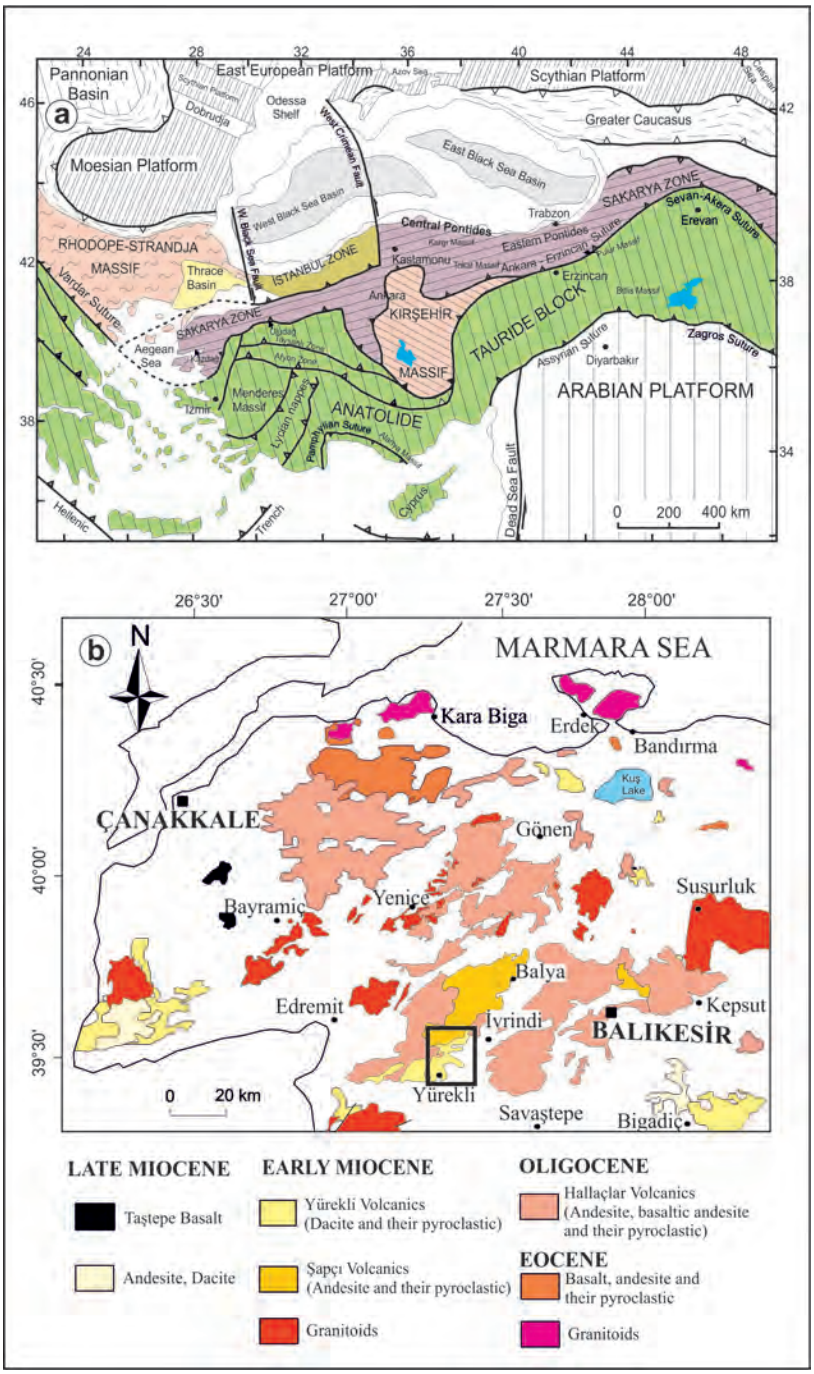

Figure 1- a) Tectonic zones of Turkey (Okay and Tüysüz, 1999) and b) The distribution of magmatic rocks in the Biga Peninsula (modified after Pehlivan et al., 2007).

found. Granitic plutons and the Edincik and Beyçayır volcanic rocks represent the first magmatism products in the Middle Eocene (Delaloye and Bingöl, 2000; Şengör et al., 1993; Köprübaşı and Aldanmaz, 2004; Altunkaynak and Dilek, 2006; Altunkaynak, 2007; Okay 2008; Altunkaynak et al., 2012, Erdem and Aslan, 2015; Aslan et al., 2017). In the Oligocene-Early Miocene period granitic intrusive rocks and genetically related volcanic rocks are found in the region (Altunkaynak and Yılmaz, 1999; Duru et al., 2004; Özgenç and İlbeyli, 2008; Altunkaynak and Dilek, 2006; Karacık et al., 2008; Akay, 2009; Prelević et al., 2012; Gülmez et al., 2013; Aslan et al., 2017). In the Biga Peninsula, Oligocene-aged volcanic products include the andesitic Yeniköy, acidic Atikhisar, basaltic Saraycık, and andesitic Bağburun

and Hallaçlar volcanics (Dönmez et al., 2005). In the Lower Miocene period the andesitic Şapçı volcanic rocks and dacitic Yürekli volcanics are present. The Yürekli volcanics outcrop in a very limited area and generally have been altered. The final products in the region are the Upper Miocene-aged Taştepe basalts. All these units are unconformably overlain by the Lower Miocene aged Soma formation (Duru et al., 2004).

The topic of the study of the Yürekli volcanic rocks is located in the west of the Sakarya zone tectonically, 45 km southwest of Balıkesir (Figure 1b). There are many studies about Tertiary magmatism in the region, with the majority related to andesitic volcanism and granitic plutonic rocks (Ercan et al., 1995; Aldanmaz et al., 2000; Dönmez et al., 2005; Altunkaynak and Genç, 2008, Karacık et al., 2008; Prelević et al., 2015; Erdem, 2015; Aslan et al., 2017). There are limited studies about the Yürekli volcanics (Duru et al., 2004; Pehlivan et al., 2007) with studies only performed about general geology and petrography due to the small outcrop area. In this study, detailed petrographic and petrochemical properties of the Yürekli volcanics are determined in an attempt to investigate their position within collisional volcanism in NW Anatolia.

2. Stratigraphy

In the Biga Peninsula, sediments, metamorphic and widespread magmatic rocks are present in the Palaeozoic to Pliocene age interval (Krushensky, 1976; Duru et al., 2004; Dönmez et al., 2005). The basement rocks in the area comprise moderate-high degree Palaeozoic-aged Kazdağ Massif and the low-moderate degree Triassic-aged Karakaya Complex (Duru et al., 2004). In the nearly 160 km^2 study area, the Triassic Karakaya Complex, Tertiary volcanic rocks and the overlying Soma formation are present (Figure 2). The Karakaya Complex outcrops in a small area southeast of the study area. The uppermost unit of the Sakarya Zone basement, the Karakaya Complex, comprises light grey-brown sandstone and semi-crystallised limestone olistoliths within them (Duru et al., 2004; Pehlivan et al., 2007). The Hallaçlar volcanics unconformably overlying the Karakaya Complex have broad distribution in the region. According to K-Ar dating (Dönmez et al., 2005), the unit has Upper Oligocene age of 26.5±1.1 My and contains andesite, basaltic-andesite and pyroclastics. With excessive alteration, the unit experienced kaolinization and silicification (Erdem and Aslan, 2015). In altered outcrops the unit has light yellow-white colour, while it appears light brown-rose coloured in outcrops without alteration effects. The Early Miocene-aged Şapçı volcanics lie above

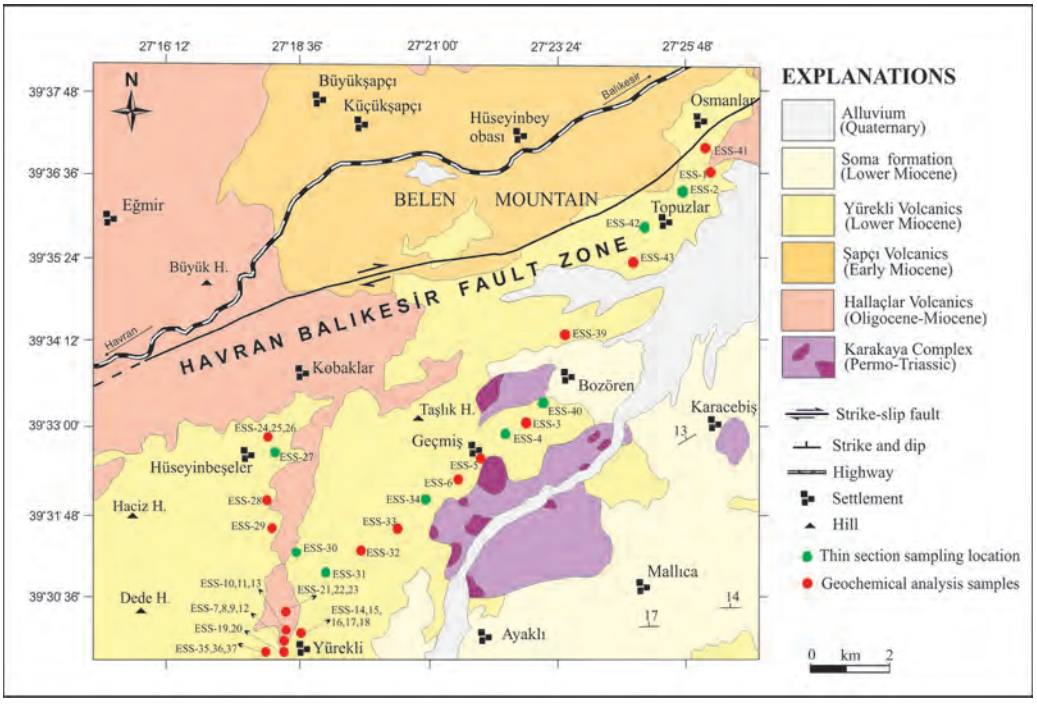

Figure 2- Geological map of the study area (modified after Pehlivan et al., 2007).

the Hallaçlar volcanics. The unit comprises andesite, trachy-andesite and their pyroclastics and is identified as 21.2±09 My by K-Ar dating (Dönmez et al., 2005) and as Early Miocene by zircon SHRIMP U-Pb dating (22.72±0.19 and 22.97±0.23 My) (Aslan et al., 2017). It outcrops in the north of the study area nearly Büyük and Küçük Şapçı villages. The unit, with light grey and light pink colour, has homogeneous hard and fractured structure.

Whole-rock K-Ar data of dacitic lava from the Yürekli volcanic rocks identified the unit as Lower Miocene (19.8±0.3, 19.5±0.1 and 20.3±0.6 My) (Krushensky, 1976). The unit is distributed along a line from northeast to southwest in the study area. The best outcrop in the region is near Yürekli village and environs (Figure 2). The Yürekli volcanics occur above the Şapçı and Hallaçlar volcanics. All units are covered by the Lowe Miocene aged Soma Formation comprising clay, marl, sandstone, tuffite, clayey limestone, siltstone and pebblestone alternations. The Soma Formation has white, grey and light-yellow colour, generally showing horizontal or close-to-horizontal bedding. It contains oolitic limestone with occasional diameters up to 2 cm. Quaternary-aged alluvium comprises the youngest unit in the study area.

3. Material and Method

Thin sections were made from 40 samples of dacitic lava from the Yürekli volcanics and 10 samples from surrounding rocks, for a total of 50 samples, investigated at Balıkesir University Department of Geological Engineering Research Laboratory using an Olympus CX31P brand polarizing microscope. A total of 21 dacitic lava samples found to be appropriate after petrographic investigations were send to ACME Laboratories (Vancouver, Canada) for main and trace-rare earth element analyses. After samples were powdered, the main and trace elements were analysed with ICP-AES, while rare earth elements were analysed with the ICP-MS method. In this analysis, main elements were measured with the ICP-AES method after $LiBO_2$ fusion. For trace and rare earth element analyses, 0.2 g powder sample was mixed with 1.5 g $LiBO_2$ in a graphite pot and heated to 1050 °C for 15 minutes. Melted samples were then dissolved in 5% HNO_3 and the solutions were analysed. With results given as weight %, main elements used SO-18/CSC as standard, while trace and rare earth elements given in ppm used the SO-18 standards.

4. Lithology and Petrography of Yürekli Volcanic Rocks

Yürekli volcanics comprise dacitic lava and pyroclastics. Pyroclastics are light-cream coloured tuffs, outcropping in very small areas east of Geçmiş village and south of Kobaklar village exposed to excessive alteration.

Dacitic lava outcrops in a large area from Osmanlar and Topuzlar villages north east of the study area continuing south to Yürekli village (Figure 2). Additionally, there are outcrops near Hüseyinbeşeler and Geçmiş villages and near Taşlık Hill, Haciz Hill and Dede Hill. The dacitic lavas form a dome structure especially near Yürekli village and surroundings (Figure 3a). In the centre of Yürekli village, the coarse-grained unit was identified to contain xenoliths of 1-3 cm dimensions. In spite of observing grey and beige tones (Figure 3b), sections affected by alteration are light yellow colour (Figure 3c). In areas affected by tectonism, there are abundant fracture-joint systems with slide surfaces. In locations with widespread alteration, there is enrichment in FeO, limonite and hematite observed, with abundant FeO accumulations on discontinuity surfaces (Figure 3d). Additionally, in sections with excessive amounts of alteration, kaolinization and silicification has occurred. Along shear fractures, there is occasional onion-peel structure formation present.

Samples taken from dacitic lava from the Yürekli volcanics generally have porphyric and hyaloporphyric texture, with occasional spherulitic texture observed. The Yürekli dacite contains the main minerals of plagioclase, quartz, amphibolite, biotite, sanidine and opaque oxides. Accessory minerals include apatite and zircon, with secondary minerals of chlorite, sericite and clay found. Plagioclases occur as euhedral and subhedral crystals and are found at different dimensions from very coarse phenocrystals to very small microliths observed in groundmass. An content is 9-25%, generally oligoclase with occasional albite. Some plagioclases show albite twinning or ring zoning (Figure 4a), while some have both characteristics. Plagioclases occasionally have cracked and fractured structure with sericitisation and kaolinization occurring. Quartz is in the form of anhedral crystals. Some quartz crystals have been corroded by groundmass (Figure 4b). Amphibole crystals are euhedral and subhedral, observed as small size microcrystals or phenocrystals (Figure 4c).

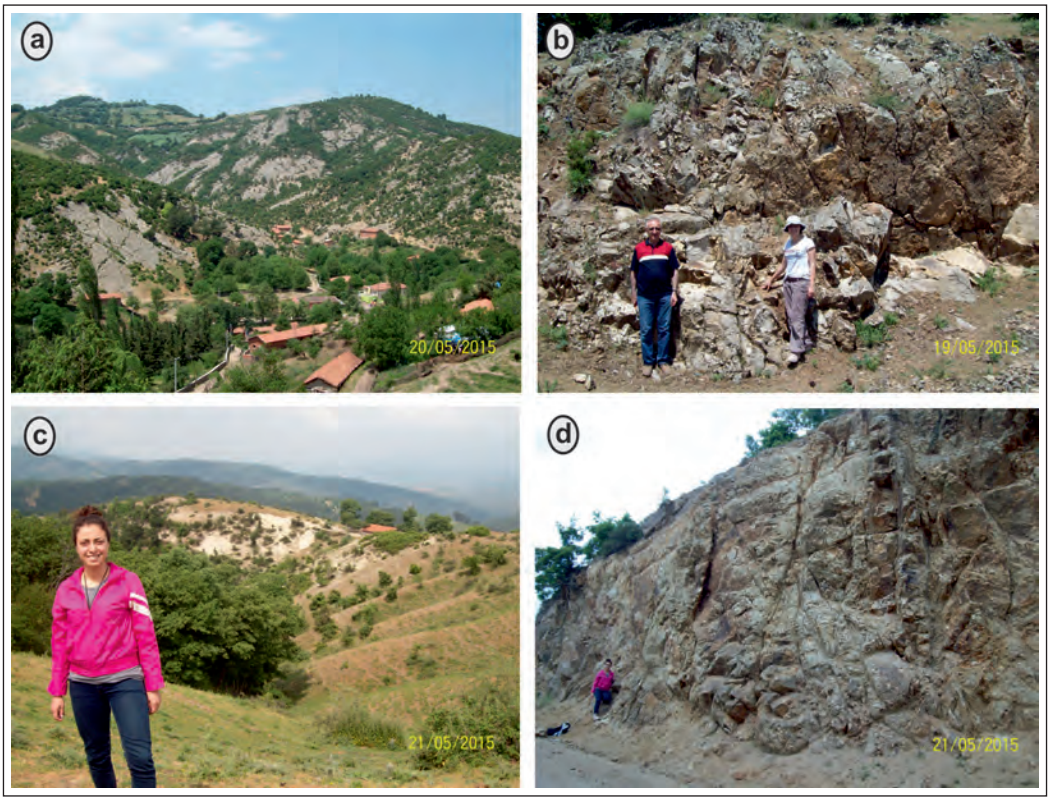

Figure 3- a) Dome shape dacitic lavas from the Yürekli volcanite (Yürekli village south slope), b) Gray colored hard and cracked dacite lava (North of Yürekli), c) Light yellow colored dacite lava affected by alteration (between Yürekli-Kobaklar), d) FeO enrichment along fractures (between Yürekli-Geçmiş villages).

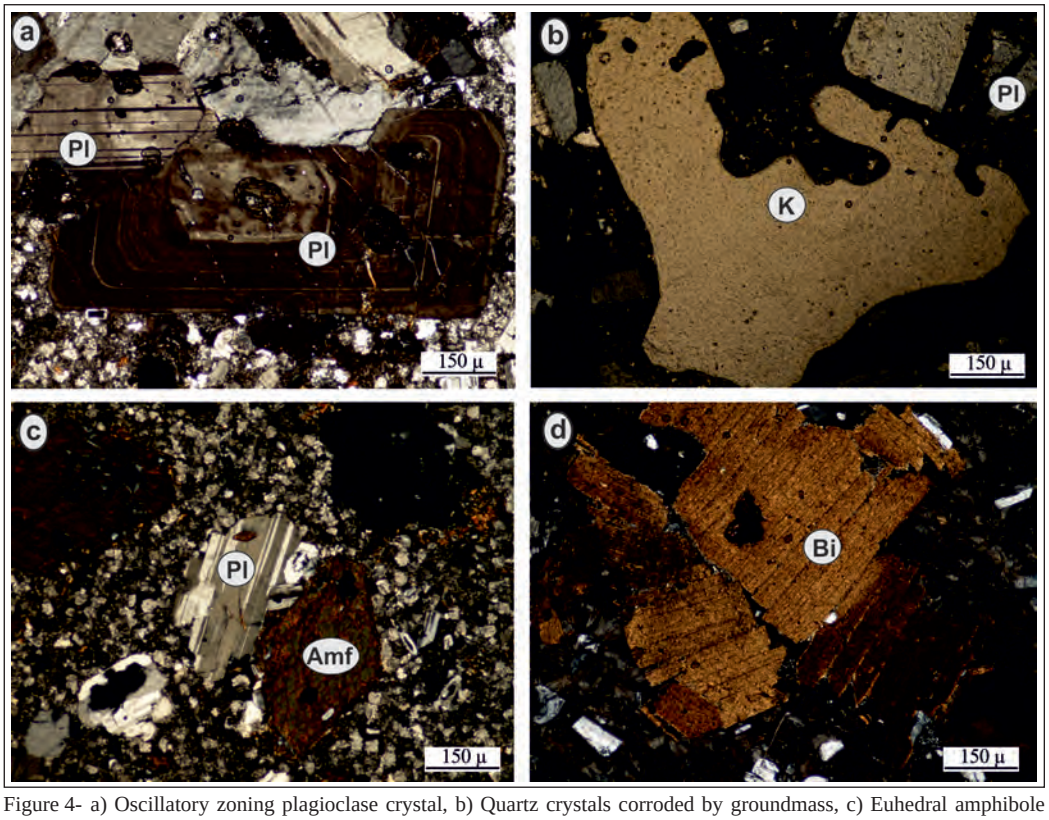

Figure 4- a) Oscillatory zoning plagioclase crystal, b) Quartz crystals corroded by groundmass, c) Euhedral amphibole crystals, d) Leaf-like biotite. Pl: Plagioclase, K: Quartz, Amf: Amphibole, Bi: Biotite.

They have pleochroism with dark brown and brown-yellow tones. Cracks and fractures have chloritisation observed. Biotites, in the form of semi-subhedral crystals, have rod-like or leaf-like (Figure 4d) shape. Generally, they have pleochroism in the light-dark or reddish-orange brown colour interval. Dark red and orange-brown colour tones show biotites have been oxidised. Some biotite minerals appear fully opaque, while some are enriched in iron but have not fully completed the opacification process. Chloritisation has occurred along the cleavage, fractures and cracks in biotites. Some biotites contain inclusions of opaque minerals and plagioclase. There are very small amounts of sanidine crystals, observed as prismatic or small microliths with clean faces. Opaque oxide minerals comprise 1-2% of the rock. Opaque minerals cluster around the edges of amphibole and biotite minerals and have irregular geometric shapes. The accessory minerals of apatite needles are found together with plagioclase, while zircons have very small size and mainly have euhedral form in groundmass. Sericite, calcite, chlorite and clay are present as weathering minerals. Groundmass contains microliths (plagioclase, sanidine and quartz), microcrystals (amphibole, biotite) and light-dark colour glass. There are plagioclase, amphibole, biotite and quartz minerals found as microliths and crystallites within the groundmass.

5. Geochemistry

The main, trace and rare earth element analysis results for dacitic lava samples from the Yürekli volcanic rocks are given in table 1. The variations in samples were SiO_2 values 60.67-73.46%, Al_2O_3 values 12.28-16.95%, MgO values 0.42-2.33%, Fe_2O_3 values 1.46-5.98%, CaO values 2.20-4.85%, K_2O values 3.17-5.87% and Na_2O values 1.94-6.65%. The LOI values were generally >1.5% due to alteration in the rocks, with these values reaching 5-5.8% for samples from between Yürekli and Geçmiş villages.

The SiO_2 against Zr/TiO_2 classification diagrams (Winchester and Floyd, 1977) for dacitic rocks of the Yürekli volcanics generally indicate dacite with some samples appearing to fall in the andesite or rhyolite areas (Figure 5a). Due to alteration of the rocks, some samples are located in different areas of the diagram. When the (Zr/TiO_2*0.0001) against Nb/Y diagram (Pearce, 1996) based on immobile elements is used, all samples appear to fall in the dacite/rhyolite area (Figure 5b). AFM triangle diagrams (Irvine and Baragar, 1971) indicate samples are in the calc-alkaline field (Figure 5c). On the Th-Co diagram (Hastie et al., 2007), all samples are located in the high-K and shoshonitic series fields (Figure 5d).

Diagrams of SiO_2 against main-trace elements observed negative and positive anomalies associated with fractional crystallisation of main mineral phases related to evolution of the investigated rocks. When variations according to increasing SiO_2 are investigated, there are negative trends for Na_2O, MgO, CaO, Al_2O_3, Fe_2O_3, P_2O_5, TiO_2, MnO, Rb and Zr, with a positive trend for K_2O while Sr, Ba, Th and Nb have irregular distributions (Figure 6). Main and trace element distributions appear to comply with the Early Miocene-aged Şapçı volcanics found in the region and similar to other volcanics (Figure 6). According to N-MORB normalised trace element distributions (Sun and McDonough, 1989), there is enrichment observed for large ion lithophile elements (LILE), Th, U and Ce values, with depletion of some high field strength elements (HFSE; Y and Ti), Nb, Tb and Ta distributions (Figure 7a). The investigated rocks are enriched in light rare earth elements and slightly less enriched in heavy rare earth elements (La_N/Lu_N= 16.77-25.67; La_N/Sm_N=4.79-7.07 and La_N/Yb_N=17.67-28.95) on rare earth element distributions (Figure 7b) normalised to chondrite (Sun and McDonough, 1989). The enrichment of light rare earth elements compared to heavy rare earth elements is typical of calc-alkaline volcanism (Wood and Joron, 1979; Wilson, 1989). Additionally, rare earth element distribution has a concave shape, indicating mineral differentiation of amphibole and plagioclase (Thompson et al., 1984; Thirlwell et al., 1994). Similarly, Eu has a very weak anomaly (Eu_N: 0.66-0.81); this situation shows differentiation of plagioclase and K-feldspar or high oxygen fugacity. The trace and rare earth element distributions for the Yürekli volcanics are similar to the Early Miocene-aged Şapçı volcanics (Figure 7a and b); thus, they may be said to have derived from the same source.

Table 1- Main oxide (weight %), trace element (ppm) and rare earth element (ppm) analyses of dacitic lava from the Yürekli volcanics.

	Yürekli volcanic rocks (dacite)									
Sample no:	**ESS-1**	**ESS-3**	**ESS-5**	**ESS-6**	**ESS-9**	**ESS-10**	**ESS-11**	**ESS-14**	**ESS-17**	**ESS-18**
SiO_2	60.67	73.46	65.61	66.18	66.79	70.00	64.6	63.03	62.89	70.96
TiO_2	0.69	0.40	0.47	0.49	0.50	0.43	0.49	0.54	0.56	0.47
Al_2O_3	16.82	12.28	15.31	16.18	16.24	13.71	15.8	16.46	16.93	15.06
Fe_2O_3(t)	5.98	1.62	2.68	2.20	2.33	1.87	4.14	4.86	4.79	1.46
MnO	0.10	0.02	0.10	0.01	0.01	0.08	0.05	0.06	0.06	0.07
MgO	1.37	0.57	0.77	0.72	0.49	0.42	0.56	0.97	1.13	0.42
CaO	4.85	2.21	2.20	2.27	2.26	2.91	3.35	2.72	2.75	2.62
Na_2O	3.65	2.21	2.07	2.48	2.94	2.15	2.99	2.93	2.96	2.80
K_2O	3.17	3.51	4.64	4.40	5.35	5.87	3.82	5.27	5.61	4.79
P_2O_5	0.25	0.14	0.16	0.10	0.17	0.14	0.17	0.19	0.19	0.17
LOI	2.10	3.30	5.80	4.70	2.60	2.20	3.70	2.60	1.80	0.90
Total	**99.65**	**99.72**	**99.81**	**99.73**	**99.68**	**99.78**	**99.67**	**99.63**	**99.67**	**99.72**
Zr	204	136	198	181	166	127	180	163	170	158
Y	21.0	14.2	13.9	15.3	16.3	15.9	17	15.4	16.3	16.6
Sr	732	502	503	559	561	465	577	592	648	628
Rb	106	111	162	160	172	183	135	162	174	137
Th	24.9	27.3	36.2	38.1	36.1	37.3	33.3	33.2	31.1	32.2
Ta	1.3	1.0	1.5	1.5	1.6	1.3	1.7	1.4	2.1	1.1
V	130	49	76	73	84	47	76	93	95	67
Pb	9.8	3.2	4.4	3.0	9.1	8.9	8.7	6.1	6.5	10.9
Ni	5.3	3.2	3.2	2.5	2.7	2.6	3.1	5.4	5.8	2.8
Co	14.2	3.6	3.6	3.6	5.3	5.5	6.3	10.9	10.5	3.4
Cs	4.9	4.2	5.2	5.5	4.1	6	3.9	7.2	7.5	6.6
Ba	1257	1109	1310	1345	1430	1294	1343	1470	1480	1342
Nb	14.9	11.3	14.4	14.0	14.3	12.7	14	13.2	13.2	12.6
Hf	4.9	3.3	5.3	4.8	4.6	3.3	4.5	4.4	4.7	4.0
La	54.90	44.40	55.10	56.10	61.00	53.70	53.60	55.70	56.80	54.10
Ce	98.90	76.70	96.40	95.80	107.20	90.20	97.60	101.40	97.90	97.50
Pr	10.43	7.98	9.60	9.71	10.64	8.79	9.58	10.06	9.90	9.97
Nd	35.70	28.70	33.90	33.90	37.60	30.80	32.50	35.00	34.80	36.60
Sm	6.43	4.73	5.51	5.39	5.80	4.97	5.51	5.90	5.71	6.11
Eu	1.56	0.96	1.11	1.20	1.33	1.06	1.28	1.27	1.33	1.43
Gd	5.65	3.70	4.42	4.27	4.77	4.21	4.98	4.54	4.48	4.97
Tb	0.78	0.47	0.56	0.58	0.64	0.58	0.64	0.60	0.59	0.69
Dy	4.12	2.68	2.85	3.16	3.18	3.03	3.33	3.33	3.1	3.39
Ho	0.75	0.49	0.55	0.55	0.60	0.52	0.64	0.64	0.56	0.63
Er	2.18	1.36	1.42	1.58	1.67	1.57	1.63	1.62	1.54	1.54
Tm	0.31	0.20	0.23	0.22	0.28	0.26	0.28	0.25	0.26	0.24
Yb	2.05	1.42	1.50	1.39	1.81	1.67	1.63	1.67	1.66	1.47
Lu	0.35	0.23	0.23	0.21	0.27	0.26	0.27	0.25	0.27	0.23
Eu_N/Eu^*	0.77	0.68	0.66	0.74	0.75	0.69	0.73	0.72	0.78	0.77
La_N/Lu_N	16.81	20.69	25.67	28.63	24.21	22.14	21.28	23.88	22.55	25.21
La_N/Yb_N	19.21	22.43	26.35	28.95	24.17	23.07	23.59	23.92	24.54	26.40
Mg#	18.64	26.03	22.32	24.66	17.38	18.34	11.91	16.64	19.09	22.34

Fe_2O_3(t): Total iron; LOI: loss on ignition; Mg# (Mg-number) =100 x MgO / (MgO+Fe_2O_3(t)), Eu*: (Sm+Gd)N/2

Çizelge 1- continued

	Yürekli volcanic rocks (dacite)										
Sample no:	**ESS-20**	**ESS-21**	**ESS-24**	**ESS-28**	**ESS-29**	**ESS-32**	**ESS-33**	**ESS-35**	**ESS-39**	**ESS-41**	**ESS-43**
SiO_2	62.00	65.00	65.92	65.13	65.23	65.47	64.95	64.48	63.01	66.66	68.03
TiO_2	0.52	0.54	0.49	0.55	0.53	0.51	0.41	0.46	0.50	0.48	0.46
Al_2O_3	16.45	16.59	15.61	16.52	16.95	16.34	14.54	14.86	15.62	15.05	14.36
Fe_2O_3(t)	4.86	3.37	3.91	3.09	3.14	3.35	3.73	4.11	3.85	4.34	4.26
MnO	0.08	0.03	0.03	0.03	0.02	0.01	0.03	0.05	0.46	0.05	0.05
MgO	0.93	0.73	0.73	0.98	0.73	0.59	1.54	2.33	1.13	1.09	1.07
CaO	3.06	2.68	2.92	3.13	2.78	2.98	3.31	3.76	3.47	3.24	3.12
Na_2O	2.74	2.96	2.84	2.91	2.94	3.07	1.94	2.51	3.10	3.33	3.22
K_2O	5.35	4.22	3.78	4.02	4.28	4.14	3.64	3.27	3.79	3.83	3.78
P_2O_5	0.19	0.18	0.17	0.17	0.07	0.17	0.22	0.15	0.17	0.13	0.13
LOI	3.50	3.40	3.30	3.20	3.00	3.10	5.30	3.70	4.50	1.50	1.20
Total	**99.68**	**99.70**	**99.70**	**99.73**	**99.67**	**99.73**	**99.61**	**99.68**	**99.60**	**99.70**	**99.68**
Zr	170	179	150	165	171	154	145	141	131	161	140
Y	15.8	19.2	14.9	24.4	12.9	13.3	14.5	16.6	18.5	19.1	13
Sr	607	559	578	604	579	608	964	681	663	578	545
Rb	168	141	130	122.6	144	138	116	101	139	138	134
Th	34.0	35.0	33.6	32.6	39.0	34.0	16.4	16.3	35.7	39.8	36.8
Ta	1.3	1.4	1.0	1.2	1.2	1.3	0.7	0.7	1.3	1.3	1.1
V	89	85	86	89	81	92	73	79	82	84	69
Pb	8.2	7.6	2.2	7.7	3.2	4.1	22.4	12.7	18.2	7.2	7.1
Ni	3.8	5.0	4.1	3.9	3.0	3.6	7.0	17.1	5.3	3.8	3.6
Co	17.7	7.4	6.1	5.2	3.9	5.5	6.5	10.1	15.7	8.8	8.8
Cr	7.1	3.6	6.0	3.6	5.0	4.0	10.0	1.4	10.4	5.9	7.1
Ba	1411	1270	1186	1215	1262	1262	1919	1231	1969	1167	1181
Nb	13.7	14	12.8	12.3	13.6	13.5	8.5	8.4	13.5	12.8	11.1
Hf	4.1	4.9	4.4	5.0	5.3	4.5	4.4	3.8	3.7	4.5	3.7
La	52.60	54.00	53.80	70.20	53.20	53.50	38.70	43.00	53.20	64.00	45.70
Ce	95.20	97.60	95.60	115.00	89.30	100.70	67.60	78.50	99.90	11.60	77.40
Pr	9.49	10.03	9.62	13.30	8.65	10.23	7.69	9.11	9.82	11.25	8.22
Nd	30.20	33.80	32.00	48.30	28.20	35.80	26.90	34.80	34.00	39.10	27.80
Sm	5.20	5.62	5.73	8.31	4.86	5.96	4.59	5.80	5.65	6.15	4.74
Eu	1.28	1.27	1.29	1.73	1.10	1.34	1.01	1.28	1.21	1.32	1.14
Gd	4.56	4.72	4.23	6.73	3.60	4.36	3.61	4.49	4.70	4.83	3.59
Tb	0.61	0.69	0.59	0.95	0.52	0.63	0.56	0.66	0.71	0.71	0.49
Dy	3.10	3.44	2.82	4.58	2.72	3.18	2.99	3.32	3.60	3.74	2.37
Ho	0.53	0.71	0.48	0.89	0.50	0.51	0.54	0.56	0.66	0.67	0.41
Er	1.69	1.82	1.44	2.76	1.40	1.20	1.49	1.65	1.93	1.85	1.19
Tm	0.24	0.31	0.20	0.36	0.21	0.20	0.21	0.24	0.30	0.30	0.21
Yb	1.66	1.83	1.37	2.42	1.30	1.37	1.46	1.59	2.16	1.97	1.37
Lu	0.27	0.30	0.23	0.40	0.23	0.19	0.22	0.23	0.34	0.33	0.22
Eu_N/Eu^*	0.78	0.73	0.77	0.68	0.77	0.77	0.73	0.74	0.70	0.71	0.81
La_N/Lu_N	20.88	19.29	25.07	18.81	24.79	30.18	18.85	20.04	16.77	20.79	22.26
La_N/Yb_N	22.73	21.17	28.17	20.81	29.35	28.01	19.01	19.40	17.67	23.30	23.93
Mg#	16.06	17.80	15.73	24.08	18.86	14.97	29.22	36.18	22.69	20.07	20.08

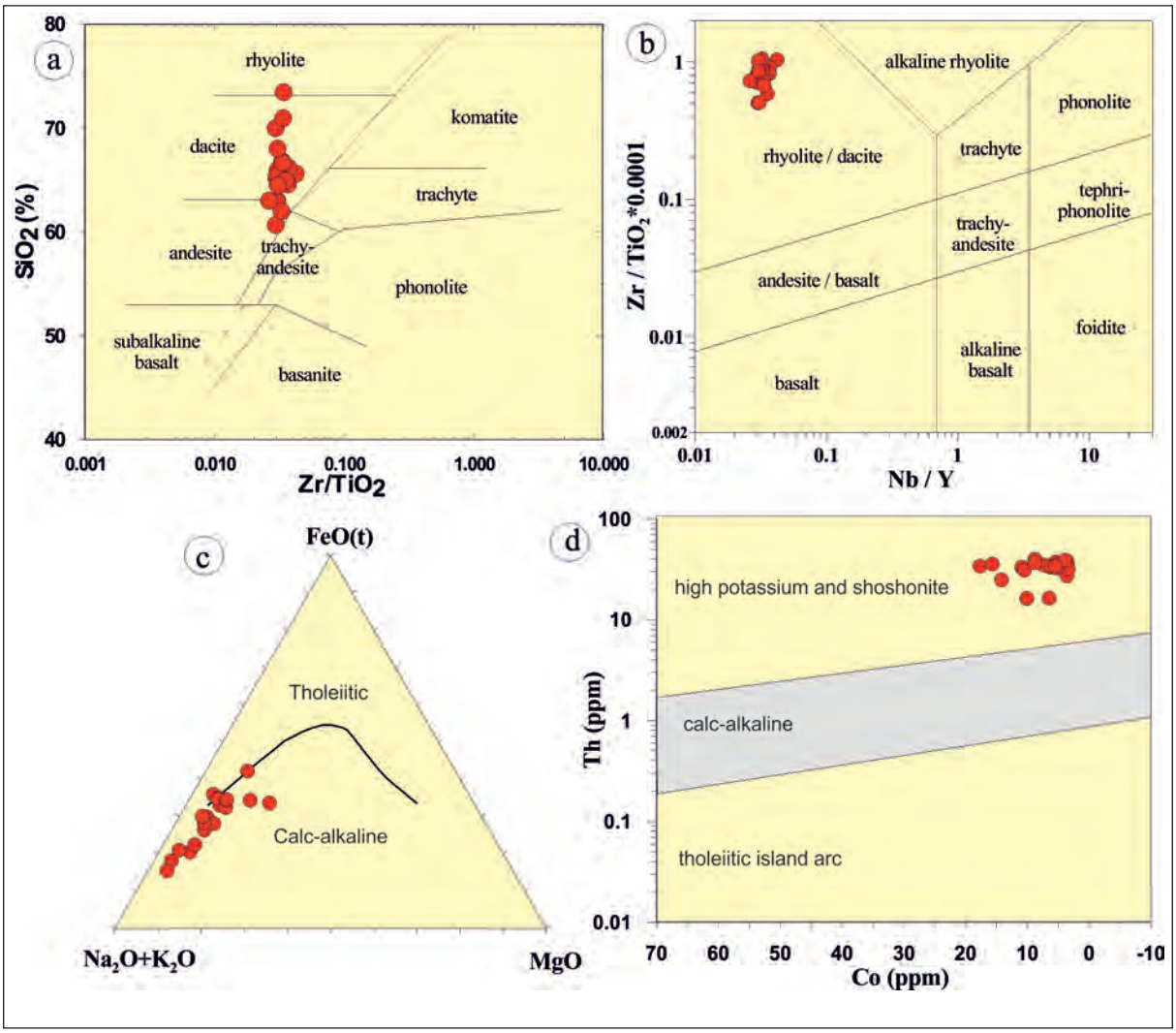

Figure 5- a) Dacitic lavas; SiO_2 vs. Zr/TiO_2 diagram (after Winchester and Floyd, 1977), b) Nb/Y vs. Zr/Ti classification diagram (Pearce, 1996), c) AFM ternary diagram (Irvine and Baragar, 1971), d) Th (ppm) vs. Co (ppm) diagram (Le Maitre vd., 2002) from the Yürekli volcanites.

6. Discussion

6.1. Source of Magma

Acidic composition magmas are derived from assimilation+fractional crystallisation of mantle-sourced basic magmas (Bacon and Druitt, 1988) or partial melts of mafic-intermediate composition magmatic or sedimentary rocks in the middle-lower crust (Stevens et al., 1997). The enrichment in large ion lithophile elements in the Yürekli volcanics (for example; Rb, Ba, Th and K) (Figure 7a) and high Ba/La and Th/Yb ratios show that the main magma for these rocks may be derived from a lithospheric mantle source containing subduction components (Pearce and Peate, 1995; Elburg et al., 2002; Zellmer et al., 2005; Baier et al., 2008; Aslan et al., 2017). Additionally the negative anomalies in Nb and Ta show subduction and/or crustal contamination (Pearce, 1983; Pearce and Peate, 1995; Elburg et al., 2002). The Ba/La ratio of the investigated rocks varies from 17.3-49.5, indicating a volcanic arc. Similarly, Ba/Nb, La/Nb, Ba/La, Sm/Nd and Nb/Th ratios show the rocks may be related to calc-alkaline volcanic rocks (Thompson et al., 1984; White and Patchett 1984; Bradshaw and Smith 1994; Smith et al., 1999; Elburg et al., 2002). The volcanic rocks display a pattern close to horizontal on heavy rare earth element distributions, which leads to the consideration that this main magma may have derived from a spinel lherzolite source containing

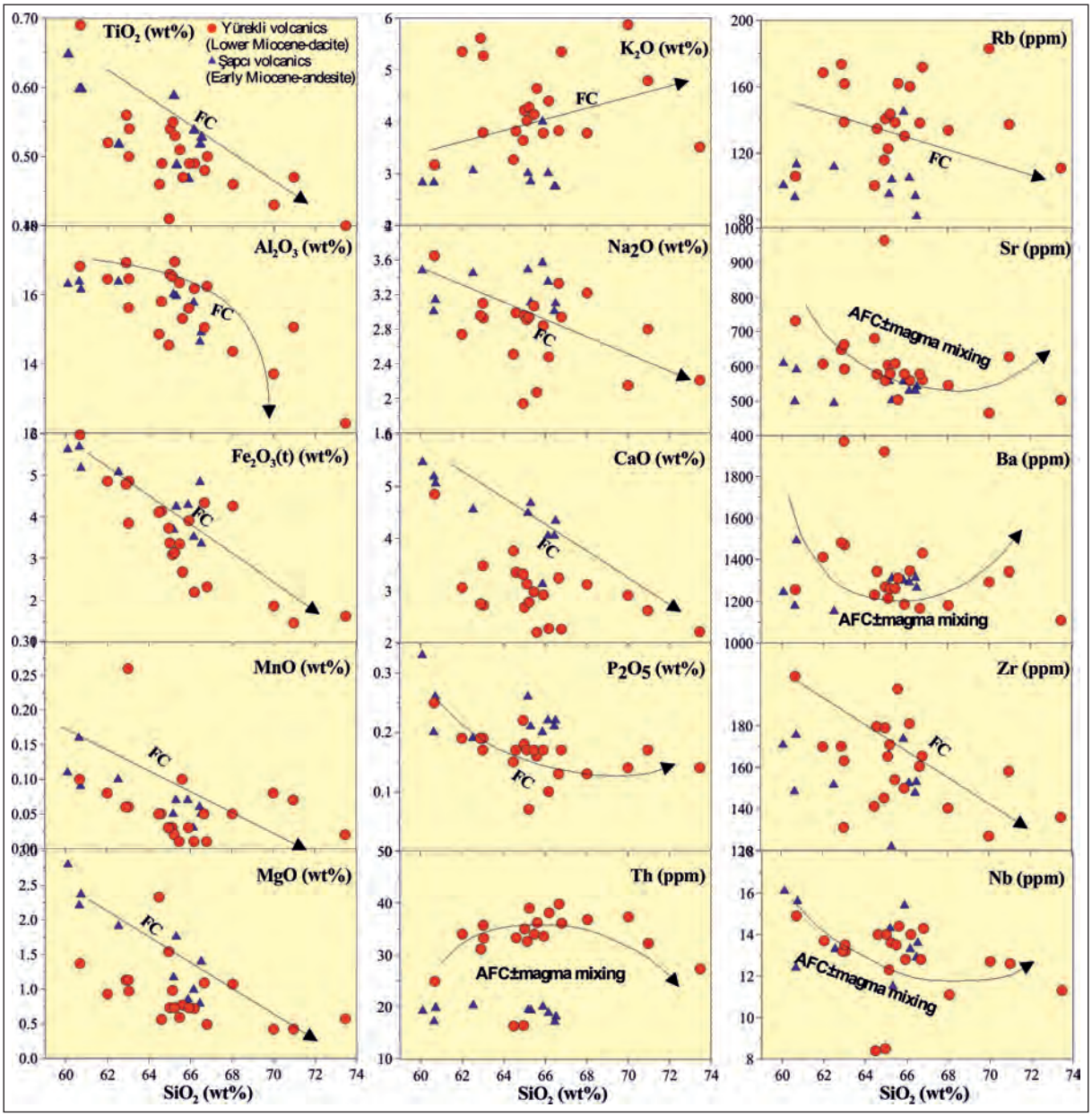

Figure 6- SiO_2 (wt%) vs. major oxide (wt%), trace (ppm) and rare earth element (ppm) variation plots of the Yürekli volcanic rocks. FC: fractional crystallization, AFC: assimilation fractional crystallization. Geochemical values of Şapçı volcanites were taken from Aslan et al., 2017.

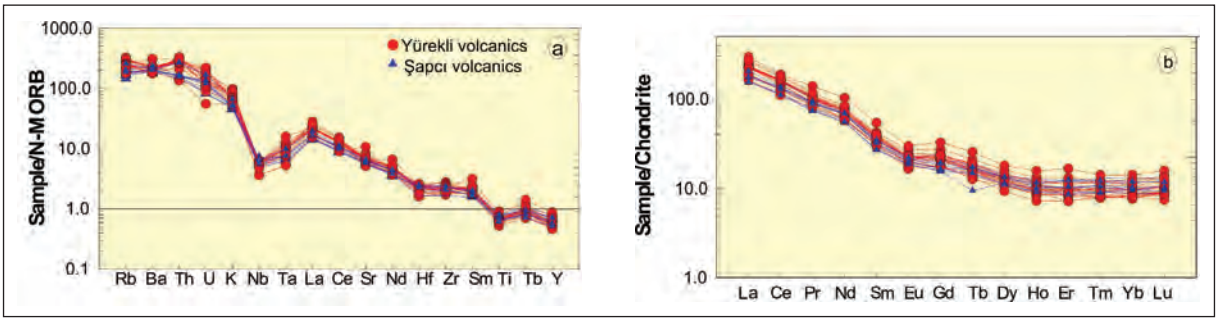

Figure 7- a) N-type MORB (Sun and Mcdonough 1989) normalized trace element spider diagram, b) chondrite (Sun and McDonough, 1989) normalized rare earth element pattern plots of the Yürekli volcanic rocks.

garnet, rather than a lherzolite source in the mantle (<50 km depth) (Wood and Joron 1979; Wilson 1989). The low Zr/Y (6-12) and Zr/Nb (10-13) values in the samples indicate sectional melt from a lithospheric mantle source.

Samples from the Yürekli volcanic rocks on the Nb_N/Zr_N–Zr diagram are located in the collision-related calc-alkaline volcanic rock field (Figure 8a). The Ta/Yb against Th/Yb diagram (Figure 8b) is used to determine whether additional components were added as a result of differentiation between mantle sources and subduction and/or crustal contamination. The analysed samples appear to show they were derived from magma evolving with fractional crystallisation (FC) and/or assimilation (AFC) events with subduction enrichment. On the same diagram, the high Th/Yb ratios in the volcanic rocks indicate subduction enrichment (Wilson, 1989). Samples from the Yürekli volcanic rocks fall in the volcanic arc area on the Ba/Nb-La/Nb diagram (Figure 8c). Similarly, on the Nb/La-La/Yb diagram (Figure 8d), samples appear to be in the lithospheric mantle area. The Lower Miocene Şapçı volcanic rocks with similar geochemical characteristics to volcanic rocks in the region (Aslan et al., 2017) are located in the same area of the diagram. This shows that Lower Miocene-aged volcanism in the region derived from main magmas with similar sources. The samples investigated have Zr/Sm values of 10-35, which similarly indicate an enriched lithospherice source (Wilson, 1989).

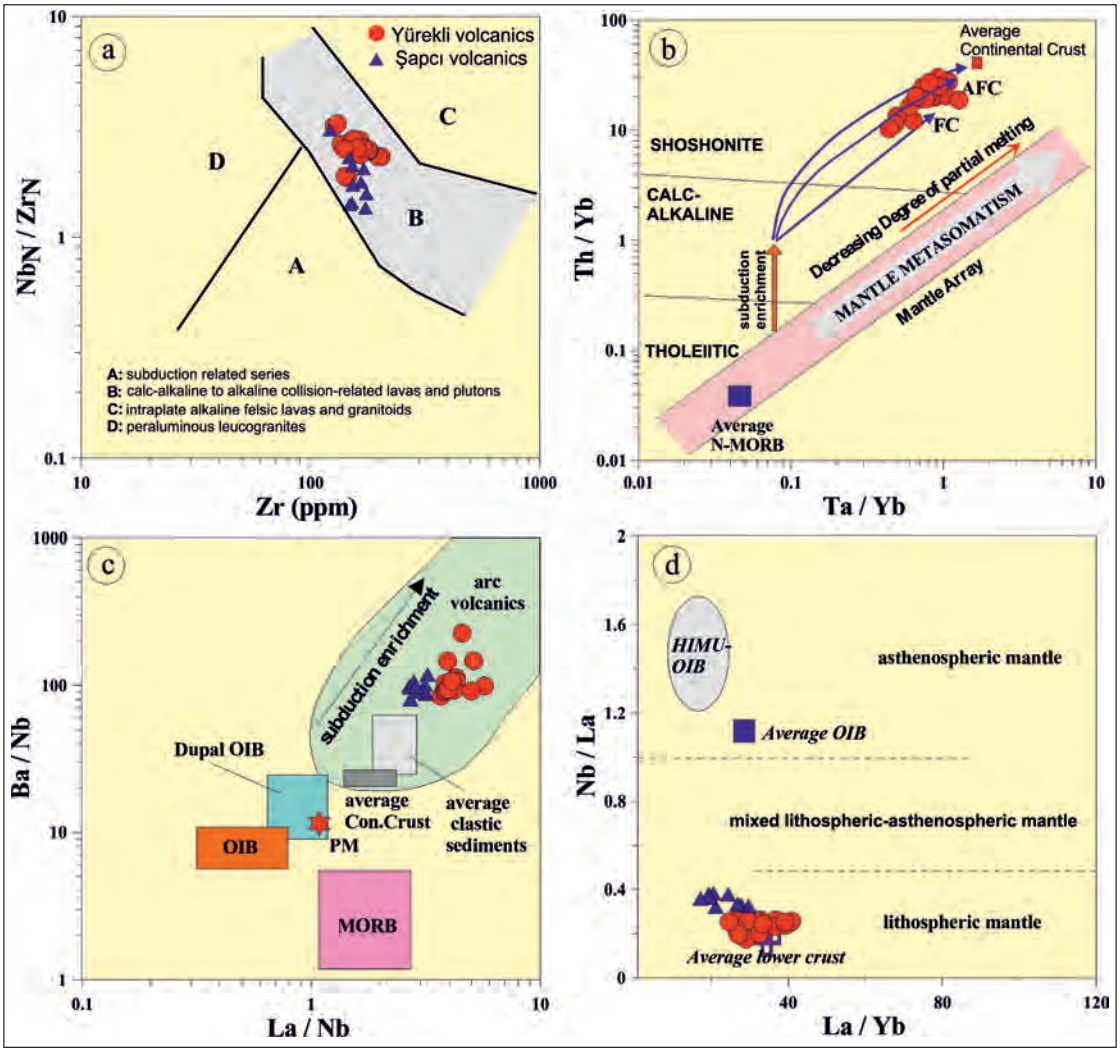

Figure 8- a) NbN/ZrN vs. Zr (ppm) diagram (Thieblemont and Tegyey 1994), (b) Th/Yb (ppm) vs. Ta/Yb (ppm) diagram (Pearce et al., 1990), (c) Ba/Nb (ppm) vs. La/Nb (ppm) diagram (Jahn et al., 1999), (d) La/Yb (ppm) vs. Nb/La (ppm) diagram (Jahn et al., 1999) for the Yürekli volcanic rocks. FC: Fractional crystallization; AFC: Assimilation-fractional crystallization; PM: Primary Mantle; MORB: Mid-Ocean Ridge Basalts; OAB: Ocean-Island Basalt.

6.2. Fractional Crystallisation and Assimilation

Negative or positive trends in SiO_2 against main and trace element variations indicate fractional crystallisation (FC) or assimilation fractional crystallisation (AFC) during evolution of the rocks (Figure 6). Variations of Na_2O, Al_2O_3, and CaO against SiO_2 are effective, especially in plagioclase crystallisation. Similarly, variation of SiO_2 against MgO ratios may be effective especially for amphibole differentiation, while the variation in SiO_2 against Fe_2O_3 ratios may be effective on amphibole and Fe-Ti oxide minerals. The variation in the trace element of Rb may be associated with amphibole crystallisation while the variation in Sr may be associated with plagioclase crystallisation (Thirlwall et al., 1994). Similarly, the reduction in TiO_2 and P_2O_5 against SiO_2 may be associated with crystallisation of titanomagnetite and apatite, respectively. The weak negative Eu anomaly indicates plagioclase and/or K-feldspar fractionation. Additionally, the negative Sr and Eu anomalies are the result of plagioclase fractionation, while negative Ba and Eu anomalies are caused by K-feldspar fractionation (Gill, 1981; Thirlwall et al., 1994). In this context, plagioclase, amphibole and biotite differentiation were effective during evolution of the investigated volcanic rocks.

Sr-MgO and Ba-Sr diagrams (Figure 9a and b) show plagioclase differentiation. Fractional crystallisation is also observed on the Zr-La diagram (Figure 9c). To identify mineral phases effective on fractional crystallisation, some binary diagrams are prepared using incompatible-compatible element associations. The negative Nb and Y variations against Zr (Figure 9d and f) represent biotite and amphibole differentiation. A positive trend of Zr against TiO_2 content indicates plagioclase and apatite differentiation, while a slight negative trend indicates Fe-Ti oxide and amphibole differentiation (Figure 9e). All these diagrams show that fractional crystallisation (FC) played an important role in the evolution of the Yürekli volcanics and differentiation of plagioclase, amphibole, biotite and Fe-Ti oxide were more effective compared to other phases. Additionally, the Ta/Yb against Th/Yb diagram (Figure 8b) shows fractional crystallisation (FC) with lower amounts of assimilation (AFC) were probably effective in the development of the Yürekli volcanics.

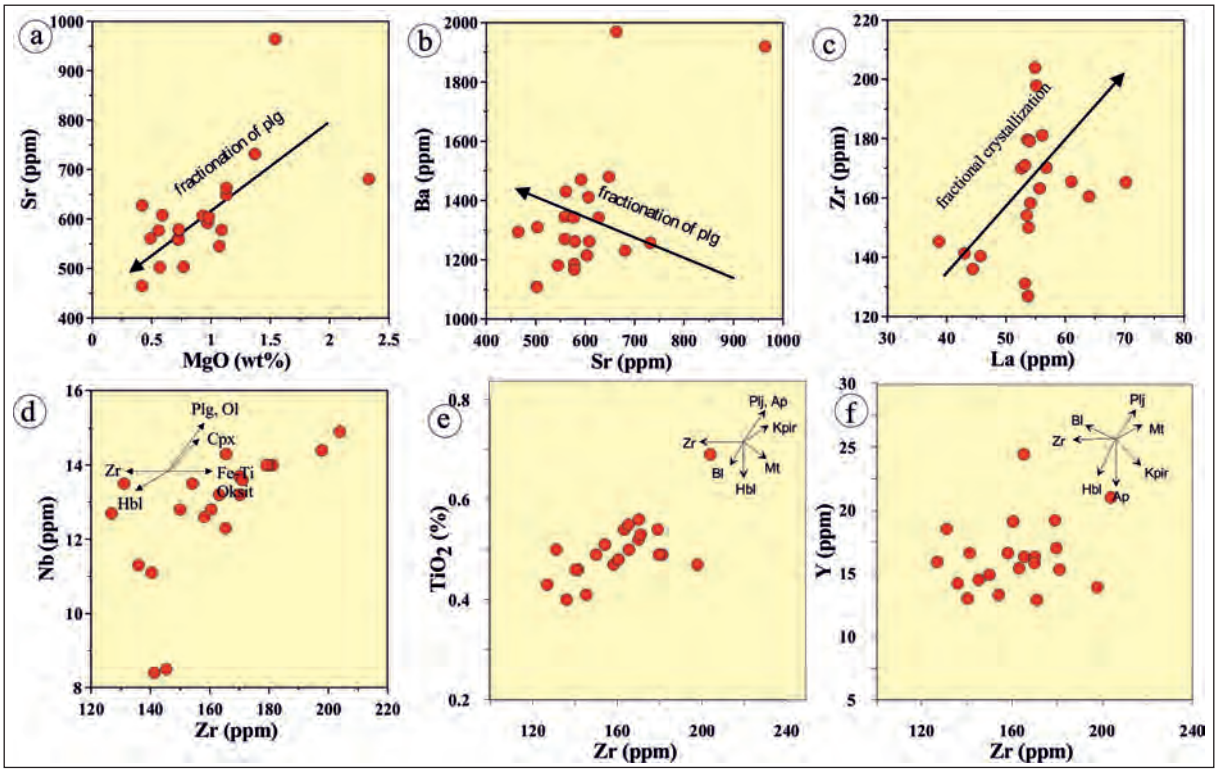

Figure 9- a) Sr (ppm) vs. MgO (wt%), b) Ba (ppm) vs. Sr (ppm), c) Zr (ppm) vs. La (ppm), d) Nb (ppm) vs. Zr (ppm) e) TiO_2 (%) vs. Zr (ppm), f) Y(ppm) vs. Zr (ppm) diagrams. Plj: Plagioclase, Kpir: Clinopyroxene, Ol: Olivine, Hbl: Hornblende, Bi: Biotite, Mt: Magnetite, Zr: Zircon, Ap: Apatite.

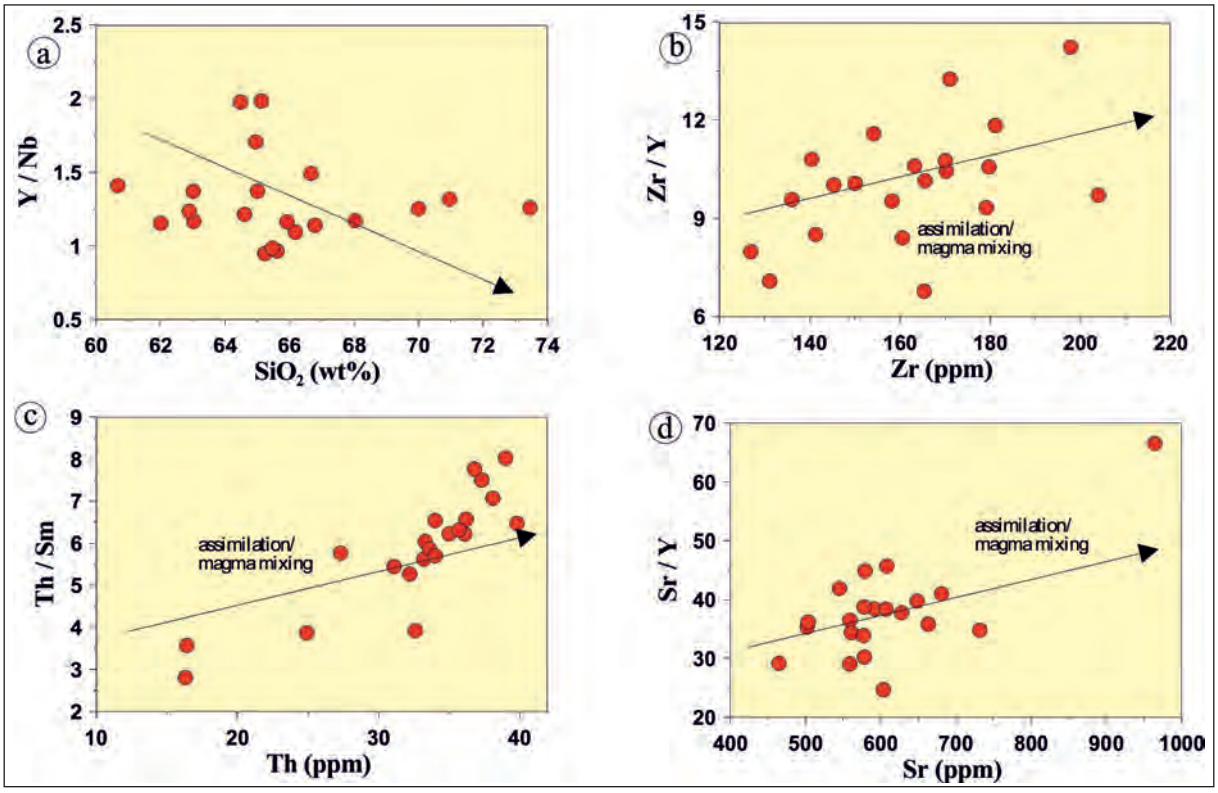

Figure 10- a) Y/Nb (ppm) vs. SiO_2 (%), b) Zr/Y (ppm) vs. Zr (ppm), c) Th/Sm (ppm) vs. Th (ppm) and d) Sr/Y (ppm) vs. Sr (ppm) diagrams.

The Zr/Y-Zr diagram shows the effect of assimilation (Figure 10b). The linear trend lines on Th/Sm-Th and Sr/Y-Sr variation diagrams (Langmuir et al., 1978) (Figure 10a, c, and d) indicate assimilation and/or low rates of magma mixing were effective in the evolution of the magma.

6.3. Magma-Tectonic Environment

The Yürekli volcanics have high potassium and calc-alkaline character. The investigated rock samples were located in the volcanic arc field (Figure 11a) on Rb/10-Hf-Ta*3 triangle diagrams (Harris et al., 1986). Additionally, the Rb/30-Hf-Ta*3 (Harris et al., 1986) diagram included a few samples in the precollisional and postcollisional area within the volcanic arc field (Figure 11b). In light of this data, we can say the Yürekli volcanic rocks are related to postcollisional magmatism.

Volcanism in Northwest Anatolia began in the Oligocene and is intensely observed in the Lower-Middle Miocene, continuing into the Upper Miocene with lower amounts in the Pliocene. Plutonism is generally not observed in the Early Miocene. Magmatism beginning with intermediate-potassium calc-alkali character in the Eocene became high potassium calc-alkaline in the Miocene and then intermediate-high potassium alkaline magmatism in the Pliocene. Tertiary magmatism played a significant role in the development of Western Anatolia. From the Upper Cretaceous to the Late Neogene, the NW Anatolian region was affected by a complex tectonic regime (Altunkaynak and Genç, 2008, Dilek and Altunkaynak, 2010; Prelević et al., 2012; Karaoğlu and Helvacı, 2014) and the Palaeogene-Neogene development of this belt is explained by complicated events like subduction, mantle metasomatism, crustal contamination and differentiation (Aldanmaz et al., 2000; Dilek and Altunkaynak , 2010; Altunkaynak et al., 2012; Seghedi et al., 2013; Prelević et al., 2012 and 2015). Studies in recent years have stated the south branch of the Neotethys Ocean developed a roll-back event and the magmatism developing from the Lower Miocene was associated with this event (Biryol et al., 2011; Ersoy et al., 2011; Prelević et al., 2012 and 2015). Magmatic rocks in the region were derived from enriched lithospheric mantle and crust (Dilek and Altunkaynak, 2010, Aslan et al., 2017). Oligocene-Middle Miocene magmatism developed as a result of the collision of the Sakarya continent with the Tauride-Anatolide continent (Ercan et al., 1995).

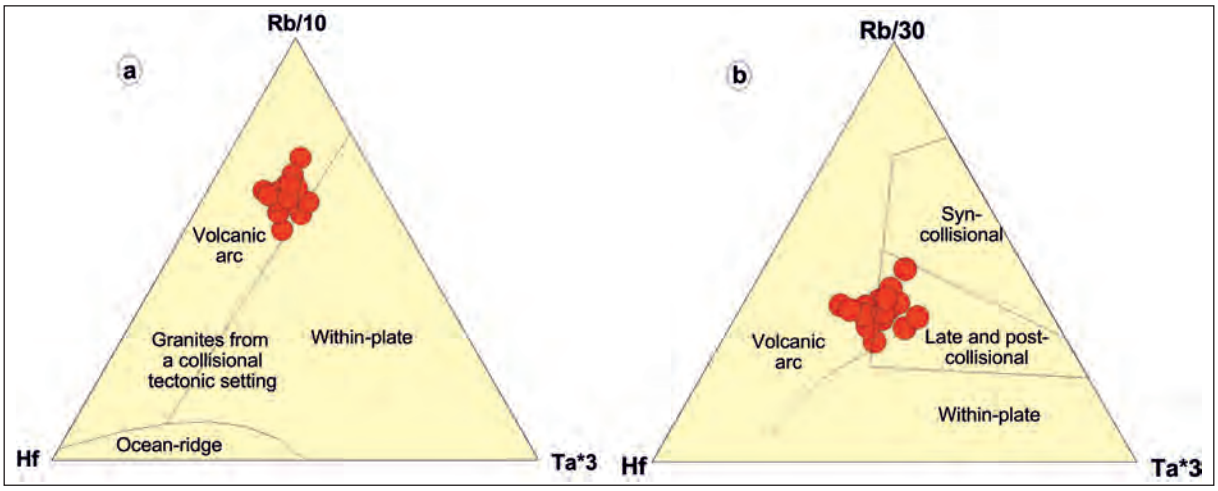

Figure 11- a) Rb/10-Hf-Ta*3 (Harris et al., 1986), b) Rb/30-Hf-Ta*3 (Harris et al., 1986) diagrams of the Yürekli volcanics rocks.

Magmatism after collision began in the Middle Eocene associated with subduction and produced intermediate-potassic calc-alkali plutonic and volcanic rocks. Post-collisional roll-back of the south branch of the Tethys Ocean crust caused elevation of the asthenosphere and melting of enriched lithospheric mantle and thus led to calc-alkali magmatism in the Middle-Late Miocene (Biryol et al., 2011; Prelević et al., 2012; Ersoy et al., 2011). The continuing extensional regime in Western Anatolia caused elevation of the asthenospheric mantle and formation of alkali magmatism linked to this.

7. Conclusion

This study determined detailed petrography of the Yürekli volcanic rocks outcropping southwest of Balıkesir, with attempts to determine the petrochemical characteristics, source and magmatic-tectonic environment of the rocks. Within the scope of this study, the basic results are summarised below:

1. Yürekli volcanic rocks comprise dacitic lava and pyroclastics. Petrographically dacitic lava has porphyric and hyaloporphyric textures, with occasional spherulitic texture. The main minerals forming the rocks are plagioclase, quartz, amphibole, biotite, sanidine and opaque oxides, with accessory minerals of apatite and zircon.

2. The Yürekli volcanics have calc-alkaline character, indicating post-collisional volcanic properties. Distribution normalised to N-MORB show enrichment in large ion lithophile elements (LILE), Th and Ce with depletion in some high field strength elements (HFSE), Nb and Ta content. Chondrite-normalised rare earth element distributions have concave form (mean La_N/Lu_N=16–25) with weak negative Eu anomaly (Eu/Eu*=0.66–0.81).

3. The main magma source for the Yürekli volcanic rocks was enriched lithospheric mantle with fractional crystallisation (FC) and low amounts of assimilation (AFC) effective during evolution.

Acknowledgements

This study comprises the Master's Thesis of Geological Engineer Ece Simay Saatçi. Born in 1990, Ece Simay Saatçi graduated from Dumlupınar University Kütahya Technical Sciences Vocational School Department of Natural Construction Stone Technology and then enrolled in Balıkesir University Department of Geological Engineering after external transition examinations. Graduating in 2014, Saatçi began Master's degree study at Balıkesir University Institute of Science and Technology the same year. After completing her Master's thesis and while preparing for her defence, Saatçi was killed in a terrible traffic accident in İzmir on 08 August 2017. Displaying exemplary behaviour in her personality and academic success, Saatçi is commemorated by dedicating this study to her memory. This study was supported by Balıkesir University Scientific Research Projects Unit (Project no: 2015/179). I thank the reviewers for their constructive criticism and valuable opinions.

References

Akay, E. 2009. Geology and petrology of the Simav Magmatic Complex (NW Anatolia) and its comparison with the Oligo–Miocene granitoids in NW Anatolia: implications on Tertiary tectonic evolution of the region. International Journal of Earth Sciences, (GeolRundsch) 98, 1655-1675.

Aldanmaz, E., Pearce, J.A., Thirlwall, M.F. Mitchell, J.G. 2000. Petrogenetic Evolution of late Cenozoic, Post-collision Volcanism in Western Anatolia, Turkey. Journal of Volcanology and Geothermal Research 102, 67-95.

Altunkaynak, Ş. 2007. Collision-driven slab breakoff magmatism in northwestern Anatolia. Turkey. Journal of Geology 115, 63-82.

Altunkaynak, Ş., Yılmaz, Y. 1999. The Kozak Pluton and its emplacement. Geological Journal 34, 257-274.

Altunkaynak, Ş., Dilek, Y. 2006. Timing and nature of postcollisional volcanism in western Anatolia and geodynamic implications. Dilek, Y., Pavlides, S. (Ed.). Post collisional tectonics and magmatism in the Mediterranean region and Asia. Geological Society of America Special Paper 409, 321-351.

Altunkaynak, Ş., Genç, Ş.C. 2008. Petrogenesis and time-progressive evolution of the Cenozoic continental volcanism in the Biga Peninsula, NW Anatolia (Turkey). Lithos 102, 316-340.

Altunkaynak, Ş., Dilek, Y. 2013. Eocene mafic volcanism in northern Anatolia: its causes and mantle sources in the absence of active subduction. International Geology Review 55, 1641-1659.

Altunkaynak, Ş., Dilek, Y., Genç, C.Ş., Sunal, G., Gertisser, R., Furnes, H., Foland, K.A., Yang, J. 2012. Spatial, temporal and geochemical evolution of oligo-miocene granitoid magmatism in western Anatolia, Turkey. Gondwana Research 21, 961-986.

Aslan Z., Erdem, D., Temizel, İ., Arslan, M. 2017. SHRIMP U-Pb zircon ages and whole-rock geochemistry for the Şapçı volcanic rocks, Biga Peninsula, Northwest Turkey: implications for pre-eruption crystallization conditions and source characteristics. International Geology Review 59 (14), 1764-1785.

Bacon, C.R., Druitt, T.H. 1988. Compositional Evolution of the Zoned Calc-Alkaline Magma Chamber of Mount Mazama, Crater Lake, Oregon. Contribution to Mineralogy and Petrology 98, 224-256.

Baier, J., Audetat, A., Kepler, H. 2008. The origin of the negative niobium tantalum anomaly in subduction zone magmas. Earth and Planetary Science Letters 267, 290-300.

Batchelor, R.A., Bowden, P. 1985. Petrogenetic interpretation of granitoid rock series using multicationic parameters. Chemical Geology 48, 43-55.

Bingöl, E. 1976. Biga yarımadasının jeolojisi ve Karakaya formasyonunun bazı özellikleri. Cumhuriyetin 50. yılı Yerbilimleri kongresi Tebliğler kitabı, Maden Tetkik ve Arama, Ankara 70-75.

Bingöl, E., Delaloye, M., Ataman, G. 1982. Granitic intrusions in Western Anatolia: A contribution of the geodynamic study of this area. Eclogae Geologisch Helvetica 75, 437-446.

Biryol, B. C., Beck, S. L., Zandt, G. Özacar, A. A. 2011. Segmented African lithosphere beneath the Anatolian region inferred from teleseismic P-wave tomography: Geophysical Journal International. 184, 1037-1057.

Bradshaw, T.K., Smith, E.I. 1994. Polygenetic Quaternary volcanism at Crater Flat, Nevada. Journal of Volcanology and Geothermal Research 63, 165-182.

Delaloye, M., Bingöl, E. 2000. Granitoids from western and North-western Anatolia: geochemistry and modeling of geodynamic evolution. International Geology Review 42, 241-268.

Dilek, Y., Altunkaynak, Ş. 2010. Geochemistry of Neogene-quaternary alkaline volcanism in western Anatolia, Turkey, and implications for the Aegean mantle. International Geology Review 52(4-6), 631-655.

Dönmez, M., Akçay, A. E., Genç, Ş.C., Acar, Ş. 2005. Biga Yarımadasında Orta-Üst Eosen volkanizması ve denizel ignimbiritler**.** Maden Tetkik ve Arama Dergisi 131, 49-61.

Duru, M., Pehlivan, Ş., Şentürk, Y.,Yavaş F., Kar, H. 2004. New Results on the lithostratigraphy of the Kazdağ Massif in Northwest Turkey. Turkish Journal of Earth Sciences 13, 177-186.

Elburg, M.A., Bergen, M.V., Hoogewerff, J., Foden, J., Vroon, P., Zulkarnain, I., Nasution, A. 2002. Geochemical trends across an arc-continent collision zone: magma sources and slab-wedge transfer processes below the Pantar Strait volcanoes, Indonesia. Geochimica et Cosmochimica Acta 66, 2771-2789.

Ercan, T. 1979. Batı Anadolu, Trakya ve Ege adalarındaki Senozoyik volkanizması. Jeoloji Mühendisliği Dergisi 9, 23-46.

Ercan, T., Günay, E. 1984. Kuzeybatı Anadolu, Trakya ve Ege adalarındaki Oligo-Miyosen yaşlı volkanizmanın gözden geçirilişi. Türkiye Jeoloji Kurultayı Bülteni 5, 119-139.

Ercan, T., Satır, M., Steinitz, G., Dora, A., Sarıfakıoğlu, E.,Adis,C.,Walter, H.J., Yıldırım, T. 1995. Biga Yarımadası ile Gökçeada Bozcaada ve Tavşan adalarındaki (KB Anadolu) Tersiyer Volkanizmasmın özellikleri. Maden Tetkik ve Arama Dergisi 117, 55-86.

Erdem, D. 2015. Şapçı (İbirler-Balıkesir) Volkaniti'nin Petrografisi, Jeokimyası ve Petrolojisi. Master thesis, Balıkesir Üniversity Institute of Natural Sciences 63 p. Balıkesir (yayınlanmamış).

Erdem, D., Aslan, Z. 2015. Kalk-alkalen Şapçı (Balıkesir) Volkanitlerin Petrografisi ve Petrolojisi: Biga Yarımadası'nda (Kuzeybatı Türkiye) Çarpışma ile İlişkili Volkanizma. Türkiye Jeoloji Bülteni 58, 1-22.

Ersoy, Y.E., Helvacı, C., Palmer, M. R. 2011. Mantle source characteristics and melting models for the early-middle Miocene mafic volcanism in Western Anatolia: Implications for enrichment processes of mantle lithosphere and origin of K-rich volcanism in post-collisional settings. Journal of Volcanology and Geothermal Research 198, 112-128.

Genç, Ş.C. 1998. Evolution of the Bayramiç magmatic complex, northwestern Anatolia. Journal of Volcanology and Geothermal Research 85, 233-249.

Genç, Ş.C., Yılmaz, Y. 1997. An example of post-collisional magmatism in northwestern Anatolia: the Kizderbent Volcanics (Armutlu Peninsula, Turkey). Turkish Journal of Earth Sciences 6, 33-42.

Gill, J.B. 1981. Orogenic Andesites and Plate Tectonics. Springer, Berlin. 390p.

Güleç, N. 1991. Crust-mantle interaction in western Turkey: implications from Sr and Nd isotope geochemistry of Tertiary and Quaternary volcanics. Geological Magazine 23, 417-435.

Gülmez, F., Genç, S.C., Keskin, M., Tüysüz, O. 2013. A postcollision slab-breakoff model for the origin of the Middle Eocene magmatic rocks of the Armutlu-Almacık belt, NW Turkey and its regional implications. Robertson, A.H.F., Parlak, O., Ünlügenç, U.C. (Ed.). Geological development of Anatolia and the Easternmost Mediterranean region: Geological Society, London, Special Publications, 372 p. doi.org/10.1144/SP372.12.

Harris, N.B.W., Pearce, J.A, Tindle A.G. 1986. Geochemical characteristics of collision-zone magmatism. Coward M.P, Ries A.C. (Ed.). Collision Tectonics. Geological Society of London Special Publication 19, 67-81.

Harris, N.B.W., Kelley, S., Okay, A.I. 1994. Post-collisional magmatism and tectonics in northwest Anatolia. Contributions to Mineralogy and Petrology 117, 241-252.

Hastie, A.R., Kerr, A.C., Pearce, J.A., Mitchell, S.F. 2007. Classification of Altered Volcanic Island Arc Rocks using Immobile Trace Elements: Development of the Th-Co Discrimination Diagram. Journal of Petrology 48, 12, 2341-2357.

Irvine, T.N., Baragar W.R.A. 1971. A guide to the chemical classification of common volcanic rocks. Canadian Journal of Earth Science 8, 523-548.

Jahn, B.M., Wu, F., Lo, C.H., Tsai, C.H. 1999. Crust-mantle interaction induced by deep subduction of the continental crust: Geochemical and Sr-Nd isotopic evidence from postcollisional mafic-ultramafic intrusions of the northern Dabie complex, central China. Chemical Geology 157, 119–146.

Karacık, Z., Yılmaz, Y., Pearce, J.A., Ece, O.I. 2008. Petrochemistry of the south Marmara granitoids, northwest Anatolia, Turkey. International Journal of Earth Sciences 97, 1181-1200.

Karaoğlu, Ö., Helvacı, C. 2014. Isotopic evidence for a transition from subduction to slab-tear related volcanism in western Anatolia, Turkey. Lithos 192-195, 226-239.

Krushensky, R. D. 1976. Neogene calc-alkalene extrusive and intrusive rocks of the Karalar-Yeşiller area, Northwest Anatolia, Turkey. Bulletin Volcanologique 40, 336-360.

Köprübaşı, N., Aldanmaz, E. 2004. Geochemical constraints on the petrogenesis of Cenozoic I-type granitoids in Northwest Anatolia, Turkey: Evidence for magma generation by lithospheric delamination in a post-collisional setting. International Geology Review 46, 705-729.

Langmuir, C.H., Vocke, R.D., Hanson, G.N., Hart, S.R. 1978. A general mixing equation with applications to Icelandic Basalts. Earth and Planetary Science Letters 37, 380–392.

Le Maitre, R.W., Streckeisen, A., Zanettin, B., Le Bas, M.J., Bonin, B., Bateman, P., Bellieni, G., Dudek, A., Efremova, S., Keller, J., Lamere, J., Sabine, P.A., Schmid, R., Sorensen, H., Woolley, A.R. 2002. Igneous rocks: A classification and glossary of terms, recommendations of the international

union of geological sciences, subcommission of the systematics of igneous rocks. Cambridge University Press, Cambridge.

Okay, A.I. 2008. Geology of Turkey: a synopsis. Anschnitt 21, 19-42.

Okay, A.I., Tüysüz, O. 1999. Tethyan sutures of northern Turkey. Durant, B., Jolivet, F., Horvath, F., Seranne, M. (ed.). The Mediterranean basin: Tertiary extension within the Alpine orogen. Geological Society Special Publication 156, 475-515.

Okay, A.I., Satır, M. 2006. Geochronology of Eocene plutonism and metamorphism in northeast Turkey: evidence for a possible magmatic arc. Geodinamica Acta 19, 251-266.

Okay, A.I., Satır, M., Maluski, H., Siyako, M., Metzger, R., Akyüz, S. 1996. Paleo-and Neo-Tethyan events in Northwest Turkey: geological and geochronological constrains. Yin, A., Harrison, T.M. (Ed.). The tectonic evolution of Asia. Cambridge University Press, Cambridge p 420-44.

Özgenç, İ., İlbeyli, N. 2008. Petrogenesis of the Late Cenozoic Eğrigöz Pluton in Western Anatolia, Turkey: Implications for magma genesis and crustal processes. International Geology Review 50, 375-391.

Pearce, J.A. 1983. The role of sub-continental lithosphere in magma genesis at destructive plate margins. Hawksworth, C.J., Norry, M.J. (Ed.). Continental basalts and mantle xenoliths. Shiva, Nantwich p. 230-249.

Pearce, J.A., Bender, J.F., De Long, S.E., Kidd, W.S.F., Low, P.J., Güner, Y., Şaroğlu, F., Yılmaz, Y., Moorbath, S., Mitchell, J.J. 1990. Genesis of collision volcanism in eastern Anatolia Turkey. Journal of Volcanology and Geothermal Research 44, 189–229.

Pearce, J.A. 1996. A user's guide to basalt discrimination diagrams. Wyman, D.A. (Ed.). Trace element geochemistry of volcanic rocks: Applications for massive sulphide exploration: Winnipeg. Geological Association of Canada, Short Course Notes12, p. 79-113.

Pearce, J.A., Peate, D.W. 1995. Tectonic implications of the composition of volcanic arc magmas. Annual Review Earth Planet Sciences Letter 23, 251-285.

Pehlivan, Ş., Duru. M., Dönmez, M., Ilgar, A., Akçay, A.E., Erdoğan, K., Özer, D. 2007. Türkiye Jeolojisi Haritaları No:96, Balıkesir-İ 19 Paftası. Maden Tetkik Aram, 40 s Ankara.

Prelevic´, D., Akal, C., Foley, S. F., Romer, R. L., Stracke, A., Van Den Bogaard, P. 2012. Ultrapotassic mafic rocks as geochemical proxies for post-collisional dynamics of orogenic lithospheric mantle: the case of southwestern Anatolia, Turkey. Journal of Petrology 53, 1019-1055.

Prelevic´, D., Akal, C., Romer, R.L., Mertz-Kraus, R., Helvacı, C. 2015. Magmatic Response to Slab Tearing: Constraints from the Afyon Alkaline Volcanic Complex, Western Turkey. Journal of Petrology 56, 527-562.

Seghedi, I., Ersoy, Y. E., Helvacı, C. 2013. Miocene-Quaternary volcanism and geodynamic evolution in the Pannonian Basin and the Menderes Massif: A comparative study. Lithos 180-181, 25-42.

Seyitoğlu, G., Scott, B. 1996. The cause of N-S extensional tectonics in western Turkey: Tectonic escape vs. backarc spreading vs. orogenic collapse. Journal of Geodynamics 22, 145-153.

Smith, E.I., Sanchez, A., Walker, J.D., Wang, K. 1999. Geochemistry of mafic magmas in the Hurricane Volcanic field, Utah: implications for small- and large-scale chemical variability of the lithospheric mantle. Journal of Geology 107, 433-448.

Sun, S.S., Mcdonough, W.F. 1989. Chemical and isotopic systematic of oceanic basalts: implications for mantle composition and processes. Saunders, A.D., Norry, M.J. (Ed.). Magmatism in the ocean basins. Geology Society London Special Publication 42, 313-345.

Stevens, G., Clemens, J.D., Droop, G.T.R. 1997. Melt Production during Granulite Facies Anatexis: Experimental Data from 'Primitive' Metasedimentary Protoliths. Contributions to Mineralogy and Petrology 128, 352-370.

Şengör, A.M.C., Yılmaz, Y. 1981. Tethyan evolution of Turkey: a plate tectonic approach. Tectonophysics 75, 181-241.

Şengör, A. M. C., Natalin, B. A., Burtman, V. S. 1993. Evolution of the Altaid tectonic collage and Paleozoic crustal growth in Eurasia. Nature 364, 299-307.

Thieblemont, D., Tegyey, M. 1994. Geochemical Discrimination of Differentiated Magmatic Rocks Attesting for the Variable Origın and Tectonic Setting of Calc-Alkaline Magmas. Comptes Rendus De L Academie Des Sciences Serie II 319 (1), 87-94.

Thirlwall, M.F., Smith, T.E., Graham, A.M., Theodorou, N., Hollings, P., Davidson, J.P., Arculus, R.J.

1994. High field strength element anomalies in arc lavas; source or process? Journal Petrogly 35, 819-838.

Thompson, R.N., Morrison, M.A., Hendry, G.L., Parry, S.J. 1984. An assessment of the relative roles of crust and mantle in magma genesis: an elemental approach. Philos Translate Society London A310, 549-590.

Yılmaz, Y. 1989. An approach to the origin of young volcanic rocks of western Turkey. Şengör, A.M.C. (ed.). Tectonic evolution of the Tethyan region. Kluwer Academics, Hague, The Netherlands p 159-189.

Yılmaz, Y. 1990. Comparison of young volcanic associations of western and eastern Anatolia under compressional regime; a review. Journal of Volcanology and Geothermal Research 44, 69-87.

Yılmaz, Y., Genç, S.C., Karacık, Z., Altunkaynak, Ş. 2001. Two contrasting magmatic associations of NW Anatolia and their tectonic significance. Journal of Geodynamics 31, 243-271.

White, W.M., Patchett, J. 1984. Hf-Nd-Sr isotopes and incompatible element abundances in island arcs: implications for magma origins and crust-mantle evolution. Earth and Planetary Science Letters 67, 167-185.

Wilson, F. H. 1989. Geologic setting, petrology anda ge of Plicene to Holocene volcanoes of the stepovak Bay area,western Alaska Peninsula. Dover, J.H., Galloway, J. P. (Ed.). Geological studies in Alaska by the U.S. Geological Survey, United State Geological Survey Bulletin 1903, 84-95.

Winchester, J.A., Floyd, P.A. 1977. Geochemical discrimination of different magma series and their differentiation products using immobile elements. Chemical Geology 20, 325-343.

Wood, D.A., Joron, J.L. 1979. Elemental and Sr izotopic variations in basic lava from Iceland and surrounding ocean floor: the nature of the mantle sources inhomogenities. Contribition and Mineralogy Petrology 70, 319-339.

Zellmer, G.F., Annen, C., Charlier, B.L.A., George, R.M.M., Turner, S.P., Hawkesworth, C.J. 2005. Magma evolution and ascent at volcanic arcs: Constraining petrogenetic processes through rates and chronologies. Journal of Volcanology and Geothermal Research 140, 171-191.

Bull. Min. Res. Exp. (2018) 157: 121-152

Bulletin of the Mineral Research and Exploration

http://bulletin.mta.gov.tr

Mineral chemistry, whole-rock geochemistry and petrology of Eocene I-type shoshonitic plutons in the Gölköy area (Ordu, NE Turkey)

İrfan TEMİZEL[a*], Emel ABDİOĞLU YAZAR[b], Mehmet ARSLAN[c], Abdullah KAYGUSUZ[d] and Zafer ASLAN[e]

[a]*Karadeniz Technical University, Department of Geological Engineering, 61080, Trabzon, Turkey. orcid.org/0000-0002-6293-8649*
[b]*Karadeniz Technical University, Department of Geological Engineering, 61080, Trabzon, Turkey. orcid.org/0000-0001-5196-8060*
[c]*Karadeniz Technical University, Department of Geological Engineering, 61080, Trabzon, Turkey. orcid.org/0000-0003-0816-4168*
[d]*Gümüşhane University, Department of Geological Engineering, 29000, Gümüşhane, Turkey. orcid.org/0000-0002-6277-6969*
[e]*Balıkesir University, Department of Geological Engineering, 10145, Balıkesir, Turkey. orcid.org/0000-0002-3418-4368*

Research Article

Keywords:
Mineral chemistry, thermobarometer, geochemistry, I-type, monzonite, Eocene, Gölköy, Turkey

ABSTRACT

The Eocene intermediate to felsic plutons are widespread in varying sizes and compositions throughout the Eastern Pontides Orogenic Belt in NE Turkey. Of these, two monzonitic bodies (namely the Eriko Tepe and Göl Tepe Plutons) in the Gölköy (Ordu) area, extend nearly in the orientation of NW-SE and E-W and were emplaced into the Upper Cretaceous and/or Eocene volcanic and sedimentary rocks. Petrographically, the studied monzonitic plutons are compositionally fine to medium grained monzonite, monzodiorite and subordinate quartz-monzonite. They consist of plagioclase (An_{35-67}), K-feldspar (Or_{61-96}), quartz, clinopyroxene ($Wo_{28-49}En_{35-51}Fs_{10-25}$), biotite (Mg#: 0.53-0.73) ± hornblende (Mg#: 0.65-0.82), Fe-Ti oxide with monzonitic, poikilitic, perthitic, rare antirapakivi and graphic textures. Mineral thermobarometer estimations imply that the plutons were crystallized in P-T conditions of mid to shallow crustal levels. Petrochemically, these monzonitic plutons show post-collisional, I-type, metaluminous (A/CNK=0.76-0.93) and shoshonitic features. The whole-rock major oxide and trace element variations suggest that fractionational crystallization played a significant role in the evolution of these monzonitic plutons. The primitive mantle-normalized trace element patterns of the studied plutons are similar to each other with enrichment in large ion lithophile elements, Th, Ce and negative Nb and Ti anomalies. Moreover, the chondrite-normalized rare earth element plots of the plutons show moderately enriched concave-shaped patterns (La_N/Lu_N=9.3-12.6) with negative Eu anomalies (Eu_N/Eu^*=0.69-0.84), all of which imply plagioclase and clinopyroxene ± hornblende fractionations during their evolution. The geochemical data suggest that the monzonitic plutons have evolved from parental magmas derived from the melts of enriched lithospheric mantle, in a post-collisional setting.

Received Date: 21.06.2017
Accepted Date: 27.12.2017

1. Introduction

The plutons observed in the Eastern Pontides Orogenic Belt (EPOB) have a wide age interval from Paleozoic to Tertiary, and they are formed by mafic and felsic rocks mainly ranging from gabbro to granite. These plutons have intruded in three time periods mainly during the Permo-Carboniferous, Cretaceous and Eocene. Of these, the Permo-Carboniferous granitoids (Yılmaz, 1972; Çoğulu, 1975; Topuz et al., 2010; Dokuz, 2011; Kaygusuz et al., 2012, 2016) were emplaced into the metamorphic rocks. The Cretaceous granitoids have a contact relation with volcanic and/or volcanoclastic rocks related to subduction (Yılmaz and Boztuğ, 1996; Karslı et al., 2010*a*; Kaygusuz et al., 2008, 2009, 2010, 2011, 2012; Kaygusuz and Aydınçakır, 2009, 2011; Kaygusuz and Şen, 2011; Karslı et al., 2012*a*; Kaygusuz et al., 2013, 2014). On the other hand, the fewer Eocene and post Eocene granitoids have cut all the series in narrow areas (Yılmaz and Boztuğ, 1996; Aslan et al., 1999; Topuz, 2002; Arslan and Aslan, 2006; Karslı et al., 2007;

* *Corresponding author: İrfan TEMİZEL, itemizel@ktu.edu.tr*
http://dx.doi.org/10.19111/bulletinofmre.371623

2011, 2012*b*; Kaygusuz and Öztürk, 2015).

In the eastern part of the EPOB (especially in Gümüşhane and Bayburt regions) there have been many studies of the geochemistry, petrogenesis and the geochronology of some of the Eocene plutons (eg. Arslan and Aslan, 2006; Karslı et al., 2007; 2011, 2012*b*; Kaygusuz and Öztürk, 2015). There are limited radiometric ages of the Eocene plutonic rocks in the region, and the age of many plutons were determined by the contact and stratigraphic relationships. However, Eocene plutons located in the Gölköy (Ordu) locality in the western part of the region and its surrounding have not been subject to any detailed petrographical, geochemical or petrological investigation. We present here the first mineral chemistry and whole-rock geochemistry of the Eocene monzonitic plutons outcropping on two different areas (Eriko Tepe and Göl Tepe) in the southeastern of Gölköy. From this we are able to establish the petrochemical and magma-tectonic characteristics and the genesis and evolution of the magmas (differentiation ± contamination).

2. Regional Geology

Turkey is a significant part of the Alpine-Himalayan orogenic belt and consists of remnants of the Paleotethys and Neotethys oceanic basins among the tectonic units (Pontides, Anatolides, Taurides and Margin folds) extending nearly in the E-W directions (Figure 1a) (Şengör and Yılmaz, 1981). Geological events related to the Paleotethys have prevailed in the Sakarya Zone and the Central Pontides in N-NW Turkey and completed its evolution by being unconformably overlain by Liassic sediments (Şengör and Yılmaz, 1981). In addition the geological events related to the Neotethys have affected the whole of Anatolia from Triassic to Miocene (Şengör and Yılmaz, 1981). The Late Cretaceous and Tertiary granitoid magmatism is one of the most significant orogenic events that have occurred during the closure of the Neotethys oceanic basins (Figure 1b).

The crustal basement of the Eastern Pontides (Ketin, 1966) is formed by Late Carboniferous granitoids, Late Carboniferous-Early Permian shallow marine-continental and the continental metasedimentary rocks (Yılmaz, 1972; Çoğulu, 1975; Okay and Leven, 1996; Topuz et al., 2007, 2010, 2011; Dokuz, 2011; Kaygusuz et al., 2012, 2016). The metamorphic rocks forming the basement have been cut by the Paleozoic granitoid rocks in pre-Liassic times (Çoğulu, 1975). The granitoid rocks mega plutonic masses and are observed in the Gümüşhane area and between the Köse area (Çoğulu, 1975; Topuz

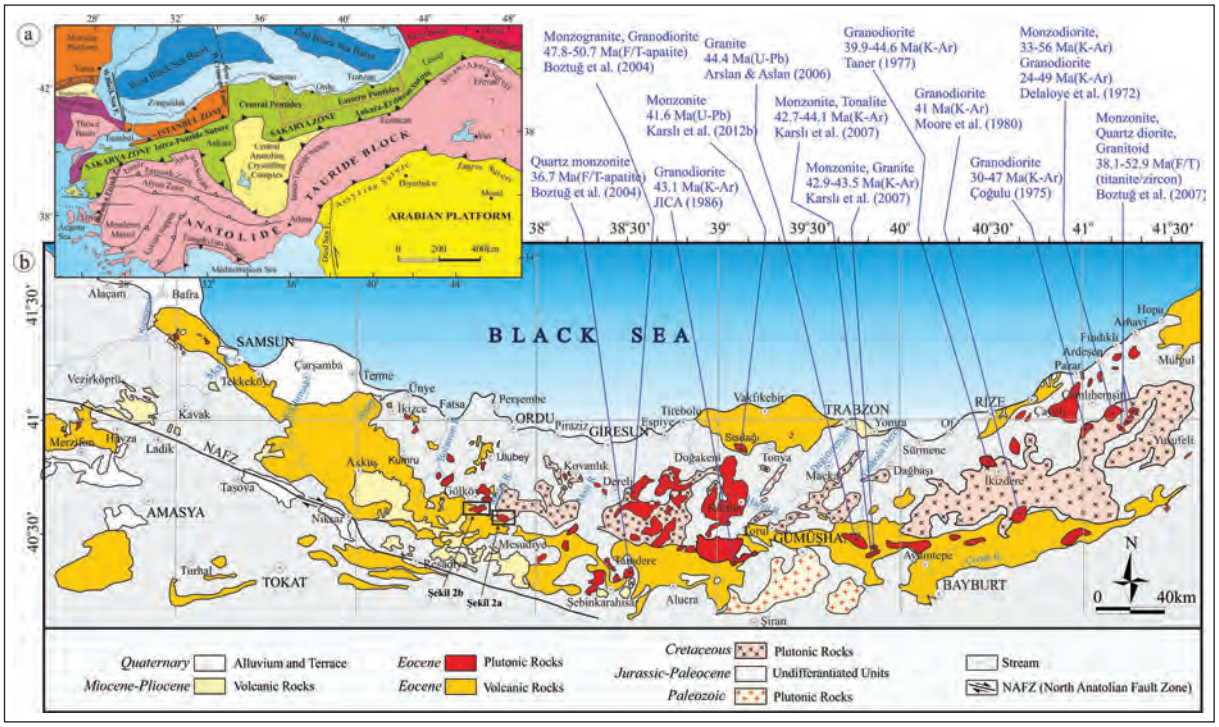

Figure 1- a) Tectonic map of Turkey (modified from Okay and Tüysüz, 1999), b) the distribution of plutonic rocks in the Eastern Pontides (modified from Güven, 1993; MTA, 2002; Arslan et al., 2013*a*; Temizel et al., 2016; Yücel et al., 2017) and the radiometric ages obtained from Eocene plutons.

et al., 2010; Dokuz, 2011), in the south of Tonya and Maçka (Soğuksu) area and the Özdil area (Kaygusuz et al., 2012, 2016). The Paleozoic rocks also form small outcrops around Artvin. The Early-Middle Jurassic pyroclastites, and clastic and sedimentary rocks intercalated with carbonates unconformably overlie the basement rocks in the Eastern Pontides and are interpreted as the volcano-sedimentary deposit related to the rift (Ağar, 1977; Robinson et al., 1995; Arslan et al., 1997; Kandemir, 2004; Dokuz and Tanyolu, 2006; Şen, 2007; Kandemir and Yılmaz, 2009). This unit is mainly represented by volcanic rocks in the northern part, and sedimentary deposits intercalating with tuff and tuffites in the south. During closure of the Paleotethys, and with the collision that occurred by the addition of the Sakarya zone in the north and Laurasia, the synchronous granitoids are Late Jurassic (Yılmaz et al., 1997; Dokuz et al., 2010) which through to the Early Cretaceous period was a period of stability in the whole orogenic belt and the carbonate deposition in the whole Eastern Pontides are dominant in this period (Pelin, 1977).

The Eastern Pontide magmatic arc developed in the Late Cretaceous along the southern boundary of the Sakarya Zone due to the northern subduction of the Neotethys (Okay and Şahintürk, 1997; Yılmaz et al., 1997; Topuz et al., 2007; Altherr et al., 2008; Dilek and Sandvol, 2009; Dilek et al., 2010; Ustaömer and Robertson, 2010; Rolland et al., 2012; Ustaömer et al., 2013; Topuz et al., 2013; Okay et al., 2013). There are different ideas about the direction and termination of the subduction of the Eastern Pontide magmatic arc, and the time of collision of the Tauride-Anatolide Platform and the Eurasian plate. These are; (1) the development of the Pontide arc as a result of the northern subduction from Paleozoic to Eocene (Ustaömer and Robertson, 1995; Okay and Şahintürk, 1997; Yılmaz et al., 1997), (2) the occurrence of the Paleotethys in the north of Pontides, and the presence of the southern subduction polarity starting from the end of the Paleozoic until the end of the Eocene (Dewey et al., 1973; Bektaş et al., 1984, 1999; Chorowicz et al., 1998; Eyüboğlu et al., 2011*a*), and 3) the presence of a two directional subduction polarity as being towards the south until Dogger and towards the north starting from the Late Cretaceous until the end of the Eocene for the Pontide arc (Şengör and Yılmaz, 1981). The Eastern Pontide magmatic arc system consists of a Late Cretaceous volcano-sedimentary deposit thicker than 2 km and the high-K, calc-alkaline, I-type granitoids (Yılmaz and Boztuğ, 1996; Okay and Şahintürk, 1997; Yılmaz et al., 1997; Boztuğ et al., 2003, 2004, 2006; Boztuğ and Harvalan, 2008; İlbeyli, 2008; Kaygusuz et al., 2008, 2009, 2010, 2011, 2012; Kaygusuz and Aydınçakır, 2011; Kaygusuz and Şen, 2011).

The collision of the Eastern Pontides magmatic arc and the Anatolide-Tauride continental block occurred in the Late Paleocene-Early Eocene (~55 Ma) and required a widespread shortening, crustal uplift and thickening, and flysch deposition in NE Turkey (Okay and Şahintürk, 1997; Dilek, 2006). The Eocene units in the Eastern Pontides generally overlie the Upper Cretaceous and Paleocene units with the basal conglomerate and are overlain by a series of andesite-basalt, pyroclastites and flysch deposits (Arslan and Aliyazıcıoğlu, 2001; Arslan et al., 2013*a*). The formation of the early Eocene adakitic rocks in the Eastern Pontides (54-48 Ma) (Topuz et al., 2005; Karslı et al., 2010*b*, 2011; Eyüboğlu et al., 2011*a, b, c*; Topuz et al., 2011; Eyüboğlu et al., 2013*a, b*; Karslı et al., 2013), corresponds to the last stage of the arc to continent collision, and they are associated with syn- and post-collisional origins. As for the Middle Eocene, the post collisional calc-alkaline volcanic rocks and high-K, calc-alkaline, shoshonitic granitoid plutons developed (Yılmaz and Boztuğ, 1996; Arslan et al., 1997; Şen et al., 1998; Aliyazıcıoğlu, 1999; Arslan and Aliyazıcıoğlu, 2001; Arslan et al., 2002; Boztuğ et al., 2004; Topuz et al., 2005; Arslan and Aslan, 2006; Karslı et al., 2007, Boztuğ and Harvalan, 2008; Temizel and Arslan, 2008, 2009; Aslan, 2010; Eyüboğlu et al., 2012; Karslı et al., 2012*b*; Temizel et al., 2012*a, b*; Yücel et al., 2012; Arslan et al., 2013*a, b*; Temizel, 2014; Yücel, 2013; Aslan et al., 2014; Temizel et al., 2014; Temizel et al., 2016; Yücel et al., 2017). The clastic rocks are widespread in the region in the post-Eocene (Okay and Şahintürk, 1997) and are generally accompanied by Neogene alkaline volcanic rocks (Aydın et al., 2008, 2009; Arslan et al., 2013*b*; Yücel, 2013, Yücel et al., 2012, 2014, 2017). The Quaternary deposits are represented by travertine and alluvial deposits.

3. Material and Methods

The field studies were carried out in two different areas where the Eocene Eriko Tepe and Göl Tepe plutonic bodies are located (Figures 2a, b).

Thin sections for the rocks of Eriko Tepe and Göl Tepe plutons were prepared in the thin section laboratory of the Geological Engineering Department

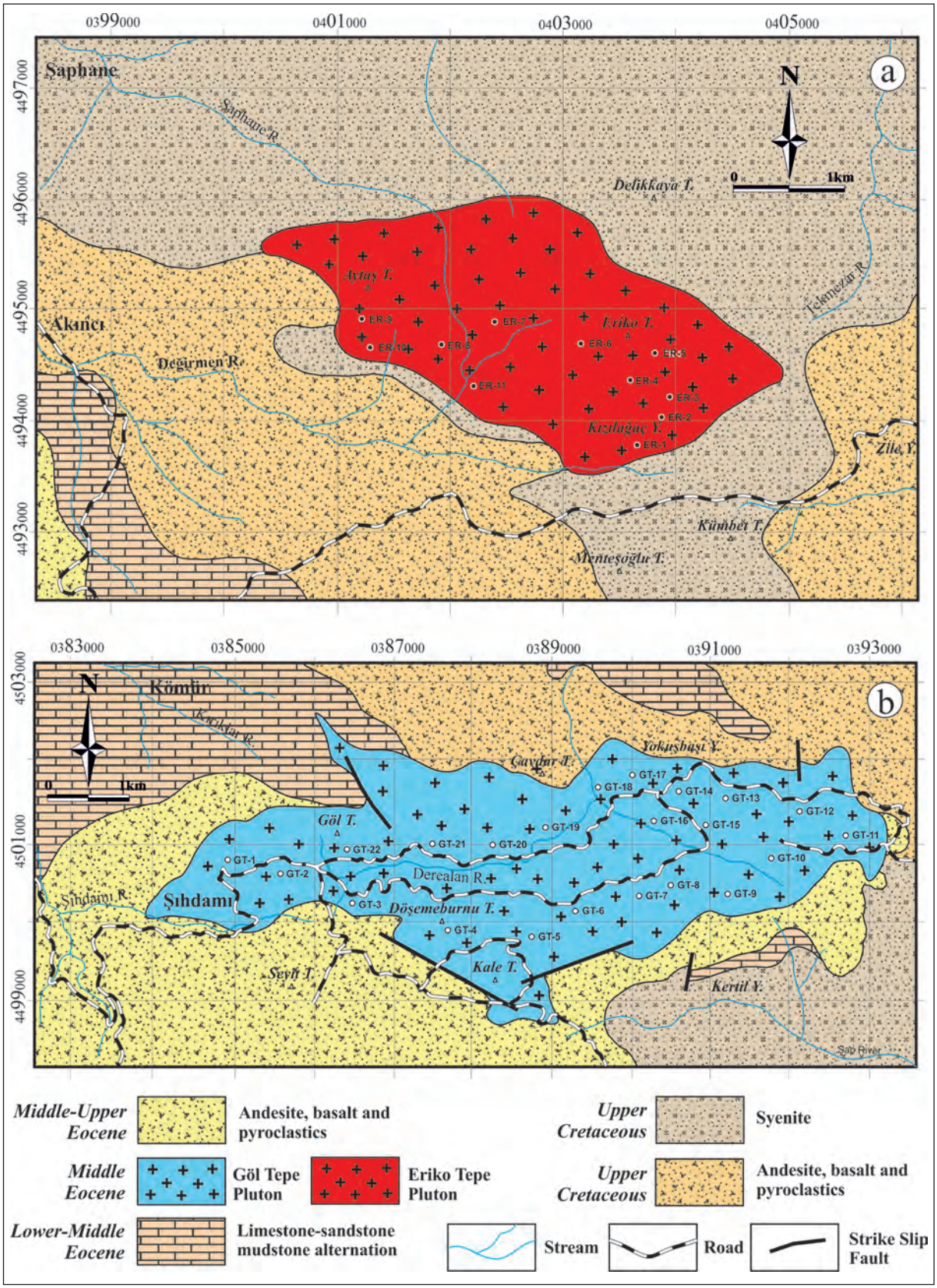

Figure 2- Geological maps showing the studied plutons and surrounding rocks of: a) the Eriko Tepe, and, b) the Göl Tepe plutons (modified from Güven, 1993; MTA, 2002, 2011).

at the Karadeniz Technical University and used to determine mineralogical compositions and textural-petrographical characteristics using a polarized microscope. The Swift point counter was used for the modal analyses and the counting was generally made within a 0.4 mm interval, but sometimes a 0.2 mm interval was also selected depending on the grain size. Approximately 400-500 points were counted in each thin section.

Mineral chemistry was determined using the CAMECA-SX-100 WDS electron microprobe in the Geoscience Marines (IFREMER) Electron Microprobe Laboratory (Universite de Bretagne Occidentale, Brest, France). The operating conditions were 15 kV and 20 nA, and a 10 μm beam diameter, and the count timing was 10s for Si, Al, Ti, Fe, Mn, Mg, Ca, Na and K. A 1 μm beam was used for pyroxene, hornbende and Fe-Ti oxide analyses. For feldspar and mica the very light defocused beam (10 μm) was used to prevent alkali loss. The natural mineral standards used were forsterite, diopside, orthoclase, albite, anorthite, biotite, apatite, wollastonite and magnetite. The analytical error is less than 1% for major elements and less than 200 ppm for trace elements.

The petrography guided the selection of fresh rock samples collected from the plutons and these were crushed by the steel jaw crusher in the Sample preparation and milling laboratory in the Geological Engineering Department at the Karadeniz Technical University. They were then pulverized in to an approximately 200 mesh size in a steel ring mill. Whole-rock analyses of rock powders from the plutons were undertaken at ACME Analytical Laboratories Ltd. (Vancouver, Canada). The major and trace element analyses were carried out by the Inductively Coupled Plasma Atomic Emission Spectrometer (ICP-AES) after fusing 0.2 gr powdered rock sample in 1.5 gr $LiBO_2$ then dissolving in 100 ml 5% HNO_3. The Rare Earth Element (REE) contents were analyzed by ICP-AES after dissolving 0.25 gr powdered rock sample in four different acids. The Loss of Ignition (LOI) was calculated from the weight difference after samples were ignited under temperature of 1000°C. The total iron content was expressed in terms of Fe_2O_3. The major elements were estimated in weight %, and the trace and REE were estimated in terms of ppm. The deviation limits in the analyses are 0.001-0.04% for major elements, 0.1-1 ppm for trace elements and 0.01-0.1 ppm for REE.

4. Geology and Petrography

4.1. Eriko Tepe Pluton

The Eriko Tepe Pluton covers nearly 7 km^2 in area and outcrops in the Eriko Tepe, Aytaş Tepe, Kızılağaç Valley and its surrounds in the south of Topçam town (Mesudiye, Ordu) (Figure 2a). The pluton was emplaced into Late Cretaceous andesite, basalt, pyroclastites, and syenites. Field observations and stratigraphical relationships of units indicate that the age of the pluton is Middle Eocene (Güven, 1993; MTA, 2002, 2011). The longitudinal axis of the Eriko Tepe Pluton extends in the northwest-southeast direction (Figure 2a) and outcrops in the form of heads on the field (Figure 3a, b). They are medium to fine grained and generally grey to dark grey due to high amounts of ferromagnesian minerals. Minor silicification and epidotization were observed where the pluton was in contact with the country rocks.

The plutonic rocks generally exhibit monzonitic, poikilitic, perthitic and rarely antirapakivi textures with plagioclase, orthoclase and quartz, with lesser ferromagnesian minerals which are clinopyroxene, biotite and hornblende (Figure 3c-f). However in some samples the hornblende is abundant with lesser biotite and pyroxene. Apatite, zircon and sphene are the opaque and accessory minerals and are less frequent than other minerals.

Plagioclases (25-30 modal %) are fine and coarse euhedral-subhedral grains that generally show albite polysynthetic twinning, but rarely Carlsbad twinning (Figure 3c) or oscillatory zoning. They are andesine (An_{44-46}) in composition based on extinction angle determinations on sections perpendicular to the (010) plane of plagioclases that show twinning based on the Albite law. The Carlsbad twinning was observed in some of the anhedral orthoclases (30-35 modal %) with variable sizes. The perthitic intergrowths, characterized by albite exsolution lamellae, were also detected in orthoclase. The coarse orthoclase crystals have occasional plagioclase, clinopyroxene and biotite inclusions in a poikilitic texture (Figure 3e-f) and surround plagioclase as monzonitic textures in some sections. Quartz grains (5-11 modal %) are anhedral and fine grained. They were emplaced generally into the residual empty spaces as it is the latest crystallized production of the magma (Figure 3c-f). Clinopyroxenes are subhedral and contain abundant opaque mineral inclusions (Figure 3c-f); their extinction angles are nearly 40° and so defined

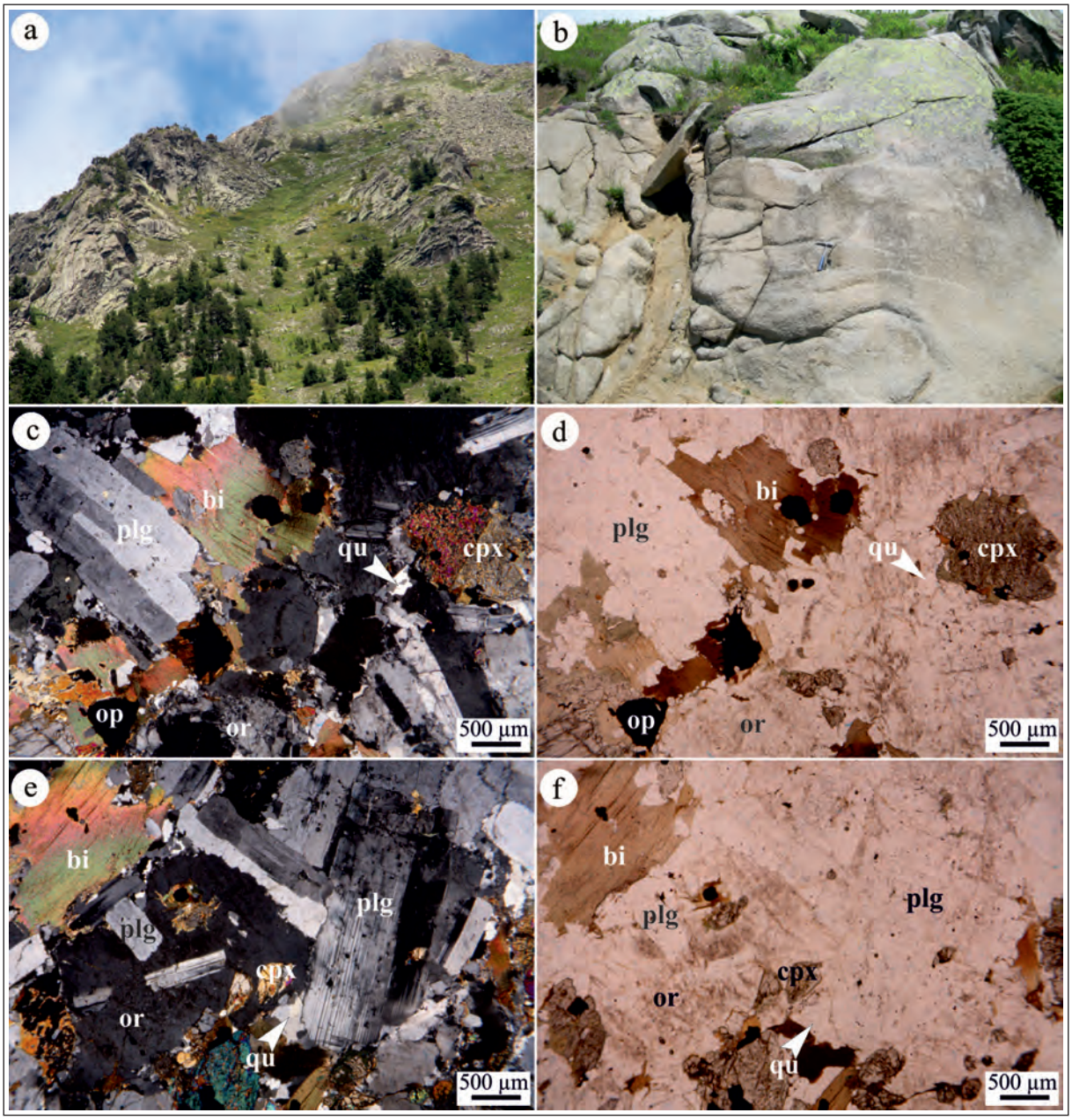

Figure 3- The field view (a and b) of the Eriko Tepe plutons and micro photos of the monzonite which exhibit the granular texture; (c and d) the plagioclase with Carlsbad twinning, bending in biotites that consists of opaque mineral inclusions and corrosions at the circumferences of clinopyroxenes; (e and f) the monzonitic texture formed by the enclosure of plagioclase by orthoclase, and the enclosure of clinopyroxene and biotite by the orthoclase in poiklitic texture, the albite-carlsbad complex twinning in plagioclases (Sample No: ER-2; C.N. and P.N.) (Explanations: C.N.: cross nicol; P.N., parallel nicol; cpx; clinopyroxene; bi: biotite; pl: plagioclase; or: orthoclase; op: opaque).

as augite. In some of their crystals the h' (100) twining was detected (Figure 3c). Biotite (8-10 modal %) are generally subhedral-euhedral and the parallel cleavage to (001) plane is distinctive. The brown pleochroism is distinctive and it is dark brown in z and y directions and yellowish in the x direction. They generally exhibit kink-banding due to deformation (Figure 3c-f). Hornblende (4-6 modal %) is few but where present is euhedral-subhedral and fine grained. and with green to pale green pleochroism. The extinction angle between c^z was measured as 20°. The mafic minerals in the rock are clustered: clinopyroxene and hornblende is surrounded, respectively, by biotite and opaque minerals and the formation of biotites around the clinopyroxene identifies disequilibrium crystallization. Opaque minerals (5-8 modal %) are

subhedral-anhedral fine crystals and are as inclusions in, and surrounding, the mafic minerals (Figure 3c-d). The majority of samples collected from the Eriko Tepe Pluton have not been affected from the alteration. Sericitization of plagioclases is rare and chloritization of ferromagnesian minerals is observed in some samples.

Modal analysis of 12 plutonic samples (Table 1), and the Quartz-Alkaline Feldspar-Plagioclase (QAP) diagram (Streickeisen, 1976) identified that the pluton is monzonite and quartz monzonite in composition (Figure 4).

Table 1- The general petrographical characteristics and modal compositions of the rocks from the Eriko Tepe and the Göl Tepe Plutons.

Name of the Pluton	**ERİKO TEPE PLUTON (ER) (n=12)**			**GÖL TEPE PLUTON (GT) (n=13)**		
Rock Type	Monzonite, Quartz monzonite			Monzonite, Quartz monzonite		
Texture	Monzonitic, poikilitic, perthitic, antirapakivi			Monzonitic, poikilitic, graphic, perthitic		
Grain Size	Medium-fine			Medium-fine		
Modal Min. (%)	**Mean**	**Min.**	**Max.**	**Mean**	**Min.**	**Max.**
Plagioclase	25.48	18.25	29.78	34.21	26.99	44.15
Quartz	5.19	1.25	10.36	3.87	0.58	9.44
Orthoclase	31.27	19.42	34.89	27.26	19.65	35.00
Hornblende	4.61	1.95	6.00	4.84	2.56	7.42
Biotite	8.04	7.06	9.99	6.76	1.12	9.36
Pyroxene	10.47	3.65	15.03	9.56	5.12	16.87
Access. Min.	2.23	1.83	2.63	1.39	0.56	2.25
Opaque Min.	5.44	2.85	8.46	6.22	4.11	8.92
Secondary Min.	3.07	2.21	4.68	2.66	0.20	6.10

n= the number of rocks on which the modal analysis were performed.

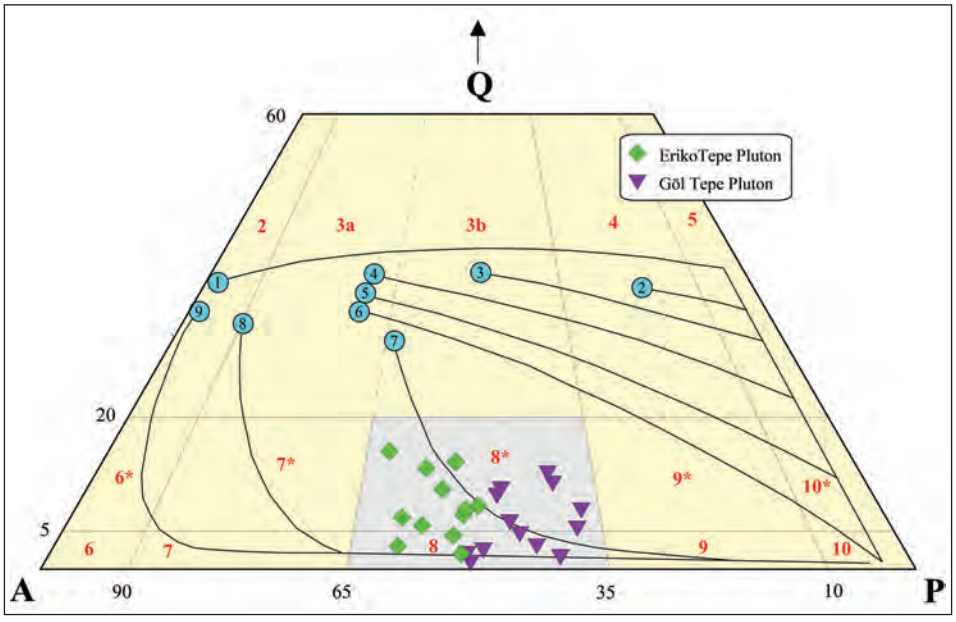

Figure 4- The Q-A-P plot of the rock samples from the Eriko Tepe and Göl Tepe Plutons. The curves show the directions of plutonic type series, which are: 1) tholeiitic series, 2) calc-alkaline trondhjemite series, 3-6) variable calc-alkaline granodioritic series, 7) monzonitic series, 8-9) variable alkaline series (Lameyre and Bonin; 1991). The fields; (2) alkaline feldspar granite, (3a) syenogranite, (3b) monzogranite, (4) granodiorite, (5) tonalite, (6*) quartz alkaline feldspar granite, (7*) quartz syenite, (8*) quartz monzonite, (9*) quartz monzodiorite/quartz monzogabbro, (10*) quartz diorite/quartz gabbro/quartz anorthosite, (6) alkaline feldspar granite, (7) syenite, (8) monzonite, (9) monzodiorie/ monzogabbro, (10) diorite/gabbro/anorthosite (Streckeisen, 1976).

4.2. Göl Tepe Pluton

The Göl Tepe Pluton outcrops in the Göl Tepe, Şıhdamı, Döşemeburnu Tepe, Kale Tepe, Çavdar Tepe, Yokuşbaşı Valley and surrounding areas in the south of the Gölköy (Ordu) town (Figure 2b). It is emplaced into a sedimentary series formed by the intercalation of Late Cretaceous andesite, basalt, pyroclastites and syenites, with Early-Middle Eocene limestone, sandstone, and mudstone (Figure 2b). The pluton is Middle Miocene based on stratigraphic relationships (Güven, 1993; MTA, 2002, 2011) and extends in the east-west direction (Figure 2b) and outcrops in the form of heads on the field with very hard, jointed and fractured structures (Figure 5a, b). Some outcrops are

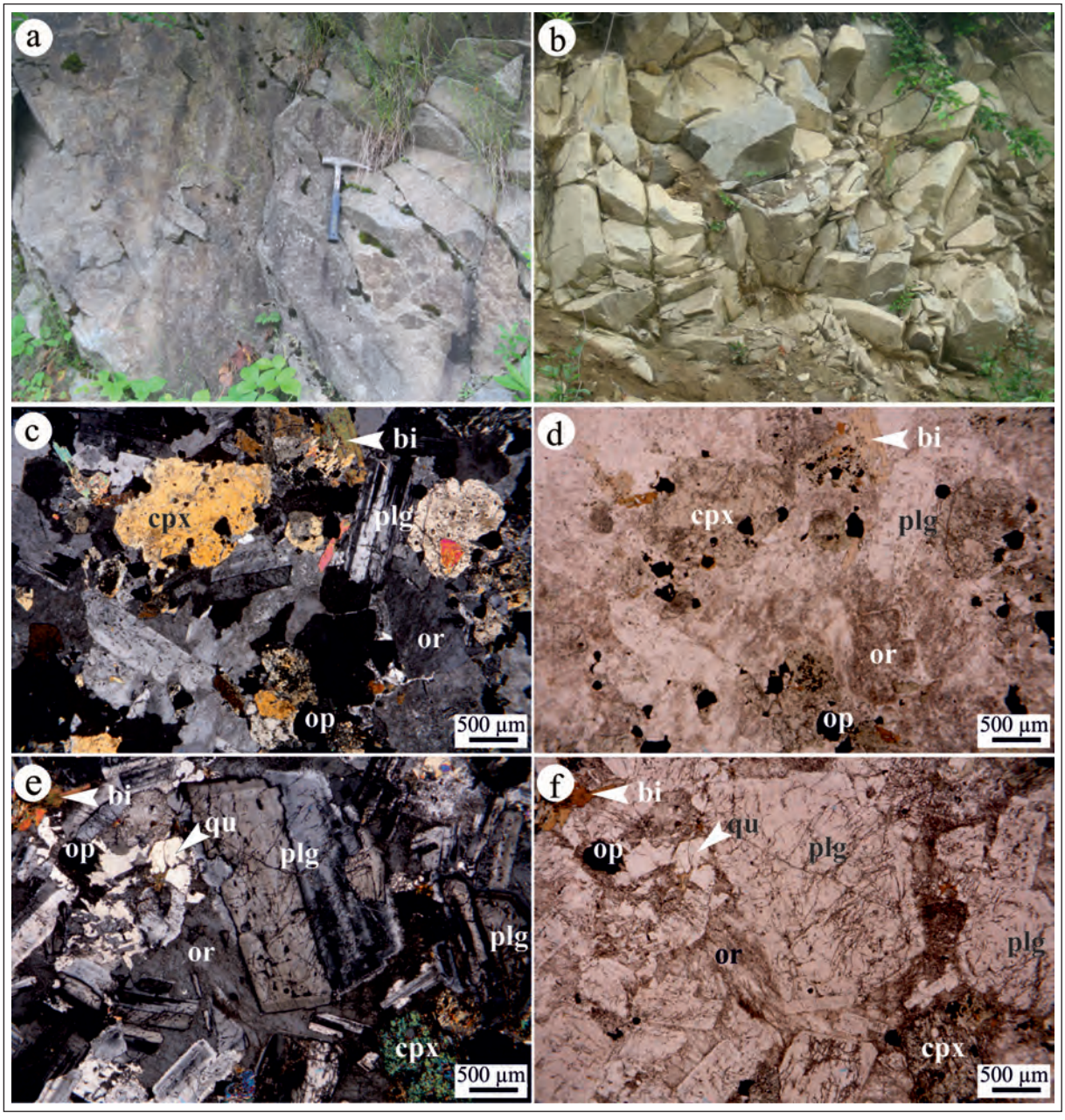

Figure 5- Monzonites from the Göl Tepe Pluton exhibit much fragmented and fractured structure (a and b), and the micro photos of monzonites that show granular textures; (c and d) the plagioclase minerals that show albite, albite-carlsbad complex twinning, clinopyroxene and biotite that have opaque mineral inclusions (Sample No: GT-3; C.N. and P.N.), (e and f) the plagioclase with oscillatory zoning in which the irregular growths are seen, the clinopyroxene mineral, which consists of much opaque minerals and plagioclase inclusions, and the monzonitic texture formed by the inclusion of plagioclase by orthoclase (Sample No: GT-4; C.N. and P.N.) (cpx; clinopyroxene; bi: biotite; plg: plagioclase; qu: quartz; or: orthoclase; op: opaque).

dark grey, depending on mineral content, and fine to medium grained. Contacts between the pluton and the country rocks are restricted by the NW-SE, NE-SW and N-S directional normal faults (Figure 2b) and crushed zones are seen occasionally in areas where the faults are observed. Rare examples of silicification and epidotization are noted.

Monzonitic, poikilitic, graphic and occasionally perthitic textures are observed and the felsic minerals present are plagioclase and quartz, whereas the dark colored minerals are clinopyroxene, hornblende and biotite and accompanying opaque minerals (Figure 5 c-f). Pyroxene, hornblende and biotite minerals are clustered and are accompanied by opaque minerals (Figure 5c, d). Accessory minerals are zircon and apatite.

Plagioclases (33-44 modal %) are euhedral-subhedral, fragmented and broken with albite twinning and oscillatory zoning, and both in some grains. Their composition is andesine (An_{40-44}) according to the examination of the perpendicular sections of crystals (010) with albite twinning. Only plagioclases with the zoned structures have irregular growth (Figure 5e, f). In some samples, there are minor opaque and apatite inclusions. Orthoclase (27-35 modal %) is anhedral and common. Some exhibit Carlsbad twinning, the others show perthitic texture (Figure 5c, f). Poikilitic grains tend to contain plagioclase, pyroxene, hornblende and opaque minerals, forming monzonitic textures surrounding plagioclase in some samples. Quartz (4-9 modal %) is anhedral, fine grained and with undulose extinction (Figure 5e, f). Clinopyroxene is subhedral-anhedral, fragmented and is coarse and fine grained. The extinction angles between c^z are nearly 40°, and so is augite, and with rare h' (100) twinning but with common plagioclase, biotite and opaque inclusions (Figure 5c, f). Biotite (6-9 modal %) is subhedral-anhedral (Figure 5c, f) and have a typical yellowish brown to brown pleochroism, and with one directional well defined cleavage. Hornblende (5-7 modal %) is subhedral and fine grained, with green to pale green pleochroism and two directional hornblende cleavages (110) detected in some sections. Opaque minerals have a irregular geometrical shape and are located around ferromagnesian minerals, or, in the form of inclusions. Alteration is in the form of kaolinization of orthoclase, chloritization of ferromagnesian minerals and sericitization of plagioclases.

Modal analysis of 13 plutonic samples (Table 1), and the QAP diagram (Streickeisen, 1976) identified that the pluton is monzonite and quartz monzonite in composition (Figure 4).

5. Mineral Chemistry

Plagioclases in the Eriko Tepe Plutonic rocks are andesine and labradorite and their compositions vary between $An_{35-49}Ab_{48-64}Or_{0-5}$ and $An_{50-52}Ab_{47-48}Or_{1-2}$, respectively. K-feldspars in these rocks are orthoclase and their compositions vary between $An_{0-7}Ab_{6-31}Or_{64-94}$ (Figure 6a, Supplementary Table 1). Plagioclase in the rocks of the Göl Tepe Pluton is andesine and labradorite and their compositions vary between $An_{37-49}Ab_{47-59}Or_{1-4}$ and $An_{51-67}Ab_{32-46}Or_{1-4}$, respectively. The K-feldspars in these rocks are orthoclase and their compositions vary between $An_{0-4}Ab_{4-38}Or_{61-96}$ (Figure 6a, Supplementary Table 1).

Hornblendes in the Eriko Tepe Plutonic rocks are magnesiohornblende based on the classification of Leake et al. (1997) and the $Mg/(Mg+Fe^{2+})$ ratios vary between 0.65-0.82 (Figure 6b, Supplementary Table 2).

Clinopyroxenes in the Eriko Tepe Plutonic rocks are diopside, diopsitic augite and augite based on the classification of Morimoto et al. (1988) and their compositions and $Mg/(Mg+Fe^{2+})$ ratio vary between $Wo_{28-48}En_{37-51}Fs_{13-22}$ and 0.70-0.76, respectively (Figure 6c, Supplementary Table 3). Clinopyroxenes in the Göl Tepe Plutonic rocks are also diopside, diopsitic augite and augite (based on the classification of Morimoto et al. 1988) and their compositions and $Mg/(Mg+Fe^{2+})$ ratios vary between $Wo_{38-49}En_{35-46}Fs_{10-25}$ and 0.58-0.81, respectively (Figure 6c, Supplementary Table 3).

Biotites in the Eriko Tepe Plutonic rocks plot on the biotite area in the $Fe/(Fe+Mg)$ vs Al^{IV} (apfu) diagram and their $Mg/(Mg+Fe^{2+})$ ratios vary between 0.53-0.60 (Figure 6d, Supplementary Table 4). In the Göl Tepe Plutonic rocks, based on the same plot, are classified as Mg enriched biotite and their $Mg/(Mg+Fe^{2+})$ ratios vary between 0.66-0.73 (Figure 6d, Supplementary Table 4).

Fe-Ti oxides in the Eriko Tepe Pluton are magnetite and titano-magnetite, and occasionally contain ilmenite lamellae (Supplementary Table 5) and in the Göl Tepe Pluton are also magnetite and titano-magnetite (Supplementary Table 5).

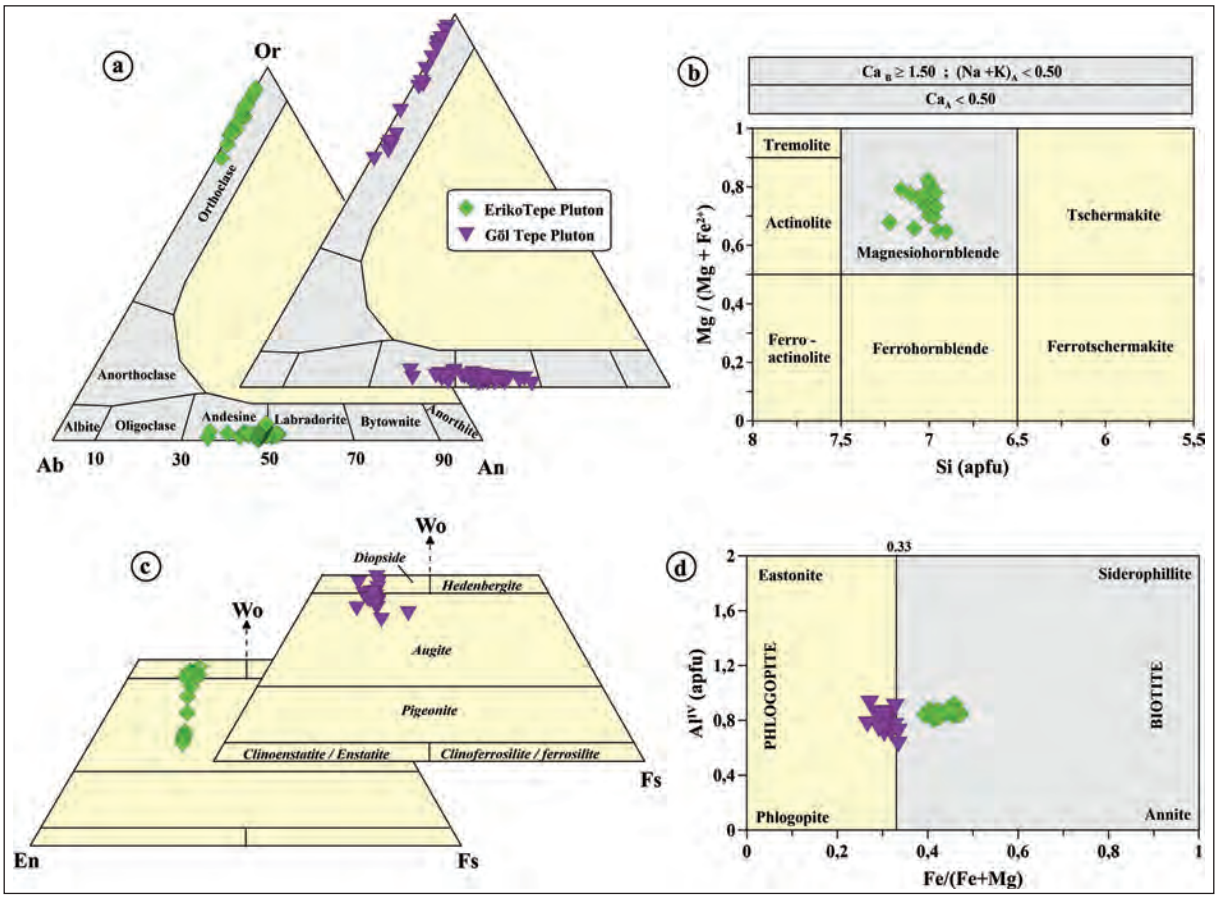

Figure 6- a) An-Ab-Or ternary plot of feldspars (Deer et al., 1992), b) Si (apfu) vs Mg/(Mg+Fe^{2+}) (Leake et al., 1997) classification diagram of hornblendes, c) Wo-En-Fs ternary plot of pyroxenes (Morimoto et al., 1988) and d) Mg–Li (apfu) vs Fe(t)+Mn+Ti-Al^{VI} (apfu) (Tischendorf et al., 1997) plot of biotites for the Eriko Tepe and the Göl Tepe plutonic rocks.

6. Whole-Rock Geochemistry

The major, trace and REE analyses for the Eriko Tepe and Göl Tepe Plutonic rocks are presented in Table 2. The geochemical characteristics of the major oxide and trace elements were compared in order to establish their magma-tectonic environments.

Plotting samples from both plutons on a TAS plot (Total alkali-silica, Middlemost 1994), the Eriko Tepe Pluton is in the monzonite field, and the Göl Tepe Pluton is in the monzodiorite, monzonite and quartz monzonite fields (Figure 7a). They are both alkaline (Figure 7a) again on this diagram based on the alkaline-subalkaline discrimination of Miyashiro (1978). The Eriko Tepe and the Göl Tepe plutonic rocks are shoshonitic on the SiO_2 (%) vs K_2O (%) diagram (Figure 7b) of Le Maitre et al. (2002), high-K and shoshonitic (Figure 7c) in character on the Co (ppm) vs Th (ppm) diagram of Hastie et al. (2007). On the (AI=Na+K/Al) vs (A/CNK) diagram of Maniar and Piccoli (1989) (Figure 7d), all samples are in the I-type field and metaluminous in character.

The rocks of the Eriko Tepe and the Göl Tepe Plutons present similar trends in major and trace element variation diagrams. With the increase in SiO_2 content, the K_2O, Na_2O, Rb, Zr, Nb, Ba, Hf, Th and Ta contents also increase, but on the contrary; TiO_2, Fe_2O_3*, MgO, MnO, CaO, P_2O_5, Sr and Y contents decrease (Figures 8 and 9). In addition; there is an increase then a decrease in the content of Al_2O_3 with the increase in SiO_2 content. The primitive mantle normalized trace element plots of the rocks from the studied monzonitic plutons exhibite similar distributions showing an enrichment in the large ion lithophile elements (LILE; Sr, K_2O, Rb and Ba), and in Th and Ce concentrations, but a depletion in some high field strength elements (HFSE; Y and TiO_2), and in Nb and Ta contents (Figure 10a). The chondrite normalized REE distributions for the rocks of the plutons are defined by a concave shaped

Table 2- The major (%), trace (ppm) and rare earth element (ppm) analyses for the rocks of the Eriko Tepe and the Göl Tepe Plutons.

	Eriko Tepe Pluton								Göl Tepe Pluton						
Sample no:	**ER-1**	**ER-2**	**ER-3**	**ER-4**	**ER-5**	**ER-6**	**ER-7**	**ER-8**	**GT-1**	**GT-2**	**GT-3**	**GT-4**	**GT-6**	**GT-7**	**GT-8**
SiO_2	58.08	56.56	56.22	58.16	57.63	55.98	59.06	59.06	53.80	55.98	55.58	55.01	53.34	64.16	55.18
TiO_2	0.77	0.83	0.82	0.69	0.78	0.79	0.63	0.68	0.80	0.68	0.67	0.72	0.72	0.40	0.71
Al_2O_3	16.44	16.28	16.92	17.12	16.59	16.40	15.79	16.98	17.09	17.40	17.74	17.18	16.83	16.14	17.02
Fe_2O_3(t)	7.21	8.06	7.81	6.27	7.33	7.70	6.33	6.21	8.68	7.20	7.29	7.71	8.27	4.26	7.80
MnO	0.13	0.15	0.14	0.20	0.13	0.14	0.10	0.14	0.16	0.14	0.14	0.14	0.16	0.10	0.13
MgO	3.11	3.59	3.47	2.58	3.17	3.49	3.11	2.52	3.38	3.07	3.01	3.22	3.62	1.51	3.44
CaO	5.56	6.20	6.25	4.69	5.61	6.37	5.43	4.43	6.53	6.18	6.38	6.78	6.75	3.57	6.18
Na_2O	3.11	2.97	3.09	3.53	3.14	2.97	3.03	3.53	3.17	3.40	3.20	3.54	3.19	3.13	2.97
K_2O	4.64	4.28	4.23	4.89	4.68	4.20	4.44	4.81	4.19	4.49	4.56	4.05	3.87	5.21	4.12
P_2O_5	0.34	0.35	0.35	0.32	0.32	0.35	0.26	0.29	0.35	0.34	0.34	0.35	0.35	0.17	0.34
LOI	0.3	0.4	0.4	1.2	0.3	1.3	1.5	1.1	1.5	0.8	0.8	1.0	2.5	1.1	1.8
Total	99.69	99.67	99.70	99.65	99.68	99.69	99.68	99.75	99.65	99.68	99.71	99.70	99.60	99.75	99.69
Zr	175.9	152.4	146.6	187.1	212.0	201.6	151.7	183.9	173.0	174.9	162.5	162.8	152.2	194.8	169.1
Y	20.8	22.7	20.1	23.8	20.8	20.4	19.0	22.9	21.6	20.9	20.9	19.9	21.1	16.6	20.8
Sr	704.1	784.3	765.3	668.3	706.0	752.7	635.5	651.8	896.0	787.9	775.9	756.8	1069.2	561.5	772.6
Rb	167.8	151.8	137.7	136.0	161.1	148.1	156.0	142.8	153.1	164.3	149.6	157.2	137.4	199.0	137.2
Th	18.8	12.4	12.0	11.5	15.3	13.3	15.7	13.9	10.5	13.3	10.8	12.5	11.3	18.6	12.0
Ta	0.8	0.7	0.7	0.7	0.7	0.7	0.7	0.8	0.4	0.6	0.7	0.7	0.7	1.0	0.5
Sc	16	18	17	14	16	18	16	14	17	15	15	16	18	7	17
V	193	232	212	166	198	228	174	157	223	180	176	201	222	90	203
Pb	4.2	2.0	1.5	11.9	3.9	1.7	5.8	4.5	5.3	5.9	12.4	9.9	9.7	10.0	3.2
Ni	10.7	13.5	13.4	7.2	11.7	12.9	12.1	7.6	10.7	10.0	9.7	11.8	14.4	5.6	15.0
Co	18.6	21.9	19.9	12.9	19.3	20.6	15.5	14.1	21.0	18.4	16.8	19.5	21.2	9.2	19.1
Cr	40	50	40	30	50	50	60	30	50	50	50	50	60	40	70
Cs	5.0	4.5	3.6	3.5	4.8	4.7	3.4	3.1	2.8	2.5	2.8	4.0	4.1	4.3	1.8
Ba	562	678	589	794	562	575	569	716	565	609	522	480	520	603	505
Nb	12.2	11.8	10.8	10.2	12.0	10.6	10.4	11.3	8.7	10.5	9.5	9.5	7.9	10.3	9.3
Hf	4.7	4.0	4.0	5.1	5.5	5.0	4.5	4.6	3.9	4.5	4.0	3.8	3.6	5.1	4.3
La	34.5	33.5	31.6	39.5	32.1	33.9	31.9	36.9	33.9	34.8	34.8	32.3	30.9	35.1	32.6
Ce	62.5	61.5	57.3	69.5	62.1	63.6	57.4	66.5	59.6	62.8	61.8	60.2	56.7	57.4	58.2
Pr	7.37	7.01	6.60	7.94	6.88	7.19	6.33	7.40	6.86	7.12	6.99	6.71	6.32	6.08	6.66
Nd	28.8	28.3	25.1	31.7	27.1	26.9	23.9	27.0	27.7	27.1	26.9	26.0	25.0	22.0	25.5
Sm	5.42	5.43	4.63	5.89	5.03	5.44	4.59	5.36	5.16	5.15	5.23	4.94	4.53	3.87	5.05
Eu	1.25	1.28	1.28	1.41	1.17	1.16	1.03	1.32	1.28	1.32	1.19	1.18	1.24	0.85	1.21
Gd	4.82	5.16	4.73	5.40	4.78	4.80	4.26	5.09	5.23	5.01	4.41	4.52	4.72	3.40	4.80
Tb	0.70	0.70	0.65	0.76	0.68	0.69	0.63	0.77	0.68	0.64	0.64	0.61	0.64	0.49	0.66
Dy	3.81	3.94	3.56	4.38	3.73	4.28	3.40	3.98	3.70	3.74	3.54	3.53	3.78	3.11	3.51
Ho	0.78	0.79	0.68	0.89	0.74	0.77	0.70	0.77	0.81	0.71	0.72	0.74	0.72	0.58	0.76
Er	2.14	2.29	2.15	2.41	2.19	2.05	1.91	2.28	2.07	2.16	2.07	2.13	1.91	1.72	2.08
Tm	0.36	0.35	0.30	0.36	0.30	0.32	0.30	0.37	0.31	0.34	0.32	0.32	0.29	0.27	0.32
Yb	2.25	2.29	2.11	2.44	2.20	2.14	2.00	2.42	2.25	2.10	2.00	2.07	2.17	1.97	2.17
Lu	0.35	0.35	0.33	0.40	0.36	0.33	0.31	0.39	0.35	0.36	0.35	0.30	0.33	0.29	0.34
Eu_N/Eu^*	0.75	0.74	0.84	0.76	0.73	0.69	0.71	0.77	0.75	0.79	0.76	0.76	0.82	0.72	0.75
La_N/Lu_N	10.23	9.94	9.94	10.25	9.26	10.66	10.68	9.82	10.06	10.04	10.32	11.18	9.72	12.57	9.95
La_N/Yb_N	10.36	9.89	10.12	10.94	9.86	10.70	10.78	10.30	10.18	11.20	11.76	10.54	9.62	12.04	10.15
Mg#	30.14	30.82	30.76	29.15	30.19	31.19	32.94	28.87	28.03	29.89	29.22	29.46	30.45	26.17	30.60

Fe_2O_3(t), total iron in terms of Fe_2O_3, LOI (Loss of Ignition): Total volatile content, Mg# =100 x MgO /[MgO + Fe_2O_3(t)].

pattern characterized with the presence of Eu anomaly (Figure 10b). The La_N/Lu_N ratios of the Eriko Tepe and Göl Tepe Plutons vary between 9.26-10.68 and 9.72-10.12.57, respectively and their La_N/Yb_N ratios vary between 9.86-10.94 and 9.62-12.04, respectively. On the other hand, the Eu_N/Eu^* ratios for the Eriko Tepe and the Göl Tepe plutons are in between 0.69-0.84 and 0.72-0.82, respectively (Figure 10b). The weak negative Eu anomaly of the plutonic rocks in the REE distributions indicates that the plagioclase

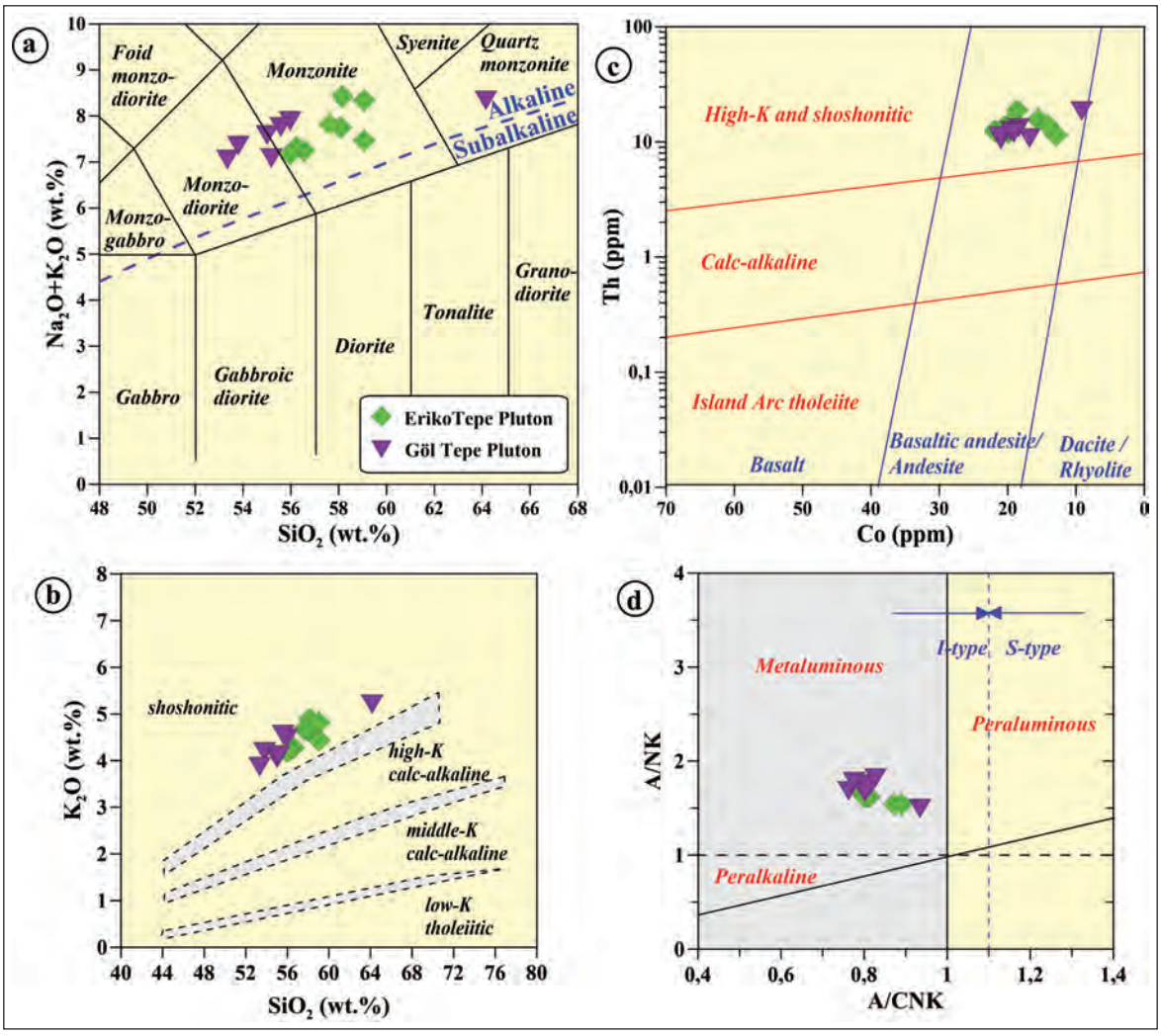

Figure 7- a) The classification diagram of Na_2O+K_2O (wt%) vs SiO_2 (wt%) (TAS) (Middlemost, 1994) (alkaline-sub alkaline line is based on Miyashiro (1978)), b) SiO_2 (wt%) vs K_2O (wt%) (Le Maitre et al., 2002), c) Th (ppm) vs Co (ppm) (Hastie et al., 2007), d) agpaitic index (AI=Na+K/Al) vs molar $Al_2O_3/(CaO+Na_2O+K_2O)$ (A/CNK) (Maniar and Piccoli, 1989) for the rocks of the Eriko Tepe and the Göl Tepe Plutons.

differentiation was not very effective in the evolution of these magmas (Figure 10b).

7. Discussion

The mineral chemistry and whole-rock analyses were used for the thermobarometry to reveal the P-T conditions. The data are also used to determine the source regions of the parental magmas, the role of magmatic processes in their evolution, and the magma-tectonic environments.

7.1. Crystallization Conditions of the Plutons

Temperature estimates are based on the two feldspar (plagioclase-alkaline feldspar) geothermometer (Putirka, 2003, 2005 and 2008), and they vary between 625-797 °C (mean= 726 ± 56ºC) for the Eriko Tepe Pluton and 623-770ºC (mean= 684 ± 47ºC) for the Göl Tepe Pluton (Table 3).

Temperatures based on the clinopyroxene thermobarometer (Putirka et al., 1996, 2003; Putirka, 1999, 2005, 2008), vary between 1039-1197ºC (mean= 1158 ± 49ºC) for the Eriko Tepe Pluton and 1018-1194ºC (mean= 1119 ± 47ºC) for the Göl Tepe Pluton (Table 4). The pressure values, on the other hand, vary between 5.3-8.4 kbar (mean= 7.5 ± 1.1 kbar) and 5.6-7.2 kbar (mean= 6.6 ± 0.6 kbar) for the Eriko Tepe Pluton and 3.2-6.6 kbar (mean= 4.8 ± 1.4 kbar) and 3.8-6.7 kbar (mean= 4.8 ± 1.3 kbar) for the Göl Tepe Pluton (Table 4).

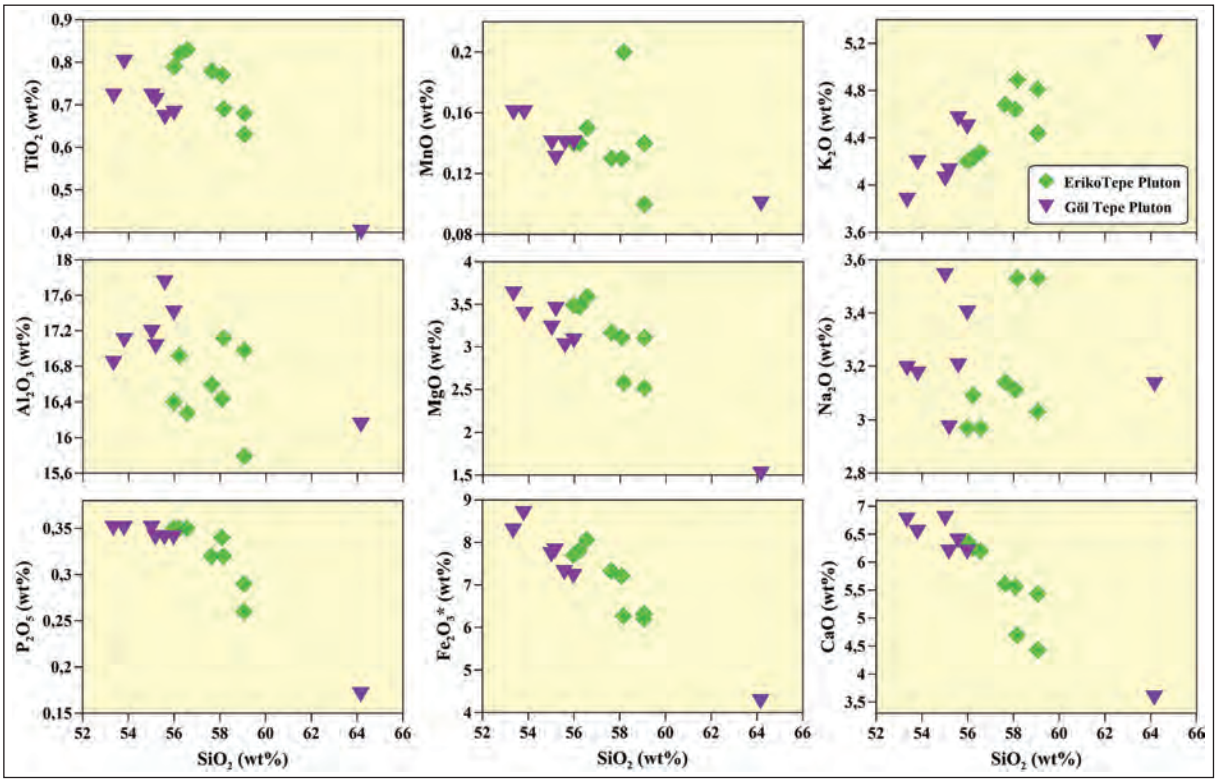

Figure 8- SiO_2 (wt%) vs major oxides (wt%) for the rocks of the Eriko Tepe and the Göl Tepe Plutons.

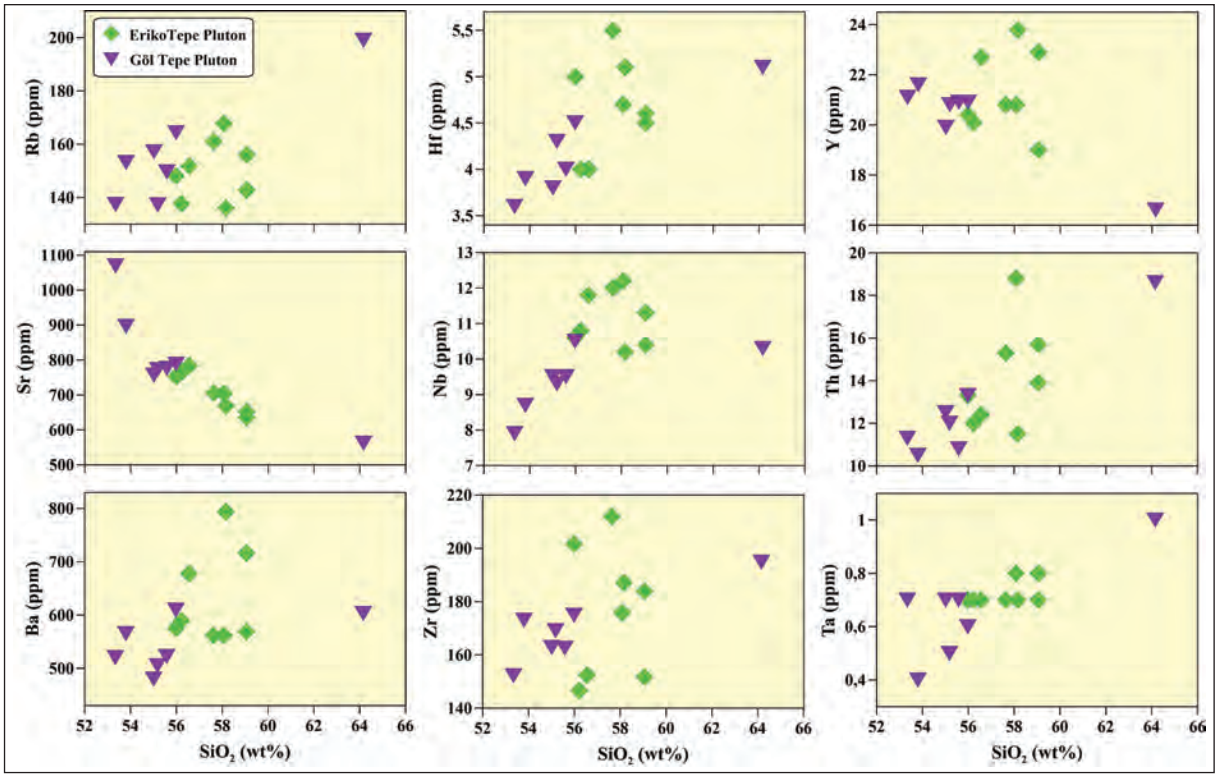

Figure 9- SiO_2 (wt%) vs trace elements (ppm) for the rocks of the Eriko Tepe and the Göl Tepe Plutons.

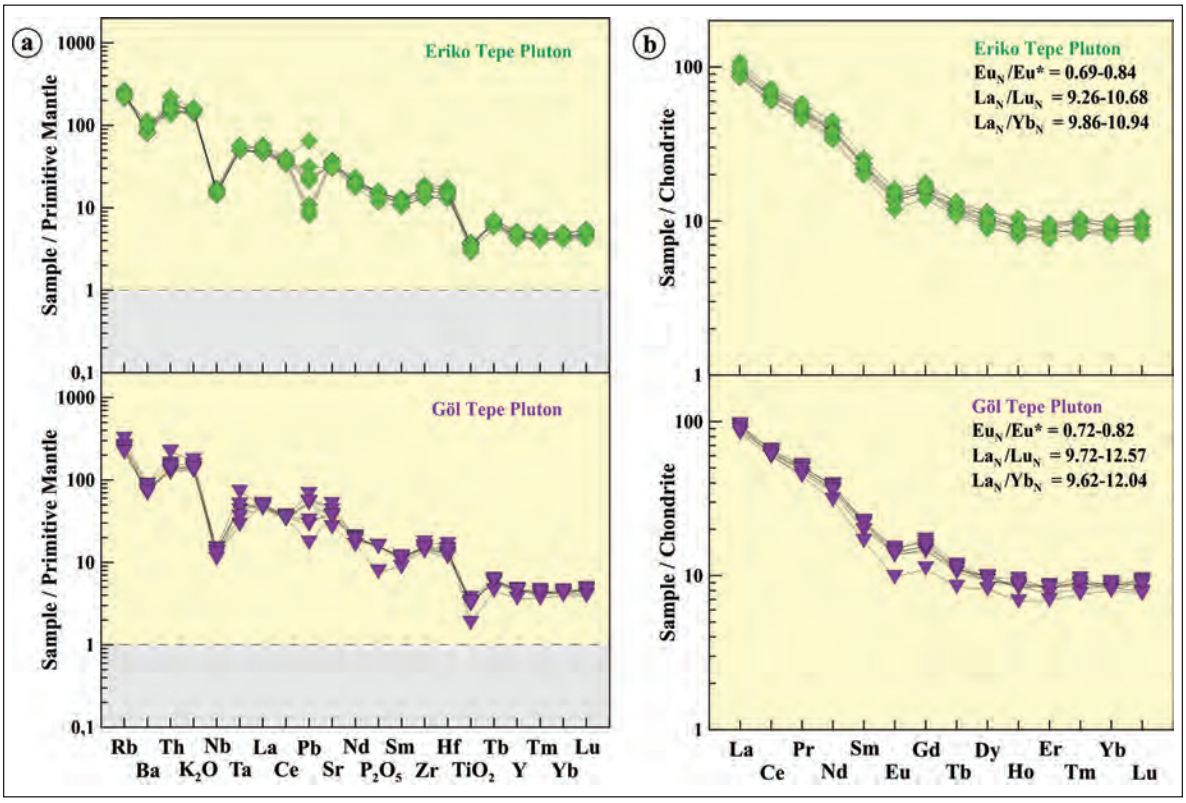

Figure 10- a) The primitive mantle normalized trace element distributions (Sun and McDonough, 1989) and b) the chondrite normalized rare earth element distributions (Taylor and McLennan, 1985) for the rocks of the Eriko Tepe and the Göl Tepe Plutons.

Table 3- The temperatures (T,ºC) estimated based on Putirka (2008) by using two feldspar compositions (plagioclase and alkaline feldspar) for the Eriko Tepe and the Göl Tepe Plutons.

Two feldspar (Plagioclase- alkaline feldspar) thermometer				
Equation 27b (thermometer)		**Mean T (°C)**	**Max. T (°C)**	**Min. T (°C)**
Eriko Tepe Pluton	(n=43)	726 ± 56	797	625
Göl Tepe Pluton	(n=24)	684 ± 47	770	623

Table 4- The temperatures (T,ºC) and pressures (P, kbar) estimated based on Putirka (2008) by using clinopyroxene and clinopyroxene-liquid compositions (plagioclase and alkaline feldspar) for the Eriko Tepe and the Göl Tepe Plutons.

Clinopyroxene Thermobarometer					
Equation 32a (barometer, non-aqueous)		**Max. P (kbar)**	**Min. P (kbar)**	**Mean P (kbar)**	**Mean Depth* (km)**
Eriko Tepe Pluton	(n=6)	8.4	5.3	7.5 ± 1.1	27.8
Göl Tepe Pluton	(n=4)	6.6	3.2	4.8 ± 1.4	17.8
Equation 32b (barometer, aqueous)					
Eriko Tepe Pluton	(n=6)	7.2	5.6	6.6 ± 0.6	24.4
Göl Tepe Pluton	(n=4)	6.7	3.8	4.8 ± 1.3	17.8
Equation 32d (thermometer, non-aqueous)		**Max. T (°C)**	**Min. T (°C)**	**Mean T (°C)**	
Eriko Tepe Pluton	(n=11)	1197	1039	1158 ± 49	
Göl Tepe Pluton	(n=13)	1194	1018	1119 ± 47	

* Depth was taken as 3.7 km for 1 kbar for the continental crust (Tulloch and Callis, 2000).

The pressure estimates based on the Al^T content of hornblende vary between 1.2-1.9 kbar (mean= 1.5 kbar ± 0.3 kbar) according to Hammarstrom and Zen (1986); 0.9-1.4 kbar (mean= 1.1 kbar ± 0.3 kbar) according to Hollister et al. (1987); 1.0-1.7 kbar (mean= 1.3 kbar ± 0.4 kbar) according to Johnson and Rutherford (1989) and 1.8-2.5 kbar (mean= 2.1 kbar ± 0.3 kbar) according to Schmidt (1992) (Table 5). Temperatures calculated using the hornblende-plagioclase thermometer of Blundy and Holland (1990) using P1-P4 values are: 776-824ºC (mean= 809 ± 17ºC) for P1, 770-826ºC (mean= 811 ± 17ºC) for P2, 782-830ºC (mean= 815 ± 17ºC) for P3 and 767-815ºC (mean=800 ± 17ºC) for P4 for the Eriko Tepe Pluton (Table 5).

Temperature estimates calculated for the Eriko Tepe Pluton for under <5 kbar pressure are based on the hornblende-plagioclase thermometer of Holland and Blundy (1994) vary between 735-790ºC (mean= 761 ±16ºC) (Table 6a). The pressure and temperature

Table 5- Pressures (P, kbar) calculated according to Hammarstrom and Zen (1986), Hollister et al. (1987), Johnson and Rutherford (1989) and Schmidt (1992) by using hornblendes for the Eriko Tepe and the Göl Tepe Plutons, and the temperatures (T, °C) estimated based on Blundy and Holland (1990) by using these mean pressure values.

	Hammarstrom and Zen (1986) (P1)	**Hollister et al. (1987) (P2)**	**Johnson and Rutherford (1989) (P3)**	**Schmidt (1992) (P4)**
Eriko Tepe Pluton (n=6)				
Max. P (kbar)	1.9	1.4	1.7	2.5
Min. P (kbar)	1.2	0.9	1.0	1.8
Mean P (kbar)	1.5 ± 0.3	1.1 ± 0.3	1.3± 0.4	2.1 ± 0.3
Mean depth (km)	5.6	4.1	4.8	7.8
Blundy and Holland (1990), Hornblende-plagioclase thermometer				
	Hammarstrom and Zen (1986)	**Hollister et al. (1987)**	**Johnson and Rutherford (1989)**	**Schmidt (1992)**
Eriko Tepe Pluton (n=6)	**(P1 =1.5 kbar)**	**(P2 =1.1 kbar)**	**(P2 =1.3 kbar)**	**(P2 =2.1 kbar)**
Max. T (°C)	824	826	830	815
Min. T (°C)	776	778	782	767
Mean T (°C)	809 ± 17	811 ± 17	815 ± 17	800 ± 17

* Depth was taken as 3.7 km for 1 kbar for the continental crust (Tulloch and Callis, 2000).

Table 6- Using the hornblendes for the Eriko Tepe Pluton; a) the temperatures (T, °C) estimated under 5 kbar pressure according to hornblende-plagioclase thermometer of Holland and Blundy (1994), and the temperature (T, °C) and pressure (P, kbar) values estimated based on the hornblende thermobarometer of Ridolfi et al (2010) and Ridolfi and Renzulli (2012); b) the oxygene fugacity [log$f(O_2)$], ΔNNO and H_2O_{melt}(w.%) values calculated based on Wones (1989), Ridolfi et al. (2008 and 2010) and Riddolfi and Renzulli (2012).

a	**Holland and Blundy (1994), Hornblende-plagioclase thermometer (Pressure (P) was taken as 5 kbar in estimations)**	**Ridolfi et al. (2010), Hornblende thermobarometer (calc-alkaline magmas)**		**Ridolfi and Renzulli (2012), Hornblende thermobarometer (calc-alkaline magmas)**	
		Pressure (P, kbar)	**Temperature (T, °C)**	**Pressure (P, kbar)**	**Temperature (T, °C)**
Eriko Tepe Pluton	**(n=13)**	**(n=14)**	**(n=14)**	**(n=14)**	**(n=14)**
Mean T (°C)	761 ± 16	0.8 ± 0.1	781 ± 11	0.9 ± 0.1	746± 19
Max. T (°C)	790	1.0	796	1.1	767
Min. T (°C)	735	0.7	763	0.6	708
b	**Wones (1989)**	**Ridolfi et al. (2008, 2010)**			**Ridolfi and Renzulli (2012)**
	Oxygen fugacity log$f(O_2)$	ΔNNO	**Oxygen fugacity log$f(O_2)$**	**H_2O melt (w.%)**	ΔNNO
Eriko Tepe Pluton	**(n=6)**	**(n=14)**	**(n=14)**	**(n=14)**	**(n=14)**
Mean	-13.6 ± 0.4	1.65 ± 0.36	-12.7 ± 0.4	4.16 ± 0.23	0.90 ± 0.52
Max.	-13.1	2.13	-11.9	4.60	2.14
Min.	-14.4	1.03	-13.4	3.77	0.00

*** Pressure (P, kbar) values used in the oxygen fugacity estimations of Wones (1989) and the temperature (T, °C) values are the calculated values according to Schmidt (1992) and Blundy and Holland (1990), respectively.

estimates based on hornblende, following Ridolfi et al. (2010), vary between 0.7-1.0 kbar (mean= 0.8 ± 0.1 kbar) and 763-796ºC (mean= 781 ± 11ºC), respectively. However, the pressure and temperature values calculated according to Ridolfi and Renzulli (2012) are in between 0.6-1.1 kbar (mean= 0.9 ± 0.1 kbar) and 708-767ºC (mean= 746 ± 19ºC), respectively (Table 6a). The oxygen fugacity values calculated according to Ridolfi et al. (2010) and Wones (1989) using the Mg content of hornblendes in the Eriko Tepe Pluton are, respectively, between (-13.4) - (-11.9) (mean= -12.7 ± 0.4) and (-14.4) - (-13.1) (mean= -13.6 ± 0.4) (Table 6b). However, the ΔNNO values calculated according to Ridolfi et al. (2008, 2010) and Ridolfi and Renzulli (2012) vary between the values of 1.03-2.13 (mean= 1.65 ± 0.36) and 0.00-2.14 (mean= 0.9 ± 0.52), respectively. The H_2O content calculated according to Ridolfi et al. (2008, 2010) varies between the values of 3.77-4.60 (mean= 4.16 ± 0.23) (Table 6b).

The temperature values estimated based on Luhr et al. (1984) and the pressure values calculated according to Uchida et al. (2007) from biotite minerals vary between 730-824ºC (mean= 765 ± 28ºC) and 0.5-1.11 kbar (mean= 0.8 ± 0.15 kbar) for the Eriko Tepe Pluton and 856-1049ºC (mean= 948 ± 52ºC) and 0.54-1.18 kbar (mean= 0.84 ± 0.25 kbar) for the Göl Tepe Pluton (Table 7). The values that are based on the oxygen fugacity model of Wones (1989), using these pressure and temperature values, are between (-15.7) - (-13.1) (mean= -14.7 ± 0.0.8) for the Eriko Tepe Pluton and (-12.3) - (-8.3) (mean= -10.4 ± 1.1) for the Göl Tepe Pluton (Table 7).

Zircon (Miller et al., 2003) and apatite (Harrison and Watson, 1984) saturation temperatures were also calculated using the whole-rock analyses of the Eriko Tepe and the Göl Tepe Plutons. Zircon saturation temperatures (T1 and T2), based on the M and FM parameters of Miller et al. (2003), are between 717-757ºC (mean= 737 ± 16ºC) and 684-734ºC (mean= 708 ± 19ºC) for the Eriko Tepe Pluton and 709-780ºC (mean= 730 ± 24ºC) and 676-766ºC (mean= 703 ± 29ºC) for the Göl Tepe Pluton (Table 8). However, the apatite saturation temperatures, which were calculated

Table 7- The pressure (P, kbar), temperature (T, °C) and oxygene fugacity values calculated according to Luhr et al. (1984), Uchida et al. (2007) and Wones (1989) by using the biotites for the Eriko Tepe and the Göl Tepe Plutons.

	Luhr et al. (1984) Temperature (T, °C)	**Uchida et al. (2007) Pressure (P, kbar)**	**Wones (1989) T and P in (*f*O2) estimations are according to (Luhr et al., 1984) (Uchida et al., 2007), respectively.**
Eriko Tepe Pluton (n=18)			
Mean	765 ± 28	0.80 ± 0.15	-14.7 ± 0.8
Max.	824	1.11	-13.1
Min.	730	0.50	-15.7
Göl Tepe Pluton (n=24)			
Mean	948 ± 52	0.84 ± 0.25	-10.4 ± 1.1
Max.	1049	1.18	-8.3
Min.	856	0.54	-12.3

Table 8- The temperature (T, °C) values estimated for the saturation of zircon (Miller et al., 2003) and apatite (Harrison and Watson, 1984) by using the whole-rock geochemical analyses of the Eriko Tepe and the Göl Tepe Plutons.

	Saturation temperature for Zircon * (Miller et al., 2003)		**Saturation temperature for Apatite (Harrison and Watson, 1984)**
	T1 (M was used)	T2 (FM was used)	
Eriko Tepe Pluton	**(n=18)**	**(n=18)**	**(n=8)**
Mean T (°C)	737 ± 16	708 ± 19	894 ± 9
Max. T (°C)	757	734	908
Min. T (°C)	717	684	883
Göl Tepe Pluton	**(n=7)**	**(n=7)**	**(n=7)**
Mean T (°C)	730 ± 24	703 ± 29	869 ± 18
Max. T (°C)	780	766	898
Min. T (°C)	709	676	845

*Saturation temperatures for zircon (T_1 and T_2) were estimated, by means of the whole-rock geochemical analyses, using the parameters M [=(Na + K + 2Ca)/(Al × Si)] of Watson and Harrison (1983) and FM [=(Na + K + (2Ca + Fe + Mg))/(Al × Si)] of Ryerson and Watson (1987), which are given in Hanchar and Watson (2003), and the experimental models suggested by Miller et al (2003).

based on the formula of Harrison and Watson (1984), are 883-908ºC (mean= 894 ± 9ºC) for the Eriko Tepe Pluton and 845-898ºC (mean= 869 ± 18ºC) for the Göl Tepe Pluton (Table 8).

The crystallization depth corresponding to the mean pressure values (4.8-7.5 kbar) from the clinopyroxene barometry are 17.8-27.8 km. However, the crystallization depth corresponding to the mean pressure values (1.1-2.1 kbar), which had been obtained from the hornblende barometry, were detected as 4.1-7.8 km (1 kbar= 3.7 km for the continental crust; Tulloch and Challis, 2000). So, this indicates that these plutonic rocks were subjected to early stage high pressure and late stage low pressure polybaric crystallization at mid to shallow crustal depths. The oxygen fugacity values calculated from the hornblendes and biotites are close to, or just in, the upper part of the NiNiO buffer zone and the plutons are the products of the similar magmas.

7.2. Origin of the Parental Magmas

There are many petrogenetical models related to the origins of granitic-monzonitic magmas: (1) fractional crystallization (FC) and/or assimilation+fractional crystallization (AFC) from mantle derived basaltic parental magmas (Grove and Donnelly-Nolan, 1986; Bacon and Druitt, 1988; Rapela and Pankhurst, 1996; Soesoo, 2000; Jiang et al., 2002; Liu et al., 2008; Li et al., 2009; Aghazadeh et al., 2010, 2011); (2) the partial melting of mafic to intermediate meta-magmatic crustal rocks (Roberts and Clemens, 1993; Xu et al., 2004; Köksal et al., 2013); (3) the mixing of mantle derived mafic magma and crustal origin felsic magmas (Neves and Mariano, 1997; Ferré et al., 1998; Barbarin, 1999; Gagnevin et al., 2004; Yang et al., 2007, 2011; Ackerman et al., 2010; Lan et al., 2011, 2012, 2013; Cheng et al., 2012; Donskaya et al., 2013; Mao et al., 2013; Wang et al., 2013; Liu et al., 2013, 2014), and, (4) the partial melting of felsic magmas, mafic to intermediate meta magmatic (Rapp and Watson, 1995; Singh and Johannes, 1996) or meta-sedimentary (Patiño Douce and Beard, 1996; Stevens et al., 1997) rocks based on the principle that mantle derived basaltic magmas provide heat to melt crustal rocks (Bullen and Clynne, 1990; Roberts and Clemens, 1993; Guffanti et al., 1996). It is also known that the shoshonitic magmas generally form in the arc and post-collisional environments (eg, Foley and Peccerillo, 1992; Turner et al., 1996). It is also asserted that the shoshonitic magmas, which were formed in the post-collisional environments, had been derived from: (i) the peridotite-amphibolite-metapelite mixture on the crust-mantle boundary (López-Moro and López-Plaza, 2004); (ii) the mixture of asthenospheric and enriched lithospheric mantle (Li et al. 2000), and, (iii) the mantle metasomatism of which the subducted sediments had caused or the enriched lithospheric mantle (Turner et al., 1996; Wang et al., 1996; Eklund et al., 1998; Liu et al., 2002).

The monzonitic rocks, which form the Eriko Tepe Pluton (SiO_2: 56-59 % and Mg#: 29-33) and the Göl Tepe Pluton (SiO_2: 53-64 %, Mg#: 26-31), are I-type, metaluminous (Eriko Tepe Pluton; A/CNK=0.78-0.89 and Göl Tepe Pluton; A/CNK=0.76-0.93) and shoshonitic and possess molar K_2O/Na_2O, molar CaO/($MgO+Fe_2O_3$*) and A/CNK ratios varying mainly in a narrow interval (Figure 11a, b). In terms of Th/U vs U (ppm) they plot in the areas which show that the melts are derived from the middle-lower continental crust (Figure 11c). In terms of La/Yb vs Nb/La they plot on the lithospheric mantle and in the area close to the intermediate continental crust composite in the diagram (Figure 11d). However, in terms of La/Nb vs Ba/Nb (Figure 11e) and Nb (ppm) vs Nb/Th (Figure 11f), the monzonitic rocks plot on the area of arc volcanics they show a tendency for subduction enrichment. When the major molar and trace element ratio diagrams are assessed together, it is apparent that the parental magmas of the monzonitic plutons may be derived from the decompressional melting of lithospheric mantle that is enriched by different ratios of amphibole and plagioclase in different H_2O contents.

These monzonitic rocks have negative Nb and TiO_2 anomalies and Sr, Rb, K_2O, Th, Ce and La enrichments in the primitive mantle-normalized diagrams. They also indicate that parental magmas of these plutons might have been derived from the mixtures of lithospheric mantle enriched by previous subduction events and that the continental crust melts in fewer ratios. However, low-intermediate Rb/Sr ratios (0.13-0.35), intermediate-high K_2O (3.9-5.2%) and SiO_2 (53-64%) contents show that the parental magmas of these rocks may have been derived from the much enriched lithospheric mantle source (Jung et al., 2009). The trace element variations of monzonitic plutons with high LILE/HFSE ratios and their REE distributions with slightly moderate degree enrichments (Eriko Tepe Pluton: La_N/Lu_N=9.26-10.68; Göl Tepe Pluton: La_N/Lu_N= 9.72-12.57) show similarity to each other.

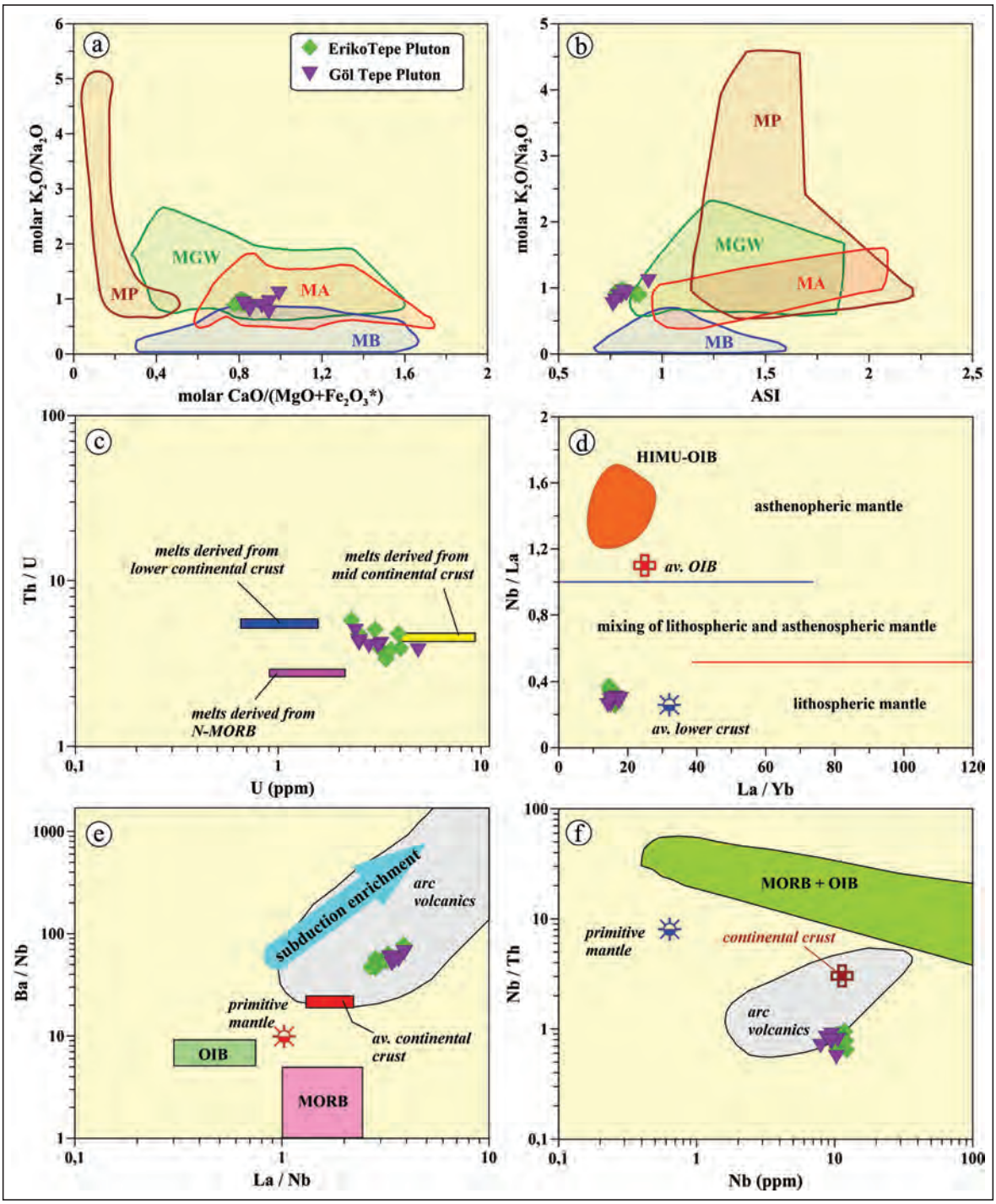

Figure 11- (a) The molar K_2O/Na_2O vs molar $CaO/(MgO+Fe_2O_3*)$, (b) molar K_2O/Na_2O vs ASI (A/CNK), (c) U (ppm) vs Th/U, (d) La/Yb vs Nb/La, (e) La/Nb vs Ba/Nb and (f) Nb (ppm) vs Nb/Th plots for the rocks of the Eriko Tepe and the Göl Tepe Plutons. The data for (a) and (b); MB: metabasalt, MA: metaandesite; MGW: metagreywacke, MP: metapelite. The fields are based on Vielzeuf and Holloway (1988), Patiño Douce and Johnston (1991), Rapp et al. (1991), Gardien et al. (1995), Rapp (1995), Rapp and Watson (1995), Patiño Douce and Beard (1996), Stevens et al. (1997), Skjerlie and Johnston (1996), Patiño Douce (1997), Patiño Douce and McCarthy (1998), Patiño Douce (1999). (c); the field belonging to the lower and intermediate continental crust and the depleted Mid Oceanic Ridge Basalt (MORB) area from Rudnick and Gao (2003) and Sun et al. (2008), respectively. (d); the boundaries among the atmospheric mantle, lithospheric mantle and the mixture of lithospheric–atmospheric mantles from Smith et al. (1999), the HIMU-OIB (Oceanic Island Basalt) area from Weaver et al. (1987), the mean OIB value from Fitton et al. (1991) and the mean lower crust value from Chen and Arculus (1995). (e); the arc volcanic field from Jahn and Zhang (1984), the primitive mantle value from Sun and McDonough (1989), the mean continental crust value from Taylor and McLennan (1985) and Condie (1993), and fields of MORB and OIB from Le Roex (1987). (f); the primitive mantle value from Hofmann (1988), continental crust value and fields of MORB, OIB and arc volcanics from Schmidberger and Hegner (1999).

It emphasizes that parental magmas of these plutons have been derived from the similar sources and through similar magmatic processes (differentiation and crust assimilation).

7.3. Fractional Crystallization (FC) and Assimilation-Fractional Crystallization (AFC)

The correlations (see Figures 8 and 9), which are observed in some major oxide and trace element variations in the Harker diagrams for monzonitic rocks of the Eriko Tepe and Göl Tepe Plutons, show that the FC is significant in the evolution of these plutons. There is a positive correlation between the SiO_2 and the K_2O, Nb, Ba, Hf**,** Th and Ta contents, however, there is a negative correlation between the SiO_2 content and TiO_2, Fe_2O_3*, MgO, MnO, CaO, P_2O_5 and Sr contents in monzonitic rocks of the Eriko Tepe and the Göl Tepe Plutons (see Figures 8 and 9). Generally the decrease of Fe_2O_3* indicates clinopyroxene fractionation. Nevertheless, the decrease of CaO with increasing SiO_2 indicates clinopyroxene and plagioclase fractionation. The decrease in Sr, but increase in K_2O, with respect to the increase in SiO_2, indicates K-feldspar fractionation. The decrease in P_2O_5, TiO_2 and Sr with the increase in SiO_2 indicates that apatite, magnetite and plagioclase fractionated, however, the decrease in Fe_2O_3*, MgO and MnO indicate that hornblende and biotite fractionated. In general, K_2O, showing a positive correlation with SiO_2, emphasizes biotite and K-feldspar fractionations. The studied plutons exhibit a concave shaped pattern in REE distributions, verifying the effectiveness of clinopyroxene and/or hornblende fractionations in their evolution (Thrilwall et al., 1994). Besides; the weak negative Eu anomaly observed in monzonitic rocks of the Eriko Tepe Pluton (Eu_N/Eu*: 0.69-0.84) and the Göl Tepe Pluton (Eu_N/Eu*: 0.72-0.82) indicates that K-feldspar±plagioclase fractionation is effective in the evolution of these rocks (see Figure 10 b).

The irregular correlations observed in some major oxide and trace element variations (see Figures 8 and 9) could also indicate crustal assimilation ± magma mixing in addition to the fractional crystallization. The correlations observed in MgO (%)-Sr (ppm) and Rb (ppm)-K_2O/Rb diagrams (Figure 12a, b) that plagioclase, K-feldspar, clinopyroxene, hornblende, biotite and Fe-Ti oxide all fractionated in the evolution of the plutons. However, the contribution of continental crust in the evolution of the plutons can be clarified by Ta/Yb vs Th/Yb diagrams (Figure 12c) (Pearce, 1983). In this diagram, the plutonic rock samples examined show a tendency towards the average continental crust value with high Th/Yb and Ta/Yb ratios (Figure 12c). Accordingly it is possible to say that the AFC has also played a lesser role compared to FC in the evolution of these plutons (Figure 12c). The AFC modelling was

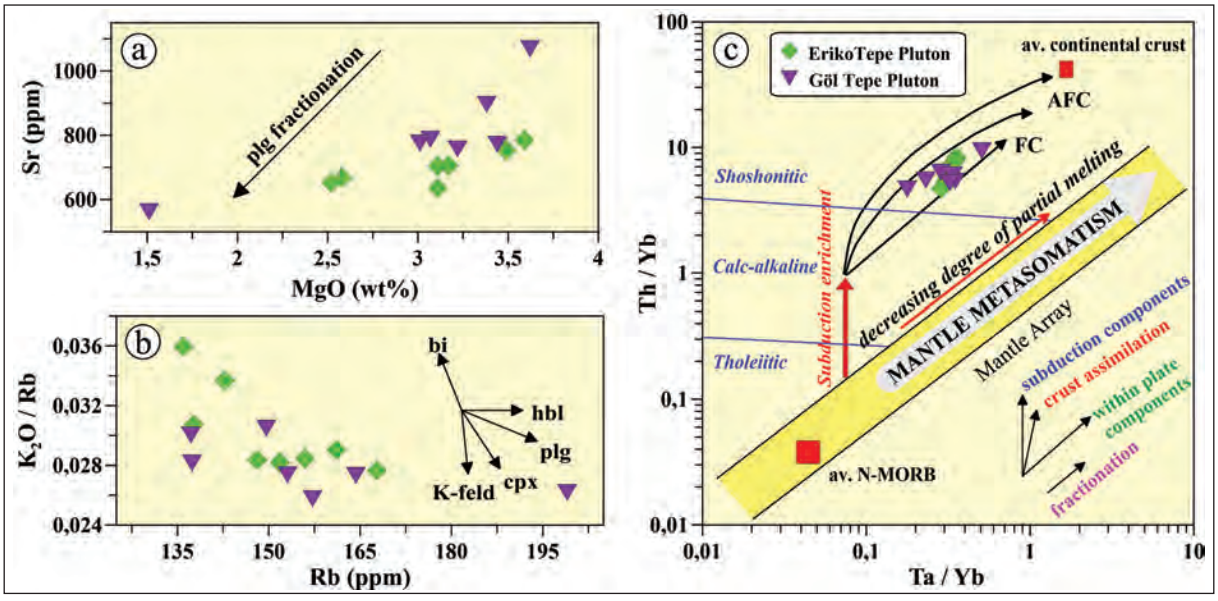

Figure 12- The plots of; a) MgO (wt%) vs Sr (ppm), b) Rb (ppm) vs K_2O/Rb and c) Ta/Yb vs Th/Yb (Pearce, 1983) (pl: plagioclase, cpx: clinopyroxene, hb: hornblende, bi: biotite, K-feld: K-feldspar) show directions of FC (fractional crystallization) and/or AFC (assimilation+fractional crystallization) and the mineral fractionation for the rocks of the Eriko Tepe and the Göl Tepe Plutons. The vectors showing FC, AFC, subduction enrichment and the mantle metasomatism were taken from Pearce et al. (1990).

based on trace element contents and/or ratios (Figures 13a, b and c) (DePaolo, 1981; Powell, 1984). All samples in diagrams of La-Nb and La-La/Nb (Figures 13a, b), which show the AFC of monzonitic rocks, plot on or near the r=0.2 curve. However, they plot on or near the r=0.05 curve in the Zr-Zr/Nb diagram (Figure 13c). Generally the r value is less than or equal to 0.2, less than the critical value of r=0.25 (Albarède, 1996) shows that FC is more effective than AFC in the evolution of these monzonitic rocks.

7.4. Magma-Tectonic Environment of Plutons

The different magma-tectonic evolution models for the Tertiary magmatism in the Eastern Pontides are suggested to be: (1) the slab-break off of the subduction plate (Boztuğ et al., 2004, 2006); (2) the southward roll-back and synchronous slab-window (Eyüboğlu et al., 2011*a, b, c*), and, (3) the lithospheric delamination (Karslı et al., 2007, 2010*b*, 2012*b*; Temizel et al., 2012*a*; Arslan et al., 2013*a*). When the geochemical and petrological characteristics of Eocene (~ 45-40 Ma) intermediate-high K and shoshonitic volcanic rocks (eg. Arslan and Aliyazıcıoğlu, 2001; Temizel et al., 2012*a*; Arslan et al., 2013*a*; Temizel et al., 2016; Yücel et al., 2017) and I-type, metaluminous and shoshonitic plutonic rocks (eg. Boztuğ et al., 2004; Boztuğ and Harlavan, 2008; Topuz et al., 2005; 2011; Arslan and Aslan, 2006; Karslı et al., 2007, 2010*a*, 2011, 2012*b*) were considered, it was asserted that the magmatism is characterized by the extensional tectonic setting related with the crustal thickening and lithospheric detachment, and has derived mainly from enriched sub-continental lithospheric mantle and lower continental crust melts and/or mixtures (Temizel et al., 2012*a*; Arslan et al. 2013*a*; Aslan et al., 2014; Yücel et al., 2017).

In order to determine the magma-tectonic environments of the monzonitic plutons, the

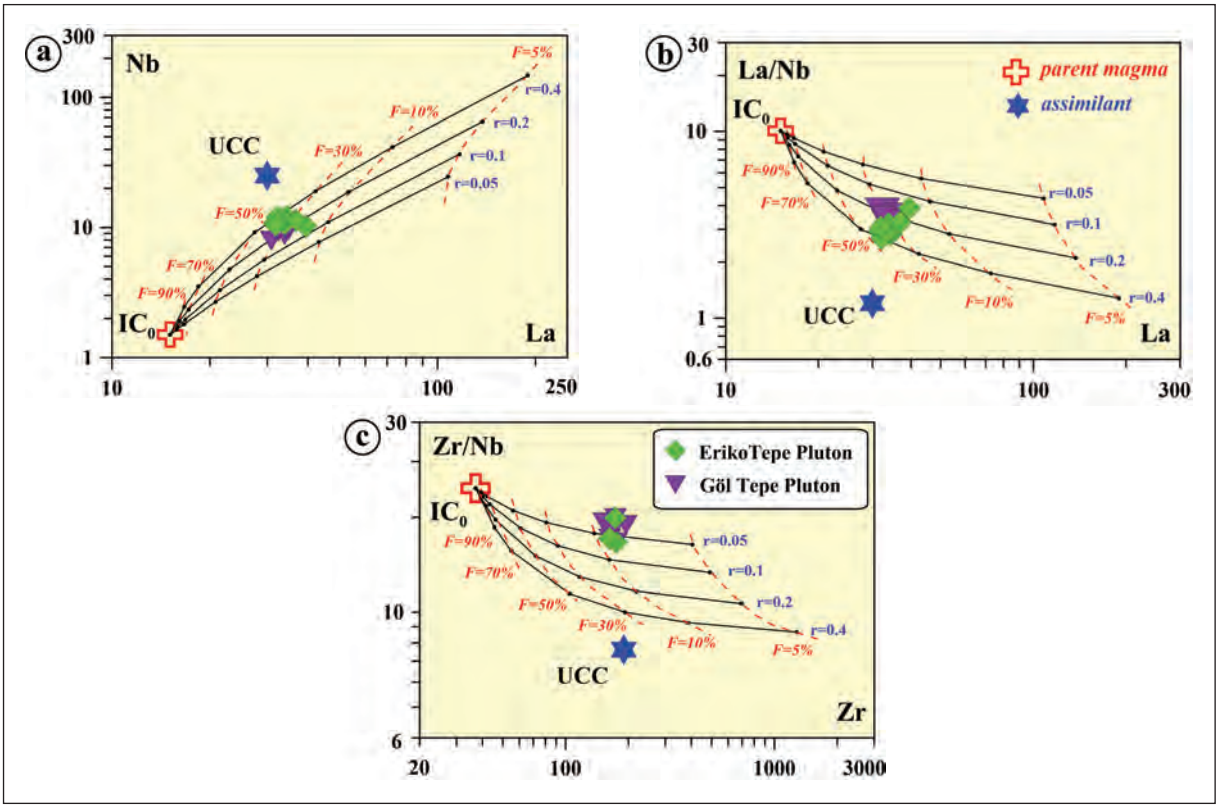

Figure 13- The plots of; a) Nb (ppm) vs La (ppm), b) La/Nb vs La (ppm) and c) Zr/Nb vs Zr (ppm), which show the trace element AFC modelling in the rocks of the Eriko Tepe and the Göl Tepe Plutons. Parental magma composition (IC_0; La = 15.1 ppm, Zr = 37.1 ppm and Nb = 1.5 ppm; CIPW mineralogy = olivine: 17.38, clinopyroxene: 17.83, plagioclase: 45.85, magnetite: 3.52) is the basalt sample SIR-108 from Arslan et al. (2013*a*). The Upper Continental Crust composition as the assimilant (La = 30 ppm, Zr = 190 ppm and Nb = 25 ppm) from Taylor and McLennan (1985) and the portition coefficients from McKenzie and O'Nions (1991). The AFC curves were drawn based on different r values (ratio of the fractional crystallization with respect to assimilation; 0.05, 0.1, 0.2 and 0.4) and the values of different F (fractionation degrees (%); 5, 10, 30, 50, 70, 90).

discrimination diagrams for the plutonic rocks were used. According to Rb-(Y+Nb) and Ta-Yb diagrams of Pearce et al. (1984) (Figure 14a, b) the samples belonging to the studied plutons plot on areas of volcanic arc and post-collisional granites. Further, they plot on fields of arc granites and granites formed by the collisional tectonics according to the Rb/10-Hf-Ta*3 ternary diagram of Harris et al. (1986) (Figure 14c), and magmatic or crust origin due to the interaction of mantle-crust (Figure 14d). Thus, considering other geological and geochemical data, it can be asserted that the studied plutons has formed from the lithospheric mantle derived magmas (with less amount of continental crust assimilation) in the Eocene post collisional environment in the Eastern Pontides.

8. Conclusions

The Eriko Tepe and Göl Tepe plutons outcropping in the southeastern part of the Gölköy (Ordu) area in the Eastern Pontides Orogenic Belt were formed from mainly monzonitic and rarely quartz-monzonitic and monzodioritic rocks in composition.

The plutons both have similar mineralogical and textural characteristics, only the Eriko Tepe pluton consists of magnesio-hornblende different than the Göl Tepe pluton. There were also observed some textural features in these studied plutons indicating disequilibrium crystallization, such as: the corrosion of clinopyroxene, the poikilitic textures observed in K-feldspars minerals and clinopyroxene minerals surrounded by the biotite minerals.

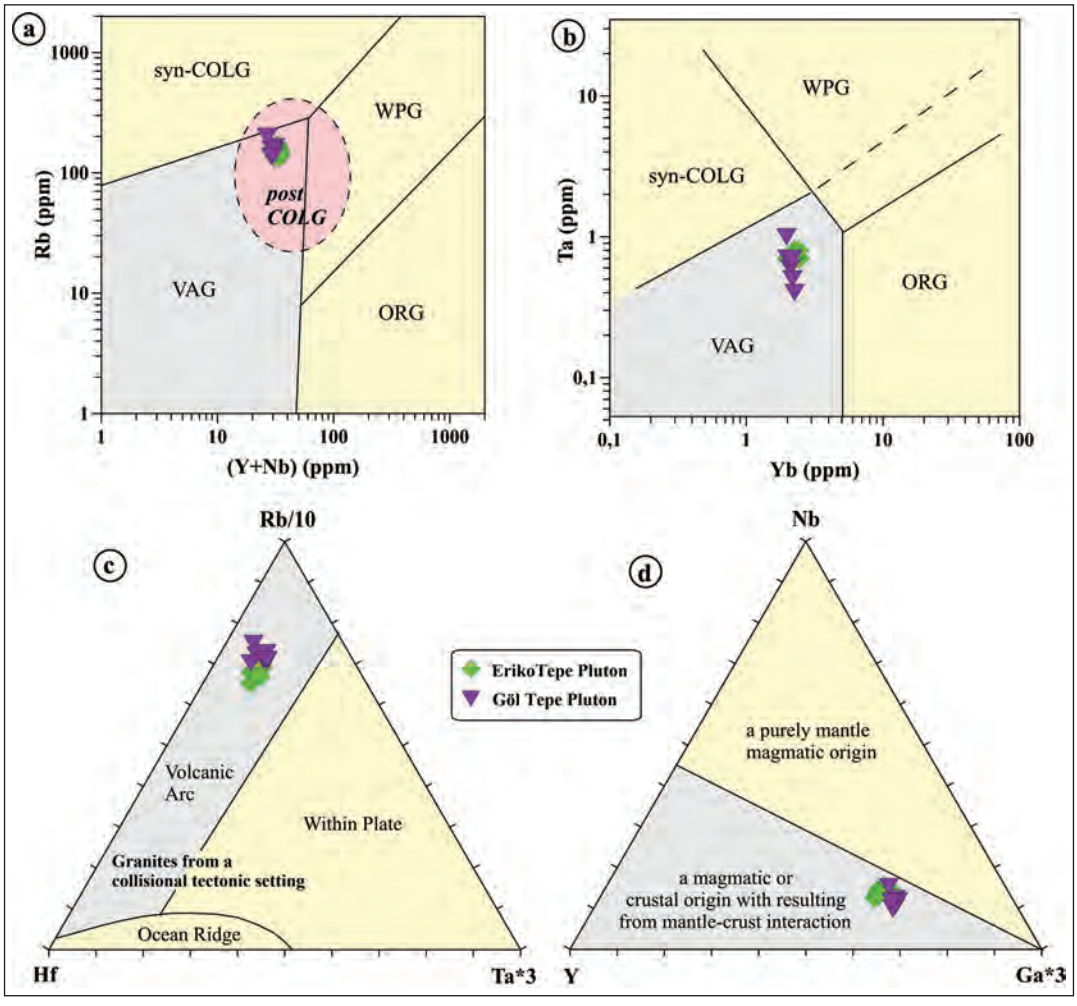

Figure 14- The magma-tectonic discrimination plots of the rocks from the Eriko Tepe and the Göl Tepe Plutons; a) Rb (ppm) vs (Y+Nb) (ppm), b) Ta (ppm) vs Yb (ppm), c) Rb/10-Hf-Ta*3 (Harris et al., 1986) and d) Nb-Y-Ga*3 (Eby, 1992) ternary diagrams. Syn-COLG: Syn-collisional granites, VAG: Volcanic Arc Granites; WPG: Within Plate Granites; ORG: Oceanic Ridge Granites; post-COLG: Post-collisional Granites.

The P-T conditions were detected by means of the chemistry of feldspar, clinopyroxene, hornblende and biotite minerals in the studied plutons. The calculated temperature and pressure values vary between 684-726ºC for feldspars, 1119-1158ºC and 4.8-7.5 kbar for clinopyroxenes, 1.1-2.1 kbar and 761-815ºC for hornblendes and 765-948ºC and 0.80-0.84 kbar for biotites. This indicates that the plutons were generally crystallized at mid to shallow crustal depths.

The whole-rock geochemical data show that the studied plutons are I-type, metaluminous and shoshonitic in character. The major and trace element variations indicate that the plutons were differantiated significantly by fractional crystallization and lesser crustal assimilation during the evolution of the magma chamber in the continental crustal.

It can be asserted that the parental magmas were derived from the enriched lithospheric mantle by decompressional melting in a post-collisional setting.

Acknowledgements

This study has been supported by the TÜBİTAK-ÇAYDAG project, number 113Y404. The authors thank to Prof. Nurdane İlbeyli and Assoc. Prof. Fuat Erkül for their constructive critiques and suggestions. We are also grateful to Dr. Sarah Sherlock for reviweving and editing of the English version.

Supplementary Data

Tables 1-5; Electronic Data for Appendices are available at https://dergi.mta.gov.tr/documents/1991_157_supplementary_tables_irfan_temizel.pdf

References

Ackerman, L., Krňanská, M., Siebel, W., Strnad, L. 2010. Geochemistry of the Drahotín and Mutěnín intrusions, West Bohemian shear zone, Bohemian massif: contrasting evolution of mantle-derived melts. Mineralogy and Petrology 99, 185-199.

Aghazadeh, M., Castro, A., Omran, N.R., Emami, M.H., Moinvaziri, H., Badrzadeh, Z. 2010. The gabbro (shoshonitic)–monzonite–granodiorite association of Khankandi pluton, Alborz Mountains, NW Iran. Journal of Asian Earth Sciences 38, 199-219.

Aghazadeh, M., Castro, A., Badrzadeh, Z., Vogt, K. 2011. Post-collisional polycyclic plutonism from the Zagros hinterland. The Shaivar-Dagh plutonic complex Alborz belt, Iran. Geological Magazine 148, 980-1008.

Ağar, U. 1977. Demirözü (Bayburt) ve Köse (Kelkit) Bölgesinin Jeolojisi. Doktora Tezi, İstanbul Üniversitesi, İstanbul (unpublished).

Albaréde, F. 1996. High-resolution geochemical stratigraphy of Mauna Kea flows from the Hawaii Scientific Drilling Project core. Journal of Geophysical Research. Solid Earth.

Aliyazıcıoğlu, İ. 1999. Kale (Gümüşhane) yöresi volkanik kayaçlarının petrografi, jeokimyasal ve petrolojik incelenmesi. Yüksek Lisans Tezi, KTÜ Fen Bilimleri Enstitüsü, 96 s. Trabzon (unpublished).

Altherr, R., Topuz, G., Siebel,W., Şen, C., Meyer, H.P., Satır, M. 2008. Geochemical and Sr-Nd-Pb isotopic characteristics of Paleocene plagioleucitites from the Eastern Pontides (NE Turkey). Lithos,105, 149-161.

Arslan, M., Aliyazıcıoğlu, İ. 2001. Geochemical and petrological characteristics of the Kale (Gümüşhane) volcanic rocks: implications for the Eocene evolution of eastern Pontide arc volcanism, northeast Turkey. International Geology Review 43, 7, 595-610.

Arslan, M., Aslan, Z. 2006. Mineralogy, petrography and whole-rock geochemistry of the Tertiary granitic intrusions in the eastern Pontides, Turkey. Journal of Asian Earth Sciences 27, 177-193.

Arslan, M., Tüysüz, N., Korkmaz, S., Kurt, H. 1997. Geochemistry and Petrogenesis of the Eastern Pontide Volcanic Rocks, Northeast Turkey. Chemi der Erde 57, 157-187.

Arslan, M., Temizel, İ., Abdioğlu, E. 2002. Subduction input versus source enrichment and role of crustal thickening in the generation of Tertiary magmatism in the Pontid Paleo-Arc setting, NE Turkey. In: De Vivo, B., R. J. Bodgar, R. J. (Eds.) Workshop-Short Course on Volcanic Systems, Geochemical and Geophysical Monitoring, Melt inclusions: Methods, applications and problems, 13-16, Napoli, Italy.

Arslan, M., Temizel, İ., Abdioğlu, E., Kolaylı, H., Yücel, C., Boztuğ, D., Şen, C. 2013*a*. ^{40}Ar-^{39}Ar dating, whole-rock and Sr-Nd-Pb isotope geochemistry of post-collisional Eocene volcanic rocks in the southern part of the Eastern Pontides (NE Turkey): Implications for magma evolution in extension-induced origin. Contribution to Mineralogy and Petrology 166, 113-142.

Arslan, M., Abdioğlu, E., Temizel, İ., Yücel, C. 2013*b*. Doğu Pontid Kuzey Zonu Tersiyer volkanitlerinin petrokimyası, Sr-Nd-Pb izotop jeokimyası,

jeokronolojisi ve jeodinamik gelişimi. TÜBİTAK ÇAYDAG Projesi No: 108Y204.

Aslan, Z., 2010. U-Pb zircon SHRIMP age, geochemical and petrographical characteristics of tuffs within calc-alkaline Eocene volcanics around Gümüşhane (NE Turkey), Eastern Pontides. Neues Jahrbuch für Mineralogie Abhandlungen 187, 329-346.

Aslan, Z., Arslan M., Şen, C. 1999. Doğu Pontidlerin Kuzey ve Güney zonlarında yüzeylenen Eosen yaşlı granitik sokulumların karşılaştırmalı jeolojik, petrografik ve jeokimyasal özellikleri. Türkiye Jeoloji Kurultayı Bildiriler Kitabı, 223-230.

Aslan, Z., Arslan, M., Temizel, İ., Kaygusuz, A. 2014. K-Ar dating, whole-rock and Sr-Nd isotope geochemistry of calc-alkaline volcanic rocks around the Gümüşhane area: implications for post-collisional volcanism in the Eastern Pontides, Northeast Turkey. Mineralogy and Petrology 108, 245-267.

Aydın, F., Karslı, O., Chen, B. 2008. Petrogenesis of the Neogene alkaline volcanics with implications for post collisional lithospheric thinning of the Eastern Pontides, NE Turkey. Lithos 104, 249-266.

Aydın, F., Thompson, R., Karsli, O., Uchida, H., Burt, J.B., Downs, R.T. 2009. C2/c pyroxene phenocrysts from there potassic series in Neogene alkaline volcanics, Ne Turkey: Their crystal chemistry with petrogenetic significance as an indicator of P-T conditions. Contributions to Mineralogy and Petrology 158, 131-147.

Bacon, C.R., Druitt, T.H. 1988. Compositional Evolution of the Zoned Calc-Alkaline Magma Chamber of Mount Mazama, Crater Lake, Oregon. Contribution to Mineralogy and Petrology 98, 224-256.

Barbarin, B. 1999. A review of relationships between granitoid types, their origins and their geodynamic environments. Lithos 46, 605-626.

Bektaş, O., Pelin, S., Korkmaz, S. 1984. Doğu Pontid yay gerisi havzasında manto yükselimi ve polijenetik ofiyolit olgusu. TJK Ketin Sempozyumu, pp. 175-188.

Bektaş, O., Şen, C., Atıcı, Y., Köprübaşı, N. 1999. Migration of the Upper Cretaceous subduction-related volcanism towards the back-arc basin of the Eastern Pontide magmatic arc (NE Turkey). Geological Journal 34, 95-106.

Blundy, J.D., Holland, T.J. B. 1990. Calcic amphibole equilibria and a new amphibole-plagioclase geothermometer. Contributions to Mineralogy and Petrology 104, 208-224.

Boztuğ, D., Harlavan, Y. 2008. K-Ar ages of granitoids unravel the stages of Neo-Tethyan convergence in the eastern Pontides and central Anatolia, Turkey. International Journal of Earth Sciences 15, 585-599.

Boztuğ, D., Avcı, N., Tatar, S., Zorlu, M., Tüvar, O. 2003. Mineralogical and geochemical evidences of the interaction between co-eval mafic and felsic magma sources in the genesis of the A-type Murmana and Dumluca granitoids, Divriği SE Sivas, Central Turkey. International Conference The South Aegean Active Volcanic Arc: Present Knowledge and Future Perspectives. SAAVA-2003, Milos Island, Greece, Book of Abstracts, 43-44.

Boztuğ, D., Jonckheere R., Wagner, G. A., Yeğingil, Z. 2004. Slow Senonian and fast Palaeocene-Early Eaocene uplift of the granitoids in the central eastern Pontides, Turkey: apatite fission-track results. Tectonophysics 382, 213-228.

Boztuğ, D., Erçin, A.İ., Kuruçelik, M.K., Göç, D., Kömür, İ., İskenderoğlu, A. 2006. Geochemical characteristics of the composite Kaçkar batholith generated in a Neo-Tethyan convergence system, Eastern Pontides, Turkey. Journal of Asian Earth Sciences 27, 286-302.

Bullen, T.D., Clynne, M.A., 1990. Trace Element and Isotopic Constraints on Magmatic Evolution at Lassen Volcanic Center. Journal of Geophysic Research 95, 19671-19691.

Chen, W., Arculus, R.J. 1995. Geochemical and isotopic characteristics of lower crustal xenoliths, San Francisco Volcanic Field, Arizona, U.S.A. Lithos 110, 99-119.

Cheng, Y.B., Spandler, C., Mao, J.W., Rusk, B.G. 2012. Granite, gabbro and mafic microgranular enclaves in the Gejiu area, Yunnan Province, China: a case of twostage mixing of crust- and mantle-derived magmas. Contributions to Mineralogy and Petrology 164, 659-676.

Chorowicz, J., Collet, B., Bonavia, F., Mohr, P., Parrot, J.F., Tesfaye, K. 1998. The Tana basin, Ethiopia: Intra-plateau uplift, rifting and subsidence. Tectonophysics 295, 351-367.

Condie, K.C. 1993. Chemical composition and evolution of the upper continental crust: contrasting results from surface samples and shales. Chemical Geology 104, 1-37.

Çoğulu, E. 1975. Gümüşhane ve Rize Granitik Plütonlarnın Mukayeseli Petrojeolojik ve Jeokronometrik Etüdü. Doçençtlik Tezi, İTÜ. Maden Fakültesi,

İstanbul (unpublished).

Deer, W.A., Howie, R.A., Zussman, J. 1992. An introduction to the Rock Forming Minerals (second edition), London, Longman, 696 s.

DePaolo, D.J., 1981. Trace element and isotopic effects of combined wall-rocks assimilation and fractional crystallization. Earth and Planetary Science Letters 53, 189-202.

Dewey, J.F., Pitman, W., Ryan, W., Bonnin, I. 1973. Plate tectonics and the evolution of the Alpine system, Geological Society American Bulletin 84, 3137-3180.

Dilek, Y. 2006. Collision tectonics of the Eastern Mediterranean region: Causes and consequences. Geological Society of America Special Paper 409, 1-13.

Dilek, Y., Sandvol, E. 2009. Seismic structure, crustal architecture and tectonic evolution of the Anatolian-African plate boundary and the Cenozoic orogenic belts in the eastern Mediterranean region. In Murphy, J. B., Keppie, J. D., Hynes, A. J. (eds.), Ancient orogens and modern analogues, Geological Society of London. Special Publications 327, 127-160.

Dilek, Y., Imamverdiyev, N., Altunkaynak, S. 2010. Geochemistry and tectonics of Cenozoic volcanism in the Lesser Caucasus (Azerbaijan) and the peri-Arabian region: Collision-induced mantle dynamics and its magmatic fingerprint. International Geology Review 52, 4–6, 536-578.

Dokuz, A. 2011. Slab Detachment and Delamination Model for the Generation of Carboniferous High-Potassium I-type Magmatism in the Eastern Pontides, NE Turkey: The Köse Composite Pluton. Gondwana Research 19, 926-944.

Dokuz, A., Tanyolu, E. 2006. Geochemical constraints on the provenance, mineral sorting and subaerial weathering of lower Jurassic and upper Cretaceous clastic rocks from the Eastern Pontides, Yusufeli (Artvin), NE Turkey. Turkish Journal of Earth Sciences 15, 181-209.

Dokuz, A., Karslı, O., Chen, B., Uysal, İ. 2010. Sources and petrogenesis of Jurassic granitoids in the Yusufeli area, Northeastern Turkey: Implications for pre- and postcollisional lithospheric thinning of the Eastern Pontides. Tectonophysics 480, 259-279.

Donskaya, T.V., Gladkochub, D.P., Mazukabzov, A.M., Ivanov, A.V. 2013. Late Paleozoic–Mesozoic subduction-related magmatism at the southern margin of the Siberian continent and the 150 million-year history of the Mongol-Okhotsk Ocean. Journal of Asian Earth Sciences 62, 79-97.

Eby, G.N. 1992. Chemical subdivision of the A-type granitoids: petrogenetic and tectonic implications. Geology 20, 641-644.

Eklund, O., Konopelko, D., Rutanen, H., Fröjdö, S., Shebanov, A.D. 1998. 1.8 Ga Svecofennian post-collisional shoshonitic magmatism in the Fennoscandian shield. Lithos 45, 87-108.

Eyüboğlu, Y., Chung, S.L., Dudas, F.O., Santosh, M., Akaryali, E. 2011*a*. Transition from shoshonitic to adakitic magmatism in the eastern Pontides, NE Turkey: implications for slab window melting. Gondwana Research 19, 413-429.

Eyüboğlu, Y., Santosh, M., Chung, S.L. 2011*b*. Crystal fractionation of adakitic magmas in the crust-mantle transition zone: petrology, geochemistry and U-Pb zircon chronology of the Seme adakites, eastern Pontides, NE Turkey. Lithos 121, 151-166.

Eyüboğlu, Y., Santosh, M., Chung, S.L. 2011c. Petrochemistry and U-Pb zircon ages of adakitic intrusions from the Pulur Massif (Eastern Pontides, NE Turkey): Implications for slab rollback and ridge subduction associated with Cenozoic convergent tectonics in the Eastern Mediterranean. Journal of Geology 119, 394–417.

Eyüboğlu, Y., Santosh, M., Yi, K., Bektaş, O., Kwon, S. 2012. Discovery of Miocene adakitic dacite from the Eastern Pontides Belt and revised geodynamic model for the late Cenozoic Evolution of eastern Mediterranean region. Lithos 146-147, 218-232.

Eyüboğlu, Y., Santosh, M., Dudas, F.O., Akaryali, E., Chung, S.L., Akdağ, K., Bektaş, O. 2013*a*. The nature of transition from adakitic to non-adakitic magmatism in a slab-window setting: a synthesis from the eastern Pontides, NE Turkey. Geosciences Frontiers 4, 353-375.

Eyüboğlu, Y., Dudas, F.O., Santosh, M., Yi, K., Kwon, S., Akaryali, E. 2013*b*. Petrogenesis and U–Pb zircon chronology of adakitic porphyries within the Kop ultramafic masif (Eastern Pontides Orogenic Belt, NE Turkey). Gondwana Research 24, 742-766.

Eyüboğlu, Y., Dudas, F.O., Santosh, M., Zhuc, D.C., Yi, K., Chatterjee, N., Jeong, Y.J., Akaryalı, E., Liuc, Z. 2016. Cenozoic forearc gabbros from the northern zone of the Eastern Pontides Orogenic Belt, NE Turkey: Implications for slab window magmatism and convergent margin tectonics. Gondwana Research 33, 160-189.

Ferré, E.C., Caby, R., Peucat, J.J., Capdevila, R., Monié, P. 1998. Pan-African, postcollisional, ferro-potassic

granite and quartz–monzonite plutons of Eastern Nigeria. Lithos 45, 255-279.

Fitton, J.G., James, D., Leeman, W.P. 1991. Basic magmatism associated with late Cenozoic extension in the western United States: Compositional variations in space and time. Journal of Geophysical Research 96, 13693-13711.

Foley, S., Peccerillo, A. 1992. Potassic and ultrapotassic magmas and their origin. Lithos 28, 181–185.

Gagnevin, D., Daly, J.S., Poli, G. 2004. Petrographic, geochemical and isotopic constraints on magma dynamics and mixing in the Miocene Monte Capanne monzogranite (Elba Island, Italy). Lithos 78, 1-2, 157-195.

Gardien, V., Thompson, A.B., Grujic, D., Ulmer, P. 1995. Experimental Melting Of Biotite + Plagioclase + Quartz ± Muscovite Assemblages and Implications for Crustal Melting. Journal of Geophysical Research 100, 15581-15591.

Grove, T.L., Donnelly-Nolan, J.M. 1986. The Evolution of Young Silicic Lavas at Medicine Lake Volcano, California: Implications for the Origin of Compositional Gaps in Calc-Alkaline Series Lavas. Contributions to Mineralogy and Petrology 92, 281-302.

Guffanti, M., Clynne, M. A., Muffler, L.J.P. 1996. Thermal and Mass İmplications of Magmatic Evolution in the Lassen Volcanic Region, California, and Constraints on Basalt Influx to the Lower Crust. Journal of Geophysical Research 101, 3001-3013.

Güven, İ.H. 1993. Doğu Pontidler'in 1/250000 Ölçekli Kompilasyonu, Maden Tetkik ve Arama Genel Müdürlüğü, Ankara.

Hammarstrom, J.M., Zen, E. 1986. Aluminum in hornblende: An empirical igneous geobarometer. American Mineralogist 71, 1297-1313.

Hanchar, J.M., Watson, E.B. 2003. Zircon saturation thermometry. Reviews in Mineralogy and Geochemistry 53, 1, 89-112.

Harris, N. B. W., Pearce, J., Tindle, A.G. 1986. Geochemical characteristics of collision zone magmatism. Collision Tectonic. Geology Society of American Bulletin . Special Pub. No: 19:67-81.

Harrison, T.M., Watson, E.B. 1984. The behaviour of apatite during crustal anatexis: equilibrium and kinetic considerations. Geochimica et Cosmochimica Acta 48, 1467-1477.

Hastie, A.R., Kerr, A.C., Pearce, J.A., Mitchell, S.F. 2007. Classification of Altered Volcanic Island Arc Rocks using Immobile Trace Elements: Development of the Th-Co Discrimination Diagram. Journal of Petrology 48, 12, 2341-2357.

Hofmann, A.W. 1988. Chemical differentiation of the Earth: the relationship between mantle, continental crust, and oceanic crust. Earth and Planetary Science Letters 90, 297-314.

Holland, T.J.B., Blundy, J.D. 1994. Non-ideal interactions in calcic amphiboles and their bearing on amphibole-plagioclase thermometry. Contribution to Mineralogy and Petrology 116, 433-447.

Hollister, L.S., Grisson, G.C., Peters, E.K., Stowell, H.H., Sisson, V.B. 1987. Confirmation of the empirical calibration of aluminum in hornblende with pressure of solidification of calc-alkaline plutons. American Mineralogist 72, 231-239.

İlbeyli, N. 2008. Geochemical characteristics of the Şebinkarahisar granitoids in the Eastern Pontides, Northeast Turkey: petrogenesis and tectonic implications. International Geology Review 50, 563-582.

Jahn, B.M., Zhang, Z.Q. 1984. Archean granulite gneisses from eastern Hebei Province, China: rare earth geochemistry and tectonic implications. Contribution to Mineralogy and Petrology 85, 224-243.

Jiang, Y.H., Jiang, S.Y., Ling, H.F., Zhou, X.R., Rui, X.J., Yang, W.Z. 2002. Petrology and geochemistry of shoshonitic plutons from the western Kunlun orogenic belt, Xinjiang, northwestern China: implications for granitoid geneses. Lithos 63, 165-187.

Johnson, M.C., Rutherford, M.J. 1989. Experimental calibration of the aluminiun inhornblende geobarometer with application to Long Valley Caldera (California) volcanic rocks. Geology 17, 837-841.

Jung, S., Masberg, P., Mihm, D., Hoernes, S. 2009. Partial melting of diverse crustal sources constraints from Sr–Nd–O isotope compositions of quartz diorite–granodiorite–leucogranite associations (Kaoko Belt, Namibia). Lithos 111, 236-251.

Kandemir, R. 2004. Sedimentary characteristics and depositional conditions of Lower-Middle Jurassic Şenköy Formation in the around of Gümüşhane. Doktora Tezi, KTÜ, 274 s. Trabzon (unpublished).

Kandemir, R., Yılmaz, C. 2009. Lithostratigraphy, facies, and deposition environment of the lower Jurassic Ammonitico Rosso type sediments (ARTS) in the Gümüşhane area, NE Turkey: Implications for the opening of the northern branch of the Neo-Tethys

Ocean. Journal of Asian Earth Sciences 34, 586-598.

Karslı, O., Chen, B., Aydin, F., Şen, C. 2007. Geochemical and Sr-Nd-Pb isotopic compositions of the Eocene Dölek and Sarıçiçek Plutons, Eastern Turkey: implications for magma interaction in the genesis of high-K calc-alkaline granitoids in a post-collision extensional setting. Lithos 98, 67-96.

Karslı, O., Dokuz, A., Uysal, İ., Aydin, F., Bin, C., Kandemir, R., Wijbrans, R.J. 2010*a*. Relative contributions of crust and mantle to generation of Campanian high-K calc-alkaline I-type granitoids in a subdution setting, with special reference to the Harşit pluton, Eastern Turkey. Contributions to Mineralogy and Petrology 160, 467–487.

Karslı, O., Dokuz, A., Uysal, İ., Aydın, F., Kandemir, R., Wijbrans, R.J. 2010*b*. Generation of the early Cenozoic adakitic volcanism by partial melting of mafic lower crust, Eastern Turkey: implications for crustal thickening to delamination. Lithos 114, 109-120.

Karslı, O., Uysal, İ., Ketenci, M., Dokuz, A., Kandemir, R., Wijbrans, J. 2011. Adakite-like granitoid porphyries in the Eastern Turkey: potential parental melts and geodynamic implications. Lithos 127, 354-372.

Karslı, O., Caran, Ş., Dokuz, A., Çoban, H., Chen, B., Kandemir, R. 2012*a*. A-type granitoids from the Eastern Pontides, NE Turkey: Records for generation of hybrid A-type rocks in a subduction-related environment. Tectonophysics 530-531, 208-224.

Karslı, O., Dokuz, A., Uysal, İ., Ketenci, M., Chen, B., Kandemir, R. 2012*b*. Deciphering the shoshonitic monzonites with I-type characteristic, the Sisdağı pluton, NE Turkey: magmatic response to continental lithospheric thinning. Journal of Asian Earth Sciences 51, 45-62.

Karslı, O., Uysal, İ., Dilek, Y., Aydın, F., Kandemir, R. 2013. Geochemical modelling of early Eocene adakitic magmatism in the Eastern Pontides, NE Anatolia: continental crust or subducted oceanic slab origin?. International Geology Review 55, 16, 2083-2095.

Kaygusuz, A., Aydınçakır, E. 2009. Mineralogy, Whole-Rock and Sr-Nd Isotope Geochemistry of Mafic Microgranular Enclaves in Cretaceous Dağbaşı Granitoids, Eastern Pontides, NE Turkey: Evidence of Magma Mixing, Mingling, and Chemical Equilibration. Chemie der Erde/ Geochemistry 69, 247-277.

Kaygusuz, A., Aydınçakır, E. 2011. Petrogenesis of a Late Cretaceous composite pluton from the eastern Pontides: the Dağbaşı pluton, NE Turkey. Neues Jahrbuch Für Mineralogie 188, 3, 211-233.

Kaygusuz, A., Şen, C. 2011. Calc-alkaline I-type plutons in the eastern Pontides, NE Turkey: U-Pb zircon ages, geochemical and Sr-Nd isotopic compositions. Chemie der Erde Geochemistry 71, 59-75.

Kaygusuz, A., Öztürk,M. 2015. Geochronology, geochemistry, and petrogenesis of the Eocene Bayburt intrusions, Eastern Pontide, NE Turkey: implications for lithospheric mantle and lower crustal sources in the high-K calc-alkaline magmatism. Journal of Asian Earth Sciences 108, 97-116.

Kaygusuz, A., Siebel, W., Şen, C., Satır, M. 2008. Petrochemistry and petrology of I-type granitoids in an arc setting: the composite Torul pluton, Eastern Pontides, NE Turkey. International Journal of Earth Sciences 97, 739-764.

Kaygusuz, A., Chen, B., Aslan, Z., Siebel, W., Şen, C. 2009. U-Pb zircon SHRIMP ages, geochemical and Sr-Nd isotopic compositions of the Early Cretaceous I-type Sarıosman pluton, Eastern Pontides, NE Turkey. Turkish Journal of Earth Sciences 18, 549-581.

Kaygusuz, A., Siebel, W., İlbeyli, N., Arslan, M., Satır, M., Şen, C. 2010. Insight into magma genesis at convergent plate margins – a case study from the eastern Pontides (NE Turkey). Neues Jahrbuch Für Mineralogie 187, 3, 265-287.

Kaygusuz, A., Arslan, M., Siebel, W., Şen, C. 2011. Geochemical and Sr-Nd isotopic characteristics of post-collisional calc-alkaline volcanics in the eastern Pontides (NE Turkey). Turkish Journal of Earth Sciences 20, 137-159.

Kaygusuz, A., Arslan, M., Siebel, W., Sipahi, F., İlbeyli, N. 2012. Geochronological evidence and tectonic significance of Carboniferous magmatism in the southwest Trabzon area, eastern Pontides. Turkey, International Geology Review 54, 15, 1776-1800.

Kaygusuz, A,. Sipahi, F,. İlbeyli, N,. Arslan, M,. Chen, B,. Aydınçakır, E. 2013. Petrogenesis of the Late Cretaceous Turnagöl intrusion in the eastern Pontides: Implications for magma genesis in the arc setting. Geoscience Frontiers 4, 423-438.

Kaygusuz, A., Arslan, M., Wolfgang, S., Sipahi, F., İlbeyli, N., Temizel, İ. 2014. LA-ICP MS zircon dating, whole-rock and Sr-Nd-Pb-O isotope geochemistry of the Camiboğazı pluton, Eastern Pontides, NE Turkey: implications for lithospheric mantle

and lower crustal sources in arc-related I-type magmatism. Lithos 192-195, 271-290.

Kaygusuz, A., Arslan, M., Sipahi, F., Temizel, İ. 2016. U–Pb zircon chronology and petrogenesis of Carboniferous plutons in the northern part of the Eastern Pontides, NE Turkey: Constraints for Paleozoic magmatism and geodynamic evolution. Gondwana Research 39, 327-346.

Ketin, İ. 1966. Anadolu'nun Tektonik Birlikleri, Maden Tetkik ve Arama Genel Müdürlüğü Dergisi 66, 20-34.

Köksal, S., Toksoy-Köksal, F., Göncüoğlu, M.C., Möller, A., Gerdes, A., Frei, D. 2013. Crustal source of the Late Cretaceous Satansarı monzonite stock (central Anatolia–Turkey) and its significance for the Alpine geodynamic evolution. Journal of Geodynamics 65, 82-93.

Lameyre, J., Bonin, B., 1991. Granites in the main plutonic series. In:Didier, J., Barbarin, B. (Eds.), Enclaves and GranitePetrology Developments in Petrology, vol. 13. Elsevier, Amsterdam.

Lan, T.G., Fan, H.R., Hu, F.F., Tomkins, A.G., Yang, K.F., Liu, Y.S. 2011. Multiple crust-mantle interactions for the destruction of the North China Craton: geochemical and Sr–Nd–Pb–Hf isotopic evidence from the Longbaoshan alkaline complex. Lithos 122, 87-106.

Lan, T.G., Fan, H.R., Santosh, M., Hu, F.F., Yang, K.F., Yang, Y.H., Liu, Y.S. 2012. Early Jurassic high-K calc-alkaline and shoshonitic rocks from the Tongshi intrusive complex, eastern North China Craton: implication for crust–mantle interaction and post-collisional magmatism. Lithos 140-141, 183-199.

Lan, T.G., Fan, H.R., Santosh, M., Hu, F.F., Yang, K.F., Yang, Y.H., Yang, Y.H., Liu, Y.S. 2013. Crust–mantle interaction beneath the Luxi Block, eastern North China Craton: evidence from coexisting mantle- and crust-derived enclaves in a quartz monzonite pluton. Lithos 177, 1-6.

Le Maitre, R.W., Streckeisen, A., Zanettin, B., Le Bas, M.J., Bonin, B., Bateman, P., Bellieni, G., Dudek, A., Efremova, S., Keller, J., Lamere, J., Sabine, P.A., Schmid, R., Sorensen, H., Woolley, A.R. 2002. Igneous Rocks: A Classification and Glossary of Terms, Recommendations of the International Union of Geological Sciences, Subcommission of the Systematics of Igneous Rocks. Cambridge University Press., 236p.

Le Roex, A.P. 1987. Source regions of mid-ocean ridge basalts; evidence for enrichment processes. In: Menzies, A.M., Hawkesworth, C.J. (Eds.), Mantle Metasomatism, Academic Press, London, 389-422.

Leake, E.B., Wooley, A.R., Arps, C.E.S., Birch, W.D., Gilbert, M.C., Grice, J.D., Hawthorne, F.C., Kato, A., Kisch, H.J., Krivovichev, V.G., Linthout, K., Laird, J., Mandarino, J., Maresch, W.V., Nickhel, E.H., Rock, N.M.S., Schumacher, J.C., Smith, D.C., Stephenson, N.C.N., Ungaretti, L., Whittaker, E.J.W., Youzhi, G. 1997. Nomenclature of amphiboles report of the subcommittee on amphiboles of the International Mineralogical Association Commission on New Minerals and Mineral Names. European Journal of Mineralogy 9, 623-651.

Li, X.H., Zhou, H.W., Liu, Y., Le, C.Y., Sun, M., Chen, Z.H. 2000. Shoshonitic intrusive suite in SE Guangxi: petrology and geochemistry. Chinese Sciences Bulletin 45, 653-659.

Li, X.H., Li, W.X., Li, Z.X., Lo, C.H., Wang, J., Ye, M.F., Yang, Y.H. 2009. Amalgamation between the Yangtze and Cathaysia Blocks in South China: constraints from SHRIMP U–Pb zircon ages, geochemistry and Nd–Hf isotopes of the Shuangxiwu volcanic rocks. Precambrian Research 174, 117-128.

Liu, H., Qiu, J.S., Luo, Q.H., Xu, X.S., Ling, W.L., Wang, D.Z. 2002. Petrogenesis of the Mesozoic potash-rich volcanic rocks in the Luzong basin, Anhui Province. geochemical constrains. Geochemica 31, 129-140.

Liu, L., Qiu, J.S., Li, Z. 2013. Origin of mafic microgranular enclaves (MMEs) and their host quartz monzonites from the Muchen pluton in Zhejiang Province, Southeast China: Implications for magma mixing and crust–mantle interaction. Lithos 160-161, 145-163.

Liu, L., Qiu, J.S., Zhao, J.L., Yang, Z.L. 2014. Geochronological, geochemical, and Sr–Nd–Hf isotopic characteristics of Cretaceous monzonitic plutons in western Zhejiang Province, Southeast China: new insights into the petrogenesis of intermediate rocks. Lithos 196-197, 242-260.

Liu, S., Hu, R.Z., Gao, S., Feng, C., Qi, Y.Q., Wang, T., Feng, G.Y., Coulson, I.M. 2008. U-Pb zircon age, geochemical and Sr–Nd–Pb–Hf isotopic constraints on age and origin of alkaline intrusions and associated mafic dikes from Sulu orogenic belt, Eastern China. Lithos 106, 365-379.

López-Moro, F.J., López-Plaza, M. 2004. Monzonitic series from the Variscan Tormes Dome (Central Iberian Zone): petrogenetic evolution from monzogabro to granite magmas. Lithos 72, 19-44.

Luhr, J.F., Carmichael, I.S.E., Varekamp, J.C. 1984. The 1982 eruptions of El Chicón Volcano, Chiapas, Mexico: Mineralogy and petrology of the anhydrite-bearing pumices. Journal of Vocanology and Geothermal Research 23, 69-108.

Maniar, P.D., Piccoli, P.M. 1989. Tectonic discrimination of granitoids. Geological Society of America Bulletin 101, 635-643.

Mao, J.R., Ye, H.M., Liu, K., Li, Z.L., Takahashi, Y., Zhao, X.L., Kee, W.S. 2013. The Indosinian collision–extension event between the South China Block and the Palaeo-Pacific plate: evidence from Indosinian alkaline granitic rocks in Dashuang, eastern Zhejiang, South China, Lithos 172-173, 81-97.

McKenzie, D., O'Nions, R.K. 1991. Partial melt distributions from inversion of rare earth element concentrations. Journal of Petrology 32, 1021-1091.

Middlemost, E.A.K. 1994. Naming materials in the magma/igneous rock system. Earth Science Reviews 37, 215-224.

Miller, C.F., McDowell, S.M., Mapes, R.W. 2003. Hot and cold granites?: Implications of zircon saturation temperatures and preservation of inheritance. Geology 31, 529-532.

Miyashiro, A. 1978. Nature of alkalic volcanic rock series. Contributions to Mineralogy and Petrology 66, 91-104.

Morimoto, M., Fabries, J., Ferguson, A.K., Ginzburg, I.V., Ross, M., Seifert, F.A., Zussman, J., Aoki, K., Gottardi, G. 1988. Nomenclature of pyroxenes. Mineralogical Magazine 52, 535-550.

MTA, 2002. 1/500.000 ölçekli Türkiye Jeoloji Haritası, Samsun ve Trabzon Paftaları, Maden Tetkik ve Arama Genel Müdürlüğü, Ankara.

MTA, 2011. 1/100.000 ölçekli Türkiye Jeoloji Haritası, Giresun G39 Paftası, Maden Tetkik ve Arama Genel Müdürlüğü, Ankara.

Neves, S.P., Mariano, G. 1997. High-K calc-Alkalic plutons in Northeast Brazil: origin of the biotite diorite/quartz monzonite to granite association and implications for the evolution of the Borborema Province. International Geological Review 39, 7, 621-638.

Okay, A.İ., Leven, E.J. 1996. Stratigraphy and paleontology of the upper Paleozoic sequences in the Pulur (Bayburt) region, Eastern Pontides. Turkish Journal of Earth Sciences 5, 145-155.

Okay, A.İ., Şahintürk, Ö. 1997. Geology of the Eastern Pontides. In: Robinson, A.G. (ed.), Regional and Petroleum Geology of the Black Sea and Surrounding Region. American Association of Petroleum Geologists Memoir 68, 291-311.

Okay, A.İ., Tüysüz, O. 1999. Tethyan sutures of northern Turkey", In: Durand, B., Jolivet, L., Hovarth, F., Séranne, M. (eds), The Mediterranean Basins: Tertiary Extension within the Alpine Orogen Tethyan Sutures of Northern Turkey. Geological Society London. Special Publications 156, 475-515.

Okay, A.İ., Sunal, G., Sherlock, S., Altıner, D., Tüysüz, O., Kylander-Clark, A.R.C, Aygül, M. 2013. Early Cretaceous sedimentation and orogeny on the active margin of Eurasia: Southern Central Pontides, Turkey. Tectonics 32, 1247-1271.

Patiño Douce, A.E. 1997. Generation of Metaluminous A-type Granites by Low-Pressure Melting of Calc-Alkaline Granitoids. Geology 25, 743-746.

Patiño Douce, A.E. 1999. What do Experiments Tell Us about the Relative Contributions of Crust and Mantle to the Origin of Granitic Magmas?. In: Understanding Granites: Intergrating New and Classical Techniques, (eds.): Castro, A., Fernandez, C., Vigneresse, J.L., Geological Society of London. Special Publication 168, 55-75.

Patiño Douce, A.E., Johnston, A.D. 1991. Phase Equilibria and Melt Productivity in the Pelitic System: Implications for the Origin of Peraluminous Granitoids and Aluminous Granulites. Contribution to Mineralogy and Petrology 107, 202-218.

Patiño Douce, A.E., Beard, J.S. 1996. Effects of P, f (O_2) and Mg/Fe Ratio on Dehydration Melting of Model Metagreywackes. Journal of Petrology 37, 999-1024.

Patiño Douce, A.E., McCarthy, T.C. 1998. Melting of crustal rocks during continental collision and subduction. In: When continents collide: Geodynamics and Geochemistry of Ultra-high Pressure Rocks, edited by Hacker, B. R., Liou, J. G., Kluwer Academic Publishers, Dordrecht, pp.27-55.

Pearce, J.A. 1983. The Role of Sub-Continental Lithosphere in Magma Genesis at Destructive Plate Margins. In: Continental Basalts and Mantle Xenoliths, (eds): Hawkesworth, C.J., Norry, M.J., Shiva Publishing, Cheshire, pp.230-249.

Pearce, J.A, Haris, N.B.W., Tindle, A.G. 1984. Trace element discrimination diagrams for the tectonic interpretation of granitic rocks. Journal of Petrology 25, 956-983.

Pearce, J.A., Bender, J.F., De Long, S.E., Kidd, W.S.F., Low, P.J., Güner, Y., Şaroğlu, F., Yılmaz, Y., Moorbath, S., Mitchell, J.J. 1990. Genesis of collision volcanism in eastern Anatolia Turkey. Journal of Volcanology and Geothermal Research 44, 189-229.

Pelin, S. 1977. Alucra (Giresun) Güneydoğu Yöresinin Petrol Olanakları Bakımından Jeolojik İncelenmesi. K.T.Ü. Yayınları, 87, 103s,Trabzon (unpublished)

Powell, R., 1984. Inversion of the assimilation and fractional crystallization (AFC) equations: characterization of contaminants from isotope and trace element relationships in volcanic suites. Journal of the Geological Society of London, 141, 447-452.

Putirka, K.D. 1999. Clinopyroxene+liquid equilibrium to 100 kbar and 2450 K. Contributions to Mineralogy and Petrology 135, 151-163.

Putirka, K.D. 2003. New igneous thermobarometers based on plagioclase + liquid equilibria. Eos. Trans. AGU, Fall Meeting. Suppl., Abstract 84, 46, F1583.

Putirka, K.D. 2005. Igneous thermometers and barometers based on plagioclase + liquid equilibria: Tests of some existing models and new calibrations. American Mineralogist 90, 336-346.

Putirka, K.D. 2008. Thermometers and barometers for volcanic systems. In Putirka, K.D., Tepley, F.E., Reviews in Mineralogy and Geochemistry 69, 61-120.

Putirka, K.D., Johnson, M., Kinzler, R., Walker, D. 1996. Thermobarometry of mafic igneous rocks based on clinopyroxene-liquid equilibria, 0-30 kbar. Contributions to Mineralogy and Petrology 123, 92-108.

Putirka, K.D., Ryerson, F.J., Mikaelian, H. 2003. New igneous thermobarometers for mafic and evolved lava compositions, based on clinopyroxene + liquid equilibria. American Mineralogist 88, 1542-1554.

Rapela, C.W., Pankhurst, R.J., 1996. Monzonite suites: the innermost Cordilleran plutonism of Patagonia. Transactions of the Royal Society of Edinburgh Earth Sciences 87, 193-203.

Rapp, R.P. 1995. Amphibole-out Phase Boundary in Partially Melted Metabasalt, its Control over Liquid Fraction and Composition, and Source Permeability. Journal of Geophysical Research 100, 15601-15610.

Rapp, R.P., Watson, E.B. 1995. Dehydration Melting of Metabasalt at 8–32 kbar: Implications for Continental Growth and Crust-Mantle Recycling. Journal of Petrology 36, 891-931.

Rapp, R.P., Watson, E.B. Miller, C.F. 1991. Partial Melting of Amphibolite Eclogite and the Origin of Archean Trondhjemites and Tonalites. Precambrian Research 51, 1-25.

Ridolfi F., Renzulli, A. 2012. Calcic amphiboles in calc-alkaline and alkaline magmas: thermobarometric and chemometric empirical equations valid up to 1130°C and 2.2 Gpa. Contributions to Mineralogy and Petrology 163, 877-895.

Ridolfi, F., Puerini, M., Renzulli, A., Menna, M., Toulkeridis, T. 2008. The magmatic feeding system of El Reventador volcano (Sub-Andean zone, Ecuador) constrained by texture, mineralogy and thermobarometry of the 2002 erupted products. Journal of Volcanology and Geothermal Research 176, 94-106.

Ridolfi, F., Renzulli, A., Puerini, M. 2010. Stability and chemical equilibrium of amphibole in calc-alkaline magmas: An overview, new thermobarometric formulations and application to subduction-related volcanos. Contributions to Mineralogy and Petrology 160, 45-66.

Roberts, M.P., Clemens, J.D. 1993. Origin of High-Potassium, Calcalkaline, I-Type Granitoids. Geology 21, 825-828.

Robinson, A.G., Banks, C.J., Rutherford, M.M., Hırst, J.P.P. 1995. Stratigraphic and structural development of the eastern Pontides, Turkey. Journal of the Geological Society, London 152, 861-872.

Rolland, Y., Perinçek, D., Kaymakcı, N., Sosson, M., Barrier, E., Avagyan, A. 2012. Evidence for ~80–75 Ma subduction jump during Anatolia-Tauride-Armenian block accretion and ~48 Ma Arabia-Eurasia collision in Lesser Caucasus-East Anatolia. Journal of Geodynamics 56-57, 76-85.

Rudnick, R.L., Gao, S. 2003. The composition of the continental crust. In: Rudnick, R.L. (Ed.), The Crust. In: Holland, H.D., Turekian, K.K. (Eds.), Treatise on Geochemistry 3. Elsevier-Pergammon, Oxford (64 pp).

Ryerson, F.J., Watson, E.B. 1987. Rutile saturation in magmas: implications for Ti-Nb-Ta depletion in island-arc basalts. Earth and Planetary Science Letters, 86, 225-239.

Schmidberger, S.S., Hegner, E. 1999. Geochemistry and isotope ststematics of calc-alkaline volcanic rocks from the Saar-Nahe basin (SW Germany)-implications for Late Variscan orogenic development. Contributions to Mineralogy and

Petrology 135, 373-385.

Schmidt, M.W. 1992. Amphibole composition in tonalite as a function of pressure: An experimental calibration of the Al-in-hornblende barometer. Contributions to Mineralogy and Petrology 110, 304-310.

Singh, J., Johannes, W. 1996. Dehydration Melting of Tonalites: Part II. Composition of Melts and Solids. Contributions to Mineralogy and Petrology 125, 26-44.

Skjerlie, K.P., Johnston, A.D.1996. Vapour-absent Melting from 10 to 20 kbar of Crustal Rocks that Contain Multiple Hydrous Phases: Implications for Anatexis in the Deep to very Deep Continental Crust and Active Continental Margins. Journal of Petrology 37, 661-691.

Smith, E.I., Sanchez, A., Walker, J.D., Wang, K.F. 1999. Geochemistry of mafic magmas in the hurricane volcanic field, Utah: implications for small- and large-scale chemical variability of the lithospheric mantle. Journal of Geology 107, 433-448.

Soesoo, A. 2000. Fractional crystallization of mantle-derived melts as a mechanism for some I-type granite petrogenesis: an example from Lachlan Fold Belt, Australia. Journal of Geological Society, London 157, 135-149.

Stevens, G., Clemens, J.D., Droop, G.T.R. 1997. Melt Production during Granulite Facies Anatexis: Experimental Data from 'Primitive' Metasedimentary Protoliths. Contributions to Mineralogy and Petrology 128, 352-370.

Streickeisen, A. 1976. To Each Plutonic Rock its Proper Name. Earth Science Review 12, 1–33.

Sun, S., McDonough, W.F. 1989. Chemical and isotopic systematics of oceanic basalt: Implications for mantle composition and processes. In: A.D. Saunders, M.J. Norry, (eds.), Magmatism in the Ocean Basins, Geological Society of London. Special Publication 42, 313-345.

Sun, C.G., Zhao, Z.D., Mo, X.X., Zhu, D.C., Dong, G.C., Zhou, S., Chen, H.H., Xie, L.W., Yang, Y.H., Sun, J.F., Yu, F. 2008. Enriched mantle source and petrogenesis of Sailipu ultrapotassic rocks in southwestern Tibet Plateau: constraints from zircon U–Pb geochronology and Hf isotopic compositions. Acta Petrologica Sinica 24, 249-264.

Şen, C. 2007. Jurassic volcanism in the Eastern Pontides: Is it rift related or subduction related?. Turkish Journal of Earth Sciences 16, 523-539.

Şen, C., Arslan, M., Van, A. 1998. Geochemical and petrological characteristics of the Eastern Pontide Eocene (?) alkaline volcanic province, NE Turkey. Turkish Journal of Earth Sciences 7, 231-239.

Şengör, A.M.C., Yılmaz Y. 1981. Tethyan Evolution of Turkey: A Plate Tectonic Approach. Tectonophysics 75, 181-241.

Taylor, S.R., McLennan, S.M. 1985. The Continental Crust, Its Composition and Evolution. Blackwell, Oxford, pp. 312.

Temizel, İ. 2014. Petrochemical evidence of magma mingling and mixing in the Tertiary monzogabbroic stocks around the Bafra (Samsun) area in Turkey: implications of coeval mafic and felsic magma interactions. Mineralogy and Petrology 108, 353-370.

Temizel, İ., Arslan, M. 2008. Petrology and geochemistry of Tertiary volcanic rocks from the İkizce (Ordu) area, NE Turkey: Implications for the evolution of the eastern Pontide paleo-magmatic arc. Journal of Asian Earth Sciences 31, 439-463.

Temizel, İ., Arslan, M. 2009. Mineral chemistry and petrochemistry of post-collisional Tertiary mafic to felsic cogenetic volcanics in the Ulubey (Ordu) area, eastern Pontides, NE Turkey. Turkish Journal of Earth Sciences 18, 29-53.

Temizel, İ., Arslan, M., Ruffet, G., Peucat, J.J. 2012*a*. Petrochemistry, geochronology and Sr-Nd isotopic systematics of the Tertiary collisional and post-collisional volcanic rocks from the Ulubey (Ordu) area, eastern Pontide, NE Turkey: implications for extension-related origin and mantle source characteristics. Lithos 128, 126-147.

Temizel, İ., Arslan, M., Abdioğlu, E., Yücel, C. 2012*b*. Bafra (Samsun) Yöresi Tersiyer Volkanitlerinin Petrografisi, Jeokimyası, Petrolojisi ve Jeodinamik Gelişimi. Karadeniz Teknik Üniversitesi BAP Projesi No: 1079, Trabzon.

Temizel, İ, Arslan, M., Abdioğlu, E., Yücel, C. 2014. Mineral chemistry and thermobarometry of the Eocene monzogabbroic stocks from the Bafra (Samsun) area in Turkey: implications for disequilibrium crystallization and emplacement condition. International Geology Review 56, 10, 1226-1245.

Temizel, İ., Arslan, M., Yücel, C., Abdioğlu, E., Ruffet, G. 2016. Geochronology and geochemistry of Eocene-aged volcanic rocks around the Bafra (Samsun, N Turkey) area: Constraints for the interaction of lithospheric mantle and crustal melts. Lithos 258-259, 92-114.

Thirlwall, M.F., Smith, T.E., Graham, A.M., Theodorou, N.,

Hollings, P., Davidson, J.P. Arculus, R.J. 1994. High field strength element anomalies in arc lavas; source or process?. Journal of Petrology 35, 3, 819-838.

Tischendorf, G., Gottesmann, B., Förster, H.J., Trumbull, R.B. 1997. On Li-bearing micas: Estimating Li from electron microprobe analyses and an improved diagram for graphical representation. Mineralogical Magazine 61, 809-834.

Topuz, G. 2002. Retrograde P–T path of anatectic migmatites from the Pulur Massif, Eastern Pontides, NE Turkey: petrological and microtextural constraints. 1st International Symposium of the Faculty of Mines (İTÜ) on Earth Sciences and Engineering Abstracts, Istanbul, Turkey, 110 p.

Topuz, G., Alther, R., Schwarz, W.H., Siebel, W., Satır, M., Dokuz, A. 2005. Post-Collisional Plutonism with Adakite-like Signatures: the Eocene Saraycık Granodiorite (Eastern Pontides, Turkey). Contributions to Mineralogy and Petrology 150, 441-455.

Topuz, G., Altherr, R., Schwarz, W.H., Dokuz, A., Meyer, H P. 2007. Variscan amphibolite-facies rocks from the Kurtoğlu metamorphic complex: Gümüşhane area, Eastern Pontides, Turkey. International Journal of Earth Sciences 96, 861-873.

Topuz, G., Altherr, R., Siebel, W., Schwarz, W.H., Zack, T., Hasözbek, A., Barth, M., Satır, M., Şen, C. 2010. Carboniferous High-Potassium I-Type Granitoid Magmatism in the Eastern Pontides: The Gümüşhane Pluton (NE Turkey). Lithos 116, 92-110.

Topuz, G., Okay, A.I., Altherr, R., Schwarz, W.H., Siebel, W. Zack, T., Satır, M., Şen, C. 2011. Post-collisional adakite-like magmatism in the Ağvanis Massif and implications for the evolution of the Eocene magmatism in the Eastern Pontides (NE Turkey). Lithos 125, 131-150.

Topuz, G., Çelik, Ö.F., Şengör, A.M.C., Altıntaş, İ. E., Zack, T., Rolland, Y., Barth, M. 2013. Jurassic Ophiolite Formation and emplacement as backstop to a subduction-accretion complex in Northeast Turkey, The Refahiye Ophiolite, and relation to the Balkan Ophiolites. American Journal of Science 313, 1054-1087.

Tulloch, A.J., Challis, G.A., 2000. Emplacement depths of Paleozoic–Mesozoic plutons from western New Zealand estimated by hornblende-Al geobarometry. New Zealand Journal of Geology and Geophysics 43, 555-567.

Turner, S., Arnaud, N., Liu, J., Rogers, N., Hawkesworth, C., Harris, N., Kelley, S., Van Calsteren, P., Deng, W. 1996. Post-collision shoshonitic volcanism on the Tibetan Plateau: implications for convective thinning of the lithosphere and the source of ocean island basalts. Journal of Petrology 37, 45–71.

Uchida, E., Endo, S., Makino, M. 2007. Relationship between solidification depth of granitic rocks and formation of hydrothermal ore deposits. Resource Geology 57, 47-56.

Ustaömer, T., Robertson, A.H.F. 1995. Palaeo-Tethyan tectonic evolution of the north Tethyan margin in the Central Pontides, N. Turkey. In: Geology of the Black Sea region (eds). Erler, A., Ercan, T., Bingöl, E., Örçen, S., MTA/JMO, 24-32.

Ustaömer, T., Robertson, A.H.F. 2010. Late Palaeozoic-Early Cenozoic tectonic development of the Eastern Pontides (Artvin area), Turkey: stages of closure of Tethys along the southern margin of Eurasia. In Stephonson, R.A., Kaymakcı, N., Sasson, M., Starostenko, V., Bergerat, F. (eds). Sedimentary Basin Tectonics from the Black Sea and Caucasus to the Arabian Platform. Geological Society, London. Special Publications 340, 281-327.

Ustaömer, T., Robertson, A.H.F., Ustaömer, P.A., Gerdes, A., Peytcheva, I. 2013. Constraints on Variscan and Cimmerian magmatism and metamorphism in the Pontides (Yusufeli–Artvin area), NE Turkey from U–Pb dating and granite geochemistry. in Robertson, A.H.F., Parlak, O., Ünlügenç, U.C. (eds). Geological Development of Anatolia and the Easternmost Mediterranean Region. Geological Society, London. Special Publications 372, 49-74.

Vielzeuf, D., Holloway, J.R. 1988. Experimental Determinations of the Fluid-absent Melting Reactions in the Pelitic System. Contributions to Mineralogy and Petrology 98, 257-276.

Wang, D., Ren, Q., Qui, J., Chen, K., Xu, Z., Zen, J. 1996. Characteristics of volcanic rocks in the shoshonite province, eastern China, and their metallogenesis. Acta Geologica Sinica 70, 23-34.

Wang, W., Liu, S.W., Bai, X., Li, Q. G., Yang, P.T., Zhao, Y. 2013. Geochemistry and zircon U–Pb–Hf isotopes of the late Paleoproterozoic Jianping diorite–monzonite–syenite suite of the North China Craton: implications for petrogenesis and geodynamic setting. Lithos 162-163, 175-194.

Watson, E.B., Harrison, T.M. 1983. Zircon saturation revisited: temperature and composition effects in a variety of crustal magma types. Earth and Planetary Science Letters 64, 295-304.

Weaver, B.L., Wood, D.A., Tarney, J., Joron, J. 1987. Geochemistry of Ocean Island Basalt from the South Atlantic: Ascension, Bouvet, St. Helena, Gough and Tristan da Cunda", In: Fitton, J.G. and Upton, B.G.J., Eds., Alkaline Igneous Rocks, The Geological Society London, Special Publication 30, 1, 253-267.

Wones, D.R. 1989. Significance of the assemblage titanite+magnetite+quartz in granitic rocks. American Mineralogist 74, 744-749.

Xu, Y.G., Huang, X.L., Ma, J.L., Wang, Y.B., Iizuka, Y., Xu, J.F., Wang, Q., Wu, X.Y. 2004. Crust–mantle interaction during the tectono-thermal reactivation of the North China Craton: constraints from SHRIMP zircon U–Pb chronology and geochemistry of Mesozoic plutons from western Shandong. Contribution to Mineralogy and Petrology 147, 750-767.

Yang, J.H., Wu, F.Y., Wilde, S.A., Xie, L.W., Yang, Y.H., Liu, X.M. 2007. Trace magma mixing in granite genesis: in-situ U–Pb dating and Hf-isotope analysis of zircons. Contribution to Mineralogy and Petrology 153, 177-190.

Yang, S.Y., Jiang, S.Y., Jiang, Y.H., Zhao, K.D., Fan, H.H. 2011. Geochemical, zircon U–Pb dating and Sr–Nd–Hf isotopic constraints on the age and petrogenesis of an Early Cretaceous volcanic-intrusive complex at Xiangshan, Southeast China. Mineralogy and Petrology 101, 21-48.

Yılmaz, Y. 1972. Petrology and structure of the Gümüşhane granite and surrounding rocks. NE Anatolia. PhD Thesis, Univ. of London.

Yılmaz, S., Boztuğ, D. 1996. Space and time relations of three plutonic phases in the Eastern Pontides, Turkey. International Geology Review 38, 10, 935-956.

Yılmaz, Y., Tüysüz, O., Yiğitbaş, E., Genç, Ş.C., Şengör, A.M.C. 1997. Geology and tectonics of the Pontides. in Robinson, A.G. (eds.), Regional and Petroleum Geology of the Black Sea and Surrounding Region. American Association of Petroleum Geologists Memoir 68, 183-226.

Yücel, C. 2013. Trabzon-Giresun arasındaki Tersiyer volkanitlerinin petrografisi, ^{40}Ar-^{39}Ar jeokronolojisi, petrokimyası, Sr-Nd-Pb izotop jeokimyası ve petrolojisi. Doktora Tezi, KTÜ Fen Bilimleri Enstitüsü, 406s, Trabzon (unpublished).

Yücel, C., Arslan, M., Temizel, İ., Abdioğlu, E., Ruffet, G. 2012. Trabzon- Giresun Arasındaki Tersiyer Alkalen Volkanitlerinin Tüm-Kayaç Petrokimyası ve ^{40}Ar-^{39}Ar Jeokronolojisi, KD Türkiye. 65. Türkiye Jeoloji Kurultayı Bildiri Özleri Kitabı 354-355.

Yücel, C., Arslan, M., Temizel, İ., Abdioğlu, E. 2014. Volcanic facies and mineral chemistry of Tertiary volcanics in the northern part of the Eastern Pontides, northeast Turkey: Implications for pre-eruptive crystallization conditions and magma chamber processes. Mineralogy and Petrology 108, 439-467.

Yücel, C., Arslan, M., Temizel, İ., Abdioğlu, E., Ruffet, G. 2017. Evolution of K-rich magmas derived from a net veined lithospheric mantle in an ongoing extensional setting: Geochronology and geochemistry of Eocene and Miocene volcanic rocks from Eastern Pontides (Turkey). Gondwana Research 45, 65-86.

Bull. Min. Res. Exp. (2018) 157: 153-164

Bulletin of the Mineral Research and Exploration

http://bulletin.mta.gov.tr

Geochemical characteristics of Gabbroic rocks in Zyarat in North East of Iran

Ghassem AZIZZADEH[a], Mostafa RAGHIMI[b], Seyed Jamal SHEIKHZAKARIAEE[c*] and Aziz RAHIMI CHAKDEL[d]

[a]*Department of Geology, Science and Research Branch, Islamic Azad University, Tehran*
[b]*Department of Geology, Science and Research Branch, Islamic Azad University, Tehran*
[c]*Department of Geology, Science and Research Branch, Islamic Azad University, Tehran*
[d]*Department of Geology, Science and Research Branch, Islamic Azad University, Tehran.*

Research Article

Keywords:
Gabbro, alkaline, geochemistry, Zyarat, OIB.

ABSTRACT

The mafic rocks outcrops exposed in the South of Gorgan, northeastern of Iran. These gabbroic rocks are intruded into the Middle–Upper Paleozoic sedimentary rocks and Gorgan schist units representing a part of the north Gondwana province. Petrography studies of these rocks show medium to coarse grained sizes and the texture varies from ophitic to intergranular under polarized microscope. The mineralogical composition of mafic dykes is dominated by large crystals of clinopyroxene + orthopyroxene + plagioclase and hornblende. These rocks can be classified as gabbroic rock. Geochemical studies show that these rocks have low to medium K_2O contents. The trace element data shows low La/Nb ratios and LREE enrichment (La/Yb 10–21.4). The high LREE/HREE ratios and low Y content corresponding high Ti/Y ratios of the gabbros suggest that they could be derived from melt fractions of a garnet stable source. Considering that the REE plot and tectonic diagrams of the region's gabbro are similar to that of OIB (Ocean island basalt), the former's origin is the same as that of OIB magmas.

Received Date: 13.03.2017
Accepted Date: 21.12.2017

1. Introduction

Based on geological divisions, the studied area is located in the eastern Alborz zone (Gansser, 1951) (Figure 1), which was the northern margin of the Gondwana during Palaeozoic (Stöcklin, 1974; Salehi Rad, 1979; Berberian and King, 1981; Davoudzadeh et al., 1986; Davoudzadeh and Weber-Diefenbach, 1987; Şengör, 1990; Alavi, 1991, 1996; Stampfli and Borel, 2002; Allen et al., 2003; Horton et al., 2008; Sinha, 2012, 2013).

Mid Paleozoic mafic intrusions, sills, dykes, volcanic tuffs and lava flows are widespread in Iran (Jenny, 1977*a*; Delaloye et al., 1981; Alavi, 1996; Wendt et al., 2005). The most prominent volcanic activity is expressed by up to 600 m– thick andesitic lavas and tuffs in the Soltan Maidan Formation in the eastern Alborz, which are ascribed to the breakup of the northern margin of Gondwana (Jenny, 1977*b*; Alavi, 1996). The Soltan Maidan volcanics are unconformably overlain by conglomerate and sandstones of Lower Devonian age (Wendt et al., 2005). However, in some places Lower to Middle Ordovician age deposits (Lashkarak Formation) underlie these volcanic rocks. Thus, the Soltan Maidan volcanic rocks are generally considered as Silurian in age (e.g., Sharabi, 1990; Zamani Pedram and Hossieni, 2003; Rahimi Chakdel, 2007; Raghimi, 2010).

Due to the difficult condition of studies and loss of outcrop, there is no detailed petrographic study on gabbroic rocks so the purpose of the present research is to carry out a petrological evaluation of these rocks by petrographic and geochemical studies. Petrogenetic studies can provide important information for understanding the mantle source of the magmas and

* *Corresponding author: Seyed Jamal SHEIKHZAKARIAEE, j.sheikhzakaria@gmail.com*
htpp://dx.doi.org/ 10.19111/bulletinofmre.413716

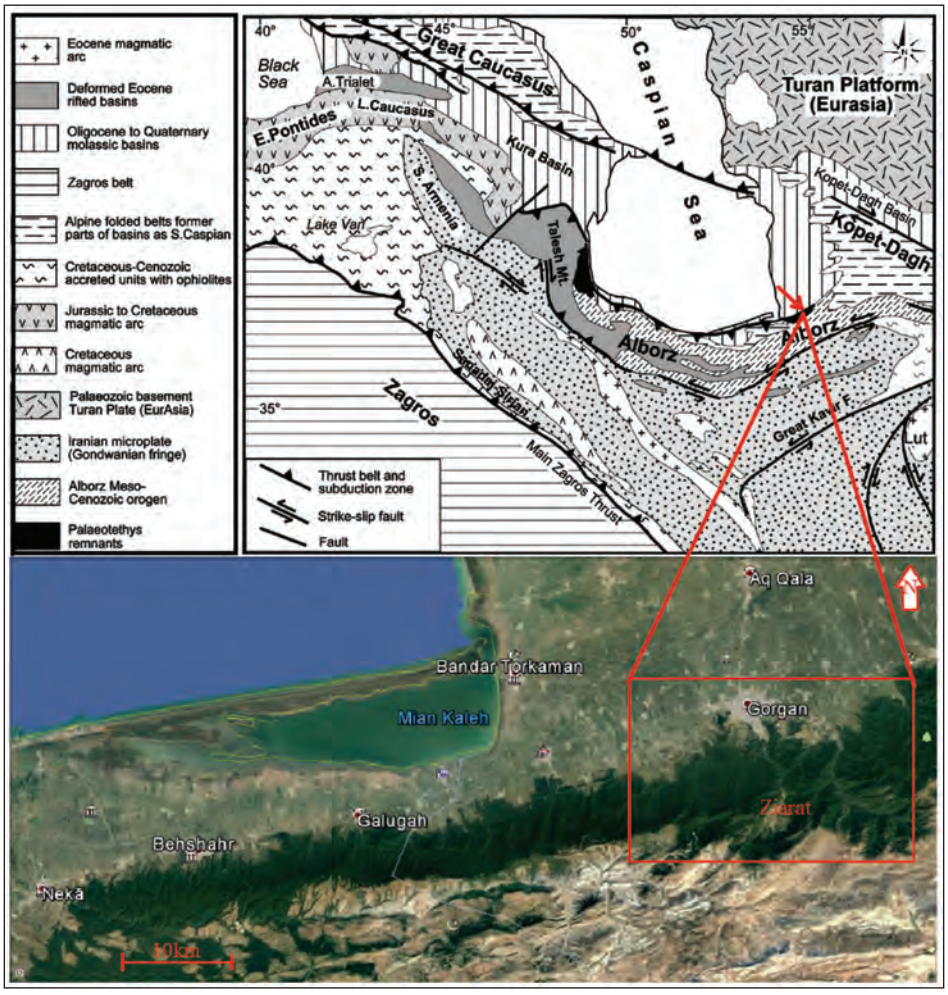

Figure 1- General tectonic map of North Iran and of the South Caspian region (modified from Brunet et al., 2003).

the tectonic evolution of the orogenic belt and adjacent regions (Gorring and Kay, 2001).

2. Geographical Location

The study area is situated approximately 5 km south of the Gorgan city, in northeastern Iran. In this area, Paleozoic rock units comprise Upper Ordovician, Silurian and Upper Carboniferous deposits. The metamorphic rocks (Gorgan schists), as one of the important geological units in Iran, are formed mainly of low-metamorphic rocks such as slate, phyllite, chlorite schist, greenschist and micaschist along with volcanic rocks and gabbrodiorite masses infiltrating them (Figure 2). These rocks are affected by a phase of regional metamorphism of lower greenschist facies and at least two phases of deformation (Geravand, 2012). In the past, most researchers dated these rocks back to Precambrian epoch (Gansser, 1951; Stöcklin, 1968; Jenny, 1977*a*), but only recently, according to the findings of the Palynomorphs in the area, they have been dated back to Late Ordovician age (Ghavidel Sivaki et al., 2011).

3. Methodology

After collecting basic information of works done in the study area using aerial photographs and geological maps, all outcrops related to these rocks were identified and sampled in a field investigation in three steps for 13 days during the summer of 2015 and 2016. The optical analyses were performed by Olympus BX-41 polarizing microscope at the Department of Geology, Science and Research Branch, Islamic Azad University, Tehran, Iran. After detailed petrographic studies 17 fresh samples were analyzed using a Varian Liberty 200 inductively coupled plasma–atomic emission spectrometer (ICP-AES) for major elements and using a Perkin Elmer Optima 3300 DV inductively coupled plasma–optical

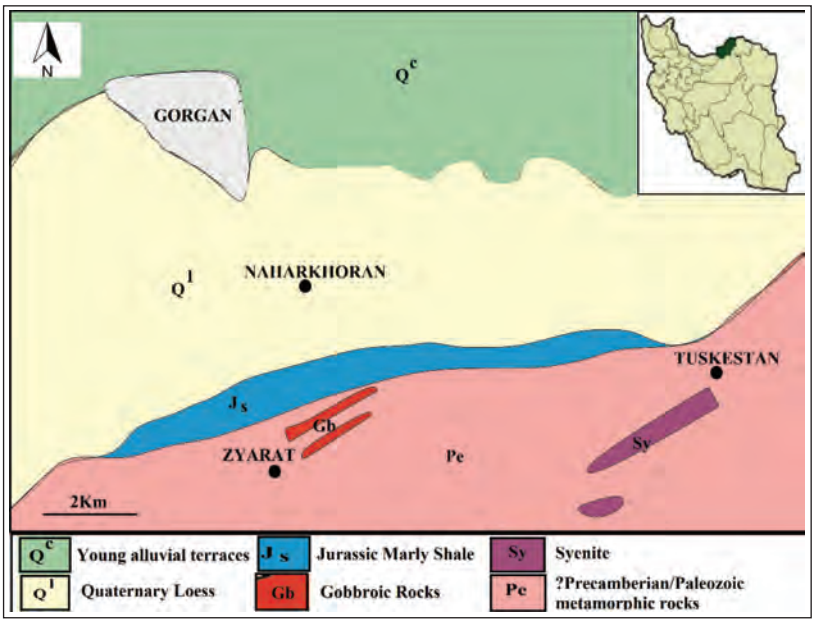

Figure 2- Location of the study area (adapted from the 1:250000 Scale map of Gorgan, Geological Survey of Iran).

emission spectrometer (ICP-OES) for trace and REE elements at Zamin Rizkavan lab, Iran. The data was interpreted using Minpet and GCDKIT 2.3 software.

4. Results

4.1. Field Study and Petrography

The mafic dykes are 1 to 5 meter in width and several hundred meters in length. They are surrounded by greenschists and show weak metamorphism (Figure 3). The samples have mesocratic to melanocratic color index (Figure 4). They have a gabbroic composition, with medium to large-grain size. They show ophitic to intergranular textures under polarized microscope (Figure 4).

The common mineralogical assemblage of gabbro and gabbrodiorite rocks in the region is plagioclase, pyroxene and opaque minerals. The plagioclases are generally subhedral to anhedral in shape (Figure 4) and sometimes they found as inclusions in pyroxene (Figure 4). Some of the clay minerals, might have formed by weathering of plagioclase prior to hydrothermal alteration. Apatite (Figure 4 e, f) and quartz are minor minerals in the rock. Gabbroic rocks of the region are heavily affected by deformation and metamorphism and show a wide range of secondary minerals such as epidote, chlorite, calcite and sericite (Figure 4 e, f). Intergranular, subophitic, and ophitic (Figure 4 a, b) and microgranoular textures are among the dominant textures in these rocks.

4.2. Geochemistry

The geochemical analysis of major, trace and rare earth elements of the study rocks are presented in table 1 and 2. FeOt is calculated by Le-Maitre's (1976) method.

Figure 3- Field photographs of samples in southern Gorgan.

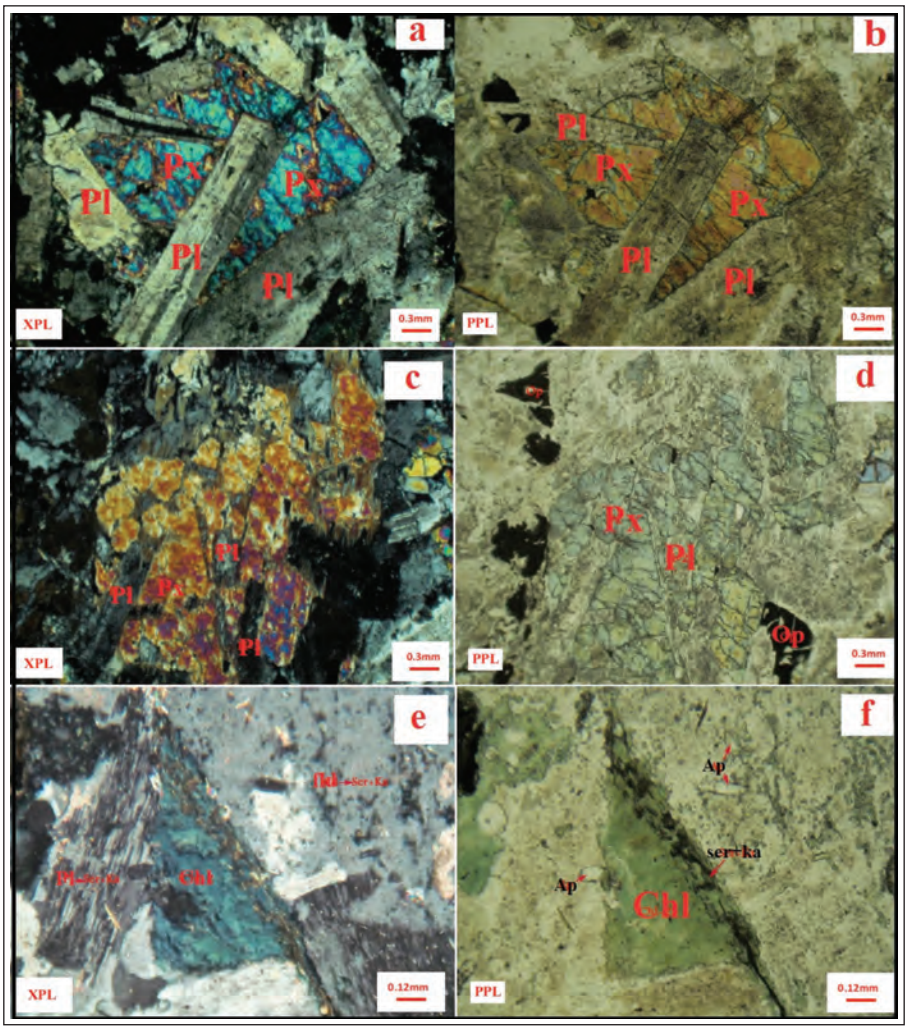

Figure 4- a, b) Ophitic textures in gabbros, c, d) Plagioclases as inclusion in pyroxene and opaque minerals, e. f) Sericite and plagioclase feldspars and along with secondary chlorite and abundant inclusions of apatite. Mineral Abbreviations (Kretz, 1983): Plagioclase: Pl, Pyroxene: Px, Chlorite: Chl, Apatite: Ap.

The classification diagram of SiO_2 (wt. %) vs. Na_2O/K_2O proposed by Winchester and Floyd (1977) is used for classification of intrusive rocks. According to this diagram, all samples are classified as gabbro (Figure 5).

Based on magma series diagrams (Irvine and Baragar, 1971), the samples are in (Figure 6a). But in the Nb/Y vs. (Zr/TiO_2* 0.0001) diagram (Winchester and Floyd, 1977) the samples are clearly in the alkaline range field (Figure 6b).

4.3. Origin

Chondrite normalized spider diagram of the samples is presented in figure 7a. The enrichment rate has been multiplied by 10-100 times. Plagioclase is the most prevalent and abundant mineral in the rocks of the study area. Sr and Ba enrichment is related to plagioclase. There is also negative anomaly in the elements Rb and K, indicating non-involvement of magma with continental crust (Kamber, 2012).

In the primitive mantle normalized diagram (Figure 7b), the studied samples show negative Rb anomaly. In the rocks affected by the deformation and metamorphism, this element is usually considered as mobile element (Kerrich and Manikyamba, 2011). Similarly, in the diagram normalized with chondrite and primitive mantle, there is no negative anomaly of high field strength elements such as Ti, P and Nb. This is a typical feature of intra-plate alkaline magmatic activity (Dai et al., 2011) and also suggests

Table 1- Results of major element analysis of the Zyarat gabbroic rocks.

Sample (wt.%)	A4	A5	B10-1	B12	B16-1	B16-2	B21-1	B21-2	B23-1	B23-2	B24-1	B24-2	B38	B39	B40	x	Bx-1
SiO_2	50.25	49.7	51.99	45.98	45.89	46.89	46.54	46.67	44.27	43.69	45.63	45.65	52.87	52.87	48.79	45.38	48.81
TiO_2	1.95	1.92	1.93	2.17	2	2	2.04	2.02	3.31	3.51	4.02	4	1.76	1.94	1.51	3.75	1.53
Al_2O_3	16.97	16.59	17.14	16.34	16.37	17.43	17.31	17.57	15.03	14.9	14.99	14.42	17.13	14.84	16.33	14.55	16.55
Fe_2O_3	3.78	4.54	3.92	3.45	3.67	3.74	3.2	3.17	4.62	4.48	4.68	4.55	3.8	4.17	3.76	4.75	3.67
FeO	5.31	5.03	4.31	5.99	5.86	5.74	5.13	5.07	7.7	7.83	7.47	7.28	5.59	5.97	6.27	7.6	5.64
MnO	0.14	0.13	0.11	0.14	0.13	0.13	0.13	0.13	0.14	0.15	0.16	0.19	0.22	0.19	0.16	0.18	0.14
MgO	5.95	6.8	2.91	5.8	6.01	5.85	4.76	4.59	5.78	5.77	4.42	4.93	2.47	3.88	5.98	4.3	6.47
CaO	6.24	7.05	4.34	9.14	9.22	9.67	10.14	9.81	8.85	8.79	9.27	9.69	7.25	4.77	8.82	7.86	8.77
Na_2O	5.06	4.44	6.51	3.61	3.37	3.27	4.03	4.13	3.15	3.01	3.27	3.52	5	6.09	3.73	4.24	3.93
K_2O	0.02	0.03	0.62	0.28	0.65	0.69	0.12	0.12	0.91	0.86	0.98	0.91	0.07	0.02	0.06	0.37	0.02
P_2O_5	0.19	0.17	0.62	0.43	0.48	0.52	0.32	0.32	0.37	0.4	0.41	0.48	0.5	0.51	0.19	1.23	0.17
BaO	<0.01	<0.01	0.07	0.04	0.08	0.08	0.02	0.02	0.09	0.08	0.07	0.08	0.02	<0.01	0.01	0.04	<0.01
Cr_2O_3	0.03	0.03	<0.01	0.02	0.02	0.02	0.03	0.03	0.01	0.01	<0.01	<0.01	<0.01	<0.01	0.03	<0.01	0.03
SrO	0.03	0.05	0.05	0.07	0.09	0.09	0.08	0.18	0.06	0.05	0.08	0.2	0.05	0.01	0.06	0.09	0.03
LOI	3.46	3.45	3.83	3.57	3.82	3.48	3.89	3.67	4.11	4.32	2.4	2.64	4.25	3.79	3.23	5.23	3.13
Total	99.38	99.93	98.35	97.03	97.66	99.6	97.74	97.5	98.4	97.85	97.85	98.54	100.98	99.05	98.93	99.57	98.89

Table 2- Results of trace element analysis of the Zyarat gabbroic rocks.

Sample	A4	A5	B10-1	B12	B16-1	B16-2	B21-1	B21-2	B23-1	B23-2	B24-1	B24-2	B38	B39	B40	B9-2	Bx-1
ppm																	
Ba	167.2	164	677.2	352.9	750	697.6	164.8	193.5	806.6	698.4	685.6	650.9	211.9	138.1	199.8	346	140.7
Co	42.1	39.2	18.6	40.1	41	39	35.6	31.5	51.3	48.6	43.2	44.5	16.2	29.2	44.1	36.7	39.3
Cr	196	205	11	165	138	128	229	221	83	87	<10	13	25	15	203	11	218
Cs	6.6	5.71	3.26	2.25	3.72	3.48	2.46	1.61	3.58	4.05	6.51	6.45	1.14	0.55	0.56	3.96	3.35
Ga	20.5	16.4	20.4	19.2	19.9	20.5	20.3	f20.7	21.4	20.4	23.3	22.6	29.7	29.5	19.2	22.3	19.5
Hf	2.6	2.3	6.5	4.1	4.3	3.9	4.3	4.4	4.1	4.3	5.5	5.6	10	13.1	2.3	5.3	2.4
Nb	19.5	18.1	51.9	31.7	37.2	34.1	30.2	32.2	24.8	25.3	49	36.7	61.5	80	29.2	50.8	29.6
Ni	103.1	96.7	16.1	90.2	95.8	94	70.8	63	86.8	81.1	22	22.7	14.7	28.9	89.4	9.7	90.9
Rb	0.3	0.8	10.8	5.5	16.4	16.3	2.7	2.5	26.1	23.9	39.1	34.8	1.2	<0.2	1.2	11.4	<0.1
Sc	17.5	20.7	11.3	24.9	20.4	18.9	31.7	27.2	49.1	46.1	33.6	36.1	19.8	23.3	26.5	22.3	22.8
Sn	<5	<5	<5	<5	<5	<5	<5	<5	<5	<5	<5	<5	<5	6	<5	<5	<5
Sr	283.5	461.4	505.1	702.6	970.1	919.9	897.8	926	577.5	567.3	846	930.9	552.7	449.3	592.6	949.1	325.6
Ta	1.7	1.6	3.7	2.2	2.3	2.1	2.2	2.4	1.8	1.9	3	2.8	4.3	5.6	1.7	3.7	1.7
TC	0.07	0.09	0.42	0.08	0.2	0.07	0.27	0.2	0.3	0.32	0.02	0.04	0.56	0.52	0.04	0.61	0.04
Th	2.64	2.01	5.16	2.78	2.75	2.6	2.48	2.78	2	1.92	3.88	3.79	7.27	5.32	1.94	4.51	1.75
TS	0.01	0.01	0.01	0.13	0.05	0.06	0.01	0.06	<0.01	<0.01	0.07	0.09	<0.01	<0.01	0.02	0.04	0.04

Table 2- continued.

Sample	A4	A5	B10-1	B12	B16-1	B16-2	B21-1	B21-2	B23-1	B23-2	B24-1	B24-2	B38	B39	B40	B9-2	Bx-1
ppm																	
U	0.32	0.29	1.04	0.78	0.93	0.82	0.87	0.78	0.63	0.64	1.03	1.05	1.98	2.61	0.27	1.24	0.61
V	159	192	99	193	180	169	205	194	483	487	392	389	79	107	248	265	210
W	1	<1	2	1	1	1	<1	<1	1	<1	1	1	2	2	<1	1	<1
Y	28	16.6	41.3	23.9	25.6	24.9	22.6	23.2	24.9	25.7	30.2	32.8	56.3	68.9	18.5	42.5	19.1
Zr	197	179	264	166	169	157	167	172	147	147	198	210	395	316	187	230	191
La	19.7	20.2	56.8	25.6	29.5	28.5	26.5	25.4	23.5	22.3	31.1	34	67.6	79.5	19.7	46.5	20.6
Ce	52.9	51.1	112.9	52.9	60.9	58.9	48.7	51.2	48.7	49	64.3	71.4	142.4	167.8	41.7	98.1	42.2
Pr	7.02	6.84	13.28	6.41	7.4	7.12	5.89	6.09	6.12	6.21	7.76	8.66	17.28	20.33	8.07	12.08	6.12
Nd	23.2	22.8	52.7	26.1	29.6	29	23.8	24.4	25.7	26.4	31.9	35.6	68.2	79.3	23.2	49.9	23.8
Sm	3.22	3.05	10.41	5.47	6.07	5.85	4.95	5.28	5.83	5.85	6.86	7.67	13.41	15.6	3.3	10.43	3.29
Eu	1.17	1.21	3.83	1.98	2.19	2.13	1.83	1.9	2.08	2.06	2.43	2.5	4.78	4.87	1.34	3.19	1.31
Gd	3.53	3.55	10.46	5.59	6.47	5.99	5.22	5.45	5.88	6.34	6.96	7.86	13.41	15.49	3.81	10.75	3.69
Tb	0.6	0.57	1.59	0.86	0.99	0.94	0.83	0.86	0.92	0.97	1.12	1.28	2.1	2.43	0.62	1.59	0.65
Dy	3.36	3.3	8.03	4.43	5.06	4.72	4.47	4.47	4.96	5.19	5.82	6.44	10.98	13	3.41	8.06	3.53
Ho	0.63	0.59	1.55	0.85	0.93	0.88	0.85	0.85	0.9	0.95	1.11	1.19	2.03	2.52	0.66	1.54	0.69
Er	1.75	1.68	4.19	2.29	2.43	2.36	2.32	2.35	2.43	2.47	2.96	3.16	5.6	6.86	1.81	4.05	1.76
Tm	0.23	0.22	0.54	0.31	0.33	0.31	0.29	0.31	0.31	0.32	0.4	0.42	0.74	0.93	0.24	0.51	0.24
Yb	1.49	1.33	3.2	1.94	1.92	1.84	1.84	2.01	1.9	1.93	2.46	2.58	4.59	5.75	1.48	3.2	1.57
Lu	0.21	0.21	0.51	0.27	0.3	0.27	0.27	0.29	0.27	0.26	0.36	0.38	0.7	0.87	0.23	0.47	0.23
Ce/Yb	35.5	38.42	35.28	27.27	31.72	32.11	26.47	25.47	25.63	25.39	26.14	27.67	31.04	29.18	28.17	30.66	26.88
Lu/Yb	0.14	0.16	0.16	0.14	0.16	0.15	0.17	0.14	0.14	0.13	0.15	0.15	0.15	0.15	0.15	0.15	0.15
La/Yb	13.22	15.18	17.75	13.19	15.36	15.49	14.40	12.63	12.36	11.73	12.64	13.17	14.72	13.82	13.31	14.53	13.12
Nb/U	60.9	62.41	49.9	40.64	40	41.5	44.71	41.28	40.65	49.5	47.61	33.01	41.55	108.1	37.3	42.3	48.52

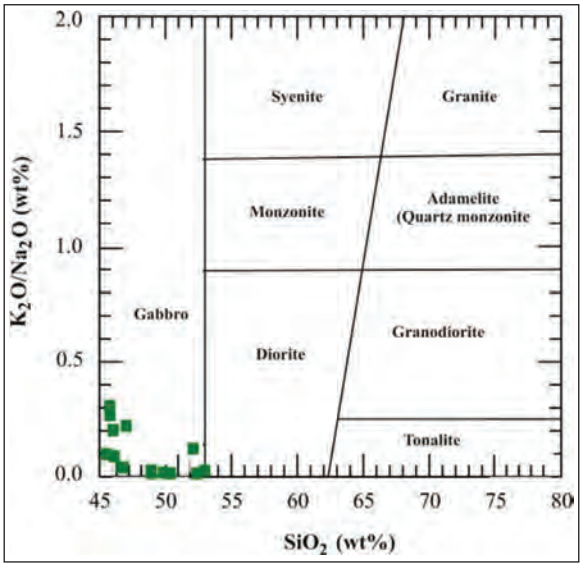

Figure 5- Rock classification diagram of the studied samples (Winchester and Floyd, 1977).

that there is no contamination of magma by continental crust (Ali et al., 2011). Slight Th in gabbros is probably due to combination of source rocks in the depth or at small melting dedree.

The samples are also normalized to OIB (Figure 7c). There is only a negative anomaly in the elements Rb and K, but the trend in the rest of the elements is consistent with the elements in the OIB.

High levels of Zr and Y in the studied samples suggest that primitive magma of gabbro is alkaline, because Zr is an incompatible element which goes into liquid phase immediately in the event of melting. The high ratio of La/Ta and Zr/Nb indicate high- alkaline magma erupting in intra-plate setting (Curtis et al., 1999).

The samples were normalized to chondrite in figure 8a and primitive mantle in figure 8b. In these diagrams, the samples show 10-100 times as much enrichment to chondrite and primitive mantle. A negative slope can be seen. In fact, the main feature of these samples is enrichment of LREE (Light Rare Earth Elements)

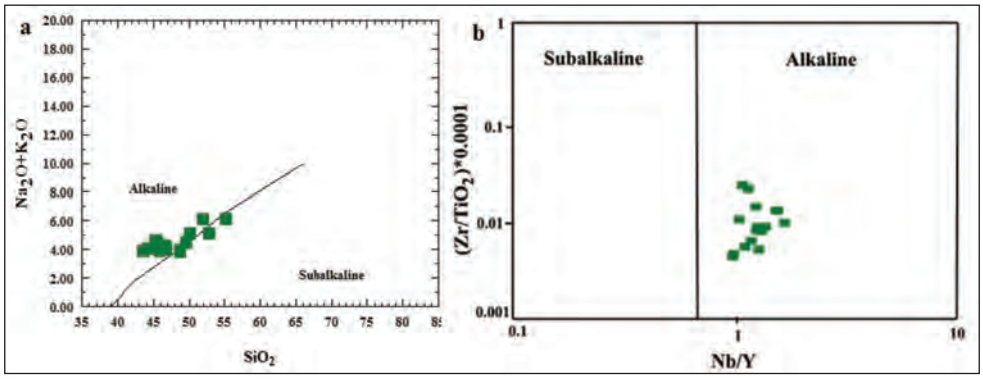

Figure 6- a) Total Alkali-SiO_2 (TAS) (Irvine and Baragar, 1971), and b) Nb vs (Zr/TiO_2) * 0.0001) (Winchester and Floyd, 1977) diagrams of the studied rocks.

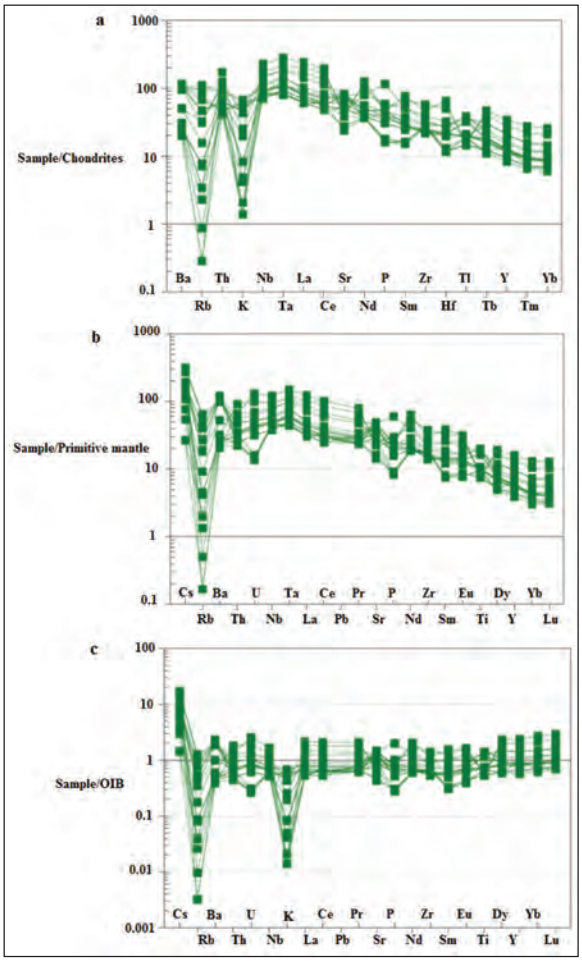

Figure 7- a) Chondrite-normalized spider diagram (Thompson, 1982), b) Primitive mantle-normalized spider diagram (Sun and McDonough, 1989), c) OIB-normalized spider diagram (Sun and McDonough, 1989) for the studied samples.

compared to HREE (High Rare Earth Elements). This indicates that the parent magma of rock including garnet and pyroxene have not participated in the melting and have retained heavy rare earth elements in refractory mantle (Rollinson, 1993; Zhao and Zhou, 2007). The LREE enrichment relative to HREE indicates a low-degree partial melting and high values of these elements in the source rock (Wright and McCurry, 1997). Similarly, it indicates the alkaline magma generated in intra-plate settings in interlayer space (Ali and Ntaflos, 2011). There is no Eu anomaly in REE plot.

According to the trend of samples on the REE diagram (Figure 8), it can be concluded that LREE are more compatible than HREE in parental gabbro magma. Depletion in heavy elements is attributed to presence of garnet in the source. LREE show enrichment to chondrites and primitive mantle. This suggests that magma derived from partial melting of mantle (Rollinson, 1993).

The samples were also normalized to OIB (Figure 8c). There is enrichment up to 2 times. The REE patterns of the studied rocks are very similar to OIB, and exhibit almost parallel trend to the OIB reference line passing through "1" (Figure 8).

5. Discussion

La/Yb ratios are high (10–21.4) in all samples (Table 2). The low La/Yb ratios reflect a melting regime dominated by relatively large melt fractions and/or spinel as the predominant residual phase (e.g., Falloon et al., 1988; Riley et al., 2005; Yang et al., 2007*a*) whereas high La/Yb ratios are indicative of smaller melt fractions and/or garnet control. The Nb/U ratios in Zyarat rocks are 40-60. These values are similar to those of the OIB (Nb/U= 47+10, Hofmann,

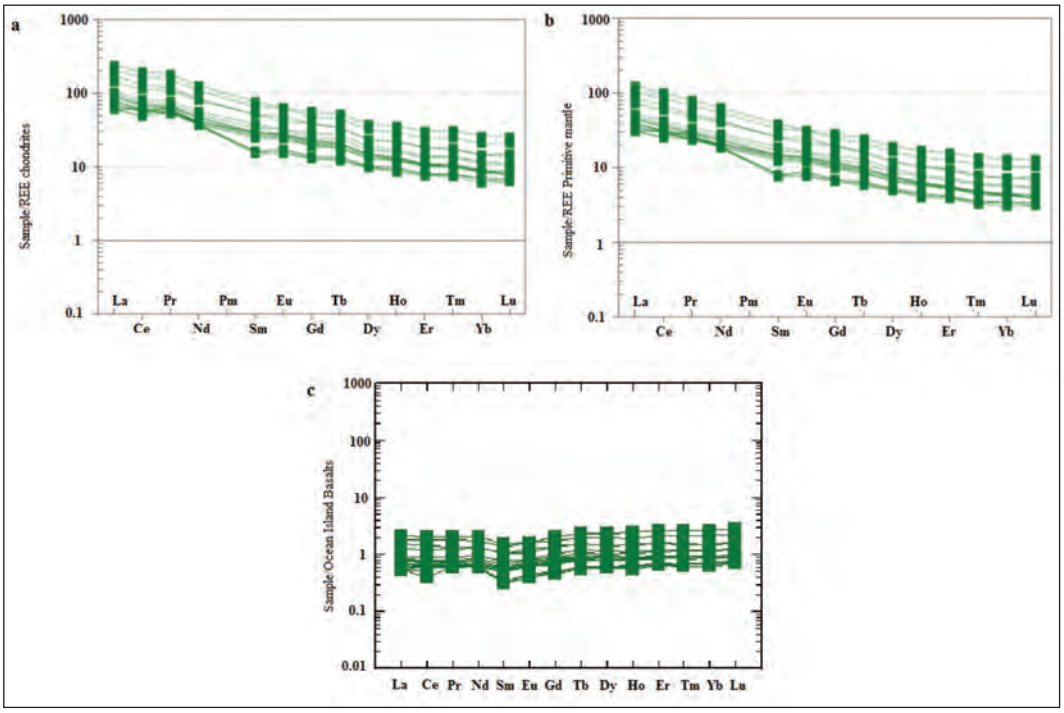

Figure 8- a) Chondrite-normalized REE diagram (Nakamura, 1974), b) Primitive mantle-normalized REE patterns (Sun and McDonough, 1989), c) OIB-normalized REE chart (Sun and McDonough, 1989) for the studied samples.

1988). The high LREE/HREE ratios and low Y content corresponding high Ti/Y ratios of the gabbros suggest that they could be derived from small melt fractions of a garnet stable source. Zr and Y do not fractionate significantly during partial melting (e.g., Yang et al., 2007*a*).

However, the dykes display low Rb/Sr (<0.1) and high Ba/Rb (>10). All of the dykes are enriched in LILE and LREE and depleted in Nb and Ta anomalies which are suggesting that metasomatism of source were triggered by subduction–related fluids or melts. Thus, the geochemical data indicate that all of the dykes may have formed by relatively low–percentage melting of an amphibole–bearing (Dai et al., 2011), refractory lithospheric mantle source in the garnet stability field. It may be metasomatized by recycled crustal materials prior to generation.

Pearce (2008) considers the melting of a low-depleted mantle to form a MORB and melt a relatively rich source (probably a mantle column at a greater depth) to form the OIB. There is a great similarity between the characteristics of the incompatible elements and the REEs of the alkaline samples and the OIB, which indicates the origin of taking the magma forming the rocks of the region from a mantle similar to the source of the OIB. In a diagram of Nb / Yb versus Th / Yb (Pearce, 2008), the samples are in the OIB range (Figure 9).

In a diagram of Nb against Nb/U (Cornelius et al., 2011), the ratio of Nb/U of studied rocks is high (Figure 10). Based on this diagram, the studied samples are in the range of OIB and away from the continental crust, which indicates the absence of crustal contamination

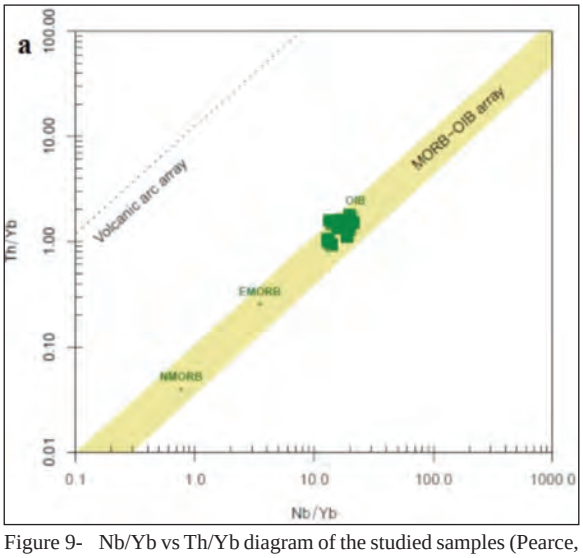

Figure 9- Nb/Yb vs Th/Yb diagram of the studied samples (Pearce, 2008).

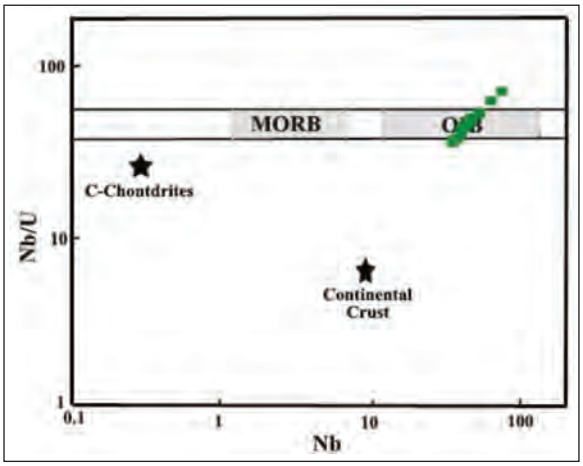

Figure 10- The Nb vs Nb/U diagram of studied samples (Cornelius et al., 2011).

in the evolution of gabbroic rocks. Dai et al. (2011) believe that magma derived from the mantle has low Lu/Yb ratio with average of 0.14-0.15, while this ratio is higher in the continental crust with average of about 0.16-0.18. The average Lu/Yb ratio in gGabbroic rocks is 0.15 which is less than that of the continental crust, and derivation of magma from these rocks from a mantle source shows no crustal contamination with the continental crust.

In order to detect the enrichment of origin of gabbroic rocks of Naharkhoran Valley, Zr-Y diagram was used (Sun and McDonough, 1989). These elements have very little mobility and are also used to study old igneous territories in high degrees of alteration (Prytulak and Elliott, 2007). All of the samples in the above-mentioned diagram are plotted in the field of enriched mantle (Figure 11a). Also in the Zr-against-Nb diagram (Abu-Hamatteh, 2005), the studied samples are in the field of enriched mantle (Figure 11b).

High Nb/Th ratio is one of the characteristics of oceanic crust (Rudnick and Fountain, 1995). This ratio is high in studied gabbros. In Nb/Th against Th diagram, the samples are in the range between enriched mantle and OIB (Figure 12a). The Rb/La against Th diagram also confirms it (Figure 12b). Both these diagrams show a lack of involvement of continental crust.

Based on geochemical analysis, the study rocks are in gabbro and the magma making these rocks had been

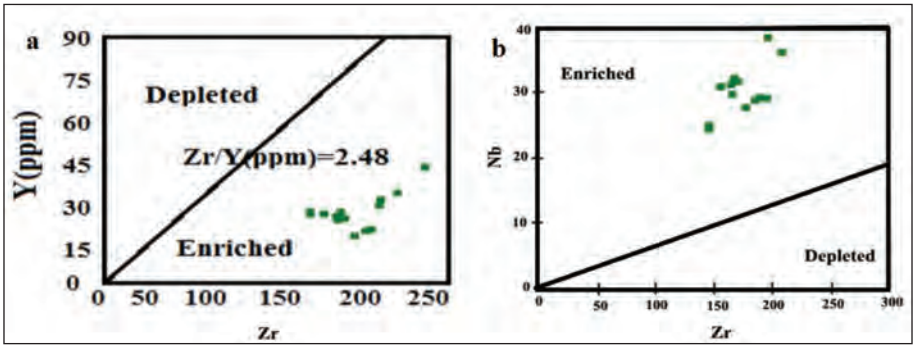

Figure 11- a) Y vs Zr (Sun and McDonough, 1989), and b) Zr vs Nb diagrams (Abu-Hamatteh, 2005) of studied rocks.

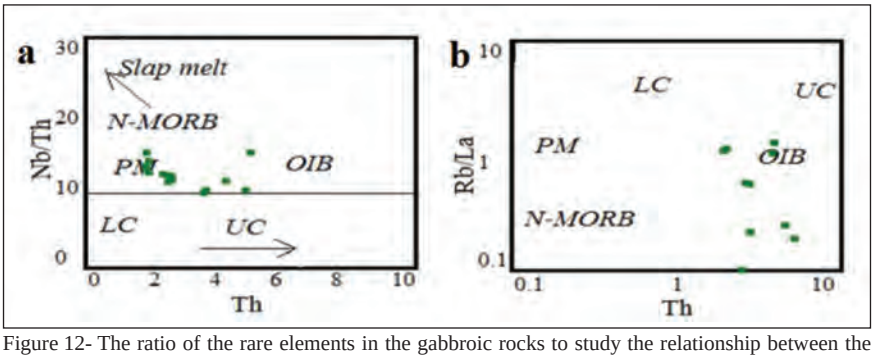

Figure 12- The ratio of the rare elements in the gabbroic rocks to study the relationship between the rocks with the enriched mantle, the upper crust and the oceanic islands (Zhao and Zhou, 2007); a) Nb / Th vs Th, and b) Rb / La vs Th diagrams of the studied samples.

alkaline in nature. Geochemical studies revealed that the gabbros were rich in K_2O and poor in Na_2O, and are mostly of alkaline type. According to Coleman and Donato (1979), high Na_2O and K_2O in gabbros resulted from exchanges with sea water or delayed magmatic vapor phase, which carries K_2O away and destroys it (Sinton and Byerly, 1980). The studied gabbros belong to alkaline magma series. The ratio of K_2O/P_2O_5 is used as an indicator for crustal contamination of magmas. Most of magmas originating from the mantle have a ratio of $K_2O/P_2O_5 < 2$. This ratio is 0.89 in average for the gabbros of the study area, indicating their origination from the mantle and absence of crustal contamination in them. The Nb value indicates the intraplate origin of these rocks. Gabbroic magma does not show depletion of Ti, Ta and Nb, suggesting non-participation of crustal materials or fluids derived from the crust in forming magma. Negative and steep slope of REE plot in these rocks suggests deep origination and reveals an origin associated with enriched mantle. High Fugacity of CO_2/H_2O in magma origin as well as a small degree of partial melting is among possible reasons for such a trend. Moreover, HREE depletion indicates that garnet and zircon have remained in the melting residue. The REE plot of the gabbros is similar to OIB, suggesting that both gabbros and OIB magmas share the same origin.

6. Conclusion

A suite of mafic gabbro dykes are intruded in the Middle–Upper Paleozoic rock units representing a part of the north Gondwana province. The alkaline gabbros include plagioclase, clinopyroxen and small needle of apatite. In general, they show OIB-like trace element patterns characterized by enrichment in LILE and LREE. Negative anomalies of Rb and K and Pb positive anomalies of Nb and Ti in the spider diagrams and other geochemical variations observed in studied rocks all indicate uncontamination by crust. Accordingly, the samples are located within the OIB range away from the continental crust, which indicates the absence of crustal deformation in the gabbroic rocks of the study. The high La / Yb ratio in the studied samples can reflect small degree of melting or garnet presence in the mantle. The tectonic environment of mafic dyke can be assigned to the initiation of the opening of Paleotethys in northern part of Gondwana province in late Ordovician time.

Acknowledgements

We would like to thank Dr. Reza Fahim Guilany for contributing the development of this article with his critiques.

References

Abu-Hamatteh, Z.S.H. 2005. Geochemistry and petrogenesis of ma.c magmatic rocks of the Jharol Belt, India: geodynamic implication. Journal of Asian Earth Sciences 25, 557-581.

Alavi, M. 1991. Sedimentary and structural characteristics of the Paleo–Tethys remnants in northeastern Iran. Geological Society of America Bulletin 103, 983-992. Doi: 10.1130/0016-7606(1991)103<0983:SASCOT>2.3.CO;2

Alavi, M. 1996. Tectonostratigraphic synthesis and structural style of the Alborz mountain system in northern Iran. Journal of Geodynamics 21, 1-33.

Ali, K.A., Moghazi, A.M., Moufti, M.R. 2011. Geochemistry and Sr-Nd-Pb isotopic composition of the Harrat Al-Madinah Volcanic Field, Saudi Arabia. Gondwana Research 21(2-3), 670-689. doi:10.1016/j.gr.2011.06.003

Ali, S., Ntaflos, T. 2011. Alkali basalts from Burgenland, Austria: Petrological constraints on the origin of the westernmost magmatism in the Carpathian-Pannonian Region. Lithos 121(1-4), 176-188.

Allen, M.B., Ghassemi, M.R., Shahrabi, M., Qorashi, M. 2003. Accommodation of late Cenozoic oblique shortening in the Alborz range, northern Iran. Journal of Structural Geology 25, 659-672. Doi: 10.1016/S0191-8141(02)00064-0

Berberian, M., King, G.C. 1981. Towards a palegeography and tectonic evolution of Iran. Cannadian Journal of Earth Sciences 18, 210-265. https://**doi**.org/10.1139/e81-019.

Brunet, M.F., Ershov, A.V., Korotaev, M.V., Nikishin, A.M. 2003. The South Caspian basin: a review of its evolution from subsidence modelling. Sedimentary Geology 156, 119-148. Doi: 10.1016/S0037-0738(02)00285-3.

Coleman, R.G., Donato, M.M. 1979. Oceanic plagiogranite revisited. Barker, F. (Ed.). Trondhjemites, Dacites and Related Rocks. Elsevier, Amsterdam, 149-168.

Cornelius, T., NtaAos, Th.V., Akinin, V. 2011. Polybaric petrogenesis of Neogene alkaline magmas in an extensional tectonic environment: Viliga Volcanic Field, northeast Russia. Lithos 122, 13-24.

Curtis, M.P., T., Leat, B., Millar, Randall, Riley, I., Storey, D. 1999. Middle Cambrian rift-related volcanism in the Ellsworth Mountains, Antarctica: tectonic implications for the paleo-Pacific margin of Gondwana. Tectonophysics 304, 275-299.

Dai, J., Wang, C., Hébert, R., Li, Y., Zhong, H., Guillaume, R., Bezard, R., Wei, Y. 2011. Late Devonian OIB alkaline gabbro in the Yarlung Zangbo Suture Zone: Remnants of the Paleo–Tethys? Gondwana Research 19, 232-243.

Davoudzadeh, M., Lensch, G., Weber–Diefenbach, K. 1986. Contribution to the paleogeography, stratigraphy and tectonics of the Infracambrian and Lower Paleozoic of Iran. Neues Jahrbuch fur Geologie und Palaontologie Abhandlungen 172, 245-269.

Davoudzadeh, M., Weber–Diefenbach, K. 1987. Contribution to the paleogeography, stratigraphy and tectonics of the Upper Paleozoic of Iran. Neues Jahrbuch fur Geologie und Palaontologie Abhandlungen 175, 121-146.

Delaloye, M., Jenny, J., Stampli, G. 1981. K–Ar dating in the eastern Elburz (Iran). Tectonophysics 79, 27-36.

Falloon, T.J., Green, D.H., Hatton, C.J., Harris, K.L. 1988. Anhydrous partial melting of a fertile and depleted peridotite from 2 to 30 kbar and application to basalt petrogenesis. Journal of Petrology 29, 1257-1282. doi:10.1093/petrology/29.6.1257

Gansser, A. 1951. Geological reconnaissance in Gorgan and surrounding area. National Iran Oil Company, interal geological report no 10, 37 (unpublished).

Geravand, M. 2012. Natural pollution assessment of heavy metals in soils of Gorgan's schist. Master's thesis, Shahrood University of Technology, 156 p. Shahrood (unpublished).

Ghavidel Sivaki, M., Hassanzadeh, H., Vecoli, M. 2011. Palynology and isotope geochronology of the upper Ordovician–Silurian successions (Ghelli and Soltan Maidan Formation) in the Khoshyeilagh area, eastern Alborz Range, northern Iran; stratigraphic and palaeogeographic implications. Rewiew of Plalaeobotany and Palynology 164, 251-271.

Gorring, M.L., Kay, S.M. 2001. Mantle sources and processes of Neogene slab window magmas from southern Patagonia, Argentina. Journal of Petrology 42, 1067-1094. doi:10.1093/petrology/42.6.1067.

Hofmann, A.W. 1988. Chemical differentiation of the Earth: the relationship between mantle, continental crust, and oceanic crust. Earth and Planetary Science Letters 90, 297-314. doi: 10.1016/0012-821X(88)90132-X.

Horton, B.K., Hassanzadeh, J., Stockli, D.F., Axen, G.J., Gillis, R.J., Guest, B., Amini, A.H., Fakhari, M., Zamanzadeh S.M., Grove, M. 2008. Detrital zircon provenance of Neoproterozoic to Cenozoic deposits in Iran: Implications for chronostratigraphy and collisional tectonics. Tectonophysics 451, 97-122. Doi: 10.1016/j.tecto.2007.11.063

Irvine, T.N., Baragar, W.R.A. 1971. A guide to the chemical classification of the common volcanic rocks. Tectonophysics 451, 97–122.

Jenny, J.G. 1977*a*. Geologie et stratigraphie de l'Elbourz oriental entre Aliabad et Shahrud, Iran. These presentee la Faculte des Sciences de l'Universite de Genve, 1-238.

Jenny, J.G. 1977*b*. Precambrien et Paleozoique inferieur de l'Elbourz oriental entre Aliabad et Shahrud, Iran du nord–est. Eclogae Geologicae Helvetiae 70, 761-770.

Kamber, E. 2012. Back arc basing in the Coatmalia zone in Africa. Journal of Geophysical 92, 34-62.

Kerrich, R., Manikyamba, C. 2011. Geochemistry of alkaline basalts and associated high-Mg basalts from the 2.7 Ga Dharwar craton, Penakacherla Terrane. India: An Archean depleted mantle-OIB array. Precambrian Research 188, 104-122.

Kretz, R. 1983. Symbols for rock-forming minerals. American Mineralogist 68, 1-2, 277-279.

Le-Maitre, R.W. 1976. The chemical variability of some common igneous rocks. Journal of Petrology 17, 589-637.

Nakamura, N. 1974. Determination of REE, Ba, Fe, Mg, Na and K in carbonaceous and ordinary chondrites. Geochimica et Cosmochimica Acta 38, 757-775.

Pearce, J.A. 2008. Geochemical fingerprinting of oceanic basalts with applications to ophiolite classification and the search for Archean oceanic crust. Lithos 100, 14-48.

Prytulak, J., Elliott, T. 2007. TiO_2 enrichment in ocean island basalts. Earth and Planetary Science Letters 263, 388-403. Doi: 10.1016/j.lithos.2007.06.016

Raghimi, M. 2010. Tectono–magmatic setting of deformed plutonic rocks of Gorgan Schists in Naharkhoran, Gorgan–Iran. Gorgan University of Agricultural sciences and Natural Resources. Technical report. 56 p (unpublished).

Rahimi Chakdel, A. 2007. Geochemistry and petrogenesis investigations of igneous veins in Ziarat village of Gorgan, Gorgan University of Agricultural sciences and Natural Resources. Technical report. 47 p (unpublished).

Riley, T.R., Leat, P.T., Curtis, M.L., Millar, I.L., Dunca, R.A., Fazel, A. 2005. Early–Middle Jurassic dolerite dykes from western Dronning maud land (Antarctia): Identifying mantle sources in the Karoo large igneous province. Journal of Petrology 46, 1489-1524. http://dx.doi.org/10.1093/petrology/ego023

Rollinson, H.R., 1993. Using geochemical data, Evaluation, Presentation, Interpretation Addison: Wesley Longman, Harlow, 352 p.

Rudnick, R.L., Fountain, D.M. 1995. Nature and composition of the continental crust: a lower crustal perspective. Reviews of Geophysics 33, 267-309.

Salehi Rad, M.R. 1979. Etude géologique de la region de Gorgan (Alborz oriental, Iran) These de docteur 3em cycle.

Şengör, A.M.C. 1990. A new model for the late Palaeozoic–Mesozoic tectonic evolution of Iran and implications for Oman. Robertson, A.H.F., Searle, M.P., Ries, A.C. (Ed.), The Geology and Tectonics of the Oman region. Geological Society, London, 797-831.

Sharabi, M. 1990. Geological map of Gorgan 1:250000, Geological survey of Iran, Tehran.

Sinha A.K. 2012. Petrological characterization of Proterozoic mafic dykes from the Singhbhum craton, eastern India, 34th International Geological Congress, Brisbane, Australia.

Sinha, A.K. 2013. Geochemistry of distinct mafic dykes from the damodar valley gondwana basins and chhotanagpur gneissic terrain, eastern India: implications for their petrogenesis and tectonic setting, Geological Society of America Abstracts with Programs.

Sinton, J.M., Byerly, G.R. 1980. Silicic differentiates of abyssal oceanic magmas: evidence for late-magmatic vapor transport of potassium. Earth and Planetary Science Letters 47, 423-30.

Stampfli, G.M., Borel, G.D. 2002. A plate tectonic model for the Paleozoic and Mesozoic constrained by dynamic plate boundaries and restored synthetic oceanic isochrones. Earth and Planetary sciences letters 196, 17-33. http://dx.doi.org/10.1016/S0012-821X(01)00588-X

Stöcklin, J. 1968. Structural history and tectonics of Iran: A review. The American Association of Petroleum Geologists Bulletin 52, 1229-1258.

Stöcklin, J. 1974. Possible ancient continental margins in Iran. Burk, C.A., Drake, C.L. (Ed.). The geology of continental margins. Springer–Verlag; Berlin, Heidelberg, New York, 873–887.

Sun, S.S., McDonough, W.F. 1989. Chemical and isotopic systematics of oceanic basalts: implication for mantle composition and processes. Saunders, A.D., Norry, M.J. (Ed.). Magmatism in the Ocean Basins. Geological society, London, Speacial publications, 42, 313-345. doi:10.1144/GSL.SP.1989.042.01.19

Thompson, R.N. 1982. Magmatism of the British tertiary volcanic province. Scotland Geological Journal 18, 49-107.

Wendt, J., Kaufmann, B., Belka, Z., Farsan, N., Karimi Bavandpur, A. 2005. Devonian /lower and palaeogeography of Iran, Part II. Northern and central Iran. Acta geologica polonica 55, 31-97.

Winchester, J.A. Floyd, P.A. 1977. Geochemical discrimination of different magma series and their differentiation products using immobile elements. Chemical Geology 20, 325-343. http://dx.doi.org/10.1016/0009-2541(77)90057-2

Wright, J.B., McCurry, P. 1997. Geochemistry of calc-alkaline volcanic in northwestern Nigeria, and a possible Pan-African suture zone. Can, Earth and Planetary Science Letters 37, 90-96.

Yang, J.H, Wu, F.Y, Wilde, S.A, Xie, L.W, Yang, Y.H, Liu, X.M. 2007. Trace magma mixing in granite genesis: in–situ U–Pb dating and Hf–isotope analysis of zircons. Contributions to Mineralogy and Petrology 153, 177-190.

Yang, J.H., Sun, J.F., Chen, F., Wilde, S.A., Wu, F.Y. 2007. Sources and Petrogenesis of Late Triassic Dolerite Dikes in the Liaodong Peninsula: Implications for Post–collisional Lithosphere Thinning of the Eastern North China Craton. Journal of Petrology 48, 1973-1997.

Zamani Pedram, M., Hossieni, H. 2003. Geological map of Gorgan 1:100000, No. 6862, Geological survey of Iran, Tehran.

Zhao, J.H., Zhou, M.F. 2007. Geochemistry of Neoproterozoic mafic intrusions in the Panzhihua district (Sichuan province, SW China). Implications for subduction-related metasomatism in the upper mantle. Precambrian Research 152, 27-47. Doi: 10.1130/0016-7606(1991)103<0983:SASCOT>2.3.CO;2

Bull. Min. Res. Exp. (2018) 157: 165-184

Bulletin of the Mineral Research and Exploration

http://bulletin.mta.gov.tr

Physicochemical properties and availability of Tahar-Güzelöz (Nevşehir) diatomite

Ayşegül YILDIZ[a*], Ali GÜREL[b] and Dilan OKUTAN[c]

[a]*Aksaray University, Faculty of Engineering, Department of Geological Engineering, 68100, Aksaray, Turkey. orcid.org/0000-0003-4823-3594*

[b]*Niğde Ömer Halisdemir University, Faculty of Engineering, Department of Geological Engineering, 51100, Niğde, Turkey. orcid.org/ 0000-0001-7068-4784*

[c]*Zemka Soil Mechanics and Quality Control Laboratory, 01100, Adana, Turkey. orcid.org/0000-0002-7203-6016*

Research Article

Keywords:
Diatomite, industrial raw laterials, late Miocene-Pliocene, Güzelöz, Kızılkaya ignimbrite, Nevşehir, Tahar, Tahar ignimbrite.

ABSTRACT

In this study, utilization of Tahar-Güzelöz (Nevşehir) diatomites occurring within the late Miocene-Pliocene age vocanosedimentary units which formed due to volcanism and outcropping in Tahar and Güzelöz (Nevşehir) areas were investigated. In the study area, three stratigraphic sections were measured, one of which was measured in the Tahar area (TK), and the two others were measured in the Güzelöz area (GÜ1 and GÜ2). Various physicomechanical, chemical, mineralogical and analytical methods were used on the samples. Analyses results of the diatomites in the investigated area were determined as follow; amount of acid-insoluble matters; 74,20 - 84,20 %, amount of water-insoluble matters; 99,80 %, loss on ignition ratios (950 °C de); 8,18 - 22,82 %, whitenesses; 80,45 - 84,79 %, particle sizes; 0,7-209 µ , pore sizes; 1,448 e-03A – 5,888 e-04A, pore volumes; 1,148 e-02 – 8,515 e-02 cc/g , specific gravities; 2,33 – 2,49 gr/cm^3 , total porosities; 57 –60 %, cumulative specific surface areas; 4,047 e+01 – 5,160 e+01 m^2/g, pH; 5-7 (acit and neutral), filtration rates; 138 – 351 ml/dk, SiO_2 contents; 38,16 – 67,77 %. It was determined that, the samples are not contain palinological material and these generally formed from long and large diatom genus and species. The evaluation of the analyses results showed that, none of the three location's diatomites is suitable as construction material, carrier, mild abrasive and cleaner, isolution material. At the same time, determined that, the Tahar and Güzelöz–1 location's diatomites can not be used as filler material. In addition, it was determined that, the subject diatomites can be used in the manufacture of silicate, and in percolator by the enrichment in terms SiO_2. Also, Güzelöz-2 location's diatomites can be used as filler material in the rubber and paper industries.

Received Date: 29.12.2016
Accepted Date: 28.09.2017

1. Introduction

The study area is located in the Güzelöz and Tahar locations within 1/25000 scale Kayseri K33-c3 and L33-b2 sheets (Figure 1). Mostly; studies regarding the volcanism have been carried out in and around the study area. Among these, Pasquaré (1968) studied the Cenozoic volcanism in the Central Anatolia and stated that the volcanism in the region began with ignimbrites in the middle Miocene and ended with basaltic lavas of the Hasandağ in Quaternary. Pasquaré et al. (1988) asserted that Neogene and Quaternary volcanics in the Central Anatolia were continental arc volcanics which had been formed by the collision of the Afro-Arabian and Eurasian plates. Ayrancı (1970) detected that the Erciyes volcanism occurred in three stages. Innocenti et al. (1975) dated volcanic rocks around Tomarza, (Kayseri), Erciyes Mountain and İncesu, and detected 8,5-2,8 my for ignimbrites, 7,8 my for tuffs, 5 my for andesites, 5,4 my for rhyolites and 10,1 my for dacites. Güner and Emre (1983) stated that there had been a calcalkaline volcanism on the Erciyes Mountain and its vicinity. Sassano (1964) carried out a study on the Neogene and Quaternary volcanisms in the Acıgöl region. Özkuzey and Önemli (1977) investigated the petrography and

* *Corresponding author: Ayşegül YILDIZ, ayildiz10@hotmail.com*
http://dx.doi.org/ 10.19111/bulletinofmre.428305

economical geology of the Acıgöl perlites. Batum (1978) studied the geology and petrography of Acıgöl and Göllüdağ volcanics. Yıldırım and Özgür (1981) on the other hand asserted that the dimension of the Acıgöl caldera and completed its evolution in 5 stages. Duritt et al. (1995) investigated Quaternary rhyolites located in the Acıgöl complex. Schumacher et al. (1990) investigated mineralogical and geochemical characteristics of the Cappadocian ignimbrites in Ürgüp-Nevşehir-Kayseri regions. Temel (1992) studied mineralogical and geochemical features of the Cappadocian ignimbrites in the Ürgüp region. Aydar (1992) detected that the Hasandağ volcanism had been formed in three stages. Göncüoğlu and Toprak (1992) stated that the Melendiz Mountain were formed by the Tepeköy, Melendizdağ and Çınarlı volcanics. Aydar and Gourgaud (1998) investigated the Hasandağ volcanism. Gevrek et al. (1994*a* and *b*) made studies regarding the maars located in the Cappadocia and the Narköy maar. Toprak (1996) made a study on defining the basins of the Cappadocia Volcanic Province (CVP) and determining the volcanism and structural characteristics. Temel et al. (1998*a*) investigated the volcanic rocks of the CVP in terms of mineralogical, geochemical and petrographical characteristics and determined that these rocks had been derived from andesitic and dacitic magmas. They also explained that volcanic activities in the region had occurred as result of the effects of compressional and extensional tectonisms related to the subduction of the Arabian-African Plate beneath the Anatolian Plate. Le Pennec et al. (2005) studied ignimbrites and volcanic rocks of the CVP and dated 10 different ignimbrites emplaced in the region by means of paleontological data and K-Ar age determinations. Gürel et al. (2007) defined the Mustafapaşa Formation and the overlying rocks forming the Cemilköy Ignimbrite, and explained sand, silt and clay ratios of each unit and the formation of dominant clay minerals.

Some investigators have mapped the study area and its vicinity. Among them, Beekman (1966), Atabey et al. (1987, 1988) and Ayhan et al. (1988) have prepared 1/25.000 scale maps of Hasandağ and Melendiz Mountain locations, Niğde-Nevşehir-Kırşehir and Kayseri regions and Niğde-Aksaray-Derinkuyu regions, respectively.

Schumacher and Schumacher (1996), Dhont et al. (1998), Froger et al. (1998), Koçyiğit and

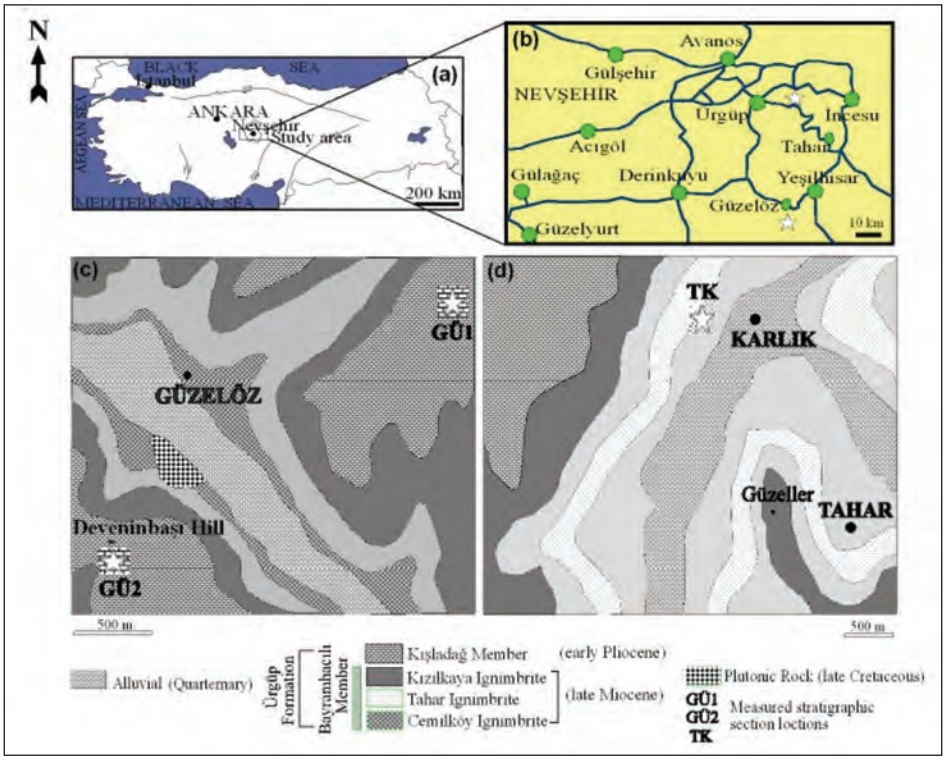

Figure 1- The stydy area location (a, b) and geological maps (c, d) and locations of the measured stratigraphic sections (modified from Pasquaré,1968; MTA, 1989; Toprak,1998; Gürel and Kadir, 2006; Yavuz-Işık and Toprak, 2010).

Beyhan (1998), Kürkçüoğlu et al. (1998), Temel et al. (1998*b*), Toprak (1998) and Dönmez et al. (2003) studied the mineralogical, geochemical, structural and petrographical characteristics of the CVP. However, Göz et al. (2014) has investigated the mineralogy and geochemistry of lacustrine formations deposited in the CVP in the late Miocene-Pliocene.

Viereck-Gotte and Gürel (2003), Kadir et al. (2006), Gürel and Kadir (2006) and Gürel et al. (2008) investigated the paleosol, caliche and clay formations located among ignimbrites in the CVP, around the study area. Yavuz-Işık and Toprak (2010) studied the palynostratigraphical characteristics of the Neogene terrigenous sediments alternating with the Cappadocian ignimbrites.

There are little studies carried out on diatomites in and around the study area. Kayalı et al. (2005) and Gürel and Kadir (2008) made a study on determining the qualitative and quantitative characteristics of clay and diatomites in the Central Anatolian Region. Yıldız and Gürel (2005) investigated the diatom assemblage and paleoenvironmental characteristics of diatomites in the Çiftlik Basin (Niğde) region. Gürel and Yıldız (2006) studied diatom assemblage and lithofacies characteristics of diatomites in the Ihlara-Selime locality. Yıldız and Gürel (2014) made a study on the fossil diatom assemblage and the paleoenvironmental characteristics for diatomites in the Karacaören-Ürgüp region (Nevşehir). Yıldız et al. (2016) have finally investigated the use areas of the diatomites for industrial raw material.

The physicochemical characteristics of diatomite levels located within the Bayramhacılı and Kışladağ members of the late Miocene-Pliocene Ürgüp formation and theirs utilities as an industrial raw material have been investigated in detail for the first time in the study area. Although, CVP is one of the place rich in diatomite in Turkey the studies regarding the physicochemical characteristics and utilities for diatomites located in this region have remained as limited until today. Therefore, the determination of physicochemical characteristics and utilities of diatomites in the Tahar and Güzelöz areas located in the CVP will contribute a lot to science and industry.

2. Material and Method

Total of three stratigraphical sections were measured one of which was from the Bayramhacılı Member (Tahar section: TS) (thickness: 50 m) and other two sections within the Kışladağ Member (Güzelöz-1 section: GÜ1, (thickness: 36 m) and Güzelöz-2: GÜ2) (thickness: 4 m.). These section were selected where diatomite units are best exposed within lacustrine deposits of the volcanic late Miocene-Pliocene Ürgüp formation in the study area. Total of 17 diatomite samples were collected along three sections and the field photos related to these sections were taken (Figures 2-4). In order to determine the

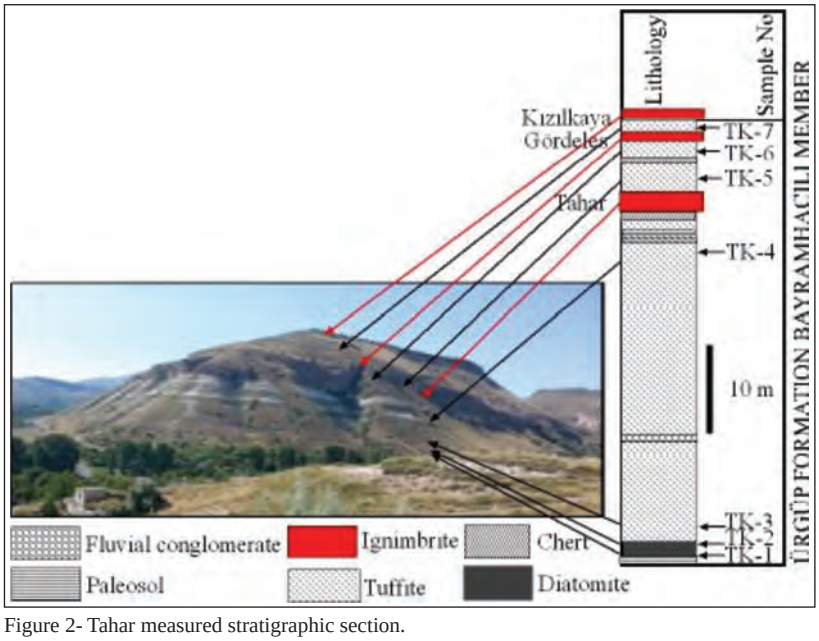

Figure 2- Tahar measured stratigraphic section.

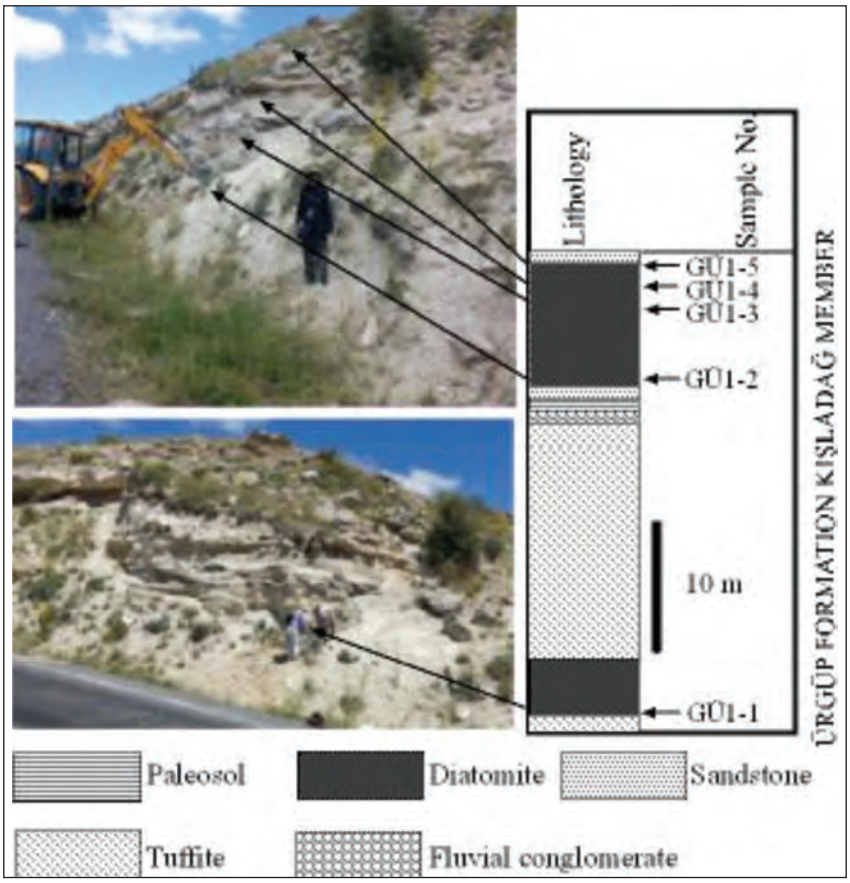

Figure 3- Güzelöz-1 measured stratigraphic section.

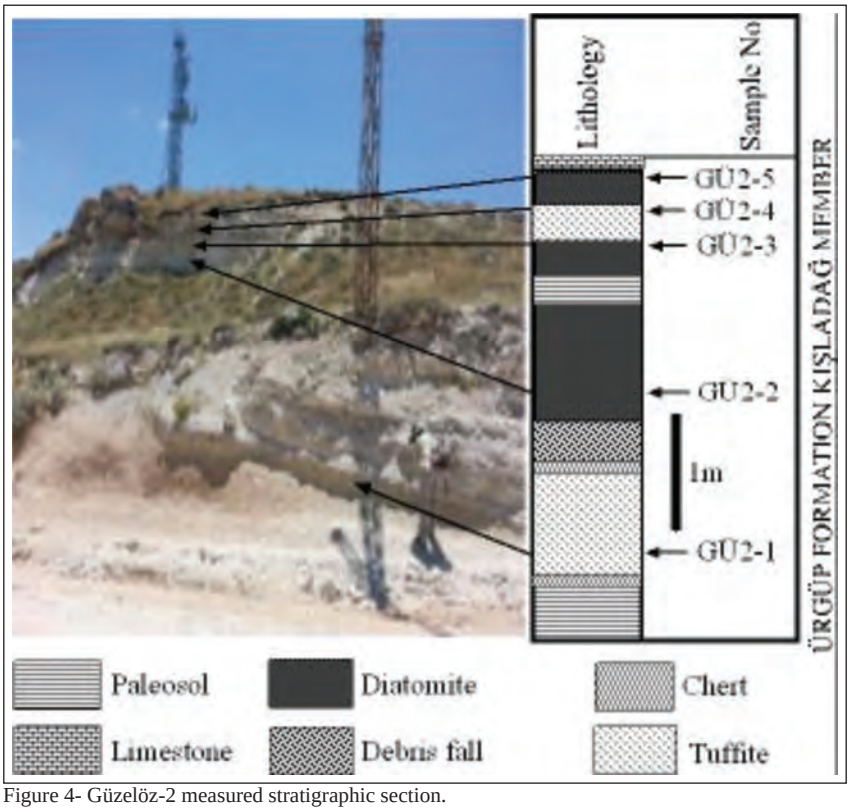

Figure 4- Güzelöz-2 measured stratigraphic section.

physicochemical characteristics and their areas of use, two diatomite samples (TK-1 and GÜ1-2) were subjected to X-Ray Diffraction (XRD) analysis in the General Directorate of Mineral Research and Exploration (MTA), Ankara, (using the Cu X-ray tube Bruker D8 Advanced XRD Analysis device as compatible with the ASTM standards), acid and water-insoluble matter amounts (results of their chemical analyses were detected by drying samples in 105°C), whiteness analysis (using Minolta Chroma Meter CR 300 device), specific surface area, porosity volume and porosity size analyses (based on the BET method using Quantochrome Nova 2200 device) (Tables 1-3). Total of six diatomite samples (TK–1, TK–2, GÜ1–2, GÜ1–4, GÜ2–2 and GÜ2–3) were subjected to pH analysis (based on TS6166 standards by the correlation made by pH indicator Strips pH 0-14) in the Soil Mechanics and Construction Materials,

Table 1- Results of qualitative XRD analysis of diatomite samples in the study area.

Sample No.		Analysis Result
Güzelöz-1 MSS	GÜ1-2	1- Calcite 2- Quartz 3- Feldspar minerals 4- Crystobalite 5- Clay minerals 6- Mica minerals 7- Amphibole minerals 8- Amorphous material
Tahar MSS	TK-1	1- Quartz 2- Crystobalite 3- Clay minerals 4- Pyroxene minerals 5- Amorphous material

Table 2 – Results of total porosity, whiteness, acid and water insoluble matter analysis of diatomite samples in the study area.

Sample No.		Total Porosity (%)	Results of Whiteness Analysis	Amount of Acid Insoluble Matter (%)	Amount of Water Insoluble Matter (%)
Güzelöz-2 MSS	GÜ2-3	57,8			
	GÜ2-2	58,1			
	GÜ2-1	57	80,45	74,20	99,80
Güzelöz-1 MSS	GÜ1-4	58			
	GÜ1-2	57,7			
Tahar MSS	TK-2	59,9			
	TK-1	60	84,79	84,20	99,80

Table 3- Results of specific surface area, pore volume and pore diameter analysis of diatomite samples in the study area.

Methods	Sample No.	
	Tahar MSS	Güzelöz-1 MSS
Specific Surface Area	TK-1	GÜ1-2
Multi Point BET	6,771 e+01 m^2/g	5,427 e+01 m^2/g
t- Method Outer Surface Area	4,787 e+01 m^2/g	2,922 e+01 m^2/g
t-Method Microporous Surface Area	1,984 e+01 m^2/g	2,505 e+01 m^2/g
NLDFT Cummulative Surface Area	5,160 e+01 m^2/g	4,047 e+01 m^2/g
Pore Volume		
t-Method Microporous Pore Volume	8,515 e-02 cc/g	1,148 e-02 cc/g
HK Method Cummulative Pore Volume	3,751 e-02 cc/g	2,966 e-02 cc/g
SF Method Cummulative Pore Volume	3,762 e-02 cc/g	2,975 e-02 cc/g
NLDFT Method Cummulative Pore Volume	5,580 e-02 cc/g	4,630 e-02 cc/g
Pore Diameter		
HK Method Pore Radius	2,158 e-04µ	2,158 e-04µ
SF Method Pore Radius	2,261 e-04µ	2,261 e-04µ
NLDFT Pore Radius	1,448 e-03µ	5,888 e-04µ

Quality Control Laboratory (Adana), seven diatomite samples (TK–1, TK–2, GÜ1–2, GÜ1–4, GÜ2–1, GÜ2–2 and GÜ2–3) were subjected to specific gravity and total porosity (%) analyses based on TS-1900-1 standards by using picnometer), six diatomite samples (TK–2, GÜ1–2, GÜ1–4, GÜ2–2, GÜ2–3 and GÜ2–5) were subjected to particle diameter distribution analysis (based on TS 1900-1 and TS 1500 standards by means of wet sieve method) and hydrometer analysis (based on TS 1900-1 standards), three diatomite samples (TK–1, GÜ1–2 and GÜ2–2) were subjected to compaction analysis [based on the Technical Specification of the General Directorate of Highways (2013)] (Tables 3-6). Total of 10 diatomite samples (TK–1, TK–2, GÜ1–1, GÜ1–2, GÜ1–3, GÜ1–4, GÜ1–5, GÜ2–2, GÜ2–3 and GÜ2–5) were subjected to X-ray fluorescent spectrometer (XRF) analysis and the Loss on Ignition (in 950°C) (by using Panalytical brand, Axios Max model Wave Length Distributed X-ray Flourescent (WD-XRF)), and three diatomite samples (TK–1, GÜ1–1 and GÜ1–2) were subjected to infiltration velocity analysis (Falling Head Permeability Test) in the Geochemical Analysis Laboratory (JAL) of the Faculty of Engineering, the Aksaray University (Aksaray). Total of 3 samples (TK–1, GÜ1–2 and GÜ1–3) were subjected to the Scanning Electron Microscope Analysis (SEM) in the Scientific and Technological Application and Research Center, Aksaray University, Aksaray (Figure 5). Four diatomite samples (TK–1, TK–2, GÜ1–1 and GÜ2–

Table 4 - Comparison of results of XRF, loss on ignition, moisture, particle size, density and pH analysis of diatomite samples from Güzelöz–1, Güzelöz–2 and Tahar measured stratigraphic sections in the study area.

	Tahar MSS		Güzelöz-1 MSS					Güzelöz-2 MSS			
	TK-1	TK-2	GÜ1-1	GÜ1-2	GÜ1-3	GÜ1-4	GÜ1-5	GÜ2-1	GÜ2-2	GÜ2-3	GÜ2-5
% SiO_2	61,25	66,18	43,67	67,77	43,84	44,73	38,16		61,02	61,83	56,59
% TiO_2	0,47	0,37	0,85	0,46	0,44	0,61	0,50		0,39	0,41	0,34
% Fe_2O_3	5,19	2,93	6,18	4,63	5,74	5,14	4,34		2,88	3,22	2,87
% Al_2O_3	11,13	14,40	11,20	8,75	11,92	12,96	10,31		7,07	7,44	6,17
% CaO	1,1	1,28	11,14	2,23	16,69	14,86	20,69		1,90	2,49	1,81
% MgO	2,5	2,02	1,9	1,5	0,2	2,05	2,08		7,43	8,18	14,12
% Na_2O	0,28	1,04	0,41	0,34	0,06	0,70	0,57		1,99	0,75	0,96
% K_2O	1,35	3,66	1,41	1,01	2,11	1,88	1,35		0,74	0,84	0,71
% P_2O_5	0,04		2,14	0,05	0,14		0,01		0,01	0,017	0,02
% MnO	0,02	0,06	0,06	0,06	0,07	0,06	0,05		0,05	0,06	0,043
% Loss on Ignition (950°C)	16,61	8,18	19,25	13,09	15,44	17,45	22,82		16,96	15,10	16,61
Average Particle Size (μ)		0,9		15		20			0,7	2	6
Particles Smaller than 20 μ (%)		9,42		55,25		14,45			26,78	27,07	23,32
Wet Density (gr/cm^3)	2,5	2,49		2,33		2,38		2,33	2,39	2,4	
Filtration Rate (ml/min)	351		138	185							
pH	5,5	5		6,5		6			6,5	7	6

Table 5- Results of pore dimeter distribution analysis of diatomite samples in the study area (wet sieve analysis + hydrometer analysis).

Sample No.		Pebble Amount (%)	Sand Amount (%)	Silt Amount (%)	Clay Amount (%)
Güzelöz-2 MSS	GÜ2-5	2,9	35,4	36,40	25,30
	GÜ2-3	5,5	22,7	41,72	30,08
	GÜ2-2	6,5	31,5	33,29	28,71
Güzelöz-1 MSS	GÜ1-4	2,5	32,8	50,14	14,66
	GÜ1-2	0,3	23,6	40,46	35,74
Tahar MSS	TK-2	0,7	46,4	40,20	12,70

Table 6- Results of compaction analysis of diatomite samples in the study area.

Material Criteria	Technical Specification for the General Directorate of Highways (2013)	Sample No.		
		Tahar MSS	Güzelöz-1 MSS	Güzelöz-2 MSS
		TK-1	GÜ1-2	GÜ2-2
Liquid Limit (%)	ù 60	NP	NP	NP
Plasticty Index	ù 35	NP	NP	NP
Material Class	A-4	ML	ML	ML
Maximum Dry Unit Volume Weight (pdmax)(gr/cm^3) / % Optimum Woter Content (wopt)	ñ 1,450	0,992 / 50,3	0,972 / 49	1,00 / 54,6
% # 200 Subsieve		52,9	59,5	62
Organic Material Prediction	Not Organic Material (lighter than color no-1)	Darker than light color no-1	Darker than light color no-1	Darker than light color no-1

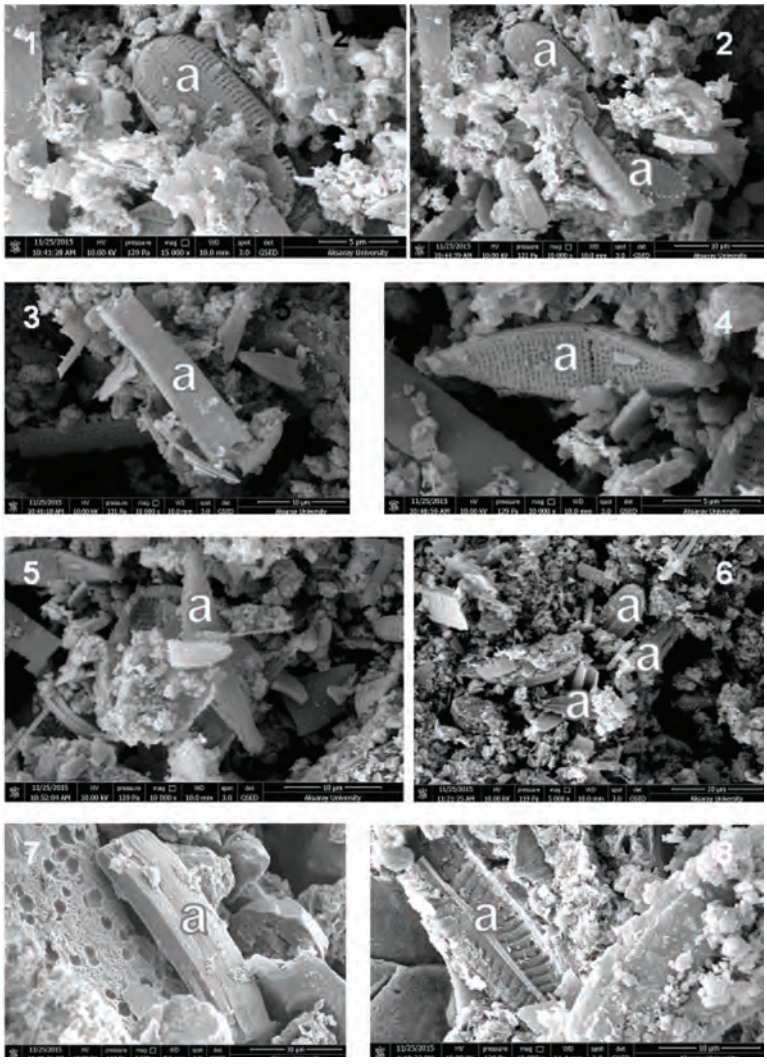

Figure 5- SEM photomicrographs from diatomite samples taken from the study area a- pennate diatom forms. 1- 6 from sample GÜ1–2, 7 from sample GÜ1–3 and 8 from sample TK–1.

1) were subjected to palynological analysis in the laboratory of the Geological Engineering Department of the Dokuz Eylül University (İzmir).

Evaluating the results of analyses performed, the physicochemical characteristics of diatomites in the study area were determined and the results were compared with standard analysis values of different diatomites which are used both in the world and in Turkey (Tables 7-9).

3. Regional Geology and Stratigraphy

The study area is located in the CVP which developed due to the closure of the Eurasian and the African-Arabian plates according to Batum (1978). The CVP is NE-SW extensional, 250-300 km long, 60 km wide and 1400-1500 m above the sea level (Aydar et al., 2012). The CVP is restricted by the Central Anatolian Fault in the east, by the Tuz Lake Fault Zone in the west and by the Central Kızılırmak Fault Zone in the north. In the south, the Derinkuyu Fault and the Niğde Fault Zones are located. The rock units of the CVP are divided into three groups as; the volcanic complexes, the volcanoclastic rocks and the cinder cone areas. Volcano-sedimentary rocks located in the region are discordant with the Paleozoic-Cretaceous basement rocks of the Niğde Massive in the south and the Kırşehir Massive in the north (Schumacher et al., 1990; Toprak, 1996). The sediments, which are located in the Ürgüp Basin, were defined as the Ürgüp formation by Pasquare (1968) and Viereck-Goette et al. (2010). According to the radiometric data these rocks were dated as the late Miocene-Pliocene (Besang et al., 1977). This stratigraphical level corresponds to the Massinian Salinity Crisis which formed in the late Miocene. The deposits of the Ürgüp formation, which

Table 7- Comparison of the analysis values of diatomites in the study area with the analysis values of different diatomites used in different areas in the World. 1) Spain, raw, 2) France, calcined, beer filtration, 3) İtalya, raw, light construction material, 4) Germany, fertilizer carrier, 5) Germany, calcined, beer filtration, 6) Germany, calcined and filler material, 7) Brazil, insulation material, 8) USA, calcined, filtering diatomite, 9) Basalt-Nevada (modified from Uygun, 2001; 8. Five years development plan, 2001).

	1	2	3	4	5	6	7	8	9	Tahar MSS	Güzelöz-1 MSS	Güzelöz-2 MSS
%SiO_2	86,6	89,9	88,6	69,7	82,9	92,1	86	88,4	83,13	61,25 - 66,18	38,16 - 67,77	56,59 - 61,83
% TiO_2	0,1	0,6	0,2	0,4	0,1	0,2	0,7	0,2		0,47 - 0,37	0,44 - 0,85	0,34 - 0,41
% Fe_2O_3	0,4	2,2	8,3	3,1	10,1	0,6	1,4	1,5	2	5,19 - 2,93	4,34 - 6,18	2,87 - 3,22
% Al_2O_3	0,9	3,9	1,7	4,9	1,8	2,6	9,4	4,1	4,60	11,13 - 14,40	8,75 - 12,96	6,17 - 7,44
% CaO	5,2	0,8	0,6	0,4	2,5	0,1	0,1	0,6	2,50	1,1 - 1,28	2,23 - 20,69	1,81 - 2,49
% MgO	0,6	0,2	0,1	0,1	0,4	0,1	0,4	0,8	0,64	2,5 - 2,02	0,2 - 2,08	7,43 - 14,12
% Na_2O	0,2				1,1	0,9		2,9	1,60	0,28 - 1,04	0,34 - 0,70	0,75 - 1,99
% K_2O	0,1	0,2	0,3	1,2	0,3	0,3	0,2	0,7		1,35-3,66	1,01 - 2,11	0,71 - 0,84
% P_2O_5	0,2	0,3	0,1	0,1	0,1	0,1		0,2		0,04	0,01 - 2,14	0,01 - 0,02
% V_2O_5 + TiO_2									0,23			
% MnO										0,02 - 0,06	0,05 - 0,07	0,043- 0,06
%Loss on Ignition (850°C)	5,5	0,7	0,5	19,1	0,5	3	2	0,3	5,30	16,61 - 8,18	13,09 - 22,82	15,10 - 16,96
Average Particle Size (µ)	3,4	2,7	2,4	4,7	4,5	1,2	2,7	14,7		0,9	15 -20	0,7 - 6
Particles Smaller than 20 µ (%)	3,7	0,8	1,6	23,4	6,8	2,7	4,6	31,8		9,42	24,45 - 55,25	23,32 - 27,07
Wet Density (gr/cm^3)	4,17	2,44	2,44	3	2,17	2,50	2,08	2,44		2,5 - 2,49	2,33 - 2,38	2,33 - 2,4
Filtration Rate (ml/min)	12	52	30	18	70	10	50	740		351	138 - 185	
pH	8,3							8,8		5,5 - 5	6 - 6,5	6,5 - 7
Quartz (%)				18								

Table 8- Comparison of the analysis values of diatomites in the study area with the analysis values of various commercial diatomite used in Turkey. 1) Kayseri, 2) Kayseri-Hırka, 3) Aydın-Dedeler, 4) Ürgüp, 5) Denizli-Sarayköy, 6) Kütahya-Alayunt, 7) Balıkesir-Balya, 8) Aksaray-Belisırma, 9) Afyon-İncehisar, 10) Afyon-Tınaztepe, 11) Ankara-Kızılcahamam, 12) Çankırı-Çerkeş (modified from Sarız and Nuhoğlu, 1992; Aruntaş et al., 1998; Bozkurt, 1999; Nuhoğlu and Elmas, 1999; Bentli, 2001; 8. Five years development plan., 2001; Uygun, 2001).

	1	2	3	4	5	6	7	8	9	10	11	12	Tahar MSS	Güzelöz-1 MSS	Güzelöz-2 MSS
%SiO_2	90,2	90,0	89,6	88,7	85,0	84,42	79,5	72,1	81,86	84,15	88,62	83,25	61,25 - 66,18	38,16 - 67,77	56,59 - 61,83
% TiO_2	0,1	0,2	0,01	0,06	0,01	0,05		0,2					0,47 - 0,37	0,44 - 0,85	0,34 - 0,41
% Fe_2O_3	0,8	1,1	1,4	3,38	2,8	1,55	3,24	4,4	1,87	3,36	0,57	1,20	5,19 - 2,93	4,34 - 6,18	2,87 - 3,22
% Al_2O_3	3,3	2,9	2,1	1,11	5,0	5,02	6,14	13,1	3,91	4,50	3,30	5,50	11,13 - 14,40	8,75 - 12,96	6,17 - 7,44
% CaO	0,6	0,7	0,01	1,35	0,01	0,96	1,2	0,9	0,86	1,07	0,74	1,30	1,1 - 1,28	2,23 - 20,69	1,81 - 2,49
% MgO	0,3	0,5	1,2	0,38	1,6	0,74	1,19	3,7	0,15	1,03	0,80	0,90	2,5 - 2,02	0,2 - 2,08	7,43 - 14,12
% Na_2O		0,6	0,06	0,28	0,13	0,62		0,17		0,47	0,77	0,95	0,28 - 1,04	0,34 - 0,70	0,75 - 1,99
% K_2O	0,1	0,2	0,15	0,32	0,4	0,60		1,9		0,44	0,71	1,30	1,35-3,66	1,01 - 2,11	0,71 - 0,84
% P_2O_5			0,01	0,42	0,01			0,1					0,04	0,01 - 2,14	0,01 - 0,02
% MnO													0,02 - 0,06	0,05 - 0,07	0,043- 0,06
% Loss on Ignition (850°C)	4,2	4,6	5,5	2,7	5,25	6,09	8,35	4,2	11,31	4,92	4,24	5,54	16,61 - 8,18	13,09 - 22,82	15,10 - 16,96
Average Particle Size (µ)	3,3					10					145	90	0,9	15 -20	0,7 - 6
Particles Smaller than 20 µ (%)	2,7												9,42	24,45 - 55,25	23,32 - 27,07
Wet Density (gr/cm^3)	2,94					1,9 2,4					1,95	1,90	2,5 - 2,49	2,33 - 2,38	2,33 - 2,4
Filt. Rate (ml/min)	48												351	138 - 185	
pH		8									7,87	7,28	5,5 - 5	6 - 6,5	6,5 - 7
Color						White					White	White	White	White	White

Table 9- Comparison of the analysis values of diatomites in the study area with standardly accepted values of diatomites used in various branches of industry for commercial purposes (modified from Özbey and Atamer,1987; Açıkalın, 1991; Aruntaş et al., 1998; Bentli, 2001).

	Commercial	Diatomites used in Turkey Sugar Factories	Filter		Filling			Abrasive Car Polish	Regulatory Fertilizer	Tahar MSS	Güzelöz-1 MSS	Güzelöz-2 MSS
			Wine	Sugar	Paper	Dye	Rubber					
%SiO_2	>85	87,3								61,25 - 66,18	38,16 - 67,77	56,59 - 61,83
% Fe_2O_3	<1,5	1,95								5,19 - 2,93	4,34 - 6,18	2,87 - 3,22
% Al_2O_3	<5	3,23								11,13 - 14,40	8,75 - 12,96	6,17 - 7,44
% CaO	<1	1,09								1,1 - 1,28	2,23 - 20,69	1,81 - 2,49
% MgO	<0,5	0,45								2,5 - 2,02	0,2 - 2,08	7,43 - 14,12
% Na_2O	<1	0,47								0,28 - 1,04	0,34 - 0,70	0,75 - 1,99
% K_2O	<1	0,44								1,35-3,66	1,01 - 2,11	0,71 - 0,84
% Loss on Ignition (850°C)	< 6	4,43								16,61 - 8,18	13,09 - 22,82	15,10 - 16,96
Average Particle Size (µ)			2,5	22		6,8	5,1	5,5		0,9	15 -20	0,7 - 6
Wet Density (gr/cm^3)			2,3	2	2,4	2,2	2,8	2,4	1,7	2,5 - 2,49	2,33 - 2,38	2,33 - 2,4
Water Absorption (%)	>280 >180											
pH		4,49	7	10	7	10	7	9,4	7	5,5 - 5	6 - 6,5	6,5 - 7
Moisture (%)	<15											
Color	White	Dirty White	Pink	White	Grey	White	Pink	White	Yellowish	White	White	White

intercalates with lake and river sediments, has a wide spread within the CVP. The Formation is divided into three groups as; the Bayramhacılı, Mustafapaşa and Kışladağ members (Viereck-Goette et al., 2010; Göz et al., 2014).

From bottom to top, the stratigraphical units observed in the study area are; the late Cretaceous plutonic rocks (Ortaköy Granitoid), the late Miocene-Pliocene Bayramhacılı Member of the Ürgüp formation (consisting of Cemilköy, Tahar and Kızılkaya ignimbrites), Kışladağ Member and Quaternary alluvial (Figure 6).

Plutonic Rocks (Ortaköy Granitoid): It was defined by Atabey et al. (1987) considering the exposures around Ortaköy. It is formed from the rocks of gabbro, banded gabbro, porphyry diorite, monzonite, syenite, monzodiorite, leucogranite and porphyry granite (Atabey, 1989). Gabbro, gneiss and marble enclaves are present in granites, and occasionally consist of coarse orthoclase crystals. Granite and granodiorites are occasionally disintegrated and mylonitized and cut metamorphic units. Ortaköy Granitoid corresponds to the Baranadağ Pluton (Seymen, 1981). Granitic rocks outcropping in the region were dated as; the Paleocene by Seymen (1981), the late Cretaceous by Ataman (1972) and the early Cenomanian by Göncüoğlu (1986) in the Niğde Massive.

Ürgüp Formation: The age of the formation is late Miocene-Pliocene (Besang et al., 1977) based on radiometric data. It outcrops between the Kırşehir Massive and Taurides and covers a wide area in Kayseri, Nevşehir and Niğde in the Central Anatolia. The volcanosediments, which consist of pyroclastics and ignimbrites with different particle sizes in terrigenous facies, were defined as the Ürgüp formation by Pasquaré (1968). The Ürgüp formation is divided into Bayramhacılı, Mustafapaşa and Kışladağ members (Viereck-Goette et al., 2010; Göz et al., 2014).

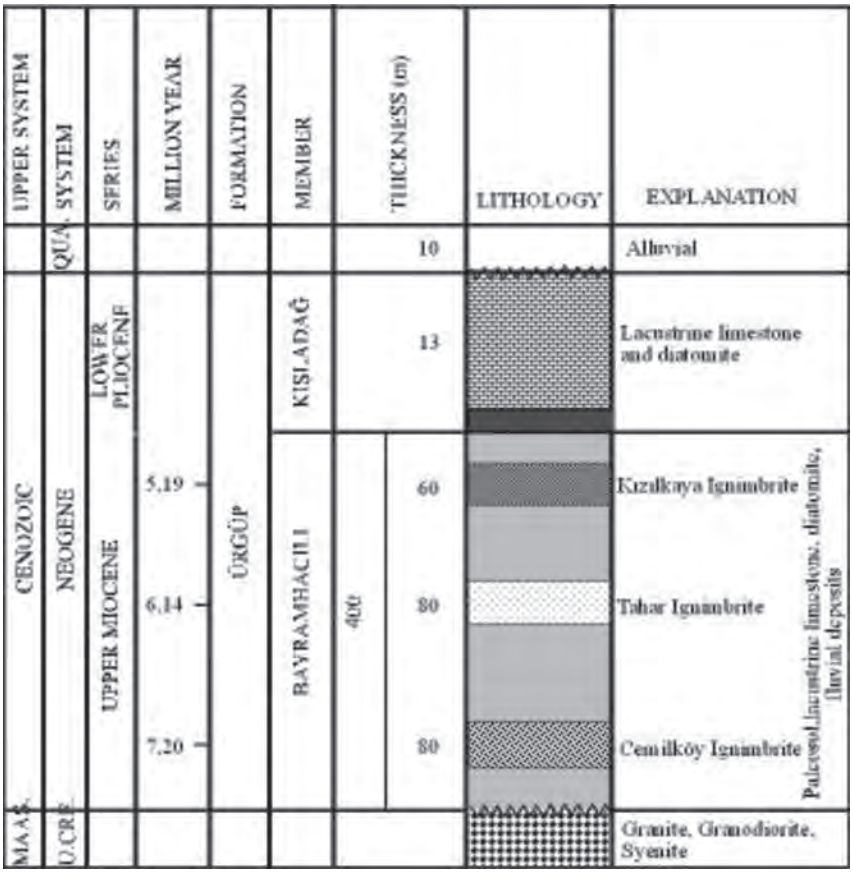

Figure 6- Unscaled generalized stratigraphic section of the study area (modified from Pasquaré, 1968; MTA, 1989; Viereck-Goette et al., 2010; Göz et al., 2014).

Bayramhacılı Member: It is formed by the river and lake sediments consisting of conglomerate, sandstone, limestone, marl and diatomites. In the Bayramhacılı member, ignimbrites (the oldest ignimbrite, Güvercinlik, Kavak, Zelve, Sarımadentepe (or Sofular), Cemilköy, Tahar, Gördeles and Kızılkaya ignimbrites), basalts (Domsa, Topuzdağı and Çataltepe basalts) and lava layers are observed (Atabey, 2013). Kavak, Zelve and Sarımadentepe ignimbrites are white-gray, however the Cemilköy ignimbrite is light gray in color. The pink colored Tahar ignimbrite, light gray colored Gördeles ignimbrite and red-pink colored Kızılkaya ignimbrite are widespread (Le Pennec et al., 1994). The age of ignimbrites in the Ürgüp formation were detected as 9-1 my based on $^{40}Ar/^{39}Ar$ and U-Pb dating (Aydar et al., 2012; Lepetit et al., 2014).

Kışladağ Member: This unit is Pliocene and formed by the lacustrine limestone and diatomites. Within lacustrine limestones of the unit the ostracod and gastropod fossils are present (Viereck-Goette et al., 2010; Göz et al., 2014).

Quaternary Alluvials: The alluvials in the study area are formed by pebble, sand, silt and soil which are observed on branches of the Kızılırmak River (Atabey, 2013).

4. Stratigraphical Sections Measured in the Study Area

Total of three stratigraphical sections one of which was from the Bayramhacılı member (Tahar section TS) and other two sections within the Kışladağ Member (Güzelöz-1 (GÜ1) and Güzelöz-2 (GÜ2)) were measured from the late Miocene-Pliocene lacustrine sediments of the Ürgüp formation (Figures 1-4).

Tahar Measured Stratigraphical Section (TS): TS was measured as 50 m thick in the 1/25000 scale Kayseri K33-c3 sheet (with starting coordinates (in UTM) of (Y): 0672742, (X): 4269675, (Z): 1320 m and end coordinates (UTM) of (Y): 0672625, (X): 4269784, (Z): 1370 m) and the total of 7 samples were taken along the section. TS begins with light brown paleosol layer at the bottom then continues with 2 m thick white diatomite layers above. Diatomite layers are then overlain by 12 m thick light gray tuffites, 50 cm thick fluvial conglomerate, 22,5 cm thick light gray tuffites. Tuffites are then overlain by 50 cm thick fluvial conglomerate, 50 cm thick light brown-cream colored paleosol, 1 m thick light gray tuffites and by 50 cm thick light brown chert layer. Above the cherts, nearly a 2 m thick pink colored Tahar ignimbrite are observed. This ignimbrite is then overlain by a 3 m thick white tuffites, 50 cm thick light brown cherts, 2 m thick light gray tuffites, then 1,5 m thick light gray Gördeles ignimbrite and 1,5 m thick white tuffites take place. In the uppermost part, the red-pink colored Kızılkaya ignimbrite is observed (Figures 1 and 2).

Güzelöz-1 (GÜ1) Measured Stratigraphical Section*:* The GÜ1 section was measured as 36 m thick in the 1/25.000 scale Kayseri L33-b2 sheet (with starting coordinates (in UTM) of (Y): 0672269, (X): 4251444, (Z): 1525 m. and end coordinates (UTM) of (Y): 0672278, (X): 4551642, (Z): 1561m.) and total of 5 samples were taken along the section. The GÜ1 section begins with 1,5 m thick light gray tuffites at the bottom and then 4,5 m thick white diatomite layer takes place. Diatomites are then overlain by a 17 m thick light gray tuffite layer. Tuffites are overlain by the light colored fluvial conglomerates, light brown paleosol layer and light gray sandstones, each layers as being in one meter thickness. The sandstones are then overlain by a 9 m thick white diatomites. Nearly one meter thick, light gray sandstones form the uppermost layer of the section (Figures 1 and 3).

Güzelöz-2 (GÜ2) Measured Stratigraphical Section: The GÜ2 section was measured as 4 m. thick in the 1/25000 scale Kayseri L33-b2 sheet (with starting coordinates (in UTM) of (Y): 0670066, (X): 4249808, (Z): 1514 m (UTM); and end coordinates of (Y): 0670099, (X): 4249776, (Z): 1518 m) and total of 4 samples were taken along the section. The GÜ2 section begins with 50 cm thick light brown paleosol layer at the bottom. Then from bottom to top, it is overlain by a 10 cm thick light brown chert layer, a 90 cm thick white colored tuffite layer, 10 cm thick light brown-cream colored second chert layer. The cherts are then overlain by a 40 cm thick debris and nearly 1 m thick white colored diatomite layer. Diatomites are then overlain by a 20 cm thick light colored paleosol layer and by a 25 cm thick second diatomite layer, 30 cm thick tuffites and by a 25 cm thick third diatomite layer. The white colored limestones form the uppermost part of the section (Figures 1 and 4).

It was observed that diatomites in three locations were light, relatively soft and easily disintegrated in hand.

5. Results of the Analyses of Samples Collected From the Study Area

In order to determine the physicochemical characteristics and the areas of use of diatomites in the study area, SEM photos of diatomite assemblages, which are consisted by three samples (TK–1, GÜ1–2 and GÜ1–3) taken from the study area, were evaluated and noticed that they were generally formed from coarse, long and coarse pennate diatom forms (Figure 5).

As a result of the XRD analysis (qualitative) applied on samples, it was noticed that results of analysis of samples collected from both locations (Tahar and Güzelöz) showed differences from each other. It is observed that clay, pyroxene minerals and amorphous materials were present in addition to quartz and crystobalite minerals in samples collected from the Tahar section (TS). However; the calcite, quartz, crystobalite, feldspar mineral, clay, mica, amphibole minerals and amorphous materials are observed in samples collected from the Güzelöz-1 (GÜ1) section (Table 1).

As a result of total porosity, whiteness, water and acid insoluble matter amount analyses applied on the samples, it was determined that results of analysis for the samples collected from both locations (Tahar and Güzelöz) showed resemblances with each other. The have high porosity between 57-60%, whiteness values varying between 80,45-84,79, acid insoluble matter in 74,20-84,20%, water insoluble matter in 99.80%, and thus they are inert against chemical reactions. The colors of diatomites can be white, light yellow, beige, and gray. However, the ones rich in organic matter can be in colors closer to green, brown and black (Cummins, 1960; Uygun, 1976; Brady and Clauser, 1991). Diatomites in the study area are in white color, so it can be said that they are pure and do not contain any organic material (Table 2).

As a result of specific surface area, pore volume and pore size analyses the following results were obtained as; the multi-point BET values between 5,427 e+01 - 6,771 e+01 m^2/g, t-method outer surface area values between 2,922 e+01 - 4,787 e+01 m^2/g, t-method micropore surface area values between 2,505 e+01 - 1,984 e+01 m^2/g, NLDFT cumulative surface area values between 4,047 e+01 - 5,160 e+01 m^2/g, t-method micropore volume values between 1,148 e-02 - 8,515 e–02 cc/g, t-method micropore surface area values between 2,505 e+01 - 1,984 e+01 m^2/g, HK method cumulative pore volume values between 2,966 e-02 - 3,751 e–02 cc/g, SF method cumulative pore volume values between 2,975 e-02 - 3,762 e–02 cc/g, NLDFT method cumulative pore volume values between 4,630 e-02 - 5,580 e–02 cc/g, HK method pore radius values between 2,158 e-04 µ, SF method pore radius values between 2,261 e-04 µ and NLDFT pore radius values between 5,888 e-04 µ -1,448 e-03 µ, for diatomites collected from the study area. Thus, they have a high porosity (Table 3).

As a result of XRF, loss on ignition, particle size, density and pH analyses applied; it was detected that diatomite samples collected from the Tahar locality contained 61,25 - 66,18% SiO_2, 0,37 - 0,47% TiO_2, 2,93 – 5,19% Fe_2O_3, 11,13 - 14,40% Al_2O_3, 1,1 - 1,28% CaO, 2,5 - 2,02% MgO, 0,28 - 1,04% Na_2O, 1,35 - 3,66% K_2O, 0,04% P_2O_5, 0,02 - 0,06% MnO. Loss on ignition values for the samples in 950°C vary between 8,18-16,61% and the average particle size values are 0,9 µ. The percentage of particle size values smaller than 20 µ are 9,42%, so the particle size of the samples are smaller than the sand size. It was also detected that their densities varied between 2,49-2,5 g/cm^3 and the infiltration rate values were 351 ml/min. The pH values vary between 5 - 5,5, reflecting the acidic environment (Tables 4-9).

The diatomite samples collected from the Güzelöz-1 locality contain 38,16 - 67,77% SiO_2, 0,44 - 0,85% TiO_2, 4,35 - 6,18% Fe_2O_3, 8,75 - 12,96% Al_2O_3, 2,23 - 20,69% CaO, 0,2 - 2,08% MgO, 0,06 - 0,70% Na_2O, 1,01 - 2,11% K_2O, 0,01- 2,14% P_2O_5, 0,05 - 0,0%7 MnO. Loss on ignition values of the samples in 950°C vary between 13,09-22,82%. Average particle size values are in between 15-20 µ and the percentage of the particle sizes smaller than 20 µ is between 14,45-55,45%, so the particle size of samples are below the sand size. Their densities are 2,33-2,38 g/cm^3, the infiltration rates vary between 138-185 ml/min, and pH values are in between 6,5-6. The samples reflect the acidic environment (Table 4-9).

Diatomite samples collected from the Güzelöz-2 locality contain 56,59 - 61,83% SiO_2, 0,34 - 0,41% TiO_2, 2,87 - 3,22% Fe_2O_3, 6,17 - 7,44% Al_2O_3, 1,81 - 2,49% CaO, 7,43 - 14,12% MgO, 0,75 - 1,99% Na_2O, 0,71- 0,84% K_2O, 0,01 - 0,02% P_2O_5, 0,043 – 0,06% MnO. Loss on ignition values of the samples in 950°C vary between 15,10-16,96%. Average particle size

values are in between 0,7-6 μ and the percentage of the particle sizes smaller than 20 μ is between 23,32-27,07%, so the particle sizes of samples are below sand size. Their densities are 2,33-2,40 g/cm^3 and pH values are in between 6-7. The samples reflect the acidic and neutral environments (Table 4-9).

As a result of compaction analyses applied in order to determine whether diatomite samples in the study area could be utilized in road fillings the following values were detected; the maximum dry unit volume weight (pdmax) 0,992 g/cm^3 and optimum water content (wopt) 50,3% for samples TK1-2 collected from the Tahar locality; the maximum dry unit volume weight (pdmax) 0,972 g/cm^3 and optimum water content (wopt) 49,0% for samples GÜ1-2 collected from the Güzelöz-1 locality; the maximum dry unit volume weight (pdmax) 1.00 g/cm^3 and optimum water content (wopt) 54,6% for samples GÜ2-2 collected from the Güzelöz-2 locality. Again, as a result of the organic material detection test carried out on the same samples the solution colors were detected as darker than no-1 light color due to the correlation made by using the No: 815 Hellige Tester Color Plate at the end of 24 hours (Table 6).

Besides; there were not observed any palynomorph as a result of palynological analysis performed on diatomite samples which were collected from each three section in the study area.

6. Discussion and Results

Diatomites are amongst the natural raw materials required by the modern technology and have a wide area of use such as; filter, filling and insulating material, structural material, absorbent, carrier, catalyzer and catalyzer carrier, silicate manufacturing, mild abrasive and cleaner. The diatomite is used in the industry as the filtration material (58%), filling material (19%), insulating material (4%) and in different purposes (19%) (Uygun, 2001).

According to the data obtained in analyses, which were carried out on diatomite samples in the study area, the areas of utilization were given below.

For commercial purposes: The standard values of diatomites, which are commercially used in different areas in the world contain; 69,7 – 92,1% SiO_2, 0,1 – 0,7% TiO_2, 0,4 – 10,1% Fe_2O_3, 0,9 – 9,4% Al_2O_3, 0,1 – 5,2% CaO, 0,1 – 0,8% MgO, 0,2 – 2,9% Na_2O, 0,1 – 1,2% K_2O and 0,1 – 0,3% P_2O_5 and have loss on ignition values between 0,3-19,1% (in 850°C), the average particle size between 1,2-14,7 μ, wet density values between 2,08-4,17 g/cm^3, filtration rate values between 10-740 ml/min and pH values between 8,3-8,8 (reflecting the basic environment) (Uygun, 2001; 8th Five Years Development Plan, 2001) (Table 7). The diatomites in the study area have low SiO_2 values (between 38,16-67,77% in three locations), Al_2O_3 (11,13 – 14,40% in the Tahar location and 8,75 – 12,96% in the Güzelöz–1 location), MgO (0,2 – 14,12% in three locations), K_2O (1,35 – 3,66% in the Tahar location and 1,01 – 2,11% in the Güzelöz–1 location), CaO (2,23 – 20,69% in the Güzelöz–1 location), P_2O_5 (0,01 – 2,14% in the Güzelöz–1 location) and high loss on ignition values (in 950°C) (13,09 – 22,82% in the Güzelöz–1 location). They also have low pH values (in between 5-7) in three locations reflecting both the acidic and neutral environments. Therefore, they are not compatible with standard analysis values for diatomites which are commercially used in different areas in the world (Tables 4 and 7).

The diatomites commercially used in Turkey contain 72,1 – 90,2% SiO_2, 0,01 – 0,2% TiO_2, 0,2 – 4,4% Fe_2O_3, 1,11 – 13,1% Al_2O_3, 0,01 – 1,35% CaO, 0,15 – 3,7% MgO, 0,06 – 1,7% Na_2O, 0,1 - 1,30% K_2O and 0,01 – 0,42% P_2O_5 and have the loss on ignition values between (in 850 °C) 2,7 – 11,31%, the average particle sizes between 3,3 – 145 μ, the wet density values between 1,9 - 2,94 g/cm^3, the infiltration rate values at 48 ml/min and pH values between 7,28-8 (reflecting the basic environment) (Sarıiz and Nuhoğlu, 1992; Aruntaş et al., 1998; Bozkurt, 1999; Nuhoğlu and Elmas, 1999; Bentli, 2001; 8th Five Years Development Plan, 2001; Uygun, 2001). Low SiO_2 values for diatomites in the study area (38,16 – 67,77% in three locations), Al_2O_3 (11,13 – 14,40% in the Tahar location), TiO_2 (0,34 – 0,85% in three locations), Fe_2O_3 (4,34 – 6,18% in the Güzelöz–1 location), CaO (2,23 – 20,69% in the Güzelöz–1 location; 1,81 – 2,49% in the Güzelöz–2 location), MgO (7,43 – 14,12% in the Güzelöz–2 location), K_2O (1,35 – 3,66% in the Tahar location; 1,01 – 2,11% in the Güzelöz–1 location), P_2O_5 (0,01 – 2,14% in the Güzelöz–1 location), high loss on ignition values (in 950°C) (13,09 – 22,82% in three locations) and low pH values (between 5 – 7 in three locations) (reflecting acidic and basic environments) indicate that these diatomites are incompatible with those of commercially used in Turkey (Tables 4 and 8).

Besides; diatomites, which are generally used for commercial purposes should contain > %85 SiO_2, <%1,5 Fe_2O_3, < %5 Al_2O_3, < % 1 CaO, < % 0,5 MgO, < %1 Na_2O, < %1 K_2O, with loss on ignition values (in 850°C) < %6, water absorption values > % 280 and > % 180, moisture ratios < % 15 and their colors should be white according to Özbey and Atamer, 1987 and Aruntaş et al., 1998 (Table 9). The diatomites located in the study area in three locations have low SiO_2 values (38,16 – 67,77%), Fe_2O_3 (2,87 – 6,18%), Al_2O_3 (6,17 – 14,40%), CaO (1,1 – 20,69%), MgO (0,2 – 14,12%), Na_2O (0,06 – 1,99%), K_2O (0,71 – 3,66%) and high loss on ignition values (in 950°C) (8,18 – 22,82%) though they have white colors. Their color is the only one resemblance with the standard characteristics of commercially raw diatomites. Therefore, they are not suitable for commercial use (Tables 2, 4 and 9).

For filtering material: In order diatomites to be used as filtering material, they should at least contain 80-84% SiO_2 (Işık, 1984, Bozkurt, 1999). For filters, the diatomites which form from pure pennat and coarse diatom genus and species are preferred (Uygun, 2001). The diatomites in the study area seem to suitable for filter use with their high porosities (57 – 60%, pore volumes 1,148 e-02 – 8,515 e-02 cc/g, pore sizes 1,448 e-03A – 5,888 e-04A), resistances against chemical effects (amount of acid-insoluble matter 74,20 - 84,20%, amount of water-insoluble matter 99,80%), purities (whiteness values range between 80,45- 84,79) and were formed from long, coarse diatom genus and species. However, the diatomites in three locations do not seem to be compatible for use in filters with their low SiO_2 values (38,16-67,77%). In order diatomites in the study area to be used in filters, they should be subjected to SiO_2 enrichment (Tables 2-4) (Figure 5).

In wine filtering processes, the pink colored diatomites with particle size of 2,5 µ, wet density of 2,3 g/cm^3, pH value of 7 are used (Açıkalın, 1991) (Table 9). The particle sizes of diatomites in the study area to be high (between 6-20 µ), pH values to be relatively low (between 5-7) and their colors to be white, and only the wet density values in three locations (2,33-2,5 g/cm^3) indicate that they are suitable for the use in wine filtering processes, however the remaining values do not seem to be proper (Tables 4 and 9).

However, in sugar filtering the white colored diatomites with particle size of 22 µ, wet density of 2 g/cm^3, pH value of 10 are used (Açıkalın, 1991) (Table 9). Besides; when looking at diatomite values used in sugar factories in Turkey it is seen that they contain 87,3% SiO_2, 1,95 Fe_2O_3%, 3,23 Al_2O_3%, 1,09 CaO%, 0,45 MgO%, 0,47 Na_2O%, 0,44 K_2O%, have loss on ignition values of 4,43% (in 850°C) and pH values between 4,49-10 with their dirty white colors (7th Five Years Development Plan, 1996; Bentli, 2001) (Table 9). The white diatomite samples collected from three locations in the study area, the average particle sizes (between 15-20 µ) and wet density values (2,33-2,38 g/cm^3) of diatomites in the Güzelöz-1 location and only the wet density values (2,33-2,4 g/cm^3) of diatomites in the Güzelöz-2 location indicate that they are suitable for sugar filtering processes. However, pH values (between 5-7) of diatomites collected from three locations and the average particle sizes of diatomites in Tahar and Güzelöz-2 locations (0,7-6 µ) to be in low values show that they are not appropriate for sugar filtering processes. Besides, the white color, Na_2O values (0,28-1,99%) and pH values (between 5-7) of diatomites in the study area show compatibility with the diatomites currently used in sugar factories in Turkey, however the other characteristics do not display any compatibility (Tables 2, 4 and 9).

It is known that the diatomites, which are used in France, Germany and the USA for filtering material, contain 82,9 – 89,9% SiO_2, 0,1 – 0,2% TiO_2, 1,5 – 4,0% Fe_2O_3, 1,8 – 4,1% Al_2O_3, 0,2 – 0,8% CaO, 0,2 – 0,8% MgO, 1,1 – 2,9% Na_2O, 0,2 – 0,7% K_2O, 0,1 – 0,3% P_2O_5. Their loss on ignition values range between 0,3-0,7% (in 850°C), with the average particle size of 2,7-14,7 µ, wet densities of 2,17-2,44 gr/cm^3, filtering rate values of 52-740 ml/min and pH values of 8.8 (basic) (Uygun, 2001) (Table 7). As diatomite samples collected from three locations in the study area have low SiO_2 (38,16 – 67,77%), TiO_2 (0,37 – 0,85%), Fe_2O_3 (2,87 – 6,18%), Al_2O_3 (6,17 – 14,40%), CaO (1,1 – 20,69%), MgO (0,2 – 14,12%), K_2O (0,71 – 3,66%), P_2O_5 (0,01 – 2,14%) and high loss on ignition values (8,18-22,82%) (in 950°C), it is seen that they do not show any similarities with diatomites which are used as filtering material in France, Germany and the USA except for the NaO content (0,06 – 1,99%), wet density (2,33 – 2,5 g/cm^3) and filtration rate values (138 – 351 ml/min) (Tables 4 and 7).

For filling material: In diatomites, which are used for filling material, the purity, whiteness, fine grain texture, high porosity, lightness, resistance against chemicals, ability for heat, sound and electricity insulations and high absorption characteristic are

required and should contain minimum 70-80% SiO_2 (Mete, 1982). As diatomites located in three locations have low organic matter ratios, white colors (whiteness value: 80,45-84,79), fine grain textures (particle sizes between 0,7-20 μ), high porosities (57-60%), with pore volumes of 1,148 e-02 – 8,515 e-02 cc/g), pore sizes of 1,448 e-03A – 5,888 e-04A, densities of 2,33-2,5 g/cm^3, high resistance against chemical effects (the amount of acid insoluble matter 74,20-84,20%, the amount of water insoluble matter 99,80%) and high absorption characteristic (specific surface area values 1,984 e+01 – 6,771 e+01 m^2/g), they seem to be suitable for use as the filling material except for their low SiO_2 values. In order that these diatomites in the study area could be used as the filling material they should be subjected to SiO_2 enrichment (Tables 2-4).

In dye sector, 200-300 μ particle size diatomite is generally added into dye in 2-3 % ratio and used. Table 9 shows the complete criteria list of diatomites used in dye, rubber and paper sectors. In the dye sector, the white colored diatomite with the average particle size of 6,8 μ, wet density of 2,2 g/cm^3 and pH value of 10; in the rubber sector pink diatomite with the average particle size of 5,1 μ, wet density of 2,8 g/cm^3 and pH value of 7 (neutral) and in the paper sector gray diatomite with the wet density of 2,4 g/cm^3 and pH value of 7 are preferred (Türkiye Diatomit Envanteri, 1968; Özbey and Atamer,1987; Açıkalın, 1991; 7th Five Years Development Plan, 1996; Bentli, 2001). Only the diatomites located in the Güzelöz-2 location in the study area are suitable for use as the filling material in rubber and paper sectors (with the average particle sizes of 0,7-6 μ, the wet densities of 2,39-2,4 g/cm^3 and pH values of 6-7). Diatomites located in three locations are not suitable for use in dye sector in terms of pH values (5-7). Besides, diatomites located in the Tahar and Güzelöz-1 locations are not also suitable for use in rubber and paper sectors in terms of pH values (5-6,5) (Tables 4 and 9).

When we have a look at the diatomite values, which are used for filling material in Germany, it seen that they contain 92,1% SiO_2, 0,2% TiO_2, 0,6% Fe_2O_3, 2,6% Al_2O_3, 0,1% CaO and MgO, 0,9% Na_2O, 0,3% K_2O and 0,1% P_2O_5 and have loss on ignition value around 3% (in 850°C), average particle size value of 1,2 μ, wet density value of 2,50 g/cm^3 and the filtration rate value of 10 ml/min (Uygun, 2001) (Table 7). The analysis results of diatomites collected from three locations in the study area do not show any compatibility with diatomite values, which are used as the filling material in Germany, except for NaO (0,06-1,99) and wet density values (2,33-2,5 g/cm^3) (Tables 4 and 7).

According to the Tecnical Specification of the General Directorate of Highways (2013) , the dry unit volume weight (pdmax) of the material to be used in the road filling should be equal or greater than 1450 g/cm^3 and should not contain any organic matter (Table 10). The maximum dry unit volume weight (pdmax) of the sample TK1-2 collected from the Tahar location in the study area is 0,992 g/cm^3 with the optimum water content (wopt) value of 50,3%; the maximum dry unit volume weight (pdmax) of the sample GÜ1-2 collected from the Güzelöz-1 location is 0,972 g/cm^3

Table 10- Properties of the material to be used in the road fill according to the Technical Specifications of Highways (2013). in various branches of industry for commercial purposes (modified from Özbey and Atamer,1987; Açıkalın, 1991; Aruntaş et al., 1998; Bentli, 2001).

Material Criteria	Technical Specification for the General Directorate of Highways (2013)
Liquid Limit (%)	≤ 60
Plasticity Index	≤ 35
Material Class	A-4
Maximum Dry Unit Volume Weight (pdmax)(gr/cm^3) / % Optimum Water Content (wopt)	≥ 1,450
% # 200 Subsieve	
Organic Material Prediction	Not Organic Material (lighter than light color-1)

with the optimum water content (wopt) value of 49% and the maximum dry unit volume weight (pdmax) of the sample GÜ2-2 collected from the Tahar location in the study area is 1 g/cm^3 with the optimum water content (wopt) value of 54,6%. Again, as a result of organic material detection test carried out on the same samples the solution colors were detected as darker than no-1 light color due to the correlation made by using the No: 815 Hellige Tester Color Plate at the of 24 hours. Samples collected from three locations have fragility and fragmentation characteristic as they have low maximum dry unit volume weight (≥ 1,450 g/cm^3) and as a result of organic matter test they are also darker than the light color number #1. Therefore they do not have compatibility for use as the filling material (Tables 6 and 10).

For construction material: There is also a possibility to benefit from the low quality diatomites in the area of construction material (Türkiye Diyatomit Envanteri, 1968; 8th Five Years Development Plan, 2001; Uygun, 2001). Therefore, the diatomites in the study area can be used as the construction material.

Besides, the diatomite can also be used as a mineral additive matter in the portland cemented concretes; for this, the sum of SiO_2+Al_2O_3+Fe_2O_3 should be minimum 70% and the loss on ignition should be maximum 10% (Aruntaş et al., 1998). The SiO_2+Al_2O_3+Fe_2O_3 sums and the loss on ignition values (in 950°C) of diatomites for the Tahar, Güzelöz-1 and Güzelöz-2 locations in the study area are respectively given as follows; for Tahar location 75,31-85,77% and 8,18-16,61%; for Güzelöz-1 location 51,54-86,91% and 15,10-16,96%; and for Güzelöz-2 location 65,63-72,49% and 1309-22,82%. So; diatomite samples collected from three locations cannot be used as the mineral additive matter without applying a direct process in portland cemented concretes as they have loss on ignition values higher than the standards (Table 4).

When we have a look at the analysis values of diatomites, which are used as the construction material in Italy, it is seen that they contain 88,6% SiO_2, 0,2% TiO_2, 8,3% Fe_2O_3, 1,7% Al_2O_3, 0,6% CaO, 0,1% MgO and P_2O_5 and 0,3% K_2O and have loss on ignition value of 0,5% (in 850°C), the average particle size values of 1,6 µ, the wet density values of 2,44 g/cm^3, the filtration rates of 30 ml/min (Uygun, 2001) (Table 7). The results of analyses of diatomites collected from three locations in the study area do not show any similarity with the analysis values of diatomites, which are used as the construction material in Italy, except for the Fe_2O_3 (% 2,87 – 6,18) and wet density values (2,33 – 2,5 gr/cm^3) (Tables 4 and 7).

As carrier: The diatomites, which are preferred as the carrier in fertilizer industry, are required to have a wet density of 1,7 g/cm^3 and pH of 7 (Özbey and Atamer, 1987; Açıkalın, 1991; 7th Five Years Development Plan, 1996; Bentli, 2001) (Table 9). Diatomites in the study area are not suitable for use as the carrier with wet density values of 2,33-2,5 g/cm^3 and pH values between 5-7 (Tables 4 and 7).

The values of diatomites, which are used as the fertilizer carrier in Germany, contain 69,7% SiO_2, 0,4% TiO_2 and CaO, 3,1% Fe_2O_3, 4,9% Al_2O_3, 0,1% MgO and 1,2% K_2O and have the loss on ignition value of 19,1% (in 850°C), the average particles size value of 4,7 µ, the wet density value of 3 g/cm^3, the filtration rate value of 18 ml/min and contain 18% quartz (Uygun, 2001) (Table 7). The results of analyses of diatomites collected from three locations do not show any similarity with diatomite values, which are used as the fertilizer carrier in Germany, except for the values of Fe_2O_3 (2,87 – 6,18%), K_2O (0,71 – 3,66%), the loss on ignition (8,18 – 16,96%) and the wet density (2,33 – 2,5 g/cm^3) (Tables 4 and 7).

In silicate manufacturing: The diatomites located in the study area can be used in silicate manufacturing with SiO_2 values of 38,16-67,77% as there was not given any limiting value (Table 4).

As mild abrasive and cleaner: The average particle size, wet densities and pH values of diatomites, which are preferred as the abrasive in auto polishes are; 5,5 µ, 2,4 g/cm^3 and 9,4, respectively (Özbey and Atamer, 1987; Açıkalın, 1991; 7th Five Years Development Plan, 1996; Bentli, 2001) (Table 9). The diatomites in the study area have low pH values (between 5-7), therefore they are not suitable for use as the mild abrasive and cleaner (Tables 4 and 9).

As insulating matter: The diatomites should contain minimum 94% SiO_2 in order to be used as the insulating matter (Bentli, 2001). Diatomites located in the study area are not suitable for use as the insulating matter as they have low SiO_2 content (38,16-67,77%) (Table 4).

The diatomites, which are used as the insulating matter in Brasil, contain 86% SiO_2, 0,7% TiO_2, 0,1% Fe_2O_3 and CaO, 9,4% Al_2O_3, 0,4% MgO and 0,2%

K_2O and have the loss on ignition of 2% (in 850°C), the average particle size of 2,7 μ, the wet density of 2,08 g/cm^3, the infiltration rate of 50 ml/min (Uygun, 2001) (Table 7). The results of analyses of diatomites collected from three locations do not show any similarity with diatomite values used as the insulating matter in Brasil except for the values of TiO_2 (0,34 – 0,85%) and Fe_2O_3 (2,87 – 6,18%) (Tables 4 and 7).

Acknowledgement

This study was produced from the project made within the scope of Scientific Research Project (BAP) numbered as 2015/94 and supported by the Scientific Research Projects Coordination Unit of the Aksaray University. The authors thank to the Scientific Research Projects Coordination Unit of the Aksaray University for their contributions.

References

Açıkalın, N. 1991. Dünyada ve Türkiye'de Diyatomit. Maden Tetkik ve Arama Genel Müdürlüğü, Ankara.

Aruntaş, H.Y., Albayrak, M., Saka, H.A., Tokyay, M. 1998. Ankara-Kızılcahamam ve Çankırı-Çerkeş yöresi diyatomitlerinin özelliklerinin belirlenmesi. Turkey Journal of Engineering and Environmental Science 22, 337–343.

Atabey, E. 1989. 1/100000 ölçekli açınsama nitelikli Türkiye jeoloji haritaları serisi, Kayseri-H19 paftası. Maden Tetkik ve Genel Müdürlüğü, Ankara.

Atabey, E. 2013. Kapadokya, Nevşehir ili ve ilçeleri, jeolojisi, maden ve enerji kaynakları, tıbbi jeolojik unsurları ve halk sağlığı. Nevşehir Belediyesi Yayını 400s.

Atabey, E., Papak, İ., Tahran, N., Aksu, B., Taşkıran, M., Adil, A. 1987. Ortaköy (Niğde)-Tuzköy (Nevşehir)-Kesikköprü (Kırşehir) yöresinin jeolojisi raporu. Maden Tetkik ve Arama Genel Müdürlüğü Rapor No: 8156 (unpublished).

Atabey, E., Tarhan, N., Yusufoğlu H., Canpolat, M. 1988. Hacıbektaş, Gülşehir, Kalaba (Nevşehir)-Himmetdede (Kayseri) arasının jeolojisi raporu. Maden Tetkik ve Arama Genel Müdürlüğü Rapor No: 8523 (unpublished).

Ataman, G. 1972. A Study on the radiometric age of Cefalikdağ, one of the granite-granadiorite bodies outcropping on the south-east Ankara, Hacettepe Science and Engineering Journal 2, 44-49.

Aydar, E. 1992. Edude volcano-structurale et magmatologique du strato-volcan Hasandağı (Anatolie Centrale-Turquie). These de Doctorat, Universitute Blaise Pascal, 200 pp. France.

Aydar, E., Gourgaud, A. 1998. The geology of Mount Hasan stratovolcano, Central Anatolia, Turkey. Journal of Volcanology and Geothermal Research 85, 129–152.

Aydar, E., Çubukçu, H.E., Şen, E., Akın, L. 2012. Central Anatolia'n Plateau, Turkey: incisin and paleoaltimetry recorded from volcanic rocks. Turkish Journal of Earth Sciences 22, 739–746.

Ayhan, A., Papak, İ., Atabey, E. 1988. Göçlük (Misli)-Derinkuyu-Sulucaova civarının jeolojisi raporu. Maden Tetkik ve Arama Genel Müdürlüğü Rapor No: 8345 (unpublished).

Ayrancı, B. 1970. Orta Anadolu'da Kayseri civarında Erciyes Volkanik Bölgesi'nin kantitatif incelemelerine istinaden petrolojisi ve jeolojisi. Maden Tetkik ve Arama Genel Müdürlüğü Dergisi 74, 13–24.

Batum, I. 1978. Geology and petrography of Acıgöl and Göllüdağ volcanics at southwest of Nevşehir Central Anatolia (Turkey). Yerbilimleri 4, 1–2, 70–88.

Beekman, P.H. 1966. The Pliocene and Quarternary volcanism in The Hasandağ-Melendizdağ Region, Maden Tetkik ve Arama Genel Müdürlüğü Doğal Kaynaklar ve Ekonomi Bülteni 66, 99–106.

Besang, C., Eckhardt, F.J., Harre, W., Kreuzer, H., Müller, P. 1977. Radiometrische altersbestimmungen an Neogen Eruptivgesteinen der Türkei. Geol. Jb. B-25, 3-36.

Bentli, İ. 2001. Kütahya-Alayunt diyatomit cevherinin zenginleştirilebilirliğinin araştırılması. 4.Endüstriyel Hammaddeler Sempozyumu, 2001, Köse, H., Arslan, V., Tanrıverdi, M. (Ed.), İzmir, 119-126.

Bozkurt, R. 1999. Diyatomit, Türkiye'de Endüstriyel Mineraller Envanteri. İstanbul Maden İhracatçıları Birliği (İMİB), Yurt Madenciliği Geliştirme Vakfı Önal, Y., Özpeker, G., (Ed.), İstanbul, 42-47.

Brady, G. S., Clauser, H. R. 1991. Materials Handbook. Mc Graw-Hill.

Cummins, A.B. 1960. Diyatomite, Industrial Minerals and Rocks (Nonmetallics other than fuels). The Am. Inst. of Mining and Metallurgical Engineers, New York.

Dhont, D., Chorowicz, J., Yürür, T., Froger, J.L., Köse, O., Gündoğdu, N. 1998. Emplacement of volcanic vents and geodynamics of Central Anatolia, Turkey. Journal of Volcanology and Geothermal Research 85, 33–54.

Dönmez, M., Türkecan, A., Akçay, E.A. 2003. Kayseri-Niğde-Nevşehir yöresi Tersiyer volkanikleri raporu. Maden Tetkik ve Arama Genel Müdürlüğü Rapor No: 10575.

Duritt, T. H., Brenchley, P.J., Gökten, Y. E., Francaviglia, V. 1995. Late Quaternary rhyolitic eruptions from the Acıgöl complex, Central Turkey. Journal of Geological Society of London 152, 655–667.

Froger, J.L., Lenat, J.F., Chorowicz, J., Le Pennec, J.L., Bourdier, J.L., Köse, O., Zimitoğlu, O., Gündoğdu, N.M., Gourgaud, A. 1998. Hidden calderas evidenced by multisource geophysical data; example of Cappadocian Calderas, Central Anatolia. Journal of Volcanology and Geothermal Research 85, 99–128.

Gevrek, A. İ., Kazancı, N. 1994*a*. Occurrence and evolution of Narköy maar in SE Cappadocia. AVCE, 1994, Ankara.

Gevrek, A.İ., Kazancı, N. 1994*b*. Material-rich and poor maars with examples from Central Anatolia, Turkey. AVCE, 1994, Ankara.

Göncüoğlu, M. C. 1986. Orta Anadolu Masifi'nin güney ucundan jeokronolojik yaş bulguları. Maden Tetkik ve Arama Genel Müdürlüğü Dergisi 105–106, 27–28.

Göncüoğlu, M.C., Toprak, V. 1992. Neogene and Quaternary volkanism of Central Anatolia: a volcano structural evoluation. Bulletin de la Section de Volcanologie 26,1–6.

Güner, Y., Emre, Ö. 1983. Erciyes Dağı'nda Pleyistosen buzullaşması ve volkanizma ile ilişkisi. Jeomorfoloji Dergisi 11, 23–34, Ankara.

Gürel, A., Yıldız, A. 2006. Diatom communities, lithofacies characteristics and paleoenvironmental interpretation of Pliocene diyatomite deposits in the Ihlara-Selime plain (Aksaray, Central Anatolia, Turkey). Journal of Asian Earth Science 30, 170–180.

Gürel, A., Kadir, S. 2006. Geology and mineralogy and origin of clay minerals of the Pliocene fluvial-lacustrine deposits in the Cappadocian Volcanic Province, Central Anatolia, Turkey. Clay and Clay Minerals 54, 555–570.

Gürel, A., Kadir, S. 2008. Geology and mineralogy of Late Miocene clayey sediments in the southeastern part of the Central Anatolian Volcanic Province, Turkey. Clay and Clay Minerals 56, 3, 307–321.

Gürel, A., Kadir, S., Kerey, E.İ. 2007. Orta Anadolu volkanik bölgesinin (CAVP) güneydoğu bölümündeki erken Miyosen yaşlı killi kayaların sedimantolojisi ve mineralojisi. Kapadokya Bölgesi'nin Jeolojisi Sempozyumu, 2007, Niğde, 133–147.

Gürel, A., Kerey, E.İ., Özcan, S. 2008. Sedimentology and mineralogy of late Miocene paleosol and calcrete rich sediments in the western part of Central Anatolian Volcanic Province (CAVP), Turkey. SGEM Conference, 2008, Bulgaria, 25.

Göz E., Kadir S., Gürel A., Eren M. 2014. Geology, minerology, geochemistry, and depositional environment of a late Miocene/Pliocene fluviolacustrine succession, Cappadocian Volcanic Province Central Anatolia, Turkey. Turkish Journal of Earth Sciences 23, 386–411.

Innocenti, F., Mazzuoli, G., Pasquare, F., Radicati Di Brozolo, F., Villari, L. 1975. The Neogene calcalkaline volcanism of Central Anatolia geochronological data on Kayseri-Niğde area. Geological Magazine 112, 4, 349–360.

Işık, I. 1984. Diyatomit. Anadolu Üniversitesi, Mühendislik-Mimarlık Fakültesi, Maden Mühendisliği Bölümü, Eskişehir 81-98s.

Kadir, K., Gürel, A., Lepetit, P., Davarcıoğlu, B. 2006. Preliminary approach to mineralogy and depositional environment of upper Miocene Cappadocian Volcanic Province, Ürgüp-Başköy-Güzelöz (Nevşehir, Central Anatolia, Turkey). Fourth Mediterranean Clay Meeting, 2006, Ankara, 1, 73.

Karayolları Teknik Şartnamesi. 2013. Karayolları Genel Müdürlüğü 30s.

Kayalı, R., Gürel A., Davarcıoğlu, B., Çiftçi, E. 2005. Orta Anadolu Bölgesi'ndeki endüstriyel ham maddelerinden kil ve diyatomitlerin spektroskopik yöntemlerle nitelik ve niceliklerinin belirlenmesi. TÜBİTAK Rapor No: ÇAYDAG-101Y067, 157s.

Koçyiğit, A., Beyhan, A.A. 1998. New Intracontinental transcurrent structure: The Central Anatolian Fault Zone, Turkey. Tectonophysics 284, 317–336.

Kürkçüoğlu, B., Şen, E., Aydar, E., Gourgaud, A., Gündoğdu, M.N. 1998. Geochemical approach to magmatic evolution of Mt. Erciyes stratovolcano Central Anatolia, Turkey. Journal of Volcanology and Geothermal Research 85, 473–494.

Le Pennec, J.L., Bourdier, J.L., Froger, J.L., Temel, A., Camus, G., Gourgaud, A. 1994. Neogene ignimbrites of the Nevşehir plateau (Central Turkey): stratigraphy, distribution and source constraints. Journal of Volcanology and Geothermal Research 63.59–87.

Le Pennec, J.L., Temel, A., Froger, J.L., Şen, Ş., Gourgaud A., Bourdier, J.L. 2005. Stratigraphy and age of the Cappadocia ignimbrites, Turkey: reconciling field

constraints with paleontologic, radiochronologic, geochemical and paleonmagnetic data. Journal of Volcanology and Geothermal Research 141, 45–64.

Lepetit, P. 2010. Kohlenstoff-Isotopie miozaner Calcretes in Kappadokien (Turkei). PhD Thesis, Friedrich-Schiller-Universitat Jena, 123 pp. , Jena.

Lepetit, P., Viereck, L., Piper John, D.A., Sudo, M., Gürel, A., Çopuroğlu, İ., Gruber, M., Mayer, B., Koch, M., Tatar, O., Gürsoy, H. 2014. 40Ar/39Ar dating of ignimbrites and plinian air-fall layers from Cappadocia, Central Turkey: Implications to chronostratigraphic and Eastern Mediterranean palaeoenvironmental record. Chemie der Erde-Geochemistry 74, 471–488.

Mete, Z. 1982. Batı Anadolu Diyatomit yataklarının bazı özelliklerinin belirlenmesi ve kullanım alanlarının araştırılması. Doçentlik Tezi, Ege Üniversitesi, İzmir.

MTA. 1989. 1/100, 000 ölçekli Türkiye Jeoloji Haritası, Kayseri-H 19 Paftası. Maden Tetkik ve Arama Genel Müdürlüğü, Ankara.

Nuhoğlu, İ., Elmas, N. 1999. Alayunt diyatomit yataklarının oluşumu ve ekonomik olarak incelenmesi. l. Batı Anadolu Hammadde Kaynaklan Sempozyumu, 1999, İzmir, 82–95.

Özbey, G., Atamer, N. 1987. Kizelgur (Diyatomit) Hakkında Bazı Bilgiler. 10. Türkiye Madencilik Bilimsel ve Teknik Kongresi, 1987, Ankara, 493–502.

Özkuzey, S., Önemli, Ö., F. 1977. Acıgöl (Nevşehir) perlitlerinin petrografisi ve ekonomik jeolojisi. I. Ulusal Perlit Kongresi, 1977, Ankara, 137–147.

Pasquare, G. 1968. Geologie of the Senozoic volkanic area of Central Anatolia. Atti della Acad. No. Delince, Menorie Serie, 1968, Roma, VIII, IX, 55–204.

Pasquare, G., Poli, S., Venzolli, L., Zanchi, A. 1988. Continental arc volcanism and tectonic setting in Central Anatolia, Turkey. Tectonophysics 146, 217–230.

Sarıiz, K., Nuhoğlu, İ. 1992. Endüstriyel Hammadde Yatakları ve Madenciliği. Anadolu Üniversitesi Yayını, No:636, 452 s.

Sassano, G. 1964. Acıgöl bölgesinde Neojen ve Kuvaterner volkanizması raporu. Maden Tetkik ve Arama Genel Müdürlüğü Rapor No: 6841.

Schumacher, R., Schumacher, U.M. 1996. The Kızılkaya İgnimbrite an unusual low-aspect-ratio ignimbrite from Cappodocia, Central Turkey. Journal of Volcanology and Geothermal Rescarch 70. 107–121.

Schumacher, R., Keller, J., Bayhan, H. 1990. Depositional characteristics of ignimbrites in Cappadocia, Central Anatolia, Turkey. In: M.Y. Savaşçın and A.H. Eronat (Eds.), International Earth Science Congress on Aegean Regions, 1990, 2, 435–449.

Sekizinci beş yıllık kalkınma planı madencilik özel İhtisas komisyonu raporu, endüstriyel hammaddeler alt komisyonu genel sanayi mineralleri IV. çalışma grubu raporu, 2001. Devlet Planlama Teşkilatı, Ankara.

Seymen, İ. 1981. Kaman (Kırşehir) dolayında Kırşehir Masifi'nin stratiğrafisi ve Metamorfizması. TJK Bülteni 24–2, 7–14.

Temel, A. 1992. Kapadokya eksplosif volkanizmasının petrolojik ve jeokimyasal özellikleri. Doktora Tezi, Hacettepe Üniversitesi, 209 s. Ankara.

Temel, A., Gündoğdu, M. N., Gourgaud, A. 1998*a*. Petrological and geochemical characteristics of Cenozoic high-K calc-alkaline volcanism in Konya, Central Anatolia, Turkey. Journal of Volcanology and Geothermal Research 85, 327–354.

Temel, A., Gündoğdu, M.N., Gourgaud, A., Le Pennec, J. L. 1998*b*. Ignimbrites of Cappadocia Central Anatolia, Turkey petrology and geochemistry. Journal of Volcanology and Geothermal Research 85, 447–471.

Toprak, T. 1996. Kapadokya Volkanik Çöküntüsü'nde gelişmiş Kuvaterner yaşlı havzaların kökeni, Orta Anadolu. 30. Yıl Sempozyumu, 1996, Trabzon, 327–329.

Toprak, V. 1998. Vent distribution and its relation to regional tectonics, Cappadocian Volcanics, Turkey. Journal of Volcanology and Geothermal Research 85, 55–67.

Türkiye Diyatomit Envanteri, 1968. Maden Tetkik ve Arama Enstitüsü 138, Ankara.

Uygun, A. 1976. Geologie und Diyatomit - Vorkommen des Neogen - Beckens vorc Emmiler-Hırka (Kayseri-Türkei). Doktora Tezi, Bonn Üniversitesi, 137 s (unpublished).

Uygun, A. 2001. Diyatomit jeolojisi ve yararlanma olanakları. Maden Mühendisleri Odası Dergisi 15, 31–39.

Viereck-Götte, L., Gürel, A. 2003. Klima-und Vegetationswechsel dokumentiert in obermiozaenen Paläoböden Kappadokiens, Zentralanatolien', Berichte der Deutschen Mineralogischen Gesellschaft. Beihefte zum European. Beihefte zum European Journal of Mineralogy 15, 211, 211pp.

Viereck-Goette, L., Lepetit, P., Gürel, A., Ganskow, G., Çopuroğlu, İ., Abratis, M. 2010. Revised volcanostratigraphy of the upper Miocene to lower Pliocene Ürgüp formation, Central Anatolian Volcanic Province, Turkey. Special paper of the geological society of America 464, 85–112.

Yavuz-Işık N., Toprak, V. 2010. Palynostratigraphy and vegetation characteristics of Neogene continental deposits interbedded with the Cappadocia ignimbrites (Central Anatolia, Turkey). Internaional Journal of Earth Science 99, 1887–1897.

Yedinci beş yıllık kalkınma planı madencilik özel İhtisas komisyonu raporu, 1996. Asbest, bentonit, fluorit, diyatomit (kizelgur), kalsit, kıymetli ve yarı-kıymetli taşlar (süs taşları), lityum, titanyum, zirkonyum ve hafniyum. Devlet Planlama Teşkilatı, Ankara.

Yıldırım, T. , Özgür, R. 1981. Acıgöl Kalderası. Jeomorfoloji Dergisi 10, 59–70.

Yıldız, A., Gürel, A. 2005. Diatom community and palaeoenvironmental interpretation of Pleistocene-Holocene lacustrine diyatomite deposits in the Çiftlik Basin (Niğde, Central Anatolia, Turkey). 12 th RCMNS Congress, 2005, Wienna, 82.

Yıldız, A., Gürel, A., 2014. Karacaören-Ürgüp yöresi (Nevşehir) diyatomitlerinin fosil diatom topluluğu ve paleoortamsal özellikleri. 67 th Türkiye Jeoloji Kurultayı, 2014, Ankara, 748,749.

Yıldız, A., Gürel, A., Dursun, Y.G. 2016. Karacaören yöresi (Nevşehir) diyatomitlerinin fizikokimyasal özellikleri ve kullanım alanları. Maden Tetkik ve Arama Genel Müdürlüğü Dergisi 152, 67-185.

Bull. Min. Res. Exp. (2018) 157: 185-190

Bulletin of the Mineral Research and Exploration

http://bulletin.mta.gov.tr

Investigation of thermal and mechanical behavıors of construction materials obtained from some natural stone waste

Gökhan EROL[a*] and Devrim PEKDEMİR[b]

[a]*General Directorate Of Mineral Research And Explorations, Department Of Industrial Raw Materials And Ceramics Materials Reseacrh, Ankara, Turkey. orcid.org/0000-0003-1013-5542.*

[b]*General Directorate Of Mineral Research And Explorations, Department Of Industrial Raw Materials And Ceramics Materials Reseacrh, Ankara, Turkey. orcid.org/0000-0002-3347-0469.*

Research Article

Keywords:
Natural stone, granite, limestone, thermal-mechanical behavior, waste.

ABSTRACT

In this study, thermal and mechanical behaviors of composite building materials obtained from different kinds of natural stone wastes were investigated. First of all, XRD analyzes, chemical analyzes and grain size distribution analyzes were carried out to identify the natural stone wastes to be used. %60 granite (magmatic), %35 recrystallized limestone (metamorphic) and %5 pure aluminum oxide (Al_2O_3) materials were used in the prepared mixture. The prepared mixture was shaped in a steel mold sized 75x20x50 mm by adding 7% shaping water and fired at 1140°C, 1150°C and 1160°C. XRD analyzes, color determination, water absorption coefficient, bending strength, Young's Modulus, bulk density, apparent density and open porosity tests were performed on the samples obtained after the mixture was fired. According to the XRD analysis results gehlenite, anorthite and wollastonite phases were detected in the samples fired. In accordance with the results of other experiments and analysis, it is detected that bending strength, Young's Modulus and mass density values have increased, on the other hand water absorption coefficient, apparent density and open porosity values have decreased after the firing process.

Received Date: 22.04.2017
Accepted Date: 18.07.2018

1. Introduction

The increase in the structures built in the process of industrialization and urbanization in our country has increased the need for natural stone usage rapidly in recent years . To be able to meet the increased needs of building industry at home and abroad, in addition to the existing ones so many new stone quarries have been opened and natural stone workshops have been put into operation. Turkey is situated in the Alpine-Himalayan mountain range where world's richest marble quarries are found. Turkey's marble reserve potential is estimated to be 5.1 billion m^3 – 13.9 billion tons. This is about 33% of the estimated world reserve of 15 billion m^3. In this branch of the industry there are 1500 natural stone quarries, 2000 factory like workshops and about 9000 small scale workshops. In Turkey the annual natural stone production is about 11.5 million tons and plate production capacity of these processing plants is about 6.5 million m^2 (Republic of Turkey Ministry of Economy, 2016). During the process of these large numbers of natural stones, inevitably large quantities of stone wastes develop and accumulate. These stone wastes need to be economically recycled . In the 'marble quarries and factories, during the process of bridge cutting, monolizing, 'ST cutting and sizing, about 30% wastes (as much as dust wastes) develop from the bottom and side units of one block cut. The amount of wastes develop in the quarries is equal to 40% of the rock mass (Akbulut and Gürer, 2007). Only 40 marble processing plants located in the organized industrial zone in Afyonkarahisar produce annually 60.000 tons solid, and 120.000 tons aqueous marble wastes (Çelik and Tur, 2012). In the marble processing plants, during the block and plate cuts of the marbles, size

* *Corresponding author: Gökhan EROL, gokhan7erol@hotmail.com*
http://dx.doi.org/10.19111/bulletinofmre.428318

of the produced dust waste material in the colloidal form is mostly below 250 μm before grinding (Demir et al., 2008). These wastes are used in the construction industry, lime production, concrete and autoclaved aerated concrete production, ceramic-glass-paper industies, agriculture, etc. Wastes not used in such fields are deposited in the waste storing areas causing various environmental problems. There are numerous studies on the evaluation of natural stone wastes in the literature. Gürü et al. (2005) used marble dust as filling material in the polyester composites and noticed that with the increased rate of filling material mechanical qualities have improved. Filiz et al. (2010) carried out a work to produce cobblestone by using waste marble dust and concluded that the material can successfully be used to produce cobblestones. Sütçü et al. (2015) studied on producing clay brick construction material by adding waste marble dust into the substance. They reported that by adding certain amount of waste marble dust into the brick material had a positive effect on to the porosity and crystal phase developments. Bilgi et al., (2012) investigated the use of waste marble dust in brick production and stated that the use of waste marble dust in industrial brick production provides great benefits to the production, the environment and the economy of the country. Along with all these works Aliabdo et al. (2014) also investigated the use of marble wastes in cement and concrete productions and they reported that by adding certain amount of marble waste into the cement have improved the physical and mechanical quality of concrete mixture. Arel (2016) also studied on the possibility of marble waste use in cement and concrete productions and concluded that by adding less than 20% waste marble dust added to the cement mixture greatly improved the physical and mechanical qualities of the concrete produced.

2. Materials and Method

2.1. Material

In traditionally produced wall tiles, mixtures containing SiO_2-Al_2O_3-CaO are heated (fired) at 1135-1155°C temperature interval (Cengiz and Kara, 2012). To be able to use the marble wastes to produce floor and wall tiles, a mixture suitable to SiO_2-Al_2O_3-CaO system was prepared. In preparation of the mixture, raw materials of 60% granite, 35% recrystallized limestone (metamorphic) and 5% Aluminium oxide (Al_2O_3) have been used. Granitoids are the magmatic rocks rich in silica ($SiO_2 \geq$ %66), alkalines (feldspars) and poor in CaO, Fe, MgO (biotite, amphibole) (Uz, 1990). Depending upon the mineral content, granitoids display colour variations from grey-white to grey, grey green and even to brown-red. Because of their magmatic origin and chemical compositions granitoids are rocks with strong resistance to acids (Gündüz, 1995). The granite (granitoid) used in the study is from the Aksaray region, it is massive with holocrystalline grain size. Mineralogical composition is; alkaline feldspars (orthoclase, microcline), quartz, plagioclase, mica (muscovite, biotite) and small amount amphibole. Recrystallized limestones are the sedimentary rocks subjected to metamorphism under high temperature and pressure, changed to become a metamorphic rock. Lime stones are basically made of calcite mineral ($CaCo_3$) with at least 90% calcite. Depending on the mineral content, recrystallized limestone may be in various colours and they are not resistant to acids (HCl, $C_6H_8O_7$, HNO_3, H_2SO_4 etc.). The recrystallized limestone used in the study is from Amasya region. It is massive with microcrystalline grain size. Mineral content consists of carbonate minerals (calcite) and has some fossils. Aluminium oxide (Al_2O_3) used in the study has been obtained by calcination of aluminium hydroxide ($AlOH_3$) used in the Bayer process. Its Al_2O_3 ratio is about 99%. It is used in the ceramic, glass, refractory industries, grinding material production, primary aluminium production, transparent armour production, ceramic cutter production.

2.2. Method

2.2.1. Material Definition Processes

Granites and recrystallized limestone have been ground, through 0.149 mm measuring range and then sieved in dry system. Following the sieving, 3 g of sample and 0.9 g of cellulose mixture were homogenously milled for 15 minutes, then compressed into a 33 mm diameter tablet under 40 kN pressure and made ready for analysis. Prepared materials were analysed by using Panalytical XRF with TSEN 15309 wave length dispersion standards. Mineralogy of the specimens was pointed out by using XRD (Rigaku, Miniflex) with Cu Kα radiation between 20–60º angles at 2% min speed. To determine the grain size distribution of the samples used in the study, Malvern Mastersizer 2000 model instrument was used which measures with Mie dispersion principle at 0.02-2000 micron measuring range. For the grain size dispersion analyses, a suspension of 200 gr specimen were prepared and were analysed with wet system.

2.2.2. Shaping and Firing

The prepared watery mixture was mixed for 30 minutes at 180/rounds/minute speed in Fritsch brand pulveriser and a homogeneous mixture was obtained, then dried at 100°C. 7% shaping water was added to the obtained mixture then the material was placed into a steel mold 75x20x50 mm in size and it was shaped at 70 MPa single axes pressure by using German made Toni Technik Baustoffprüfsysteme GmbH, hydraulic press. The shaped material was kept 24 hours at room temperature then dried for 24 hours at 100°C in a drying oven. Dried material has been fired (heated) in a Protherm brand PLF 160/15 electrical drying oven at 1140, 1150 and 1160°C temperatures with 5°C/min. rate, then were kept in the oven for 1 hour (Figure 1).

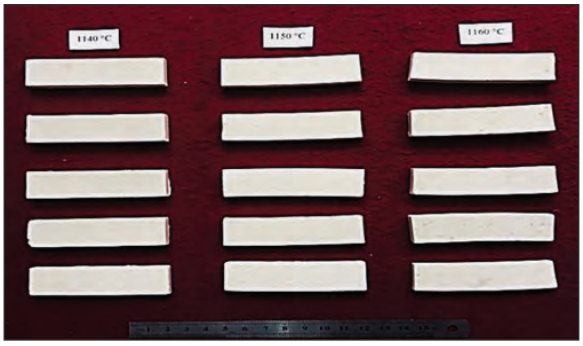

Figure 1- View of the materials fired (heated) at 1140, 1150 and 1160°C temperatures.

2.2.3. Tests Carried Out on The Fired Samples

To point out mineralogical composition of the fired material, ground specimens were studied by using Rigaku Miniflex brand diffractometer with Cu anode. X-Ray dispersion analyses of the samples were carried out. 3 points bending strength test was conducted by using German made Toni Technik Baustoffprüfsysteme universal test instrument. By using Grindo-Sonic, J. W. Lemmens Inc., St. Louis, Mo. 'Young's Modulus' measurements were made in accordance with ASTM C1259-15 standards. According to impulse excitation method in the undamaged tests samples are subjected to fixed impacts with a small hammer with fixed intervals. By using this method Young's Modulus values of the prepared samples have been determined. By using Minolta CR300 chronometer L (white), a (green) and b (blue) colour values of the fired samples have been determined. To determine water absorption coefficient of the fired samples, the samples were dried at 70°C in the oven and then weighed at 24 hours' interval and continued drying until samples came to a stable mass. Dried samples at room temperature were kept in water for 48 hours and weighed with 24 hours' interval and kept them in water until they reached to fixed saturation. Apparent density analyses of the fired samples were determined in accordance to ASTM D 5550-14 standart by using 'Micromeritics AccuPyc II 1340 helium picrometer'. To measure apparent density, in the instruments using gas replacement method inert gasses helium or nitrogen are used as replacement gases. By using Micromeritics GeoPyc 1360 instrument, mass density tests of fired samples were carried out in accordance with ASTM D 6683-14 standard. The instrument operates in Archimedes principle and uses semi liquid replacement media of non-hazardous microspheres with high degree of flow rate. In accordance to apparent and mass density tests results open pore space values have been determined.

3. Research and Findings

3.1. Characteristics of Raw Materials

Grain size distribution of the prepared mixture is given in table 1. According to these results 10% of the mixture has grain size below 2,114μm, 50% below 26.326 μm and 90% below 87.950 μm. Chemical analyses of granite and limestone are given in table 2. In the XRD chart pattern of the limestone used in the mixture shows that main mineral content of the mixture is calcite (Ka) (Figure 2). In the granite pattern of the XRD main mineral content is quarts (K) and orthoclase (O) (Figure 3).

Table 1- Grain size distribution of the mixture materials (% distribution).

Mixture	d (10) (μm)	d (50) (μm)	d (90) (μm)
Grain size	2.114	26.326	87.950

Table 2- Chemical analyses of the Granite and Limestone samples.

Samples	MgO (%)	Al_2O_3 (%)	SiO_2 (%)	CaO (%)	Fe_2O_3 (%)
Granite	0.32	14.18	73.10	1.35	1.55
Limestone	0.31	0.03	0.10	55.9	0.01

3.2. Bending Strength and Young's Modulus Tests

Three points bending and Young's Modulus test results of the samples are given in figure 4. In the

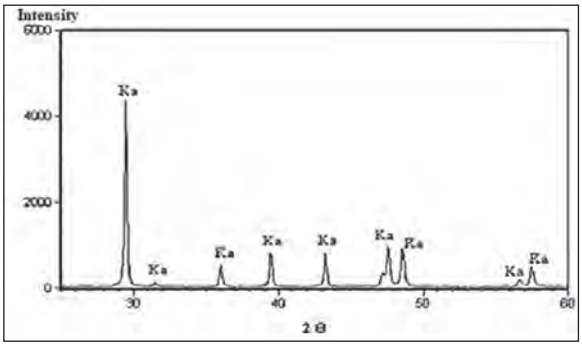

Figure 2- XRD chart view of the limestone samples used in the study (Ka= Calcite).

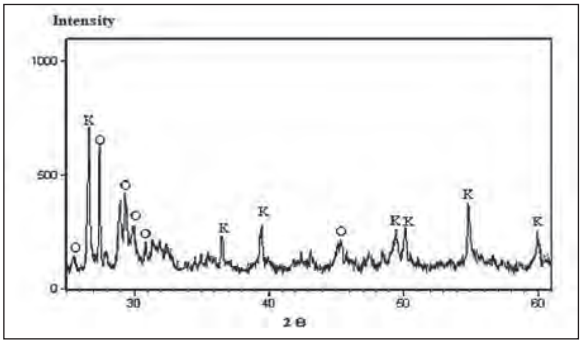

Figure 3- XRD chart view of the granite samples used in the study (K= Quarts, O= Orthoclase).

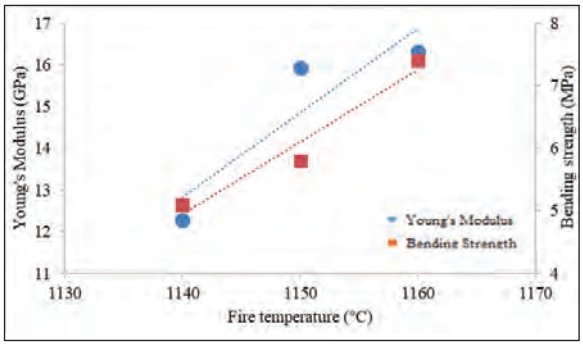

Figure 4- 3 points bending and Young Module values [Young Module, Bending strength, Firing (heating) temperature (°C)].

tests it was noticed that with the increasing firing temperature bending strength and Young's Modulus values increase accordingly.

3.3 Colour Measurement

Results of the L, a, b colour measurements of the samples heated (fired) at different temperatures are given in table 3. With increased heating, whiteness of the samples represented by 'L' value decreases. 'a' representing greenness value of the heated samples. During the heating procedure of the samples, when temperature increases from 1140ºC' to 1150ºC' green colour value increases, on the other hand when temperature goes up from 1150ºC' to 1160ºC then green colour value decreases. 'b' represent blueness value. During the heating process when temperature goes up from 1140ºC' to 1150ºC' yellow colour value decreases, when temperature goes up from 1150ºC' to 1160ºC' blue colour value increases.

Table 3- Colour measurement values of the cooked (heated) samples.

Cooking Temperature (°C)	Parameters		
	L	a	b
1140	82,95	+ 0,15	+ 11,12
1150	81,87	- 1,33	+ 10,22
1160	79,39	- 0,61	- 10,36

3.4. Water Absorption and Density Tests

According to water absorption and porosity test results, when samples are heated (fired) to 1140ºC-1150ºC and 1160ºC water absorption coefficient and porosity values decrease (Figure 5). It is considered that decrease in water absorption is related to decrease in open porosity values. According to apparent density and mass density results, when samples are fired (heated) to 1140ºC-1150ºC and 1160ºC apparent density value decreases but mass density values increases (Figure 6).

3.5. Characteristics of The Heated (fired) Samples

Calcium Carbonate ($CaCO_3$) triggers phase development reactions. At 800ºC'-900ºC' with the destruction of Calcium Carbonate (Ca CO_3 Calcium Oxide (CaO) develops. Calcium Carbonate reacts

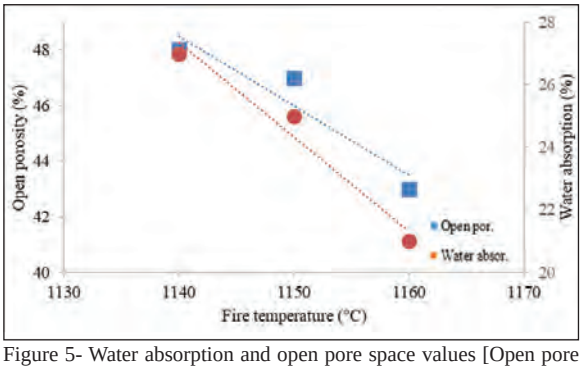

Figure 5- Water absorption and open pore space values [Open pore space, Water absorption, Firing (heating) temperature °C].

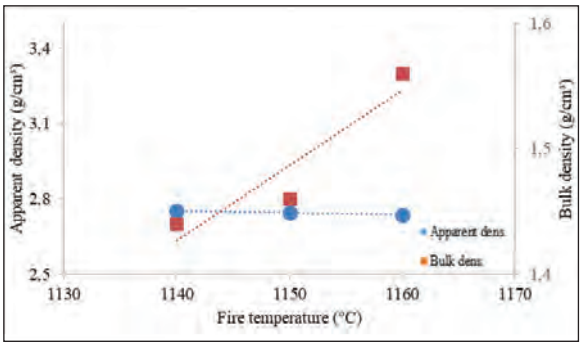

Figure 6- Visible and mass density values (Visible density, Mass density, Firing (heating) temperature °C).

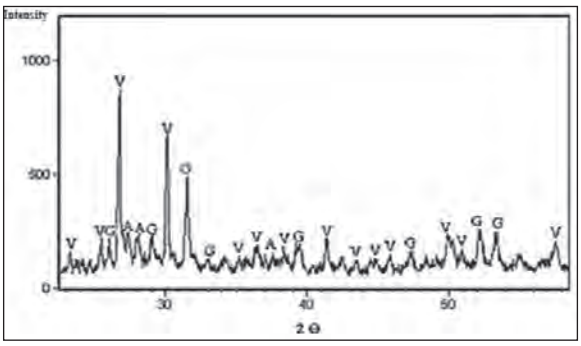

Figure 9- XRD chart view of the material fired (heated) at 1160 °C (V = Wollastonite, G = Gehlenite, A= Anorthite).

with the amorphous phase (Metakaolinite). As a result, gehlenite and anorthite like crystal phases develop (Kara vd., 2006). Figure 7 and figure 8 show XRD patterns of the samples heated (fired) to 1140ºC (Figure 7) and 1150ºC (Figure 8) indicating gehlenite and wollastonite developments. In figure 9, the XRD pattern shows that when a sample is heated to 1160ºC phases making up the structure are gehlenite, wollastonite and anorthite. It is considered that with the increase of temperature, anorthite will be more prominent.

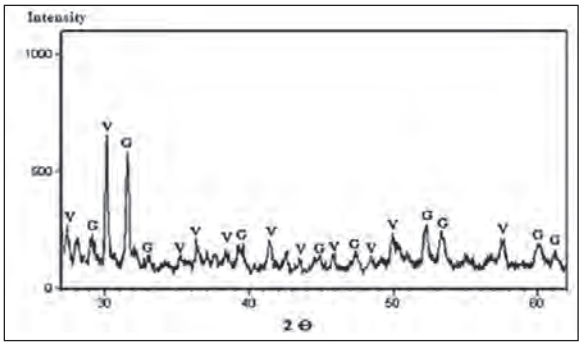

Figure 7- XRD chart view of the material fired (heated) at 1140°C (V = Wollastonite, G = Gehlenite).

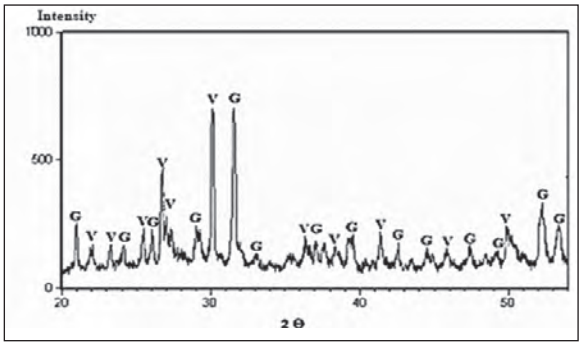

Figure 8- XRD chart view of the material fired (heated) at 1150°C (V = Wollastonite, G = Gehlenite).

4. Results

It was noticed that Despite the decline in water absorption values with the increase in cooking temperature, there was a slight change in the apparent and bulk densities; it is believed that the temperature and the total porosity are unchanged while the open pores are partially closed, but the glassy phase, which increases with temperature, does not completely fill the closed pores. In this study it was understood that changes in the bending strength and Young's Modulus are related to the main skeleton forming the structure of the mineral rather than pores forming. Measuring the frequency difference developed as a result of sound waves advancing within the material has shown that change in the Young's Modulus values with increased temperature is smaller than the changes in the bending strength values. As porosity in the materials acts as a barrier to the advancing sound waves this is in accordance with the small changes in the porosity and density and determined small increase in the Young's Modulus values with increased temperature. Bending strength is related to porosity of the material but more so to the skeleton structure. When firing temperature goes up from 1150 °C to 1160 °C Young's Modulus and bending strength values show respectively increase to 2.4% and 28%. When materials is fired (heated) at 1150 °C in respect to 1140 °C there was increase in the wollastonite and gehlenite developments. At 1160 °C along with increased wollastonite and gehlenite, anorthite also starts developing. In this study it was noticed that anorthite phase development has considerably effected the strength of the material.

The main purpose of this study is to study of the possibilities of using natural stone wastes as construction material in producing ceramic tiles. The material was evaluated in accordance with TS EN

14411 ceramic tiles standard given in Attachment L. As water absorption capacity of the tiles were above 10% at three different firing temperature, so they are in BIII[b] group but as bending strength values are smaller than 12 N/mm^2 so they are below than the values stated in standard.

In this study, it was shown that two different types natural stone wastes used in this study are not suitable to produce ceramic tiles. It has been determined that the anorthite phase, which is an important phase in the production of fast-fired ceramic tile, begins to form at 1160 ° C. However, it is considered that the other stone wastes can be used as filling substance in producing ceramic tiles.

References

Akbulut, H., Gürer, C. 2007. Use of aggregates produced from marble quarry waste in asphalt pavements. Building and environment, 42(5), 1921-1930.

Aliabdo, A.A., Abd Elmoaty, Abd Elmoaty M., Auda, E.,M. 2014. Re-use of waste marble dust in the production of cement and concrete. Constr. Build. Mater. 50, 28e41.

Arel, H. Ş. 2016. Recyclability of waste marble in concrete production. Journal of Cleaner Production, 131, 179-188.

ASTM C1259-15. 2015. Standard Test Method for Dynamic Young's Modulus, Shear Modulus, and Poisson's Ratio for Advanced Ceramics by Impulse Excitation of Vibration, ASTM International, West Conshohocken, PA.

ASTM D5550-14. 2014. Standard Test Method for Specific Gravity of Soil Solids by Gas Pycnometer, ASTM International, West Conshohocken, PA.

ASTM D6683-14. 2014. Standard Test Method for Measuring Bulk Density Values of Powders and Other Bulk Solids as Function of Compressive Stress, ASTM International, West Conshohocken, PA.

Bilgin, N., Yeprem, H. A., Arslan, S., Bilgin, A., Günay, E., Marşoglu, M. 2012. Use of waste marble powder in brick industry. Construction and Building Materials, 29, 449-457.

Cengiz, Ö., Kara, A. 2012. Tek Pişirim Duvar Karosu Bünyelerinde Borik Asit İlavesinin Sinterleme Davranışına Etkileri. Afyon Kocatepe Üniversitesi Fen Bilimleri Dergisi, 29-35.

Çelik, M. Y., Tur, Ş. 2012. Afyonkarahisar Organize Sanayi Bölgesi Doğal Taş Atık Depolama Sahasındaki Mermer Atıklarının Özelliklerinin İncelenmesi. Afyon Kocatepe Üniversitesi Fen Bilimleri Dergisi, 12-2.

Demir, İ., Başpınar, M. S., Görhan, G., Kahraman, E. 2008. Mermer tozu ve atıklarının kullanım alanlarının araştırılması. 6. Mermer ve Doğaltaş Sempozyumu, 26-27.

Filiz, M., Özel, C., Soykan, O., Ekiz, Y. 2010. Atık Mermer Tozunun Parke Taşlarında Kullanılması. Electronic Journal of Construction Technologies/ Yapi Teknolojileri Elektronik Dergisi, 6(2).

Gündüz, L. 1995. Dekoratif Taş Endüstrisinde Granit. Endüstriyel Ham Maddeler Sempozyumu, İzmir.

Gürü, M., Akyüz, Y., Emin, A. 2005. Mermer tozu/polyester kompozitlerde dolgu oranının mekanik özelliklere etkileri. Politeknik Dergisi, 8(3).

Kara, A., Özer, F., Kayacı, K., Özer, P. 2006. Development of a multipurpose tile body: Phase and microstructural development. Journal of the European Ceramic Society, 26(16), 3769-3782.

Sütçü, M., Alptekin, H., Erdogmus, E., Er, Y., Gencel, O. 2015. Characteristics of fired clay bricks with waste marble powder addition as building materials. Construction and Building Materials, 82, 1-8.

T.C. Ekonomi Bakanlığı. 2016. Doğal Taş Sektör Raporu. Ankara.

TS EN 14411. 2006. Ceramic Tiles-Definitions, Classification, Characteristics and Marking. Turkish Standards Institute.

TS EN 15309. 2008. Characterization of waste and soil - Determination of elemental composition by X-ray fluorescence. Turkish Standards Institute.

Uz B. 1990. Granit Mermer. Mermer Dergisi, Sayı 13, s 18-19.

Bull. Min. Res. Exp. (2018) 157: 191-206

Bulletin of the Mineral Research and Exploration

http://bulletin.mta.gov.tr

An ore adit planning with the help of three dimensional ore body modeling: A case study from Çulfa Çukuru Pb-Zn-Cu-Ag deposit

Sinan AKISKA[a] and Elif AKISKA[b*]

[a]*Ankara Üniversitesi Mühendislik Fakültesi Jeoloji Mühendisliği Bölümü, 06830, Gölbaşı, Ankara. orcid.org/0000-0001-8262-7349*
[b]*Ankara Üniversitesi Mühendislik Fakültesi Jeoloji Mühendisliği Bölümü, 06830, Gölbaşı, Ankara. orcid.org/0000-0002-6180-4710*

Research Article

Keywords:
Modeling, geostatistics, ore, kriging, idw.

ABSTRACT

Çulfa Çukuru Pb-Zn-Cu-Ag mineralization has occurred along the metamorphic and metamorphic-dacitic volcanic rock contacts of the Sakarya zone on the Biga Peninsula. The base metal mineralizations (Pb-Zn-Cu-Ag±Au) developed along the contact and fracture planes of these rocks can be observed as veins, lenses and disseminated ore geometries in the calc-silicate rock assemblages. Base metal mineralizations are mainly controlled lithologically and are generally associated with recrystallized limestones. In this study, the surface and the subsurface were modeled using the topographical data and the geochemical data (Pb% and Zn%) collected from 42 boreholes of Çulfa Çukuru which is located 20 km South-Southeast of Kalkım (Çanakkale). The surface and the subsurface data were interpolated by Kriging and Inverse Distance Weighted methods, respectively. The intersectional areas of Pb% and Zn% modeling data obtained from this study were determined by dividing the areas above the cut-off grade into 4 different sectors (low, intermediate, high, and very high). Using the distribution of the intersections of these sectors, the possible adit lines were determined and also an interpreted map of the adit was drawn for 450 level. This modeling study helps to plan the ore adit to be opened in a mining area. Moreover, according to the important changings that may occur in conditions (e.g. fluctuations in metal prices or decrasing-increasing costs), models can also be modified during operations.

Received Date: 26.05.2017
Accepted Date: 11.02.2018

1. Introduction

One of the most problematic issues encountered during the assessment of mineral deposits is that we do not have any observations for the entire subsurface. However, the data obtained from boreholes, well logs, and by geophysical methods can provide us some important information about underground. The use of the borehole data for the interpretation can only be achieved by combining this data with appropriate interpolation methods. That is why, the choice of an appropriate interpolation method is very important for the most accurate estimate to the real values. Using the estimation error values and the cross-validation data, the accuracy of the applied interpolation method can be checked.

With the development of computer technology, the utilization of 3D (3-dimensional) modeling of complex structures has increased considerably over the last few decades. A large amount of data can now be evaluated and interpreted together with the help of computers capable of high level processing. With the support of these studies, many problems that we encounter in during the actual work can be solved. In the geosciences, modeling studies are used frequently in the detection of subsurface location and the evaluation of natural resources such as ore deposits (Saraç and Tercan, 1996; Chen et al., 2007; Feltrin et al., 2009; Wang et al., 2011; Liu et al., 2012; Wang and Huang, 2012; Xiao et al., 2012; Akıska et al., 2013; Kashani et al., 2016), oil, natural gas and coal (Sims, 1992; Saraç et al., 2004; Kaufmann and Martin, 2008; Jian et al., 2012; Dağ and Özdemir, 2013), hydrology and hydrogeology studies (Turner, 1992; Watt et al., 2007; Ahmed, 2009; Gallerini and Donatis, 2009), determining structural elements (Renard and Courrioux 1994; de Kemp, 2000; Galera et al., 2003;

* *Corresponding author: Elif AKISKA, egunen@eng.ankara.edu.tr*
http://dx.doi.org/ 10.19111/bulletinofmre.372510

Bistacchi et al., 2008; Calcagno et al., 2008; Zanchi et al., 2009; Dhont et al., 2012), and solving road, tunnel and dam problems (Veldkamp et al., 2001; Elkadi and Huisman, 2002; Rengers et al., 2002; Özmutlu and Hack 2003; Zhu et al., 2003; Hack et al., 2006; Choi et al., 2009).

In this study, using the data from the geochemical analyses obtained from the 42 boreholes in Çulfa Çukuru Pb-Zn-Cu-Ag mineralization, the 3D subsurface modeling were made. The areas above the cut-off grade were determined and the optimal adit lines were detected using these models. These modeling studies were controlled by statistical and cross-validation techniques. The appropriate parameters can be determined by interpreting the geological, structural, and economic conditions of the deposit and using these parameters, it is possible to detect how to extract the ore from the underground in an optimal way by making a model both before and during an underground operation.

2. Regional Geology

Based on the geological studies of Biga Peninsula (Siyako et al., 1989; Okay et al., 1990, 1996, 2008; Dönmez et al., 2005, 2008; Altunkaynak and Genç 2008; Dilek et al., 2009), the basement of the area consists of Paleozoic-Mesozoic metamorphic rocks and ophiolitic rocks. The area was affected by intense magmatism from Paleocene to the end of Miocene. During this period, while many granodiorite bodies, mostly composed of granodiorite, intruded into the basement rock, these were covered with andesitic-dacitic-rhyodacitic-rhyolitic volcanic rocks unconformably. Also during this period, volcanic activity on the Biga Peninsula was often accompanied by an intense sedimentation. The last volcanic products in the area are represented by Pliocene basalts. All of the units were unconformably covered by the Plio-Quaternary fluvial units (Figure 1a).

Based on detailed studies of the Çulfa Çukuru area by Akıska (2010), Akıska et al. (2010, 2013), Akıska and Demirela (2014), the units, from older to younger, are Çamlık granodiorite (Devonian), Permo-Triassic Kalabak metamorphic rocks, including metasandstone and calc-schist lenses (Permo-Triassic), Eybek pluton (Oligo-Miocene), and Kalkim volcanics (Middle Miocene) (Akıska, 2010).

Çamlık granitoid was investigated by Okay (1990), and the ore geology of Çulfa Çukuru area was studied by Yücelay (1976), Çetinkaya et al. (1983*a*, *b*), Tufan (1993). The researchers have mentioned the existence of tectonic contact between this unit and Kalabak schist. This unit includes quartz, plagioclase, and chlorite with grey-brown color macroscopically and is cut by aplite and quartz veins (Akıska, 2010).

The Kalabak Formation was first described by Radelli (1970) as “Kalabak schists”. This formation overlays the lithological units of Precambrian Kazdağ massif with angular unconformity outside of the study area and is overlain with Çamlık granitoid in the south of the study area. This formation is also covered by Kalkım volcanics and Akköy Formation with angular unconformity in the North (Tufan, 1993). According to Yücelay (1976), Çetinkaya et al. (1983*a*, *b*), Tufan (1993), The Kalabak Formation includes clayey schist, biotite schist, sericite-chlorite schist and sericite-graphite schist with metasandstone, marble, serpentinite, and meta-diabases lenses (Akıska, 2010).

Eybek pluton (Tufan (1993), Andiç and Kayhan (1996), Pehlivan and Çetin (1997), and Genç and Altunkaynak (2007) is mainly composed of granite, quartz monzonite and granodiorite. The main minerals in the rocks are quartz, alkali feldspar, plagioclase (generally albite-andesine type), biotite, hornblende and augite, while the accessory minerals are titanite, zircon, apatite and opaque minerals (Akıska, 2010).

Kalkım volcanics (Yücelay (1976), Çetinkaya et al. (1983*a, b*), Tufan (1993), Andiç and Kayhan (1996), and Pehlivan and Çetin (1997) were correlated with the Hallaçlar Formation by Krushensky (1976) (Akıska, 2010). They are represented by rhyolite, dacite, andesite, trachyandesite, ignimbrite, tuff, and agglomerates (Figure 1a, b) (Akıska, 2010).

Çulfa Çukuru Pb-Zn-Cu-Ag mineralization is observed to be related to the metamorphic rocks and volcanic rocks belonging to the Sakarya zone in the Biga Peninsula. The base metal mineralizations at the contact between these rocks and along the cracks and fault planes are seen as veins, lenses and disseminations in the calcsilicate rock assemblages. Although the relationship between the mineralization and wall rock is seen between volcanic and metamorphic rock, the direct relationship of the volcanic rock with mineralizations is not well proven. Base metal mineralizations are mainly controlled by lithology and are generally associated with recrystallized limestone (Figure 1a, b).

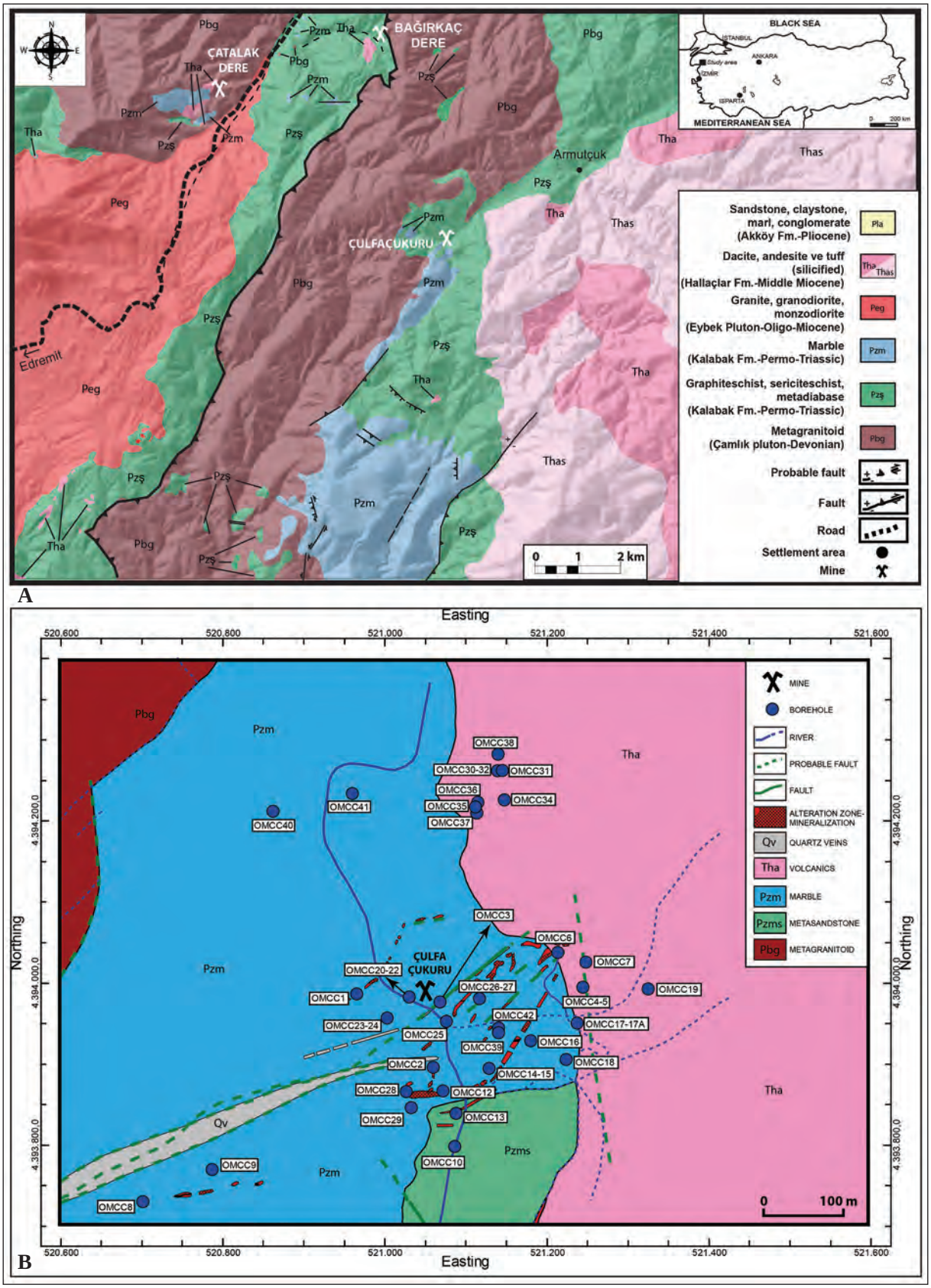

Figure 1- A) Geological map of the Çulfa Çukuru area and its surroundings (modified from Duru et al., 2007), B) Geological map (Yücelay, 1975) and the borehole locations of the Çulfa Çukuru Pb-Zn deposit (the coordinates are given in UTM coordinate system – 35N).

3. Methods

3D underground modeling studies have, in recent years, been accelerated with the development of computer technology. The complex studies can be done easily with computers. As a result, there has been a rapid increase in modeling studies, and subsurface ore modeling has become one of the most frequently used. The accurate estimation of the ore in an underground environment minimizes expenditure for mining companies, the correct orientation of the adit direction in underground mining areas playing the most important role in this cost reduction.

In earth sciences, interpolation is used for both prediction and visualization (Falivene et al., 2010). A number of algorithm have been developed to perform interpolation such as; kriging (Krige, 1951; Matheron, 1960), splines (Ahlberg et al., 1967; Mitasova and Mitas, 1993), inverse distance weighting (IDW) (Kane et al., 1982) and polynomial regression (Wang and Huang, 2012). In many cases, the kriging method is the best predictor, while in some cases IDW and spline are considered more suitable methods (Zimmerman et al., 1999; Peralvo, 2004; Chaplot et al., 2006; Binh and Thuy 2008; Shahbeik et al., (2014). In order to determine the ore distribution correctly, it is important to choose the best estimation method and thus minimizing the estimation errors.

In this study, the surface and subsurface modeling were performed using topographic data and geochemical data of Pb-Zn deposit in the Çulfa Çukuru area, respectively, and the direction of the adits to be opened underground was determined with the help of mathematical operations. The data set which was created for this study consists of topographic, borehole and geological data. For the interpolation method, Ordinary Kriging (OK) method was used and for surface modeling and IDW method were used for subsurface modeling in this study (Figure 2).

Kriging is a statistical interpolation method used to determine unknown points from the points in a data set, and is the usual name of generalized least squares regression algorithms (Cressie, 1990; Li and Heap, 2008). This algorithm is an estimation method used to detect unknown values with the help of known values and semi-variograms. The distinction from most other methods is the use of spatial continuity among the data (Wang and Huang, 2012). It also minimizes the variances among the estimations and makes the estimate in the most appropriate way at each unknown point. Kriging variance depends not

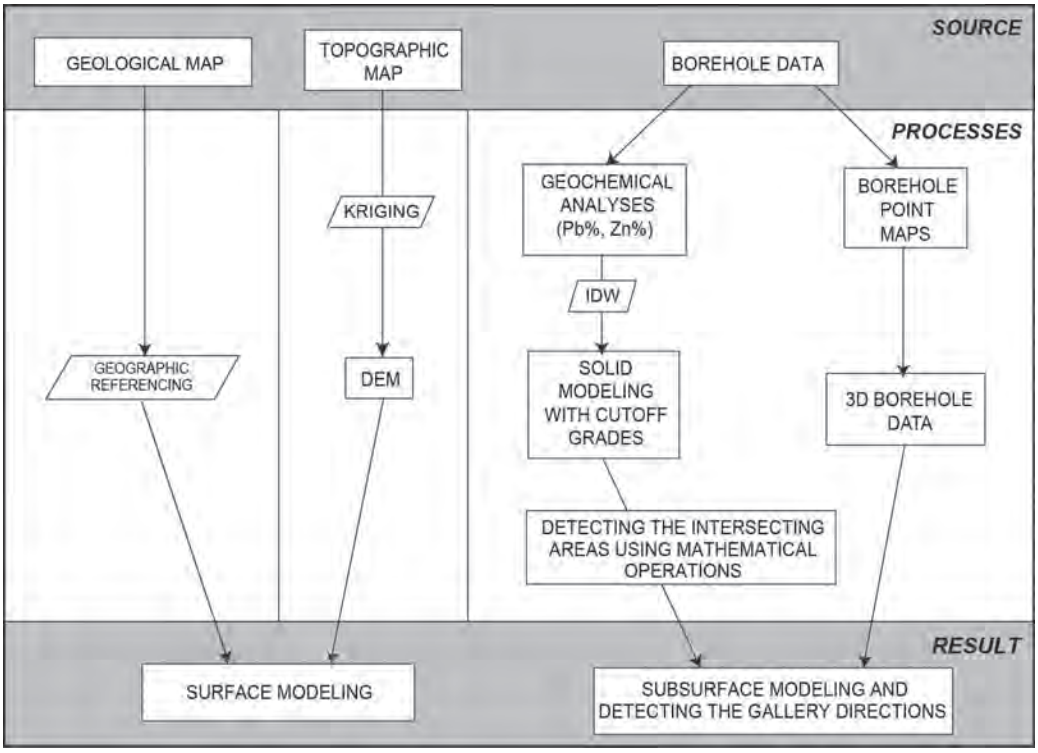

Figure 2- Flow chart of the modeling processes.

on the real values of the data, but on a function of the amount of data and the distances between the data collection points. The most important advantage of this method is the weights determined with the help of certain mathematical operations. The data is analyzed systematically and the weights are decided using semi-variograms. The availability of Kriging depends on the compatibility of the selected semi-variogram. Semi-variogram (experimental semi-variogram) is a graphic used in applied geostatistics for determining the spatial dependencies among the data (Kitanidis, 1997). A semi-variogram is calculated from the mean of all the specified separation distances and directions and half of the squared difference of z-values over all observed pairs (Wang and Huang, 2012). The accuracy rate of the data produced by the Kriging method depends on the amount of data, the frequency of the data and the accuracy of the semi-variogram (Brooker, 1986; Chaouai and Fytas, 1991). There are different Kriging techniques, OK is one of the most commonly used. The estimation of unknown values in the OK method is realized according to the assumption of the unknown-constant mean and the stationary variables. In addition, OK is a linear model based on local neighborhood structure (Tahmasebi and Hezerkani, 2010).

The IDW method uses the weights obtained from the produced inverse function depending on the distance between the sampled points and unsampled points (Li and Heap, 2008). The sampled points closer to the unsampled points are given more weight, and vice versa. According to the assumption of this method, the values belonging to unsampled points are more similar to the closer points than the farther points. IDW is a sensitive method and gives extremely accurate results for a wide range of data interpretations (Lam, 1983). The basic factor affecting the accuracy of the IDW method is the power parameter (p) in the formula. The weight decreases as the distance increases. When p value increases, the closer points get more weight and the resulting spatial interpolation is local (Isaaks and Srivastava, 1989). The most important feature of this method is that it can interpolate dispersed data in regular grids or irregularly spaced data very quickly (Li and Heap, 2008). Although the application of this method is easy, "bull's-eye" patterns can also be seen due to the concentric contours created by the IDW method (Burrough and McDonnell, 1998; Van Dijk et al., 1999; Dressler, 2009).

The neighborhood estimation is very important in terms of limiting the data used (Johnston et al., 2001). It is created by drawing a circle or ellipse around the estimated point. The values within these are then considered, while the ones outside are not taken into account (Fencík and Vajsáblová, 2006). In addition, to prevent trending in a certain direction, the circle or ellipse can be divided into sectors.

In surface modeling studies, DEM is created with the help of topographic data and a 3D surface map obtained. DEM is created by the determination of unknown values from known values with the help of interpolation methods. The IDW method is applied to the subsurface modeling. Through this method, the intersecting areas of Pb% and Zn% values above the cut-off grade were detected. The basic logic for this method is to determine the area with most potential for ore being found in the underground environment. This method of intersecting areas was applied by Akıska et al. (2013) to determine the potential ore areas in an underground environment. The study was checked both with cross-validation methods and in the field survey, the results were highly promising.

Cross-validation is a process which tests whether a study is consistent with its goals (Olea, 1999). Cross-validation is the most common method used to control the accuracy of an interpolation method (Voltz and Webster, 1990). It is a method of testing the reliability of a selected model by estimating the values at the sample points with the help of neighborhood values and comparing the predicted values using measured values (Davis, 1987). According to this method, a known value is removed from the dataset temporarily and the value of this point is estimated with the help of neighborhood data. Thus, the error between the measured value and estimated value can be observed. This process is repeated for all remaining samples (Isaaks and Srivastava, 1989). Cross-validation is very important for getting rid of unnecessary data redundancy (Olea, 1999; Webster and Oliver, 2001), and all the data obtained can be used for prediction. This method can also be used for selecting the best variogram model among the possible models and to select the lag size, also to search radius in order to minimize the kriging variance (Davis, 1987; Olea, 1999). In addition, this method helps in finding the best parameters from the test data for IDW and spline methods (Robinson and Metternicht, 2006).

Some prediction errors are used in this study. These are Mean Error (ME), Root-Mean-Square Error (RMSE), Mean Standardized Error (MSE), Root-Mean-Square Standardized Error (RMSSE), and

Average Standard Error (ASE) for surface data, Mean Error (ME) and Root-Mean-Square Error (RMSE) for subsurface data and Coefficient of Determination (R^2) for both data sets.

4. Results

4.1. Geostatistical Analysis of the Surface Data

The study area is located 13 km south of Kalkım (Çanakkale) and covers 0.7 km^2 (1000 m x 700 m). The topographic data was digitized from Yücelay (1975) and the information about the survey method was not given in the study. The distance between contour lines is 10 meters. The scale of the topographic map is 1:2000. The total number of x, y and z values is 8502. The heights are generally irregularly distributed (non-flat topography), the minimum height is 450 meters and the maximum height is 670 meters. The mean height is 547.16 meter and standard deviation is 55.824. The surface was divided into 2 x 2 x 5 m blocks (2450000 total voxels) for the modeling study.

In this study, the experimental semi-variograms were calculated in four different directions (N-S, E-W, NE-SW and NW-SE) no directional effects were observed for semi-variograms. Both the sill and range values were almost the same in the variograms calculated in all four directions. Lag size of the semi-variogram is 52.72 m and "Spherical Model" provided the best fit for the experimental semi-variogram. The range value is 517.52 m, the sill value is 5396.57 m and the nugget value is 0 m. (Figure 3a).

In this study, the neighborhood shape was selected as a circle because of the absence of any directional effects within the spatial autocorrelation of the data. The circle was divided into 4 sectors with 45^o offset. The number of neighbors was between 2 and 5.

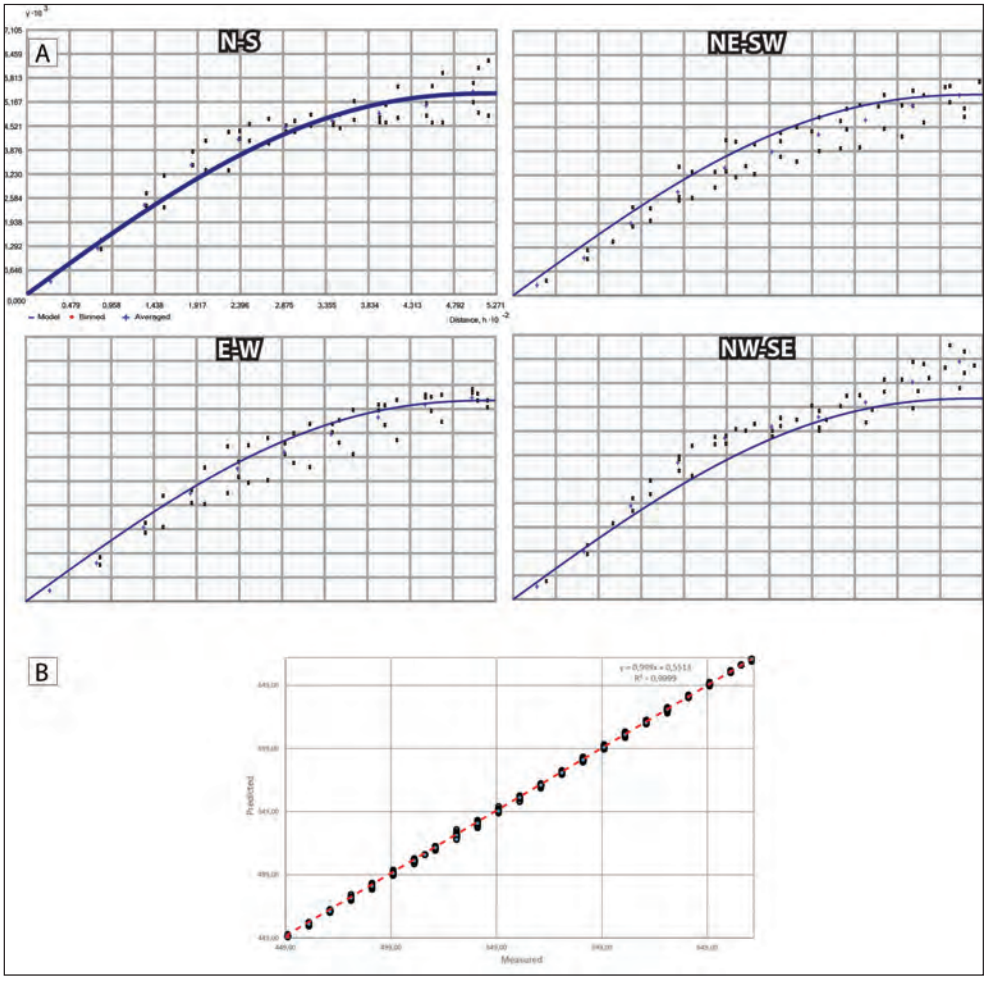

Figure 3- a. Generated experimental semi-variograms according to the directions, b. The scatter plot of the measured-predicted values of surface data.

The accuracy of surface values in this study was tested using cross-validation method (Figure 3b) and ME, RMS, ASE, MSE, and RMSS prediction errors were used to compare the models. The cross-validation method was used on all of the data (8502 points). The prediction errors in this study are 0.25 for ME, 0.52 for RMSE, 0.006 for MSE, 0.09 for RMSE and 6.22 for ASE (Table 1). To ensure that the created DEM is as accurate as possible; ME and MSE should be close to 0, RMS should have the lowest value, ASE should be close to RMS value, and RMSS value should be close to 1 (Johnston et al., 2001; Webster and Oliver, 2001; Hu et al., 2004). The results obtained from the cross-validation technique and prediction errors indicate that the prediction values similar to real values are produced as possible. The cross-validation diagram is shown in figure 3b and the prediction errors are seen in table 1. The created 3D surface map using topographic values is also shown in figure 4.

Table 1- Surface modeling prediction errors of Çulfa Çukuru area.

Samples	n	8502
Mean Error	ME	0.02485
Root-Mean-Square Error	RMSE	0.51497
Mean Standardized Error	MSE	0.00617
Root-Mean-Square Standardized Error	RMSSE	0.08534
Average Standard Error	ASE	6.21714

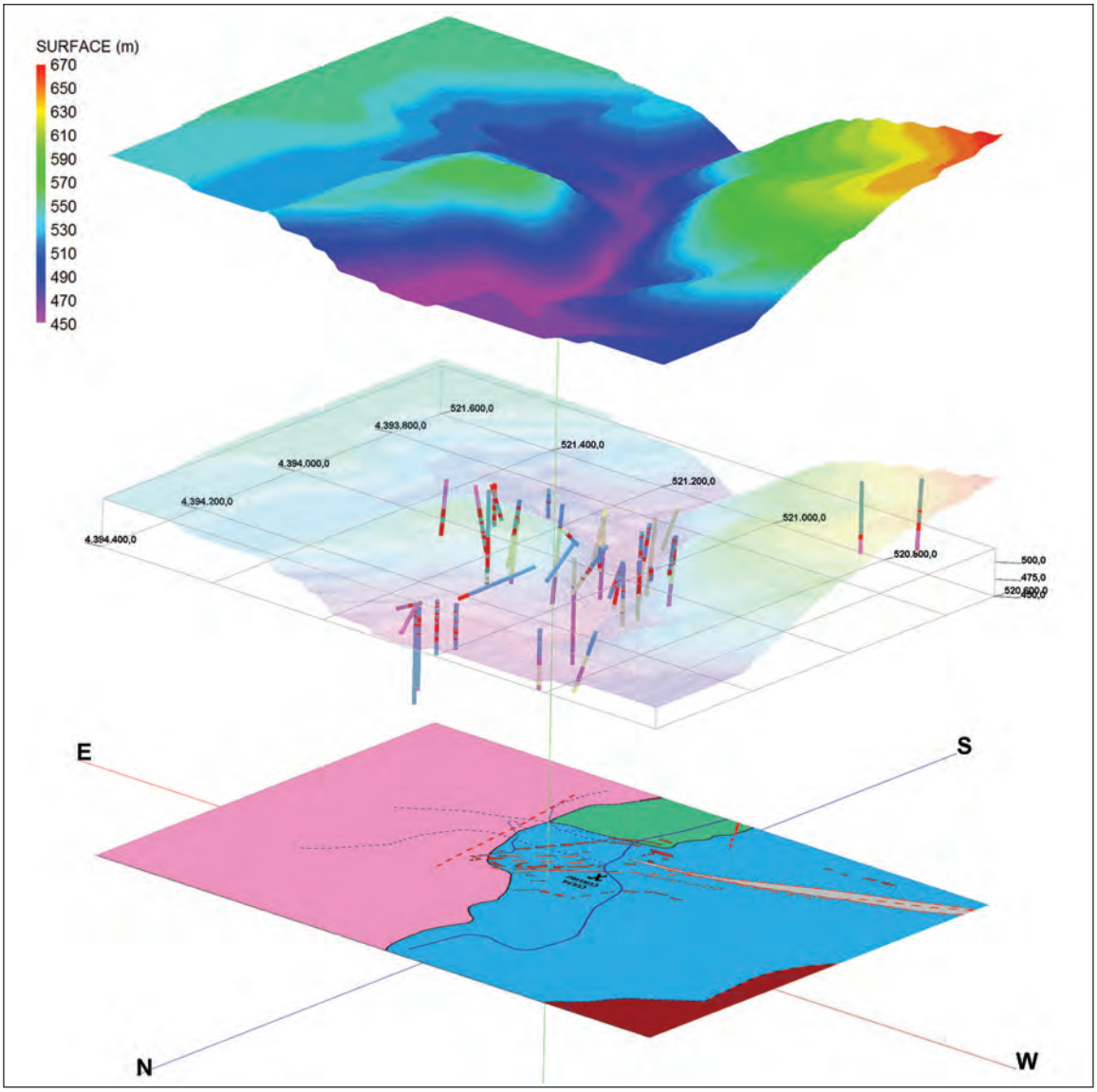

Figure 4- 3D topographic map, boreholes, and geology map of Çulfa Çukuru Pb-Zn deposit (to avoid confusion, +1000 m. offset and -1000 m offset along z axis were applied on geology map and topographic map, respectively) (see Figure 1 for the legend of geological units).

4.2. Three-Dimensional Subsurface Modeling of Mineralization

The study area is located in a 0.7 km^2 area and has an irregular topography. In the study area where both flat areas and hills are located, Akpınar stream flows from north to south. The main mineralization in the area was discovered in this stream bed, and then subsurface continuity of the mineralization was found in more detailed studies (Figure 4).

The block model with IDW algorithm was applied to Pb% and Zn%. The values obtained from the geochemical analyses on the ore-alteration zones with a total of 42 boreholes were used for the Pb% and Zn% values. The shallowest drilling is 19.5 m (OMCC1) and the deepest drilling is 161.5 m (OMCC37). The total depth of drillings is 3622.4 m and average depth of drillings is 86.25 m. The ore-alteration zones were observed 7 out of 42 boreholes (OMCC10, OMCC24, OMCC26, OMCC38, OMCC39, OMCC40, and OMCC41) (Figure 4). Using Pb% and Zn% geochemical analyses values, the individual model files were created for each element percentage with the help of the IDW interpolation method. The data was modeled using cut-off grades, 7% for Pb and 4% for Zn and 2637765 voxels which were 2 x 2 x 5 m in dimension.

Inverse distance, using constant or variable exponential weighting, assigns a voxel node value based on the weighted average of neighboring data points. In this study, the sector shape is circular because there was no directional effect on the regional autocorrelation in the data and the factor of anisotropy is 1. The power and the number of neighborhood values were tested and the optimal values are; power value 8, neighborhoods 6 for Pb%, power value 4, neighborhoods 2 for Zn%.

The distribution of the ore zones that was followed during the modeling studies, using geochemical analysis data for each element, covers quite large areas in the subsurface environment (Figure 5). It seems quite difficult to determine the target area in this way. Therefore, for both Pb% and Zn%, the values above the cut-off grade are divided into four equal sectors. These sectors are referred to as “Low”, “Intermediate”, “High”, and “Very High” (Table 2). The ore zones which were created separately for each sector can also be observed in a wide range area. This is a common situation especially when the amount of data is limited (e.g. insufficient number of boreholes, irregularly spaced boreholes etc.). This is why, instead of evaluating the data of each sector separately, using the intersection of the sectors in the same category seems to be more suitable at detecting target area (e.g. the intersection of the “low” grading sector of Pb% and the “low” grading of Zn%). Although it is possible to find the ore zones outside of these areas, the promising areas are the intersectional areas (Akıska et al., 2013).

In order to create intersection areas, the first created model files are converted to Boolean model files. When the intersection areas are detected, the corner coordinate values of each cube are detected and it is also determined whether the values contained herein are within the given range. In these Boolean model files, 1 is assigned to the values in the given intervals and 0 is assigned to the remaining values.

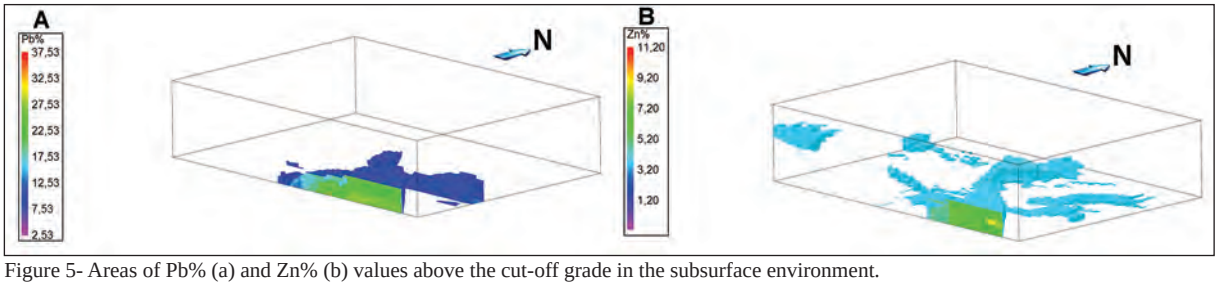

Figure 5- Areas of Pb% (a) and Zn% (b) values above the cut-off grade in the subsurface environment.

Table 2- Sector names and properties using in subsurface modeling study.

Sector #	Sector Name	Pb% Intervals	Zn% Intervals	Pb% Boolean Model File	Zn% Boolean Model File
1	Low	7.00–14.81	4–6,33	Pb_bool_sector1	Zn_bool_sector1
2	Intermediate	14.81–22.62	6.33–8.66	Pb_bool_sector2	Zn_bool_sector2
3	High	22.62–30.43	8.66–10.98	Pb_bool_sector3	Zn_bool_sector3
4	Very High	30.43–38.24	10.98–13.31	Pb_bool_sector4	Zn_bool_sector4

The generated Boolean model files are then transferred to MS Excel. With the help of a macro written in MS Excel, the "1" values (ore grade values in the specified range) were taken into account while "0" values were excluded from the modeling study.

The Boolean files for each sector ("low", "intermediate", "high", and "very high") and each element were created using the method described above. Then, in order to detect the intersection areas of each sector, multiplication was applied to the Boolean model files (e.g., the values in Pb_bool_sector1.mod and Zn_bool_sector1.mod were multiplied by each other to find the intersection areas of Sector1) (Figure 6). The process of detection for the intersecting areas was applied to every sector, and these areas were determined. Details and applications of this method were given in Akıska et al. (2013).

In the region with the obtained data; a mass of ore with a total volume of 1100000 m^3 including 382000 m^3 for Sector1, 696000 m^3 for Sector2 and 22000 m^3 for Sector3, was identified. Since the 0 value is obtained by multiplying the Boolean files belonging to Sector 4, referred to as "Very High", the result is that there is no intersected area between these ranges (Figure 7).

Attempted detection of the adit directions and locations was done using sector values that were obtained using the intersection method. When the adit locations were detected, the elevation intervals of the adits were randomly determined as being 10 meters (450-520 levels) and the adit dimensions as 2 x 2 meters. These intervals can be increased, decreased or changed according to the subsurface environment conditions and lithological conditions during adit planning. The related sectors for each level were brought together and the adit line of that level was created. In addition, it was determined which sector will be seen in which location on a certain level (Figure 8).

The case study for 450 level was made. The top view and the side view of the adit line including all sectors in the 450 level are seen in figure 9a and 9b, respectively. Each point on the level shown in Figure 9b implies the area where the ore is located. The interpreted map using Figure 9a and 9b was drawn for 450 level (Figure 9c). The strike of the first entrance is N105E. The general trend of the adit is E-SE. In the interpreted map, the location of the adit entrance and the general orientation of the adit were determined from the model image (Figure 9a). It was checked with the topographic map whether this point (adit entrance) coincided with a point on the surface. The detected point may not be exactly on the surface, but on the subsurface. This is because the points in the model file are due to the presence of ore in the specified intervals in the sectors. If the point determined as the entrance of the adit does not contain ore at these intervals, the point containing the ore closest to the surface can be detected and the entrance of the adit can be determined accordingly. Likewise, these maps can be created for all levels so that adit planning can be done.

The accuracy of the subsurface modeling studies was checked statistically and using cross-validation techniques. The estimation errors and cross-validation graphic can be seen in figure 10 and table 3, respectively. The cross-validation technique is applied to all the data used in the interpolation creation (7170 points). The fact that the R^2 values are close to 1, the Mean Error values are very close to 0, and the RMS values are relatively low values, they indicate that the applied interpolation algorithm and related parameters were selected very closely to the real values.

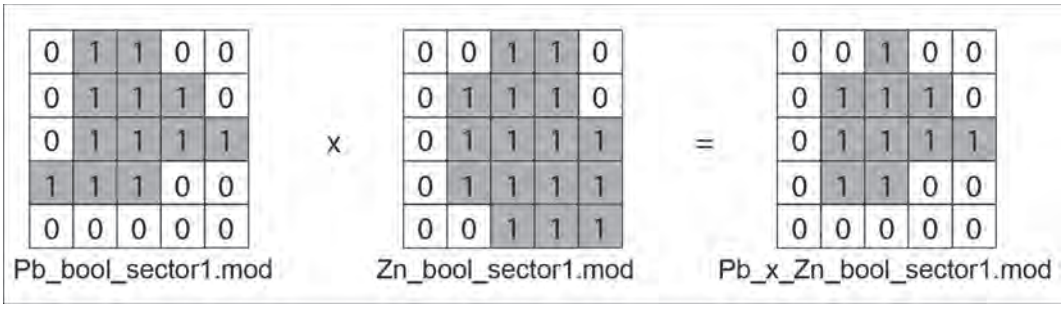

Figure 6- Schematic representation of multiplication operation that are applied to the Boolean files belonging to Sector 1 (the numbers were arbitrarily selected) (Akıska et al., 2013).

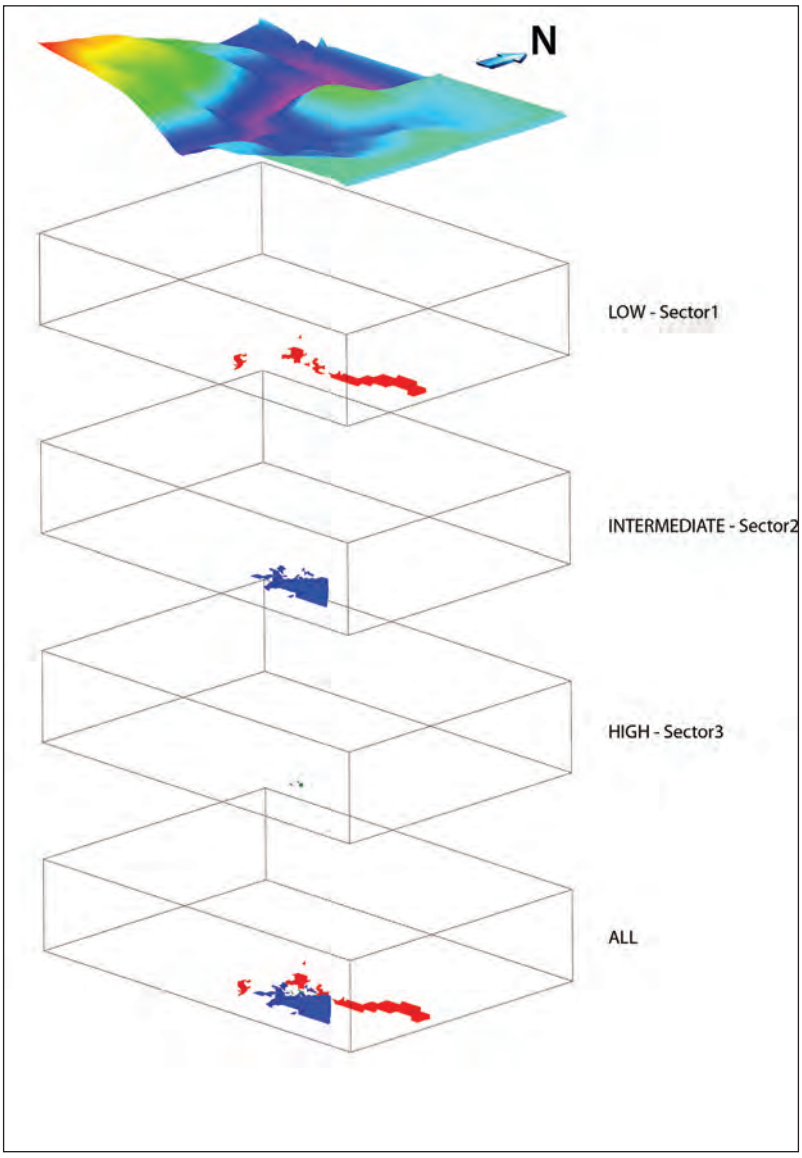

Figure 7- The subsurface locations of the sectors of Pb% and Zn% values above the cut-off grade.

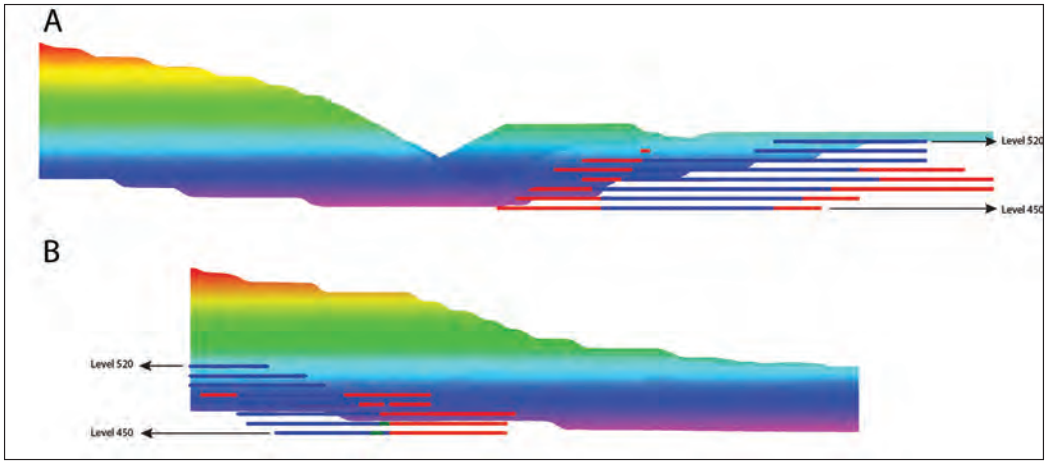

Figure 8- The southern (a) and the eastern (b) views of the adits obtained as a result of modeling study and the intersecting areas of sector groups (See figure 7 for the color of sector areas).

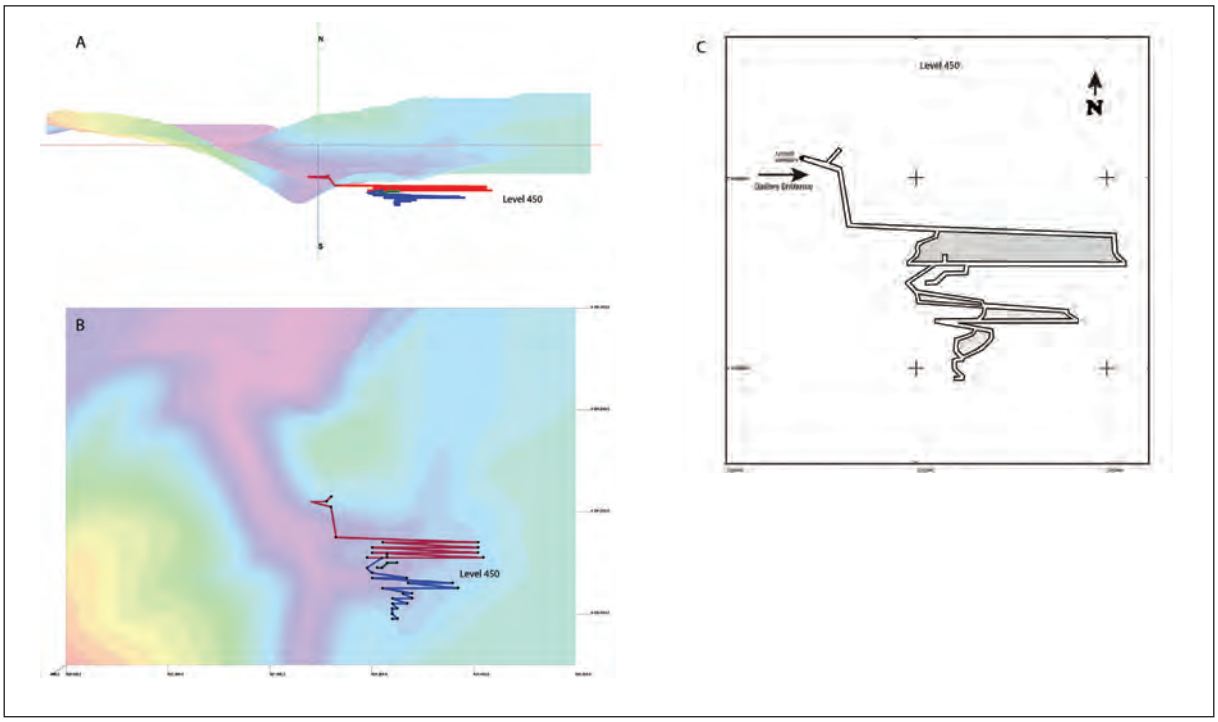

Figure 9- A) 3D topographic map and the sample adit line at Level 450 (the opacity value of the 3D topographic map has been reduced to 30% and the angle of view has been tilted 13° to the top along the x axis) (side of view: from South) (see figure 4 for the legend of the topographic elevations and figure 7 for the explanations of the sector colors), B) Side of view: from Top, C) Interpreted adit map of 450 level.

Table 3- Prediction errors of modeling study using IDW method.

		%Pb	%Zn
Samples	n	7170	7170
Mean Error	ME	0.00011	0.00023
Root-Mean-Square Error	RMSE	1.02861	0.56252

5. Conclusions

The surface modeling study using Kriging method and the subsurface modeling study using IDW method are intended to show the spatial trends and variability of the ore zones and also to determine the probable adit locations. For this purpose, to determine the appropriate adit lines the geochemical data and the location of the subsurface ore was used.

With the help of geostatistical analyses made on the topographic data used to create DEM, the suitable interpolation algorithm and the semi-variogram were determined and all results were controlled statistically and using cross-validation technique. As a result, the most suitable interpolation algorithm is “Ordinary Kriging” and the semi-variogram is “Spherical model”. The lag size is 52,72 m, sill value is 5396,57 m, and nugget value is 0 m. The suitable shape for neighborhood estimation was determined as circle that have four sectors divided by 45° offset and the number of neighborhoods was between 2 and 5.

Pb% and Zn% values were detected with the help of geochemical analyses of the ore zones in the 42 surface and subsurface boreholes. The ore zones in the subsurface environment for Pb% and Zn% were determined using this data. From the detected areas, the parts above the cut-off grade were modeled. The large areas were specified as a result of this modeling study. It is not appropriate to use this data directly because of the limited number of boreholes, whose distances were not regularly spaced, and because the boreholes were not regularly distributed over the whole study area. Instead, the areas above the cut-off grades for both Pb% and Zn% were divided into 4 sectors to identify more specific areas (low, intermediate, high, very high). Then, the intersection areas in the subsurface environment of the same sectors for Pb% and Zn% were specified and an attempt to determine the appropriate adit lines was tried. The IDW interpolation algorithm was used for the modeling of subsurface data. The power and the neighborhood values were tested for both Pb% and Zn% values and the optimal values are; power value 8

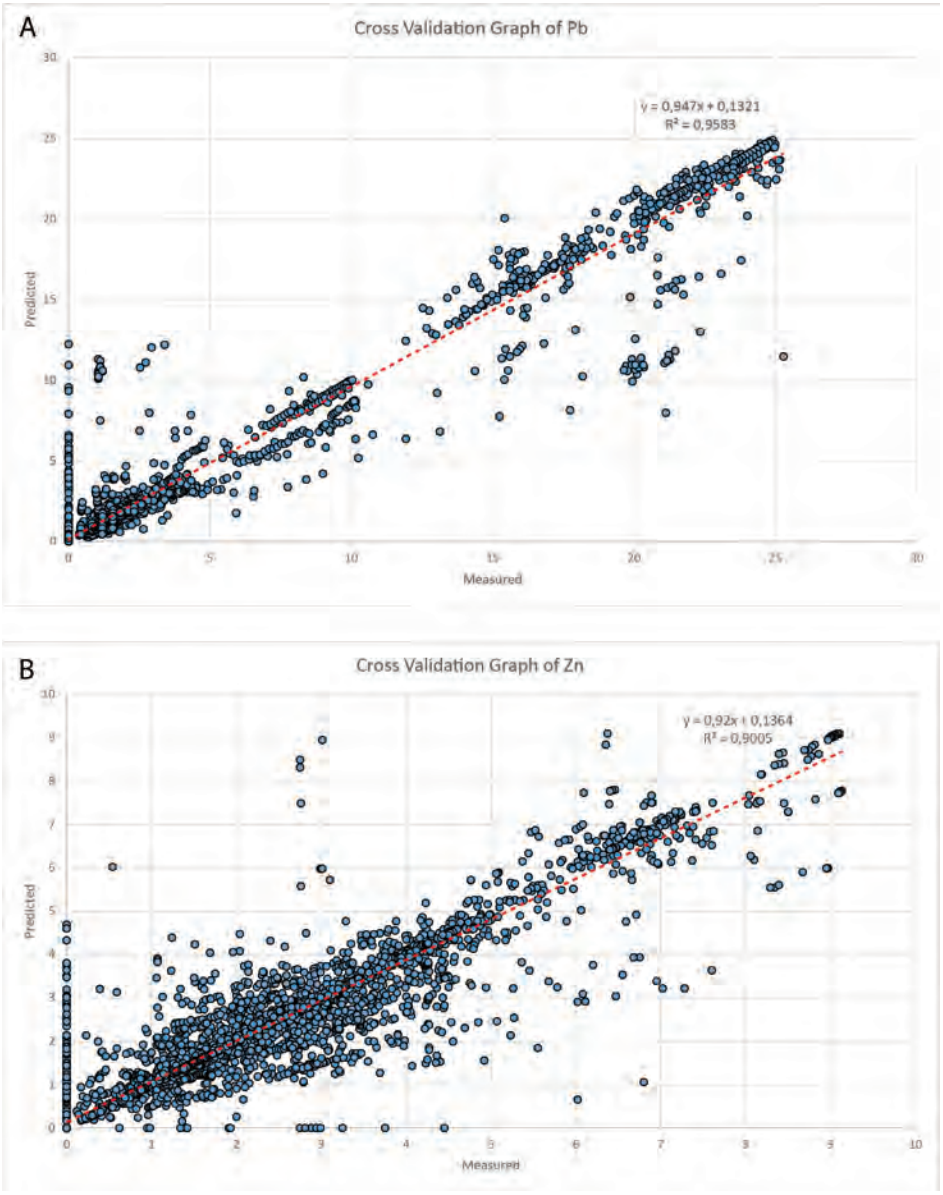

Figure 10- Cross-validation graph of the measured-estimated values of Pb% and Zn%.

and number of neighborhoods 6 for Pb%, power value 4 and number of neighborhoods 2 for Zn%.

The cross-validation results and the prediction errors obtained from the surface modeling study are shown in figure 3 and table 1, respectively, while the cross-validation results and the prediction errors obtained from the subsurface modeling study are shown in figure 10 and table 3, respectively. In this study, the modeling studies are evaluated considering all the data and the results obtained from the modeling studies are presented taking these values into consideration.

The number of sectors and the sector intervals were determined randomly in this study. These features may show changes in each different area. The sector intervals may be determined based on deposit conditions, economic conditions, and metal prices etc. Generally, modeling studies are carried out before the mining operations and the ore zones are operated in the frame of the model. However, depending on the importance of changes in the conditions on that day (e.g. sudden increases and decreases in costs, changes in metal prices), these models can be regenerated or the sector intervals on the created model can be changed. In this way, a model that can be actively used and can be changed during the mining operations is presented

in this study. Although all the modeling studies up to this point were controlled by the geostatistical and cross-validation methods, the geological data such as lithology, the general position of ore, and structural elements should always be prioritized.

Acknowledgements

The authors would like to thank Oreks Madencilik for providing the data for this study and for granting permission to study on the field.

References

Ahlberg, J., Nilson, E., Walsh, J. 1967. The Theory of Splines and its Applications. Academic Press, New York, 280 p.

Ahmed, A.A. 2009. Using lithologic modeling techniques for aquifer characterization and groundwater flow modeling of the Sohag area, Egypt. Hydrogeology Journal 17, 1189–1201.

Akıska, S. 2010. Yenice (Çanakkale) Bölgesi'ndeki Cu-Pb-Zn Oluşumları. Doktora Tezi, Ankara Üniversitesi, 234 s. Ankara (unpublished).

Akıska, S., Demirela, G., Sayılı, İ.S., Kuşcu, İ. 2010. Fluid inclusion and S isotope systematics of some carbonate-related Pb-Zn-Cu mineralizations in NW Anatolia, Turkey. Melfos, V., Marchev, P., Lakova, I., Chatzipetros, A. (Ed). Geologica Balcanica Abstract Volume, 21.

Akıska, S., Sayılı, İ.S., Demirela, G. 2013. 3D Subsurface Modeling of Mineralization: A Case Study from Handeresi (Çanakkale, NW Turkey) Pb-Zn-Cu Deposit. Turkish Journal of Earth Sciences 22, 574-587.

Akıska, S., Demirela, G. 2014. Handeresi, Bağırkaçdere ve Fırıncıkdere (Kalkım, Yenice - ÇANAKKALE) Pb-Zn±Cu Distal Skarn Yataklarında Akışkanların Kökeni. Yerbilimleri 35(3):, 199-218.

Altunkaynak, Ş., Genç, Ş.C. 2008. Petrogenesis and time-progressive evolution of the Cenozoic continental volcanism in the Biga Peninsula, NWAnatolia (Turkey). Lithos 102, 316-340.

Andiç, T., Kayhan, F. 1996. Havran-İvrindi (Balıkesir), Kalkım-Pazarköy (Çanakkale) yöresinde yapılmış genel ve tahkik jeokimya çalışma raporu, Maden Tetkik ve Arama Genel Müdürlüğü Rapor No: 9900, Ankara (unpublished).

Binh, T.Q., Thuy, N.T. 2008. Assessment of the influence of interpolation techniques on the accuracy of digital elevation model. VNU Journal of Science, Earth Sciences 24, 176–183.

Bistacchi, A., Massironi, M., Dal Piaz, G.V., Dal Piaz, G., Monopoli, B., Schiavo, A., Toffolon, G. 2008. 3D fold and fault reconstruction with uncertainty model: an example from an Alpine tunnel case study. Computers & Geosciences 34, 351–372.

Brooker, P.I. 1986. A parametric study of robustness of kriging variance as a function of range and relative nugget effect for a spherical semivariogram. Mathematical Geology 18, 477–488.

Burrough, P.A., McDonnell, R.A. 1998. Principles of Geographical Information Systems. Oxford University Press, 356 p.

Calcagno, P., Chilès, J.P., Courrioux, G., Guillen, A. 2008. Geological modelling from field data and geological knowledge Part I. Modelling method coupling 3D potential-field interpolation and geological rules. Physics of the Earth and Planetary Interiors 171, 147–157.

Chaouai, N.E., Fytas, K. 1991. A sensitivity analysis of search distance and number of samples in indicator kriging. CIM Bulletin 84, 37–43.

Chaplot, V., Darboux, F., Bourennane, H., Leguedois, S., Silvera, N., Phachomphon, K. 2006. Accuracy of interpolation techniques for the derivation of digital elevation models in relation to landform types and data density. Geomorphology 77, 126–141.

Chen, J., Lu, P., Wu, W., Zhao, J., Hu, Q. 2007. A 3-D Prediction Method for Blind Orebody Based on 3-D Visualization Model and Its Application. Earth Science Frontiers 14(5), 54-62.

Choi, Y., Yoon, S.-Y., Park, H.-D. 2009. Tunneling Analyst: a 3D GIS extension for rock mass classification and fault zone analysis in tunneling. Computers & Geosciences 35, 1322–1333.

Cressie, N.A.C. 1990. The origins of kriging. Mathematical Geology 22, 239–252.

Çetinkaya, N., Karul, B., Önal, R., Yenigün, K. 1983*a*. Çanakkale-Yenice-Kalkım Bağırkaç Dere jeoloji raporu. Maden Tetkik ve Arama Genel Müdürlüğü Rapor No: 7814, Ankara (unpublished).

Çetinkaya, N., Karul, B., Önal, R., Yenigün, K. 1983*b*. Çanakkale-Yenice-Kalkım Handeresi Pb-Zn-Cu yatağı jeoloji raporu. Maden Tetkik ve Arama Genel Müdürlüğü Rapor No:7822, Ankara (unpublished).

Dağ A., Özdemir A.C. 2013. A Comparative Study for 3D Surface Modeling of Coal Deposit by Spatial Interpolation Approaches, Resource Geology 63, 394-403.

Davis, B.M. 1987. Uses and abuses of cross-validation in geostatistics. Mathematical Geology 19, 241–248.

de Kemp, E.A. 2000. 3-D visualization of structural field data: examples from the Archean Caopatina Formation, Abitibi greenstone belt, Québec, Canada. Computers & Geosciences 26, 509–530.

Dhont, D., Monod, B., Hervouët, Y., Backé, G., Klarica, S., Choy, J.E. 2012. 3D geological modeling of the Trujillo block: Insights for crustal escape models of the Venezuelan Andes. Journal of South American Earth Sciences 39, 245-251.

Dilek, Y., Altunkaynak, Ş., Öner, Z. 2009. Syn-extensional granitoids in the Menderes core complex, and the late Cenozoic extensional tectonics of the Aegean province. Geological Society of London, Special Publications 321, 197-223.

Dönmez, M., Akçay, A.E., Genç, Ş.C., Acar, Ş. 2005. Biga Yarımadası'nda Orta-Üst Eosen volkanizması ve denizel ignimbiritler. Maden Tetkik ve Arama Genel Müdürlüğü Dergisi 131, 49-61.

Dönmez, M., Akçay, A.E., Duru, M., Ilgar, A., Pehlivan, Ş. 2008. Türkiye Jeoloji Haritaları Çanakkale-H17 Paftası. Maden Tetkik ve Arama Genel Müdürlüğü Jeoloji Etütleri Dairesi, 101 s.

Dressler, M. 2009. Art of Surface Interpolation. Doktora Tezi, Technical University of Liberec, 80p. Liberec (unpublished).

Duru, M., Pehlivan, S., Dönmez, M., Ilgar, A. Akçay, A.E. 2007. Balıkesir İ18 paftasının Jeolojik Haritası. Maden Tetkik ve Arama Genel Müdürlüğü Rapor No: 97, Ankara (unpublished).

Elkadi, A.S., Huisman, M. 2002. 3D-GSIS geotechnical modeling of tunnel intersection in soft ground: the second Heinenoord tunnel, Netherlands. Tunnelling and Underground Space Technology 17, 363–369.

Falivene, O., Cabrera, L., Tolosana-Delgado, R., Alberto, S. 2010. Interpolation algorithm ranking using cross-validation and the role of smoothing effect. A coal zone example. Computers & Geosciences 36, 512-519.

Feltrin, L., McLellan, J.G., Oliver, N.H.S. 2009. Modelling the giant, Zn-Pb-Ag century deposit, Queensland, Australia. Computers & Geosciences 35, 108–133.

Fencík, R., Vajsáblová, M. 2006. Parameters of interpolation methods of creation of digital model of landscape. The 9th AGILE Conference on Geographic Information Science, 2006, Visegrad, Hungary, 374–381.

Galera, C., Tennis, C., Moretti, I., Mallet, J.L. 2003. Construction of coherent 3D geological blocks. Computers & Geosciences 29, 971–984.

Gallerini, G., De Donatis, M. 2009. 3D modeling using geognostic data: The case of the low valley of Foglia river (Italy): Computers & Geosciences 35, 146-164.

Genç, Ş.C., Altunkaynak, Ş. 2007. Eybek graniti (Biga yarımadası, KB Anadolu) üzerine: Yeni jeokimya verileri ışığında yeni bir değerlendirme. Yerbilimleri, 28(2), 75-98.

Hack, R., Orlic, B., Özmutlu, S., Zhu, S., Rengers, N. 2006. Three and more dimensional modelling in geo-engineering. Bulletin of Engineering Geology and the Environment 65, 143–153.

Hu, K., Li, B., Lu, Y., Zhang, F. 2004. Comparison of various spatial interpolation methods for non- stationary regional soil mercury content. Environmental Science 25(3), 132-137.

Isaaks, E.H., Srivastava, R.M. 1989. Applied Geostatistics. Oxford University Press, New York, 561 p.

Jian, W., Yuanhui, S., Bin, W., Yongjun, W., Lei, X., Chunmeng, D. 2012. 3D geological modeling of fractured volcanic reservoir bodies in Block DX18 in Junggar Basin, NW China. Petrolium Exploration and Development 39(1), 99-106.

Johnston, K., Ver Hoef, J.M., Krivoruchko, K., Lucas, N. 2001. Using ArcGIS Geostatistical Analyst. ESRI Press Redlands, CA, USA, 300 p.

Kane, V.E., Begovich, C.L., Butz, T.R., Myers, D. 1982. Interpretation of regional geochemistry using optimal interpolation parameters. Computers & Geosciences 8 (2), 117-135.

Kashani, S.B.M., Abedi, M., Norouzi, G.H. 2016. Fuzzy logic mineral potential mapping for copper exploration using multi-disciplinary geo-datasets, a case study in seridune deposit, Iran. Earth Science Informatics 9, 167-181.

Kaufmann, O., Martin, T. 2008. 3D geological modelling from boreholes, cross-sections and geological maps, application over former natural gas storages in coal mines. Computers & Geosciences 34, 278–290.

Kitanidis, P.K. 1997. Introduction to Geostatistics: Applications in Hydrogeology. Cambridge University Press, Cambridge, USA, 249 p.

Krige, D.G. 1951. A statistical approach to some basic mine valuation problems on the Witwatersrand. Journal of the Chemical, Metallurgical and Mining Society of South Africa 52, 119–139.

Krushensky, R.D. 1976. Neogene calc-alkaline extrusive and intrusive rocks of the Karalar-Yeşiller area, Northwest Anatolia. Bulletin Volcanologique 39, 336–360.

Lam, N.S. 1983. Spatial interpolation methods review. The American Cartographer 10, 129–149.

Li, J., Heap, A. 2008. A Review of Spatial Interpolation Methods for Environmental Scientists. Geoscience Australia Record/23, 137p.

Liu, L., Zhao, Y., Sun, T. 2012. 3D computational shape- and cooling process-modeling of magmatic intrusion and its implication for genesis and exploration of intrusion-related ore deposits: An example from the Yueshan intrusion in Anqing, China. Tectonophysics 526-529, 110-123.

Matheron, G. 1960. Krigeage d'un Panneau Rectangulaire par sa Périphérie. Note Geostatistique No. 28, CG. Ecole des Mines de Paris, Paris.

Mitasova, H., Mitas, L. 1993. Interpolation by Regularized Spline with Tension: I. Theory and Implementation. Mathematical Geology 25, 641-655.

Okay, A.İ., Siyako, M., Bürkan, K.A. 1990. Biga Yarımadası'nın jeolojisi ve tektonik evrimi. Türkiye Petrol Jeologları Derneği Bülteni 2, 83–121.

Okay, A.İ., Satır, M., Maluski, H., Siyako, M., Monie, P., Metzger, R., Akyüz S. 1996. Paleo- and Neo-Tethyan events in northwest Turkey: geological and geochronological constraints. Yin, A., Harrison, M. (Ed.). Tectonics of Asia. Cambridge University Press, Cambridge, 420–441.

Okay, A.İ., Bozkurt, E., Satır, M., Yiğitbaş, E., Crowley, Q.G., Cosmas, K.S. 2008. Defining the southern margin of Avalonia in the Pontides: Geochronological data from the Late Proterozoic and Ordovician granitoids from NW Turkey. Tectonophysics 461, 252-264.

Olea, R.A. 1999. Geostatistics for Engineers and Earth Scientists. Kluwer Academic Publishers, London, UK, 303 p.

Özmutlu, S., Hack, R. 2003. 3D modelling system for ground engineering. Rosenbaum, M.S., Turner, A.K. (Ed.). New Paradigms in Subsurface Prediction Characterization of the Shallow Subsurface Implications for Urban Infrastructure and Environmental Assessment, Lecture Notes in Earth Sciences 99, 253–260.

Pehlivan, A.N., Çetin, A. 1997. Edremit (Balıkesir) Ezine-Bayramiç-Yenice (Çanakkale) çevresinin altın ağırlıklı polimetal ve ağır mineral çalışmaları raporu. Maden Tetkik ve Arama Genel Müdürlüğü Rapor No: 10061, Ankara (unpublished).

Peralvo, M. 2004. Influence of DEM interpolation methods in drainage analysis. GIS Hydro 04, University of Texas, Austin, Texas, 26 p.

Radelli, L. 1970. La nappe de Balya la zone plis Egéenne et extension de la zone du Vardar en Turquie occidentale. Géologie Alpine 46, 169-175.

Renard, P., Courrioux, G. 1994. Three-dimensional geometric modeling of a faulted domain: the Soultz Horst example (Alsace, France). Computers & Geosciences 20, 1379–1390.

Rengers, N., Hack, R., Huisman, M., Slob S., Zigterman, W. 2002. Information technology applied to engineering geology. van Rooy, J.L., Jermy, C.A. (Ed.). Engineering Geology for Developing Countries – Proceedings of 9th Congress of the International Association for Engineering Geology and the Environment, 121–143.

Robinson, T.P., Metternicht, G. 2006. Testing the performance of spatial interpolation techniques for mapping soil properties. Computers and Electronics in Agriculture 50, 97-108.

Saraç, C., Tercan, A.E. 1996. Grade and reserve estimation of the Tulovasi borate deposit by block kriging. International Geology Review 38, 832–837.

Saraç, C., Demirel, I.H., Sen, O., Varol, N. 2004. Geostatistical Simulation of the Total Organic Carbon Values: An Example from Petroleum Source Rocks on the Coastal Area of Western Taurus Region, Turkey. Petroleum Science and Technology 22(3&4), 367-379.

Shahbeik, S., Afzal, P., Moarefvand, P. Qumarsy, M. 2014. Comparison between Ordinary Kriging (OK) and Inverse Distance Weighted (IDW) based on estimation error Case study: in Dardevey iron ore deposit, NE Iran. Arabian Journal of Geosciences 7, 3693–3704.

Sims, D.L. 1992. Application of 3D geoscientific modelling for hydrocarbon exploration. Turner, A.K. (Ed.) Three- Dimensional Modelling with Geoscientific Information systems, Kluwer Academic Publishers, 443 p.

Siyako, M., Bürkan, K.A., Okay, İ.A. 1989. Biga ve Gelibolu Yarımadaları'nın Tersiyer jeolojisi ve hidrokarbon olanakları. Türkiye Petrol Jeologları Derneği Bülteni 1(3), 183-199.

Tahmasebi, P., Hezarkhani, A. 2010. Application of adaptive neuro-fuzzy inference system for grade estimation; case study, Sarcheshmeh porphyry copper deposit, Kerman, Iran. Australian Journal of Basic and Applied Sciences 4, 408–420.

Tufan, A.E. 1993. Karaydın Köyü (Yenice-Çanakkale) çevresinin jeolojik ve petrografik özellikleri ile kurşun-çinko zuhurlarının jenetik incelemesi. Doktora Tezi, Selçuk Üniversitesi, 158 s. Konya (unpublished).

Turner, A. K. 1992. Three- Dimensional Modelling with Geo-scientific Information Systems. Kluwer Academic Publishers, 468 p.

Van Dijk, M.J., Rientjes, T.H.M., Boekelman, R.H. 1999. Interpolation schemes, H.P., Bähr and T., Vögtle (Ed.). GIS for Environmental Monitoring. Schweizerbart 183 - 189.

Veldkamp, J.G., Hack, H.R.G.K., Özmutlu, S., Hendriks M.A.N., Kronieger, R., Van Deen, J.K. 2001. Combination of 3D-GIS and FEM modelling of the 2nd Heinenoord Tunnel, The Netherlands. Abstract to the International Symposium, EngGeoCity – 2001 'Engineering Geological Problems of Urban Areas', 30 July-2 August 2001, Ekaterinburg, Russia, 1-8.

Voltz, M., Webster, R. 1990. A comparison of kriging, cubic splines and classification for predicting soil properties from sample information. European Journal of Soil Science 41, 473–490.

Wang, G., Huang, L. 2012. 3D geological modeling for mineral resource assessment of the Tongshan Cu deposit, Heilongjiang Province, China. Geoscience Frontiers 3, 483-491.

Wang, G., Zhang, S., Yan, C., Song, Y., Sun, Y., Li, D., Xu, F. 2011. Mineral potential targeting and resource assessment based on 3D geological modeling in Luanchuan region, China. Computers & Geosciences 37, 1976–1988.

Watt, J.T., Glen, J.M.G., John, D.A., Ponce, D.A. 2007. Three-dimensional geologic model of the northern Nevada rift and the Beowawe geothermal system, north-central Nevada. Geosphere 3(6), 667–682.

Webster, R., Oliver, M.A. 2001. Geostatistics for Environmental Scientists. John Wiley and Sons, 360 p.

Xiao, F., Chen, J., Zhang, Z., Wang, C., Wu, G., Agterberg, F.P. 2012. Singularity mapping and spatially weighted principal component analysis to identify geochemical anomalies associated with Ag and Pb–Zn polymetallic mineralization in Northwest Zhejiang, China. Journal of Geochemical Exploration 122, 90–100.

Yücelay, M.A. 1975. Çanakkale İli Yenice İlçesi Kalkım Bucağı Güneyindeki Çulfa Çukuru Kurşun Çinko Mineralizasyonu Jeolojik Etüdü, Maden Tetkik ve Arama Genel Müdürlüğü Rapor No: 5617, Ankara (unpublished).

Yücelay, M.A. 1976. Çanakkale-Kalkım-Handeresi Pb-Zn-Cu bölgesinin etüdü. Maden Tetkik ve Arama Genel Müdürlüğü Rapor No: 5720, Ankara (unpublished).

Zanchi, A., Francesca, S., Stefano, Z., Simone, S., Graziano, G. 2009. 3D reconstruction of complex geological bodies: Examples from the Alps. Computers & Geosciences 35, 49-69.

Zhu, S., Hack, R., Turner, A. K., Hale, M. 2003. How far will uncertainty of the subsurface limit the sustainability planning of the subsurface? Proceedings of Sustainable Development & Management of the Subsurface (SDMS) Conference, 5-7 Nov 2003, Utrecht, Netherlands. 203-210.

Zimmerman, D., Pavlik, C., Ruggles, A., Armstrong, P. 1999. An experimental comparison of ordinary and universal kriging and inverse distance weighting. Mathematical Geology 31, 375–390.

Bull. Min. Res. Exp. (2018) 157: 207-215

Bulletin of the Mineral Research and Exploration

http://bulletin.mta.gov.tr

Evaluation of Thrace Region fine coal tailings

Murat Olgaç KANGAL[a*], Mustafa ÖZER[b], Fırat BURAT[c] and Soner AKIN[d]

[a]*Istanbul Technical University, Faculty of Mining, Department of Mineral Processing Engineering, 34469, Maslak, İstanbul, Turkey. orcid.org/0000-0003-4993-064X*

[b]*Istanbul Technical University, Faculty of Mining, Department of Mineral Processing Engineering, 34469, Maslak, İstanbul, Turkey. orcid.org/0000-0003-2642-6782*

[c]*Istanbul Technical University, Faculty of Mining, Department of Mineral Processing Engineering, 34469, Maslak, İstanbul, Turkey. orcid.org/0000-0001-7051-0063*

[d]*Uysal Mining Co., Yeni Mah. Mescit Geç., No:2, 59100 Malkara, Tekirdağ, Turkey. orcid.org/0000-0002-7220-7655*

Research Article

Keywords:
Lignite, fine tailings, Reichert spiral, dewatering.

ABSTRACT

79.9% of the lignites in our country have a calorific value of less than 2500 Kcal/kg. In order to reduce energy dependence of the country, it would be right to use these lignite reserves of 11.8 billion tons by use of effective coal preparation methods and with clean coal combustion systems together with developing technology. A typical coal preparation plant produces 20% of the feed coal, all below 0.5 mm. Generally, due to high cost, the product under this size is not used but thanks to the developing coal cleaning technology, this size group can be utilized with low ash content. Within the framework of this study, the discarded fine fraction coal sample which was below 0.5 mm was taken from Uysal Mining Company in Tekirdağ and subjected to enrichment and dewatering experiments to obtain a marketable product. In experimental studies, in order to produce a high quality product, the slime portion which contains mainly clay minerals was removed with 81.25% ash content using screen with aperture of 150 microns. Afterwards, the coal having 49.09% ash content was subjected to multistage Reichert Spiral tests and a clean coal product with 24.1% ash content was produced. In settling experiments, the product below 150 microns was used and at the end of these tests the slurry with 30% solid in pulp ratio was produced. It can be concluded that the clean coal which is produced after enrichment tests could be used in energy sector, power plants, briquetting plants, cement plants etc.

Received Date: 26.05.2017
Accepted Date: 11.02.2018

1. Introduction

In developed countries, the coal produced from mine is not directly burned. Using physical, chemical and heating processes the quality of coal is upgraded and the negative effects originated from coal burning is diminished. To succeed this the main impurities such as ash, sulfur and moisture contents are decreased. In this manner, the maintenance and repair costs in mills and boilers, ash storage problems, particulate matter emissions and heavy metal emissions are reduced in thermal power plant operation. The enrichment methods are generally divided into two categories according to particle size, coarse and fine (Aslan et al., 1999; Önal, 1994).

In fine coal enrichment, the gravity techniques (jigging, shaking table, cyclone, spirals) is widely utilized because of its high effectiveness and low cost. The flotation method is preferred where the gravity methods cannot be applied for removing clays and pyrites captured in thin sections of coals. Because the flotation method is ineffective for oxidized coal and a good separation performance cannot be obtained in significantly high clay bearing coals, this led to the development of new technologies in coal enrichment. In fine coal processing, currently, Reichert spiral, column flotation, multi-gravity separator and the Falcon separator are mainly used (Baştürkcü and Acarkan, 2011, Parekh and Abdel Khalek, 2002, Ateşok, 2009, Honaker, 1995, Honaker et al., 1996).

* *Corresponding author: Murat Olgaç KANGAL, kangal@itu.edu.tr*
http://dx.doi.org/10.19111/bulletinofmre.428324

Nowadays, the need for energy is increasing more and more due to the development of the industry. Fossil fuels are not only the raw materials for energy but also they are needed for main inputs of different industries (Sharpe, 2007). One of the most important points that separates the coal from oil and natural gas is its homogeneous distribution on the earth. In addition, given the current visible reserves and the fact that petroleum will be consumed in 40 years, natural gas in 60 years, and coal will be consumed in 200 years, the strategic importance of the coal is even more evident. Coal has a very big share in the energy sector in terms of current production levels, its excess amount relative to other fossil resources, price stability, ease of transport and storage and its low cost to user (Ateşok, 2009).

The world coal production has doubled within the last thirty years. The increase in the coal production is largely due to demand for electricity in Asia, especially in China. The electricity generation of this country has increased 2.6 times over the past decade, reaching around 5.650 TWh in 2014 and 81% of this production is derived from the coal-based thermal power plants. In the last decade, the increase in electric energy production in the Asia-Pacific region has been about twice, and the coal has been the most heavily used source in the electricity generation (TKİ, 2016; British Petroleum, 2012; BGR Report, 2016).

Approximately 80% of Turkish lignites contain calorific value lower than 2500 kcal/kg. In order to diminish the energy dependency of our country, it would be right way to evaluate these lignite reserves which is about 11.8 billion tons using an effective coal preparation method and apply clean coal combustion systems together with developing technology. It is well know that a typical coal preparation plant produces below 0.5 mm fine coal that accounts 20% of the total feed. Generally, due to the high cost, the recovery of fine coal under this size is not preferred by many coal producers, however, with the developed coal cleaning methods this fraction can be evaluated (Ateşok, 2009).

The dewatering and drying are the obligatory processes for the use of coal. As it is known; a 1% increase in moisture in coals reduces the thermal efficiency equivalent to 4% increase in ash. To increase the capacity of transport, storage, crushing, grinding and burning systems and to provide coal in accordance with technological requirements also demonstrates the importance of dewatering and drying. With the processing of -0.5 mm fraction, the removal of the moisture from final products with an effective dewatering and drying technique must be executed. Because, the dehydration of the particles in small size is more difficult due to the increased surface area (Ateşok and Kangal, 2011; Ford and Fleming, 2002; Gallego-Juárez et al., 2003; Keller and Stahl, 1997).

In recent years, the privatization process of coal-based thermal power plants together with coalfields has gained momentum and thus the share of the private sector in production has begun to increase. The thermal power plants have the largest share in lignite consumption with 76%, 10% in the industry and 14% in the heating sector (TKİ, 2016).

The total annual ROM production capacity of the projects created for the public lignite sites is 78.735 million tons. The project capacity of TKİ is 46.150 million tons on a rom basis and the project capacity on the marketing basis is 41 million tons. 34.035 million tons of this salable capacity are for thermal power plants with an installed capacity of 4209 MW and of 6.73 million tons are for heating and industrial sectors. The lignite to take place in the second raw after the hydraulics in terms of cost in the electricity production, and besides giving importance to domestic resource production and use gives the impression that lignite will increase the share of electricity production in next years (TKİ, 2016).

As fuel in the cement sector; petroleum coke, imported hard coal, imported and domestic lignite, small amount of fuel-oil and natural gas are used and fuels constitute 30% of the cost. The petroleum coke has a thermal value of 7.500 Kcal/kg, an imported hard coal product of 6.300 Kcal/kg, a domestic hard coal product of 6.000 Kcal / kg and a domestic lignite of 3.500 to 4.500 Kcal/kg. The industry has an annual fuel requirement of 5.500 Kcal/kg and 6.5 million tons of coal with 3% sulfur content.

In addition, there are a total of 30 Sugar Factories in our country, 21 of which use coal as fuel. In factories which use coal as the fuel utilize two classes of coal as; low (2.200-3.800 Kcal/kg) and high calorific (4.000-4.500 Kcal/kg and above). The annual lignite needs of these factories are around 900,000 tons (TKİ, 2016).

It is known that in the soil sector, there are nearly 600 brick and tile factories in our country, most of them produce bricks and some of them produce both bricks and tiles. Their production capacity increases and decreases depending on the developments in the construction sector. The fuel used in soil industry in Turkey is the lignite in 3000 to 4000 Kcal/kg thermal value and the ovens have been designed accordingly with few exceptions.

It seems possible to maintain the market share of lignite in the heating sector by increasing the number and quality of plants related to coal remediation, preparing coal according to environmental criteria, developing smokeless boiler and stove technology, and maintaining competition with imported coal.

Besides, the lignite needs of industrial enterprises (chicken, oil, textile, salt factories etc.) in medium and small scales tend to show an increase parallel to the growth rate of the country and economic development. However, given the fact that some industrial plants established in big cities are required to pass natural gas due to environmental regulation, it is expected that the coal demands of this sector will continue in the range of 2.5-3 million tons.

Within scope of this study, the spiral beneficiation and dewatering studies were carried on waste character fine size lignite coal (-0.5 mm) obtained from coal washery that belong to Uysal Mining Co. in Tekirdağ.

2. Experimental Studies

2.1. Materials and Method

Within the scope of this study, fine lignite coal in waste character obtained from the coal preparation plant of the Uysal Mining Co., which is located in the Pirinççesme village of Malkara inTekirdağ, was used. In this coal washing plant, where fine coal is sieved and removed, and the enrichment with heavy medium in coarse size is carried out, and the final produced clean coal is used for heating. However, the fine coal is not subjected to any enrichment process and is stored at the end of the dewatering process. Within context of this study, which aims the recovery of coal in the composition of this residual material obtained as a fine-sized object, the chemical and physical characterization of the tailing, and the possibilities of enrichment with Reichert coal spiral were investigated. At the end of the enrichment, the coal analyses of the products were carried out and the results were evaluated. In addition to the enrichment experiments, settling tests were carried out for the dewatering of the slurry containing mostly clay minerals, and a process flow diagram was generated. The Reichert coal spiral was used in the experimental works and it is made of polyurethane and has a capacity of 1.2 ton/h. It consists of six 1000 mm diameter troughs wrapped around a vertical hub and the height of spiral is about 2380 mm. Solid in pulp ratio was adjusted as 25%. The upper heating value analyses of the products obtained in studies were carried out according to ASTM-D 5865, in the ICA calorimeter C700; the sulfur analysis according to ASTM-D 4239, in X-MET C-S device; and volatile matter and ash analyzes were made by burning in MF-120 Nuve oven in the crucible. Lower thermal values were calculated according to ISO 1928. All analyzes were given based on dry basis.

2.1.1. Physical Properties of the Sample

The screen analysis was carried out in order to determine the size distribution of the tailing sample obtained from the plant as a pulp with 73.6% moisture content, and the particle characteristics of the sample were determined according to the wet screen analysis. The results are shown in figure 1. The upper size of the representative sample was found as 1 mm. d_{80} and d_{50} sizes were found as 600 microns and 150 microns, respectively.

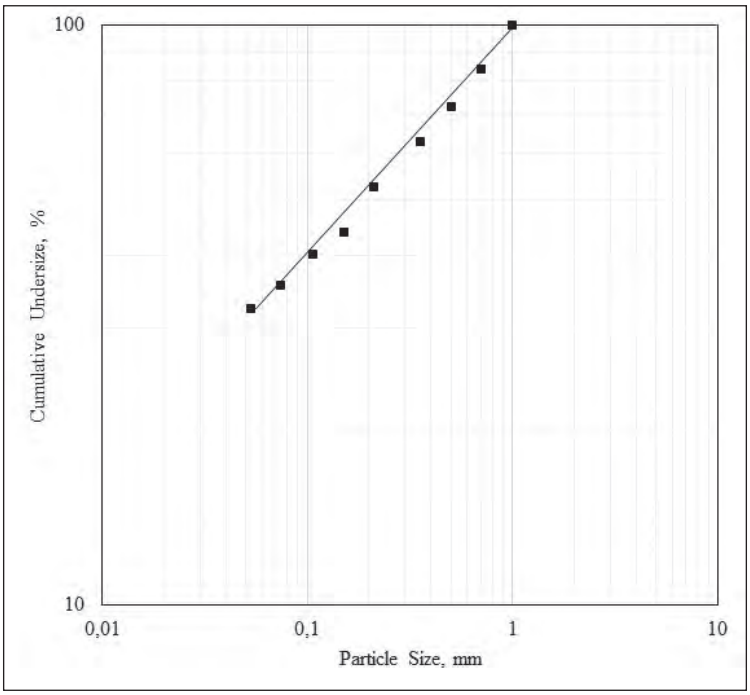

Figure 1- Undersize curve of the sample.

2.1.2. Chemical Properties of the Sample

The results of the chemical analysis performed to determine the composition of the test sample that is under 1 mm, and results are given in table 1.

Table 1- Chemical analysis of original coal sample.

Category	Analysis in dry basis
Ash %	61.48
Volatile matter, %	27.56
Fixed Carbon, %	10.96
Total sulfur, %	2.44
Lower thermal value, Kcal/kg	1689.0
Upper thermal value, Kcal/kg	1950.1

According to the chemical analysis results; it was found that the sample contains 61.49% ash with 1950 kcal/kg upper heating value. This thermal value, along with a constant carbon content of 10.96%, indicates the presence of coal in this tailing character material.

2.2. Results and Discussion

The tailing sample is distributed over a wide range of sizes (0-1 mm). As seen in Table 2 that the ash contents in coarse fractions are lower compared to fine fractions. This suggests that the coal is scattered in coarse sizes and that the composition of the tailing is predominant in clay minerals as the ash-forming minerals. Particularly; it is observed that the material under 150 microns size contains clay in big amounts. The ash content of the material fractions at +150 micron fraction was determined as 44.13%, while the ash content of the material containing clay minerals under the -150 micron size was determined as 81.25%.

27.6% of the total feed is above 0.5 mm with 39.1% ash content could be beneficiated when heavy medium cyclones at -20 + 0.5 mm is effectively operated. From this point, it was decided to carry out the enrichment works using spiral concentrator with the sample below 0.5.

Actually in Uysal Mining Company's coal washing plant, where the representative sample is provided, is designed to discharge the sample below 0.5 mm as a tailing. Due to the fact that the vibrating screen does not work effectively +0.5 mm materials contaminated with this waste character material. This increases the amount of tailing being discharged and the amount of coal that is lost in fine size. Adapting efficient working conditions related with vibrating screen with the aperture size of 0.5 mm the material less than 0.5 mm in size can be produced successfully. Due to this reason, the enrichment tests were carried out with tailing material below 0.5 mm size.

Table 2- Screen and fractional ash analyses of the tailings.

Size range, mm	Amount, %	Ash, %	Ash distribution, %	Combustible portion, %
+0.700	15.8	36.33	9.5	25.4
-0.700+0.500	11.8	42.60	8.3	17.1
-0.500+0.355	9.3	45.80	7.0	12.7
-0.355+0.212	10.4	49.75	8.6	13.2
-0.212+0.150	8.8	51.80	7.5	10.7
-0.150+0.100	3.7	71.25	4.4	2.7
-0.100+0.074	4.6	75.80	5.8	2.8
-0.074+0.053	3.1	80.40	4.1	1.5
-0.053	32.5	83.25	44.8	13.9
Total	100	60.43	100.0	100.0

According to the results from screen analyzes performed on the sample, using a vibrating screen with the aperture size of 0.5 mm, +0.5 mm size group was removed from the system. The size distribution of all passing 0.5 mm is given in table 3.

As the particles larger than 0.5 mm will be evaluated in coarse size beneficiation unit and -0.5 mm fraction can be processed in fine size coal beneficiation unit. Therefore, the upper size was selected as 0.5 mm in the spiral enrichment process. According to the size distribution and ash contents of the material in Table 3, it is clearly seen that 60.7% of the sample is accumulated below 0.150 mm and consists of mainly clay minerals with 81.25% ash content. Because of this reason, the cut size of the sample to be used in the spiral enrichment experiments was determined as 0.150 mm and the samples within the range of -0.5 + 0.150 mm were prepared using the Mozley hydrocyclone.

The spiral beneficiation experiments were performed with Reichert Coal Spirals shown in figure 2 and the process flow diagram is given in figure 3.

As a result of the enrichment test performed by using three concentration stages, two clean coal, a mixed and a schist products were obtained. The results of the experiments in terms of amount, ash content,

Figure 2- Reichert spiral unit in the experimental studies.

Table 3- The particle distribution after removing +0.5 mm size from the system.

Size range, mm	Amount, %	Ash, %	Ash distribution, %	Combustible portion, %
-0.500+0.355	12.8	45.80	8.5	22.1
-0.355+0.212	14.4	49.75	10.4	23.0
-0.212+0.150	12.1	51.80	9.1	18.6
-0.150+0.100	5.1	71.25	5.3	4.7
-0.100+0.074	6.4	75.80	7.1	4.9
-0.074+0.053	4.3	80.40	5.0	2.7
-0.053	44.9	83.25	54.5	24.0
Total	100	68.62	100.0	100.0

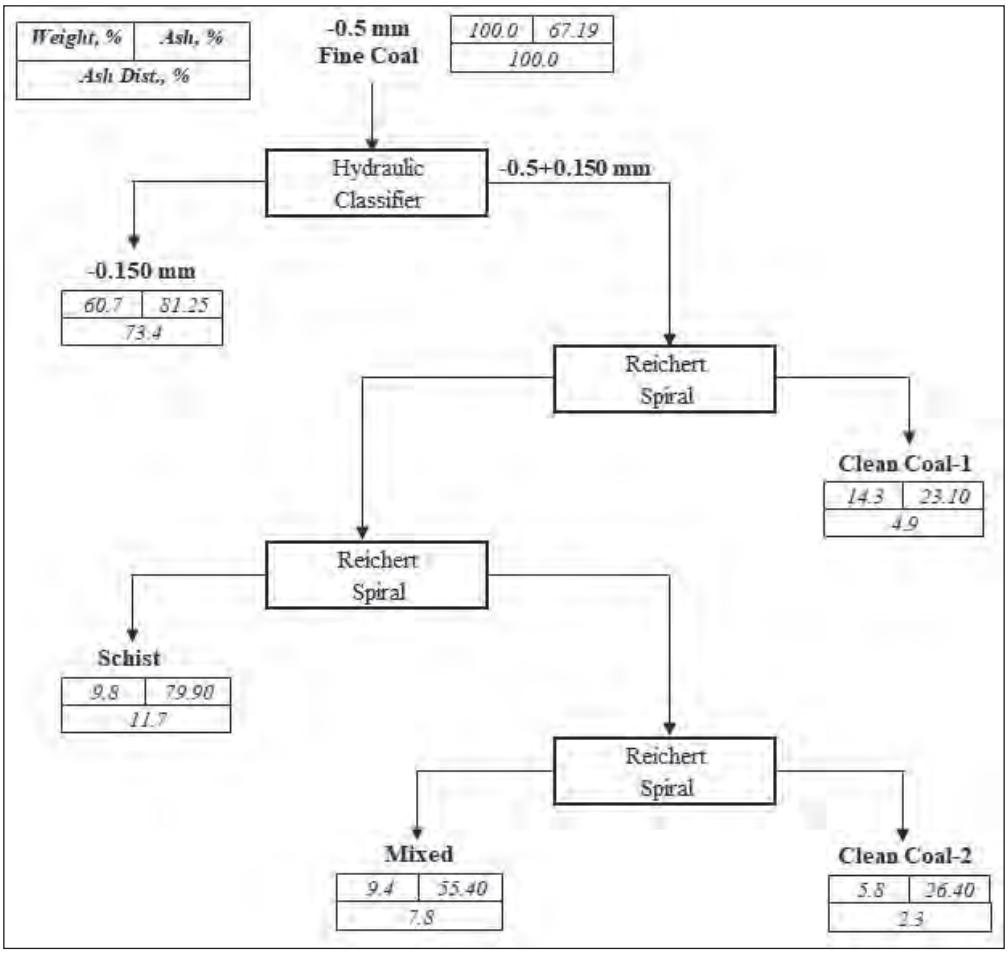

Figure 3- Process flowsheet of -0.5 mm fine coal.

ash distribution and combustible recovery are given in table 4.

According to the results given in table 4, the total clean coal is composed of Clean Coal 1 with 23.1% ash content at the amount of 14.3% and Clean Coal 2 with 26.4% ash content at the amount of 5.8%. As combined about 20.1% of the feed is taken with 26.4% ash content as a clean coal with 46.5% combustible recovery. The tailings from spiral is about 9.8% of the feed and contains about 80% ash. 60.7% of the total feed is obtained as slime with 81.3% ash content. When tailings from spiral and slime was combine the total tailings is found as 70.5% of the feed and assays 81.1% ash.

After the beneficiation process the slime materials must be thickened before filtration process. For this reason, the settling tests of slime having 5% solid in pulp ratio were carried out. An anionic flocculant commercially named as Fusifloc was used. It accelerates the settling and gives rise to obtain a clear

Table 4- Obtained final products.

Products	Amount, %	Ash content, %	Ash distribution, %	Combustible productiviy, %
Clean Coal 1	14.3	23.1	4.9	33.5
Clean Coal 2	5.8	26.4	2.3	13.0
Mixed	9.4	55.4	7.8	12.8
Schist	9.8	79.9	11.7	6.0
-0.150 mm	60.7	81.25	73.4	34.7
Total	100	67.19	100.0	100.0

water in the settling test as the problems related with clarity of the water and settling rate were observed during tests performed without adding any polymers. The settling curves, which formed as a result of settling tests at natural pH values (7.1) of the pulp at different flocculant concentrations of 50 g/t, 100 g/t, 150 g/t and 200 g/t, are given in figure 4.

As shown in figure 4, the concentration of flocculant less than 150 g/t is not sufficient in terms of both the settling rate and the clarity of the water.

The size calculation of a thickener with a capacity of 25 tons/h, which will be used for the settling of -0.150 mm material with 150 g/t flocculant addition, were carried out. The settling distances and rates in such a way to obtain 20. 25 and 30% solid in pulp ratios using a feed with 5% solid in pulp ratio were calculated and given in table 5.

As a result of the calculations, a thickener with a radius of 17.33 mm is necessary to obtain 30% solid in pulp ratio material.

3. Conclusions

As the coarse coal (+0.5 mm) with heavy medium separators in the coal preparation plant located in Pirinççesme village in Malkara, Tekirdağ of the Uysal Mining Co. is enriched, the material below 0.5 mm with 61.48% ash content and 1950 kcal/kg upper heating value is processed as a tailing. However, within the scope of this study, it was understood that the material obtained from the plant in -0.5 mm size was actually below 1 mm. The presence of high clay minerals in the composition of material allows the removal of high amount of slime (60.7%) with 81.25% ash content using a simple size classification. The material within a size range of -0.5 + 0.150 mm is fed to 3-stages Reichert spiral and makes it possible to produce a clean coal with 14.3% amount.

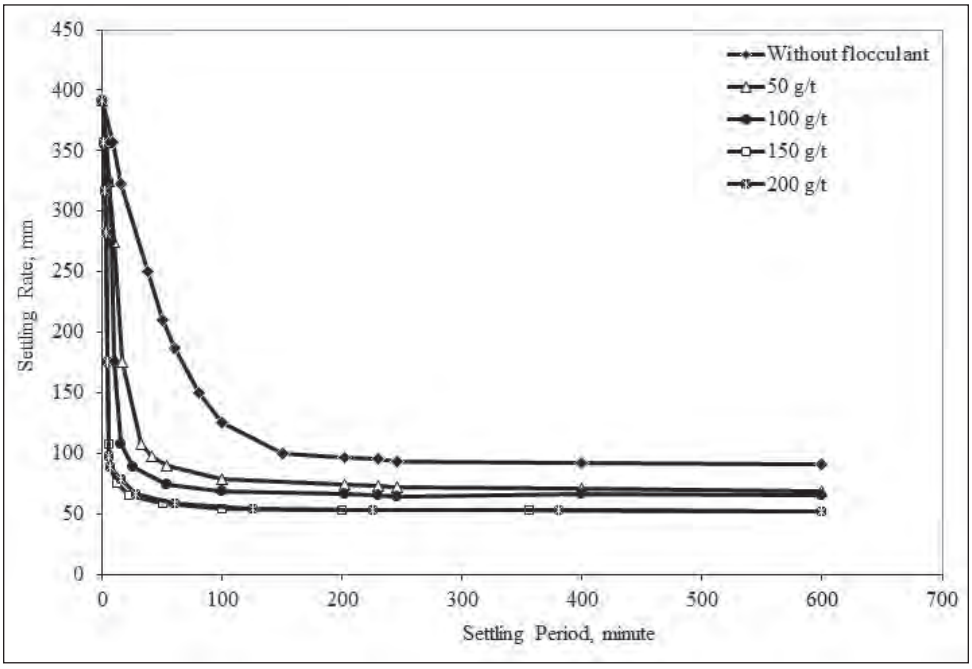

Figure 4- Settling experiments results with/without flocculant addition.

Table 5- Thickener diameters calculated according to different concentrations.

Post settling product PKO, %	Settling distance, m	Settling time, hour	Area, m^2	Thickener radius, m
20	0.09373	0.097	121.859	6.23
25	0.07385	0.203	255.025	9.01
30	0.06059	0.75	943.053	17.33

Ash, 24.10%

Volatile Matter, 42.10%

Fixed Carbon, 32.97%

Total sulfur, 2.07%

Upper Heat Value, 5036 Kcal/kg

It was revealed that this type of coal obtained in these specifications could be used in energy sector, thermal power plants, briquetting plants, cement factories etc. and provide an economic gain.

As a result of these studies; the process diagram given in figure 5 is presented as an alternative for the purpose of recovering coals from fine coal slimes.

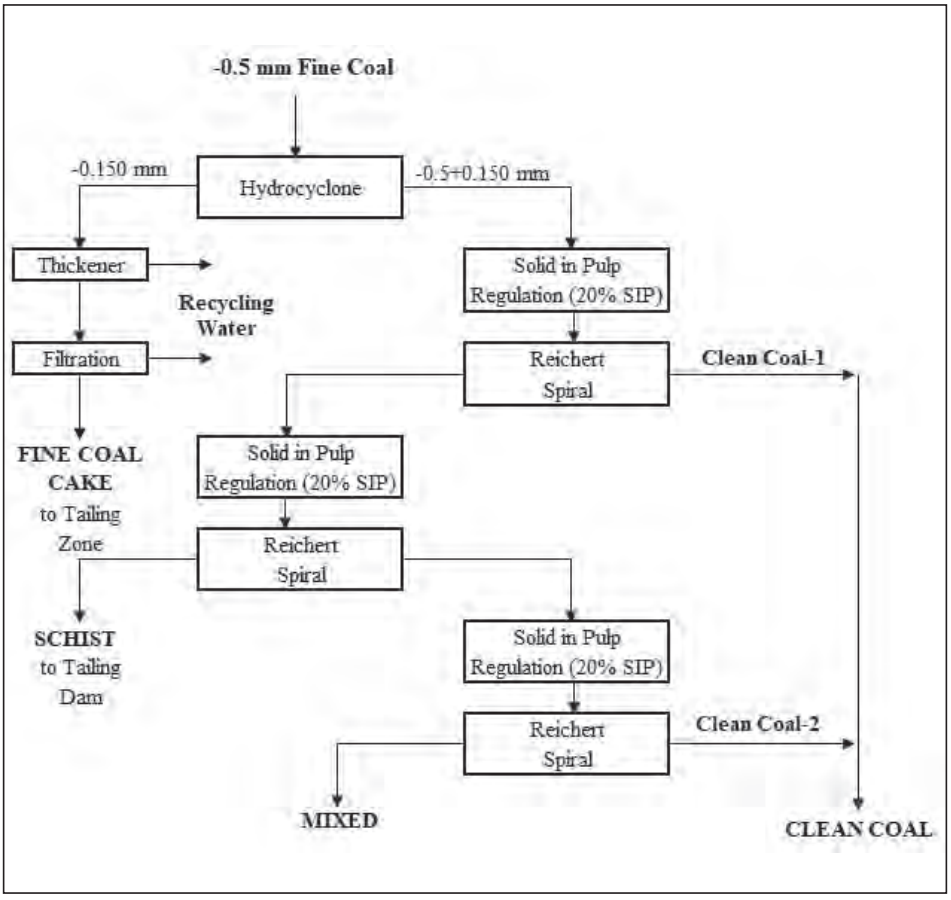

Figure 5- Proposed fine coal process flowsheet.

References

Aslan, N., Canbazoğlu, Ulusoy, M., Yeniçubuk, U. 1999. Gemerek linyit kömürlerinin MGS ile yıkanabilirliğinin araştırılması, Türkiye 16. Madencilik Kongresi ve Sergisi, Ankara, 321-326.

Ateşok, G. 2009. Kömür Hazırlama ve Teknolojisi, Yurt Madenciliğini Geliştirme Vakfı Yayınları, İstanbul, 376 s.

Ateşok, G., Kangal, M.O. 2011. Susuzlandırma ve Kurutma, YMGV Yayınları, İstanbul, 125 s.

Baştürkcü, H., Acarkan, N. 2011. Removal of sulfur from coal with Falcon concentrator, Proceedings of XIV Balkan Mineral Processing Congress, Bosnia 14-16 June, 363-368.

BGR Report. 2016. Federal Institute for Geosciences and Natural Resources. Reserves, Resources and Availability of Energy Resources, Hannover, 88 p.

British Petroleum, 2012. Statistical Review of World Energy, 48 p.

Ford, M., Fleming, R. 2002. Mechanical Solid-Liquid Separation of Livestock Manure, Ridgetown College - University of Guelph.

Gallego-Juárez, J.A., Elvira-Segura, L., Rodríguez-Corral, G. 2003. A Power Ultrasonic technology for deliquoring, ultrasonics, 41, 255-259.

Honaker R. Q. 1995. Enhanced gravity separators: New alternatives for fine coal cleaning, Proceedings 12th International Coal Preparation Conference, Intertec Inc., Lexington, Kentuck, 282-292.

Honaker, R. Q., Wang, D., Ho, K. 1996. Application of the Falcon concentrator for fine coal cleaning, Minerals Engineering 9, 11, 1143-1156.

Keller, K., Stahl, W. 1997. Vibration screens for dewatering-Theory and practice. Minerals and Metallurgical Processing 27-34.

Önal, G. 1994. Cevher ve kömür hazırlamanın ülkemiz madenciliği açısından önemi, Kömür kalitesinin iyileştirilmesi, kömür kullanımı, kömür zenginleştirme tesislerinin kurulması, işletimi ve denetimi – Meslek İçi Eğitim Semineri, İstanbul.

Parekh, B. K., Abdel Khalek, M. A. 2002. Using a Falcon concentrator, as a new technology, for removal of environmental pollutants of Egyptian coal / Mısır kömürlerinden çevreyi kirleten bileşenlerin uzaklaştırılması için Falcon zenginleştiricisi kullanımı", Ore Dressing/Cevher Hazırlama 7, 20-28.

Sharpe, M.A. 2007. Coal Preparation: A Discussion on Conventional and Advanced Technology, Coal Preparation Workshop, India.

TKİ, 2016. 2015. Kömür (Linyit) Sektör Raporu, Türkiye Kömür İşletmeleri Genel Müdürlüğü, Ankara, 90 s.

Bulletin of the Mineral Research and Exploration

http://bulletin.mta.gov.tr

Optimization of some parameters on desulfurization process of Muğla Yatağan Bağyaka lignite by ultrasonic waves

İlkay ÜNAL SANSAR[a*]

[a]*General Directorate of Mineral Research and Exploration, Department of Mineral Analyses and Technology, Directorate of Mineral Analysis Division, 06800 Ankara-Turkey. orcid:0000-0001-5022-4545*

Research Article

Keywords:
Lignite, ultrasonic, desulfurization, ash, optimization.

ABSTRACT

In this study, the desulfurization process developed using ultrasonic waves for Muğla Yatağan Bağyaka lignite had the optimum conditions for parameters affecting the ash and sulfur removal potentials determined with the Surface Response Method and a model created. The process parameters to obtain optimum desulfurization and ash removal were chosen as the ultrasonic treatment time, solid content, concentration of chemical reactive (H_2O_2) and reactive volume, and the optimum values were determined. Using this data with the aid of the Design Export 7.0 program, the regression model was found as a second degree polynomial equation. The coefficients of determination (R^2) for desulfurization and ash removal regressions were 0.96 and 0.97, respectively, in the determined model. The model prediction values and experimental results for desulfurization and ash removal in the investigated parameter intervals were compared and the fit was identified. In the experimental removal of sulfur types with optimum desulfurization it was found that pyritic 17.02%, sulfate 16.67% and organic 9.52%.

Received Date: 08.05.2017
Accepted Date: 14.04.2018

1. Introduction

Physical methods are commonly used in coal cleaning facilities to remove the ash content. Though physical methods remove coal ash to a significant degree, the sulfur content remains (Aksoy et al., 1981; Akalın and Öz, 1989; Atak and Güney, 1989; Tosun et al., 1994; Özbayoğlu and Mamurekli, 2002; Tuncalı et al., 2002). To remove a significant portion of sulfur in the chemical-based coal desulfurization process, longer treatment time and the use of solvents increases costs and difficulties are encountered in neutralising coal at the end of the process (Mukherjee and Borthaku, 2003; Nabeel et al., 2009; Tosun, 2012). Biological methods remove pyritic sulfur up to 70-80% in coal via consumption by special bacteria; however, removal of organic sulfur is very low and difficult (Göktepe, 2002). Biological methods can be applied to very finely ground coal and require times lasting days, and also require significant security precautions to protect the biological environment and prevent environmental effects (Tosun et al., 1994; Tosun, 2012).

Using new generation technologies like ultrasonic waves in the sulfur removal increases the process efficiency of physical coal cleaning processes and/or ensure equipment savings (Angle et al., 1988; Buttermore and Slomka, 1991; Ambedkar et al., 2011*a*, 2011*b*; Şahinoğlu and Uslu, 2013). When ultrasonic waves are used in the chemical demineralization and desulfurization processes, they are stated to increase process efficiency (Baruah and Khare, 2007; Ambedkar et al., 2011*a*, 2011*b*; Saikia et al., 2014*a*, 2014*b*, 2016). When conventional methods (using HNO_3 and H_2O_2 as reactives, in the order of wetting; 300 min and mixing; 500, 1000 rpm, 60 min) for coal desulfurization are compared with ultrasonic processes (with 20 kHz frequency prop; with reactives (HNO_3, 23 min and H_2O_2, 30 min) and aqueous), total sulfur removal with ultrasonic methods (with 20 kHz frequency; with reactives 87% (HNO_3), 74%

* *Corresponding author: İlkay ÜNAL SANSAR, ilkay.unal@mta.gov.tr*
http://dx.doi.org/10.19111/bulletinofmre.417405

(H_2O_2) and aqueous 55%) is higher compared to conventional methods [with wetting, 46% (HNO_3) and 35% (H_2O_2); mixing rates of 500 and 1000 rpm, 25% (HNO_3), 29% (H_2O_2) and 24% (HNO_3), 27 (H_2O_2%), respectively] and when reactives are used, this removal conspicuously increases (Ambedkar et al., 2011*b*). After HF/HNO_3 acid leach processes Iranian coal with sulfur content of 1.89% reached a sulfur content of 1.26% (sulfur removal 33.33%), while after pretreatment with ultrasonic waves and then the leach process sulfur content was found to fall to 1.16% (sulfur removal 38.62%) (Royaei et al., 2012).

When ultrasonic waves are applied to a mixture of coal and water, the physical bonds between coal and mineral material are broken and with the mass transfer mechanism two possible events occur as mineral material is more easily dissolved and removed. In environments with ultrasonic waves, oxidation occurs called the advanced oxidation process and this transforms the sulfur in coal into water-soluble sulfate (Özkan, 1998; Gül, 2001; Ambedkar et al. 2011*a*, 2011*b*; Royaei et al., 2012; Saikia et al., 2014*a*, 2014*b*, 2016). During effective desulfurization, strong oxidant like environment friendly H_2O_2 is aided by the ultrasonic system ensure sulfur removal in a short time interval. When hydrogen peroxide reacts with almost all forms of sulfur and converts them into soluble sulfate it does not produce any harmful by-products (Saikia et al., 2016). The desulfurization process with ultrasonic waves is a method ensuring removal with minimum treatment time and less use of solvents and is recommended for its capabilities at industrial scales (Ambedkar et al., 2011*b*; Saikia et al., 2014*a*, 2014*b*).

Modelling and optimization of chemical processes carry great importance in terms of economic and technically efficient operation of these processes. Response Surface Method (RSM) is a statistical tool that has been used for optimization of ash and sulfur removal with a variety of methods in recent years and in assessing the single and binary/multiple effects of process parameters. The most commonly applied form of the response surface method is Central Composite Design (CCD) created with second degree equations (Karacan et al., 2007; Montgomery, 2009; Türk, 2016).

In this study, Muğla Yatağan (MY) Bağyaka lignite was used with total sulfur content of 2.69% and organic sulfur responsible for a large proportion of 2.10% of this sulfur. MY Bağyaka lignite was determined to have washability of moderately difficult degree (65% recovery, 20% ash removal and no sulfur removal, Akalın and Öz, 1989) or very difficult degree (18.84% ash removal and no sulfur removal, Tuncalı et al., 2002); as a result the necessity to reduce the high sulfur amounts unable to be removed with washing was stated. In this way, this research and development (R&D) study of the chemical desulfurization process conducted using ultrasonic waves for MY Bağyaka lignite to determine the optimum conditions for parameters affecting the ash and sulfur removal potentials with the response surface method and a model was developed. With this aim, the process parameters to obtain optimum desulfurization (sulfur removal) and ash removal of ultrasonic treatment time, solid content, chemical reactive (H_2O_2) concentration and reactive (H_2O_2) volume were chosen and optimum values were determined.

2. Material and Method

2.1. Material

The MY Bağyaka lignite used in our study was obtained by blending samples stacked at the entrance to Yatağan Thermal Power Plant. Lignite samples were reduced to -250 μm particle size after crushing, milling and screening processes, and after that were placed in airtight bags for use in experiments. The chemical analysis results of the lignite were determined in accordance with ASTM standards (D7582, D4239, D5865), and sulfur analysis types were determined according to TS 329 ISO 157 (Table 1). The particle size distribution of lignite was determined using a Malvern Mastersizer 2000 (Hydro 2000 MU) particle size analyser (Table 2).

2.2. Experimental Procedure

According to the design matrix shown in table 3, 30 experiments were performed with the parameters of ultrasonic treatment time (5, 10, 20, 30, 35 min), solid content (5, 10, 20, 30, 35%), concentration of chemical reactive (0, 0.5, 1.5, 2.5, 3 M 30% H_2O_2) and chemical reactive volume (20, 40, 80, 120, 140 ml H_2O_2). Keeping the total volume as 200 ml for all the experiment, the lignite (-250 μm) and a homogeneous mixture of distilled water and hydrogen peroxide (30%) were placed in a 500 ml erlenmeyer flask and they were processed in an ultrasonic bath with power of 500 W and frequency of 28 kHz for the desired treatment time. The lignite mixture obtained at the end of the experiment was filtered with rough filter paper and washed with hot distilled water. The

Table 1- Chemical analysis of Muğla Yatağan Bağyaka lignite.

	Air dried (ad)	Dry basis (db)	Dry ash free (daf)
Proximate Analysis			
Moisture (%)	8.39	–	–
Ash (%)	35.97	39.27	–
Volatile matter (%)	39.45	43.06	70.90
Fixed Carbon (%)	16.19	17.67	29.10
Sulfur Analysis			
Total sulfur (%)	2.47	2.69	–
Pyritic sulfur (%)	0.43	0.47	–
Sulfate sulfur (%)	0.11	0.12	–
Organic sulfur (%)	1.93	2.10	–
Lower calorific analysis			
Lower calorific value (kcal/kg)	3069	3404	5604

Table 2- Particle size distribution for Muğla Yatağan Bağyaka lignite.

Lignite	d(0,1), µm	d(0,5), µm	d(0,9), µm	d(sauter), µm	SSA[a], m^2/g
MY Bağyaka	2.718	17.399	120.798	6.494	0.924

d(0,1), d(0,5), d(0,9): particle diameters at 10%, 50%, 90% points, d(sauter): Sauter mean diameter, a: Specific surface area.

Table 3- Independent process parameters and coding levels.

Parametre	Code	Unit	Coded Parameter Levels				
			-α	-1	0	+1	+α
Time	X_1	min	5	10	20	30	35
Solid content	X_2	%	5	10	20	30	35
Reactive concentration	X_3	M	0	0.5	1.5	2.5	3
Reactive volume	X_4	ml	20	40	80	120	140

washed lignite remaining on the filter paper was dried overnight in an oven at 80±5ºC. The obtained lignite samples had ash and total sulfur contents identified. The flow schematic of the process is given in figure 1.

Desulfurization (sulfur removal, DE), Ash Removal (AR) and Recovery (R) were determined based on the following equations (1), (2) and (3), respectively. In these equations, C_F and C_P are the

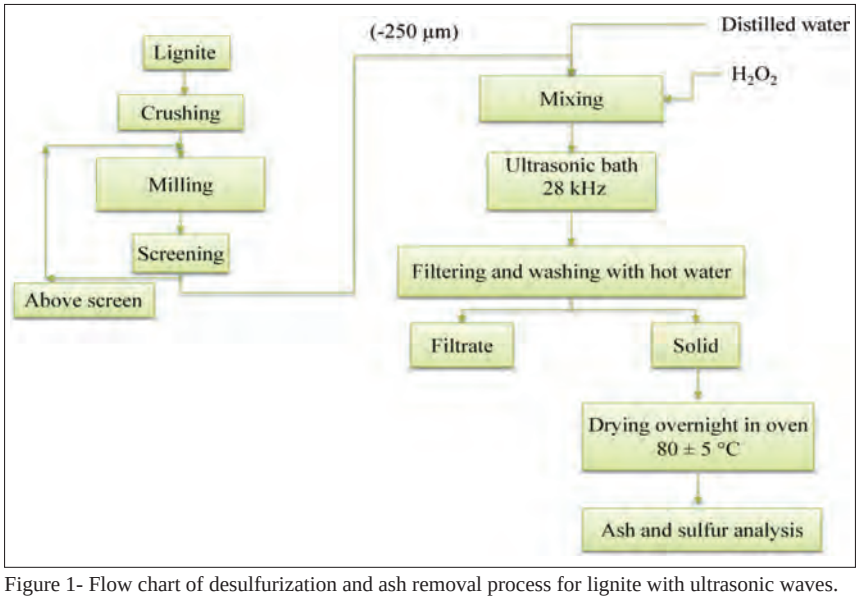

Figure 1- Flow chart of desulfurization and ash removal process for lignite with ultrasonic waves.

total % sulfur content in original feed and ultrasonic processed lignite; A_F and A_p are the % ash content in original feed and ultrasonic processed lignite; and C_a and C_f are the ash-free (g) amounts of ultrasonic processed and original feed lignite.

$$DE(\%) = [(C_F - C_P)/C_F]x100 \quad (1)$$

$$AR(\%) = [(A_F - A_P)/A_F]x100 \quad (2)$$

$$R(\%) = (C_a / C_f)x100 \quad (3)$$

2.3. Experimental Design

The response surface method (RSM) is defined as a method using mathematical and statistical techniques to develop a sufficient functional relationship between the response and independent variables. Within the experimental planning, preliminary experiments for factors affecting the process are performed, and levels are explored. After the levels are determined, the experimental studies in the pattern predicted by the program are completed and assessed with the aid of the program to reveal the optimum conditions of the process (Aygün, 2012). Generally to represent the system, second degree equations given in Equation (4) are used.

$$Y = \beta_0 + \Sigma\beta_i X_i + \Sigma \beta_{ii} X_i^2 + \Sigma \beta_{ij} X_i X_j \quad (4)$$

Here Y: predicted response, β_{ii}: square coefficient, β_i: linear coefficient, β_0: model constant, βij: coefficient showing mutual interaction between parameters, and Xi and Xj: independent variables of the process. Regression analysis with the second degree polynomial equation in the model estimates the coefficients to create the regression equation. With the aid of the created equation predicted results are obtained for the response and the accuracy of the predictions are checked to see if the model is sufficient or not.

The most commonly applied form of RSM is Central Composite Design (CCD) with a second degree response surface model created. The method has two factorial points. These are axis points (α) and central points. With k factor numbers (number of independent variables) and n_0 central point, the total number of design points is $N = 2^k + 2k + n_0$. Here the factor levels are coded as -1 for minimum and +1 for maximum. Axis points are beyond the two level points determined by the designer and are +α and –α values determined by the program. The central points are repeated points to estimate the experimental error. Finally in CCD each parameter has five levels. These are the factor points represented by +1 and -1, axis points represented by +α and –α and the central point represented by 0 (Montgomery, 2009; Türk, 2016).

In this study the independent variables of the system, their mutual interactions, and effects on obtaining the product were statistically analysed, modelled with RSM and had experiments designed with CCD. To determine optimum desulfurization (Y_1) and ash removal (Y_2) conditions, with the CCD method of RSM $2^4+2(4) + 6 = 30$ experiments were planned for 4 parameters. While 24 experiments were normal experiments, 6 were repeated experiments at the central points of individual variables. The parameters used in the experimental design were determined as ultrasonic treatment time (X_1), solid content (X_2), chemical reactive concentration (30% H_2O_2) (X_3) and reactive volume (H_2O_2) (X_4). The minimum, maximum, axis and central point values for variables given in table 3 form the experimental design matrix. Using this data with the aid of the Design Export 7.0 program, statistical analysis was performed and a regression model obtained.

3. Results and Discussions

According to the 30 experiments in the design matrix given in table 3 for treatment time (min), solid content (%), reactive concentration (M) and reactive volume (ml) parameters, the experimental (observed) data for desulfurization (DE) and ash removal (AR) of MY Bağyaka lignite are shown in table 4. With the aid of Design Export 7.0 program using this experimental data, statistical analysis was performed and a regression model obtained. The regression models of the desulfurization (Y_1) and ash removal (Y_2) are in the form of second degree polynomial equations given in Equations (5) and (6).

• Desulfurization

$$Y_1 = 6.60 - 0.40X_1 - 0.34X_2 + 1.02X_3 + X_4 - 0.094X_1X_2 + 0.23X_1X_3 + 0.37X_1X_4 + 0.32X_2X_3 - 0.84X_2X_4 + 0.046X_3X_4 - 0.40X_1^2 - 0.53X_2^2 - 0.28X_3^2 + 0.13X_4^2 \quad (5)$$

• Ash removal

$$Y_2 = 2.57 - 0.42X_1 - 0.79X_2 + 0.15X_3 + 0.13X_4 + 0.044X_1X_2 + 0.027X_1X_3 - 0.29X_1X_4 - 0.25X_2X_3 - 0.18X_2X_4 + 0.16X_3X_4 + 0.37X_1^2 + 0.24X_2^2 - 0.72X_3^2 - 0.13X_4^2 \quad (6)$$

Table 4- Experimental design matrix, desulfurization and ash removal results for MY Bağyaka lignite.

Run	Coded level of parameters				Experimental parameters				Observed values	
	X_1	X_2	X_3	X_4	X_1, min	X_2, %	X_3, M	X_4, ml	DE, %	AR, %
1	0	0	0	0	20	20	1.5	80	7.06	2.65
2	+1	+1	-1	-1	30	30	0.5	40	3.35	1.71
3	-1	-1	+1	+1	10	10	2.5	120	6.32	5.09
4	0	0	0	+α	20	20	1.5	140	9.29	1.43
5	0	0	0	0	20	20	1.5	80	5.95	2.24
6	-1	+1	-1	+1	10	30	0.5	120	3.35	2.55
7	-1	+1	+1	+1	10	30	2.5	120	5.95	2.52
8	+1	-1	+1	-1	30	10	2.5	40	4.09	2.83
9	+1	+1	+1	+1	30	30	2.5	120	7.06	1.15
10	-1	-1	-1	+1	10	10	0.5	120	6.32	3.13
11	0	-α	0	0	20	5	1.5	80	6.32	5.37
12	+1	-1	-1	+1	30	10	0.5	120	5.95	2.11
13	0	0	0	0	20	20	1.5	80	7.06	2.62
14	0	0	0	0	20	20	1.5	80	6.69	2.57
15	0	0	0	0	20	20	1.5	80	6.32	2.34
16	0	0	0	0	20	20	1.5	80	6.69	2.60
17	+1	-1	+1	+1	30	10	2.5	120	11.15	3.44
18	0	+α	0	0	20	35	1.5	80	4.09	1.27
19	+1	+1	+1	-1	30	30	2.5	40	7.81	1.25
20	-1	+1	+1	-1	10	30	2.5	40	6.69	1.73
21	-1	+1	-1	-1	10	30	0.5	40	3.72	1.20
22	-1	-1	+1	-1	10	10	2.5	40	5.20	2.24
23	0	0	+α	0	20	20	3.0	80	6.32	0.81
24	0	0	-α	0	20	20	0.0	80	5.20	1.53
25	+α	0	0	0	35	20	1.5	80	5.58	2.70
26	-1	-1	-1	-1	10	10	0.5	40	2.97	2.88
27	+1	-1	-1	-1	30	10	0.5	40	4.46	1.48
28	-α	0	0	0	5	20	1.5	80	5.20	4.99
29	+1	+1	-1	+1	30	30	0.5	120	4.83	1.12
30	0	0	0	-α	20	20	1.5	20	4.09	3.54

DE: Desulfurization, AR: Ash removal.

The coefficients of determination (R^2) for desulfurization and ash removal were determined as 0.96 and 0.97, respectively. The results of analysis of variance (ANOVA) to determine the significance of the model and the significance of terms in the model are given in tables 5 and 6.

High F value indicates the significance of the relevant term. Whether the F value has sufficiently high value or not is assessed with the p value. While low p values indicate rejection of the hypothesis, at the same time they represent the significance of the variable (whether the parameter has a greater effect on the result) (Aslan and Ünal, 2009; Kumar et al., 2009; Amani-Ghadima et al., 2013; Sabuncu, 2014). If the p value is smaller than 0.05 it is significant, if it is larger than 0.1 it is insignificant. In this situation the significant model terms are X_3, X_4 and X_2X_4 (Table 5) for desulfurization; and X_1, X_2, and X_3^2 (Table 6) for ash removal. The observed values for desulfurization, ash removal and the predicted values obtained in the model using Equations (5) and (6) are given together in table 7.

3.1. Optimization of Process Parameters

The desulfurization and ash removal results for MY Bağyaka lignite under optimum conditions found with the numerical optimization method for desulfurization (ODE), ash removal (OAR) and recovery are given in table 8. For desulfurization from MY Bağyaka lignite, the optimum process parameters found with the numerical optimization method were time 30 min, solid content 10%, chemical reactive concentration 2.5 M and reactive volume 120 ml producing 95.87% recovery and 9.54% optimum desulfurization. At this optimum desulfurization, the model prediction value for ash removal was 3.25%.

Table 5- Analysis of variance (ANOVA) for desulfurization of MY Bağyaka lignite.

Source	Total of squares	df	Mean of squares	F value	p value
Model	71.00	14	5.07	3.93	0.0063 significant
X_1-Time	3.45	1	3.45	2.67	0.1229
X_2-Solid content	2.42	1	2.42	1.88	0.1908
X_3-Reactive concentration	21.51	1	21.51	16.68	0.0010
X_4-Reactive volume	20.38	1	20.38	15.80	0.0012
X_1X_2	0.14	1	0.14	0.11	0.7458
X_1X_3	0.86	1	0.86	0.67	0.4256
X_1X_4	2.19	1	2.19	1.70	0.2121
X_2X_3	1.69	1	1.69	1.31	0.2703
X_2X_4	11.22	1	11.22	8.70	0.0099
X_3X_4	0.034	1	0.034	0.027	0.8728
X_1^2	1.81	1	1.81	1.40	0.2551
X_2^2	3.24	1	3.24	2.51	0.1340
X_3^2	0.93	1	0.93	0.72	0.4093
X_4^2	0.19	1	0.19	0.15	0.7067
Residual	19.34	15	1.29		
Lack of fit	18.52	11	1.68	8.20	0.0283
Pure Error	0.82	4	0.21		
Total	90.34	29			

Table 6- Analysis of variance (ANOVA) for ash removal of MY Bağyaka lignite.

Source	Total of Squares	df	Mean of square	F value	p value
Model	28.72	14	2.05	2.79	0.0288 significant
X_1-Time	3.81	1	3.81	5.19	0.0378
X_2-Solid content	12.68	1	12.68	17.26	0.0008
X_3-Reactive concentration	0.44	1	0.44	0.59	0.4529
X_4-Reactive volume	0.34	1	0.34	0.46	0.5090
X_1X_2	0.032	1	0.032	0.043	0.8387
X_1X_3	0.012	1	0.012	0.016	0.9018
X_1X_4	1.37	1	1.37	1.87	0.1914
X_2X_3	0.97	1	0.97	1.31	0.2696
X_2X_4	0.52	1	0.52	0.71	0.4124
X_3X_4	0.39	1	0.39	0.54	0.4753
X_1^2	1.58	1	1.58	2.15	0.1631
X_2^2	0.66	1	0.66	0.90	0.3575
X_3^2	5.87	1	5.87	7.99	0.0128
X_4^2	0.20	1	0.20	0.27	0.6128
Residual	11.02	15	0.73		
Lack of fit	10.90	11	0.99	35.11	0.0018
Pure Error	0.11	4	0.028		
Total	39.74	29			

Table 7- Observed and predicted results for desulfurization and ash removal for MY Bağyaka lignite.

Run	Experimental parameters				DE, %		AR, %	
	X_1, min	X_2, %	X_3, M	X_4, ml	Observed	Predicted	Observed	Predicted
1	20	20	1.5	80	7.06	6.60	2.65	2.57
2	30	30	0.5	40	3.35	3.42	1.71	1.75
3	10	10	2.5	120	6.32	7.34	5.09	4.71
4	20	20	1.5	140	9.29	8.39	1.43	2.47
5	20	20	1.5	80	5.95	6.60	2.24	2.57
6	10	30	0.5	120	3.35	3.50	2.55	2.14
7	10	30	2.5	120	5.95	5.82	2.52	2.20
8	30	10	2.5	40	4.09	5.04	2.83	2.90
9	30	30	2.5	120	7.06	7.64	1.15	0.91
10	10	10	0.5	120	6.32	6.32	3.13	3.67
11	20	5	1.5	80	6.32	5.92	5.37	4.29
12	30	10	0.5	120	5.95	7.58	2.11	2.10
13	20	20	1.5	80	7.06	6.60	2.62	2.57
14	20	20	1.5	80	6.69	6.60	2.57	2.57
15	20	20	1.5	80	6.32	5.80	2.34	3.36
16	20	20	1.5	80	6.69	6.60	2.60	2.57
17	30	10	2.5	120	11.15	9.54	3.44	3.25
18	20	35	1.5	80	4.09	4.89	1.27	1.93
19	30	30	2.5	40	7.81	6.49	1.25	1.29
20	10	30	2.5	40	6.69	6.15	1.73	1.40
21	10	30	0.5	40	3.72	4.01	1.20	1.97
22	10	10	2.5	40	5.20	4.32	2.24	3.20
23	20	20	3.0	80	6.32	7.50	0.81	1.18
24	20	20	0.0	80	5.20	4.43	1.53	0.74
25	35	20	1.5	80	5.58	6.31	2.70	2.77
26	10	10	0.5	40	2.97	3.48	2.88	2.78
27	30	10	0.5	40	4.46	3.27	1.48	2.38
28	5	20	1.5	80	5.20	5.11	4.99	4.04
29	30	30	0.5	120	4.83	4.38	1.12	0.74
30	20	20	1.5	20	4.09	5.40	3.54	2.08

DE: Desulfurization, AR: Ash removal.

Table 8- Desulfurization, ash removal and recovery results under optimum conditions found with the numerical optimization method for MY Bağyaka lignite.

	Experimental parameters				Lignite (daf), g		Product (db), %		Removal, %				R, %
					Feed	Product	Sulfur	Ash	Sulfur		Ash		
	X_1	X_2	X_3	X_4					O	P	O	P	
ODE	30	10	2.5	120	11.13	10.67	2.39	37.92	11.15	9.54	3.44	3.25	95.87
OAR	10	10	2.5	120	11.13	10.65	2.52	37.27	6.32	7.34	5.09	4.71	95.69

ODE: Optimum values for lignite desulfurization conditions, OAR: Optimum values for lignite ash removal conditions, R: Recovery, X_1: Time, X_2: Solid content, X_3: Reactive concentration (H_2O_2), X_4: Reactive volume (H_2O_2), O: Observed, P: Predicted, db: dry basis, daf: dry ash free.

For ash removal from MY Bağyaka lignite, the optimum process parameters found with the numerical optimization method were time 10 min, solid content 10%, chemical reactive concentration 2.5 M and reactive volume 120 ml producing 95.69% recovery and 4.71% optimum ash removal. At this optimum ash removal, the model prediction value for desulfurization was 7.34%. The optimum desulfurization and ash removal of MY Bağyaka lignite of the observed results were 11.15% and 5.09%, respectively. According to optimization results to confirm the accuracy of the process, repeated experimental results were 10.29% and 4.94%, respectively. For desulfurization and ash removal of MY Bağyaka lignite, according to optimization results to confirm the accuracy of the process, repeated experimental results were 10.29%

and 4.94%, respectively. From the obtained results, the model in the form of second degree polynomial equation may be said to have accuracy and validity proven for desulfurization and ash removal.

In experiments performed according to the design matrix in table 3, other parameters were fixed (solid content 20%, chemical reactive concentration (H_2O_2) 1.5 M and reactive volume (H_2O_2) 80 ml) and ultrasonic process time was increased from 5 min to 20 min, which increased sulfur removal from 5.20 % to 7.06% while ash removal fell from 4.99% to 2.65%. When pure water is used as reactive instead of hydrogen peroxide, the other parameters were fixed (time 20 min, solid content 20%, chemical reactive concentration (water) 0.0 M and reactive volume (water) 80 ml), and after ultrasonic wave treatment sulfur removal was 5.20% and ash removal was 1.53%. When pure water is used instead of hydrogen peroxide, sulfur removal fell from 7.06% to 5.20% while ash removal fell from 2.65% to 1.53%. The use of hydrogen peroxide as reactive increased sulfur and ash removal. In the hydrogen peroxide environment, oxidation occurs with the ultrasonic waves and this transforms the sulfur present in the coal into water-soluble sulfate (Ambedkar et al. 2011*a*, 2011*b*; Saikia et al., 2014*a*, 2014*b*, 2016). For effective desulfurization strong oxidants, like cost efficient and environmentally-friendly hydrogen peroxide, with the aid of an ultrasonic system produce sulfur removal in a short time interval.

For desulfurization and ash removal from MY Bağyaka lignite, the Malvern particle size analyser results for original and optimum conditions are given in table 9. As seen in the table 9, the specific surface area values (m^2/g) of lignite fell from 0.924 to 0.631 for desulfurization and from 0.924 to 0.818 for ash removal. This reduction is greater for desulfurization compared to ash removal. During desulfurization of lignite with ultrasonic waves, the pore volume of the lignite is reduced and as a result the specific surface area reduced. When the desulfurization parameters are fixed (solid content 10%, chemical reactive concentration (H_2O_2) 2.5 M and reactive volume (H_2O_2) 120 ml), increasing the time from 10 min to 30 min increases sulfur removal from 6.32% to 11.15% while ash removal falls from 5.09% to 3.44%. This reduction in ash removal may be due to fine minerals being held in the interior sections of the lignite or in large pores on the surface during the reaction.

Additionally during the desulfurization of MY Bağyaka, observed analysis types of lignite under original and optimum conditions, sulfur analysis types, removal of ash and sulfur analysis types are given in table 10 as dry basis. In table 10, it appears the organic sulfur amount in original lignite is higher compared to pyritic and sulfate sulfur. During combustion of lignite, a large portion of organic sulfur transforms to sulfur dioxide (SO_2) (Ateşok, 1986; Şahinoğlu, 2006). As organic sulfur is bound to the molecular structure of lignite, as long as chemical bonds holding the molecules together are not broken, it is not possible to remove it from lignite (Özbayoğlu, 1982). With desulfurization of MY Bağyaka lignite, total, pyritic, sulfate and organic sulfur reduced. Total sulfur fell from 2.69% to 2.39%, pyritic sulfur fell from 0.47% to 0.39%, sulfate sulfur fell from 0.12% to 0.10% and organic sulfur fell from 2.10% to 1.90%. It appeared

Table 9- Malvern particle size analysis result under original and optimum conditions for desulfurization and ash removal of MY Bağyaka lignite.

Lignite	d(0,1), μm	d(0,5), μm	d(0,9), μm	d(sauter) μm	SSA[a], m^2/g
Original	2.718	17.399	120.798	6.494	0.924
Optimum desulfurization	4.127	36.742	242.809	9.502	0.631
Optimum ash removal	3.170	20.447	144.227	7.335	0.818

d(0,1), d(0,5), d(0,9): particle diameters at 10%, 50%, 90% points, d(sauter): Sauter mean diameter, a: Specific surface area.

Table 10- Sulfur analysis types and removal of sulfur analysis types (observed) under original and optimum conditions for desulfurization of MY Bağyaka lignite (dry basis).

MY Bağyaka Lignite	Sulfur, %					Sulfur removal, %				Ash removal, %
	Pyritic	Sulfate	Organic	Total		Pyritic	Sulfate	Organic	Total	
Original	0.47	0.12	2.10	2.69		-	-	-	-	-
Optimum condition	0.39	0.10	1.90	2.39		17.02	16.67	9.52	11.15	3.44

that ultrasonic waves (28 kHz) in the hydrogen peroxide environment had a positive effect on removal of sulfur types from lignite.

Saika et al. (2014*a*) used 20 kHz frequency prop with ultrasonic treatment time of 180 min and H_2O_2 reactive on four different Indian coals (with low ash, high sulfur content and high organic sulfur content, with similar rank and origin obtained from different areas) and obtained removal of sulfur analysis types (pyritic 16.66-51.21%, sulfate 32.83-47.61%, organic 4.05-47.60% and total 19.81-31.09%) and ash removal (7.78-32.47%). In this study similar to the literature, desulfurization of MY Bağyaka lignite in a short time of 30 min obtained total sulfur removal of 11.15%, pyritic sulfur removal of 17.02%, sulfate sulfur removal of 16.67%, organic sulfur removal of 9.52% and ash removal of 3.44%. The differences in sulfur types and ash removal in coals may be due to the nature of mineral material composition and organic sulfur compounds in coal (Grounds and Wandless, 1952; Ely and Barnhart, 1963; Lowry, 1963; Ünal, 1999; Ambedkar et al., 2011*a*, 2011b; Saikia et al., 2014*a*, 2014*b*, 2016).

3.2. Three Dimensional (3D) Surface Figures

In desulfurization and ash removal from MY Bağyaka lignite, 3 dimensional (3D) surface graphics based on the interaction of optimum process parameters obtained using the numerical optimization method in Equations (5) and (6) were obtained. The correlation between the variables and effects are more clearly understood with the aid of these graphics. Though the model included four variables, on each graphic two variables were fixed at the centre and the other two variables had values within the limits. The response surface graphics produced 12 responses as a function of the two fixed variables and the two variables within the limits. When the two variables for desulfurization and ash removal are fixed in the centre, and the other two variables have values within the determined limits, the obtained three dimensional surface graphics are shown in figure 2 (a-f) and figure 3 (a-f).

As seen on figure 2 (a-f), for desulfurization as the ultrasonic treatment time, chemical reactive concentration and reactive volume increase, sulfur removal increased; however as solid content increased sulfur removal reduced. For ash removal, as chemical reactive concentration and reactive volume increased, ash removal increased; as ultrasonic treatment time and solid content increased, ash removal reduced (Figure 3 (a-f)). Within the investigated parameter intervals on 3D surface graphics, it appears all variables play an important role in desulfurization and ash removal from MY Bağyaka lignite.

4. Conclusion

In this study, the sulfur and ash removal potential with ultrasonic waves was investigated for MY Bağyaka lignite.

1. In determination of optimum conditions, experiments were performed for 4 parameters using the central composite design of the response surface method. With this aim, the optimum values were determined for the process parameters of ultrasonic treatment time, solid content, chemical reactive concentration and reactive volume to obtain optimum desulfurization (sulfur removal) and ash removal. With the aid of Design Export 7.0 program using this data, statistical analysis was performed and a regression model was obtained. The desulfurization (Y_1) and ash removal (Y_2) given in the model equations were stated as functions of time (X_1), solid content (X_2), chemical reactive concentration (X_3) and reactive volume (X_4) coded units. The regression model was found to be a second degree polynomial equation. The coefficients of determination for desulfurization and ash removal were determined as 0.96 and 0.97, respectively.

2. With the numerical optimization method for MY Bağyaka lignite with 95% and above recovery, the optimum desulfurization and ash removal prediction values were 9.54% (time 30 min, solid content 10%, chemical reactive concentration 2.5 M and reactive volume 120 ml) and 4.71% (time 10 min, solid content 10%, chemical reactive concentration 2.5 M and reactive volume 120 ml).

3. During desulfurization and ash removal from MY Bağyaka lignite, specific surface area values were reduced. During desulfurization of lignite with ultrasonic waves, the pore volume of the lignite reduced and as a result there was a reduction in specific surface area.

4. In the literature, it was determined to be difficult to remove sulfur with physical separation

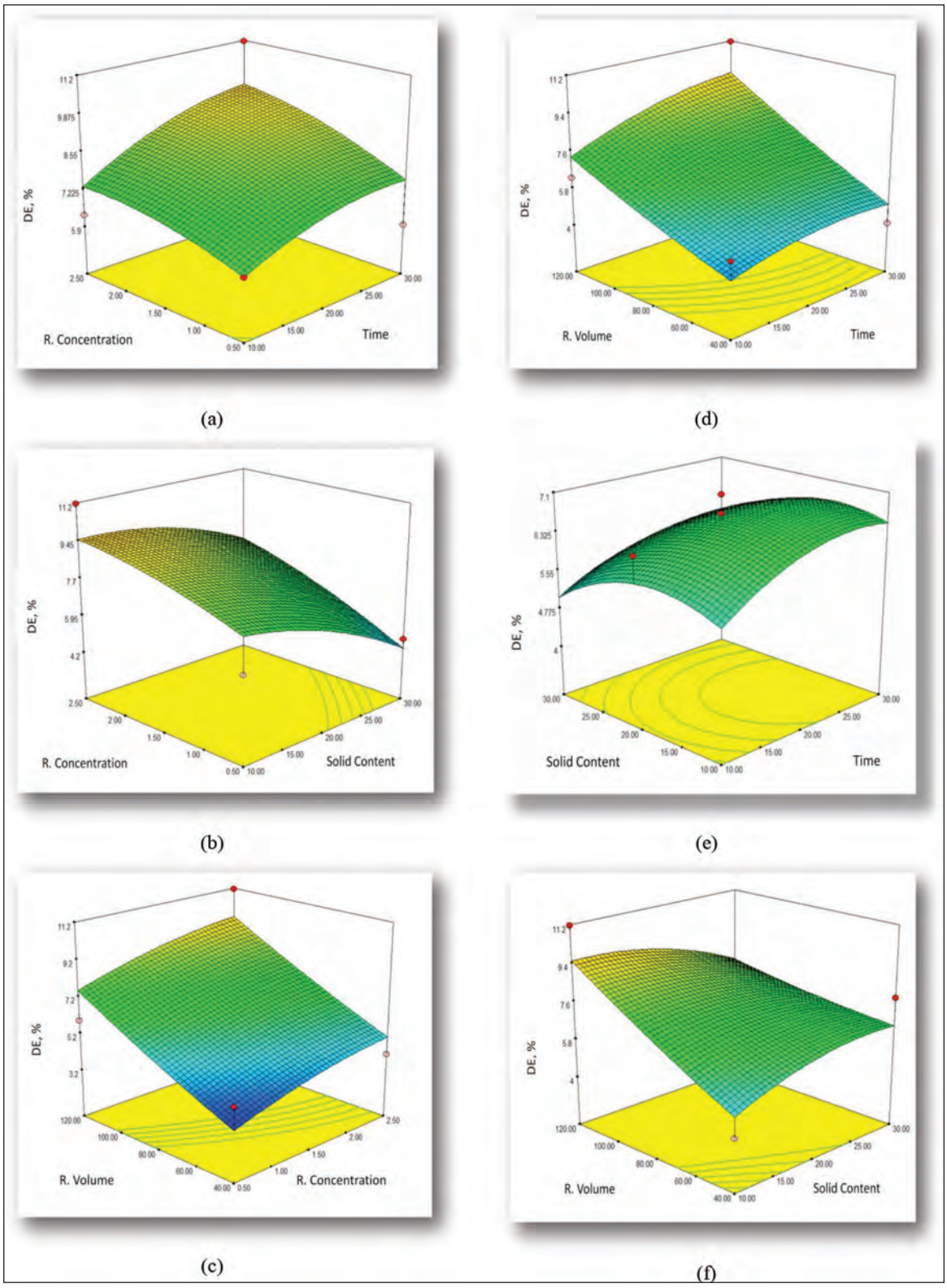

Figure 2- Response surface graphs showing of the effect of two variables on desulfurization (DE) of MY Bağyaka lignite (other two variables are held at center level): (a) reactive concentration and time; (b) reactive concentration and solid content; (c) reactive volume and reactive concentration; (d) reactive volume and time; (e) solid content and time; (f) reactive volume and solid content.

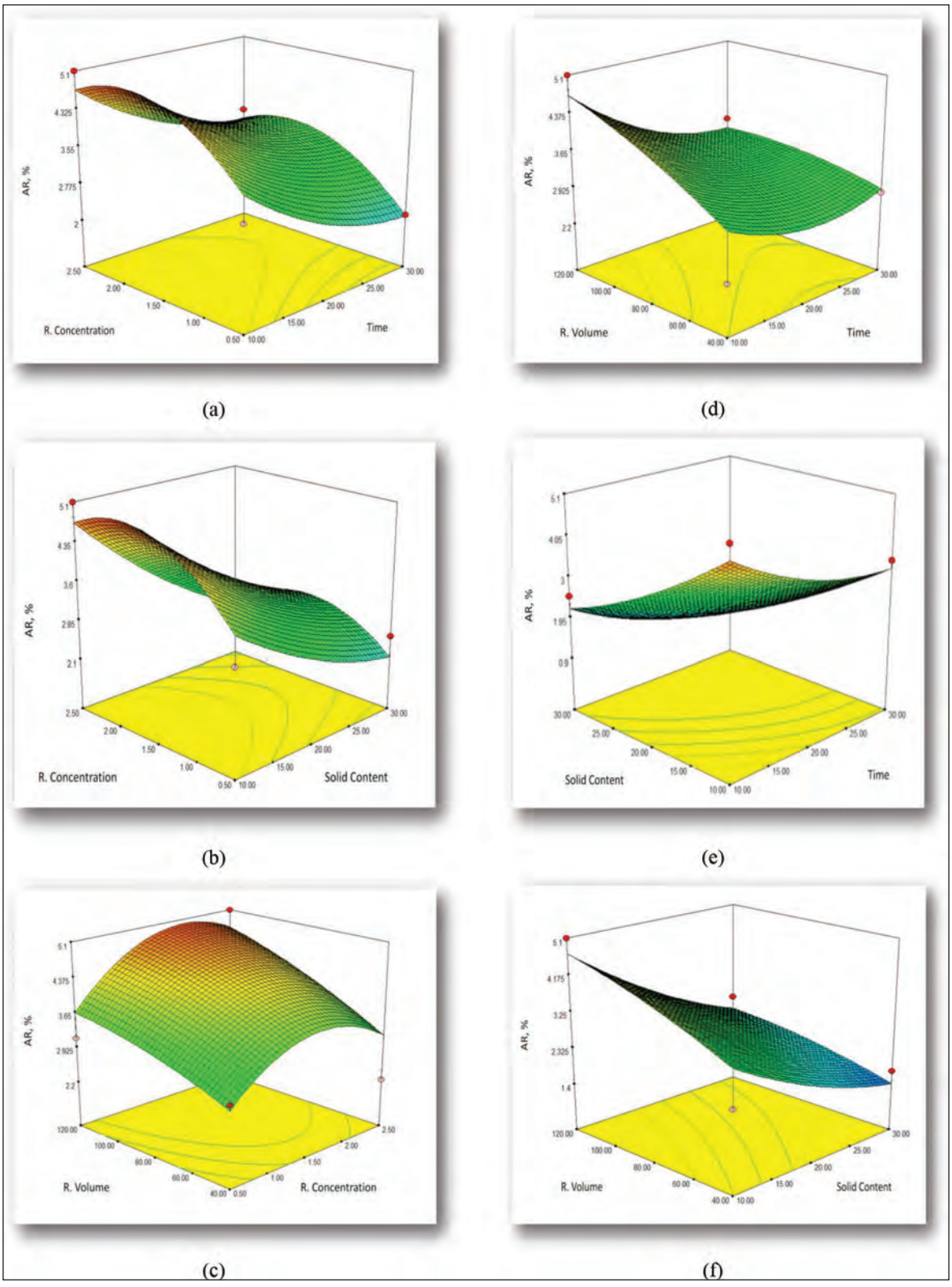

Figure 3- Response surface graphs showing of the effect of two variables on ash removal (AR) from MY Bağyaka lignite desulfurization (other two variables are held at center level): (a) reactive concentration and time; (b) reactive concentration and solid content; (c) reactive volume and reactive concentration; (d) reactive volume and time; (e) solid content and time; (f) reactive volume and solid content.

methods due to the high organic sulfur amounts in MY Bağyaka lignite. The chemical desulfurization process with ultrasonic waves had a positive effect on removal of all sulfur types (pyritic 17.02%, sulfate 16.67% and organic 9.52%) with low treatment time, low solid content, and low chemical reactive concentration and volume.

5. On dry basis, with desulfurization optimization total sulfur content reduced from 2.69 to 2.39%, with ash content reducing from 39.27 to 37.92%; with ash removal optimization, total sulfur content reduced from 2.69 to 2.52%, with ash content reducing from 39.27 to 37.37%.

6. According to optimization results based on repeated results to confirm the accuracy of the process, the model in the form of a second degree polynomial equation was seen to have accuracy and validity confirmed for desulfurization and ash removal within the interval of the investigated parameters.

Acknowledgements

This study was supported by Mineral Research and Exploration General Directorate (MTA) (Project Special Code No: 2014-35-16-07; 2015-35-16-07). The author thanks to her colleagues of MTA for their support.

References

Akalın, M. Öz, Z. 1989. Hava Kirliliğini Azaltmak Amacıyla Isınmada Kullanılan Linyitlerin Yıkanabilirliği. Türkiye 6. Kömür Kongresi Bildiriler Kitabı.

Aksoy, S., Bektimuroğlu, O., Doğan, H., Özden, Ü., Parmaksızoğlu, A. 1981. Çan Linyitlerinin Kül Ve Kükürtten Fiziksel Yöntemlerle Arındırılması (Ara Rapor-1). MTA Enstitüsü, Teknoloji Dairesi Başkanlığı, Cevher Zenginleştirme Servisi, Ankara.

Amani-Ghadima, A.R., Aber, S., Olad, A. Ashassi-Sorkhabi, H. 2013. Optimization of Electrocoagulation Process for Removal of An Azo Dye Using Response Surface Methodology and Investigation on the Occurrence of Destructive Side Reactions, Chemical Engineering and Processing, 64, 68-78.

Ambedkar, B., Chintala, T.N., Nagarajan, R., Jayanti, S. 2011*a*. Feasibility Of Using Ultrasound-Assisted Process For Sulfur And Ash Removal From Coal, Chemical Engineering And Processing:Process Intensification, 50, 236-246.

Ambedkar, B., Nagarajan, R., Jayanti, S. 2011*b*. Ultrasonic Coal-Wash For De-Sulfurization, Ultrasonics Sonochemistry, 18, 718-726.

Angle, C. W., Donini, J. C., Hamza, H. A. 1988. The Effect Of Ultrasonication On The Surface Properties, Ionic Composition And Electrophoretic Mobility Of An Aqueous Coal Suspension, Colloids suraces, 30 (3-4), 373-385.

Aslan, N., Ünal, İ. 2009. Optimization Of Some Parameters On Agglomeration Performance Of Zonguldak Bituminous Coal By Oil Agglomeration, Fuel, 88, 490-496.

Atak, S., Güney, A. 1989. Bazı Linyitlerin Yapısal Özellikler ve Kükürt Bakımından İncelenmesi. Türkiye 6. Kömür Kongresi Bildiriler Kitabı.

Ateşok, G. 1986. Kömür Hazırlama, Kurtiş Matbaacılık, 190 s.

Aygün, A. 2012. Tekstil Endüstrisi Reaktif ve Dispers Boya Banyo Atıksularının Elektrokoagülasyon Prosesi ile Arıtımı: Yanıt Yüzey Yöntemi ile Optimizasyon, Doktora Tezi, Selçuk Üniversitesi Fen Bilimleri Enstitüsü, 218 s, Konya.

Baruah, B.P., Khare, P. 2007. Desulfurization of oxidized indian coals with solvent extraction and alkali treatment. Energy Fuels, 21, 2156–2164.

Buttermore, W. H., Slomka, B. J. 1991. Effect Of Sonic Treatment On The Flotability Of Oxidized Coal. International Journal of Mineral Processing, 32 (3-4) 251-257.

Ely, F. G., Barnhart, D. H. 1963. Chemistry coal utilazation supplementary vol. Lowry, H. H. (Ed.), Wiley, Chapter, 19; 820-891, New York.

Göktepe, F. 2002. Kömür flotasyonunda bakteri ilavesinin piritik kükürt uzaklaştırmasına etkisi. Türkiye 13. Kömür Kongresi Bildiriler Kitabı, 29-31 Mayıs, Zonguldak.

Grounds, A. Wandless, A. M. 1952. The mineral matter in coal and its relation to preparation problems. Journal of the Institute of Fuel, 25; 170-177.

Gül, E. 2001. Ses Dalgaları İle Türk Linyitlerinin Zenginleştirilmesinin Kömür Dönüşümü Ve Ürün Dağılımı Üzerine Etkisi, Doktora Tezi, Ankara Üniversitesi Fen Bilimleri Enstitüsü Kimya Mühendisliği Anabilim Dalı, 93 s. Ankara.

Karacan, F., Özden, U., Karacan, S. 2007. Optimization Of Manufacturing Conditions For Activated Carbon From Turkish Lignite By Chemical Activation

Using Response Surface Methodology, Applied Thermal Engineering, 27, 7, 1635-1659.

Kumar, M., Ponselvan, F.I.A., Malviya, J.R., Srivastava, V.C. Mall, I.D. 2009. Treatment of Bio-digester Effluent by Electrocoagulation Using Iron Electrodes, Journal of Hazardous Materials, 165, 345-352.

Lowry, H. H. 1963. Chemistry of coal utilization sup., John Wiley and Sons Inc., New York.

Montgomery, D.C. 2009. Design and analysis of experiments, 7th ed., John Wiley&Sons, New York, 2009.

Mukherjee S., Borthaku P.C. 2003. Effect of leaching high sulphur subbituminous coal by potassium hydroxide and acid on removal of mineral matter and sulphur. Fuel, 82, 783-788.

Nabeel A., Khan T.A., Sharma D. K. 2009. Studies on the Production of Ultra Clean Coal by Alkali-acid Leaching of Low-grade Coals. Energy Sources Part A., 31, 594-601.

Özbayoğlu, G. 1982. Determination of Washability Characteristics of Some Turkish Lignites with Ash and Sulphur Content, Doktora Tezi, Orta Doğu Teknik Üniversitesi, Fen Bilimleri Enstitüsü, Ankara.

Özbayoğlu G, Mamurekli M. 2002. Super-Clean Coal Production From Turkish Bituminous Coal. Fuel, 72, 7, 1221-1223.

Özkan, Ş.G. 1998. Ultrasonik İşlemlerin Flotasyon Üzerindeki Etkileri, İstanbul Üniversitesi Mühendislik Fakültesi Yerbilimleri Dergisi, Cilt:11, Sayı 1, İstanbul, 131-135

Royaei, M. M., Jorjani E., Chelgani, S. C. 2012. Combination of Microwave and Ultrasonic Irradiations as a Pretreatment Method to Produce Ultraclean Coal M. International Journal of Coal Preparation and Utilization, 32,143–155.

Sabuncu, M. E. 2014. Süt ve Süt Ürünleri Endüstrisi Atık sularının Elektrokoagülasyon Yöntemi İle Arıtımında RSM Kullanılarak Proses Optimizasyonu, Yüksek Lisans Tezi, Yıldız Teknik Üniversitesi Fen Bilimleri Enstitüsü, 106 s. İstanbul.

Saikia, B. K., Dutta, A. M., Baruah, B. P. 2014*a*. Feasibility Studies Of De-Sulfurization And De-Ashing Of Low Grade Medium To High Sulfur Coals By Low Energy Ultrasonication. Fuel, 123, 12-18.

Saikia, B.K., Khound , K., Baruah, B.P. 2014*b*. Extractive de-sulfurization and de-ashing of high sulfur coals by oxidation with ionic liquids. Energy Convers. Manage. 81, 298–305.

Saikia, B. K., Dalmora, A. C., Choudhury, R., Das, T., Taffarel, S. R., Silva, L. F. O. 2016. Effective removal of sulfur components from Brazilian power-coals by ultrasonication (40 kHz) in presence of H2O2. Ultrasonics Sonochemistry 32, 147–157

Şahinoğlu, E. 2006. Müzret (Artvin-Yusufeli) Kömürünün Yağ Aglomerasyonu İle Temizlenmesi, Yüksek Lisans Tezi, Karadeniz Teknik Üniversitesi,Trabzon.

Şahinoğlu, E., Uslu, T. 2013. Increasing Coal Quality By Oil Agglomeration After Ultrasonic Treatment, Fuel Processing Technology, 116, 332–338.

Tosun, Y.I., Rowson N.A., Veasey, T.J. 1994. Bio-column flotation of Coal for Desulfurization and Comparison with Conventional and Column Flotation. 5th International Conference Of Mineral Processing, Nevşehir, 465-471.

Tosun, Y. I. 2012. Kısmi ergiyik kostik liç yöntemi ile türk linyitlerinin kükürtsüzleştirilmesi-mermer atık tozu kullanımı. Süleyman Demirel Üniversitesi, Fen Bilimleri Enstitüsü Dergisi, 16-1, 103-108.

Tuncalı, E., Çiftçi, B., Yavuz, N., Toprak, S., Köker, A., Gencer, Z., Ayçık, H., Şahin, N. 2002. Türkiye Tersiyer Kömürlerinin Kimyasal ve Teknolojik Özellikleri. Maden Tetkik ve Arama Genel Müdürlüğü, Ankara.

Türk, T. 2016. Merkezi Kompozit Tasarımı Kullanılarak Bakır Cürufundan Arsenik Liçinin İncelenmesi, Hacettepe Üniversitesi Yerbilimleri Uygulama ve Araştırma Merkezi Bülteni, Yerbilimleri, 37 (3), 193-202.

Ünal, İ. 1999. Kömürün Yağ Aglomerasyonu ve Ekstraksiyon Çarının İyileştirilmesi, Doktora Tezi, Ankara Üniversitesi Fen Bilimleri Enstitüsü, 120 s. Ankara.

ACKNOWLEDGEMENT

We would like to thank to the honored reviewers whose names are written below by contributing to the Bulletin of the Mineral Research and Exploration during the article review process between 13th of December 2017 and 13th of November 2018 in the name of the Executive Publication Editorial.

ABDULSAMAD Esam O. (Libya)
ABOUZEID Abdel-Zaher M. (Egypt)
AFZAL Peyman (Iran)
ALBORA Ali Muhittin (Turkey)
AMAR Mounir (Morocco)
ARAUJO Ofelia (Brazil)
ARISOY Muzaffer Özgü (Turkey)
ARSLAN Mehmet (Turkey)
ARSLAN Şebnem (Turkey)
ASGHARI Omid (Iran)
ASLAN Zafer (Turkey)
ATALAY Fırat (Turkey)
AYDIN Ali (Turkey)
AYDIN Harun (Turkey)
AYDIN Olgu (Turkey)
AYSAL Namık (Turkey)
BAĞCI Utku (Turkey)
BATI Zühtü (Turkey)
BAYARI Serdar (Turkey)
BEKAR Kürşat (Turkey)
BENDEREV Aleksey (Bulgaria)
BENEDETTI Andrea (Italy)
BISWAS Arkoprovo (India)
BİLİR Turhan (Turkey)
BİNAL Adil (Turkey)
BUCCI Giovanna (Italy)
CALCATERRA Domenico (Italy)
CAMERLENGHI Angelo (Italy)
CENGİZ Oya (Turkey)
CHATZIPETROS Alexandros (Greece)
CHRİSTANİS Kimon (Greece)
ÇELİK Mehmet (Turkey)
ÇİFTÇİ Emin (Turkey)
ÇİFTÇİ Yahya (Turkey)
ÇİNER Atilla (Turkey)
ÇUBUKÇU Evren (Turkey)
DARDENİZ Gonca (Turkey)
DEMIR Gökhan (Turkey)
DEMİR Yılmaz (Turkey)
IŞIK Veysel (Turkey)
İLHAN Semiha (Turkey)
JALALI Mohammad (Iran)
JESUS Prentis De (USA)
JODIERI Behshad (Iran)
KADIOĞLU Yusuf Kağan (Turkey)
KADİR Selahattin (Turkey)
KALENDER Leyla (Turkey)
KARABIYIKOĞLU Mustafa (Turkey)
KARADAĞ Mehmet Muzaffer (Turkey)
KARAHANOĞLU Nurkan (Turkey)
KARAKAŞ Zehra (Turkey)
KARAKUŞ Hüseyin (Turkey)
KARAOĞLAN Fatih (Turkey)
KARAYİĞİT Ali İhsan (Turkey)
KAVAK KaaN Şevki (Turkey)
KIYAK Alper (Turkey)
KHATIB Jamal (England)
KOH Sang Mo (South Korea)
KORALAY Banu Demet (Turkey)
KORKANÇ Mustafa (Turkey)
KOŞUN Erdal (Turkey)
KURŞUN İlgin (Turkey)
KURTULUŞ Bedri (Turkey)
KUŞÇU Ercan (Turkey)
KUŞÇU İlkay (Turkey)
KUZUCUOĞLU Catherine (France)
KÜRÜM Sevcan (Turkey)
LAMPROPOULOU Paraskevi (Greece)
LENTZ Dave (Canada)
LESS György (Hungary)
LISHCHUK Viktor (Swedish)
MADANI Nasser (Kazakhistan)
MAHTO Vikas (India)
MALVIC Tomislav (Croatia)
MANFREDA Salvatore (Italy)
MATTIOLI Michele (Italy)
MICHETTI Alessandro Maria (Italy)
MUKHERJEE Soumyajit M. (India)
ÖZYURT Nur (Turkey)
ÖZYURTKAN Mustafa Hakan (Turkey)
PAPAZZONI Cesare Andrea (Italy)
PARLAKTUNA Mahmut (Turkey)
PEKŞEN Ertan (Turkey)
PIGNATTI Johannes (Italy)
PTáčEK Petr (Czech Republic)
RIZAOĞLU Tamer (Turkey)
SAN Bekir Taner (Turkey)
SAN Dilek (Turkey)
SARI Ali (Turkey)
SARIKAYA Mehmet Akif (Turkey)
SARP Gülcan (Turkey)
SCHRANK Eckart (Germany)
SCHROEDER Paul A. (USA)
SEGHEDI Ioan (Romania)
SENTHILKUMAR R.D. (Oman)
SEYİTOĞLU Gürol (Turkey)
SILYE Lorand (Germany)
SMITH Martin (England)
SOMAY Adile Melis (Turkey)
SÖNMEZ Harun (Turkey)
SÖZBİLİR Hasan (Turkey)
SÜTÇÜ Emine (Turkey)
ŞAFAK Ümit (Turkey)
TABAR Emre (Turkey)
TAKORABT Mebarka (Algeria)
TAPETE Deodato (Italy)
TARTAROTTI Paola (Italy)
TEMANI Rim (Tunus)
TEMEL Abidin (Turkey)
THOMSEN Erik (Denmark)
TOPÇU İlker Bekir (Turkey)
TOPRAK Selami (Turkey)
TOSUN Levent (Turkey)
TÖRK Koray (Turkey)
TRUONG Xuan Quang (Vietnamese)
TUĞAN Murat Fatih (Turkey)
TUĞRUL Atiye (Turkey)

DEMİRELA Gökhan (Turkey)
DİNÇER Feyza (Turkey)
DUMAN Tamer Yiğit (Turkey)
EKMEKÇİ Mehmet (Turkey)
EKMEKÇİ Zafir (Turkey)
EL NADY Mohamed Mostafa (Egypt)
EREN Yaşar (Turkey)
ERTUNÇ Güneş (Turkey)
GANGULI Shib Sankar (India)
GENÇ Ömürden (Turkey)
GÖKÇE Ahmet (Turkey)
GÖRMÜŞ Muhittin (Turkey)
GÜLBAY Reyhan Kara (Turkey)
GÜLEN Levent (Turkey)
GÜRBOĞA Şule (Turkey)
GÜRBÜZ Alper (Turkey)
GÜREL Ali (Turkey)
H.T Basavarajappa (India)
HANİLÇİ Nurullah (Turkey)
HäSSIG Marc (France)
HEMASINGHE Hasali (Sri Lanka)
HOTZA Dachamir (Brazil)
HUDOCKOVA Natalia (Slovakia)
IFEANYI Chinwuko A. (Nigeria)
MUTLU Halim (Turkey)
NABATIAN Ghasem (Iran)
NARSIMHA Adimalla (India)
NAZİK Atike (Turkey)
NEFESLİOĞLU Hakan (Turkey)
NEMEC Wojciech (Norway)
NEZAFATİ Nima (Iran)
OGUBAZGHI Ghebrebrhan (Eritrea)
OKAN Özlem Öztekin (Turkey)
OKYAY Ünal (Turkey)
OMRANI Hadi (Iran)
ORHAN Ayşe (Turkey)
ORUÇ Bülent (Turkey)
OSMANLIOĞLU Ahmet E. (Turkey)
OYAN Vural (Turkey)
OYMAN Tolga (Turkey)
ÖZALP Selim (Turkey)
ÖZCAN Ercan (Turkey)
ÖZÇELİK Yılmaz (Turkey)
ÖZGEN ERDEM Nazire (Turkey)
ÖZMEN Öner (Turkey)
ÖZTÜRK Bilal (Turkey)
ÖZTÜRK Hüseyin (Turkey)
ÖZTÜRK Yeşim Yücel (Turkey)
TUNOĞLU Cemal (Turkey)
TÜRKMEN İbrahim (Turkey)
TÜYSÜZ Okan (Turkey)
ULUGERGERLİ Emin (Turkey)
USTAÖMER Timur (Turkey)
UYSAL İbrahim (Turkey)
VAJDA Vivi (Swedish)
VAN DE SCHOOTBRUGGE Bas (Holland)
VERBURG Rens (USA)
VURAL Alaattin (Turkey)
WINCHESTER J.A. (England)
YAĞMURLU Fuzuli (Turkey)
YALÇIN Mustafa Gürhan (Turkey)
YAMAGUCHI Yasushi (Japan)
YAVUZ Ali Bahadır (Turkey)
YAVUZ Nurdan (Turkey)
YEKELER Mefrune (Turkey)
YENİLMEZ Firdevs (Turkey)
YILDIRIM Esra (Turkey)
YILDIRIM Özge (Turkey)
YILMAZ İsak (Turkey)
YILMAZER Erkan (Turkey)
YİĞİT Özcan (Turkey)
YİĞİTBAŞ Erdinç (Turkey)

PUBLICATION RULES FOR THE BULLETIN OF THE GENERAL DIRECTORATE OF MINERAL RESEARCH AND EXPLORATION

1. Aims of Publication

- To contribute to the providing of scientific communication on geosciences in Turkey and international community.
- To announce and share researches in all fields of geoscientific studies in Turkey with geoscientists worldwide.
- To announce scientific researches and practices on geoscientific surveys carried out by the General Directorate of Mineral Research and Exploration (MTA) to the public.
- To use the journal as an effective media for international publication exchange by keeping the journal in high quality, scope and format.
- To contribute to the development of Turkish language as a scientific language.

2. Scope

At least one of the following qualifications is required for publishing the papers in the *Bulletin of Mineral Research and Exploration*.

2.1. Research Articles and Review Articles

2.1.1. Original Scientific Researches

- These articles cover and contribute to the main subjects of the earth sciences, the original scientific researches and its results related to all aspects of disciplines in geoscience like exploration and evaluation of the underground sources and environmental problems, and
- The studies, which apply new aspects and methods for the solution of problems about the earth sciences and researches, which apply new aspects and methods for the solution of the problems, in the engineering sciences carried out in MTA.

2.1.2. Review articles

- These papers include comphrehensive scholarly review articles that summarize and critically assess previous geoscientific researches with a new perspective and reveal a new approach.

2.2. Discussion/Reply

- This type of article is intended for the discussion of papers that have already been published in the latest issue of the *Bulletin*. The discussion/reply type articles, which criticize all or a part of a recently published article, are published in the following first issue if it is submitted within six months after the publication of the *Bulletin*.
- The discussions are sent to the corresponding author of the original paper to get their reply before publication. The discussions abut the paper with two or more authors are sent only to the corresponding author.
- If the review article is not published within the prescribed preiod then it is published alone. Later sent replies are not published. Re-criticising of the replies is not allowed.
- The authors should obey the rules of scientific ethics and discussions in their discussion/reply papers. The papers in this category should not exceed four printed pages of the journal including figures and tables etc. The format of the papers should be compatible with the “Spelling Rules” of the *Bulletin.*

2.3. Short Notes

- The short notes part of the *Bulletin* covers short, brief and concisely written research reports for papers including the data obtained from ongoing and/or completed scientific researches and practices related to geoscience and new and/or preliminary factual findings from Turkey and worldwide.
- The short notes will follow a streamlined schedule and will normally be published in the following first or second issue shortly after submission of the paper to the *Bulletin*.
- This type of articles should not exceed four printed pages of the journal including figures, tables and an abstract.

3. Submission and Reviewing of Manuscripts

Manuscript to be submitted for publishing in the Journal must be written clearly and concisely in Turkish and/or English and prepared in the *Bulletin of Mineral Research and Exploration* style guidelines. All submissions should be made online at the **http://.dergi.mta.gov.tr** website.

- The manuscript submitted for reviews must not have been published partially or completely previously in another journal.

- The rejected manuscripts are not returned back to author(s) whereas a letter of statement indicating the reason of rejection is sent to the corresponding author.

- Submitted manuscripts must follow the *Bulletin* style and format guidelines. Otherwise, the manuscript which does not follow the journals' style and format guidelines, is given back to corresponding author without any reviewing.

- Every manuscript which passes initial Editorial treatise is reviewed by at least two independent reviewers selected by the Editors. Reviewers' reports are carefully considered by the Editors and associated editors.

- The manuscript that need to be corrected with the advices of reviewer(s) is sent back to corresponding author(s) to assess and make the required corrections suggested by reviewer(s) and editors. The authors should prepare a letter of well-reasoned statement explaining which corrections are considered or not.

- If there are any suggestions given by editors and referees that are not accepted and corrected by the author, then it should be sent to the Editor's Office with corrected copies of the report explaining the reason for not accepting these suggestions and corrections.

- Figures and tabless should be 1/3 of the main text.

- To be published in the *Bulletin of Mineral Research and Exploration*, the printed lenght of the manuscript should not exceed 30 printed pages of the journal including an abstract, figures and tables. The publication of longer manuscripts will be evaluated by Editorial Board if it can be published or not.

- The authors must do the reviewer's corrections and proposals in 60 days and must upload to the system.

- At the printing stage after the last control, the first print of the manuscript are sent to the author/ authors in pdf version and asked from the author/ authors to make the press control.

4. Publication Language and Periods

- *The Bulletin of Mineral Research and Exploration* is published at least twice a year and each issue is published both in Turkish and English. Thus, the manuscripts are accepted in Turkish or English. The spelling and punctuation guidelines of Turkish Language Institution are preferred for the Turkish issue. However, the technical terms related to geology are used in accordance with the decision of the Editorial Board.

5. Spelling Draft

- Manuscripts should be written in word format in A4 (29.7 x 21 cm) size and double-spaced with font size Times New Roman 10-point, margins of 25 mm at the sides, top and bottom of each page.

- The formulas requiring the use of special characters and symbols must be submitted by the symbols part of the Microsoft Office Word Program on computer.

- Initial letters of the words in sub-titles must be capital. The first degree titles in the manuscript must be numbered and left-aligned, 10 point bold Times New Roman must be used. The second degree titles must be numbered and left-aligned, they must be written with 10 point normal Times New Roman. The third degree titles must be numbered and left-aligned, they must be written with 10 point italic Times New Roman. The fourth degree titles must be left-aligned without having any number; 10 point italic Times New Roman must be used. The text must continue placing a colon after the title without paragraph returns (See: Sample article: http://bulletin.mta.gov.tr).

- One line spacing must be left after paragraphs within text.

- Paragraphs must begin with 0.5 mm indent.

- The manuscript must include the below sections respectively;

  - Title Page
  - The Name and Surname of the author and * sign (Adress, e-mail adres must be given at the bottom of the page)
  - Abstract
  - Key Words

- Introduction
- Body
- Discussion
- Conclusion
- Acknowledgements
- References

5.1. Title of the Article

- The title must be short, specific and informative and written with small letters font size Times New Roman 10-point bold. The title mustn't contain the subjects insufficiently processed in the article.

5.2. The Name of the Author, Address and E-Mail Adress

- The name and surname of the author/authors must be written without affiliations. Name must be written in small letters, the surname must be written in capital letters.
- At the affiliation (work adres) written after the name and the surname of the author/authors only the name of the company must be written, the author's job mustn't be written.
- Information about the adresses must be given at the next line as 10-point and italic.
- At the articles with two or more than two authors, the numbers must be written above the surnames of the authors, the informations about their adresses must be given at the next line by leaving one space line. Also, at this part the corresponding author must be indicated by the (*) symbol and the telephone, FAX and e-mail address of the corresponding author must be given.
- Abbreviations must not be made while writing the name of the uthor and the affiliation adres. Adresses must be given in Turkish in the Turkish version, in English in the English version.
- At the end of the article the name of the corresponding author and contact informations must be added.

5.3. Abstract

- The abstract must be understandable before having a look at the text.
- The abstract should state briefly the overall purpose of the research, the aim of the article, its contributions to the known theories, new data, principle results and major conclusions.
- Tha abstract must contain short and brief sentences.
- Addressing other sections and illustrations of the text or other writings must be avoided.
- The information, which have not been mentioned in the text, must not be in the abstract.
- The article must be written as one paragraph, preferably. Please provide an abstract which doesn't exceed 200 words.
- The abstract must be written with 10-point, normal Times New Roman in single-spaced lines.
- "Abstract" must not be given for the writings that will be located in "Short Notes" section.
- The English abstract must be under the title of "Abstract".

5.4. Key Words

Immediately after the abstract, please provide up to 5 key words and with each words seperated by comma. These key words will be used for indexing purposes.

5.5. Introduction

- The introduction section should state the objectives of the work, research methods, location of the study area and provide an adequate and brief background by avoiding a detailed literature survey.
- Non-standard or uncommon classifications or abbreviations should be avoided. But if essential, then they must be defined at their first mention and used consistently thereafter. Seperate paragraphs could be organized for each of the subjects at the introduction part. If it is necessary, the subtitle can be given for each of them (for example method, material, terminology etc.).
- When pre-information is needed for facilitating the understanding of the text, this section can also be used (for example, statistical data, bringing out the formulas, experiment or application methods, and others).

5.6. Body

- In this chapter, there must be data, findings and opinions that are intended to convey to the reader about the subject. The body section forms the main part of the article.
- The data used in other sections such as "Abstract", "Discussions", and "Results" are caused by this section.
- While processing the subject, the care must be taken not to go beyond the objective highlighted in the "Introduction" section. The knowledge, which do not contribute to the realization of the purpose of the article or are useless for conclusion, must not be included.
- All data used and the opinions put forward in this section must prove the findings obtained from the studies or they must be based on a reference by citation.
- The guidance and methods to be followed in processing subjects vary according to the characteristics of the subjects mentioned. Various topic titles can be used in this section as many as necessary.

5.7. Discussions

- Discussion of the data and findings that are objectively transferred in the Main Text section of the article should be done in this section. This must be written as a seperate section from the results section.

5.8. Conclusions

- The main conclusion of the study provided by data and findings of the research should be stated concisely and concretely in this section.
- **T**he subjects that are not mentioned sufficiently and/or unprocessed in the body section must not be included in this section.
- The conclusions can be given in the form of substances in order to emphasize the results of the research and to make the expression understandable.

5.9. Acknowledgements

In this section, the significant contributions made in the realization of investigation that form the topic of the paper is specified. While specifying contributions, the attitude diverted the original purpose of this section away is not recommended. Acknowledgements must be made according to the following examples.

- This study was carried out within scope of .....project.
- I/we would like to thank to …… for contributing to the development of this article with his/her critiques.
- Academic and/or authoritorial affiliations are written for the contributions made because of requirement of ordinary task.

For example:

- o "Prof. Dr. İ. Enver Altınlı has led the studies".
- o "The opinions and warnings of Dr. Tandoğan Engin are considered in determining the chemistry of chrome minerals."

- The contributions made out of the requirement of ordinary task:

For example:

o "I would like to thank to Professor Dr. Melih Tokay who gives the opportunity to benefit from unpublished field notes"; "I would like to thank to the preliminary-Plan Chief Engineer Ethem Göğer, State Hydraulic Work, 5th Zone". Academic and / or task-occupational titles are indicated for such contributions.

- The contributions, which are made because of requirement of ordinary task but do not necessitate responsibility of the contributor mustn't be specified.

For example:

o Sentences such as "I would like to thank to our General Manager, Head of Department or Mr. / Mrs. President ……who has provided me the opportunity to research" must not be used.

5.10. References

- All references cited in the text should be given in the reference list.
- The authors must be careful about the accuracy of the references. Publication names must be written in full.

- Reference list must be written in Times New Roman, 9-point type face.
- The reference list must be alphabetized by the last names of the first author of each work.
- If an author's more than one work is mentioned, then ranking must be made with respect to the publication year from old to new.
- In the case that an author's more than one work in the same year is cited, the lower-case alphabet letters must be used right after publication year (for example; Saklar, 2011a, b).
- If the same author has a publication with more than one co-author, firstly the ones having single author are ranked in chronological order, then the ones having multiple authors are ranked in chronological order.
- In the following examples, the information related to works cited is regulated in accordance with different document/work types, considering punctuation marks as well.
- If the document is located in a periodical publication (if it is an article), then the information about the document must be given in the following order: surnames of the author/authors, initial letters of author's/authors' first names. Year of publication. Name of the document. Name of the publication where the document is published, volume and/ or the issue number, numbers of the first and last pages of the document.

For example:

  - o Pamir, H.N. 1953. Türkiye'de kurulacak bir hidrojeoloji enstitüsü hakkında rapor. Türkiye Jeoloji Bülteni 4, 1, 63-68.
  - o Barnes, F., Kaya, O. 1963. İstanbul bölgesinde bulunan Karbonifer'in genel stratigrafisi. Maden Tetkik ve Arama Dergisi 61, 1-9.
  - o Robertson, A.H.F. 2002. Overview of the genesis and emplacement of Mesozoic ophiolites in the Eastern Mediterranean Tethyan region. Lithos 65, 1-67.

- If more than one document by the same authors is cited, first the documents having single name must be placed in chronological order, second the documents having two names must be listed in accordance with the chronological order and second author's surname, and finally the docments having multiple names must be listed in accordance with chronological order and third author's surname.
- If the document is a book, then; the surname of the author/authors, initial letters of the author's/ authors' first names. Year of publication. Name of the book (initial letters are capital). Name of the organization, which has published the book, name of the publication where the document is published, volume and/ or the issue number, total pages of the book.

For example

  - o Meric, E. 1983. Foraminiferler. Maden Tetkik ve Arama Genel Müdürlüğü Eğitim Serisi 23, 280 s.
  - o Einsele, G. 1992. Sedimentary Basins. Springer-Verlag, 628 p.

- If the document is published in a book containing the writings of various authors, the usual sequence is followed for the documents in a periodic publication. Then the editor's surname and initial letters of their name/names are written. "Ed.", which is an abbreviation of the editor word, is written in parentheses. Name of the book containing the document (initial letters are capital). Name of the organization which has published the book. Place of publication, volume number (issue number, if any) of the publication where the document is published, numbers of the first and last page of the document.

For example:

  - o Göncüoğlu, M.C., Turhan, N., Şentürk, K., Özcan, A., Uysal, Ş., Yalınız, K. 2000. A geotraverse across northwestern Turkey. Bozkurt, E., Winchester, J.A., Piper, J.D.A. (Ed.). Tectonics and Magmatism in Turkey and the Surrounding Area. Geological Society of London Special Publication 173, 139-162.
  - o Anderson, L. 1967. Latest information from seismic observations. Gaskell, T.F. (Ed.). The Earth's Mantle. Academic Press. London, 335-420.

- If the name of a book, where various authors' writings have been collected, is specified, those must be indicated respectively: book's editor/

editors' surname/surnames and initial letters of their name/names. "Ed.", which is an abbreviation of the editor word, must be written in parentheses. Year of Publication. Name of the book (initial letters are capital). Name of the organization which has published the book, total pages of the book.

For example:

- o Gaskel, T.F. (Ed.) 1967. The Earth's Mantle. Academic Press, 520 p.

- If the document is an abstract published in a Proceedings Book of a scientific activity such as conference/symposium/workshop …etc., the information about the document must be given in the following order: surnames of the author/authors, initial letters of author's/authors' first names. Year of publication. Title of the abstract. Name, date and place of the meeting where the Proceedings Book is published, numbers of the first and last pages of the abstract in the Proceedings Book.

For example:

- o Yılmaz, Y. 2001. Some striking features of the Anatolian geology. 4. International Turkish Geology Symposiums 24-28 September 2001, London, 13-14.

- o Öztunalı, Ö., Yeniyol, M. 1980. Yunak (Konya) yöresi kayaçlarının petrojenezi. Türkiye Jeoloji Kurumu 34. Bilim Teknik Kurultayı, 1980, Ankara, 36

- If the document is one of the unpublished documents as a report, lecture notes, and so on, the information about the document must be given by writing the word "unpublished" in parentheses at the end of information about the document after it is specified in accordance with usual order which is implemented for a document included in a periodic publication.

For example:

- o Özdemir, C. Biçen, C. 1971. Erzincan İli, İliç ilçesi ve civarı demir etütleri raporu. *General Directorate of Mineral Research and Exploration Report No: 4461*, 21 p. Ankara (unpublished).

- o Akyol, E. 1978. Palinoloji ders notları. EÜ Fen Fakültesi Yerbilimleri Bölümü, 45 p., İzmir (unpublished).

- The followings must be specified for the notes of unpublished courses, seminars, and so on: name of the document and course organizer. Place of the meeting, name of the book, corresponding page numbers must be given.

For example:

- o Walker, G. R. Mutti, E. 1973.Turbidite facies and facies associations. Pacific Section Society for Sedimentary Geology Short Course. Annaheim. Turbitides and Deep Water Sedimantation, 119-157.

- If the document is a thesis, the followings are written: surname of the author, initial letter of the author's first name. Year of Publication. Name of the thesis. Thesis type, the university where it is given, the total number of pages, the city and "unpublished" word in parentheses.

For example:

- o Seymen, İ. 1982. Kaman dolayında Kırşehir Masifi'nin jeolojisi. Doçentlik Tezi, İTÜ Maden Fakültesi, 145 s. İstanbul (unpublished).

- Anonymous works must be regulated according to the publishing organization.

For example:

- o MTA. 1964. 1/500.000 ölçekli Türkiye Jeoloji Haritası, İstanbul Paftası. Maden Tetkik ve Arama Genel Müdürlüğü, Ankara.

- The date after the name of the author is not given for on-printing documents; "in press" and / or "on review" words in parenthesis must be written. The name of the article and the source of publication must be specified, volume and page number must not be given.

For example:

- o Ishihara, S. The granitoid and mineralization. Economic Geology 75th Anniversary (in press).

- Organization name, web address, date of access on web address must be indicated for the information downloaded from the internet. Turkish sources must be given directly in Turkish and they must be written in Turkish characters.

For example:

- o ERD (Earthquake Research Department of

Turkey). **http://www.afad.gov.tr**. March 3, 2013.

- While specifying work cited, the original language must be used; translation of the title of the article must not be done.

6. Illustrations

- All drawings, photographs, plates and tables of the article are called as "illustration".
- The illustrations must be used when the use of them is inevitable or when they facilitate the understanding of the subject.
- While selecting and arranging the illustrations' form and dimensions, the page size and layout of the *Bulletin* must be considered. The unnecessary loss of space must be prevented as much as possible.
- The pictures must have high quality, high resolution suitable for printing.
- The number of illustrations must be proportional to the size of the text.
- All illustrations must be sent as in separate files independent from the text.
- While describing illustrations in the text, the abbreviations must be avoided and descriptions must be numbered in the order they are mentioned in the text.
- Photographs and plates must be given as computer files containing EPS, TIFF, or JPEG files in 600 dpi and higher resolutions (1200 dpi is preferable) so that all details can be seen in the stage of examination of writing.

6.1. Figures

- Drawings and photos (except for the plates in the text) will be evaluated together as "Figure" and they must be numbered in the order they are mentioned in the text.
- The figures published in the *Bulletin of Mineral Research and Exploration* must be prepared in computer considering the dimensions of single-column width 7.4 m or double-column width 15.8 cm. Figure area together with the writing at the bottom should not exceed 15.8x21in maximum.
- Unnecessasry details must not be given in figures or care must be taken not to use much space for information transfer.
- Figures must be arranged in such a way to be printed in black/white or colored.
- The figure explanations being justified in two margins must be as follows:

  Figure 1- Sandıklı İlçesinin (Afyon); a) güneybatısının jeolojik haritası, b) İnceleme alanının genel dikme kesiti (Seymen 1981), c) Türkiye'nin önemli neotektonik yapıları (Koçyiğit 1994'den değiştirilerek).

  Figure 1- a) Sandıklı ilçesinin güneybatısının jeolojik haritası, b) İnceleme alanının genel dikme kesiti (Seymen 1981), c) Türkiye'nin önemli neotektonik yapıları (Koçyiğit 1994'den değiştirilerek).

- Drawings must be made by well-known computer programs painstakingly, neatly and cleanly.
- Using fine lines, which can disappear when figures shrinks, must be avoided. Symbols or letters used in all drawings must be in Times New Roman and not less than 2 mm in size when shrink.
- All standardized icons used in the drawings must be explained preferably in the drawing or with figure caption if they are too long.
- Linear scale must be used for all drawings. Author's name, figure description, figure number must not be included into the drawing.
- Photos must be in quality and quantity that will reflect the objectives of the subject.

6.2. Plates

- Plates must be used when needed a combination of more than one photo and the publication on a special quality paper.
- Plate sizes must be equal to the size of available magazine page space.
- Figure numbers and linear scale must be written under each of the shapes located on the Plate.
- The original plates must be added to the final copy, which will be submitted, if the article is accepted.
- Figures and plates must be independently numbered. Figures must be numbered in Latin numerals and plates with Roman numerals (e.g., Figure1, Plate I).

- There must be no description text on Figures.

6.3. Tables

- All tables must be prepared preferably in word format in Times New Roman fonts.
- Tables together with table top writing must not exceed 15x8 cm in size.
- The table explanations being justified in two margins must be as follows:

Table 1- Hydrogeochemical analysis results of geothermal waters in the study area.

7. Nomenclature and Abbreviations

- Non-standard and uncommon nomenclature abbreviations should be avoided in the text. But if essential, then they must be described as below. In cases where unusual nomenclatures and unstandardized abbreviations are considered to be compulsory, the way followed and method must be described.
- Full stop must not be placed between the initials of words for standardized abbreviations (MER, SHW, etc.).
- Geographical directions must be abbreviated in English language as follows: N, S, E, W, NE …etc.
- The first time used abbreviations in the text are presented in parenthesis, the parenthesis is not used for subsequent uses.
- The metric system must be used as units of measurement.
- Figure, plate and table names in the article must not be abbreviated. For example, "as shown in the generalized stratigraphic cross-section of the region (Figure 1……..."

7.1. Stratigraphic Terminology

Stratigraphic classifications and nomenclatures must be appropriate with the rules of International Commision on Stratigraphy and/or Turkish Stratigraphic Committee. The formation names, which have been accepted by International Commision on Stratigraphy and/or Turkey Stratigraphy Committee, should be used in the manuscript.

7.2. Paleontologic Terminology

Fossil names in phrases must be stated according to the following examples:

o For the use of authentic fossil names;

e.g. Limestone with *Nummulites*

o When the authentic fossil name is not used;

o e.g. nummulitic Limestone

o Other examples of use;

e.g. The type and species of Alveolina/ Alveolina type and species

- Taxonomic ranks must be made according to the following examples:

Super family: Alveolinacea Ehrenberg, 1939	*Not reference, Not stated in the Reference section*
Family: Borelidae Schmarda, 1871	
Type genus: *Borelis* de Montfort, 1808	
Type species: *Borelis melenoides de Montfort, 1808*; *Nautilus melo* Fitchel and Moll, 1789	
Borelis vonderschmitti (Schweighauser, 1951) (Plate, Figure, Figure in Body Text)	*Schweighauser, 1951 not reference*
1951 *Neoalveolina vonderschmitti* Schweighauser, page 468, figure 1-4	*Cited Scweighauser (1951), stated in the Reference section.*
1974 *Borelis vonderschmitti* (Schweighauser), Hottinger, page, 67, plate 98, figure 1.7	*Cited Hottinger (1974), stated in the Reference section.*

- The names of the fossils should be stated according to the rules given below:

  - o For the first use of the fossil names, the type, spieces and the author names must be fully indicated;

    Alveolina aragoensis Hottinger

    Alveolina cf. *aragoensis* Hottinger

    Alveolina aff. *aragoensis Hottinger*

  - o When a species is mentioned for the second time in the text;

    A.aragoensis

    *A.*cf.*aragoensis*

    *A.*aff.*aragoensis*

  - o It is accepted as citiation if stated as *Alveolina aragoensis* Hottinger (1966).

- The statement of plates and figures (especially for the articles of paleontology):

  - o for the statement of species mentioned in the body text;

  Borelis vonderschmitti (Schweighauser, 1951).

  (plate, figure, figure in the body text).

  - o When cited for other articles;

  1951 *Neoalveolina vonderschmitti* Schweighauser, page 468, figure 1-4, figure in body text

  1974 *Borelis vonderschmitti* (Schweighauser), Hottinger, page 67, plate 98, figure 1-7

- For the citation in the text

  (Schweighauser, 1951, page, plate, figure, figure in the body text)

  (Hottinger, 1974, page, plate, figure 67, plate 98, figure 1-7, figure in the body text.)

8. Citations

All citations in the body text must be indicated by the last name of the author(s) and the year of publication, respectively. The citations in the text must be given in following formats:

- For publications written by single author;

  - It is known that fold axes of Devonian and Carboniferious aged units around Istanbul is in NS direction (Ketin, 1953, 1956; Altınlı, 1999).

  - Altınlı (1972, 1976) defined the general characteristics of Bilecik sandstone in detail.

- For publications written by two authors;

  - The upper parts of the unit contain Ilerdian fossils (Sirel and Gündüz, 1976; Keskin and Turhan, 1987, 1989).

- For publications written by three or more authors;

  According to Caner et al. (1975) the Alıcı formation reflects the fluvial conditions.

  The unit disappears by wedging out in the East direction (Tokay et al., 1984).

- If reference is not directly obtained but can be found in another reference, the cross-reference should be given as follows:

  - It is known that Lebling has mentioned the existence of Lias around Çakraz (Lebling, 1932: from Charles, 1933).

9. Reprints

The author(s) will receive (2) two hard copies of the related issues.

10. Copyright and Conditions of Publication

- It is necessary that the work submitted for the publication must be original and has not been previously unpublished in whole or partially.

- It is necessarry that the authors who send their publications to the *Bulletin of Mineral Research and Exploration* hereby accept the conditions of publication of the Bulletin in advance.

- All copyrights of the accepted manuscripts belong to MTA. The author or corresponding author on behalf of all authors (for papers with multiple authors) must sign and give the agreement under the terms indicated by the Regulations of Executive Publication Committee. Upon acceptance of an article, MTA can pay royalty to the authors upon their request according to the terms under the "Regulations of Executive Publication Committe" and the "Regulations of Royalty Payment of Public Office and Institutions"

All the information and forms about the *Bulletin of Mineral Research and Explorations* can be obtained from **http://dergi.mta.gov.tr**